

SOME ENGINEERING ASPECTS OF THE HYDROGEN-OXYGEN FUEL CELL

F. T. Bacon

Consultant to Energy Conversion Ltd.

Introduction

There is no doubt that the hydrogen-oxygen cell possesses a number of important characteristics which have made it much easier to develop into practical units capable of generating a useful amount of power, compared with hydrocarbon-air cells. It is perhaps worthwhile briefly to recapitulate these characteristics, and this will make plain the reasons for the choice of the particular system which was developed at Cambridge, England.

First of all, it is well known that hydrogen reacts electrochemically much more easily than any hydrocarbon fuel; this of course makes electrode design much easier.

Secondly, the use of pure hydrogen and oxygen makes it possible to use an alkaline electrolyte, which has obvious advantages in the lower cost of materials which can be employed for the electrodes, current collectors and other cell parts.

Thirdly, the use of pure gases means that an unvented system is possible, and this eliminates the additional problems which have to be faced when an inert diluent, such as CO_2 in a reformed hydrocarbon fuel, have to be vented from the system at the correct rate under all load conditions; this would seem to present quite an intricate control problem, if undue waste of fuel is to be avoided. Moreover, groups of cells would presumably have to be fed in series with the fuel gases, each group having its own control valve; it would clearly be too complicated to have a monitoring device on each cell to regulate the gas flow individually. Some of these arguments would also apply if air is used instead of pure oxygen; and in addition, control of the rate of water removal from the vented system may be difficult under conditions of varying air temperature and humidity. This is in contrast to the hydrogen-oxygen system, in which the only reaction product is steam which can easily be separated from the hydrogen in a simple air-cooled condenser, provided that the operating temperature of the cells is somewhat above ambient; parallel flow of hydrogen through all the cells in a battery can be used without difficulty, and small inequalities of flow through individual cells are of little consequence. Besides this, the higher partial pressures of the reacting gases, using pure hydrogen and oxygen, lead to a higher cell performance and a higher limiting current.

It must be admitted that even with very pure gases, occasional venting of the system to atmosphere is usually necessary, owing to the gradual build-up of inert diluents; but this, in our experience at Cambridge, need only be done very occasionally, especially if electrolytic gases are used, and can easily be done by hand.

Fourthly, there is the possibility of operating the battery at considerably elevated pressures. This has the advantage of reducing activation polarization of the electrodes and so yielding possible savings in weight, bulk and electrode cost. The use of elevated pressures also makes it possible to operate with an increased partial pressure of water vapour and hence a higher electrolyte conductivity and a more compact condenser. It is relatively simple to supply pure hydrogen and oxygen at elevated pressure, but, with a hydro-carbon-air cell, there would be complications and a heavy parasitic load due to the compressors.

Fifthly, there is the important fact that hydrogen cells can be made self-starting from cold; this was not a feature of the cells developed at Cambridge, where the decision had been taken to operate at the highest practicable temperature so as to minimize the problems associated with electrode activity. However, other workers have demonstrated hydrogen-oxygen cells with lower temperatures of operation, which will start from cold though relatively cheap catalysts are used; alternatively, very small amounts of precious metal catalysts may be employed with good results in this respect; it is assumed that one of the many new types of electrode, which depend on a degree of semi-wetness in the active layers, would be used.

It should be added that efforts were made, quite early in the work to think in terms of a complete working system rather than in terms of single cells, or even a battery of cells; and before the work was closed down at Cambridge, a complete working system was evolved, including gas admission, and control of temperature, electrolyte concentration and pressure difference across electrodes, under both steady and rapidly varying loads, with a unit of 40 cells which would develop up to 6 kw of power. (1)

Personnel

As it was only possible to employ very small teams, for financial reasons, it was essential to break as little fresh ground as possible, and the practical experience of both battery and electrolyser manufacturers was freely drawn upon; up till 1941, the author worked alone, the work being supported by Merz and McLellan, the well-known consulting engineers. From 1946-51, additional help was given by one part-time consultant, the work being done in the Departments of Colloid Science, and Metallurgy, Cambridge University. After this a small team was gradually built up in the Department of Chemical Engineering, Cambridge, the team consisting of two chemists, one metallurgist, one engineer (author) and three assistants, besides two part-time consultants, one being a physicist and the other an electrochemist. This team was unfortunately completely disbanded in 1956 owing to lack of support. From 1946-56 the work was financed by the Electrical Research Association, with additional help from the Ministry of Fuel and Power, and the Admiralty. In 1957, another team was built up with the help of the National Research Development Corporation, at Marshall of Cambridge Ltd., the total numbers of the team reaching a maximum of fourteen, including one chemist, one metallurgist and three engineers, besides five part-time consultants, one being a chemist, one a metallurgist, one a control engineer and two chemical engineers. Once again the team was completely

disbanded in 1961 owing to lack of industrial support in England. It should be added that the help given by the consultants was invaluable; all were men of wide theoretical knowledge and much practical experience, and without their help some serious mistakes would undoubtedly have been made.

Further Developments in Hydrogen-Oxygen Cells

The author has not carried out any experimental work since 1961, but it has been most interesting to watch the work of others during this time, particularly the wonderful developments which have taken place in the United States.

The stage has now been reached where completely automatic and reliable batteries, using hydrogen and oxygen, have been produced, these batteries being completely equipped with controls which will deal with all load conditions including rapidly varying loads; in addition to this, many are self-starting from cold. The first cost is still high, but this is systematically being reduced. Is it possible that some commercial application could now be found for this type of cell, apart from space and military uses?

Storage of Gases

The principal technical difficulty preventing the use of hydrogen-oxygen batteries for say traction purposes is, in the author's view, associated with the storage of the gases, in particular the storage of hydrogen; it seems inconceivable that liquid hydrogen could ever become a commercial fuel. It is, therefore, very important to watch for any new developments in science and engineering which could have a bearing on this difficult problem of hydrogen storage. As recently as 1959, the best ratio which could be quoted for weight of hydrogen carried to weight of container was 1 to 100; this was for nickel-chrome-molybdenum forged steel cylinders, with a working pressure of 3,000 p.s.i. (2). Since that time, considerable development has taken place in the design of gas vessels and a ratio of 1 to 43 can be quoted for weight of hydrogen to weight of steel with a gas pressure of 3,600 p.s.i.; a low carbon chrome-molybdenum steel is used at present, and welded construction; these figures refer to spheres, and assume that all the gas can be used, which is not strictly accurate but which does not introduce a serious error. Taking an average voltage of 0.8V per cell, and assuming the above weight ratio of 1 to 43 for hydrogen, and assuming also that oxygen is carried as well, the weight of gas vessels + hydrogen + oxygen comes out at about 8.1 lb/kwh. generated; with hydrogen alone, the weight would be 4.7 lb/kwh generated.

These gas vessels are not only used in missiles and military aircraft, but also in civil aircraft where very high standards of safety are of course required. Partly as a result of the American space programme, even further improvements in design appear to be under way; but it seems impossible to prophesy when, or even whether, resin fibre glass containers will become a practical proposition for the storage of hydrogen under ordinary commercial conditions. The whole question of ultra high strength materials is being intensively studied in many parts of the world (3), and it seems possible that, in the future, further reductions in the weight of gas vessels will be achieved.

Other factors which must be taken into account are volume, cost, safety and convenience, but it is not possible to go into these closely in this short paper. In the past, it has always been the weight which has made gas storage relatively unattractive.

Possible Applications for Hydrogen-Oxygen Cells

It has always seemed to the author that road and rail traction are the most promising applications for fuel cells; this applies particularly in the case of short range transport in cities, using public service vehicles. In the United Kingdom quite large numbers of battery driven delivery vehicles are used - the numbers have now risen to over 40,000 - and these are able to compete on level terms with engine driven vans, in spite of the weight and high first cost of the lead/acid batteries; this is basically because of the lower cost per mile of electricity compared with taxed gasoline, and also because of the lower maintenance costs of battery driven vehicles, under the rather special stop-start conditions under which delivery vans have to operate; and this is in spite of a much higher capital cost, part of which is due to the cost of the battery itself, and part to the fact that mass production methods cannot be used for the small numbers of vehicles produced. It is hoped that the fuel cell will eventually extend the field of battery traction into areas where the weight of lead batteries precludes the possibility of electric traction, owing to the fact that a rather higher speed and longer range are required.

The effective capacity of a typical lead-acid traction battery, at 80 amp discharge, has been given as 12.8 kwh.; this was for a 20 cwt. pay load delivery vehicle with a speed of 15-18 m.p.h. and a range of 25-30 miles (4). This capacity would require a weight of hydrogen + oxygen + gas vessels of $12.8 \times 8.1 = 104$ lb. Assuming that the weight of modern low temperature low pressure hydrogen-oxygen batteries on normal load is about 40 lb./kw., and also assuming that a power of 5.3 kw. is required on normal load (4), the weight of the battery alone would be 212 lb.; complete with gas vessels, the total weight would be 316 lb. Taking an up-to-date figure of 10.5 wh/lb for a lead traction battery, on a 2-3 hour discharge basis, a conventional battery would weigh 1,220 lb. If these figures can indeed be substantiated, it would appear that hydrogen-oxygen batteries cannot be ruled out for short range road traction, on a weight basis; in fact, they appear to be more or less substantiated by William T. Reid (5) in an estimate dealing with a passenger road vehicle with a range of 150 miles at 40 m.p.h. It is admittedly extremely difficult to compete on level terms with internal combustion engines, especially if a long range is required between re-fuellings; but a silent fume-free propulsion system would have many attractions for public service vehicles in cities, where they could easily return each night to a central refuelling station, thus avoiding the high cost normally associated with the distribution of hydrogen in cylinders. Reid (5) concludes that running costs, using electrolyzers for gas production, would compare favourably with gasoline-powered engines, even in the United States, and the comparison should be even better in the United Kingdom, though the analysis admittedly ignores the tax problem. So far, battery driven vehicles have been exempt from any form of fuel tax in the U.K. As regards the engineering problems

associated with the storage and transfer of compressed gases, much experience was obtained in England, before and during the Second World War, in the use of compressed coal gas as a fuel for propelling buses, and no special difficulties were encountered (2).

Conclusion

It has for many years been realized that there are two alternative applications for fuel cells; one is the task of producing batteries which will consume a hydrocarbon fuel and air; the other concerns the possibility of storing electrical energy; the author has always been drawn towards the latter application. It is true that the overall efficiency of the double process is not likely at present to exceed 50 per cent (6) and might indeed initially be somewhat below this figure (7); but it is hoped that, before long, some of the knowledge acquired by fuel cell workers will be applied to the process of electrolysis; this would entail extensive tests for endurance, in view of the present trouble-free life of at least ten years, which is now expected with existing designs. Further, it is likely that, in the foreseeable future, very cheap off-peak power will become available in the United Kingdom; in an article on "Large Scale Storage of Energy" A. B. Hart (8) states that with nuclear stations off-peak power may be available for storage at a generating cost of 0.25 penny (or 2.9 mils) per kwh, though this does not mean that it could be sold to a consumer at this very low price.

If practical power plants for short range road transport can be achieved, it would not be a very big step to design a larger plant suitable for propelling railcars, where the problems of weight and space are much less severe than with road transport; many battery driven railcars are now in use in Germany, where conditions are favourable for this application.

Lastly, it is hoped that the suggestions contained in this paper, which may be regarded as very reactionary, will not be taken as detracting in any way from the magnificent work which is being done in many parts of the world on hydrocarbon-air cells; but the latter project still seems some way from complete fulfilment, and it would, in the author's opinion, be of immense benefit to the whole fuel cell scene if some substantial commercial application could be found quite soon, even in a limited sphere such as the one suggested.

Acknowledgements

The author wishes to thank the Board of Energy Conversion Ltd. for permission to publish this paper. He would also like to thank his colleagues, particularly Mr. T. M. Fry, for much help and advice during the preparation of the paper.

References

1. Bacon, F. T. (et al.) "Fuel Cells," a C.E.P. technical manual. Amer. Inst. Chem. Eng., 1963, p. 66 ff.
2. Clarke, J. S. Proc. Inst. Automobile Eng., XXXIV, 1939-40, p. 43 ff.
3. Cottrell, A. H. et al. Proc. Roy. Soc., Series A, No. 1388, Oct. 1964. Vol. 282. "A Discussion on New Materials."
4. Sheers, W. D. and Heyman, H. W. Proc. Inst. Elec. Eng., 99, Part II, No. 71, Oct. 1952, p. 457 ff.
5. Reid, William T. Battelle Technical Review, 1965, 14 (4), pp. 9-15.
6. Bacon, F. T. U.N. Conf. on New Sources of Energy, Rome, Aug. 1961. Preprint 35/Gen/9.
7. Euler, J. World Power Conference, Lausanne, Sept. 1964, Paper 110, 11E. "The Storage of Electrical energy by means of galvanic fuel cells." (in German)
8. Hart, A. B. Science Journal, May 1965, pp. 70-75. "Large scale storage of energy".

HYDROCARBON-AIR FUEL CELL SYSTEMS

Dr. Galen R. Frysinger

Energy Conversion Laboratory
U. S. Army Engineer Research and Development Laboratories
Fort Belvoir, Virginia 22060

INTRODUCTION

In reviewing the state-of-the-art I wish to include all hydrocarbon-air system configurations. This is defined broadly to include all fuel cell systems which utilize a hydrocarbon fuel and an air oxidant. The four variations which have been under investigation at this laboratory are shown schematically in Figure 1.

EXTERNAL REFORMER INDIRECT SYSTEM

The external reformer indirect systems are based on the use of separate hydrocarbon reformers to liberate the bound hydrogen energy of a liquid hydrocarbon fuel. Hydrogen produced from hydrocarbons by the conventional steam reforming process has been of commercial importance for some time. Only recently, however, has emphasis been placed on simplification and miniaturization of these process plants to become compact hydrogen generators for fuel cell systems. The first hydrogen generators for fuel cell systems which were constructed over the last few years using natural gas, methanol, or JP-4 as the fuel were quite bulky and heavy because they utilized largely state-of-the-art, off-the-shelf type process components. These hydrogen generators, themselves, weighed between 100 and 200 lbs/KW equivalent of hydrogen produced. In one instance, with the Engelhard reformer fabricated under contract to USAERDL, a special fuel and water pump and air blowers were developed to greatly reduce the weight and the electrical power consumed by these auxiliaries. Only recently has emphasis been placed on the design of very lightweight systems. Based on hydrogen reformer systems which are still at the design (Contract DA-44-009-AMC-967(T) with Pratt and Whitney Aircraft) or very early development stage, it is estimated that about 40-45 lbs/KW must be assigned to this major component.

A second major component of an indirect system is the hydrogen-air fuel cell stack or module. Based on electrode performances of greater than 200 amps per square foot at 0.8 volts per single cell, this component should have a weight of 15-20 lbs per KW for a 28 volt stack in the 2-10 KW size range.

A third major component for an a.c. fuel cell powerplant is the combination voltage regulator and inverter. Recent experience with hardware procured by USAERDL indicates that inverter weights are within the range of 10-15 lbs/KW of net a.c. output. By adding together the weights of these major components it is evident that only about 20 to 30 lbs/KW are allowable for the auxiliaries if a

power density of 100-110 lbs/KW is to be obtained for a total a.c. output, fuel cell powerplant. A power density of 100 lbs/KW is roughly that obtained with conventional engine generators.

Therefore, for a fuel cell powerplant to be weight competitive, a major emphasis must be placed on process simplification. Major weight reduction is best achieved by elimination of unneeded components. To cite one example, in an Army fuel cell powerplant for operation in the field, adequate moisture must be reclaimed for use in the steam reformer to avoid the need for makeup water. In the present Allis Chalmers 5 KW system (USAERDL Contract DA-44-009-AMC-240(T)), Figure 2, part of this moisture is reclaimed from the air exhaust, but the major portion comes from the evaporation and condensation in an air stream of water removed from a circulating KOH stream. This requires that a water removal plate be included next to each hydrogen electrode in each single cell to allow the excess moisture to come in contact with and dilute the circulating KOH. In this system part of the water is reclaimed also from the reformer combustion exhaust.

In a much simplified system now being studied (Contract DA-44-009-AMC-967(T) with Pratt and Whitney Aircraft) all of the moisture from the cell is removed in the air exhaust which is used as the combustion air for the reformer burner. A single condenser is therefore all that would be required to condense the required water from the burner exhaust. This simplification would eliminate two condensers, blowers, valves and piping as well as simplifying the cell stack construction.

Future wide application of indirect systems will be dependent on research to achieve greatly improved current densities and to protect the reformer catalyst from the sulfur impurities found in presently available liquid hydrocarbon fuels. Research now in progress indicates that current densities several times the 200 ASF at 0.8 V, which is now state-of-the-art, may be achieved in hydrogen-air cells with very low or no platinum metal content of the electrodes. Likewise, research studies indicate that the "guard catalyst", renewable cartridge, technique may be applicable to protect the compact hydrogen generator catalyst from excessive degradation due to sulfur impurities.

INDIRECT ACID ELECTROLYTE SYSTEMS

The description and weight predictions already given are based on a pure hydrogen alkaline electrolyte system which involves a major weight penalty due to the inclusion of a scrubber to remove the small amounts of carbon dioxide present in the incoming air and for a hydrogen diffusion membrane purification system. For an indirect system based on an acid electrolyte hydrogen-air fuel cell module, the carbon dioxide scrubber would not be required and also the possibility exists that an impure hydrogen contaminated with small or moderate amounts of carbon monoxide, may be utilized directly. The attractiveness of the acid electrolyte system, however, depends largely on the power density which can be achieved in the hydrogen-air cell stack and the efficiency with which hydrogen and air can be electrochemically converted in the acid electrolyte system. Because of the

significant system simplifications, research emphasis is being placed on electrode structures and electrocatalysts for the anodic oxidation of hydrogen-carbon monoxide mixtures with air. Under Contract DA-44-009-AMC-479(T) with General Electric a tungsten oxide-platinum black electrocatalyst system has shown high activity for this mixture. Using very thin electrodes and lightweight plastic cell components and a circulating electrolyte coolant, a module of comparable power density to that of an alkaline system may be achieved even with the lower voltages of the acid electrolyte single cell.

INTERNAL REFORMER INDIRECT SYSTEM

The principal disadvantages of an external reformer are the need to operate the reformer at temperatures of about 1400°F to produce significant quantities of hydrogen, and the need to control the hydrogen production rate to match exactly the fuel requirements of the cell at all times. The internal reforming cell developed by Pratt and Whitney (Contract DA-44-009-AMC-756(T) for operation with hydrocarbons and air may overcome some of these problems. In this cell, the hydrocarbon-steam reaction occurs in a catalyst bed which is in direct contact with the fuel cell anode. With a concentrated potassium hydroxide electrolyte the cell can be operated at 500°F, at which the equilibrium for hydrocarbon-steam reactions is such that only a small percentage of hydrogen is produced. However, as the fuel cell anode consumes the hydrogen by diffusion through the silver-palladium anode, the equilibrium is shifted so that it is possible to convert a high proportion of the fuel to hydrogen and to utilize this hydrogen in the anode reaction. This type of cell can be more efficient since the endothermic reform reaction takes its heat requirement directly from the waste heat of the cell. Such a system is largely self-controlling since hydrogen is produced only as fast as it is required by the anode.

The status of this system and its ability to utilize hydrocarbon fuels will be discussed in detail in another paper in this symposium.

The principal research problem is to find the optimum reforming catalyst. The catalyst should have very high activity (fast kinetics for the hydrocarbon to hydrogen reaction) at 500°F and be stable for long term operation. The commercially available reforming catalysts designed for higher temperature (1500°F) operation are not necessarily the best for this lower temperature reforming. Serious catalyst activity decay problems have been encountered. The relative attractiveness of the internal reforming hydrocarbon-air system will depend largely on what improvements are possible in the long term stability of the reformer catalysts.

PARTIAL OXIDATION OF LIQUID FUELS AND MOLTEN CARBONATE FUEL CELLS

The air partial oxidation of liquid hydrocarbon fuels is insensitive to the fuel type or the amounts of sulfur found in military fuels. Under Contract DA-44-009-AMC-54(T) (Texas Instruments), marine white gasoline, JP-4, kerosene, Number 2 diesel fuel, and CITE engine fuel, ranging in sulfur content from 30 ppm to 3,200 ppm, were successfully converted to electrical power in a partial

oxidation molten carbonate fuel cell system. The unpurified product of partial oxidation is utilized directly in the molten carbonate fuel cell. The sulfur is carried into the anode as hydrogen sulfide but does not adversely affect performance. The molten carbonate electrolyte system, Figure 3, due to its higher temperature of operation tends to be more rugged and heavier than competing systems. The auxiliaries are simplified; no liquid water must be condensed and the stacks can probably be air cooled. The cell stack in this case represents about 50% of the total weight. This means that the current densities which can be achieved are a very important factor in determining the total weight of the system. Today 30 watts/sq ft is routinely achievable and 40-60 watts/sq ft can most likely be achieved by minor engineering improvements. Power densities of greater than 100 watts/sq ft are required, however, if the molten carbonate system is to be competitive in the 3-10 KW power range. Significantly more research emphasis must be placed on understanding the electrode limitations with this mixed fuel and air and the design and testing of more active electrode structures.

DIRECT OXIDATION

The status of direct oxidation hydrocarbon fuel cell research and preliminary engineering is being ably discussed by others in this symposium. I wish to add to this only by stressing two major points.

Tremendous progress has been made over the last several years in anodically oxidizing hydrocarbon fuels at an electrode. Whereas, three years ago the ability to oxidize saturated hydrocarbons at lower temperature (150-200°C) and atmospheric pressure was questioned, today 10-15 watts/sq ft with n-octane can be routinely obtained with electrodes with useful lives of over 1000 hours. Twenty watts/sq ft is a legitimate goal for this year. The current density at a cell voltage of 0.5 to 0.6 volts, however, must be greatly increased for a direct oxidation system to become attractive. A several fold increase in current density must be achieved while at the same time greatly reducing the platinum content of the electrodes. The progress has been very encouraging but a tremendous amount of research must still be devoted to understanding the complex nature of hydrocarbon anodic oxidation.

Most of the work to date has been done on pure single component hydrocarbon fuels. Work now in progress is determining the tolerance of electrodes to olefinic, naphthalenic and aromatic components. The future "fuel cell fuel" may not be what we burn in our automobiles today, but economics dictate that it will be a multi-component fuel which can be produced from a petroleum refinery. Greater research emphasis must be placed on the direct oxidation of raffinates and other complex fuel mixtures.

CONCLUSIONS

Indirect hydrocarbon fuel cell systems are closest to the hardware stage but require additional research to simplify auxiliary systems, to increase current densities with less costly electrodes, and to protect reformers

from the effect of sulfur impurities present in liquid hydrocarbon fuels. An internal reformer system can achieve major efficiency and control advantages if present research aimed at long life low temperature reformer catalysts is successful. Major current density gains are required for the molten carbonate system to be competitive for portable power plants. Tremendous progress has been made with direct oxidation but much higher current densities must be achieved with multi-component fuels for a practical system.

ACKNOWLEDGEMENT

Portions of the analyses and research results presented here were done under contract to the U. S. Army Engineer Research and Development Laboratories by Allis Chalmers, Engelhard Industries, General Electric, Pratt and Whitney Aircraft, Texas Instruments and Varo, Incorporated.

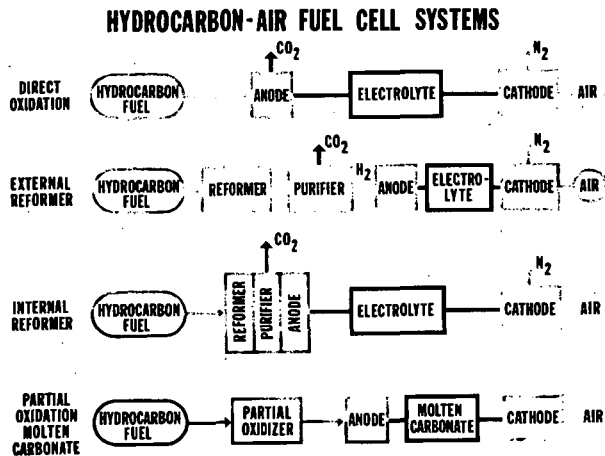


Fig. 1.-ALTERNATIVE HYDROCARBON-AIR FUEL CELL SYSTEMS

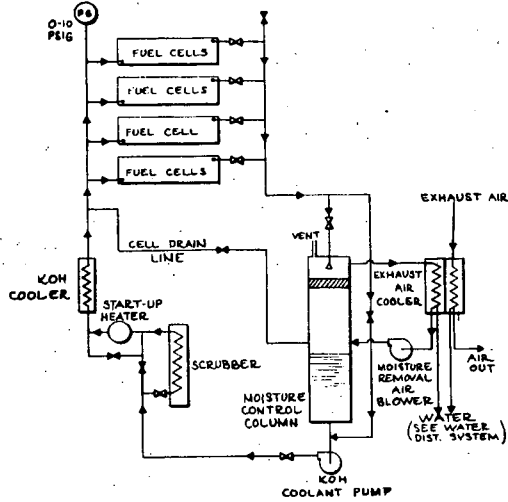


Fig. 2.-MOISTURE SUBSYSTEM

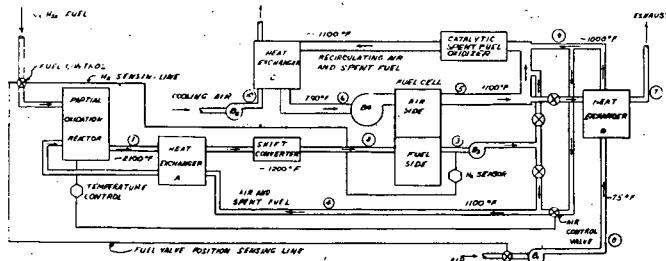


Fig. 3.-PARTIAL OXIDATION-MOLTEN CARBONATE SYSTEM

CARBON-AIR ELECTRODES FOR LOW TEMPERATURE FUEL CELLS

by K. V. Kordesch
Union Carbide Corporation, Development Department
Parma Technical Center, Parma, Ohio

I. INTRODUCTION

The economy of a terrestrial, low temperature fuel cell system depends strongly on the feasibility of using air at atmospheric pressure. High current densities are required to keep battery weight and size down; simple operation, preferably at atmospheric pressure, is desired to avoid costly and energy-consuming accessories. Last, but not least, the use of noble metal catalysts and expensive structural materials must be restricted to a minimum.

At the present time, low temperature, acidic-electrolyte, fuel cell systems have not reached the development stage which would indicate their practical utilization in the near future. For this reason, the discussion will be limited to alkaline electrolytes only. With hydrophobic carbon electrodes, it is a matter of technical choice whether liquid or immobilized electrolytes are used; therefore, no differentiation will be made.

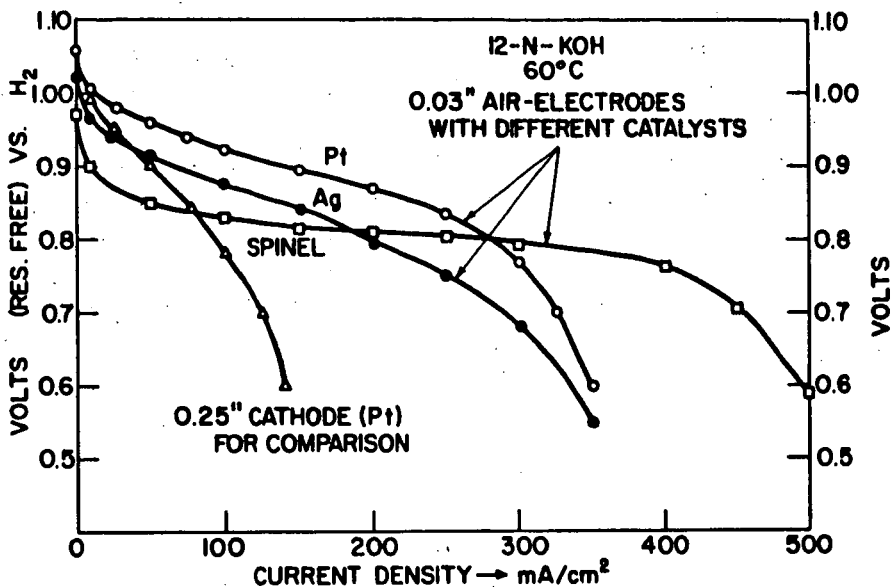
II. DISCUSSION

1. The Performance of Carbon-Air Electrodes.

a) Comparison of Polarization Curves. - The potential of an electrode at a given load is dependent on the activity of the catalytic system used. Carbon-oxygen (air) electrodes function as hydrogen, peroxide-producing, gas-diffusion electrodes, and for this reason show a strong dependence on the peroxide-decomposing capability of the electrode surface. (1)

Figure 1 shows the polarization curves of three differently catalyzed carbon electrodes. Characteristic is the high voltage level of the Pt-catalyzed cathodes—Pt is deposited in a quantity of 1 milligram per cm² of geometric surface. A very remarkable performance is shown

by the third electrode, containing no specially added metals—only the peroxide-decomposing catalytic activity of the basic CoOAl_2O_3 spinel-containing carbon is demonstrated. (2) While the initial performance level is lower, the current-carrying ability is greater at very high current densities.



D-1882

Fig. 1 Electrode Polarization Curves Employing Different Catalysts (Linear Diagram).

The upper-three curves of Fig. 1 were obtained with so-called "fixed-zone", 0.03-inch thick composite electrodes consisting of a repellent porous nickel plaque (0.008-inch thick) coated with layers of catalyzed carbon. (3) The fourth curve in Fig. 1 was obtained with a platinum-catalyzed, 0.25-inch thick carbon electrode (1 mg Pt/cm²). While pure oxygen performance (not shown) of 0.25-inch and 0.03-inch electrodes is essentially equal, the performance with air is very different. The thicker electrode is clearly diffusion-limited.

The same voltage-current curves of Fig. 1 (linear diagram) are replotted in Fig. 2 using a logarithmic abscissa. The similarity in elec-

trochemical behavior of the four electrodes becomes more apparent in the second figure. The Tafel slopes are identical (40 to 50 mv per decade at low current densities), but the voltage levels are different in accordance with the chosen catalyst. Also different is the extent of the "mass-transport limitation" (as expected, considering the difference in electrode thicknesses). The cross-over of the "spinel-catalyzed" thin electrode is not accidental—this characteristic is consistently observed.

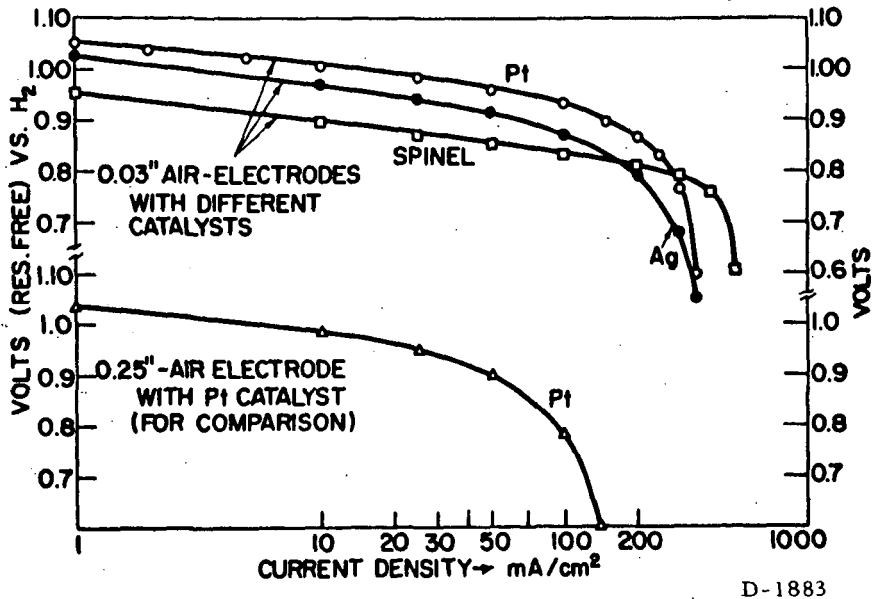
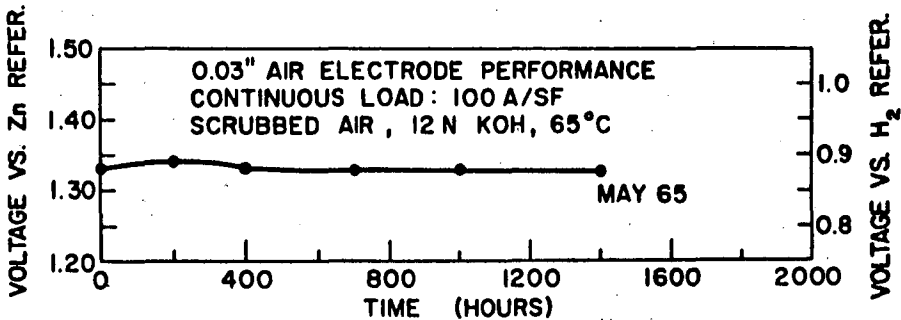


Fig. 2 Electrode Polarization Curves Employing Different Catalysts (Logarithmic Diagram).

b) Operational Life of Air Electrodes. - Life of the electrodes depends, first of all, upon the current density. Current density determines the operational voltage (as Figs. 1 and 2 demonstrate). The "polarization level" (terminal voltage minus the voltage drop in the resistive components of the cell) is a more decisive parameter than the "terminal voltage". This "resistance-free" voltage can be determined by means of current interrupter devices (4), or suitably placed reference electrodes.

The relationship between current density and operational life seems to be an exponential function. Doubling the current density usually decreases life to one-fourth the time, or vice versa; cutting the current density in half prolongs the electrode life fourfold. This should be considered only as a "rule-of-thumb" fitting our present experience.

Figure 3 shows the performance life of 1965 Union Carbide thin electrodes operating on a continuous load corresponding to 100 A/SF (105 ma/cm²). It should be noted that CO₂-free (scrubbed) air has been used.



D-1885

Fig. 3 Operational Life of Union Carbide Fixed-Zone, Air Electrodes(1965).

2. The Effect of Carbon Dioxide from the Air.

The approximate 0.03% CO₂ contained in air is known to be detrimental to alkaline cell performance. Consequently, most tests are performed with CO₂-free air; and less data are available about the nature and extent of carbon dioxide's damaging effects.

However, for economical operation of larger fuel cell batteries, the cost of air scrubbing is important. In addition, size and weight problems are introduced by air-scrubbing accessories. Therefore, an attempt has been made to answer a few principal questions concerning this matter:

- a) The effect of carbonate in the electrolyte;
- b) The rate of CO₂-pickup through the operating electrode;

c) The effect of CO_2 on electrode life (catalysts, variation in electrolytes, etc.), and

d) Possible explanation of the effects.

a) The Effect of Carbonate in the Electrolyte. - For comparison, two identical cells were operated in 6 molar KOH containing 0.4 mol potassium carbonate, and 6 molar KOH containing 1.0 mol potassium carbonate. The air supplied to the cell was cleaned in a gas wash tower containing KOH; no additional CO_2 was absorbed during operation. No noticeable difference in performance was observed.

b) Rate of CO_2 -Contamination through the Operating Electrode. - The speed of CO_2 -pickup from the air through the wall of cathodes was first tested with 0.25-inch carbon cathodes continuously exposed to room air in a concentric, triangular, 7-cell battery (5). Table I gives the data which show that the CO_2 -takeup from the air (for 6 M KOH) was rapid during the first few days, then slowed down considerably.

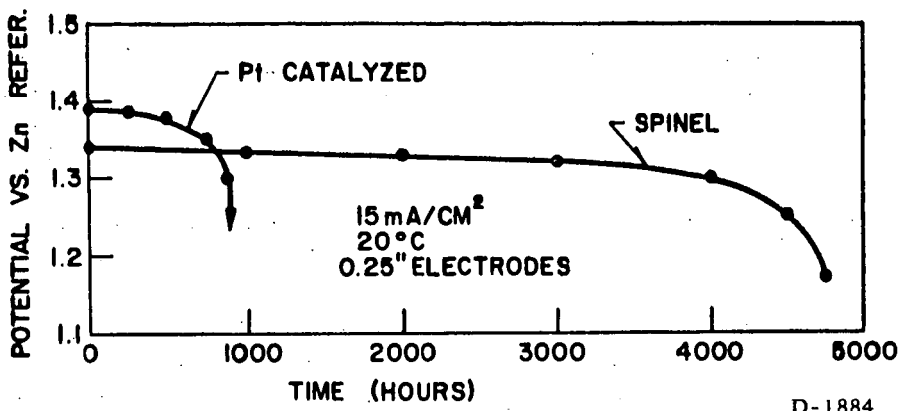
TABLE I
RATE OF CO_2 -CONTAMINATION OF 6 M KOH
IN AIR-EXPOSED CELLS (15 ma/cm² LOAD)

Time Elapsed Since Exposure of Cathodes (6 M KOH) to Air	Titred M CO_2
72 Hours = 3 Days	0.4 M
720 Hours = 4 Weeks	1.0 M
2160 Hours = 3 Months	2.5 M

Adding KOH pellets to the partially neutralized caustic solution until the OH^- ion concentration corresponded to 6 M KOH restored the original performance.

c) The Effect of CO_2 on Electrode Life. - The 0.25-inch carbon electrodes used in the concentric (triangular) cells, mentioned above, carried no special metal catalyst. Most of the test cells survived 4000 hours at a current density of 15 ma/cm²; some operated for 7000 hours. Cell life was only about 800 hours under the same conditions of operation and air exposure when 0.25-inch, platinum-catalyzed (1 mg/cm²) cathodes were employed.

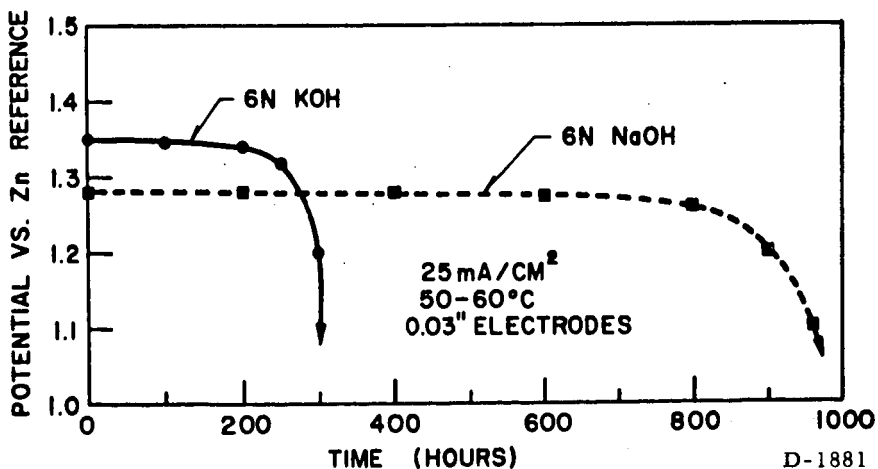
Figure 4 illustrates the average results of these tests. The voltage level of the noble metal-catalyzed cathodes was higher, but life was far shorter.



D-1884

Fig. 4 Performance with CO₂-Containing Air, Comparing Noble Metal-Catalyzed vs. Spinel-Catalyzed Cathodes.

In another series, platinum-catalyzed, thin electrodes (1963) were operated with CO₂-containing air, using 6 N KOH for one set of cells, and 6 N NaOH for the other. Figure 5 shows the results—the cathodes in NaOH outlived the cathodes in KOH by a wide margin, again at the cost of the voltage level, however.



D-1881

Fig. 5 Performance with CO₂-Containing Air, Comparing Platinum-Catalyzed Cathodes—6 N KOH vs. 6 N NaOH.

A third combination (uncatalyzed electrodes in NaOH electrolyte) did not look promising from the cell-performance standpoint at that time. This combination will be tried in the future using newer, more active electrodes.

d) Possible Explanation of Effects - Physical examination of the CO₂-damaged electrodes always revealed a mechanical blockage. It seems that the degree of repellency of an electrode determines the degree of resistance against CO₂ damage. NaOH is less wetting than KOH, and platinum-catalyzed electrodes are less repellent than electrodes without platinum catalyzation. CO₂-damage is also current-density dependent; a heavily polarized air electrode has a shorter life in the same electrolyte than does one showing a lesser degree of polarization.

Experiments with porous metal electrodes indicate that "wet"-operated electrodes (gas pressure balance) have an extremely low tolerance for CO₂. The pores of such electrodes plug within a few hours, and physical damage (possibly by expanding carbonate) is irreversible. Carbonate-plugged, 0.25-inch carbon electrodes were usually permanently damaged, and could not be revived. However, the newer thin composite electrodes have frequently been washed and reused.

III. CONCLUSIONS

Carbon-containing cathodes seem to be the most desirable electrodes for high-power density, economical, air-fuel cells. The fuel source for such low temperature cells may be hydrogen from hydrocarbon reformer units, or hydrogen from alcohol or ammonia converters.

At present, CO₂ removal is necessary during air operation in order to attain long life at high current densities. However, recognition of the nature of carbon dioxide effects on today's electrodes is the first step towards possible future remedy.

In the author's opinion, of all the available cathodes, the carbon electrode is the least sensitive to carbon dioxide damage.

REFERENCES

- (1) K. V. Kordesch in "Fuel Cells," (G. J. Young, ed.), p. 14, Reinhold Publishing Corp., New York, 1960.
- (2) K. V. Kordesch in "Fuel Cells," (W. Mitchell, ed.), p. 346, Academic Press, New York, 1963.
- (3) M. B. Clark, W. G. Darland, and K. V. Kordesch, "Composite Carbon-Metal Electrodes for Fuel Cells," paper presented at the 1964 Washington Meeting of Electrochem. Soc. To be published in Electrochem. Tech.
- (4) K. Kordesch and A. Marko, J. Electrochem. Soc. 107, 480(1960).
- (5) L. M. Litz and K. V. Kordesch in "Fuel Cell Systems," (G. J. Young and H. R. Linden, eds.), p. 166, Am. Chem. Soc., Washington, 1965. (Advances in Chemistry Series No. 47.)

PERFORMANCE OF A REFORMED NATURAL GAS-ACID
FUEL CELL SYSTEM

Part I. Hydrogen Generator Design

by

John Meek
B. S. Baker
A. C. Allen

Institute of Gas Technology
Chicago, Illinois

INTRODUCTION

Natural gas can be used in low-temperature fuel cell systems in several ways. Although the direct methane cell has proven feasible,^{1,2} present and foreseeable technology of such systems will be very costly because of the quantity and type of catalyst required for direct anodic oxidation. The indirect cell, which requires the reforming of methane followed by the utilization of hydrogen, seems more attractive at the present time. With alkaline electrolyte systems it is necessary to use high-purity hydrogen as the fuel. This may be obtained by steam reforming in an external reformer and purifying the gas with a palladium-silver diffuser, or by reforming the gas in situ in a fuel cell that employs a palladium-silver-hydrogen diffusion anode. For application in the gas industry, it is essential that both first costs and operating costs remain low. Accordingly, the program at IGT has focused its attention on development of a hydrogen generator-fuel cell system in which the feed from the reformer is rich in hydrogen but unpurified, the enrichment being achieved by conventional chemical processing techniques. It is realized that this implies the use of a fuel cell of the acid electrolyte type which is presently more expensive than the alkaline electrolyte fuel cell. Nevertheless we believe that the cost of the acid electrolyte cell can be greatly reduced especially where the fuel is hydrogen. The other factors affecting the decision to pursue this system have been outlined in an earlier publication in this series.³ Design of a natural gas-fueled hydrogen generator is described here in which the product is suitable for use in any acid electrolyte fuel cell.

HYDROGEN-GENERATION PROCESS

The hydrogen generation process used in the IGT system has been described in detail.³ It consists of three stages: First, natural gas is steam-reformed at 800°C to produce a hydrogen-carbon

monoxide-carbon dioxide mixture. The effluent from this first reactor is then cooled and fed to a carbon monoxide shift reactor operating at about 270°C, wherein the carbon monoxide content of the gas is reduced from a typical 15% (dry basis) to about 2000 parts per million. For certain acid fuel cells operating above 100°C this gas might prove to be an acceptable feed, but, for lower temperature cells it is desirable to further reduce the carbon monoxide content of the feed gas. This is achieved in the last stage by passing the effluent from the carbon monoxide shift reactor through a low-temperature (190°C), selective methanation reactor in which the carbon monoxide content of the gas is reduced to approximately 20 parts per million by reaction with hydrogen to produce methane. Typical gas compositions along with the free energy for these reactions are summarized in Tables 1 and 2. It can be seen that the reforming and carbon monoxide shift reactions proceed, for practical consideration, to equilibrium. The reaction based on the methanation of carbon monoxide alone is a long way from equilibrium and improvement might be expected. The large deviation from equilibrium is probably due to reaction of carbon dioxide with hydrogen to produce carbon monoxide.

HYDROGEN GENERATOR DESIGN

For the hydrogen generation process to be attractive it is necessary that an integrated three-stage, gas-fired hydrogen generator that is self-controlling be designed and constructed. Limited data is available on the design of complete hydrogen generation systems with small capacity.^{4,5}

In the IGT system an annular reactor design was chosen because it represented a readily packageable easily fabricated unit with low pressure drop.

The first problem encountered in the design was the development of a gas-fired burner that could operate on low-pressure gas (6 in. wc), bring the relatively compact reformer reactor to operating temperature, and maintain the desired heat input to sustain the endothermic steam-reforming reaction. It was found that reactors of the present design, or of almost any design, did not have sufficient heat transfer area to permit heating by a convective process. To obtain a higher effective heat transfer coefficient, both sides of the annular reactor were encased in annular sections filled with the refractory material of high surface area. The sections could be brought to the desired temperature by convection and would in turn heat the reformer by radiation from the refractory. A typical burner design for this system is shown in Fig. 1. The reforming stage of the hydrogen generator, which is capable of reforming 25 cu ft of methane per hour, is shown in Fig. 2.

The second problem encountered in the present system was to find a means for reducing the temperature of the hot flue gases to maintain the second- and third-stage reactors at their proper operating temperatures. The solution was to cool both the flue gas from the natural gas burner and the product gas from the reformer reactor by generating and superheating process steam. The flue gas and the product gases are effectively cooled by this procedure but the achievable temperature control was not accurate

enough for the shift and methanation stages. Obtainment of temperature control in these two reactors within the desired limits, was made possible by jacketing the reactors with constant boiling fluids. Dow-Therm A and Dow-Therm E have been chosen for this purpose. The jacketed shift and methanation units are shown in Figs. 3 and 4. Temperature control of these reactors is achieved by dependence of pressure on temperature of the Dow-Therm liquid-vapor systems. The Dow-Therm vapor pressurizes a Sylphon bellows which transmits a pressure signal to actuate damper valves which control the direction of flow of hot flue gases. Water flow valves which, in turn, control the flow of cooling water to the Dow-Therm vapor condensers also activated by this means.

This mode of control is especially suited to a hydrogen generator that supplies a constant amount of product gas. The Sylphon bellows (Fig. 1) has the further advantage of not requiring any parasitic power from the fuel cell system; it is also relatively inexpensive. The only auxiliary power on the present reformer is that needed for a small air blower which provides combustion air. This blower draws about 40 watts at maximum air demand. The complete system is shown schematically in Fig. 5. The actual unit with a 100 cu ft/hr capacity is shown in Fig. 6.

PERFORMANCE CHARACTERISTICS

Hydrogen generators very similar in design to the one described in the present paper have been successfully operated at IGT, producing the gas given in Table 1. The best overall efficiency achieved with this type reformer in 150 hours of intermittent operation has been 41%. This figure was obtained with a unit that has an output of 50 cu ft of hydrogen per hour. The system presently under test has an output capacity of 100 cu ft of hydrogen per hour; overall efficiency figures of about 50% are anticipated.

Gas of the type produced by this hydrogen generator has been extensively tested in low-temperature acid fuel cells. Use of these gases is the subject of Part II of this paper.

ACKNOWLEDGMENT

The authors wish to thank Southern California Gas Company, Southern Counties Gas Company of California and Con-Gas Service Corp., who are sponsoring this investigation, for permission to publish these results.

REFERENCES

1. Binder, H., Köhling, A., Krupp, H., Richter K. and Sandstede, G., "Anodic Oxidation of Derivatives of Methane, Ethane and Propane in Aqueous Electrolytes" in Fuel Cell Systems, 283-291, Advances in Chemistry Series 47. ACS, Washington D.C., 1965.
2. Grubb, W. T. and Michalske, Carol J., "Hydrocarbon Fuel Cells," in Proceedings: 18th Annual Power Sources Conference 17-19, PSC Publication Committee, Red Bank N.J., 1964.
3. Meek, J. and Baker B.S., "Hydrogen from Natural Gas from Fuel Cells," in Fuel Cell Systems, 221-231, Advances in Chemistry Series 47 ACS Washington, D.C., 1965.
4. Geissler, H. H., "Compact H₂ Generators for Fuel Cells," in Proceedings: 17th Annual Power Sources Conference, 75-77, PSC Publication Committee, Red Bank, N.J., 1963.
5. Geissler, H. H., and Goodman, L.E., "Hydrogen Generators," in Proceedings: 18th Annual Power Sources Conference, 28-31, PSC Publication Committee, Red Bank, N.J., 1964.

Table I

Composition, Mole percent

Reactor	H ₂	CO ₂	CH ₄	CO	H ₂ O	N ₂	T°C	$\frac{\Delta F}{RT}$
Reformer In	0	0.107	*	0	87.268	0.046	800	-∞
Reformer Out	34.644	3.773	0.045	6.847	54.654	0.036	800	-7.287
Shifter In	34.644	3.773	0.045	6.847	54.654	0.036	270	-5.18211
Shifter Out	41.346	10.475	0.045	0.146	47.952	0.036	270	-2.30975
Methan. In	41.346	10.475	0.045	0.146	47.952	0.036	190	-26.50958
Methan. Out	41.030	10.505	0.190	0.001	48.236	0.036	190	-20.05782

*See Table II

Table II

Fuel	CH ₄	C ₂ H ₆	C ₃ H ₈	C ₄ H ₁₀	C ₅ H ₁₂	C ₆ H ₁₄	C ₇ H ₁₆	N ₂	CO ₂
Comp, mole %	12.027	0.394	0.097	0.033	0.009	0.010	0.009	0.046	0.107

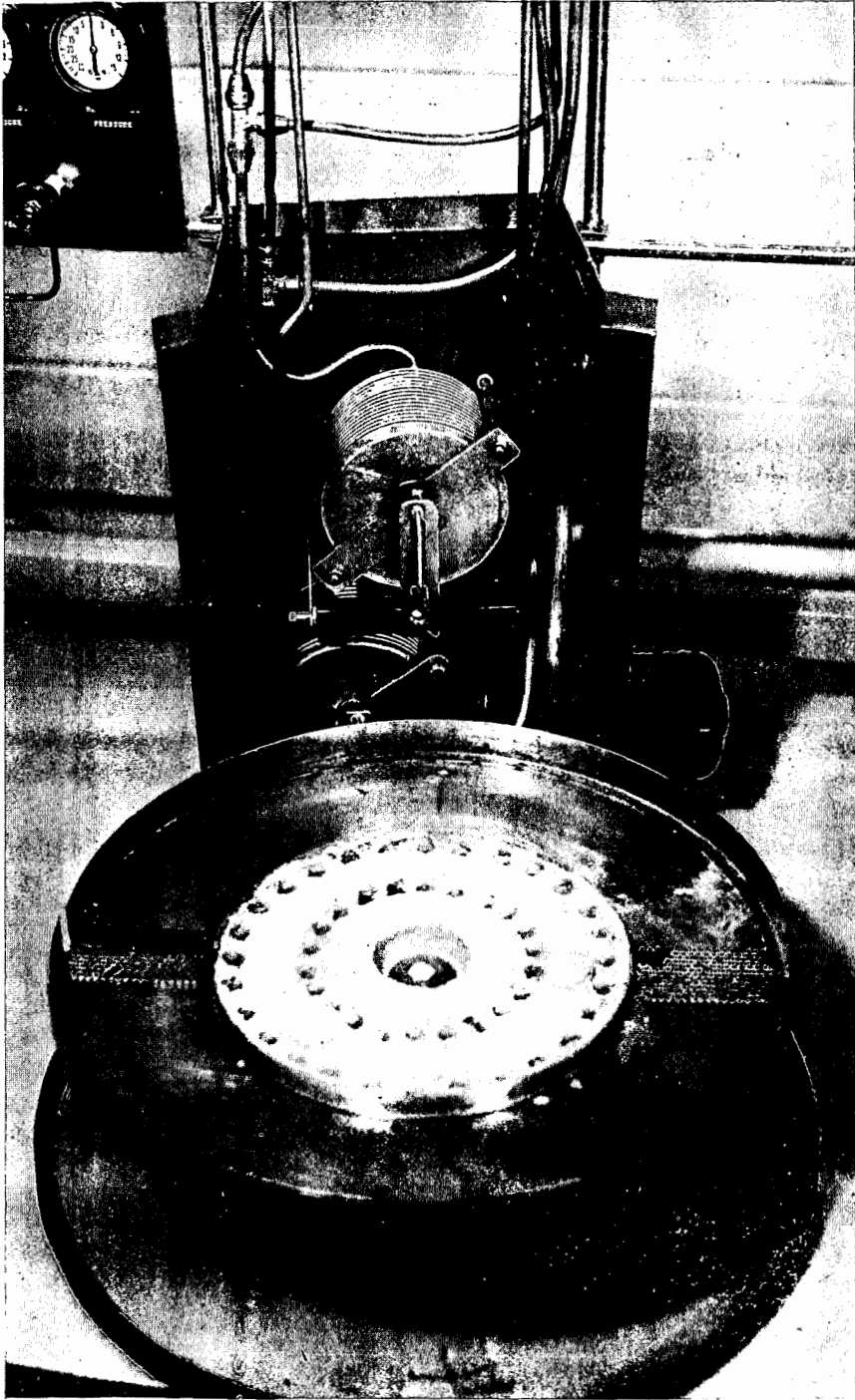


Fig. 1.-NATURAL GAS BURNER USED AS PRIMARY HEAT SOURCE FOR HYDROGEN GENERATOR

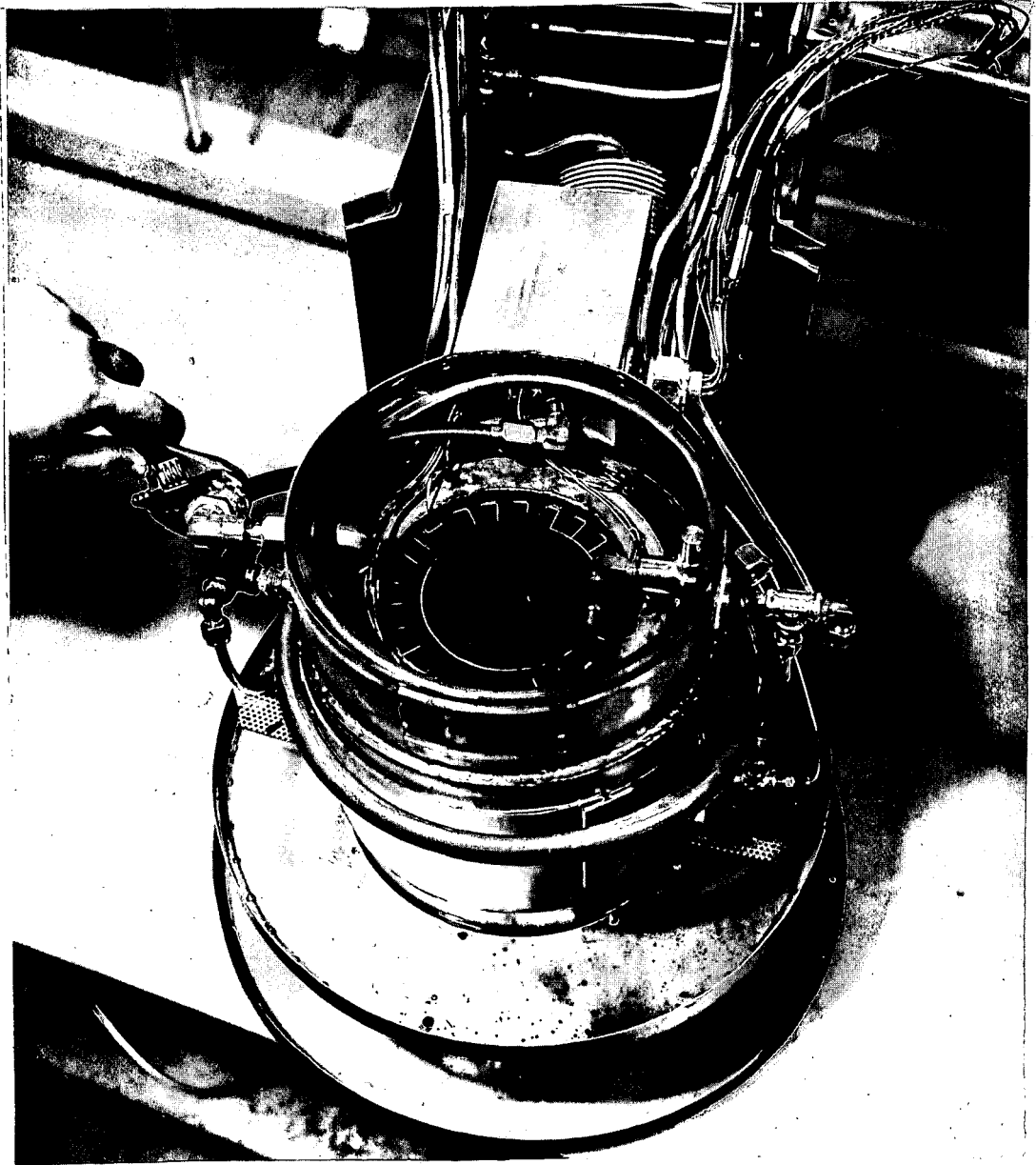


Fig. 2.-REFORMER AND CONTROL SECTION OF THE HYDROGEN GENERATOR

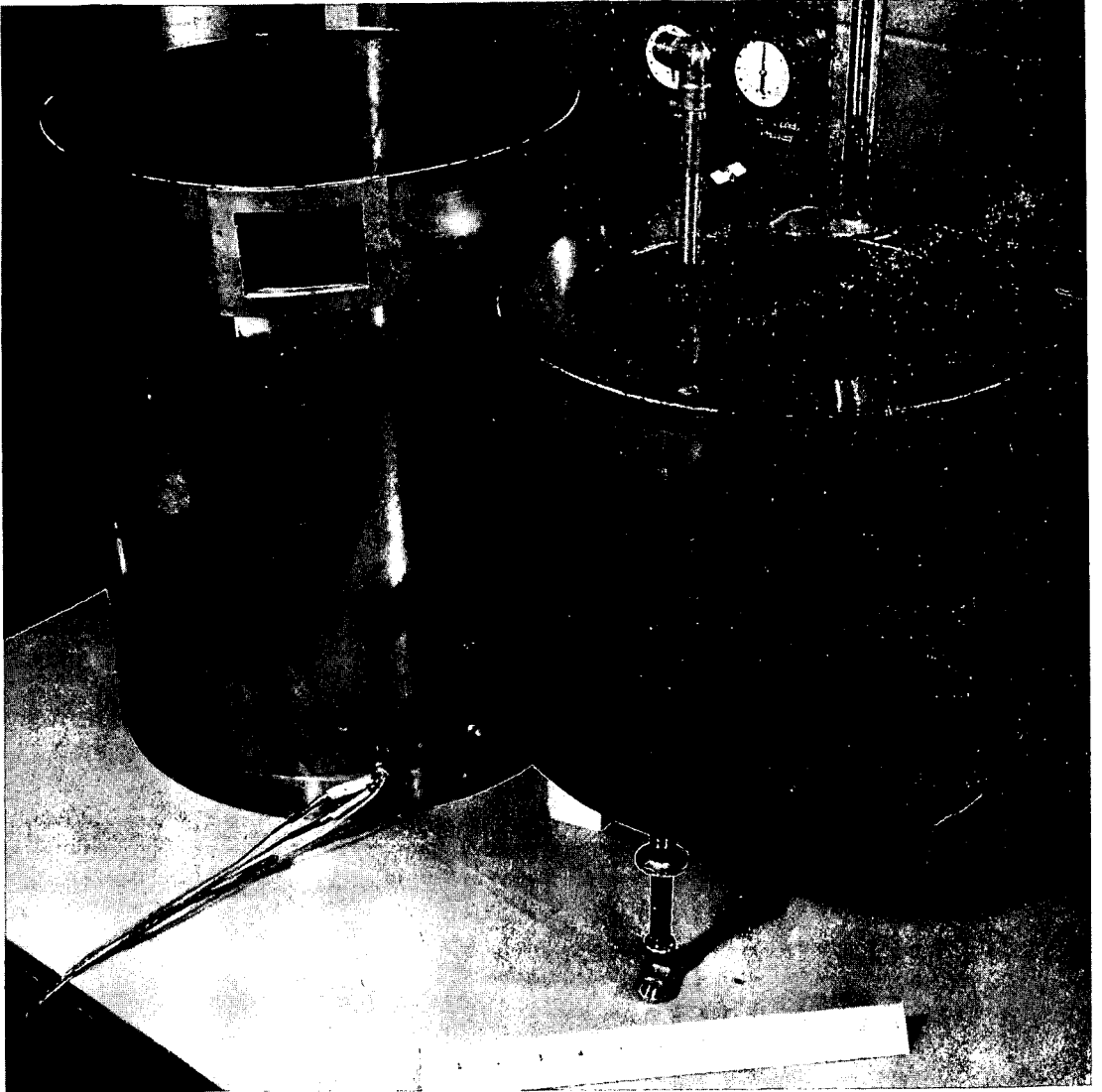
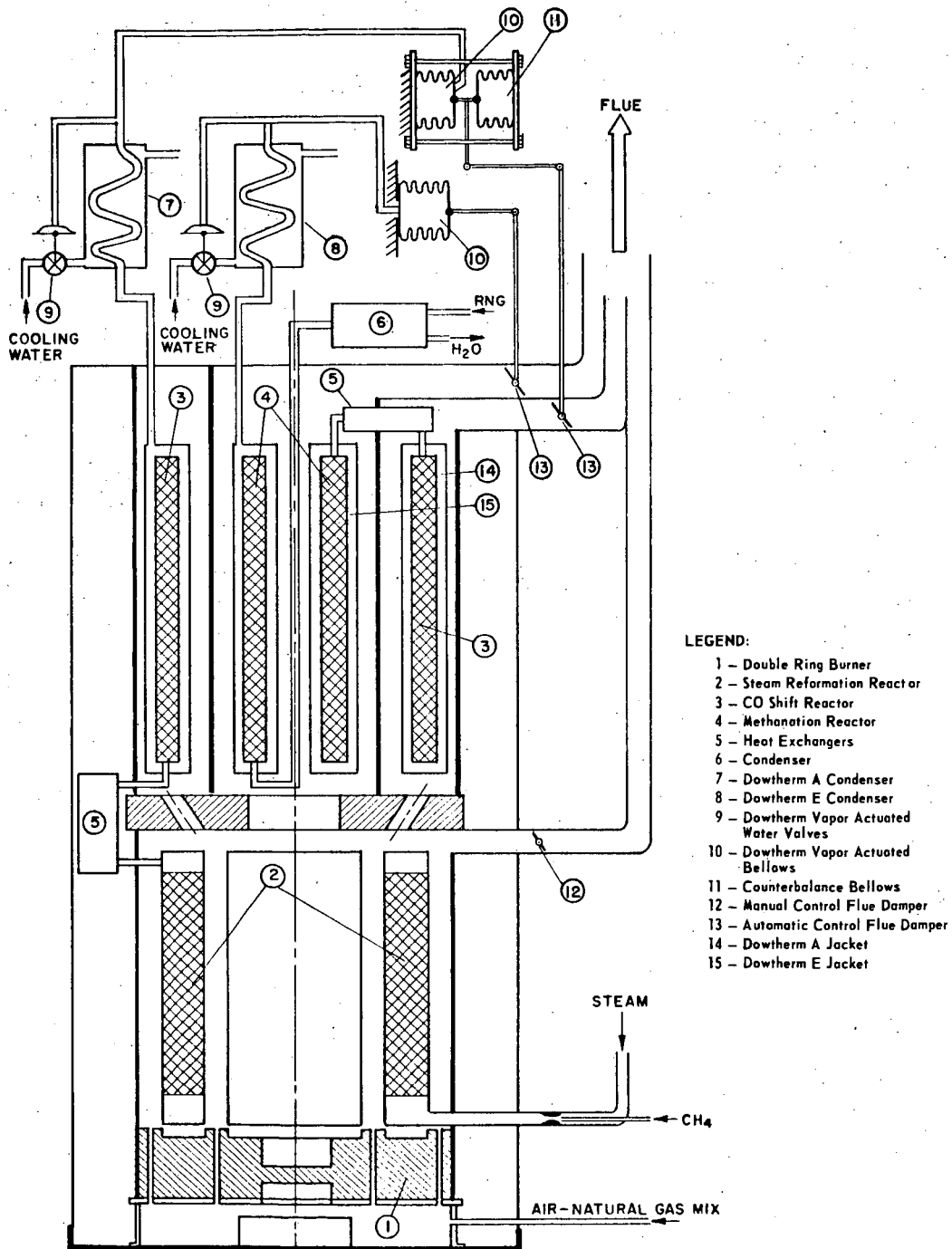


Fig. 3.-JACKETED CARBON MONOXIDE SHIFT REACTOR



Fig. 4.-JACKETED METHANATION REACTOR



LEGEND:

- 1 - Double Ring Burner
- 2 - Steam Reformation Reactor
- 3 - CO Shift Reactor
- 4 - Methanation Reactor
- 5 - Heat Exchangers
- 6 - Condenser
- 7 - Dowtherm A Condenser
- 8 - Dowtherm E Condenser
- 9 - Dowtherm Vapor Actuated Water Valves
- 10 - Dowtherm Vapor Actuated Bellows
- 11 - Counterbalance Bellows
- 12 - Manual Control Flue Damper
- 13 - Automatic Control Flue Damper
- 14 - Dowtherm A Jacket
- 15 - Dowtherm E Jacket

Fig. 5.-SCHEMATIC REPRESENTATION OF IGT HYDROGEN GENERATOR SHOWING REACTORS AND CONTROL LOOPS

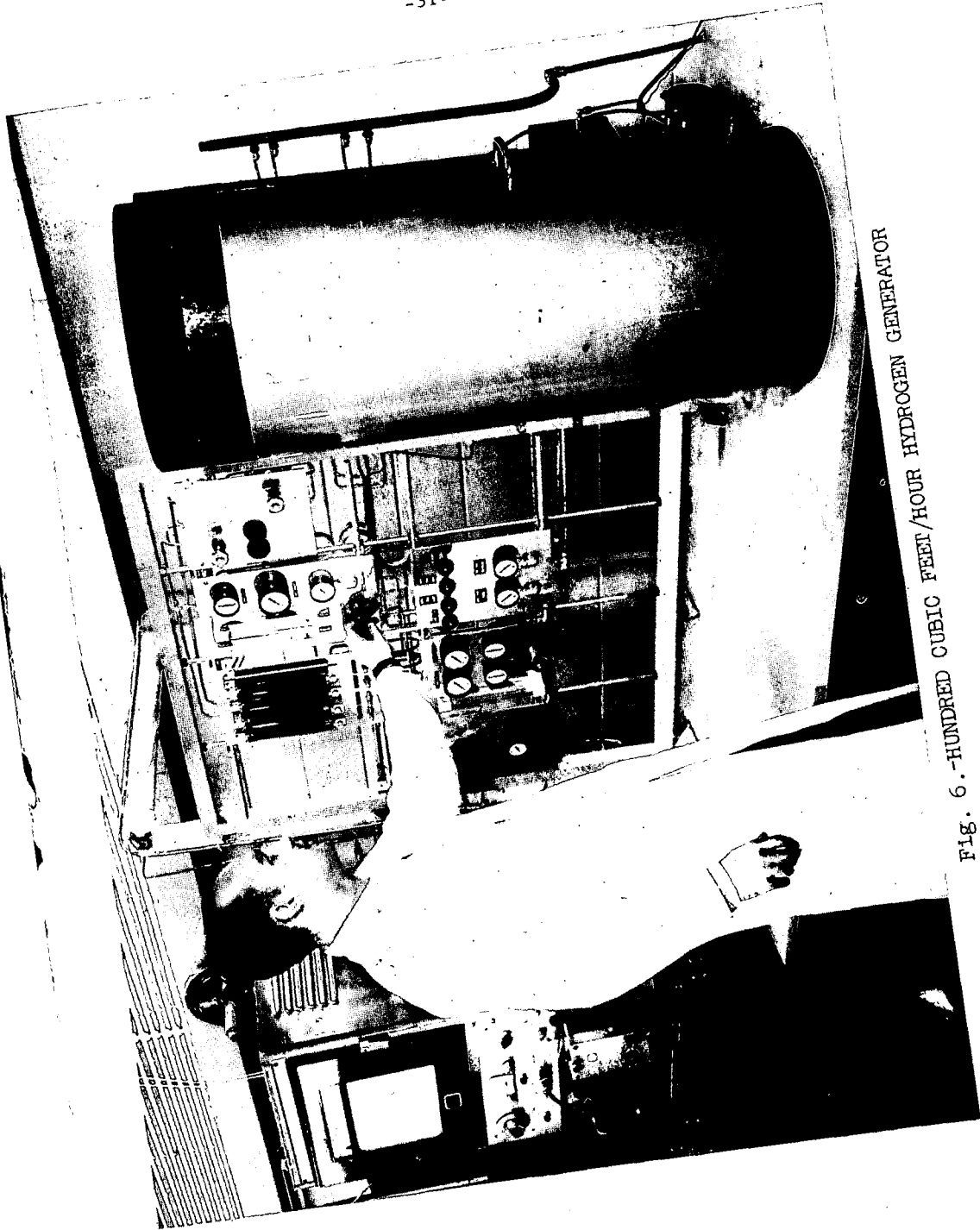


FIG. 6. -HUNDRED CUBIC FEET/HOUR HYDROGEN GENERATOR

PERFORMANCE OF A REFORMED NATURAL GAS-ACID
FUEL CELL SYSTEM

Part II. Fuel Cell Battery

F. B. Leitz and W. Glass
Ionics, Inc., Cambridge, Mass.

D. K. Fleming
Institute of Gas Technology, Chicago, Ill.

INTRODUCTION

This is a report on a joint effort of Ionics, Inc. and The Institute of Gas Technology to develop an air-breathing fuel cell system powered by natural gas. The long range objective of the project is the development of an economical power source using this readily available fuel, and which has a high degree of reliability and safety for relatively long periods of unattended operation. The system selected for this program was a low temperature, hydrogen-oxygen fuel cell with an acid electrolyte.

The hydrogen-oxygen system is well advanced. It provides relatively high efficiency with fuels and oxidants that are easy to obtain. The fuel can be generated from natural gas or other hydrocarbons and the oxidant is available from the air. The process to generate hydrogen for this fuel cell has been presented in an earlier publication in this series.¹ The description of a 100-CFH reformer unit has been discussed in another paper during this session.²

A low temperature system was selected for the investigation because of its long life, reduced corrosion problems, and low pressure operation. These advantages are counterbalanced in part by the present high cost of the catalyst.

An acid electrolyte system was dictated by the need for compatibility with the carbon dioxide which is formed during the reforming of natural gas and which is also present in room air. With the acid system, expensive steps to purify the hydrogen are not required. Also, the air does not have to be scrubbed to remove carbon dioxide.

A dual ion-exchange membrane battery was chosen for its inherent safety and reliability. With the acid electrolyte contained between two membranes, and the gases on the outside of these membranes, the chances of gas intermixing are minimized. A pinhole in one membrane does not bring two reactant species together in the presence of an active catalyst which would cause failure. The safety of operation is consistent with the goals of the project.

BATTERY CONSTRUCTION AND OPERATION

General Description

The battery is an internally manifolded stack of cells wired in series and with parallel flows of gas and electrolyte. An individual cell is diagramed in Figure 1. The acid compartment, in the center of this diagram, is filled with a polyethylene-

polypropylene woven cloth (70% void) to maintain the electrolyte spacing. On either side of the acid compartment are cationic ion-exchange membranes with woven glass backing. Each of these membranes is intimately contacted by an electrode, either anode or cathode. These, in turn, are held in place by ribbed plates. The plates are embossed niobium sheets, 5 mils thick. They electrically connect one cathode to the adjacent anode and simultaneously distribute the flow of gas to the electrodes. The gas and electrolyte compartment frames are made of 65 durometer butyl rubber. This is sufficiently firm to retain dimensional stability but still has enough flexibility for sealing. The electrodes are platinum-black bonded to a tantalum screen as manufactured by the American Cyanamid Company.³ The catalyst loading in the present battery is 9 grams per square foot. The total thickness for a single cell is 140 mils or about 1/7 inch.

The internal manifolding technique is shown in Figure 1. The manifolds for the movement of fresh and spent material are holes punched in the margins of the components. Channels connect the appropriate compartments and manifolds. In the present geometry, 70 percent of the total area is active. The active area of a cell is 1/4 square foot.

In operation, the reactant gases are fed to the top of their respective compartments. Spent gas is removed from the bottom of the battery to sweep out the liquid formed by the reaction or which has passed through the membrane by osmosis. The 25 percent sulfuric acid electrolyte flows from the bottom of the compartment to the top. This removes gas which may be in the compartments during start-up. The current is taken from the battery from the terminal collector plates. These are heavier than the interior sheets to reduce the battery's electrical resistance.

Heat and Mass Balance

A detailed analysis of the heat and mass balance problems within the cathode compartment of the cell was performed on a digital computer using finite difference techniques. This study indicated that the air required for a thermal balance is greater than that for a water balance by a factor of approximately 30. Therefore, the heat of reaction must be removed by other means.

Figure 2 shows the heat and mass balances during steady-state operation on reformed natural gas. The operating conditions are typical of those realized in the laboratory. All of the heat generated in the battery, plus that which is equivalent to the water condensed, is removed by the rise in the acid's temperature. If the humidity of the inlet air were lower during operation, water would be removed from the battery and the acid concentration would rise. The exit air is a few degrees higher than the acid temperature because most of the irreversibility of the reaction is at the cathode. The inlet air temperature and humidity are maintained at the conditions of the exit air. The fuel, on the other hand, need not be excessively heated or humidified for stable operation.

Pressure Drop

The pressure drop of the gas streams within the battery is important in the design of the entire system. Air must be supplied at enough pressure to overcome the losses in the humidification process and within the battery. Of greater importance, the reformer must be designed to supply gas at enough pressure to overcome the losses on the anode side of the battery from a line pressure of six inches.

The pressure drop in the present battery design is shown in Figure 3. From this graph, it can be observed that the flow in the cathode chamber is laminar; the pressure drop varies directly with the flow rate. With the same design, the pressure drop for an 80 percent hydrogen-20 percent carbon dioxide fuel mixture, similar to the generator product, should be significantly less than that of the air. The pressure drop with this fuel mixture is so low that uneven distribution within the battery results. To correct the distributional problem, the resistance in the inlet to the fuel compartment from the fuel manifold is increased. In the present design, the restriction is 1/2 inch of 19 mil. I.D. tantalum tubing. With this restriction, the pressure drop to fuel flow is about the same as the pressure drop to air flow. The flow within the anode compartment, according to the slope of the line in Figure 3, is not laminar but is in the transition region.

The pressure drop at expected operating conditions is three to five inches wc. From the earlier paper on the reformer construction, it will be noted that this fuel pressure is readily obtainable from the hydrogen generating system. Enough energy is available in the reformer flue gas to generate steam for ejecting the air required. As the air must be heated and humidified, according to Figure 2, an ejector is a convenient technique for air movement.

If extrapolated, the pressure drops, at increased power levels, would be quite high. This problem can be avoided by embossing the bipolar plates more deeply and shortening the length of the restrictive tubing in the anode compartment.

The plates are now pressed manually and are not identical. This non-uniformity presents a problem with uneven flow distribution within the battery. Relatively high pressure drops must be used in the experimental units for uniform gas distribution.

BATTERY PERFORMANCE

The initial investigations of this program were performed on cells having an area of four square inches. Performance of the batteries is better than that of the small cells. This is due to improved control facilities. Four of these batteries have been constructed and tested. Each has 13 cells with 1/4 square foot of active area. The power is nominally rated at 100 watts each when operated on reformed natural gas and air.

Hydrogen-Oxygen Performance

Polarization curves for a 13 cell battery operating on various fuel and oxidant gases are shown in Figure 4. The data for Figure 4 were taken with 500 hours total operation on the electrodes, and just after a 100 hour run, to minimize the effects of fresh catalyst. The hydrogen-oxygen performance of the battery at 60°C is the standard of comparison for the operating conditions. When these data are plotted IR-free, with each electrode against a reference, it is found that the anode reaction is essentially reversible over the range of current density. By contrast, the oxygen electrode shows substantial polarization, even when the circuit is open. The irreversibility of oxygen electrodes is well-known. It is an area for further catalyst investigation.

Internal Resistance

Preliminary measurements of the internal resistance of the battery show 0.002 ohms-square foot for each cell. This value was determined by interrupting the load on the battery and instantaneously measuring the voltage rise on an oscilloscope. This resistance figure is probably high. More accurate determinations will be possible when faster battery switching techniques have been perfected. Figure 4 shows a curve for the hydrogen-oxygen performance on an IR-free basis.

Conductivity measurements of the membranes and electrolyte indicate that a negligibly small fraction of the internal resistance is in the metallic components of the battery. The liquid electrolyte area resistance is 0.00046 ohm-square foot and the membranes, which act very much like porous media containing 25 percent electrolyte, are responsible for the balance.

Hydrogen-Air Performance

The goals of the project require a system that operates with air at the cathode. The prime disadvantage in the use of air is the loss of cathode potential because of dilution. This potential loss ranges from 40 to 80 millivolts per cell if sufficient air is used. The voltage loss increases as current is increased. The loss at 60 amps per square foot (ASF) is approximately 70 millivolts per cell or .91 volts for the battery. A polarization curve for hydrogen-air operation is included in Figure 4.

The loss of cathode potential, as stated above, depends upon the use of sufficient air. This is designated as a maximum effective feed rate - that is, the point at which any further increase in air flow does not measurably increase the electrode potential. A determination for this air flow rate is presented in Figure 5. For a single cell, the air flow rate at which a potential drop occurs is only slightly more than the stoichiometric equivalent. This is less than 20 percent excess air for 300 millivolt drop from a linear extrapolation of the polarization curve, and less than 25 percent excess air for

100 millivolt drop. At twice stoichiometric flow (100 percent excess air), no deviation from the straight line curve can be observed.

If the oxidant gas supply is interrupted briefly while current can flow through the battery, a noticeable improvement occurs in the battery's performance. This may amount to .65 volts at 60 ASF with a decay time of up to 6 hours depending upon the past history of the battery. Since this lack of reactant shifts the cathode potential almost to the anode potential, a strongly reducing condition is produced at the cathode which apparently cleans the electrode.

Dilute Fuel Performance

The product of the hydrogen generator is primarily 80 percent hydrogen and 20 percent carbon dioxide, with trace amounts of methane and carbon monoxide. The methane and carbon dioxide dilute the anode feed whereas carbon monoxide has a polarization effect which will be discussed later.

The investigation of reactant dilution is straightforward since only hydrogen and carbon dioxide need be considered. The concentration effects due to the dilution of the hydrogen are shown in Figures 6 and 7. Polarization data is included on Figure 4. In treating the data, it is convenient to define a unit gas flow rate as a stoichiometric equivalent (or stoich). This is a gas flow equal to the rate at which the reactant gas is consumed under specified conditions. For example, with a 13-cell battery operating at 15 amperes current, 1 stoich equals 1460 milliliters per minute of hydrogen. Figure 6 shows the stoichiometric relationships. Lines of constant fresh feed (j), and recycle ratio (R), are shown for an 80-20 percent mixture of hydrogen and carbon dioxide.

Experimentally, the indicated feed and recycle rates were simulated by feeding a mixture of the corresponding values of the pure gases. The average potential loss at 60 ASF was then calculated for each condition. This voltage, expressed as millivolts per cell, appears on Figure 6 near the intersection of the corresponding lines. The average potential loss is strongly influenced by excess feed and only slightly affected by the recycle ratio.

The arithmetic mean of battery inlet and outlet conditions was used for average reactant concentration. A graph of potential loss against the average concentration is presented in Figure 7. The correlation is good. The three poorest points occurred at low total flow rates. With this condition, poor distribution between cells was the most likely cause, that is, one or two cells behaved differently from the rest. According to Figure 7, there is a wide range of conditions under which the potential loss can be held to approximately 20 millivolts at 60 ASF.

Figure 7 is plotted on semilog paper for convenient presentation of the data. Also included on this graph is the line for the Nernst Equation which expresses the theoretical open

circuit potential loss. At low average feed concentrations, there appears to be a significant diffusion problem at 60 ASF current. In the range of probable operation, without recycle, the concentration effect is not large.

Figure 4 includes a curve for the polarization of the 13-cell battery on 80 percent hydrogen-20 percent carbon dioxide fuel mixture vs. air. Approximately 200 percent excess fuel was used in the collection of these data.

To check for carbon monoxide production in the anode chamber, the carbon monoxide concentrations of the battery inlet and outlet gases were measured with a sensitive infra-red analyzer. With an inlet concentration from a bottled mixture of 80 percent hydrogen-20 percent carbon dioxide containing 3 ppm of carbon monoxide, the battery outlet concentration was 4 to 5 ppm of carbon monoxide without load. The thermodynamic equilibrium of the reverse water gas shift reaction at 60°C is 20 ppm. Under the flow conditions in the battery, the reaction does not proceed rapidly over the platinum catalyst.

Performance with Reformed Natural Gas Fuel

The purpose of this project is to achieve satisfactory battery operation on a fuel derived from natural gas. The product gas of the hydrogen generator contains 3000 ppm of methane and 20 ppm of carbon monoxide in addition to the hydrogen and carbon dioxide. The methane exerts a negligible dilution effect only, but the carbon monoxide, even in small amounts, significantly affects the battery's operation. It is believed that the carbon monoxide is adsorbed at the reaction site and results in a poisoning effect.

Figure 4 includes a line for the polarization of the 13-cell battery at 60°C when operating on reformed natural gas (RNG) fuel and air. These data were taken after 300 total hours on RNG fuel and immediately after a 100 hour run at 40 ASF. The polarization at 60 ASF is 1.2 volts for the 13 cells, or less than 100 millivolts per cell, when compared with pure hydrogen feed. As expected from the previous section, the concentration polarization due to the presence of carbon dioxide is less than 20 millivolts per cell. The remainder is due to the effect of the carbon monoxide. The maximum power of the battery is 112 watts at 80 ASF.

The poisoning effect just mentioned has occurred for 60°C operation. From tests on small cells, the effect at room temperature is approximately 300 millivolts per cell. The operating temperature of 60°C was selected to minimize the poisoning effect without reaching the temperature at which the fuel reduces the sulfuric acid to hydrogen sulfide.

The long term effects of carbon monoxide in the feed stream are now being investigated. At present, the total operating time on reformed natural gas is 800 hours.

Apparently, the anode can be rejuvenated by two techniques. If the battery load is removed for about an hour, the output

voltage of an 80-20 fuel mixture is produced when the load is restored. Another technique to remove the anode poisoning is to short circuit the battery without fuel. In this case, the carbon monoxide apparently is oxidized. It is not known if either of these rejuvenation techniques can be repeated indefinitely. There is evidence of increasing potential falloff rate with repeated anode treatment.

FUTURE IMPROVEMENTS

When this program was started two years ago, the approximate material cost was \$50,000 per kilowatt of power on hydrogen-oxygen feeds. The present cost is \$3,000 per kilowatt with an RNG-air feed. The cost must still be reduced significantly for this fuel cell battery to be an economical power source. There are several points of potential improvement in the battery.

The electrical resistance of the electrolyte accounts for a substantial loss of cell potential. A majority of the resistance is in the ion-exchange membranes. Research at Ionics has produced a membrane which could reduce the resistance by more than half, doubling the power output. It is likely that additional effort will result in further improvements in membrane technology.

Experimental electrodes with a greater tolerance for carbon monoxide are now being studied. These electrodes may reduce the load on the methanation system of the hydrogen generator and permit lower temperature operation. Improvement of the carbon monoxide polarization may be possible with increased unit power output.

Electrode costs are a significant fraction of the total battery material costs. Although the electrodes have a high scrap value, the platinum is a high cost investment. While it is unlikely that platinum will be replaced as a catalyst, at least on the oxygen side, the possibility of a more effective use of the catalyst is significant. Experiments with electrodes using different amounts of platinum indicate that the effectiveness of the platinum (at constant potential) increases significantly as the platinum loading decreases. Some success may be expected from attempts to place small amounts of catalyst on the electrode surface most favorable to the reaction. The anode polarization curve indicates that reduction in catalyst loading may be possible now without penalty to performance.

ACKNOWLEDGEMENT

The authors wish to thank Southern California Gas Company, Southern Counties Gas Company of California, and Con-Gas Service Corp., who are sponsoring this investigation, for permission to publish these results.

REFERENCES

1. Meek, J., and Baker, B. S., "Hydrogen from Natural Gas for Fuel Cells," Fuel Cell Systems, pp. 221-231, American Chemical Society, Washington, D. C., 1965.

2. Meek, J., Baker, B. S., and Allen, A., "Performance of a Reformed Natural Gas-Acid Fuel Cell System, Part I, Hydrogen Generator Design," presented at Fuel Chemistry Division of the American Chemical Society, 150th Annual Meeting, Atlantic City, N. J., Sept. 12-17, 1965.
3. Haldeman, R. G., Colman, W. P., Langer, S. H., and Barber, W. A., "Thin Fuel Cell Electrodes," Fuel Cell Systems, pp. 106-115, American Chemical Society, Washington, D. C., 1965.

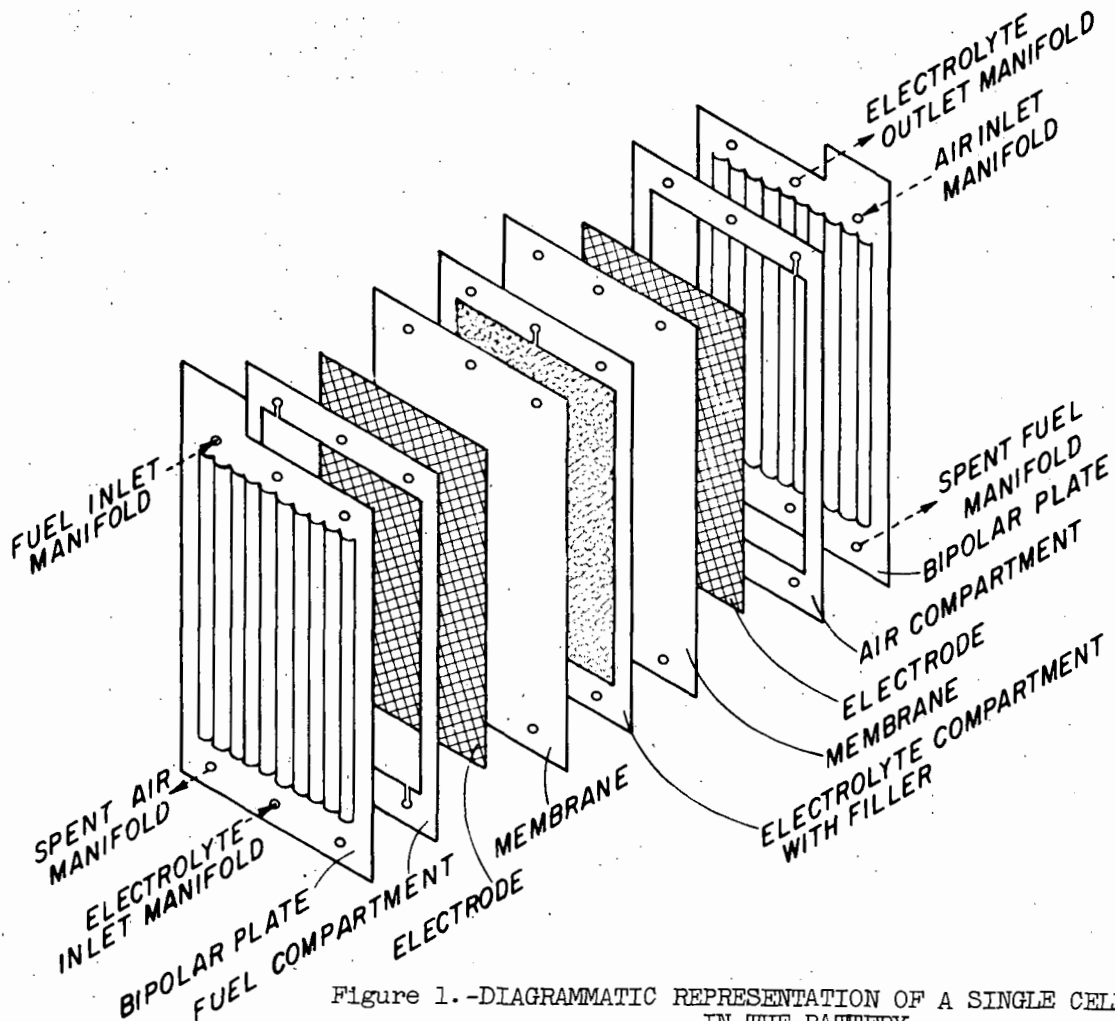


Figure 1.-DIAGRAMMATIC REPRESENTATION OF A SINGLE CELL IN THE BATTERY

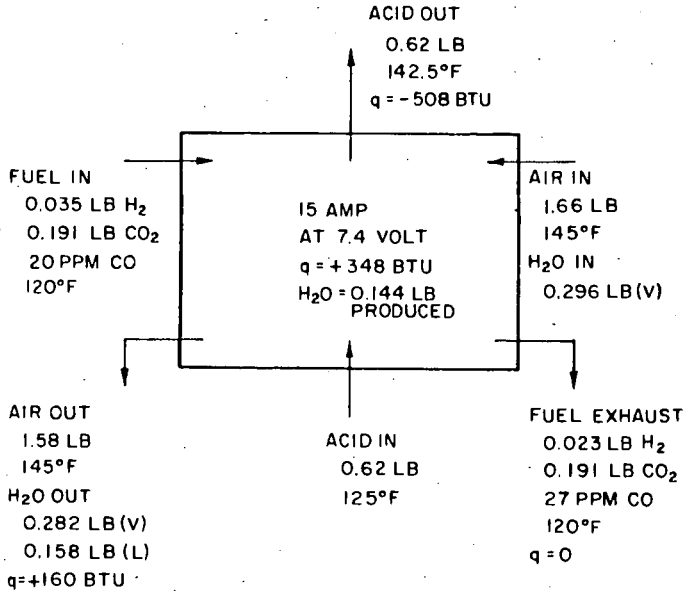


Figure 2.-HEAT AND MASS BALANCES AROUND THE OPERATING BATTERY
(13 CELLS, 1/4 SQ FT EACH, 1 HR OPERATION, STEADY STATE)

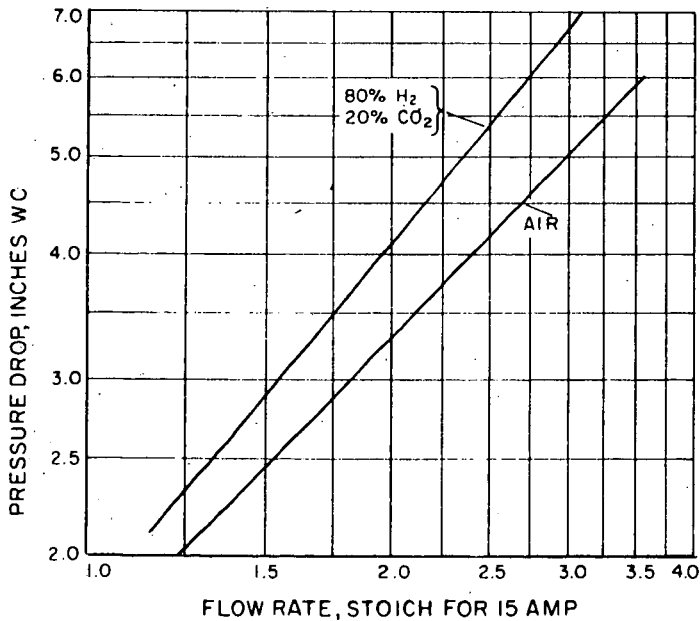


Figure 3.-PRESSURE DROPS IN THE BATTERY GAS STREAMS

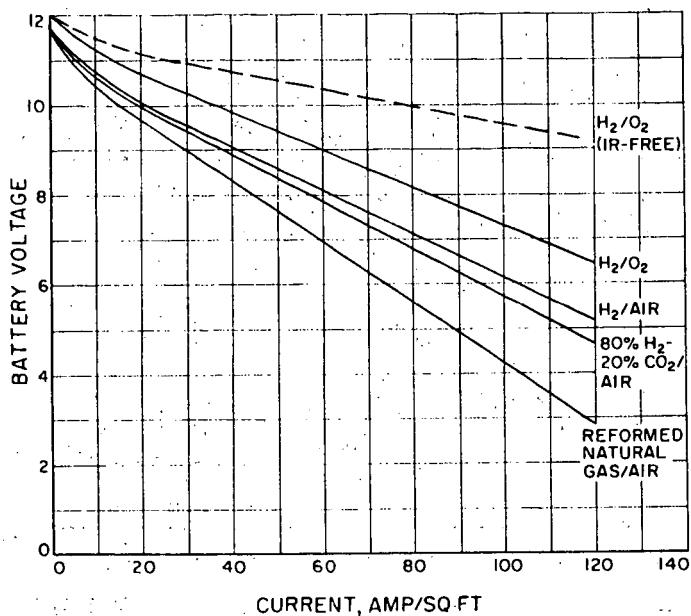


Figure 4.-OPERATING PERFORMANCE OF A 13-CELL BATTERY AT 60°C

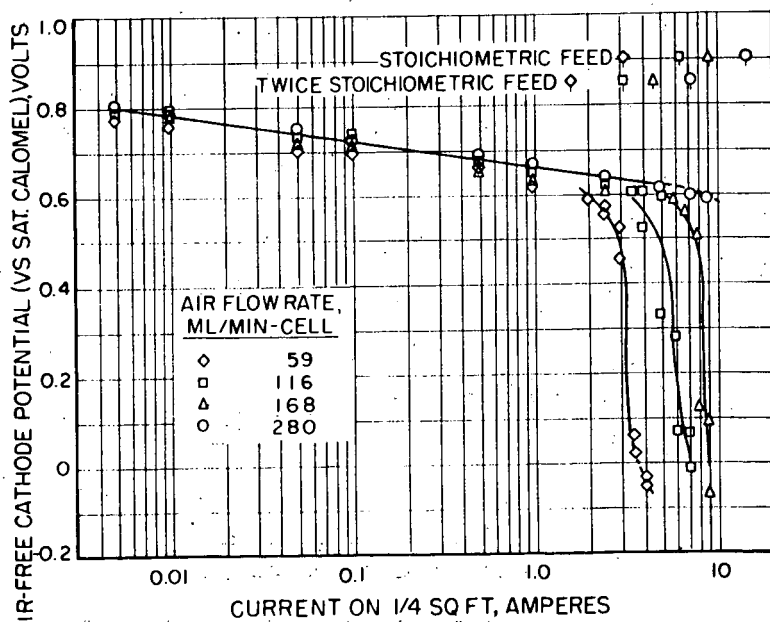


Figure 5.-POLARIZATION CURVE SHOWING POTENTIAL DROP AS CURRENT APPROACHES STOICHIOMETRIC EQUIVALENT OF AIR FEED

THE PERFORMANCE OF SOLID-ELECTROLYTE CELLS AND BATTERIES
ON CO-H₂ MIXTURES; A 100-WATT SOLID-ELECTROLYTE
POWER SUPPLY*

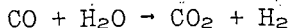
D. H. Archer, L. Elikan, and R. L. Zahradnik

Westinghouse Research Laboratories
Beulah Road, Churchill Borough
Pittsburgh 35, Pennsylvania

INTRODUCTION

Fuel cells employing a ZrO₂-based electrolyte are customarily operated at temperatures around 1000°C in order to promote high oxygen ion conductivity in this solid, ceramic material. At such high temperatures commercial fuels - coal and hydrocarbons - are thermodynamically unstable; they tend to crack forming solid carbon and hydrogen gas. The deposition of carbon in solid-electrolyte batteries can be prevented by mixing with the incoming fuel a portion of the CO₂ and H₂O products emerging from the battery. These gases reform the fuel producing CO and H₂ which are then oxidized in the solid-electrolyte cells to produce power. Essentially, therefore, in utilizing commercial fuels solid-electrolyte cells operate on CO-H₂ mixtures.

Experiments have been performed to characterize the performance of solid-electrolyte cells on fuel gas mixtures containing CO, H₂, CO₂, and H₂O in various proportions. Open circuit voltages have been determined in single cells at various temperatures; the measured values of voltage agree with those computed from thermodynamic data within 3%. The dependence of the operating voltage of solid-electrolyte cells on the current drain (or current density) has also been studied at various temperatures for different fuel mixtures. In general, cells operating on CO-CO₂ mixtures develop less output voltage than those operating on H₂-H₂O because of increased polarization voltage losses. The addition of H₂-H₂O to CO-CO₂ mixtures, however, greatly reduces these losses. And the insertion of a catalyst into the cell which promotes the shift reaction



causes further reduction in the observed polarizations to the extent that cell performance on CO-H₂ fuel duplicates that on pure H₂.

Tubular, solid-electrolyte batteries containing 20 bell-and-spigot cells of 7/16 in. diameter and 7/16 in. length have been produced. They are leak-tight. Their resistance has been

*The work recorded in this paper has been carried out under the sponsorship of the Office of Coal Research, U.S. Department of the Interior, and Westinghouse Research Laboratories. Mr. George Fumich, Jr., is head of O.C.R.; Neal P. Cochran, Director of Utilization, and Paul Towson have monitored the work for O.C.R.

of oxygen to gm-atoms of carbon in the fuel gas mixture - and n_H^1 , a similar ratio for hydrogen and carbon. Experimental values of open-circuit voltage are plotted together with theoretical curves in Figures 2 and 3. Except at $n_O = 1.0$ (usually corresponding to pure CO) and $n_O = 2.0$, $n_H^1 = 0.0$ (pure CO₂) where E_t changes very rapidly with n_O , E_t values are within $\pm 5\%$ of the predicted values. This agreement is considered to be within the limits of accuracy of the measurements of composition, temperature, and voltage involved.

VOLTAGE-CURRENT RELATIONS

The single solid-electrolyte cell shown in Figure 1 was also used to determine voltage-current curves for various mixtures of CO, H₂, CO₂, and H₂O at different temperatures. Some of the experimental results are shown in Figures 4-7.

When a current is drawn from the terminals, the voltage of the cell drops below the open-circuit voltage because of resistance losses in the electrolyte and electrodes and because of polarization voltage losses associated with irreversible electrode process.

$$V = E_t - IR - V_p \quad (2)$$

where V = the terminal voltage of the cell, volts

E_t = the open circuit voltage of the cell (which can be determined from Figures 2 or 3), volts

I = the load current passing through the cell, amperes

R = the electrical resistance of electrodes and electrolyte, ohms

V_p = the polarization voltage loss, volts.

An approximate value for the resistance of the cell shown in Figure 1 can be computed from

$$R = \rho_b \delta_b / A_b + (\rho_e / \delta_e)(L_e / P_e) \quad (3)$$

where ρ_b = electrolyte resistivity, about 70 ohm-cm at 1000°C

δ_b = electrolyte thickness, 0.09 cm

A_b = active cell area, 27.6 cm²

ρ_e / δ_e = resistivity-thickness quotient for the cell electrodes, estimated to be 0.8 ohms

L_e = mean distance traveled by the electronic current in the electrodes passing from the plus to the minus terminal of the cell, estimated to be 4 cm

P_e = mean width of the electrode perpendicular to the direction of electronic current flow, calculated as 3.4 cm

$$\begin{aligned} R &= [(70)(0.09)/27.6] + [(0.8)(4/3.4)] \\ &= 0.23 \text{ ohms} + 0.94 \text{ ohms} \\ &= 1.2 \text{ ohms.} \end{aligned}$$

The cell resistance has also been determined by measuring the voltage loss over the cell while passing a current with air at both inner and outer electrodes. The constant slope of this curve at higher current densities is termed the air-air resistance. Generally, this resistance value checks the resistance as computed above. Immediately after its construction the air-air resistance of the cell of Figure 1 checked the calculated resistance. Before the data for Figures 4-7 were obtained - three months later, the electrolyte component of cell resistance had gradually doubled. Presumably, the active cell area had decreased to about one-half the superficial electrode area.

Values of the polarization voltage V_p have been computed by Equation 2 from data of the type presented in Figures 4-7. For these computations the air-air resistance values were used, and E_t values were corrected by the use of Figures 2 and 3 where the cell current produced any appreciable change in n_0 , the oxygen content of the fuel stream passing through the cell. Table 1 presents the V_p values and also gives derived values of αn and i_0 in the simplified Tafel equation³

$$V_p = \frac{RT}{\alpha n} [\ln(i/i_0)] \quad (4)$$

where α is an empirically determined fraction of the electrical work output by which the free energy of activation is increased. An α value of about 0.5 is usually assumed in cases where specific knowledge is lacking.

n is the number of electrons transferred for each occurrence of the irreversible event causing the polarization voltage loss; n is assumed to be 2 in the electrochemical oxidation of CO.

i is the current density I/A_p , amperes/cm².

i_0 is the exchange current density, the equal but opposite rates at which the polarization-causing process and its reverse occur at open circuit (assuming a reversible electrode at this condition).

The following general observations can be made based on the data for pure, dry CO-CO₂ fuel mixtures presented in Figures 4-6 and Table 1:

- 1) Polarization losses in solid-electrolyte cells with conventional electrodes are much greater than those observed with H₂-H₂O fuel.
- 2) Polarizations with CO-CO₂ tend to decrease with increasing temperature.

determined by passing a current through the battery with air at both electrodes, and their fuel cell performance has been measured with pure H₂ and with H₂-CO mixtures as fuel, and with air as the oxidant. Over twenty-four of these batteries have been tested. Their average internal resistance is 8.2 ± 1.8 ohms; and their power output, 6.7 ± 0.8 watts. Twenty of these batteries have been assembled into a system which produces over 100 watts with H₂ or H₂-CO fuel and air.

OPEN-CIRCUIT VOLTAGES

A single solid-electrolyte cell has been employed to measure the open circuit voltages developed by mixtures containing CO, H₂, CO₂, and H₂O in various amounts. This cell was fabricated by applying conventional, sintered-platinum electrodes outside and inside of the central portion of a tube of (ZrO₂)_{0.85}(CaO)_{0.15} electrolyte material as shown in Figure 1. A platinum screen was placed in the tube to serve as a current collector. A cell lead wire was attached directly to this screen. Platinum wires were wound around the electrode on the outside of the tube and could be used either as current leads or as voltage probes.

Fuel mixtures obtained by mixing varying amounts of pure hydrogen with premixed CO-CO₂ mixtures flowed inside the tubular cell, which was maintained at the desired temperature in an electrically-heated furnace. An air atmosphere surrounded the tube.

The thermodynamically predicted open-circuit voltage of the cell can be calculated by

$$E_t(4F) = RT \ln (P_{O_2,a}/P_{O_2,f}) \quad (1)$$

where 4F = 4(the Faraday number) = quantity of charge transferred per mole of O₂ passing through the electrolyte 386,000 coulombs/mole

R = universal gas constant, 8.134 watt-sec./°K mole

T = absolute temperature of cell, °K

P_{O₂,a} = the partial pressure of oxygen in the air surrounding the cell, 0.21 atm.

P_{O₂,f} = the partial pressure of oxygen in the fuel gas atmosphere within the cell.

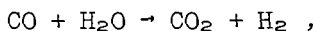
The value of P_{O₂,f} can be calculated from the composition of the fuel by standard thermodynamic methods.^{1,2} If the water gas equilibrium,



is achieved in the cell, then the fuel composition, P_{O₂,f}, and hence E_t can be determined from two parameters n₀ - the ratio of gm-atoms

- 3) The CO-CO₂ polarizations decrease with decreasing velocity of fuel flow.
- 4) Polarizations tend to increase more rapidly with current at fuel compositions where the $E_t - n\phi$ curve is sharply dropping; conversely the polarization voltage loss tends to remain more nearly constant with varying i at CO-CO₂ fuel compositions where the $E_t - n\phi$ curve is horizontal.
- 5) The αn values in the Tafel equation average about 1.0 as might be expected from simple theory which assigns α the value 0.5 and n the value 2. For the particular cell employed in this investigation the exchange current densities, i_0 , averaged about 0.7 milliamperes/cm². Insufficient data are available to draw any firm conclusions about trends of αn and i_0 with operating conditions in the cell.

The data presented in Figures 6 and 7 demonstrate that small quantities of hydrogen added to CO-CO₂ greatly reduce polarization voltage losses. With a hydrogen-carbon ratio $n_H^1 = 0.5$ the performance of the cell is essentially the same as with pure H₂. A hydrogen content of 5 mol % in a CO-H₂ mixture flowing at 1.0 cc/sec will alone support a current of 400 milliamperes; at this current the observed value of V_D from Figure 7 is about 0.15 volts if the effect of current on $n\phi$ and hence on E_t is considered. At a total current of over 1000 milliamperes (equivalent to about 40 milliamperes/cm²) the cell polarization voltage loss has risen only slightly to 0.20 volts. If the current in excess of 400 milliamperes were supported by the oxidation of CO, the data of Table 1 indicate that polarizations losses in excess of 0.30 volts could be expected at 1000 milliamperes. Apparently, the water gas shift process,



has provided sufficient hydrogen to maintain cell polarization losses low.

To investigate further the effect of hydrogen additions on the polarization losses associated with CO-CO₂ fuel mixtures - a three-cell battery, illustrated in Figures 8 and 9, was utilized. In operating on hydrogen and air this battery had higher resistance than is usually encountered in solid-electrolyte batteries of this type^{4,5} but polarization losses were negligible as shown in Figure 11. In operating on CO-CO₂ and air, however, polarizations were observed as shown in Figure 11 and in Table 2. The Tafel constants derived from the data are in good agreement with those obtained with the single cell. The difference between E_t for the CO-CO₂ fuel mixture and the observed open circuit voltage per cell in the battery is about 0.23 volts; the Tafel equation indicates that such a polarization corresponds to a current density of 6.2 milliamperes/cm²

(or 12 milliamperes/total current) passing through the cells at open circuit. This current is attributable to shunt paths in the seal regions.⁵

In a successful effort to reduce polarization losses, the CO-CO₂ fuel stream was humidified by passing it through a water bath at room temperature. At most 3 mol % H₂O was added to fuel stream. A catalyst material, Cr₂O₃, was sintered on the outside of the fuel feed tube and placed in the battery as shown in Figures 10 and 8. The performance of the battery is shown in Figure 11. (Catalyst Tubes 1 and 2 differ slightly in the quantity of Cr₂O₃ applied to the tube and the conditions of sintering.) Essentially the performance curves for the CO-CO₂ fuel mixture differ from the H₂ fuel curve only by an amount equal to three - for three cells - times the difference in E_t for the different fuels; CO-CO₂ mixtures can be utilized in solid-electrolyte cells with low polarization losses if some H₂ or H₂O is present and if a suitable shift catalyst is employed.

Additional experience on the performance of CO-H₂ fuel mixtures at higher current densities has been gained by a series of tests on a 20-cell solid-electrolyte battery whose construction and H₂-air performance have been previously described.⁵ The two H₂ performance curves of Figure 12 check with predictions based on the calculated cell resistance and on the variation of the open circuit voltage E_t with the composition of the fuel as it is gradually oxidized along the length of the battery. Polarization voltage losses are apparently negligible. The CO-H₂ performance curve was obtained without any shift catalyst present in the battery. The voltage with the CO-H₂ mixture at a current density of 450 milliamperes/cm², 0.9 ampere, is 0.1 of a volt per cell less than with pure hydrogen at the same net flow of H₂, 3 cc/sec. It can be expected that the addition of catalyst will bring about appreciable improvement of this 20-cell battery.

TWENTY-CELL BATTERIES

Twenty-five batteries identical in construction to the one whose performance is presented in Figure 12 have been fabricated and tested. All except one proved leak-tight. At the operating temperature of 1000°C battery air-air resistance - the voltage loss divided by the current value of 1.0 ampere - ranges from 6.4 to 9.4 ohms; the average and root mean-square deviation values are 7.8 ± 1.0 ohm. This average battery resistance is about 30% greater than the value calculated from the electrolyte resistivity and electrode resistance/thickness values. The open circuit voltage developed by these batteries on H₂ or H₂-CO fuel and air ranges between 19 and 20 volts; losses in the generated voltage of the solid-electrolyte bell-and-spigot cells due to shunt currents in the seal region⁵ are thus less than 7% of the reversible voltage. The maximum power output of the batteries is 6.7 ± 0.8 watts with complete combustion of H₂ fuel at about 0.87 amperes or 435 milliamperes/cm².

The resistance, open circuit voltage, and power output of these batteries are in reasonable agreement with theoretical calculations.⁵ And the methods used in fabricating the batteries yield a reasonably uniform product.

100-WATT SOLID-ELECTROLYTE FUEL-CELL POWER SUPPLY

Twenty of the 20-cell batteries described above have been used to construct a 100-watt solid-electrolyte fuel-cell power supply shown in Figure 13. The batteries are mounted on a 4.5 in. diameter metal base plate (see Figure 14) which provides support and manifolding for up to twenty-four batteries. The flow to each battery from the fuel plenum is regulated by a fine needle valve - one of which is shown on Figure 14. The valve position push rods are adjusted to equalize the flows to the batteries. The fuel flows up the feed tube to the top of the battery; it then flows downward inside the tube of cells reacting with the oxygen which passes through the electrolyte as current is drawn from the battery. The combustion products are carried down into the upper plenum of the base plate and then into the exhaust pipe.

Air surrounds the batteries inside the 3-zone furnace (see Figure 13) which is used to maintain the cells at the desired operating temperature. Plugs of insulation 5 in. in diameter and 4-1/2 in. thick are used to reduce heat losses from the top and bottom of the cylindrical heated region of the furnace. The temperature distribution throughout the batteries is indicated in Figure 15; the small circles represent individual batteries in a plan view of their arrangement in the furnace. At the top are the temperatures of the uppermost cell in three batteries indicated by Pt-Pt-10% Rh thermocouples. The middle temperatures are those on the tenth cell from the top; at the bottom are shown temperatures of the lowest cells in the batteries. With the exception of one low temperature reading on a battery opposite the "crack" of the split-tube furnace the temperatures are within $\pm 30^{\circ}\text{C}$ of the average value. Even better uniformity can be achieved by a more careful adjustment of the heat input to the various sections of the furnace.

The twenty batteries are divided into two groups of ten; in each group the batteries are electrically connected in series. The two groups, each containing 200 series-connected cells, are used in parallel to supply power to the load. The electrical performance of this power supply is shown in Figure 16. The open-circuit voltage is 200 volts; the maximum power is 102 watts at 1.2 amperes with H_2 flow at a rate corresponding to 2.1 amperes. This power output is about 20% lower than that which might be expected from the measurements of the power output of single batteries. A reduction in temperature of batteries caused by heat losses through the "split" in the furnace and a non-uniform distribution of air flow through the batteries have been shown to cause in part this reduction in power. With excess H_2 flow, the performance of the battery is improved as shown in Figure 17 and a maximum power of 110 watts is achieved.

The 100-watt power supply demonstrates the feasibility of generating fuel-cell power by means of banks of solid-electrolyte batteries. This, plus the demonstrated ability of the batteries to produce

power efficiently from carbon monoxide - carbon dioxide - water - hydrogen mixtures with the employment of a chrome oxide catalyst, demonstrates the technical feasibility of generating this power from coal.

REFERENCES

1. D. H. Archer and E. F. Sverdrup, "Solid-Electrolyte Fuel Cells" in Proceedings of the 16th Power Sources Conference, 34 (1962).
2. D. H. Archer, E. F. Sverdrup, and R. L. Zahradnik, "Coal Burning Fuel Cell Systems" Chemical Engineering Progress, 60,6, 64 (1964).
3. L. G. Austin, "Electrode Kinetics and Fuel Cells" Proceedings of the IEEE, 51, 820 (1963).
4. D. H. Archer, J. J. Alles, W. A. English, L. Elikan, E. F. Sverdrup, and R. L. Zahradnik, "Westinghouse Solid-Electrolyte Fuel Cell" in Advances in Chemistry Series (R. F. Gould, ed.), 47, 332 (1965).
5. D. H. Archer, R. L. Zahradnik, E. F. Sverdrup, W. A. English, L. Elikan, and J. J. Alles, "Solid-Electrolyte Batteries" in Proceedings of the 18th Power Sources Conference, 36 (1964).

Alcher

Table 1

Polarization Voltage Losses, V_p , and Tafel Equation Constants at Various Fuel Flow Rates, Compositions and Temperatures

Cell Operating Conditions			Polarization Voltage Losses at Various Current Densities, volts				Tafel Constants	
% CO in CO + CO ₂ 100 (n ₀ - 1.0) ²	Temperature T, °K	Fuel Flow Q, cc/sec	i = 2 ma/cm ²	i = 4 ma/cm ²	i = 6 ma/cm ²	i = 12 ma/cm ²	cm	i ₀ , ma/cm ²
100	1215	0.7	0.19	0.27	0.30	0.39	1.1	0.33
100	1215	0.17	0.12	0.17	0.21	0.27	0.8	0.47
100	1050	0.7	0.32	0.32	0.32			
100	1050	0.17	0.19	0.20	0.21			
90	1330	0.7	0.13	0.23	0.31		1.4	0.94
25	1215	0.7	0.11	0.175	0.22		0.9	0.64
25	1215	0.17	0.065	0.14	0.195		1.1	1.20
25	1050	0.7	0.29	0.375				
25	1050	0.17	0.28	0.34				
10	1215	0.7	0.09	0.16	0.19	0.24	0.8	0.80
10	1215	0.17	0.09	0.11				
10	1050	0.7	0.275	0.34				
10	1050	0.17	0.235	0.255				

Table 2

Polarization Voltage Losses with CO-CO₂ in a Three-Cell Solid-Electrolyte Battery

Fuel: 90 mol % CO, 10 mol % CO₂
 $n' = 1.1$
 5.7 cc/sec
 Oxidant: air
 Temperature: 1000°C
 Cell area (active): 2.0 cm²

Current density, $I/A_p = 1$, milliamperes/cm ² :	25	50	100	150
Polarization Voltage loss, V_p , volts:	0.37	0.44	0.51	0.55

Derived Tafel constants: $\alpha_n = 0.92$
 $i_0 = 0.6$ milliamperes/cm²

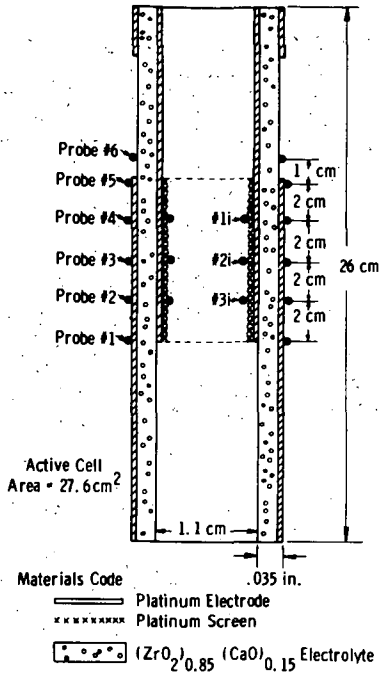


Fig. 1—Schematic cross section of fuel cell TC#8

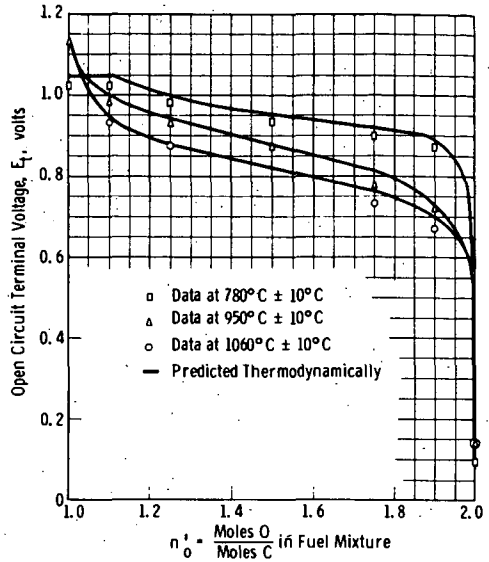


Fig. 2—Generated voltage of a fuel cell using a C-O fuel mixture as a function of fuel mixture composition

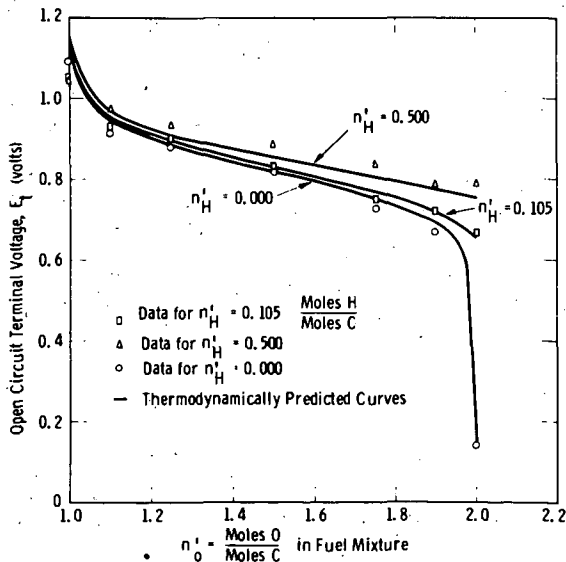


Fig. 3—Generated voltage of a fuel cell using a C-H-O fuel mixture at 1060°C as a function of fuel mixture composition

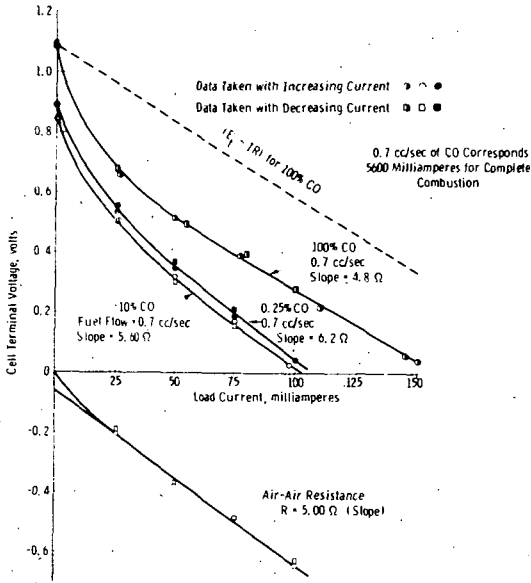


Fig. 4 - Load curves for fuel cell TC #8 using CO-CO₂ fuel mixtures at 780°C

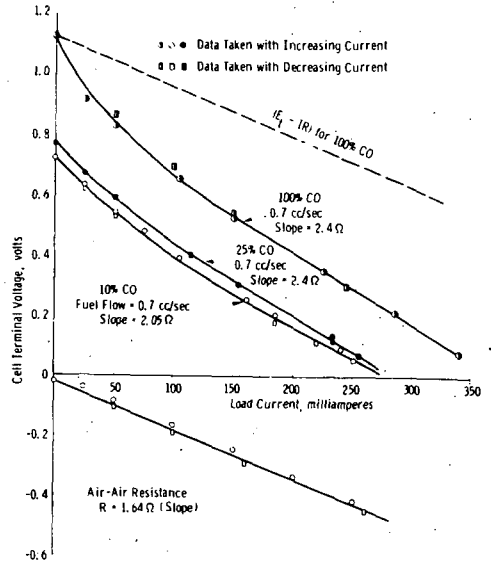


Fig. 5 - Load curves for fuel cell TC #8 using CO-CO₂ fuel mixtures at 940°C

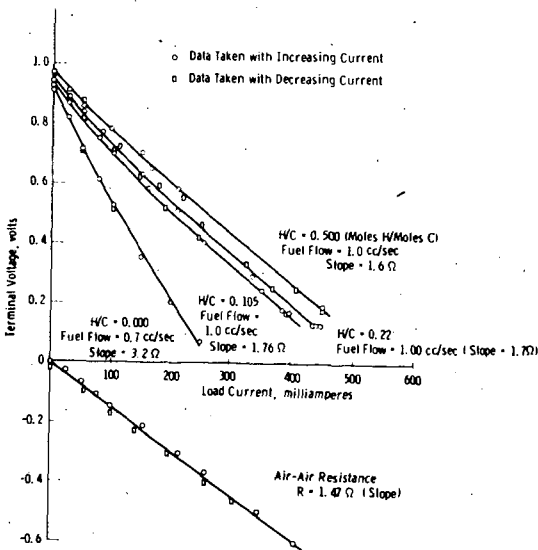


Fig. 6 - Load curves for fuel cell TC #8 using C-H-O fuel mixtures at 1060°C with $n^+ = 1.10$ (Moles O/Moles C) in fuel chamber

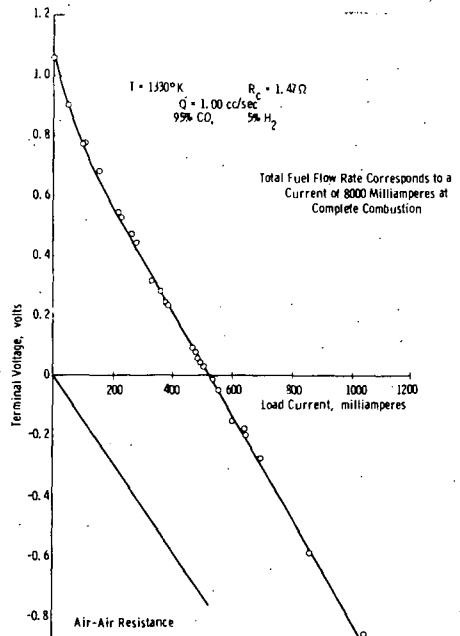


Fig. 7 - Load curve demonstrating effectiveness of water-gas reaction in improving fuel cell performance in TC #8

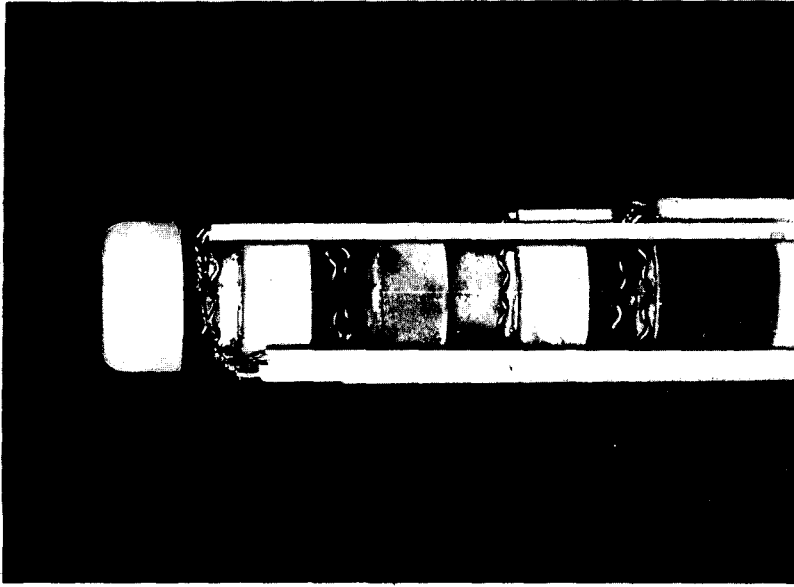


Fig. 9—Three-cell solid-electrolyte battery with current leads, voltage taps, and thermocouple probes

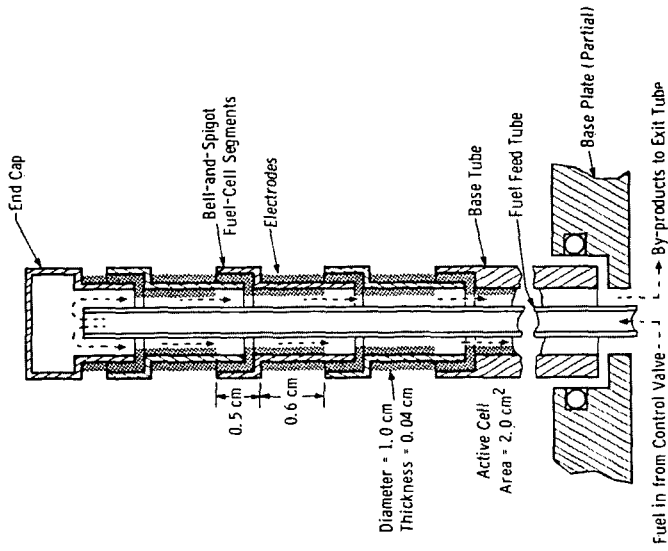


Fig. 8—Schematic axial cross-section of a three-cell solid electrolyte battery showing feed-tube

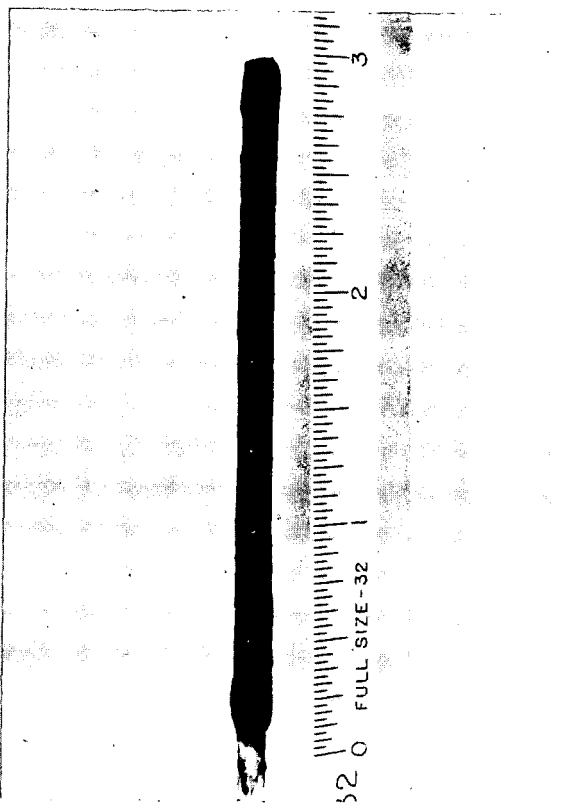


Fig. 10—Fuel feed tube for three-cell battery with Cr_2O_3 catalyst coating

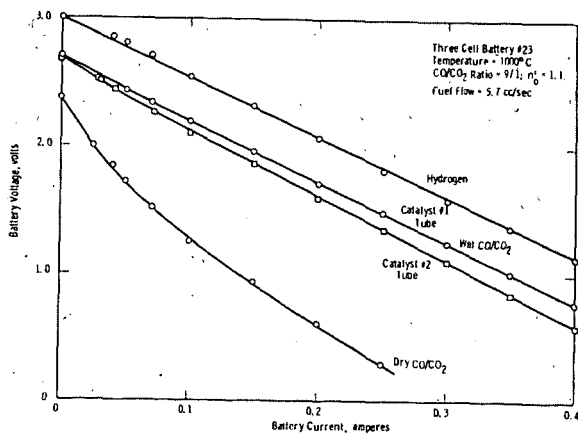


Fig. 11—Performance of three cell battery using chrome-oxide catalyst sintered to fuel feed tube

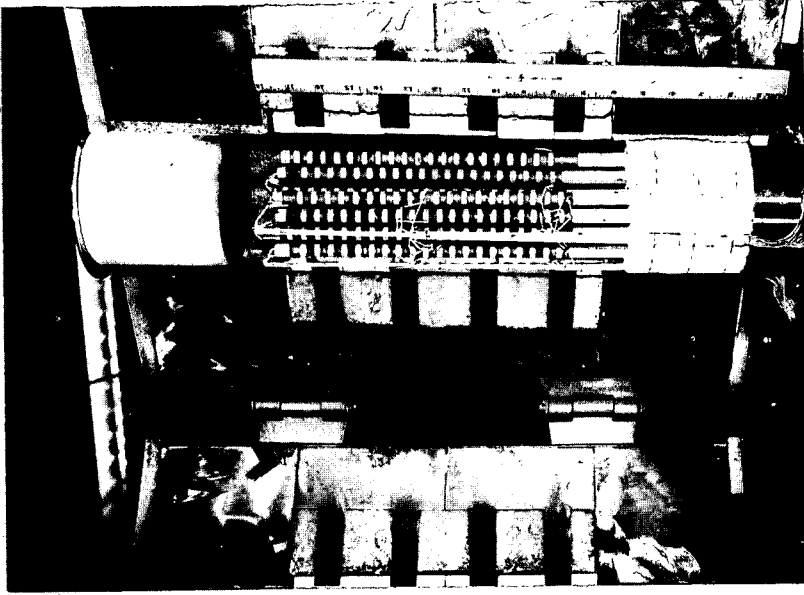


Fig. 13—100-watt solid-electrolyte fuel-cell power generator with furnace door open

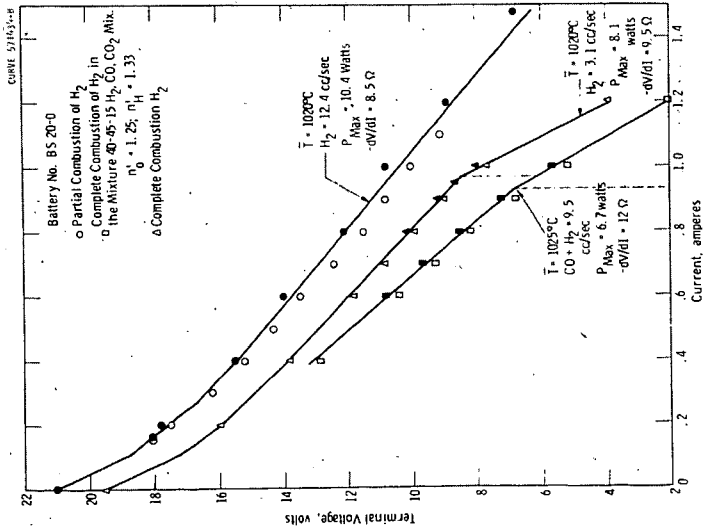


Fig. 12—Twenty-cell solid-electrolyte battery performance

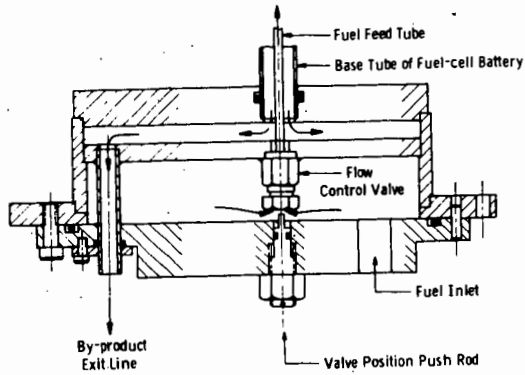


Fig. 14 - Section view of base plate

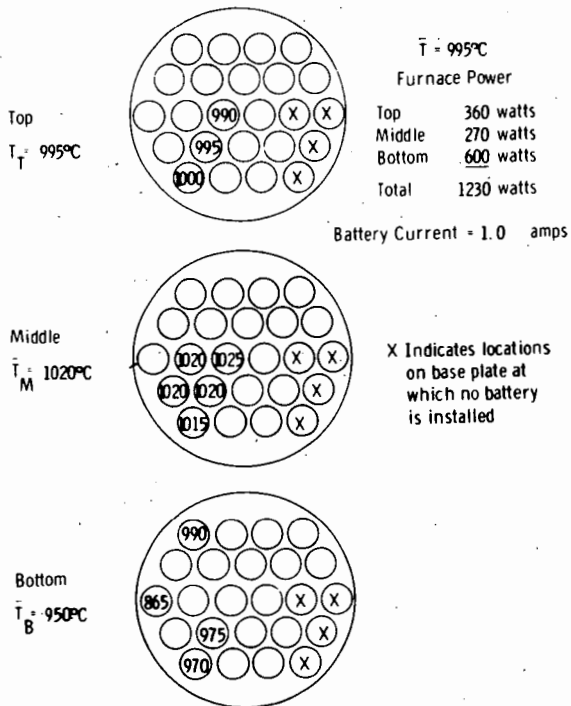


Fig. 15 - Battery temperature distribution as a function of axial position --at operating temperature

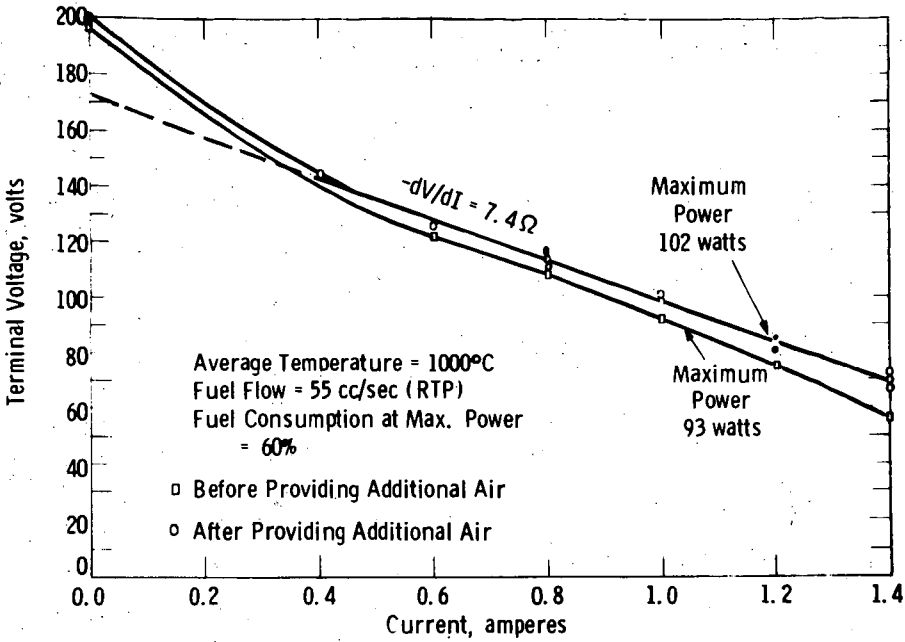


Fig. 16—100-watt battery performance before and after increasing air flow

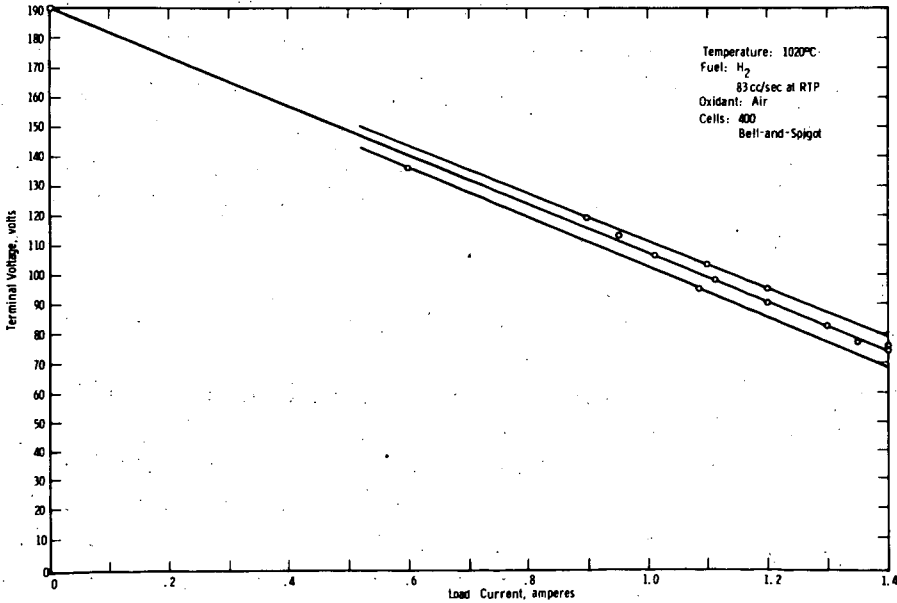


Fig. 17—Performance of 100-watt solid-electrolyte fuel-cell power system

ALCOHOL AIR FUEL CELLS - DEVELOPMENT AND APPLICATION

W. Vielstich

Institut für Physikalische Chemie der Universität Bonn

INTRODUCTION

Taitelbaum (1) in 1910 was the first to convert the chemical energy of liquid fuels (e.g. petroleum, stearic acid and starch) in a galvanic cell into electricity. But the use of fuels like alcohols or aldehydes was proposed many years later by Kordesch and Marko (2) and by Justi et al (3).

Kordesch and Marko studied the system formaldehyde/air. The cell with the alkaline or acid electrolyte contains an oxygen diffusion electrode and a porous fuel electrode. The fuel or fuel/electrolyte mixture penetrates the fuel electrode from the back. In this manner an enlargement of the two phase boundary is obtained. Moreover, under proper operating conditions the fuel concentration is relatively small in the vicinity of the oxygen electrode, even if no diaphragm is used. This is particularly important if the oxygen electrode contains a metal which catalyses the fuel reaction.

In an other method of construction the alcohol is dissolved in the electrolyte and both electrodes dip into the fuel-electrolyte mixture (3,4).

The use of liquid fuels in general obviates the need for a three-phase boundary, and thus facilitates the construction of the fuel electrode. An additional advantage is that the fuel can be brought to the catalytic electrode in high concentration. Thus, if the reaction is fast enough, high current densities can be obtained (up to 1 A/cm^2 at room temperature). Such battery systems can be used conveniently for maintenance-free, continuous operation if air at ambient temperature and pressure is supplied to the oxygen electrode. Some examples of this type of fuel cell are discussed in the following.

METHANOL AIR CELL FOR OPERATION AT LOW CURRENT DENSITIES

General Remarks

In recent experiments (5,6) it has been shown, that the anodic oxidation of methanol proceeds via formaldehyde, and formate or formic acid respectively. On open circuit at platinum metal electrodes one observes a hydrogenation/dehydrogenation-equilibrium (7), while under load also methanol is not electrochemically active itself. At potentials $\varphi < + 400$ mV versus the H_2 potential in the same solution a preliminary dehydrogenation takes place. At more positive potentials the fuel reacts with the oxygen which has been chemically adsorbed by the electrode surface (8,9). Therefore, a suitable combination of catalyst, electrolyte and temperature has to be arranged to obtain the required current density in the desired potential range over the total oxidation up to CO_2 or CO_3^{--} respectively. In this connection two problems have to be solved when using an alkaline solution, which is the most suitable electrolyte for practical cells.

- (i) An appreciable enrichment of formate has to be avoided: the use of mixed platinum and palladium catalysts is one possible solution (10).
- (ii) The electrode polarization increases with the concentration of CO_3^{--} -ions at current densities $j > 5 - 10$ mA/cm² at 20 - 50°C (11). To obtain a flat voltage/time curve over the total capacity of 6 electrons per molecule (i.e. $CH_3OH + 8 OH^- \rightarrow CO_3^{--} + 6 H_2O + 6 e^-$), the critical current density should not therefore be exceeded.

Experimental Results with Laboratory Cells

For the investigation in the laboratory glass vessels containing 1 liter of electrolyte/fuel mixture (10 N KOH and 4.5 M methanol) were used. KOH is used because cells with NaOH have higher polarizations, particularly on the oxygen side. The KOH concentration is chosen in such a manner that even after complete reaction of the fuel the OH^- -concentration will be 1 - 2 molar.

Platinum on a porous carrier was found to be a better catalyst than Raney-nickel. Up to now 2 - 5 mg Pt/cm² have been used. At this fuel electrode the oxidation potentials for methanol and formate up to current densities of 5 mA/cm² are about the same. So the formate content of the electrolyte when using methanol as fuel is very low. This results in a flat voltage-time curve (see Fig. 1).

Since, for the intended application (see below), only a few mA/cm² are needed, porous carbon without metallic additions is used on the oxygen side. Plate-like or cylindrical electrochemically active carbon electrodes (surface area: 250 cm²) are made hydrophobic with polyethylene dissolved in benzene to such a degree that the methanol/electrolyte mixture will not penetrate through the electrode even after 10.000 hours (the thickness of the electrode plates is 5 - 10 mm).

The EMF of this methanol/air cell is about 0.9 volt; at a current drain of 0.5 amp the terminal voltage is 0.75 - 0.6 volt. For short periods of time 2 amps can be withdrawn at 0.6 - 0.5 volt. The long term experiments are performed taking into consideration that the end use will be periodic loads (2 seconds at 0.5 amp and 4 seconds O.C.). The periodic current interruption not only makes the diffusion of air easier but it also increases the life time and preserves the activity of the fuel electrode.

Typical discharge curves are shown in Fig. 1. The difference between theoretical and experimental current yields can be explained on the basis of analysis of the electrolyte by evaporation of methanol through the porous carbon. The analysis also shows that the diffusion of CO₂ from the air through the carbon can be neglected.

The influence of temperature on the oxidation rate at constant electrode potential is very pronounced. Current density-potential plots obtained after operation for one day at 10 mA/cm² are given in Fig. 2.

Discussion

The special feature of a methanol/air cell as described above is a high Ah-capacity per unit volume or per unit weight: 5.000 Ah/litre methanol, up to 1.000 Ah/l fuel-electrolyte mixture, or about 3 kg/kWh for an operating time 6.000 hours.

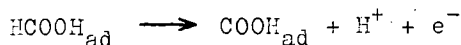
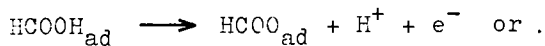
The experimental results reveal, however, the following disadvantages:

- (i) The current densities at the fuel electrode at ambient temperatures are relatively low, if small amounts of noble metal catalysts are used.
- (ii) The vapour pressure is unfavourable for moderate temperature applications.
- (iii) With decreasing temperature the power output of the cell drops considerably.

FORMIC ACID AND FORMATE AS FUEL

Anodic oxidation of formic acid, nature of the intermediate product

In acid electrolytes methanol and formaldehyde are less reactive than formic acid (9,12,13). The oxidation rate at potentials $\varphi < 0.6$ volt (vs. SHE) is determined by the poisoning effect of an intermediate product. The particles adsorbed at a Pt-electrode are probably formate radicals and certainly not carbon monoxide or oxalic acid (14). A potentiostatic potential scan is especially suited to give a qualitative view of the reaction mechanism. Fig. 3 shows three current peaks during the anodic scan. The first maximum is due to the reaction step (14)



In the region of the second and third peaks the fuel reacts with chemisorbed oxygen as described above for the methanol oxidation. The adsorbed intermediate too is oxidized in this potential range. Fig. 4 clearly demonstrates the poisoning

effect of the adsorbed product on a smooth platinum electrode at 0.5 volt.

Application of a mixed Pt/Ru-catalyst

Recently Frumkin (15) has discovered that the use of a mixed platinum ruthenium catalyst diminishes the poisoning effect. This has been confirmed by the following experiment. An active carbon electrode (geom. surf. 24 cm^2 , $12 \text{ mg Pt-metal/cm}^2$) was prepared (a) with 3 % Pt (b) with 3 % Pt/Ru (9:1) ratio by weight. The current densities observed at the two electrodes at 0.5 volt were for electrode (a) 2 mA/cm^2 and for electrode (b) 10 mA/cm^2 . In a long duration experiment with an HCOOH/air cell (50 cm^2 electrodes, 20°C) the ratio of power outputs using the two types of electrode was about 3. The current yield which is about the same for the two cells is surprisingly low, less than 20 % on a 2 electron/molecule basis.

Formate ion-oxidation on mixed noble metal catalysts

In early investigations of the anodic oxidation of methanol in alkaline solution with Raney-nickel (9) or platinum (6,10) electrodes formate ion was usually found as the primary oxidation product. The further oxidation of the formate ions occurred at a less favourable potential. Grimes and Spengler (10), however, have observed that the use of mixed platinum and palladium catalysts allows the complete oxidation of methanol to carbonate. A formate ion/oxygen fuel cell with a nickel substrate as anode ($9 \text{ mg Pd/Pt (5:1)/cm}^2$) produced twice the power output of a similar methanol cell at the same temperature.

These results demonstrate that the oxidation rate of formate ions is very sensitive to the composition and the structure of the metal catalyst. Moreover, the electrocatalytic effects are different for formate ion and methanol.

Our studies have shown that the formate oxidation rate on platinum and palladium alloys varies over more than two orders of magnitude. The formate oxidation has been investigated on a series of smooth metal electrodes by use of the potentiostatic scanning method. An example of the current voltage dia-

grams obtained in 6 N KOH + 4 M HCOOH is given in Fig. 5. The height of the high anodic current peak (during the anodic scan) is taken as measure of the catalytic activity of the metal. The activity of the metal surface is controlled by the potential range covered and the scanning speed (100 mV/sec). Fig. 6 shows the strong influence of the electrode material on the peak current density for 20 and 40°C.

The relationship between electrode material and current density obtained offers of course only a first insight into the selection of the most suitable catalyst. In battery practice one has to deal with porous electrodes and continuous discharge. Therefore factors other than metal composition are also important.

In preliminary tests of formate ion/air cells about 10 times the power output compared with methanol as fuel has been observed. Continuous discharge at 20 mA/cm² at 20°C is readily obtained.

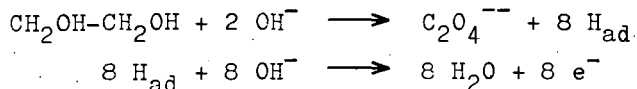
Discussion

By use of mixed Pt/Ru-anode catalysts the power output of a HCOOH/air cell at ambient operating conditions is of the same order as that of an alkaline methanol/air cell. The reaction product of the formic acid cell is CO₂ and therefore electrolyte renewal is not required. On the other hand one needs for both electrodes noble metal catalysts. Another disadvantage is the high rate of the current-less decomposition. The influence of the current density on the reaction yield has not yet been investigated.

Due to the moderate current densities at ambient temperature and pressure the formate ion/air cell with mixed Pt-metal catalysts at the fuel electrode offers a new field of applications. In contrast to methanol the vapour pressure is low, so that operating temperatures up to 100°C can be used. Compared to methanol, however only 2 electrons per molecule are obtainable.

EXPERIMENTS WITH GLYCOL AS FUEL

In acid electrolytes the anodic oxidation of glycol leads to CO_2 as end product. The working potential is, however, less favourable than with formic acid as fuel (9). The oxidation at alkaline pH results in the formation of oxalate. But at moderate temperatures (60 - 90°C) a strong dehydrogenation takes place



and current densities up to 600 mA/cm² can be obtained (9,16). Grüneberg et al (9,16,17) have developed a glycol/air cell operating at ambient temperature and pressure.

The air electrode was pressed from activated carbon and polyethylene powder (500 kg/cm², 160°C) and built up in two layers. The layer on the electrolyte side was made only weakly hydrophobic and contained Ag₂O as catalyst. The electrode had such good mechanical stability that it could be used as an end plate in the cell. Between the air electrodes there is a fuel electrode of the same size: coarse grained Ni-DSK (3) is held in place by nickel screens.

The open circuit potential of such a cell (6 N KOH + 2 M glycol) is about 1.1 volt. At a load of 3 mA/cm² such a cell will have a potential of 0.8 volt at room temperature. For short periods of time current densities up to 30 mA/cm² can be withdrawn.

For the investigation of high current density glycol/air cells we have used as fuel electrodes, flame-sprayed Raney-nickel on a nickel substrate. Electrodes up to a geometric area of 20 x 30 cm² have been studied. As already stated by Boies and Dravnieks (18) the activity of the electrode is critically dependent on the grain size, and the substrate must be carefully prepared to obtain good and stable contact to the catalytic layer. The increase of the dehydrogenation rate with temperature has a strong influence on the shape of the current/voltage-curve (Fig. 7).

The features of the glycol cell operating at moderate temperatures are:

noble metal catalysts are not required, high current densities can be obtained in direct oxidation from an easily handled liquid fuel, and strong gas evolution does not take place. The price of the fuel and the necessary renewal of the electrolyte are the main disadvantages.

APPLICATIONS OF ALCOHOL AIR/CELLS

General Remarks

Ambient air cells with methanol or formate ion as fuel are particularly suited for a maintenance-free, continuous operation at low or moderate current densities. Therefore they could be used to supply signal devices, stationary or mobile communication systems, isolated weatherstations etc. Such alcohol/air cells can start to compete with dry batteries and wet batteries of the system zinc/NaOH/air.

The high power glycol cell should be applicable e.g. as an emergency unit. In contrast to such a fuel cell the presently used Diesel engine has several disadvantages: it requires maintenance, unreliability of the rotating parts, uncertain starting in an emergency.

Beside battery construction cost, fuel cost and availability, the amount of noble metal used for the electrodes is a peculiar problem in commercial fuel cell application. In the alkaline methanol and formate cells developed so far 2 - 5 mg/cm² platinum and palladium are needed. To what extent this amount has to be decreased to make such cells economic depends very much on the special application.

Test of a 60 Watt methanol/air battery for sea buoys

On the basis of our laboratory investigations described above Brown, Boveri a. Cie. have built a 6 volt 10 amp battery for a flashing buoy. The module contains 10 cylindrical cells (Fig. 8). In each cell 18 pairs of electrodes are connected in parallel in order to equalize the different performance of the individual cells and to prevent the failure of single electrodes. From the 400 litre fuel/electrolyte-mixture 180 kWh

can be obtained. By using an electronic device the power output of the battery is stabilised (30 Watt in signal operation between 5 and 30°C) against changes of temperature and changes in fuel concentration which occur over a two years period of operation (intermittent 2 sec load, 4 sec O.C.).

The battery is presently in field test for several months. It is felt that the operation cost (methanol and caustic) will be cheaper than the present propane-consuming buoys.

Literature

1. I. Taitelbaum, Z. Elektrochem. Ber. Bunsenges. physik. Chemie **16**, 295 (1910).
2. K. Kordesch and A. Marko, Oesterr. Chemiker Zeitung **52**, 125 (1961)
3. E. Justi and A. Winsel, "Fuel Cells - Kalte Verbrennung", Steiner, Wiesbaden, 1962
4. M. Janes, Trans. Electrochem. Soc. **77**, 411 (1940)
5. M.J. Schlatter, Symposium Amer. Chem. Soc. Chicago 1961, B 149
6. O. Bloch, P. Degobert, M. Prigent and J.C. Balaceanu, 6th WPC Frankfurt 1963, Section VI-paper 3 - Pd 10
7. A.N. Frumkin and B.I. Podlovchenko, Ber. Akad. Wiss. UdSSR **150**, 349 (1963)
V.S. Bagotzky and Y.B. Vasiljev, Electrochim. Acta (London) **8**, 869 (1964)
8. W. Vielstich, Chem. Ing. Techn. **35**, 362 (1963)
A. Kutschker and W. Vielstich, Electrochim. Acta (London) **8**, 985 (1963);
J. Giner, Electrochim. Acta **9**, 63 (1964)
9. W. Vielstich, "Brennstoffelemente - Moderne Verfahren zur elektrochemischen Energiegewinnung", Verlag Chemie, Weinheim, 1965
10. P.G. Grimes and H.M. Spengler, ECS-Meeting, Washington 1964, Battery Div. Ext. Abstr. No. 27
11. J.N. Murray and P.G. Grimes, "Methanol Fuel Cell", Res. Div. Allis Chalmers, Milwaukee, 1963
12. W. Vielstich, Chem. Ing. Techn. **35**, 362 (1963)
13. R. Jasinski, J. Huff, S. Tomter and L. Swette, Ber. Bunsenges. physik. Chemie **68**, 400 (1964)

14. W. Vielstich and U. Vogel, Ber. Bunsenges. physik. Chemie 68, 688 (1964)
15. A.N. Frumkin, paper presented at the 4th Intern. Symp. on Batteries, Brighton, 1964
16. H. Spengler and G. Grüneberg, Dechema Monogr. 38, 579 (1960)
17. G. Grüneberg and M. Jung, BPA 592 862
18. D.B. Boies and A. Dravnieks, Elektrochem. Techn. 2, 351 (1964)

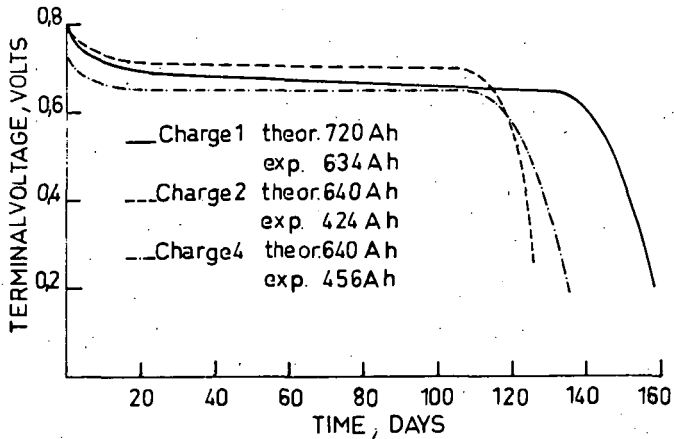


Fig. 1 Terminal voltage at periodic loads (2 sec load and 4 sec O.C.) of a methanol/air cell, operating time $\tau > 12,000$ hours with 4 electrolyte charges, temperature 10 - 20°C

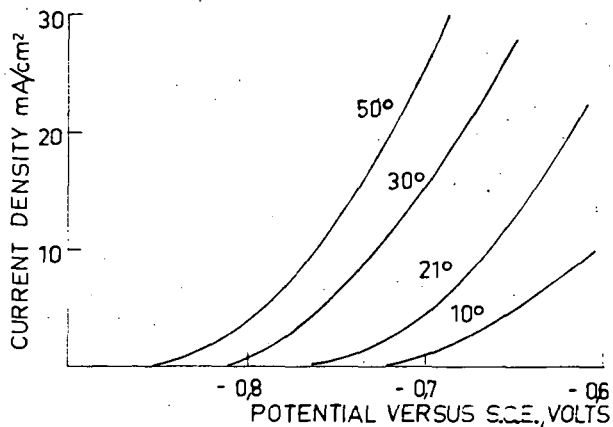


Fig. 2 Effect of temperature on the performance of a platinum activated carbon electrode in 6 N KOH + 2 M CH₃OH solution, F = 12 cm², 4.8 mg Pt/cm²; curves taken after 1 day operation at 10 mA/cm².

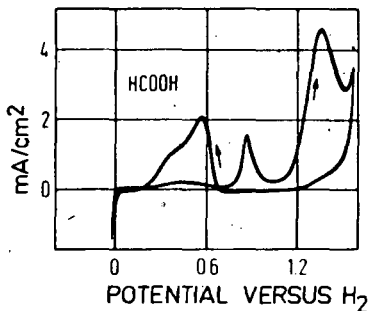


Fig. 3 Triangular potential scan on smooth Pt in 1 N H₂SO₄ + 1 M HCOOH, 50 mV/sec, 20°C

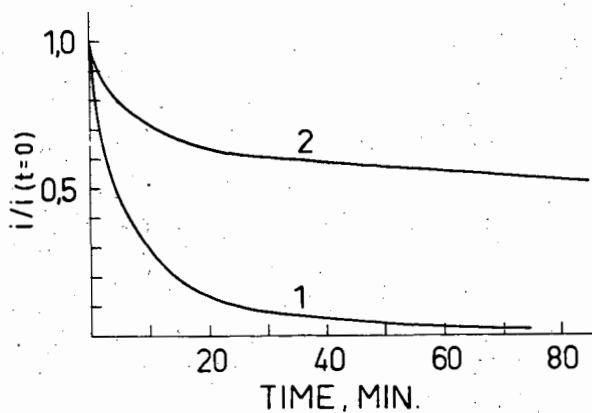


Fig. 4 Decrease of current with time on smooth Pt in 1 N H_2SO_4 + 1 M HCOOH at constant potential
(1) at 0.5 volt (first current peak in Fig. 3)
(2) at 0.9 volt (second peak in the anodic scan of Fig. 3)

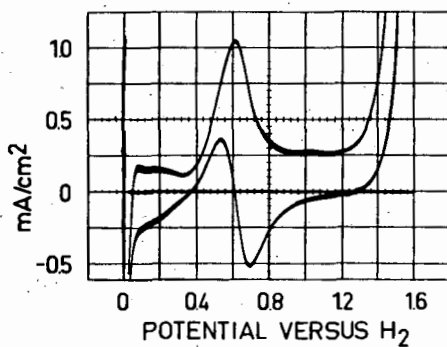


Fig. 5 Triangular potential scan on smooth Pt/Ir (75:25)-alloy in 6 N KOH + 4 M HCOOK, 1.00 mV/sec, $40^\circ C$

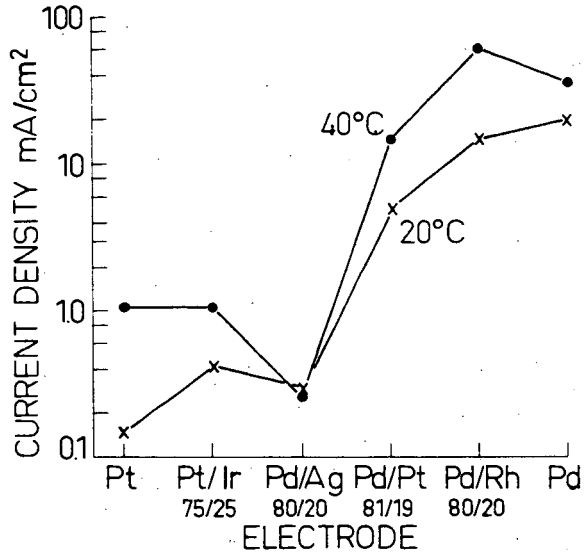


Fig. 6 Peak current density of a triangular potential scan according to Fig. 5 on different smooth metal electrodes in 6 N KOH + 4 M HCOOK

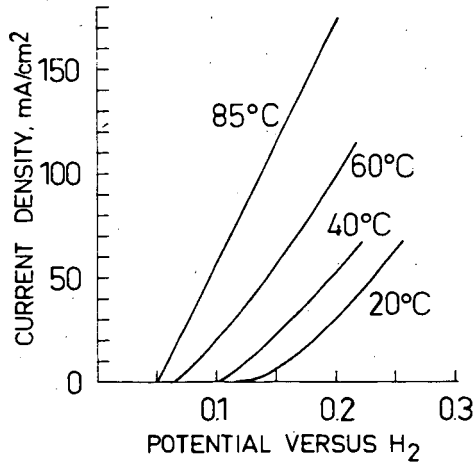


Fig. 7 Current density-potential curves on flame sprayed Raney-nickel (grain size 200 μ) in 6 N KOH + 2 M Glycol, plots taken after 2 day operation at 50 mA/cm²

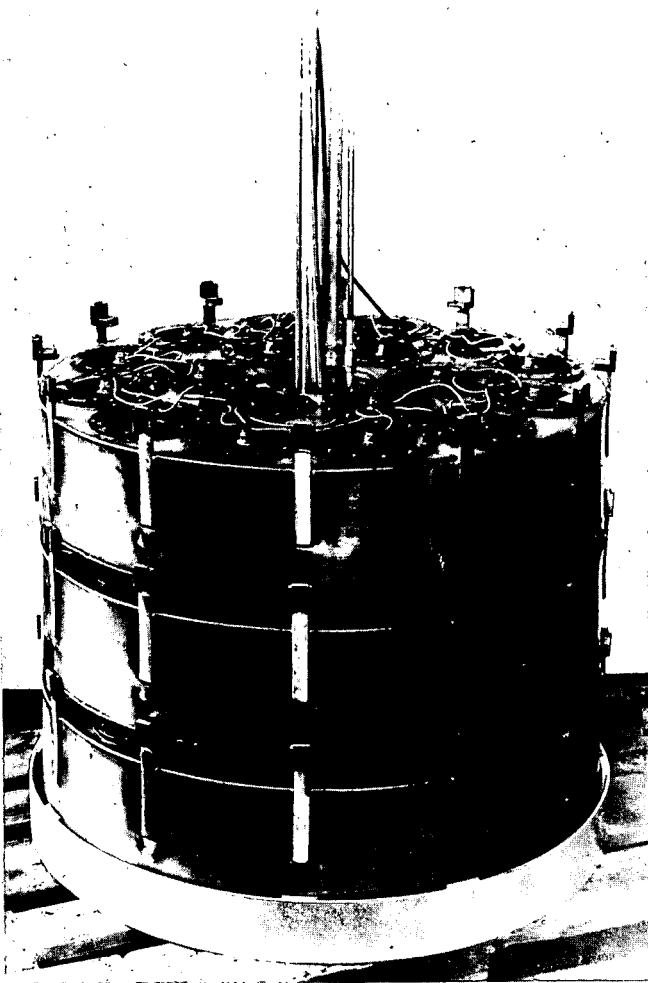


Fig. 8 Three cells of a 10 cell 60 Watt-methanol/air battery with cylindrical air diffusion electrodes for a flashing sea buoy
(by courtesy of Brown, Boveri and Cie., Baden/Schweiz)

The Anodic Oxidation of Methanol on
Raney-Type Catalysts of Platinum Metals

A. Binder, A. Köhling, G. Sandstede

Battelle-Institut e.V., Frankfurt/Main, Germany

1. INTRODUCTION

For a couple of years methanol has played an important part in fuel cell research and development. It has proved to be the only alcohol that can be completely oxidized to carbon dioxide and water in a fuel cell operating with an aqueous alkaline electrolyte at temperatures below 100°C and a platinum catalyst (1). The disadvantage of a fuel cell system of this type is the consumption of the alkaline electrolyte due to formation of the carbonate. Therefore, acid electrolytes would be more desirable; however, on platinum the oxidation of methanol requires a much higher overvoltage in acids than in alkaline solution.

It has been the objective of these investigations to develop a suitable catalyst which does not require the large overvoltage during the anodic oxidation of methanol. From our previous investigations (2) it was concluded that there might be a more active catalyst among the group of platinum metals and their alloys and that the Raney method might be suitable for preparation of alloy catalysts at low temperatures.

2. EXPERIMENTAL CONDITIONS

In our comparative appraisal of the catalysts we used electrodes of the type described in an earlier communication (3). Accordingly, it contained the Raney catalyst in a gold skeleton to which sodium chloride was added for formation of macropores. The proportion of catalyst was kept constant with all electrodes. The catalysts were prepared in situ from Raney alloys of type PtAl₄ or Au_{0.5}B_{0.5}Al₄ by treatment with potassium hydroxide solution in the preformed electrode disk. In separate experiments following the periodic potential sweep method the electrochemically active surface area of the catalyst of such a test electrode was determined to be about 35 sq.m. per g. in the case of platinum. X-ray diffraction measurements for the example of the ruthenium-platinum catalyst showed a solid solution of ruthenium in platinum which is not quite homogeneous but still contains proportions of free ruthenium.

The electrolyte was 5 N potassium hydroxide solution and 4.5 N sulfuric acid (reagent grade: "pro analysi", E. Merck, Darmstadt). In all experiments the methanol was used in a

concentration of $c = 2$ mole/liter (reagent grade of methanol: "pro analysi", E. Merck, Darmstadt).

The electrochemical measurements were made in the half-cell arrangement likewise described previously (3) according to the galvanostatic method. The current densities reported in this paper refer to the projected surface area and the potential relates to a hydrogen electrode in the same solution. The ohmic drop between Luggin capillary and electrode was not accounted for.

The plots were taken first at decreasing and then at increasing current densities. This implies that a certain proportion of the reaction products was present in the electrolyte.

3. RESULTS

3.1 Measurements in 6.5 N KOH Solution

Figures 1 and 2 show the differences in the catalytic behavior of platinum metals in the oxidation of methanol in 5 N potassium hydroxide at 25°C and 80°C, respectively. Measurements on electrodes with Raney gold serve for reference.

It is noted that two platinum metals at a time show a similar activity. The three groups thus obtained conspicuously correspond to the dyads

Ru	Rh	Pd
Os	Ir	Pt

of the platinum metals in the Periodic Table. Osmium and ruthenium, and also gold are found to be unsuitable as fuel cell catalysts, since there will not be a constant potential at high polarization. At 80°C, however, polarization with respect to the potential at a current density of 50 mA/cm² which is reasonable in fuel cell operation, does not exceed that measured on iridium and rhodium.

3.2 Measurements in 4.5 N Sulfuric Acid

3.2.1 Pure Platinum Metals

In sulfuric acid polarization with all platinum metals is much larger than in potassium hydroxide solution. Particularly striking is the increased polarization in the case of palladium at 25°C (Fig. 3), which even at comparatively small current densities reaches a potential range where corrosion occurs.

Even at 80°C (Fig. 4) palladium shows only slightly lower polarization so that this metal is the least active catalyst in the conversion of methanol in sulfuric acid, whereas osmium,

featuring only low conversion at 25°C, is the most active catalyst among the platinum metals. If the potential at a current density of 50 mA/cm² is taken as a measure for the "activity" of the electrode and thus of the catalyst, the order at 80°C is as follows: Os > Ir = Ru > Pt > Rh > Pd.

In sulfuric acid the platinum metals do not form three groups as has been observed in the conversion of methanol in potassium hydroxide solution.

3.2.2 Alloys of Platinum Metals

The experimental results on pure platinum metals suggest that catalysts of the lowest activity are found among the palladium alloys. Figures 5 and 6 depict the potential/current density curves of alloys of palladium with the addition of one of the other platinum metals (50 atomic per cent).

A distinct increase in the activity is observed by the addition of the second component. Worth noting is the effect of ruthenium which at a current density of 50 mA/cm² and 80°C (Fig. 5) results in a decrease in polarization by 280 mV and 25°C even causes a decrease by 300 mV (Fig. 6). It should be borne in mind that pure ruthenium proved almost inactive at 25°C.

It now turns out that the most active catalysts are found especially among alloys containing ruthenium (Figs. 7 and 8). A combination of pronounced activity is obtained by a ruthenium-platinum alloy. At a current density of 50 mA/cm² and at 80°C (Fig. 7) such a Raney ruthenium-platinum electrode shows a potential of 230 mV. Even at 25°C (Fig. 8) the corresponding potential does not exceed 400 mV. These values for the polarization are only about 50 mV higher than the corresponding values for the most active catalyst in potassium hydroxide solution, viz. platinum.

This Raney ruthenium-platinum catalyst is the most active of all platinum metal alloys evaluated. This is illustrated by Table 1 which summarizes the potentials of all alloy catalysts of the composition A50B (atomic per cent) and confronts them with those of the pure metals, as observed at a current density of 50 mA/cm² and temperatures of 25°C (lower values) and 80°C (upper values).

Next in the activity scale ranges the osmium-platinum alloy. A very low activity at 80°C is registered not only for palladium-gold but also for palladium-rhodium.

Our test electrode consisting of Raney ruthenium-platinum on a gold skeleton enabled current densities of at least

5000 mA/cm² to be reached (Fig. 9), the potential remaining constant for extended periods of time. At a current density of 2000 mA/cm² the potential did not increase by more than 20 mV within 600 h (Fig. 10), provided that the concentration of methanol was kept approximately constant.

Ruthenium-platinum electrodes can also be used in the oxidation of methanol in a potassium bicarbonate electrolyte from which the resultant carbon dioxide gas escapes. Also in this case polarization is much lower than in the case of platinum as catalyst (Fig. 11).

Figure 12 shows the potential of electrodes with Raney platinum metal catalysts at 80°C and a current density of 50 mA/cm² as a function of the composition of the catalyst. It is worth noting that in most cases the potential reaches a minimum only with catalysts where the two components are present in about equal proportions, whereas in gas-phase reactions a synergistic effect is often caused even by minute additions. Attention is also called to the fact that an addition of rhodium to palladium hardly affects the potential within a comparatively wide range.

Discussion

The order of the activity of platinum metals in the oxidation of methanol in potassium hydroxide solution determined by our measurements is Pt > Pd > Ru = Rh > Ir > Os > Au and thus varies from the order Pd > Rh > Au > Pt reported in an earlier publication (4). Particularly striking is the extreme discrepancy in the case of platinum, which may possibly be explained by the fact that Tanaka (4) - in contrast to us - used the smooth metals. In addition, it has to be borne in mind that catalysts prepared by the Raney method contain aluminum in varying proportions (order of magnitude from 0.1 to 1 %), which may have a bearing on the activity.

In acid solutions, too, the order of the activity of platinum metals Os > Ru = Ir > Pt > Rh > Pd as determined by us varies from that reported by earlier authors (5). However, Breiter's values (5) are non-stationary values, since they were derived by the periodic potential sweep method. These measurements do not involve enrichment of intermediates in the electrolyte to such an extent as would always be encountered in fuel cell operation (6), (7).

Since the consecutive products of the oxidation of methanol continue to react at different rates in the presence of the different platinum metals, the enrichment varies from one metal to the other. Formic acid, for example, in contact with Raney platinum in alkaline electrolytes is oxidized more slowly than methanol, but more rapidly in the acid medium. In

contact with Raney palladium, on the other hand, formic acid reacts at a higher rate than methanol even in the alkaline electrolyte (3). Owing to this enrichment of the consecutive products all methanol electrodes act as multiple electrodes so that the measured potentials are mixed potentials.

Because of these difficulties there is still some doubt about the oxidation mechanism of methanol, and this applies even to platinum, a material often examined thoroughly in extensive investigations. The differences in the activity of platinum metals in sulfuric acid as found by our measurements encourage us to make the following speculations:

As the activity drops in the order $Os > Ru = Ir > Pt > Rh > Pd$, the paramagnetic susceptibility of the metals qualitatively rises in almost the same order (cf. Table II); palladium with the largest susceptibility value is the least active catalyst.

Table II: Paramagnetic Susceptibility of Platinum Metals
(10^{-6} cgs)

Ru	Rh	Pd
43.2	111	567
Os	Ir	Pt
9.9	25.6	202

Since the paramagnetism of platinum metals results from unpaired d-electrons - the very high value for palladium is connected with quasi-ferromagnetic regions (8), (9) - it is not unreasonable to assume a relationship between paramagnetic susceptibility and catalytic activity.

Even for the activity of alloys of platinum metals such a tendency can be qualitatively deduced: the addition of rhodium to palladium improves the activity but slightly up to an amount of 50 at. %, whereas the addition of ruthenium has a favorable effect (Fig. 12). With respect to susceptibility (Fig. 13), the addition of small quantities of rhodium results in a minor increase, and only additions of larger quantities effect a decrease (10). Addition of ruthenium, even in low concentrations, reduces the susceptibility significantly (11).

The synergistic effect on the anodic oxidation of methanol observed with ruthenium-platinum alloys might be ascribed to an optimum value of susceptibility leading to optimum sorption of all reactants. Since quantitative values for the paramagnetic susceptibility of our alloys are not yet available, the speculative nature of this statement is emphasized once more. Evidence for relatively weak sorption is provided by

the fact that intermediates of the anodic oxidation of higher or multivalent alcohols are desorbed by ruthenium-platinum to such an extent that they condense to form brown-black products (12).

Hence, ruthenium-platinum alloys are almost specific for the conversion of methanol and its consecutive products, but these catalysts have also been found superior to platinum in other reactions (13), (14). Even in the oxidation of methanol the consecutive product - formaldehyde - is desorbed more easily than in conversions on platinum so that in coulometric measurements according to those described in (1) complete conversion to carbon dioxide and water is not obtained at a temperature of 80°C unless formaldehyde is not allowed to escape (12).

In the meantime further references on the excellent properties of platinum-ruthenium catalysts in the anodic oxidation of methanol have been mentioned (15). The catalyst described in these publications has been prepared according to Brown's method (16) by reduction of suitable salts with sodium borohydride.

The experimental results available now show characteristic differences among the binary alloys of the platinum metals as concerns the activity in the anodic oxidation of methanol in acid medium. Some reveal a synergistic effect whereas others not even show an addition of the activity as a function of composition. This dissimilar behavior might be due to the differences in the galvanic-magnetic properties of the alloys. Further data are necessary for a quantitative explanation of the phenomena observed.

Acknowledgment

This work was conducted under a contract and in co-operation with the Robert Bosch GmbH, Stuttgart, Germany. Its permission to publish these results is gratefully acknowledged. We greatly appreciate the interest and the valuable suggestions by Drs. Herrmann, Ilge, Jahnke, Neumann and Simon, members of the sponsoring company. Furthermore we wish to acknowledge the valuable assistance of Miss K. Spurk and Mr. K. Richter, members of Battelle-Institut, Frankfurt (Main), Germany.

Literature Cited

- (1) H. Binder, A. Köhling and G. Sandstede, paper presented at ACS meeting, New York, 1963; *Advances in Chemistry Series* 47, 283 (1963)
- (2) H. Krupp, H. Rabenhorst, G. Sandstede, G. Walter and R. McJones, *J. electrochem. Soc.* 109, 553 (1962)

- (3) H. Binder, A. Köhling, H. Krupp, K. Richter and G. Sandstede, paper presented at ACS meeting, New York, 1963; *Advances in Chemistry Series* 47, 269 (1965).
- (4) S. Tanaka, *Z. Elektrochem.* 35, 38 (1929)
- (5) M. W. Breiter, *Electrochim. Acta* 8, 973 (1963)
- (6) M. Prigent, O. Bloch and J.-C. Balaceanu, *Bull. Soc. Chim. France*, 1963, p. 368
- (7) M. J. Schlatter, in "Fuel Cells" (G. J. Young, ed.), p. 190, Reinhold, New York, 1963.
- (8) N. F. Mott, *Proc. physic. Soc.* 47, 571 (1935)
- (9) E. C. Stoner, *Proc. Roy. Soc. London (A)* 154, 656 (1936)
- (10) D. W. Budworth, F. E. Hoare and J. Preston, *ibid.* 257, 250 (1960)
- (11) W. Köster and D. Hagmann, *Z. Metallkunde* 52, 721 (1961)
- (12) H. Binder, A. Köhling and G. Sandstede, publication in progress
- (13) A. Amano and G. Parravano, *Advan. Catalysis* 9, 716 (1957)
- (14) D. W. McKee and F. J. Norton, *J. Phys. Chem.* 68, 481 (1964)
- (15) C. E. Heath, *Proc. 18th Ann. Power Sources Conf.*, May 1964, p. 33
- (16) H. C. Brown and C. A. Brown, *J. Am. Chem. Soc.* 84, 1493 (1962)

2M CH₃OH
 4.5N H₂SO₄; 80°C
 50 ma/cm²

	Ru							
Ru	350 / >900	Rh						
Rh	300 / 500	420 / 540	Pd					
Pd	290 / 490	520 / 580	570 / 800	Os				
Os	290 / >900	320 / 540	340 / 720	320 / 830	Jr			
Jr	300 / 440	380 / 520	400 / 580	350 / 500	350 / 560	Pt		
Pt	230 / 400	330 / 510	480 / 610	250 / 440	290 / 490	370 / 540	Au	
Au	310 / >900	460 / 580	650 / 780	400 / >900	300 / 540	380 / 580	>900 / >900	

Table I Potentials at alloy catalysts (50 atomic %) with methanol in 4.5 N H₂SO₄ at 25°C (lower figures) and 80°C (upper figures); current density: 50 ma/sq.cm.

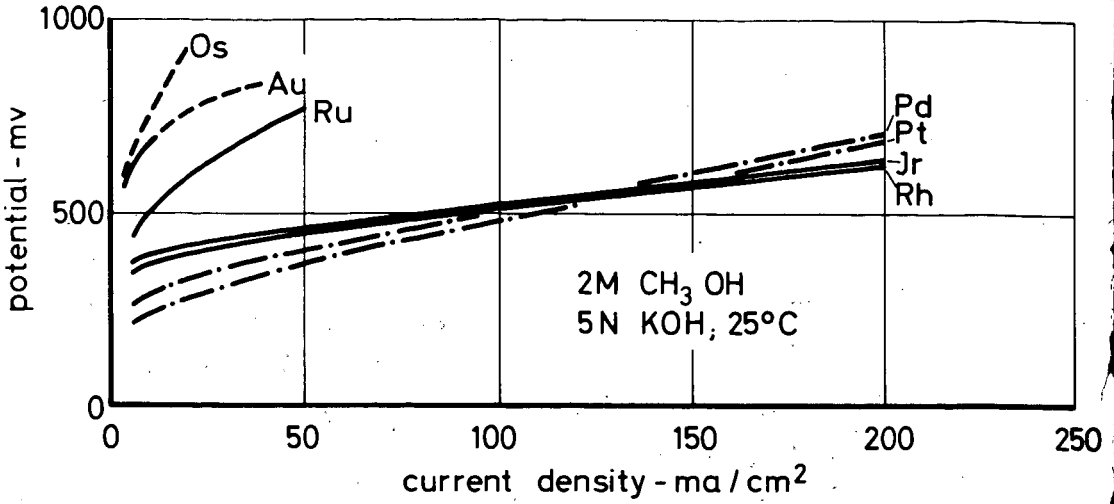


Fig. 1 Potential/current density plots of electrodes containing Raney platinum metals with methanol in 5 N KOH at 25°C

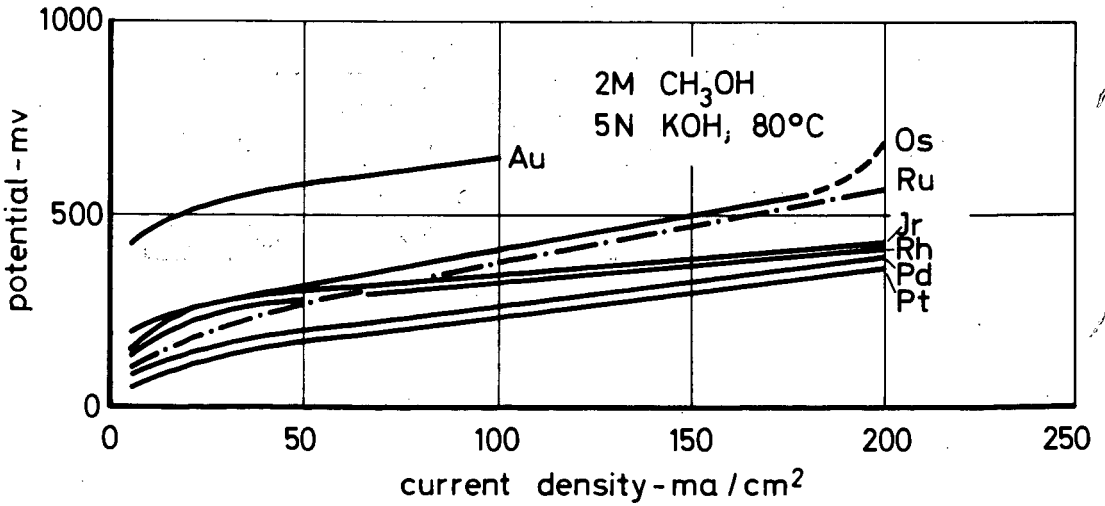


Fig. 2 Potential/current density plots of electrodes containing Raney platinum metals with methanol in 5 N KOH at 80°C

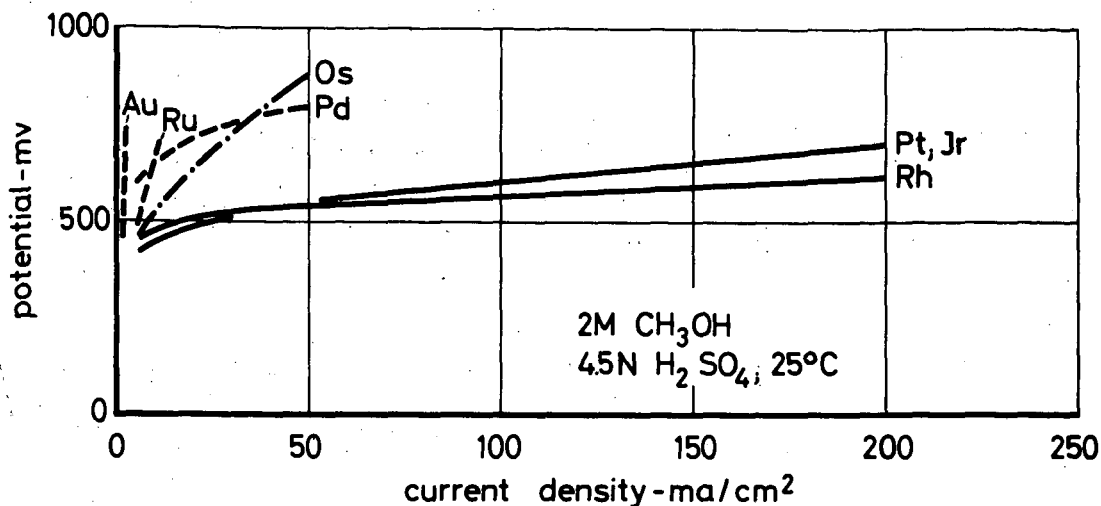


Fig. 3 Potential/current density plots of electrodes containing Raney platinum metals with methanol in 4.5 N H₂SO₄ at 25°C.

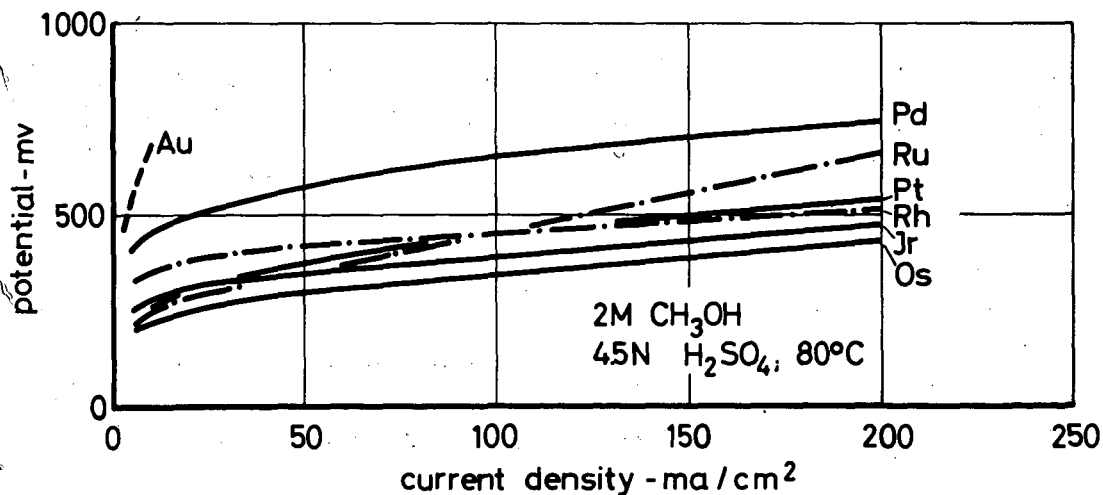


Fig. 4 Potential/current density plots of electrodes containing Raney platinum metals with methanol in 4.5 N H₂SO₄ at 80°C.

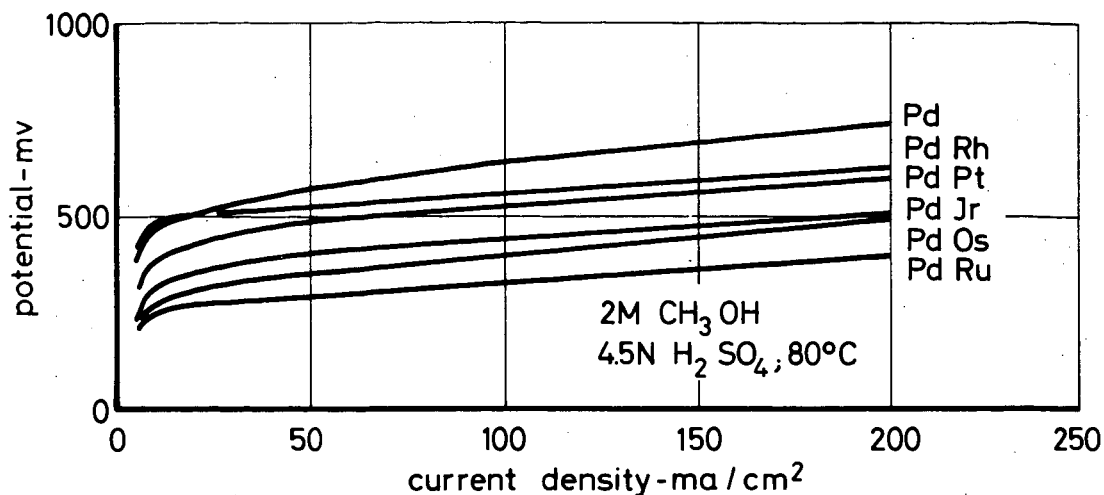


Fig. 5 Potential/current density plots of electrodes containing Raney palladium alloys with methanol in 4.5 N H₂SO₄ at 80°C

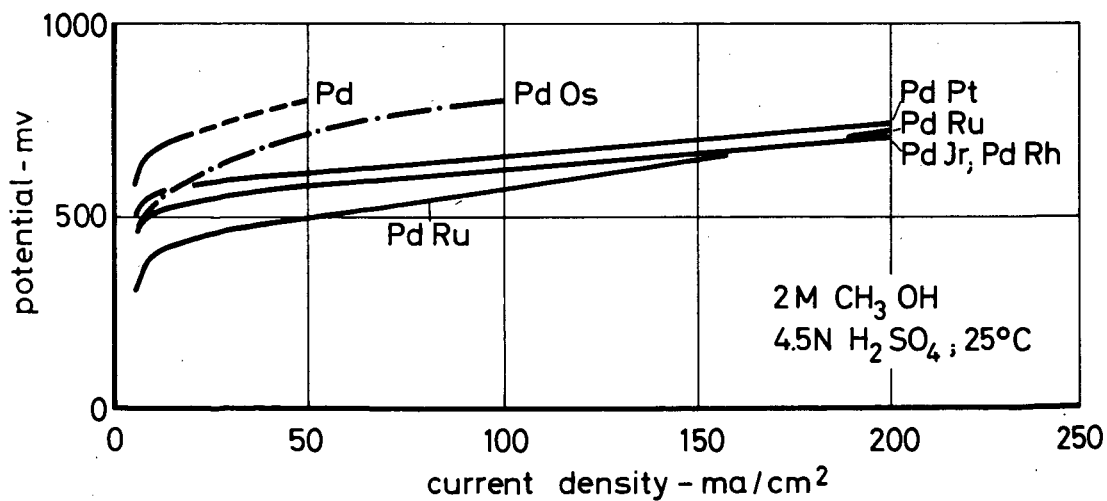


Fig. 6 Potential/current density plots of electrodes containing Raney palladium alloys with methanol in 4.5 N H₂SO₄ at 25°C

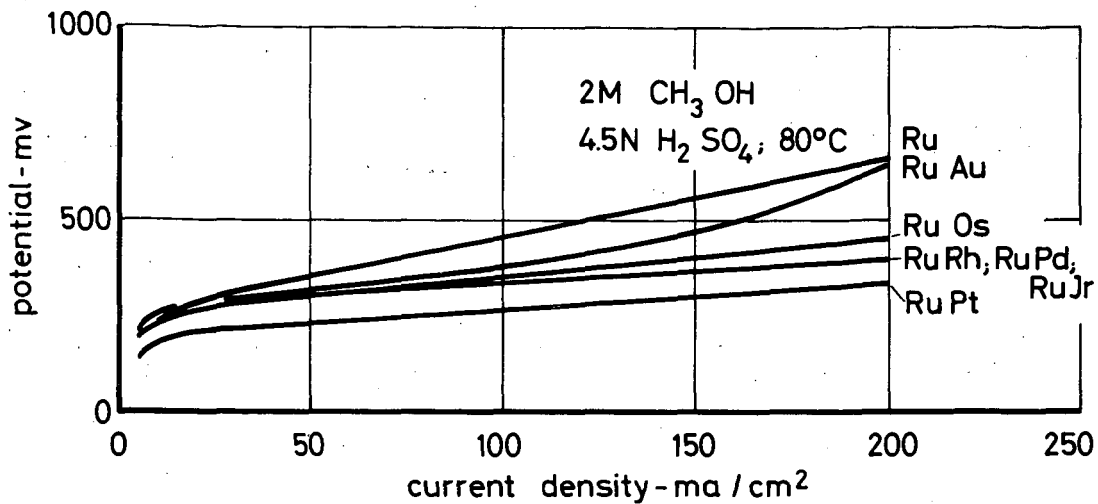


Fig. 7 Potential/current density plots of electrodes containing Raney ruthenium alloys with methanol in 4.5 N H₂SO₄ at 80°C

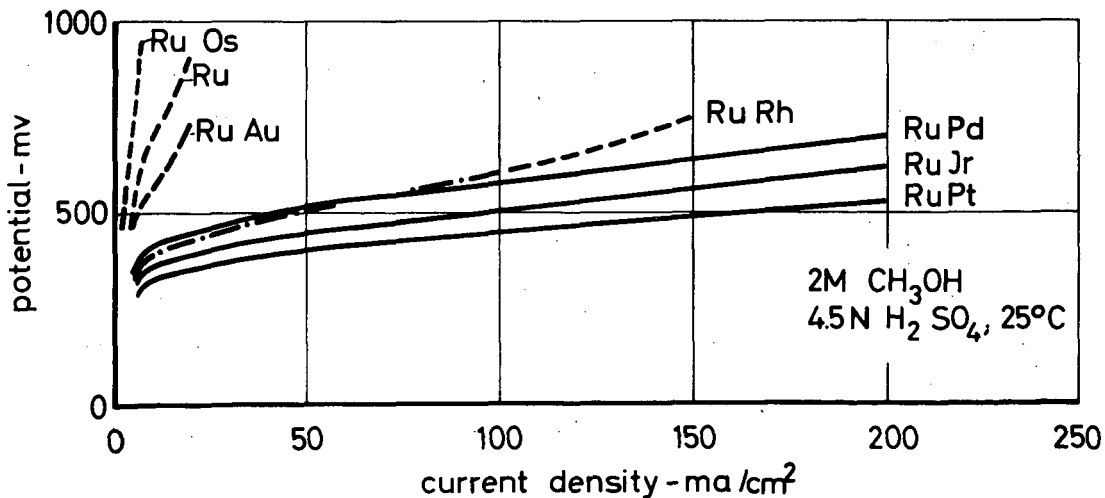


Fig. 8 Potential/current density plots of electrodes containing Raney ruthenium alloys with methanol in 4.5 N H₂SO₄ at 25°C

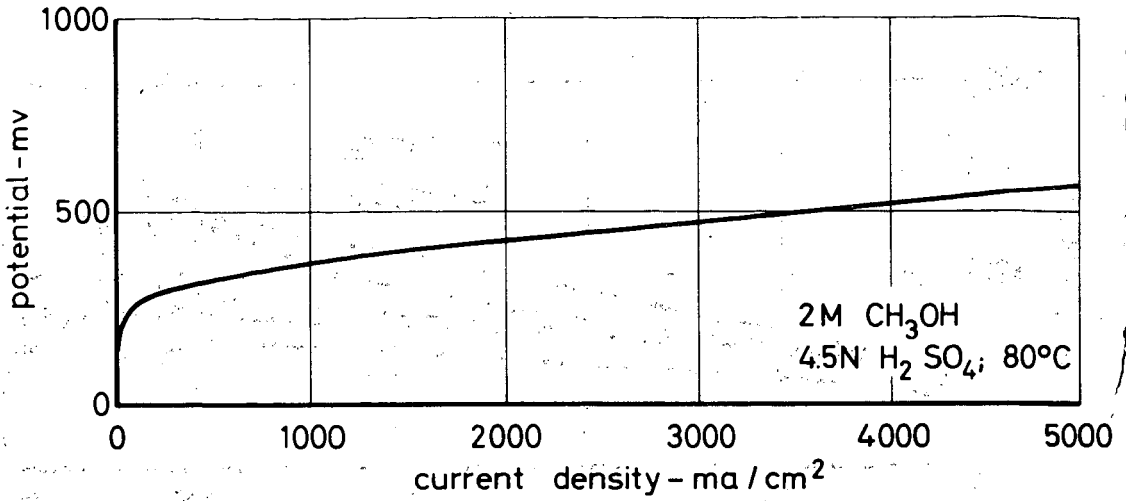


Fig. 9 Potential/current density plot of a Raney ruthenium-platinum electrode with methanol in 4.5 N H₂SO₄ at 80°C

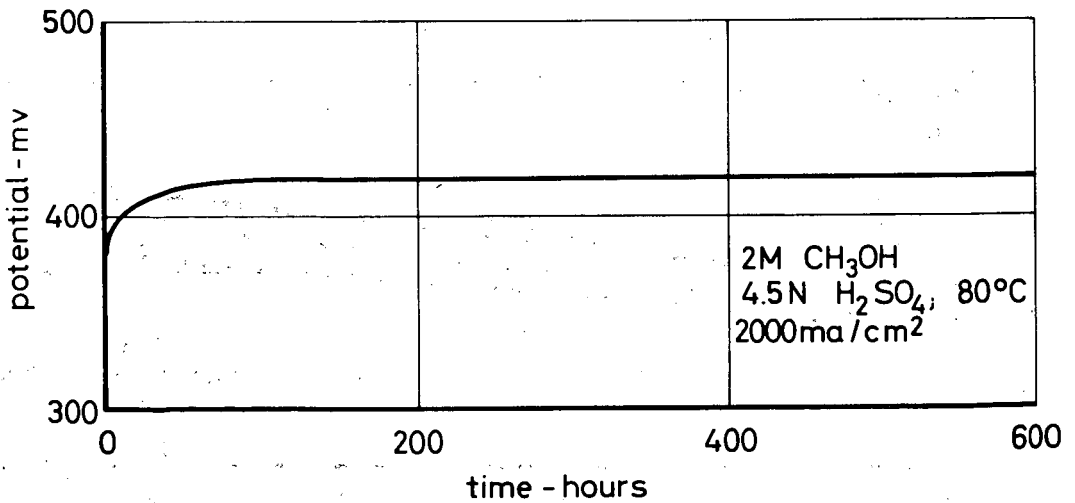


Fig. 10 Change of potential with time on a Raney ruthenium-platinum electrode with methanol in 4.5 N H₂SO₄ at 80°C and a load of 2000 ma/sq.cm.

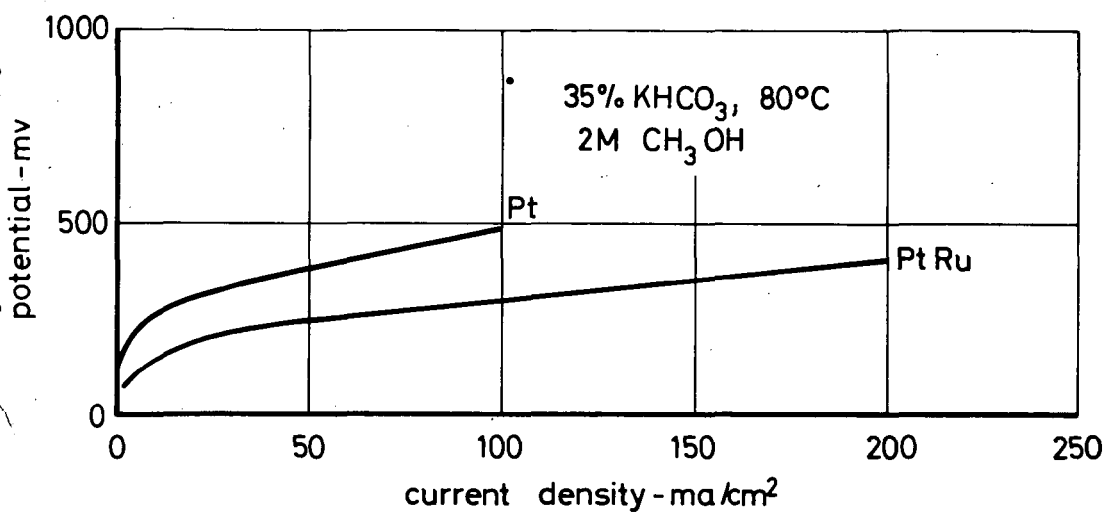


Fig. 11 Potential/current density plots of Raney platinum and Raney ruthenium-platinum with methanol in 35 % (by weight) KHCO₃ at 80°C

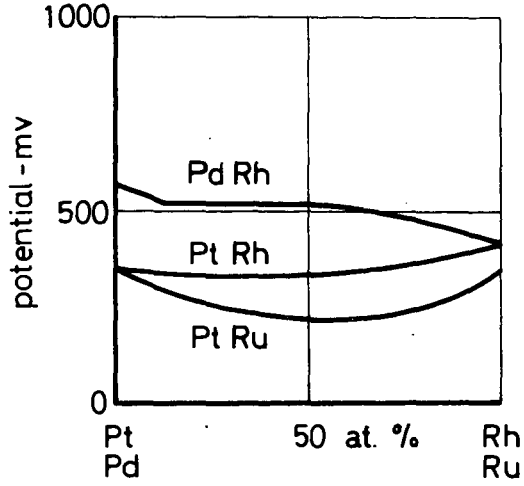


Fig. 12 Potential plots of platinum alloys with methanol in 4.5 N H_2SO_4 at 80°C as a function of composition

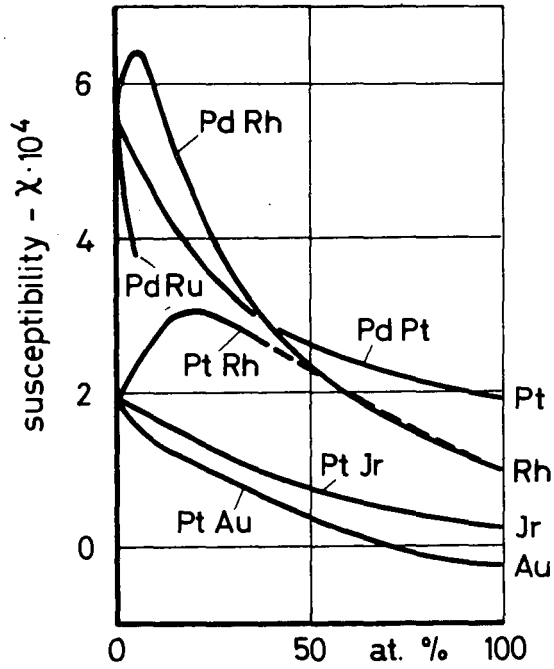


Fig. 13 Magnetic susceptibility of alloys of platinum metals as a function of composition (data from the literature)

THE ANODIC OXIDATION OF METHANOL ON
PLATINUM IN ALKALINE SOLUTION

D. Poull and J.R. Huff*
Research Division, Allis-Chalmers Manufacturing Co.
Milwaukee, Wisconsin

ABSTRACT

The electrochemical oxidation of methanol on platinum was studied as a function of temperature, composition of electrolyte and pretreatment of the electrode. The majority of the data were obtained with the linearly varying potential technique. Results indicate that the oxidation of methanol in alkaline solution proceeds at a potential some 200-300 mV. less positive than in acid, (potentials versus the hydrogen electrode in the same solution). Peak currents for a bright platinum electrode are independent of stirring and increase with increasing voltage sweep rates. From the effect of temperature on the reaction rate, it is evident that the formation of platinum oxide is not the rate determining step. Current transients at low potentials indicate that the initial step involves the abstraction of a hydrogen atom; and that the oxidation of the remaining methanol fragment determines the reaction rate.

INTRODUCTION

In recent years, the anodic oxidation of methanol on platinum in both acidic and basic media, has been studied in considerable detail. The impetus for these investigations is derived from a search for suitable fuels to replace hydrogen in the fuel cell. Breiter et. al. (1,2) have studied the oxidation processes in acid solution; and found the current to be proportional to the amount of methanol adsorbed on the surface of the electrode. These authors propose that the initial step in the reaction is the direct oxidation of the methanol molecule (adsorbed) to a methanol radical and a hydrogen ion.

The anodic oxidation in alkaline solution has been studied by Vielstich (3) and Buck and Griffith (4). Vielstich (3) concludes that rather than the direct electrochemical oxidation of the methanol, the platinum reacts to form a platinum hydroxide which in turn oxidizes the methanol chemically. The formation of the platinum hydroxide must then be rate determining. Vielstich supports his hypothesis by the fact that the current peak in the current-voltage characteristic is normally independent of the oxidizable substance. The fact that methanol in 6-8 Molar alkali is oxidized spontaneously at temperatures exceeding 80°C is explained by assuming a base catalyzed dehydrogenation mechanism.

Buck and Griffith (4) studied the anodic oxidation processes in both acid and alkali media. For the basic system, these authors

* Present Address: Globe-Union, Milwaukee, Wisconsin.

calculated a Tafel slope of 0.21 - 0.28V; and they concluded that the rate determining step in alkaline solution involves the reaction of a methyrate and two hydroxide ions with the transfer of two electrons.

Some further work was done recently by Liang and Franklin (5), who studied the anodic oxidation of formic acid and formaldehyde in addition to that of methanol. Oxley, et. al. (6) investigated the anodic processes in acid by studying the potential decay curves. The effect of the reductive adsorption of CO₂ was studied by Giner (7).

Although a good deal of work has been done in this field, the factors which govern the shape of the current - voltage curve obtained by the linearly varying potential technique (L.V.P.) are, in general, still unknown. In this paper, we describe some work carried out in order to ascertain which variables dictate the general shape of the i-V curve determined by the technique cited above. Furthermore, we will examine the theories outlined above concerning the oxidation of methanol in the light of some current transient measurements, and the effect of temperature.

EXPERIMENTAL

The electronic equipment used in these experiments is based on the use of operational amplifiers to control the potential of the working electrode. The basic circuitry is due to De Ford (8). A modification permitting compensation of the IR voltage drop between reference and working electrodes has been described elsewhere (9). A block diagram indicating the essential components of the instrument is shown in Fig. 1. The integrator shown in Fig. 1 may be used to generate a single sweep or a triangular wave. In normal experimentation, a triangular wave was applied to the working electrode.

The electrolysis cell was of the conventional H-type with a sintered glass disc between anode and cathode compartments. A working electrode of bright platinum foil (1cm²) was spot-welded to a platinum wire sealed in soft glass. The counter electrode consisted of a platinized platinum foil, of 1cm² geometric area.

The electrode assembly and cell were washed initially with aqua regia followed by a dilute solution of hydrofluoric acid. Further washing with copious quantities of distilled water was carried out before the cell was assembled for use. The hydrofluoric acid solution did not appear to have any deleterious effects on the platinum-soft glass seal.

The electrochemical cell was thermostatted in a water bath to $\pm 0.2^{\circ}\text{C}$. Nitrogen was normally bubbled through the cell at all times. The nitrogen was pre-conditioned by passing it through a solution identical to that in the cell.

A mercury-mercuric oxide reference electrode was used in all experiments. Since adequate IR (reference to working electrode) compensation was achieved electronically, no great care was taken to place the tip of the reference electrode very near the working electrode surface. All potentials in this paper will be cited with respect to the potential of the hydrogen electrode in the same

solution. Rather than calculate the potential of the Hg/HgO electrode versus that of this hydrogen electrode for each set of conditions, its value was determined experimentally. Before the potential of the Hg/HgO reference electrode was measured, it was established that the potential of the hydrogen electrode is not significantly affected by the presence of methanol at temperatures below 60°C.

Harleco carbon dioxide free sodium hydroxide and ACS analytical reagent grade methanol were used in all experiments. The appropriate concentrations of reactant and electrolyte were prepared by dilution of the concentrated material with doubly distilled water.

Since it is normally difficult to obtain reproducible results when the history of the electrode is not clearly defined, a pre-treatment was devised to promote reproducibility. Initially, oxygen was evolved from the electrode at 5mA/cm² for 5 seconds. The electrode potential was then reduced to the initial value for the subsequent linearly varying potential sweep. After maintaining the potential at this value for 2 minutes, a repetitive triangular wave was applied to the working electrode. Nitrogen was bubbled through the electrolyte to remove oxygen produced during the pre-treatment as effectively as possible. This type of pre-treatment normally gave results reproducible to +5%.

RESULTS AND DISCUSSION

The major portion of this work consisted of an investigation of the system, bright platinum/2M methanol, 4.5 M sodium hydroxide. Unless stated otherwise in the text, it will be assumed understood that this is the experimental system. The advantage of the high concentration of methanol is that normally the background current caused by charging of the double layer and adsorption of oxide or hydroxide species is negligibly small over an appreciable potential range, as compared to the oxidation current of the methanol. The last statement is not necessarily true at temperatures near 0°C.

The system cited above was chosen to study the effects of voltage sweep rate, temperature, and voltage sweep range on the current-voltage characteristic. In addition, a study was made of the effects of electrolyte and methanol concentration on the general features of the current-voltage curve, and on the current at constant potential.

The normal voltage sweep range was within the limits of +300 to +1400 mV. It is felt that the adsorption and possible evolution of hydrogen at lower potentials and the evolution of oxygen at higher potentials only complicates the interpretation of the data. Of course, in basic solution even at +300 mV. a small amount of hydrogen is adsorbed.

LINEARLY VARYING POTENTIAL EXPERIMENTS

General Current-Voltage Curve and the Effect of Temperature

In Fig. 2 we show the least complex of the *i*-V curves obtained in this study. The curve is for the 2M CH₃OH/4.5M NaOH system at 60°C and a voltage sweep rate of 100 mV./sec. Both the

i-V curves for the initial sweep and a "steady state" curve are shown. By steady state, we refer to the condition when subsequent voltage scans do not alter the curve significantly.

From Fig. 2, we note that the current at low potentials for the initial sweep lies below that for the steady state curve. At higher potentials, the i-V curves cross and the current for the initial sweep exceeds that of the steady state scan. This sequence of events is a function of the experimental conditions. The i-V curve for increasing potentials in Fig. 2 (later referred to as the forward sweep) has a single maximum and no plateaus or inflections. This feature is rather different from the curve obtained by Breiter (2) for the oxidation of a molar methanol in molar perchloric acid solution. Fig. 2 also shows the i-V curve for the decreasing potential sweep (later referred to as the reverse sweep). The current maximum for the reverse sweep does not lie outside the forward i-V curve as has been observed for some methanol-acid systems (1). The actual potential of the current peak for the reverse sweep depends markedly on the experimental conditions; and will be considered in some detail later on in this paper.

As shown in Fig. 2 the currents in the low potential region, i.e. at potentials below that of the current maximum are greater for the reverse than the forward sweep. This "hysteresis loop" is less pronounced in the alkaline than in the acid system (c.f. Breiter (4)). Although the effect decreases with increasing temperature, it is still present at 60°C.

Fig. 3 depicts the i-V characteristic for the same system at 0°C. The actual currents at the same potentials are obviously much lower than at 60°C. Decreasing the temperature has altered the general shape of the i-V curve quite considerably. The current for the initial forward sweep lies below that of the steady state curve at all potentials; and the loop formed as a result of the difference between currents for forward and reverse sweeps is appreciably larger than at 60°C. Furthermore, at the lower temperatures the i-V curve for the reverse sweep is much less symmetrical about the potential of the current maximum, and the curve shows an inflection. The "back" side (negative resistance portion) of the forward curve, i.e. at potentials exceeding that of the current maximum, shows a shoulder at 0°C which is absent at 60°C.

Having discussed the general properties of the i-V curves in some detail, we shall now consider possible explanations for the "hysteresis loop" for forward and reverse sweep currents, and the effect of temperature on the shoulder and inflection on the i-V characteristic shown in Fig. 3.

A number of suggestions have been made to account for the hysteresis loop referred to above. Giner (7) has suggested that a reduced form of CO₂ is adsorbed on the electrode surface while the electrode is maintained at its initial potential; say below 250 mV. in molar acid. The reduced CO₂ may be formed from either CO₂ or carbonate in solution or from methanol. This reduced CO₂ then acts as a poison to the oxidation reaction. It has also been suggested that the effects might result from a lower concentration of adsorbed methanol during the reverse sweep, and that oxidation proceeds more readily on a bare surface.

Although it cannot be denied that both explanations, in view of experimental results for the acid system, appear reasonable; the results for the basic system do not support this explanation. Let us consider the reduced CO_2 hypothesis. We have found that the hysteresis loop is not significantly dependent on the initial potential and on the time that the potential was maintained at its initial value. In our work, the initial potential was always maintained above the potential of the hydrogen electrode in the same solution. Giner (7) reports that in the acid system the reduced CO_2 species is produced below 250 mV.; but in the basic system the corresponding potential should be several hundred millivolts less positive. According to this author, the reduced species is oxidized at potentials exceeding 400 mV. Hence, it does not seem likely that the reduced CO_2 hypothesis is applicable to the basic system. Furthermore, one should observe an effect of the holding time (time that the potential is maintained at its initial value) at the initial potential. This is not observed. A possible explanation is that the adsorption of the reduced species is so rapid that when the holding time exceeds one second, no further effect will be observed.

To account for the hysteresis loop by assuming that the reaction occurs more rapidly on a bare surface would seem contradictory to the fact that the current at relatively high surface coverages, 0.3 - 0.8, appears to be proportional to the surface coverage.

A possibility that the hysteresis loop is due to removal of a poisonous intermediate at potentials when the surface oxide is present does not seem applicable since the loop is present even when the most positive potential is less than that where oxide adsorption is possible. It could be thought that the increased currents on the reverse sweep are due to activation of the electrode by adsorption, and reduction of the surface oxide resulting in a different reaction product. Although this possibility cannot be discounted for the alkali system, it does not seem valid in the acid system where the difference in current for reverse and forward sweeps is much too large. The reason for postulating a different reaction product for a more active electrode is that the reaction product is known to depend on the electrode catalyst material (11).

A possible explanation for this phenomenon, which to the best of our knowledge has not been explored previously, is that a reaction consisting of an adsorbed methanol species and a methanol molecule involving a bare surface site is responsible. It is proposed that this reaction occurs in conjunction with the normal reaction of the adsorbed methanol. In this manner, the lower surface coverage in the reverse sweep should yield a somewhat higher reaction rate and at coverages between 0.3 and 0.8 the reaction rate could be proportional to the adsorbed material. It must be emphasized, however, that this explanation is speculative and more data regarding the various steps in the reaction mechanism are necessary.

The fact that the hysteresis loop in alkali is somewhat smaller than that in acid may be due to a closer concurrence of the adsorption isotherm for the forward and reverse sweeps. To our knowledge, no data regarding these isotherms are available for the basic system.

The inflection on the i - V curve for the reverse sweep may be due to an appreciable oxide reduction current. Such an explanation is not satisfactory, however, since the inflection changes to a minimum when this cathodic current is made negligibly small. It is possible that this inflection results from the same process as that which causes the shoulder on the forward curve at 0°C . The shoulder is presumably caused by interaction of the surface oxide, a methanol species and a bare site. It seems improbable that the current can be ascribed to removal of adsorbed methanol, or a different reaction occurring on the oxide surface. At these potentials the surface concentration of methanol must be very small, and if a different reaction on the surface oxide causes the shoulder, then one would not expect the current to decrease with increasing potential. The oxide concentration (surface coverage) at the potential of the inflection in the i - V curve for the reverse sweep should be very similar to that at the potential of the shoulder on the forward curve. It is, therefore, not inconceivable that a relation exists.

The lack of an inflection at higher temperatures (60°C) is probably due to the fact that the surface oxide is reduced at a higher potential and hence the peak current for the main reaction for the reverse sweep is much higher, thereby making the "surface phenomena" less significant.

The shift of the potential of the current maximum on the reverse sweep to lower values as the temperature is lowered is also thought to be a result of a shift in the potential at which the surface oxides are reduced. It is known that the reduction of the surface oxides occurs at less positive potentials as the temperature is lowered (12). Hence, the current peak should also be shifted to less positive potentials.

The Dependence of the Tafel Slope on Temperature

A few log i -potential curves for the anodic oxidation of methanol at 60°C are depicted in Fig. 4. The Tafel slopes for the initial, and steady state forward and reverse sweeps are 125 ± 15 mV. and 170 ± 20 mV., respectively. These values were found to be essentially independent of temperature for the initial and steady state reverse sweeps.

The Tafel slope for the steady state forward sweep for this range of potentials is markedly dependent on the temperature. Decreasing the temperature from 60° to 0°C caused its value to rise from 170 ± 20 mV. to 240 ± 25 mV. The latter value is in reasonable accord with that reported by Buck and Griffith (4) for the oxidation of methanol on a platinized platinum ball at 25°C , at a voltage sweep rate of 8 mV./sec. and methanol concentration below 0.025M. Hence, as the temperature is raised, the Tafel slopes for steady state reverse and forward sweep converge.

A value of 125 ± 15 mV. is readily, although possibly naively, interpreted in terms of a one electron transfer mechanism having a symmetrical energy barrier. However, since the surface concentration of methanol changes with potential during the scan it cannot be assumed that this slope is characteristic of the electron transfer reaction. Breiter (1), assuming Langmuir kinetics, and correcting the observed currents for the effect of the surface coverage, calculated a value of 0.67 for α . If we consider that the effect of

decreased surface coverage results in an apparently increased Tafel slope, it would appear that our value of 125mV is similar to that observed by Breiter (1), indicating that the rate determining steps are the same in acid and base.

The Effect of Voltage Sweep Range

In general, the Tafel slopes are not significantly affected by the voltage sweep range provided the maximum and minimum potentials are not within the range of oxygen or hydrogen evolution.

The current maxima normally decrease with decreasing most positive potentials attained during the sweep and the number of cycles required to attain a steady state i-V curve increases. Fig. 5 depicts the effect of decreasing the maximum potential attained during a potential scan. Reference has already been made to the inflection on the i-V curve for the reverse sweep (see Fig. 3). This inflection changes to a marked minimum as the most positive potential during the sweep is decreased from 1400 to 900mV. The nature of the hysteresis loop is not significantly affected by the maximum potential provided it exceeds the potential of the current maximum during the forward sweep.

The Effect of Voltage Sweep Rate

As found by other investigators, the current maximum rises with increasing voltage sweep rate. The fact that stirring does not effect the current-voltage characteristic shows that increased currents at higher sweep rates cannot be accounted for by a diffusion process in the bulk of the solution. In addition, the increased currents can neither be accounted for by higher double layer charging currents, since these are negligible at the higher methanol concentrations. It would appear that this phenomenon is a result of a higher concentration of adsorbed materials at the peak potential as the sweep rate is increased. It has been shown indirectly that the concentration of methanol on the surface at constant potential increases with increasing sweep rates (1). Furthermore, the inhibiting effect of the surface oxide should decrease as the sweep rate is raised since the oxide adsorption reaction is rather irreversible.

Earlier reference has been made to the shoulder on the i-V curve at potentials exceeding that for the current maximum (see Fig. 3). The data on Fig. 2 would seem to indicate that this feature disappears as the temperature is raised. However, even at 60°C, the shoulder may be made to reappear when the voltage sweep rate is increased to 500 mV/sec. Such behavior is characteristic of a surface reaction; and it was interpreted in this manner earlier. The greater prominence of the shoulder at the lower temperatures may be ascribed to the fact that the current for the main reaction is relatively more temperature dependent.

Raising the voltage sweep rate causes the potential of the current maximum for the reverse sweep to decrease. This is not too surprising since it was assumed that the decrease in current beyond the maximum on the forward sweep is caused by surface oxides; and the peak current for the oxide reduction shifts to lower potentials

as the sweep rate is increased. At increased sweep rate, the inflection on the i - V curve for the reverse sweep becomes more prominent. This feature appears only at the lower temperature.

The Effect of Solution Composition

As the methanol concentration is raised, the current at constant potential increases. However, at concentrations exceeding 10 Molar, the current begins to decrease. For the concentration range 0.1 -2M, the slope of the $\log i$ vs. $\log c$ plot at constant potential is unity, indicating that the reaction is directly proportional to the methanol concentration. The shape of the current voltage curves over the range of concentrations where the $\log i$ vs. $\log c$ plot is linear is not significantly affected unless the surface reaction i.e. oxide adsorption, becomes appreciable. This occurs at the higher sweep rates.

Fig. 6 depicts the curve obtained for a solution 0.1M in methanol. During the reverse sweep, cathodic currents are observed and the normal reverse sweep peak current is absent. Furthermore, a current minimum and a plateau are observed on the forward sweep. Similar features have been observed for the anodic oxidation of methanol in acid. The phenomena are different in nature, however, in that for the basic system the minimum and plateau are due to the oxide adsorption currents which cannot be the explanation for the acid system since the observed currents are too high.

The effect of the concentration of sodium hydroxide between 0.01 and 4.5M is small. The general shape of the current-voltage curve does not seem to be affected significantly as the concentration is varied between the limits cited.

Current Transients

In these experiments, the potential was raised to a value between 1200 and 1400 mV., and maintained at this point for about 10 minutes. The potential was then decreased instantaneously to a value between 200 and 400 mV.; and the current recorded. Fig. 7 depicts the current transient for the conditions cited. The initial portion when the current is negative has been omitted and the current to the left of the graph is a combination of the reduction of surface oxide and the oxidation of methanol. The peak current at 400 mV. is about 2.5 mA/cm^2 , some 20-50 times greater than that observed after one second. The area under the curve corresponds to the charge required to oxidize a monolayer of hydrogen. The reason for the experiment was to gain some insight into the relative rates of adsorption and oxidation at lower potentials. It must not be concluded that the peak current represents the maximum rate of methanol adsorption at this potential. Obviously the rate of adsorption is considerably faster, since the peak value includes a cathodic oxide reduction current.

Furthermore, it would appear that the initial reaction involves the abstraction of one or more hydrogen atoms which are oxidized instantaneously at a potential of 400 mV. The sluggish reaction is then ascribed to the oxidation of the remaining methanol radical.

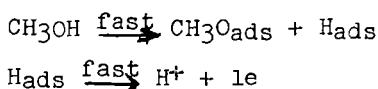
CONCLUSIONS

We have already cited the reaction mechanism proposed by Vielstich (3), who assumes that the anodic oxidation of platinum to a platinum hydroxide is the rate determining step. The methanol subsequently reacts chemically with the metal hydroxide. The author supports his hypothesis by the fact that normally the potential of the peak current is independent of the oxidizable substance. This phenomenon is equally well explained by the assumption that a surface oxide or hydroxide inhibits the oxidation reaction. For, the formation of this inhibitor is essentially independent of fuel. Furthermore, it has been shown by Vielstich that at higher temperatures the potential required to oxidize methanol decreases. Although the author explains this phenomenon by assuming a base catalyzed dehydrogenation mechanism, we have found no evidence for his hypothesis since the i - V curves and Tafel slopes for the initial sweeps are not significantly dependent upon temperature between 0° and 60°C .

Furthermore, examination of the i - V curves for acid and base systems shows that the potentials at which appreciable currents are obtained shift about the same amount for both systems (about 300 mV.) as the temperature is raised from 25° to 85°C . It should also be stated that the equilibrium potential for the basic system is some 250 mV. more negative than that for the acid system; and if the reaction mechanism, Tafel slope and exchange current are the same for both systems, the oxidation of methanol in the basic system at 80°C should be quite appreciable near the potential of the hydrogen electrode in the same solution. It would then be reasonable to assume that if the dehydrogenation is base catalyzed it is also acid catalyzed.

In the basic system complete dehydrogenation of methanol would result in the formation of a carbon monoxide species on the electrode surface. It has been shown that the final product of the oxidation of methanol is either formate or carbonate (3). This implies that carbon monoxide fragments on the surface are further oxidized. Since the carbon monoxide normally inhibits anodic processes (7) it may be assumed that the substance is strongly adsorbed; and should, therefore, decrease the rate of dehydrogenation since the electrode surface is no longer available for catalysis. It appears to us, therefore, that a base catalyzed dehydrogenation mechanism is not responsible for the increased currents in the base system.

It is our hypothesis, in view of the current transient measurements, that even at the lower temperature the radicals are most difficult to oxidize and enhanced dehydrogenation should not influence the rate appreciably, at least not at the lower potentials. It seems to us that the initial reaction sequence can best be described by the following mechanism



The $\text{CH}_3\text{O}_{\text{ads}}$ is then further oxidized, and at potentials below 600 mV. this oxidation process is the rate determining step in the reaction. The actual intermediate formed from the adsorbed CH_3O will probably depend on the final product, whether this be

the carbonate or the formate ion. In general, it would be reasonable to assume that the intermediate lies between CH_3O and formaldehyde (or adsorbed formaldehyde) since the latter is much more readily oxidized than methanol (3).

ACKNOWLEDGMENT

Our thanks are due to Mr. J.C. Pearson for faithfully carrying out the experiments, and to Mr. J. Seibold for many helpful discussions during the writing of this paper.

REFERENCES

1. S. Gilman and M.W. Breiter, J. Electrochem. Soc., 109, 1099 (1962)
2. M.W. Breiter and S. Gilman, ibid, 109, 622 (1962).
3. W. Vielstich, Chemie-Ing-Techn., 35, 362 (1963).
4. R.P. Buck and L.R. Griffith, J. Electrochem. Soc. 109, 1005 (1962).
5. C. Liang and T.C. Franklin, Electrochimica Acta, 9, 517 (1964).
6. J.E. Oxley et. al., ibid., 9, 897 (1964).
7. J. Giner, ibid, 9, 63 (1964).
8. D.D. de Ford, Division of Analytical Chemistry, 133rd National Meeting, A.C.S., San Francisco, Calif., April 1958.
9. Dirk Pouli et.al., Anal. Chem., in course of publication.
10. W. Böld and M.W. Breiter, Electrochimica Acta, 7, 25 (1962).
11. P.G. Grimes, Private communication.
12. J.R. Huff and Dirk Pouli, unpublished data.

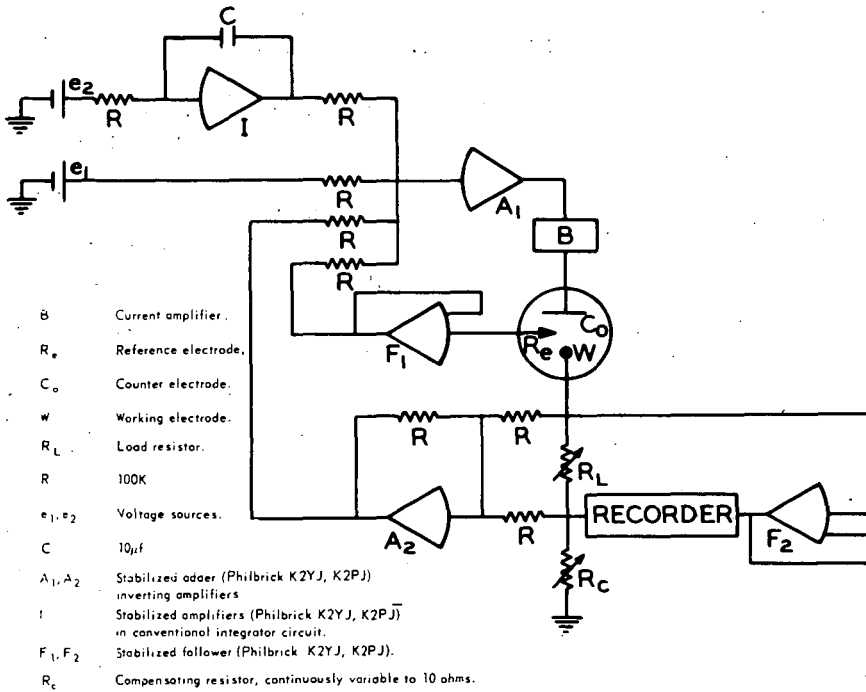


FIGURE 1

Voltammetric Circuit for Continuous Ohmic Voltage Compensation

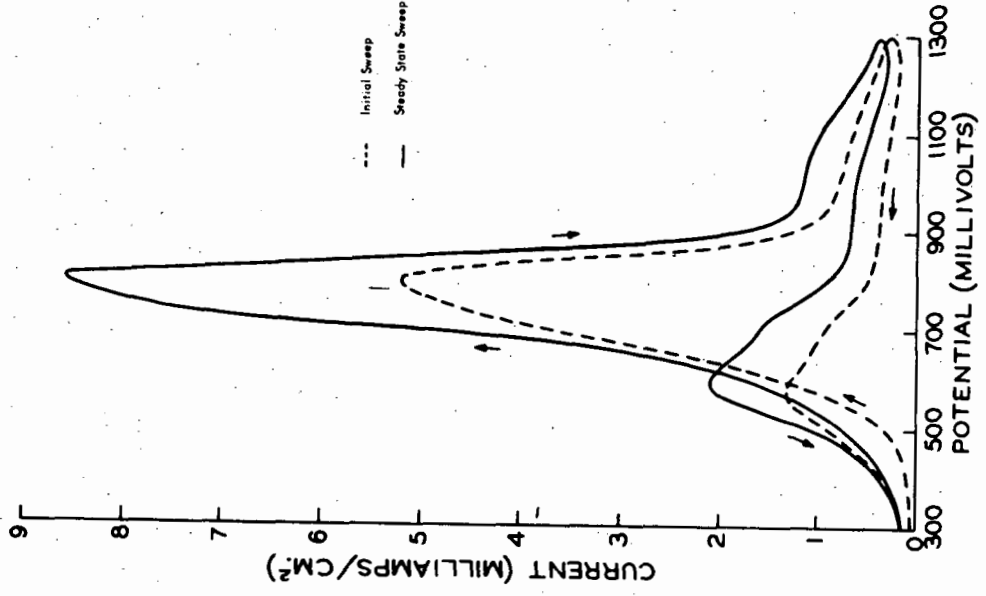


FIGURE 3
Current - Potential Curve for the System, Bright Pt/2M CH₃OH/4.5M NaOH at 0°C and a Voltage Sweep Rate of 100 mv/sec.

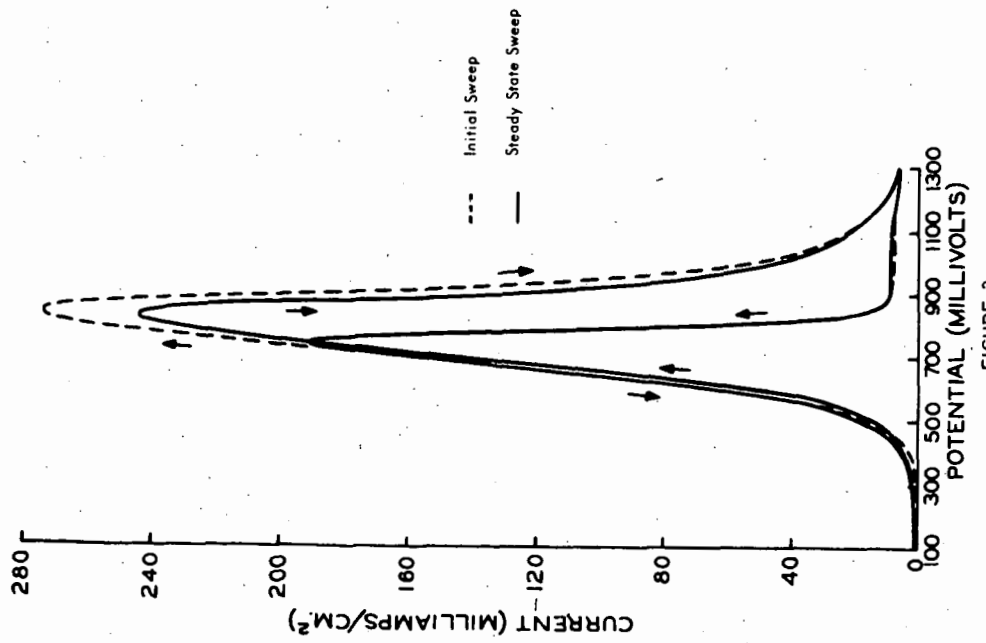


FIGURE 2
Current - Potential Curve for the System, Bright Pt/2M CH₃OH/4.5M NaOH at 60°C and a Voltage Sweep Rate of 100 mv/sec.

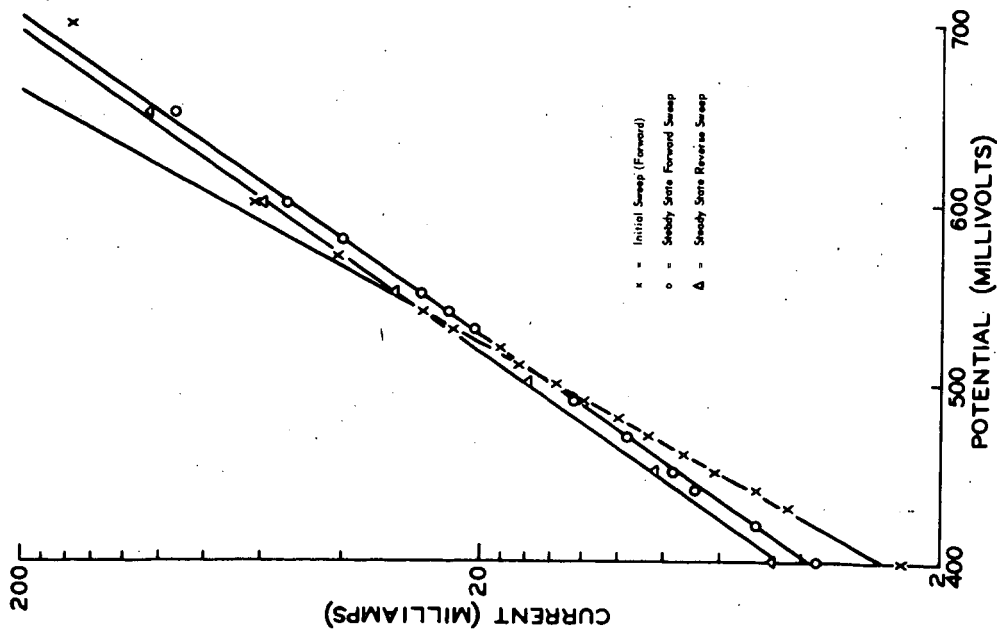


FIGURE 4
Log i Vs Potential for the System, Bright Pt/2M CH₃OH/4.5M NaOH
at 60°C and a Voltage Sweep Rate of 100 mv/sec.

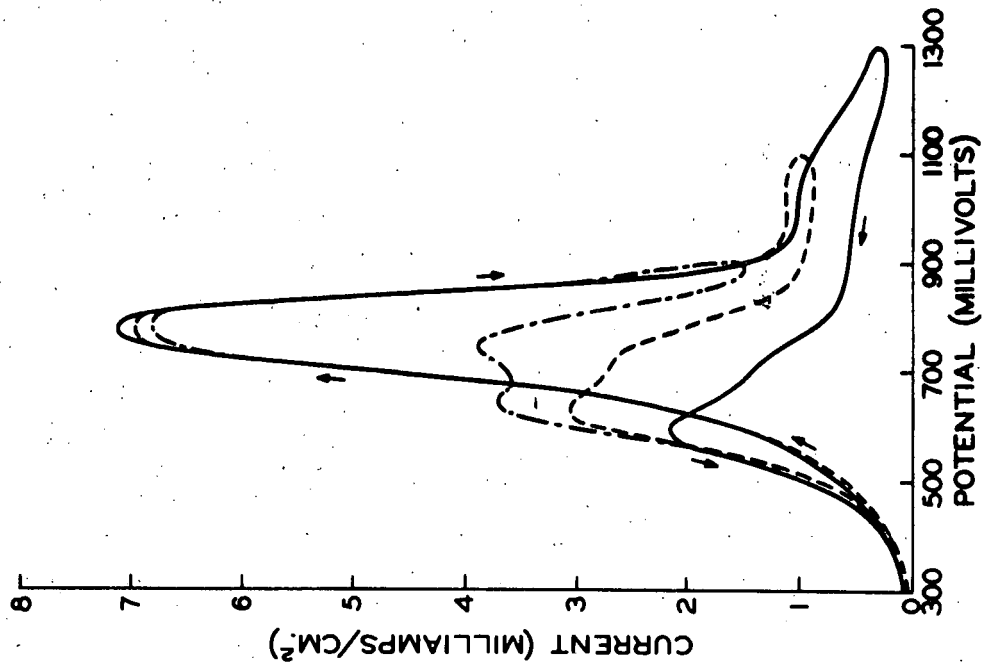


FIGURE 5
The Effect of the Final Potential on the Shape of the Current -
Potential Curve at 0°C, Sweep Rate 100mv/sec.

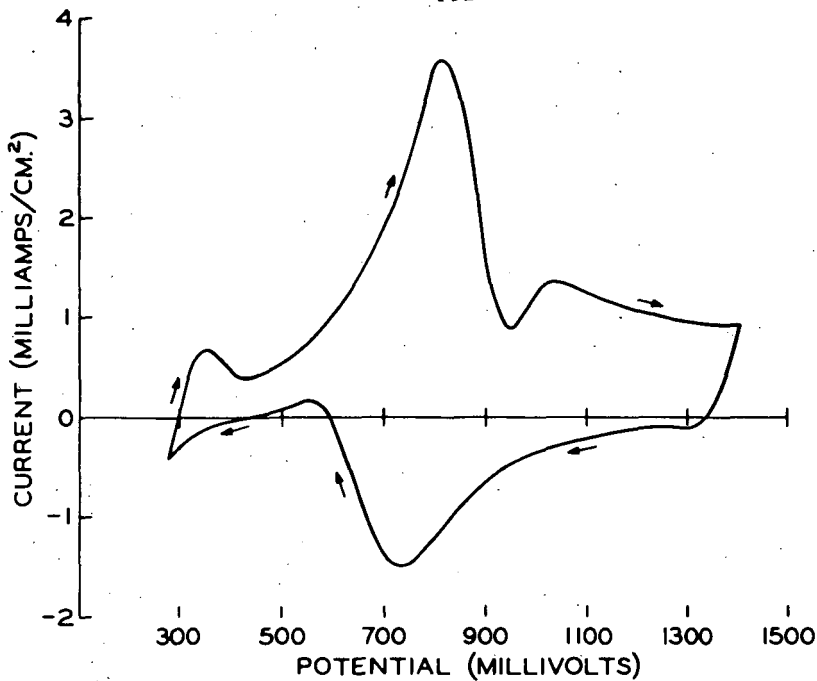


FIGURE 6

Current - Potential Curve of the System, Bright Pt/0.1M
CH₃OH : 4.5M NaOH at 30°C and 500 mv/sec:

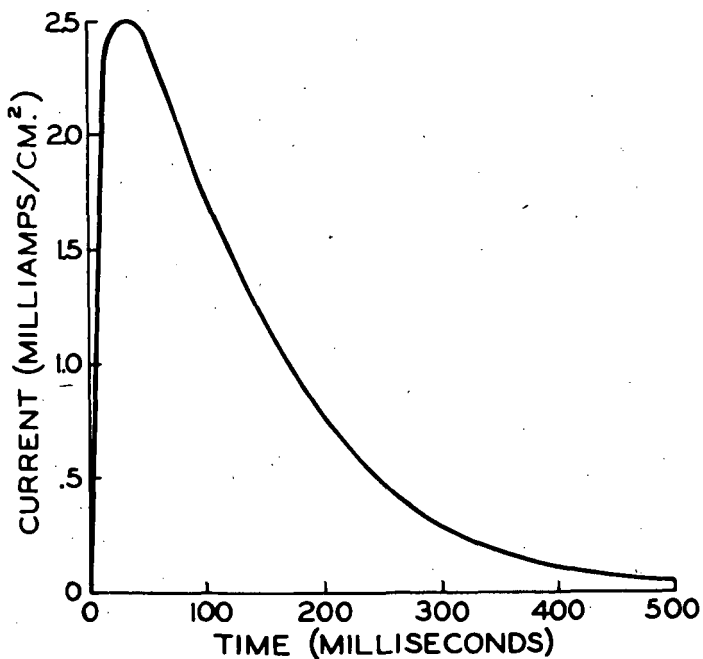


FIGURE 7

Current Transient at 400mv for the System Bright
Pt/1M CH₃OH/ 1M NaOH at 30°C.

FORMATE ION - OXYGEN FUEL CELLS

P. G. Grimes and H. H. Spengler
Research Division, Allis-Chalmers Mfg. Co.
Milwaukee, Wisconsin

Introduction

Formate ion is one of the more readily oxidizable carbonaceous fuels in basic electrolyte. In the range 80-100° C, formate ion-oxygen fuel cells, using a platinum-palladium catalyst, have a performance approaching that of hydrogen or hydrazine fuel cells. Formate ion-oxygen fuel cells with a platinum-palladium catalyst have been shown to have about twice the output of methanol fuel cells at ambient temperature (1).

Formate salts are easily handled as solids or in solution, are stable, have low toxicity and are potentially low in cost. Formic acid may also be used as the fuel. It also is stable, and potentially low priced. However, its corrosive properties demand that it be handled with some care. Formate solutions in base are stable at 100° C. At this temperature, the fuel is not volatile in contrast to methanol.

The investigations of the formate fuel cells were extended to study the effects of temperature on the cell output. Further studies involved variation of catalyst and electrolyte composition and fuel concentration.

Experimental

A sandwich type fuel cell was used in these studies. Grooved and manifolded stainless steel end plates held the electrodes and allowed uniform flow of electrolyte-fuel and oxygen over the electrode surfaces. An asbestos sheet (0.060 inch thick) served as the separator-spacer between the electrodes (2).

The electrolyte-fuel mixture, heated in an external chamber, was pumped through the cell anode compartment and then back to the external heater chamber. Oxygen was supplied to the cell at or slightly above atmospheric pressure. Appropriate cell temperature was maintained within $\pm 1^\circ$ C with an auxiliary heating pad. The external heating and pumping system was constructed of Teflon, glass and stainless steel materials. The reference saturated calomel electrode (SCE) was connected to the electrolyte system by means of an external Luggin capillary tube.

Porous nickel plaques (0.028 inch thick) were used as catalyst support material. Electrode plating solutions were prepared by mixing appropriate amounts (in accordance with the required catalyst ratio) of the noble metal chloride solutions containing 2 mg. of

metal per ml. and then adjusting the pH level to 1 with hydrochloric acid. A vacuum filtration technique was used to draw the plating solution through the porous nickel plaque at a slow flow rate. The ratio of the Pd/Pt chemideposited on the plaques was the same as that in the mixed plating solutions (3). Plated plaques were then washed with distilled water and stored in a dry atmosphere. A waterproofing coating of Teflon was applied over the catalyzed surface of those platinum-palladium electrodes which were to be used as cathodes to prevent electrode "flooding." All electrodes were plated with a total of 60 mg/in² of noble metal catalysts. The geometric area of the electrodes was 6.25 in²; and the current data presented are expressed in terms of amperes per square foot (ASF).

Fuel cell electrodes were evaluated with a sine wave (4) and a square wave commutator. The square wave current was generated by a mercury switch function generator. Operating power was supplied by a 12 volt storage battery; a second 12 volt battery supplied the power to operate the auxiliaries of the square wave generator. Voltage readings were taken with a Tektronix 564 Storage Oscilloscope and a R.C.A. Senior vacuum tube voltmeter when using the square wave or sine wave commutators, respectively.

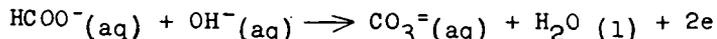
For the half cell studies a current equivalent to 60 ASF was supplied to the cell for a pre-polarization period of five minutes. Experimental data at 60 ASF were then taken, i.e. anodic and cathodic half cell voltages, total cell voltage (ohmic free), and the ohmic voltage (IR drop) of the cell.

The cells were normally kept at the appropriate current density for a three minute polarization period before the potentials were measured. For the lower temperature (30° C) tests, the cell was operated at alternately high and low current densities to maintain a nearly constant temperature in the cell, however, it was not necessary to follow this procedure at 100° C.

Results and Discussion

Anode and Cathode Studies

Formate solutions in basic electrolyte are stable at elevated temperatures, allowing operation of cells near the boiling point of the electrolyte at atmospheric pressure. Studies at ambient and elevated temperatures were conducted to determine the polarization curves for anodes and cathodes using different noble metal catalyst mixtures with formate and oxygen. The standard potential for the anode reaction is 1.02 volts.



Previous studies have shown that formate ion is readily oxidized on an anode catalyzed with a platinum-palladium mixture or with palladium (1, 3). Platinum catalyzed anodes are severely polarized under applied load. Increasing the palladium content of the catalyst improves the activity of the anodes at 30° C (Figure 1). All electrodes had a total noble metal catalyst-loading of 60 mg/in². The palladium anode was the least polarized on initial tests. Upon

extended testing for over a thousand hours at ambient temperature, a ratio of five parts palladium to one part platinum by weight proved to be the superior catalyst (1).

Formate ion fuel cells were shown in these studies to have about twice the performance of methanol fuel cells under the same conditions at ambient temperature. Performance of the methanol anode is not greatly changed (Figure 2) when the cell temperature is raised to 60° C (limited by the vapor pressure of methanol). However, anode performance of the formate cell is markedly improved by the temperature increase.

Anode polarization curves obtained for cells operating at 90° C with 4M potassium formate and 4M potassium hydroxide electrolyte are shown in Figure 3. The porous nickel electrodes were catalyzed with a total of 60 mg/in² of catalyst. The performance of all the anodes improves with temperature (compare with Figure 1). Obviously, the data show that on initial tests, the palladium anode gave the highest potential for currents between 1 and 200 ASF at 90° C. The same trend, noted at the lower temperature, of decreasing anode activity with increasing platinum content was observed, except that the platinum anode was comparable in performance to the palladium and 50 Pd/10 Pt/in² anodes.

The effect at 30° and 90° of increasing platinum content of anodes is depicted schematically in Figure 4. The markedly improved activity of a platinum anode at 90° C was unexpected and is inexplicable at this time.

Previous cathode studies with hydrogen-oxygen cells at ambient temperature have shown that platinum-palladium mixtures are more active than either platinum or palladium (4). In the 4M potassium formate - 4M potassium hydroxide system, the oxygen cathode performance improves with increasing platinum content. The best cathode at 30° has a content of 40 mg Pd/20 mg Pt/in² catalyst. The platinum cathode was highly polarized at 30° C.

The oxygen cathode polarization curves at 90° C for 60 mg/in² of platinum and/or palladium are shown in Figure 5. At the higher temperatures, the activity of the cathode catalyst increases with increasing platinum content. However, again the platinum cathode is least active at the higher currents. The best cathode catalyst had equal amounts of platinum and palladium. The trend of cathodic activity of platinum-palladium mixtures is opposite that of anodic activity of these same mixtures.

The effect of formate ion concentration on the potential of the oxygen electrode at 90° C is shown in Figure 6. A waterproofed porous nickel electrode with equal amounts of platinum and palladium was used as the cathode. Potassium formate concentration in the 4M potassium hydroxide electrolyte ranged between 0.5M to 4M.

It may be seen from Figure 6 that the formate fuel exerts a considerable polarizing effect on the behavior of the cathode; and that the effect is greater with increasing concentration of potassium formate. Furthermore, the polarization of the anode decreases slightly with increasing concentration of fuel. Similar results have been observed for the methanol-oxygen fuel cell (5). Explanations for an increased polarization of the cathode as the concentration of the dissolved fuels are raised have not been considered in

detail. It is for this reason that we should like to present possible hypotheses for this phenomenon. The decrease in anode polarization as the fuel concentration is raised (Figure 6) may be due to either a decrease in diffusion limitation or increase in concentration of fuel in the pre-electrode layer. Since the i-V curves do not exhibit a diffusion limiting current for any of the concentrations studied, it would appear, therefore, that the effect of fuel concentration may be explained approximately by the concentration term in the rate equation.

Although the net reaction at the oxygen electrode is cathodic, this electrode may still function as an anode for formate ion, provided an adequate supply of fuel is present at the electrode surface. If this occurs, the net cathodic current is less, and increased polarization will be observed.

It has been assumed that the anodic and cathodic reactions are totally independent of one another over the voltage range studied. Since formate ion is probably adsorbed on the cathode, it would be reasonable to assume that the surface covered with formate is not available for catalysis of the cathodic reaction. However, the predominating factor controlling the effect of fuel on the cathode polarization in the system discussed in this paper appears to be the formate oxidation current, rather than adsorption of fuel. This explanation is supported by the fact that increased formate concentration results in greater cathode polarization. Furthermore, the performance of the cathode as a function of the catalyst is the opposite of that shown for the anode in Figure 6.

Operating Cells

A cell was constructed using a platinum anode and a 30 mg Pd/30 mg Pt/in² cathode. The selection of these electrodes was based on the catalyst spectrum studies. The performance of the cell using a 4M potassium formate - 4M potassium hydroxide electrolyte is shown in Figure 7. An ohmic free cell voltage of 0.82 volts at 200 amps per square foot was obtained at 90° C.

Based on this data, an operating formate ion-oxygen fuel cell system in strong alkali electrolyte could presently be expected to produce 120-170 ASF at 0.8 volts per cell at 90° C. The system construction would be similar to that of a hydrazine fuel cell (2). This performance approaches that of hydrogen-oxygen and hydrazine-oxygen fuel cells at the same temperatures. Further studies of the effects of temperature, formate ion concentration, and cell design to minimize contact of formate with the cathode should lead to marked improvement in the performance of the formate ion-oxygen fuel cell.

The oxidation of formate ion in this system produces carbonate ion and consumes hydroxyl ion. Continued operation of the system would convert the cell electrolyte to carbonate. If the cell is to be operated at high pH, periodic replacement of the electrolyte would be required. However, if a small reduction in performance is not a detriment, the cell can be operated using a carbonate electrolyte. Figure 8 shows the current-voltage curve of the cell with 4M potassium formate - 4M potassium carbonate electrolyte at 90° C. The

ohmic free cell voltages at 200 and 100 ASF are 0.5 and 0.65 volts, respectively.

The polarization of the formate anode is only slightly greater in the carbonate than in the hydroxide electrolytes. However, the performance of the oxygen cathode is markedly poorer in the carbonate electrolyte. The difference in performance of the two cells shown in Figure 8 is due primarily to the cathode polarization.

In spite of the greater polarization of the cathode in carbonate electrolyte such a system may reasonably be expected to produce 100 to 130 ASF at 0.5 volts at 90° C.

Conclusions

The formate ion-oxygen fuel cell will produce 0.82 volts at 200 ASF (ohmic free) at 90° C with hydroxide electrolyte. Operation of the formate ion cell with a carbonate electrolyte reduced the performance of the cathode, lowering the output to 0.5 volts at 200 ASF (ohmic free) at 90° C.

Palladium and platinum are the best anode catalysts at this temperature. A mixed catalyst containing equal amounts of platinum and palladium is the poorest anode catalyst. At 30° C, however, palladium was the best anode catalyst and activity decreased with increase in platinum content. The mixed catalyst, referred to above, however, is the best for the oxygen electrode at both 30° and 90° C in the presence of formate.

The output of formate ion-oxygen fuel cells approaches that of hydrogen and hydrazine-oxygen fuel cells. This allows the formate ion-oxygen cells to be applied in special applications.

Acknowledgements

The authors wish to express their appreciation to Dr. D. Pouli, Mr. T. Reimer and Mr. W. Jenkin of the Research Division for their technical assistance.

References

1. P. G. Grimes, H. H. Spengler, "Formate Ion-Oxygen Fuel Cell," Fall Meeting of The Electrochemical Society, Washington D.C., October, 1964.
2. S. S. Tomter, A. P. Anthony, "The Hydrazine Fuel Cell System," in "Fuel Cells, CEP Technical Manual," American Institute of Chemical Engineers, New York (1963)
3. P. G. Grimes, J. N. Murray, H. H. Spengler, "Studies on the Anodic Character of Mixed Noble Metal Catalysts: Platinum and Palladium," Fall Meeting of The Electrochemical Society, Washington D.C., October, 1964.
4. G. F. Pollnow, R. M. Kay, "A Transistorized 60 cps Sine Wave Commutator for Resistance and Potential Measurements," J. Electrochem. Soc. 109, 648 (1962)
5. J. N. Murray, P. G. Grimes, "Methanol Fuel Cells" in "Fuel Cells CEP Technical Manual," American Institute of Chemical Engineers, New York (1963).

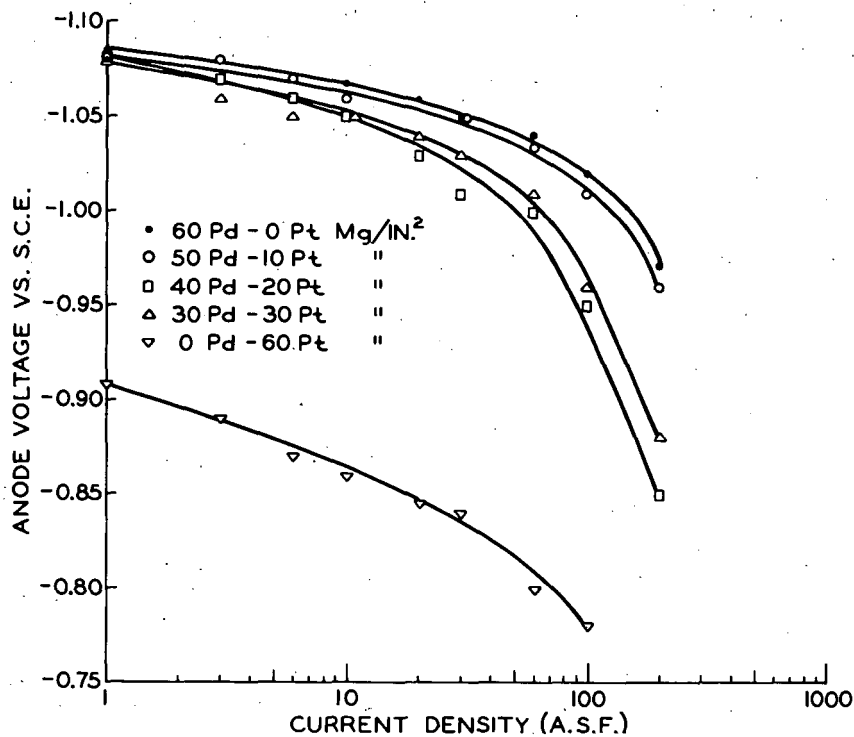


Fig. 1.-EFFECT OF CATALYST ON ANODE POTENTIALS IN 4M POTASSIUM FORMATE AND 4M POTASSIUM HYDROXIDE AT 30°C

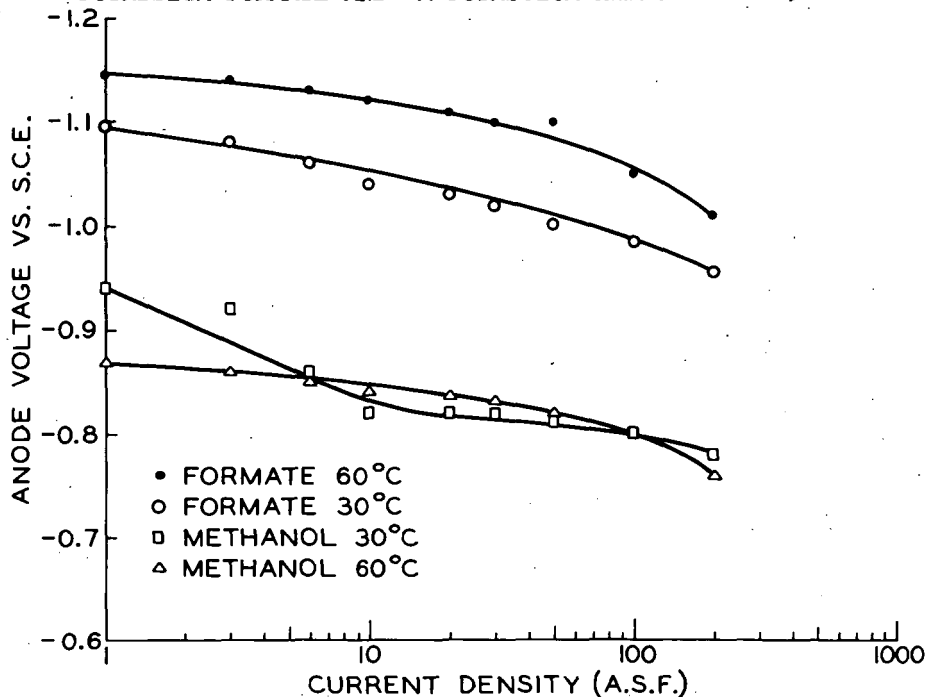


Fig. 2.-ANODE CURRENT-VOLTAGE CURVES FOR THE SYSTEMS 4M METHANOL AND 4M POTASSIUM FORMATE IN 4M POTASSIUM HYDROXIDE AT 30° AND 60°C

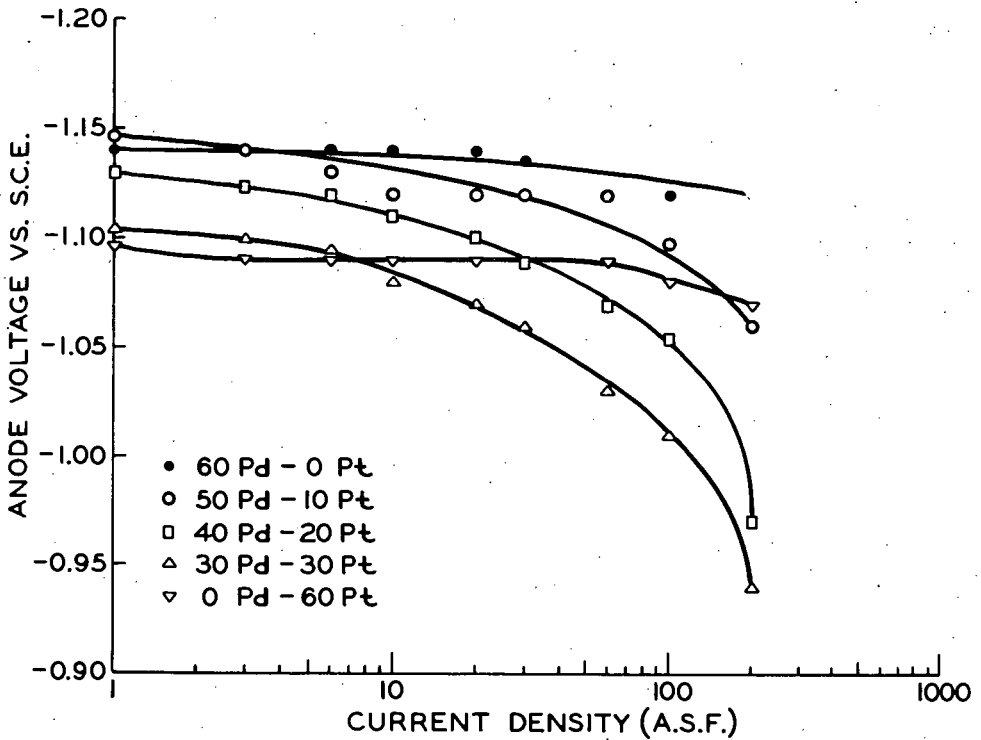


Fig. 3.-EFFECT OF CATALYST ON ANODE POTENTIAL IN 4M POTASSIUM FORMATE AND 4M POTASSIUM HYDROXIDE AT 90°C

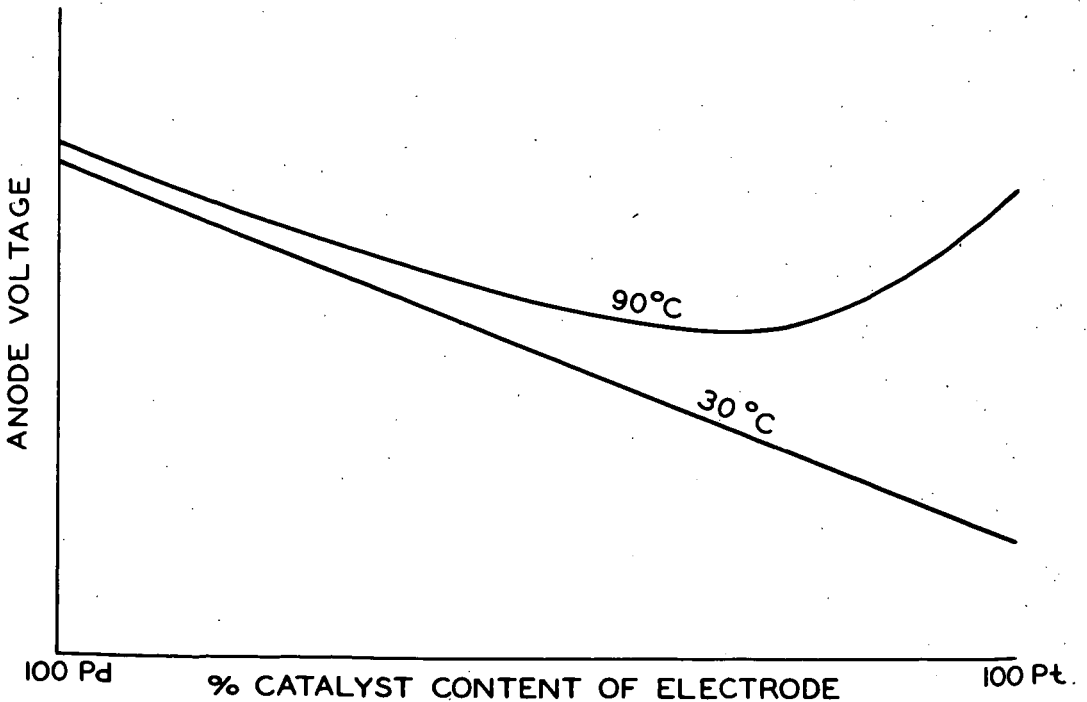


Fig. 4.-SCHEMATIC: ANODE VOLTAGE VS. CATALYST COMPOSITION

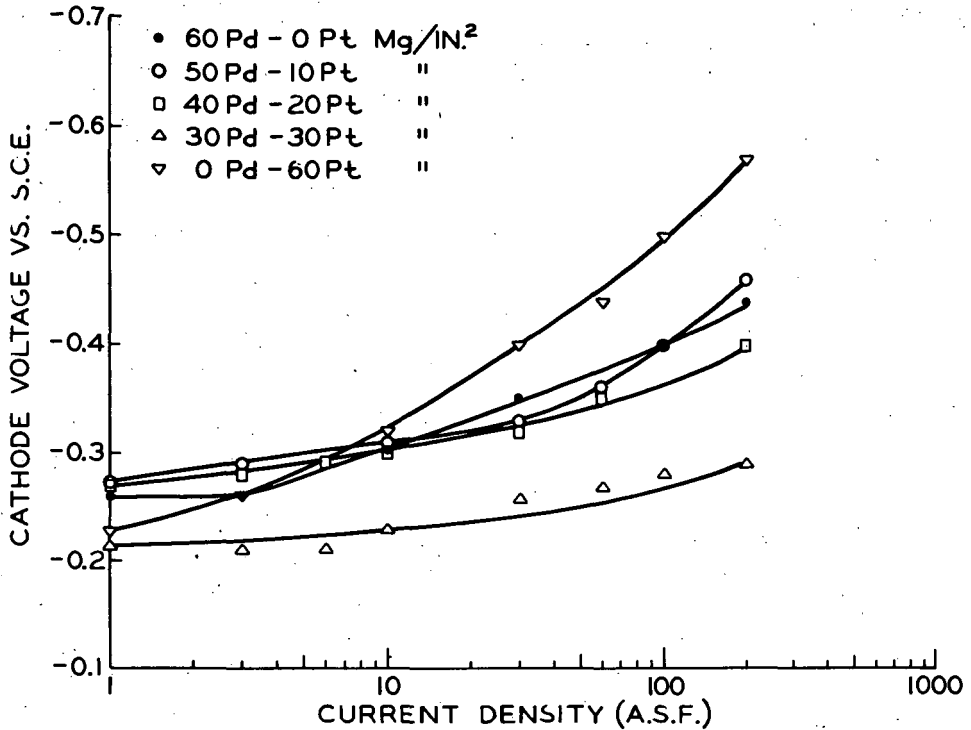


Fig. 5.-EFFECT OF CATALYST ON CATHODE POTENTIALS IN 4M POTASSIUM FORMATE AND 4M POTASSIUM HYDROXIDE AT 90°C

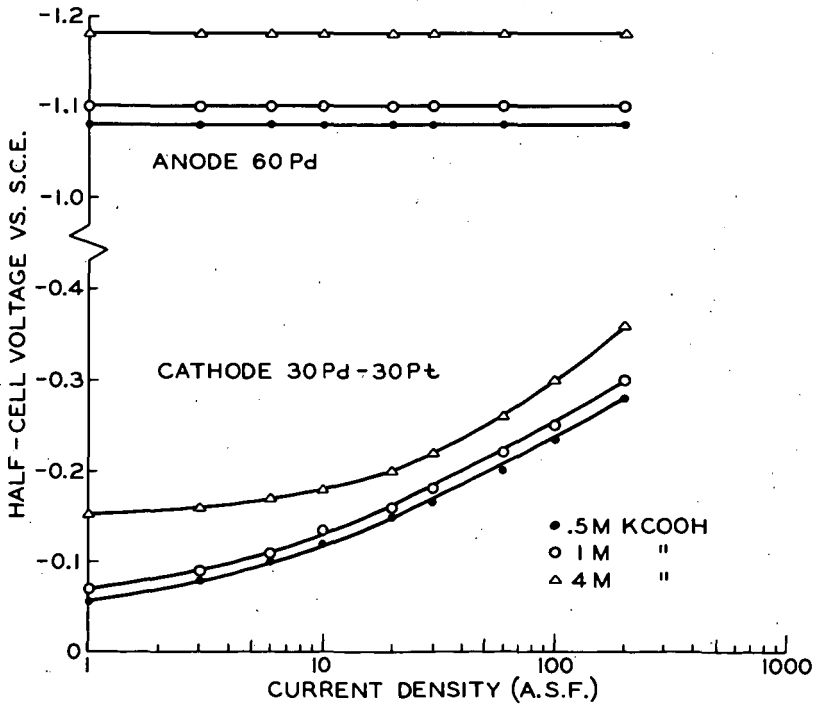


Fig. 6.-EFFECT OF POTASSIUM FORMATE CONCENTRATION ON ANODE AND CATHODE POTENTIALS IN 4M POTASSIUM HYDROXIDE AT 90°C

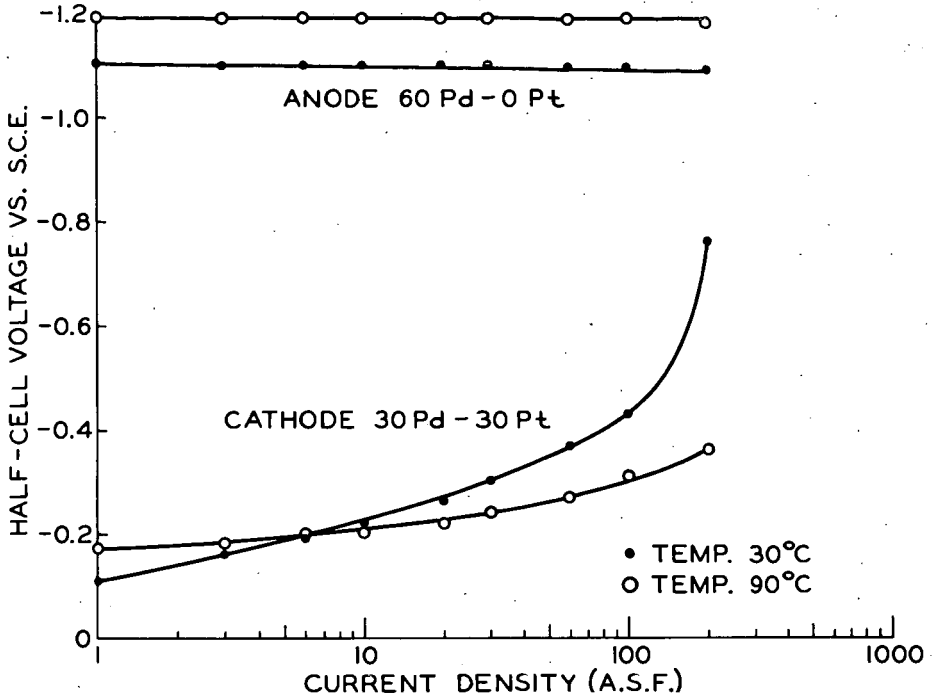


Fig. 7.-HALF-CELL VOLTAGES FOR THE BETTER ANODE AND CATHODE COMBINED IN A SINGLE CELL WITH 4M POTASSIUM FORMATE AND 4M POTASSIUM HYDROXIDE

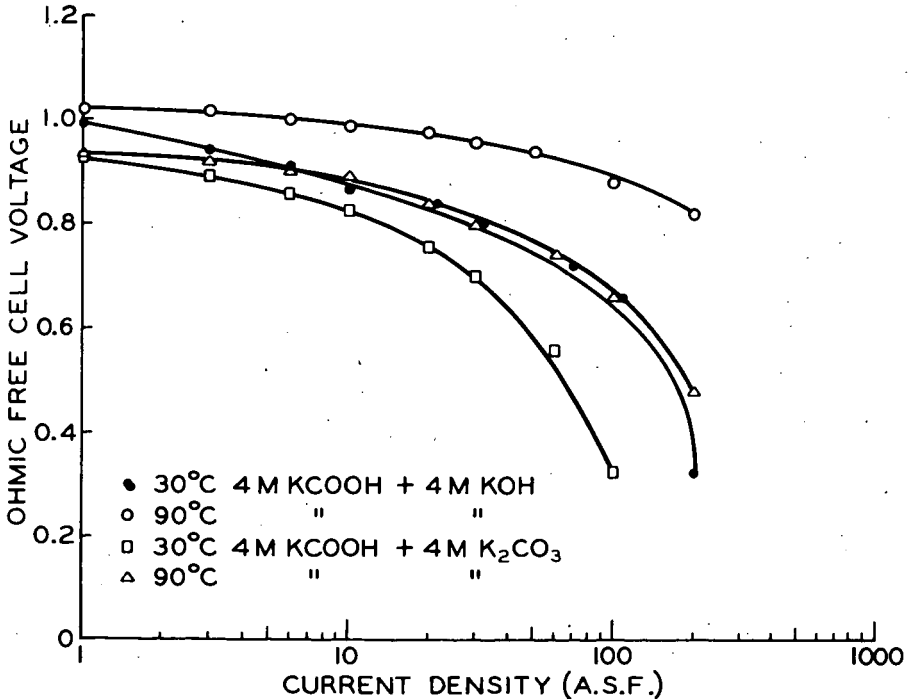


Fig. 8.-CURRENT-VOLTAGE CURVES FOR THE SYSTEMS FORMATE/4M POTASSIUM HYDROXIDE AND POTASSIUM FORMATE/4M POTASSIUM CARBONATE (OHMIC FREE)

AN ALKALINE METHANOL-AIR PRIMARY BATTERY SYSTEM

R. E. Biddick & D. L. Douglas

Research & Development Laboratory - Gould-National Batteries, Inc.
Minneapolis, Minnesota

A primary battery system operating on methanol dissolved in KOH, and air, has been developed to the laboratory hardware stage. Fuel-electrolyte solution flows by gravity through palladium-activated porous nickel electrodes. Teflon waterproofing and semi-permeable separators minimize fuel and electrolyte loss through the cathode. Condensed in a chimney, water is recycled from the emerging air stream. Extensive tests carried out on a battery rated at 30 W (one-third max. power) indicate that in series, 24 cells, individually about one-fourth sq. ft. in area, deliver 12 V. At rated output, utilization of 5 molar CH_3OH /6 molar KOH fuel is ca. 55 Wh/lb. Single cells have been operated one year at room temperatures, and cells in test batteries have maintained 3000 hours of satisfactory output. A preliminary cost analysis indicates that the system can be competitive with existing primary and secondary batteries.

INTRODUCTION

The advantages of a methanol fuel and an alkaline electrolyte are well known in fuel cell lore. The two in combination suffer the disadvantage that alkali is consumed in the fuel cell reaction. Thus, for long term operation either a large reservoir must be provided or the electrolyte must be continuously purified of formate, carbonate and other reaction products.

Three fairly comprehensive studies of alkaline methanol systems have been reported in the literature. Murray and Grimes (1) describe a methanol-oxygen system in which methanol is metered into a circulating electrolyte. Temperature of the battery is controlled by a heat exchanger in the electrolyte loop. No means of reformation of carbonate ion to hydroxide ion was provided, so that the size of the electrolyte reservoir limits the operating time - about five hours in the system described. Electrodes are of a bipolar design. The anode consists of a sintered nickel plaque impregnated with a palladium-platinum catalyst, and the cathodes are fabricated from porous nickel plaques containing silver catalyst and Teflon waterproofing. Considerable methanol is lost through evaporation, but that which is oxidized goes to carbonate.

Vielstich (2) describes a methanol-air fuel battery and its application in a signaling device. In this case, the electrodes are immersed in a container of

fuel-electrolyte solution, the spent solution being replaced as required. Platinum catalyst on an unspecified porous carrier serves as the anode, and the cathodes consist of wetproofed porous carbon activated with silver. Natural convection and diffusion serve to provide an adequate supply of air to open-topped cathodes. A 28-cell battery of this design, fabricated by Brown, Boveri, Ltd. (Baden, Switzerland), was tested as a power source for a river navigation buoy over a six month period. About a 10% loss in methanol (presumably by evaporation) was experienced. Oxidation of fuel consumed is to carbonate ion.

An alkaline methanol system in which dissolved sodium chlorite is used as the oxidizer has been reported by Boies and Dravnieks (3). The development was not carried past the single cell stage. A fuel solution approximately 5M in methanol and 5M in KOH is circulated past an anode which consists of a platinized substrate of flame-sprayed Raney nickel. The oxidant solution (4M in sodium chlorite and 5M in KOH) similarly flows through a cathode chamber. The cathode is flame-sprayed Raney nickel-silver and fuel and oxidant chambers are separated by a dialysis membrane. External heating of the reactant solutions is used to maintain a cell operating temperature of 55°C. An output of 144 mA/cm² at 0.6 V is reported. Methanol is not oxidized past the formate stage, and a considerable parasitic loss due to chemical oxidation of methanol by chlorite occurs.

This paper describes a study of a continuous flow alkaline-methanol fuel battery system which has been carried through the laboratory model stage. The work was carried on as part of a joint research and development program of the Pure Oil Company and Gould-National Batteries, Inc. A primary design objective was a reliable system capable of unattended operation over periods of several months. Only slightly less important were first cost and operating cost. A minimum of power-operated controls and auxiliaries are used. Natural forces, i.e., gravity and surface tension, serve to effect and control the flow and distribution of reactants.

CELL DESIGN

Cell design is shown schematically in Figure 1. A nickel sheet forms one side of the anode compartment, and a diaphragm forms the other side. The anode is a standard sintered-nickel battery plaque in which palladium catalyst has been deposited. The cathode contains silver catalyst bonded to nickel screen by Teflon particles in the sub-micron size range. In single-cell tests, electrode size has been two or four inches square, while in batteries the electrodes have been as large as one-fourth square foot in area.

The diaphragm separating the electrodes may be either a semi-permeable membrane or a more porous separator such as asbestos. In most of the cells constructed to date, we have used Permion 300 or 320 type membranes such as have been used in experimental silver-zinc batteries.

Electrical connection between cells is provided by a corrugated nickel screen which serves also to maintain sufficient separation between cells to permit air convection.

Electrolyte containing dissolved fuel is admitted to the cell at the top of the anode, flowing down under the influence of gravity through the anode compartment and dripping out of the cell into a collecting trough.

SYSTEM DESIGN

Cells are stacked three per inch and are held in place by compression between end plates connected by tie bolts. Fuel-electrolyte solution is distributed to the cells in parallel flow by means of a system of wicks and manifold which is operable over a wide range of flow rates.

The battery and fuel distributor are enclosed in a cabinet as shown in Figure 2 of a 24-cell system. Natural draft over the height of the battery cabinet is sufficient to provide adequate air convection past the cells. Controls and design features are provided to maintain flow rates and temperatures within the limits of satisfactory operation over a range of environmental conditions.

Air enters the cabinet through a thermostatically controlled opening near the bottom. Air leaves the cabinet through an opening near the top, entering a chimney of narrow rectangular cross section. Some water is condensed on the walls of the chimney and returned to the battery through the fuel distributor. To provide auxiliary cooling at high ambient temperature, metallic fins extend from each cell through the back wall of the cabinet into a secondary air chamber through which natural air flow is thermostatically controlled. To prevent excessive heat loss in a cold environment, the cabinet and secondary air chambers are covered with a layer of polyurethane foam insulation.

The feed rate of fuel-electrolyte solution is controlled automatically in response to battery output by means of a controller developed by Honeywell. Several types of valves and positioners have been tried. One type which resulted in good control characteristics consisted of a needle valve having a stem with a one-degree taper which was turned by a small reversible DC motor.

OPERATING CHARACTERISTICS

A polarization curve for a typical natural-flow cell at room temperature is shown in Figure 3. In order to permit comparison with other types of cells in which electrolyte concentration changes are negligible, the data in Figure 3 were obtained at a high feed rate. Maximum power output at these conditions was about 10 W/ft².

Ordinarily, if this natural-flow system is to be operated with once-through flow of electrolyte, feed rate will be very slow in order to provide good utilization

of reactants. The effect of feed rate on output voltage is shown in Figure 4. These data were obtained with a six-cell uninsulated battery with natural convection of air. Voltage dependence shows two markedly different regions. At feed rates between about 170-300% of the theoretical methanol rate (100-180% of theoretical potassium hydroxide rate), voltage is roughly proportional to feed rate. At higher feed rates voltage increases only slightly with feed rate, and at very high rates voltage would decrease because of the cooling effect of the feed.

The explanation for this operating characteristic lies in the influence of reactant and product concentrations on reaction rate. At low fuel rates concentration changes in the electrolyte are extensive, and a voltage gradient is observed through the cell along the path of the electrolyte. The potentials of anode and cathode vs. a reference electrode both become more positive as the reference electrode is moved from the electrolyte inlet to the electrolyte outlet. Single-cell data illustrating this effect are shown in Table I. At a feed rate of 275% of theoretical methanol, the change in potential between inlet and outlet amounted to 0.14 V.

TABLE I. EFFECT OF FEED RATE ON ELECTRODE POTENTIALS

Feed: 5M CH₃OH - 6M KOH
 Current Density: 10 mA/cm²
 Cell Temperature: 30°C

Feed Rate, % of Theoretical Methanol	Electrode Potentials vs. SCE in:				Measured Cell Voltage
	Feed		Effluent		
	E _{Anode}	E _{Cath.}	E _{Anode}	E _{Cath.}	
750	-.83	-.34	-.83	-.33	.51
470	-.80	-.32	-.80	-.32	.49
345	-.81	-.35	-.79	-.32	.46
295	-.80	-.36	-.74	-.29	.44
275	-.78	-.39	-.65	-.24	.40

Utilization of fuel, in terms of specific power output of the fuel solution in Wh/lb, can be derived from the voltage dependence and is plotted in Figure 4. If output voltage were strictly proportional to fuel rate in the low rate region, then fuel utilization would be independent of fuel rate in this region. However, Figure 4 shows that fuel utilization does increase slightly as fuel rate is decreased.

Maximum fuel utilization with 5M CH₃OH-6M KOH fuel was about 55 Wh/lb. It was limited largely by methanol loss occurring by evaporation through the

diaphragm but also by electro-osmotic flow of electrolyte through the diaphragm and cathode. These losses could be reduced through the use of a more retentive diaphragm. Concentration of formate in the spent electrolyte is less than 0.05 mole/liter, indicating high selectivity to carbonate formation.

Battery temperature is a function of current and of the flow rates of feed solution and air. Table II lists operating temperatures of the 24-cell battery shown in Figure 2 at a fuel rate of about 300% of theoretical based on methanol content of the 5M CH₃OH-6M KOH feed solution used; however, if the fuel rate were calculated on the basis of potassium hydroxide rather than methanol, it would be 180% of the theoretical rate required by the current. In these experiments air was forced through the cabinet at a metered rate rather than being allowed to flow by natural convection.

TABLE II. OPERATING TEMPERATURE OF 24-CELL BATTERY

Ambient Temperature: 25°C

Feed: 5M CH₃OH-6M KOH

Feed Rate: 300% of Theoretical CH₃OH

<u>Current Density</u> mA/cm ²	<u>Air Rate,</u> % of Theoretical	<u>Battery</u> <u>Voltage</u>	<u>Temperature, °C</u>
10	200	10.8	61
10	500	11.2	58
20	200	8.6	79
20	500	12.0	63

At an ambient temperature of 75°F, battery temperature is roughly 60-65°C at current densities of 10-20 mA/cm² and at the air rates and feed rates ordinarily used. At a low air rate the boiling point of the fuel can be exceeded, resulting in severe reduction of output voltage. Cell voltages at these currents are ordinarily between 0.4 and 0.5 V.

USE AS A POWER SOURCE WITH INTERMITTENT LOAD

One possible application of this primary fueled-battery system is as a power source for signalling devices, many of which operate intermittently. A load of this type was simulated by means of a timer operating for one second on and nine seconds off in series with a 250 W, 12 V lamp. Since the current surge required to operate this load was greater than could be supplied directly by the fueled battery, a storage battery was connected in parallel with the fueled

battery. The storage battery was a 12 Ah, 10 V assembly of sealed nickel - cadmium cells*. A schematic diagram of the system is shown in Figure 5.

This system operated automatically for a three day test period, during which time the voltage under load remained within the range of 9.0 to 9.7 V. Although the storage battery was operated under severe overcharge conditions for most of the test period, it performed satisfactorily.

LIFE TESTS

Single cells have been tested at room temperature for periods up to one year under a continuous drain of 10 mA/cm². Voltage decline has occurred mainly at the anode, amounting to 10 to 30% of the initial voltage output. Cracks in epoxy edge seals have required some increase in feed rate during the progress of the test in order to maintain cell performance at this level.

Cells in test batteries have maintained satisfactory output for 3000 hours of operating time accumulated in successive test batteries. The longest time which a battery has been operated thus far is 2000 hours; the battery was utilized in system tests rather than battery life tests and was subjected to more extreme operating conditions than would be expected in an optimum system design.

In some early batteries containing cells with thin-membrane diaphragms, cell reversals resulted in deposition of palladium and silver in the diaphragms to the extent that electrical shorting occurred. The problem was eliminated by removing the cause of cell reversal, namely, unequal feed rate to individual cells which resulted in excessive fuel depletion in some cells.

OTHER FUELS

Since the major cause of low methanol utilization in this system is the high volatility of methanol, one might expect less volatile fuels to overcome this difficulty. Ethyl alcohol, for example, boils 14°C higher than methyl alcohol. In a single cell test, however, fuel loss was not reduced by the substitution of ethyl alcohol. Ethylene glycol is not an acceptable fuel because it forms an insoluble oxidation product which plugs the cell passages.

COSTS

Based on a specific power output of 50 Wh/lb of fuel solution and a cost of \$0.10/lb of methanol and potassium hydroxide, fuel cost would amount to \$0.80/kWh.

Catalyst cost is about \$3/W, most of which is recoverable. Cost of the complete system would be many times this amount in small scale production.

* Manufactured by Alkaline Battery Division, Gould-National Batteries, Inc.

Even so, with a life of only one year the alkaline methanol-air system might be economically competitive with existing primary and secondary batteries.

CONCLUSIONS

Because a natural-flow fueled-battery system can operate with a minimum of moving parts, it should be inherently reliable. The system can operate automatically and unattended, giving power on demand and maintaining itself in standby condition under no load.

Power capability can be substantially higher than is practical with air-depolarized primary batteries or with secondary batteries. The system is simply recharged for a new period of use by refilling the fuel-electrolyte reservoir with fresh solution. Life tests of single cells indicate a useful life of at least one year and possibly considerably longer.

Costs may be competitive with existing low-energy power sources.

ACKNOWLEDGEMENTS

This work was conducted under a joint fuel cell research program of Gould-National Batteries, Inc. and Pure Oil Company. The assistance of Messrs. E. L. Burkholder, P. S. Chow and W. G. Howard in various phases of battery construction and testing is gratefully acknowledged.

LITERATURE CITED

- (1) Murray, J. N. and Grimes, P. G., in "Fuel Cells", CEP Technical Manual, pp. 57-65, Am. Inst. Chem. Engrs., New York, 1963.
- (2) Vielstich, W., "Methanol Air Fuel Cell", preprint, Fourth International Symposium on Batteries, Brighton, England, Sept. 29 - Oct. 1, 1964, Pergamon Press.
- (3) Boies, D. B. and Dravnieks, A., in "Fuel Cell Systems", pp. 262-268, Amer. Chem. Soc., Washington, 1965.

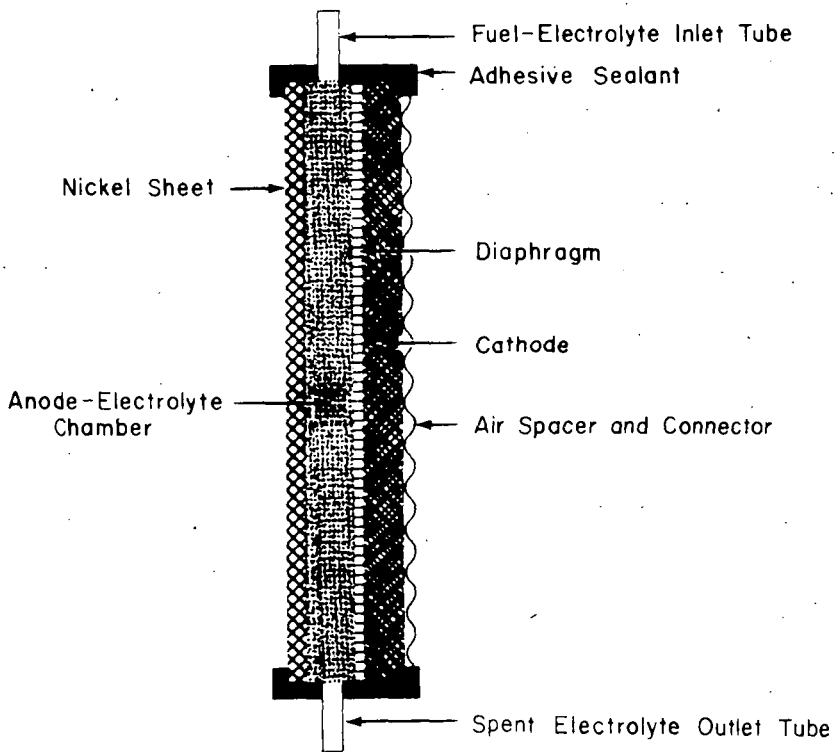


FIGURE 1. CONSTRUCTION OF DISSOLVED-FUEL CELL WITH NATURAL FLOW

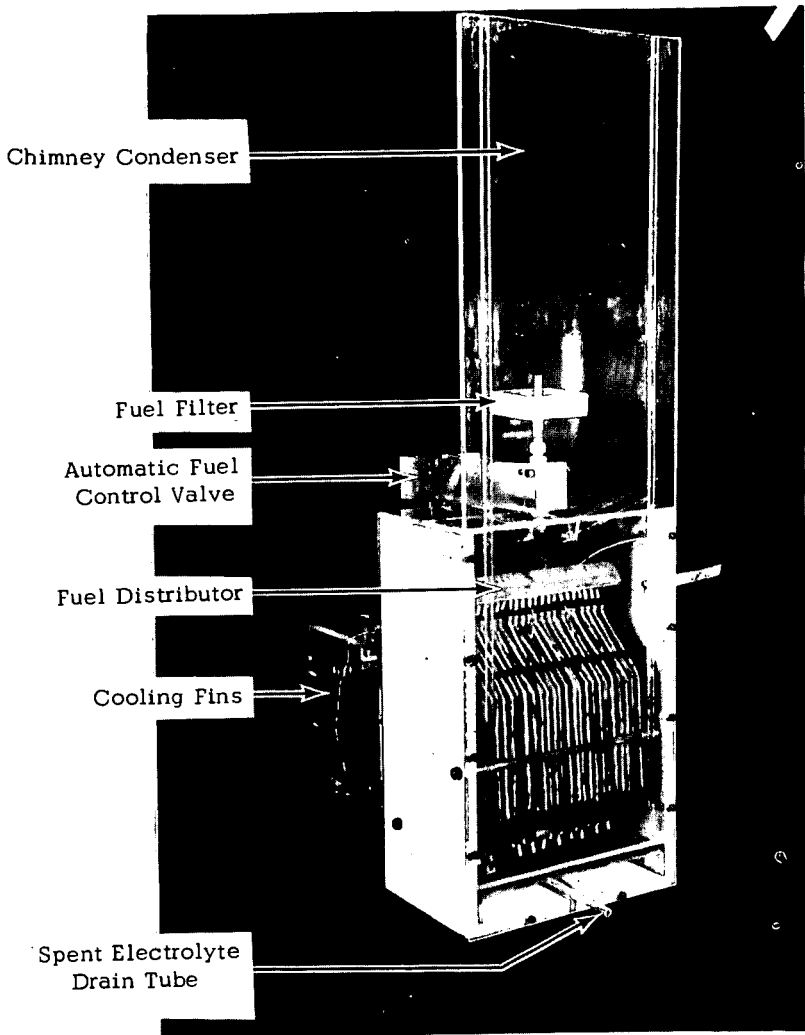


FIGURE 2. NATURAL FLOW ALKALINE METHANOL-AIR SYSTEM

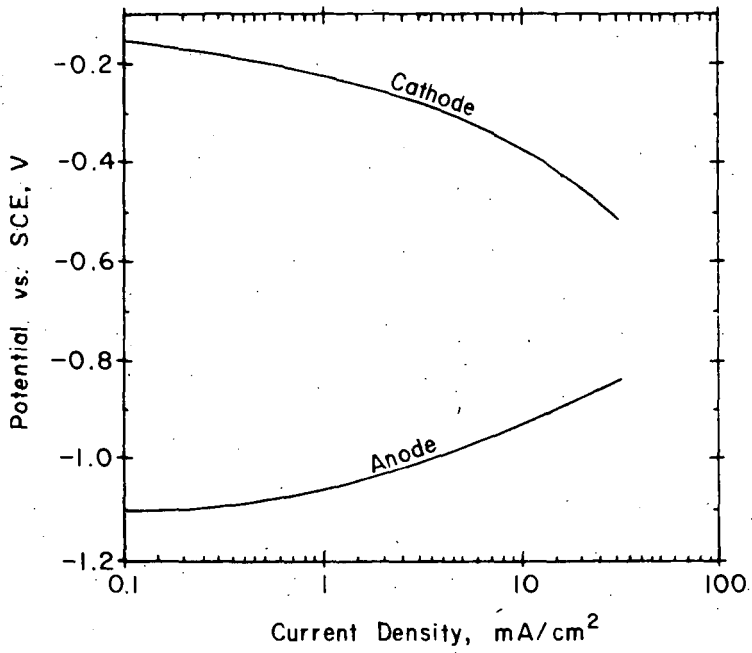


FIGURE 3. POLARIZATION CURVES FOR NATURAL-FLOW CELL

Temperature: 30°C
Fuel Rate: High

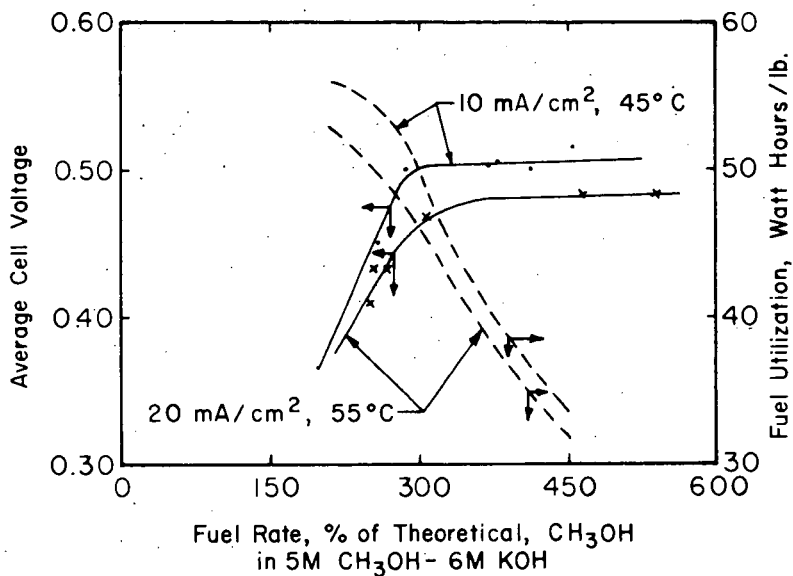


FIGURE 4. EFFECT OF FEED RATE ON AVERAGE CELL VOLTAGE AND ON FUEL UTILIZATION

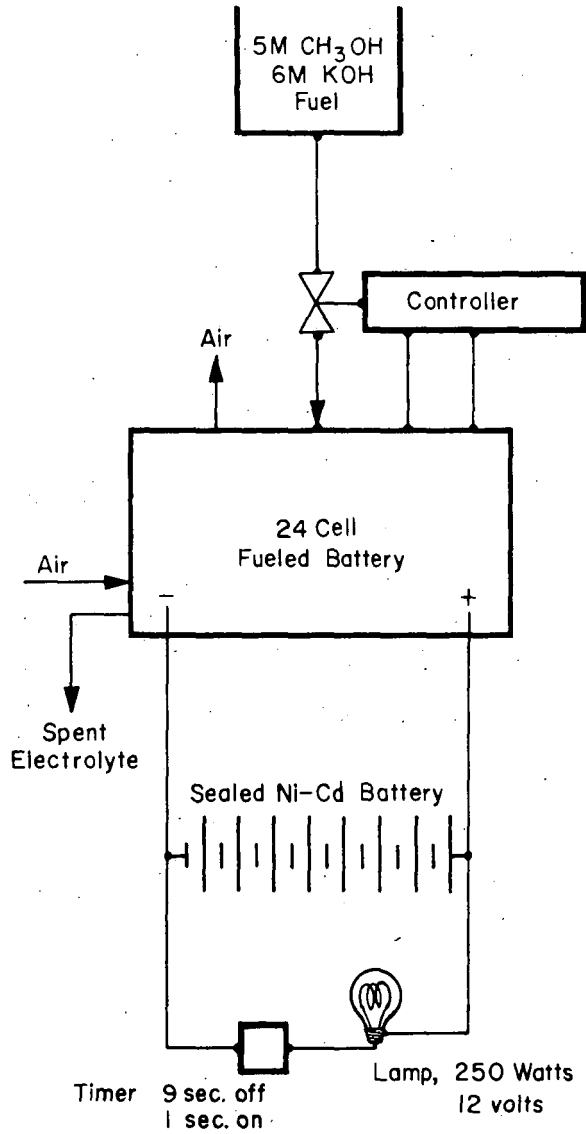


FIGURE 5. SCHEMATIC DIAGRAM OF COMPLETE POWER SYSTEM INCLUDING AN INTERMITTENT LOAD

SOME ASPECTS OF THE DESIGN AND OPERATION
OF DISSOLVED METHANOL FUEL CELLS

by

K.R. Williams, M.R. Andrew and F. Jones

"Shell" Research Ltd., Thornton Research Centre, P.O. Box 1, Chester, U.K.

INTRODUCTION

It has long been recognized¹ that a soluble fuel such as methanol may conveniently be used in low temperature fuel cells. However most early attempts to realize this type of fuel cell involved the use of an alkaline electrolyte, which would have been rapidly converted to carbonate. Thus potassium or sodium hydroxide solutions do not meet the requirements of invariance implicit in the definition of a fuel cell. At low temperatures, that is at ambient temperature and slightly above, carbonate electrolytes are unsuitable; not only is the performance of the oxygen electrode poor and the anode subject to concentration polarization, but formation of the bicarbonates, which are of low solubility, makes it difficult to conceive of a reasonably invariant system when such an electrolyte is used. If operation at around 120°C is acceptable, then Cairns and his co-workers^{2,3} have shown that caesium and rubidium carbonates can be used as invariant electrolytes for methanol fuel cells. However, the performance of present oxygen electrodes in this electrolyte falls short of that obtained in strong acids and bases. Furthermore, as Williams and Gregory⁴ have shown only strong acids and bases can be used as electrolytes for low temperature fuel cells if high current densities are required.

These considerations suggest that a strong acid is likely to be the most satisfactory electrolyte for a direct methanol fuel cell. Of the strong acids, sulphuric seems the best choice if operation at temperatures between ambient temperature and 60 or 70°C is required. This acid has a high specific conductivity, is non-volatile and, although it is

corrosive, the problems attendant upon its use are not insurmountable. In our experience the performance of oxygen electrodes in sulphuric acid is marginally better than in phosphoric acid, the major alternative; also the electrical conductivity of sulphuric acid is higher than that of phosphoric acid at low temperature. Perchloric acid offers no significant advantage over sulphuric acid with our electrodes and as there is a possible fire hazard with perchloric acid and methanol we preferred sulphuric acid.

Another advantage of acid electrolytes is that water removal is easier than with an alkaline electrolyte. This is because, with an acid electrolyte, hydrogen ions discharge on the air electrode to form water which is readily removed. On the other hand in alkaline systems, water has to be transported from the fuel electrode through the electrolyte to the air electrode. This process takes place against the concentration gradient as the concentration of electrolyte is highest, and hence vapour pressure of water lowest, at the region from which water is evaporated.

There are various reasons for accepting an upper limit of operating temperature of 70°C for the dissolved methanol cell. In the first place methanol, even in solution, is sufficiently volatile at temperatures above 60°C as to necessitate stringent precautions against loss by evaporation. Secondly, an upper temperature limit of about 70°C means that a wide range of cheap, commercially available plastics offers sufficient temperature and corrosion resistance to be useful for fuel cell construction. Additionally, corrosion problems, particularly in the vicinity of the air electrode, are aggravated by increased temperatures and offer a further incentive to relatively low temperature operation. Finally, if a cell is designed to run at about 60°C, it will have a reasonable output at room temperature and will start easily from cold.

The ability to operate an invariant acid electrolyte system at a relatively low temperature may be of importance where extreme longevity is required. In our experience the rate of electrode deterioration increases with increasing operating temperatures but even at the present state of the art, lives of the order of years appear possible if temperatures can be kept fairly close to 30°C.

EXPERIMENTAL

For our air electrodes we have developed a structure in which microporous polyvinyl chloride (P.V.C.) is used as the substrate⁵. This substrate is made conducting by being coated with an evaporated metal layer, which may be thickened by electrodeposition of more metal. Finally, a catalyst is applied to the electrode surface. In acid electrolytes we have used gold as the conducting metal layer. Since quite thin layers of gold are acceptable, the intrinsic value of the substrate (microporous polyvinyl chloride together with the gold film) is only about \$1.50 per sq.ft.

The performance of oxygen and air electrodes of this type in acid and in acid to which methanol has been added is shown in Figure 1 in which the scale of the ordinate is exaggerated in order to emphasize the differences in electrode performance. It can be seen that the voltage of the air electrode throughout the current range is within 50 mV of that of the electrode using pure oxygen. This is characteristic of electrodes of this type provided that the catalytic activity is high. Whilst the presence of methanol in the electrolyte has a substantial effect on the open circuit voltage of the air electrode, at useful current densities 1M methanol depresses the potential of the air electrode by only 20-50 mV.

We have found that the microporous plastic also makes an ideal substrate for methanol electrodes. This quite naturally led to our using both sides of the material to make a complete cell. One side of the substrate is used for the air electrode and the other side for the methanol electrode, the cell thickness being the thickness of the porous plastic itself. Thus it is now a relatively simple matter to make complete cells with an inter-electrode distance of 0.030 inch and having a very low internal resistance.

The performance of both methanol and air electrodes in a complete cell at 25°C and 60°C is shown in Figure 2. Over this temperature range, the air electrode is relatively unaffected by the temperature of operation whereas the voltage of the methanol electrode at reasonable current densities decreases by about 100 mV as the temperature is raised. The internal resistance of the fuel cells is, of course, varied by electrode separation. A typical voltage loss due to internal resistance at a current density of 100 mA/sq.cm would be 45 mV per cell.

Methanol-air batteries with sulphuric acid electrolyte have been built from cells of this type. The alternative design in which a separate piece of porous plastic is used for each electrode, with a relatively thick electrolyte layer between the electrodes, has also been used in the construction of batteries. Both designs of cell are shown schematically in Figure 3. With both types of battery internal electrical connections from the electrodes to the conducting cell separators were made from gold-plated plastic mesh. Thus series electrical connection is built into the batteries. The mesh chosen allows the free passage of gas past the air electrodes, escape of carbon dioxide bubbles from the electrolyte and current collection from the surface rather than from the periphery of the

electrodes. The construction of this type of cell is described elsewhere⁵ and Figure 4 shows a 300 watt methanol-air battery of 40 cells.

During operation of an 8-cell prototype methanol-air fuel cell using 6N sulphuric acid, the fuel-electrolyte mixture developed an ester-like smell. The electrolyte was extracted with ether and the extract analysed by gas-liquid chromatography. In addition to the intermediates normally encountered (formaldehyde and formic acid), traces of acetic, propionic, butyric and isobutyric acids were detected together with some unidentified compounds. These materials were not present in either the methanol used as fuel or in the ether used for the extraction.

These side products are present in small quantities but may be strongly adsorbed on the electrocatalyst thereby causing the observed slow decline in electrical output with time. Experiments in which small quantities of these materials were deliberately introduced into a fresh electrolyte - fuel mixture showed that they had a poisoning effect on the methanol electrode.

We have carried out some preliminary experiments to determine the source of these poisons. The first possibility that occurred to us was that these materials might arise as a result of attack by the acid electrolyte on one or other of the plastics present in the cell (polystyrene, Perspex, P.V.C., or polyethylene). We were able however to detect traces of these organic acids after prolonged anodic oxidation of methanol in 6N sulphuric acid in all-glass apparatus with a platinized-platinum anode.

DISCUSSION

In spite of the difficulties of choosing inexpensive, acid-resistant constructional materials, developing suitable electrocatalysts and minimizing the effects of impurities on the electrodes, we have built a series of satisfactory methanol-air batteries. The first battery - a small 8-cell prototype - was built in September 1963 and is still operational, giving 2.85 watts at 1 amp compared with its initial performance of 3.15 watts at the same current density. This testifies to the longevity of the system, for the only servicing the battery has received is an occasional wash with distilled water.

Since the prototype was built we have been able to build larger batteries using improved electrocatalysts and this work has led to the construction of a 40-cell battery delivering 300 watts at 12 volts at 60°C. With this battery, as with all the other batteries we have constructed, there has always been an ester-like smell and organic acids have been detected frequently. It is interesting to speculate on the origins of these materials.

Whilst radical dimerizations are frequently encountered in electrochemical processes⁶, this type of reaction does not seem likely here. If a radical were polymerizing then the expected yields of acids would be butyric << propionic << acetic. Even though the isolation of the organic acids is only qualitative it seems that they are present in quantities which decrease only slowly as one goes up the homologous series. Thus the likely route appears to be an attack of a radical on a methanol molecule.

The existence of the radical $\text{H} - \underset{\text{M}}{\overset{\text{O}}{\text{C}}} - \text{OH}$ has been postulated in the

Fischer-Tropsch synthesis⁷ of organic compounds from carbon monoxide and hydrogen. Formaldehyde, which has been detected in solution by several workers^{8,9}, might have this structure in the adsorbed state and, by progressive condensations with methanol and subsequent rearrangements, would lead to aldehydes which, under the anodic conditions present, would be electrochemically oxidized to the organic acids which have been detected. However, until a more thorough investigation of the spectrum of products is available, the reaction mechanism must remain obscure.

Finally, although these side reactions cause some trouble, the longevity of our prototype battery testifies to the fact that they do not have a disastrous effect on cell life. However, attention will have to be devoted not only to improving the efficiency of electro-catalysts for the methanol oxidation but also to the suppression of side reactions. Probably, if a catalyst is sufficiently good for the overall reaction of methanol to carbon dioxide, the side products will be formed in negligible quantities.

REFERENCES

1. K. Kordesch and A. Marko. Oesterr. Chemiker-Z., 52 (1951) 185.
2. E.J. Cairns and D.I. MacDonald. Electrochem. Technol., 2 (1964) 67.
3. E.J. Cairns and D.C. Bartosik. J. Electrochem. Soc., 111 (1964) 1205.
4. K.R. Williams and D.P. Gregory. J. Electrochem. Soc., 110 (1963) 209.
5. K.R. Williams and J.W. Pearson. Joint Symposium of the Inst. of Chem. Eng. and the Amer. Inst. of Chem. Eng., June 1965, (in press).
6. A.P. Tomilov and M.Ya. Fiochin. Russian Chem. Rev., 32 (1963) 30.
7. G.C. Bond. Catalysis by Metals. Academic Press, London, 1962, p.365.
8. T.O. Pavela, Ann. Acad. Sci. Fennicae, A II 59 (1954) 7.
9. M.J. Schlatter, Fuel Cells, Vol. 2, ed. G.J. Young, Reinhold, New York, 1963, p.190.

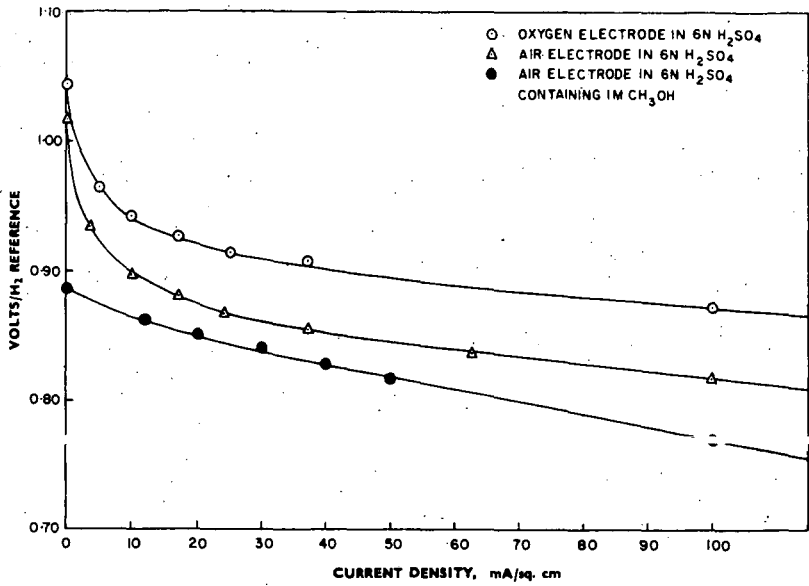


FIG. 1—Polarization curves for oxygen and air electrodes in sulphuric acid solution at 25°C

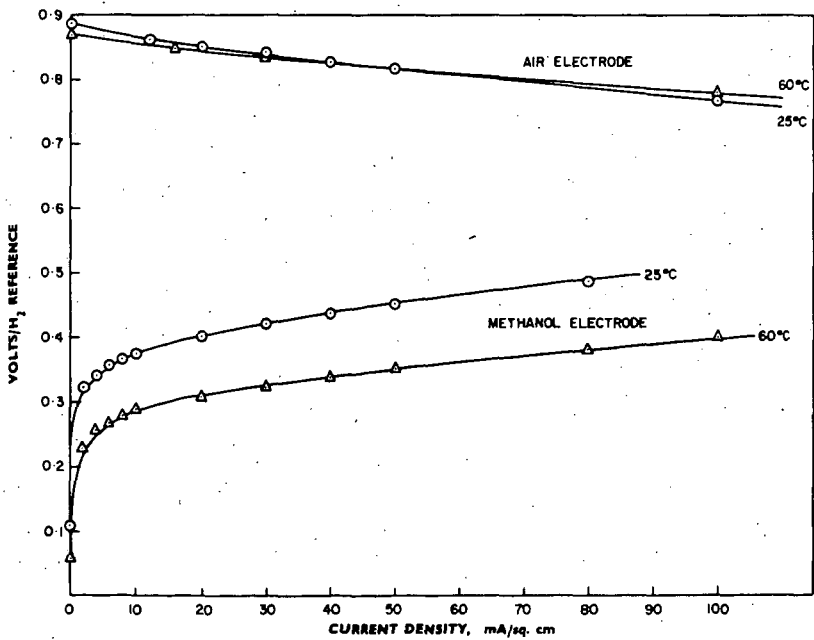


FIG. 2—Polarization curves for air and methanol electrodes in a 1M CH₃OH-6N H₂SO₄ mixture at 25° and 60°C

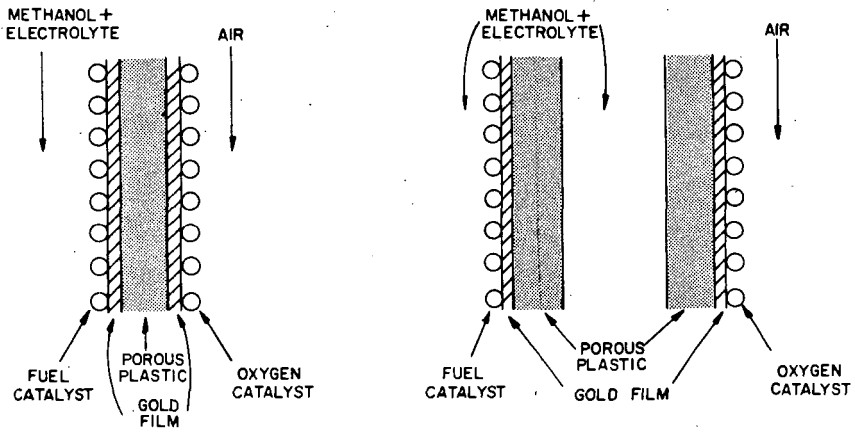
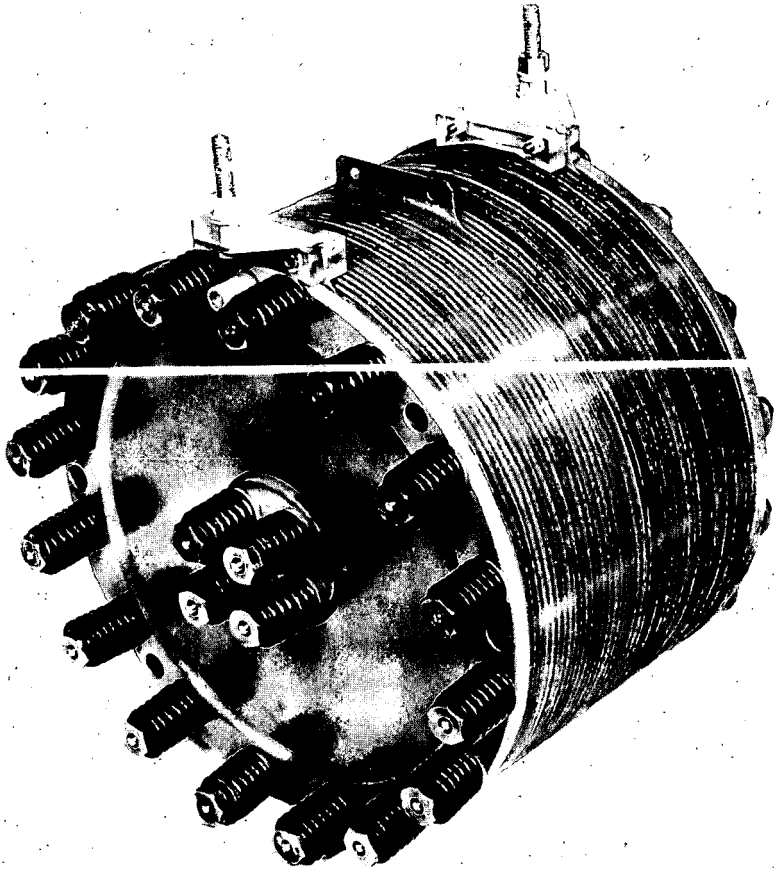


FIG. 3—Schematic drawing of two types of single cell



MH 1014

FIG. 4- 40-cell methanol-air fuel battery

A COMPARISON BETWEEN EXTERNAL AND INTERNAL REFORMING METHANOL FUEL CELL SYSTEMS

Nigel I. Palmer, B. Lieberman and M. A. Vertes

Leesona Moos Laboratories
Division of Leesona Corporation
Great Neck, New York

INTRODUCTION

With the results of several years work in many laboratories now available, it is possible to compare the rather limited number of fuel cell systems capable of operating on carbonaceous fuels. Although many of the approaches are conceptually simple, it must be conceded that none meet the original objectives of ultra-high efficiency and system simplicity. Because of this, it may be misleading to base comparisons only on the characteristics of the central component, i.e., the fuel cell. The object of this paper is to compare designs for two complete 6 kw fuel cell systems operating on methanol and air.

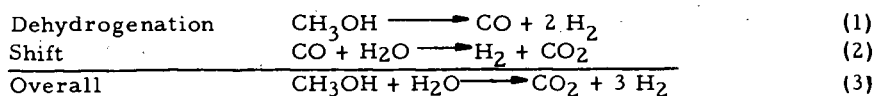
Figure 1 illustrates the basic system options that are available. The direct anodic oxidation approach remains conceptually the most attractive. However, unsolved problems of catalyst cost and stability, corrosion and electrochemical efficiency have so far prevented it entering a development stage. The remaining approaches may all be termed 'indirect' in that the anodic oxidation step involves hydrogen produced from the fuel in a previous stage. System (2), using an acid electrolyte cell retains some of the problems of the direct system; namely, materials and catalyst stability in acid, plus poisoning by trace amounts of carbon monoxide. System (3) which is undoubtedly the most developed, retains the advantages of a basic electrolyte cell by prepurifying the hydrogen -- usually with a palladium/silver diffuser. A variation of this system combining the last two stages by the use of palladium/silver anodes (System 4) has been described by Chodosh and Oswin.⁽¹⁾ More recently, Vertes and Hartner have described an alternative approach⁽²⁾ originally developed at Leesona Moos Laboratories in which the reforming, purification and anodic oxidation steps are integrated within the anode structure (System 5). This is referred to as an 'integral reforming' or 'internal reforming' fuel cell system.

In principle all the systems shown are capable of operating on any carbonaceous fuel. Methanol, however, offers several advantages for fuel cell use, and the systems compared have been designed for this fuel. Significant factors determining this choice were:

1. The favorable thermodynamics of methanol reforming at relatively low temperature.
2. The favorable kinetics and catalyst stability obtained for the methanol reforming reaction.
3. The complete miscibility of methanol and water with resultant simplification of system design.
4. The availability of relatively cheap, high purity methanol.

INTERNAL REFORMING PRINCIPLES

Before discussing the overall systems, it will be necessary to describe briefly the operating principles of the internal reforming electrodes. Figure 2 illustrates the sequential steps involved. An equimolar mixture of methanol and water is vaporized and passed through a catalyst bed contained in a thin plenum chamber behind the palladium/silver membrane. Here dehydrogenation of the methanol occurs first, followed by shift conversion of the resultant carbon monoxide.



Hydrogen from this reaction zone diffuses through the palladium-silver membrane to the electrolyte side where it is anodically oxidized. The 75% palladium/25% silver membrane, 1 mil thick, activated with palladium black⁽³⁾ imposes no restraint on the reaction and limiting currents exceeding 1 amp/cm² have been obtained. The electrolyte employed can in principle be either acid or base, but 85% KOH has been preferred because of its lower vapor pressure, lower corrosion, and the higher performance obtained.

The overall reforming reaction is endothermic. In this system the necessary heat can be supplied directly by the waste heat produced in the cell by entropy and polarization losses. Various side reactions such as the methanation reaction can be suppressed by proper selection of the catalyst. Best results have been obtained using a mixed oxide type catalyst. It may be observed here that because of the physical separation of catalyst from electrolyte, optimization of the catalyst is substantially easier than for a direct oxidation anode. Thermodynamically, conversion to hydrogen is 99% complete at 160°C. The lower temperature limit for operation is established at about this point by kinetic considerations. A higher operating limit of 300°C is established by electrolyte and materials limitations within the cell itself. Selection of the optimum operating temperature requires an analysis of several other interrelated factors and is discussed in a later section on system design.

SYSTEM EFFICIENCIES

The primary reason for using a fuel cell is the high efficiency of energy conversion, although account must be taken of other factors such as weight, volume, capital cost, etc. The priority of these will be determined by the requirements of a particular application.

The net thermal efficiencies of both fuel cell systems can be expressed as functions of the same set of component efficiencies; however, the interrelations and limits of these component efficiencies are quite different for the two cases. Figure 3 shows the location of the points of energy loss - expressed as efficiencies.

The efficiencies considered are:

$$\text{Net system efficiency } \eta_N = \frac{\text{Net electrical energy delivered}}{\text{Heating value of CH}_3\text{OH supplied}}$$

$$\text{Conversion efficiency } \eta_C = \frac{\text{H}_2 \text{ produced in the reformer}}{\text{H}_2 \text{ stoichiometrically available from CH}_3\text{OH/H}_2\text{O}}$$

$$\text{Heat exchange efficiency } \eta_E = \frac{\text{Heat supplied}}{\text{Heat available}}$$

$$\text{Utilization efficiency } \eta_U = \frac{\text{H}_2 \text{ anodically consumed}}{\text{Total H}_2 \text{ produced}}$$

$$\text{Cell thermal efficiency } \eta_T = \frac{\text{Gross electrical energy produced}}{\text{Heating value of H}_2 \text{ consumed}}$$

$$\text{Auxiliaries efficiency } \eta_A = \frac{\text{Net electrical energy delivered}}{\text{Gross electrical energy produced}}$$

Evidently, defined in this way the net system efficiency is expressed as a product of the component efficiencies.

$$\eta_N = \frac{3 \Delta H_{\text{ox}}'}{\Delta H_{\text{ox}}''} \cdot \eta_C \cdot \eta_U \cdot \eta_T \cdot \eta_A \quad (4)$$

where: $\Delta H_{\text{ox}}'$ = lower heating value of H₂ (at cell temperature)
 $\Delta H_{\text{ox}}''$ = lower heating value of CH₃OH (at room temperature)

At any steady operation condition, a state of thermal neutrality must be obtained for the system.

Case I. External Reforming System. The requirement of thermal neutrality is achieved in this system by oxidizing the purge gases from the hydrogen extractor and supplying the heat produced to the reformer. Provision must also be made for removing the cell waste heat which in this system is not utilized. Writing a simplified energy balance for the system,

$$\eta_C \Delta H_R + \Delta H_V = \eta_E \left[(1 - \eta_U) 3 \eta_C \Delta H_{\text{ox}}' + (1 - \eta_C) \Delta H_{\text{ox}}'' \right] \quad (5)$$

where: ΔH_R = heat required to reform methanol, Kcals/g. mole
 ΔH_V = heat to vaporize and superheat methanol and water, Kcals/g. mole

Considering the components of efficiency: The conversion efficiency η_C will have a theoretical limit established by the thermodynamics of reactions (1) and (2). This exceeds 0.99 at 200°C. In practice however, the primary limitation results from kinetic factors, i. e., need to minimize the reformer volume. With external reforming this restriction is not serious and values for η_C as high as 0.95 may be obtained. The cell efficiency η_T has a theoretical limit imposed by the cell entropy losses (approximately 0.9) and a practical limit determined by a tradeoff between the capital cost and operating cost. Since the cell waste heat is not utilized, thermal balance requirements do not impose an additional limit. The auxiliaries efficiency η_A can theoretically approach 1.0 for a simple system; in practice it will be as low as 0.7 in small systems, rising to higher values as the gross power level increases.

The H₂ utilization efficiency η_U has a theoretical limit in external reforming systems, imposed by the need to supply reformer heat. This limit will be determined by the conversion efficiency and the heat exchange efficiency between the catalytic burner and the reformer. The interrelationship between η_U , η_C and η_E is given in equation (5) and is shown graphically in Figure 4. For a given conversion level and heat exchange efficiency, the value of η_U in this graph represents the maximum utilization possible for thermal balance.

Table 1 shows the effect of component efficiencies on the system net thermal efficiency. Three cases are considered; the first refers to ultimate theoretical limits assuming complete reversibility of each component, the second refers to probable practical limits that may be approached, and the third gives state-of-the-art values employed in the present designs. In the second case a limiting operating voltage of 1.0 V is assumed.

Table 1. External Reforming System - Component Efficiencies

Efficiencies		Theoretical Limit	Practical Limit	Present Design (State of the Art)
Conversion	η_C	1.0	0.95	0.91
Cell	η_T	0.9	0.75	0.62
Auxiliaries	η_A	1.0	0.95	0.83
Heat Exchange	η_E	1.0	0.80	0.70
Utilization	η_U	0.78	0.77	0.76
Net	η_N	0.80	0.51	0.40

Case II. Internal Reforming System. Considering now the internal reforming system, it is evident that the same expression (5) for net efficiencies must hold. However, the expression for thermal neutrality is quite different since heat is now supplied by the cell:

$$\eta_C \Delta H_R + \Delta H_V = 3 \eta_C \eta_U \eta_E' (1 - \eta_T) \Delta H_{Ox}' \quad (6)$$

The cell thermal efficiency may be expressed in terms of operating voltage (E):

$$\eta_T = \frac{2 E F}{\Delta H_{Ox}'} \quad (7)$$

Substituting this into equation (6), an expression is obtained relating the conditions for thermoneutrality to the cell voltage:

$$\eta_C \Delta H_R + \Delta H_V = 3 \eta_C \eta_U \eta_E' [\Delta H_{Ox}' - 2FE] \quad (8)$$

The heat exchange efficiency term η_E' is defined essentially as before, but has components which themselves must be optimized for thermal balance;

$$i. e. \eta_E' = \frac{\text{heat produced} - \text{losses to air} - \text{losses to surroundings}}{\text{heat produced}}$$

As in the previous system, no theoretical limits exist for η_C . Because of cell temperature, size, and heat transfer considerations, however, the practical limit for η_C may be lower for internal reforming systems. This is due, it must be emphasized, to kinetic rather than thermodynamic considerations. It may be mentioned at this point that where thermodynamic limitations do apparently occur, as for example with hydrocarbons, they may in practice be circumvented. This results from hydrogen extraction through the membrane,

distorting the equilibrium until complete conversion has occurred. This is discussed more fully elsewhere. (4) (5) With the catalysts currently used at LML, a limit of about 0.9 is obtained for methanol. η_U has no theoretical limit in this system, but a practical limit of 0.97 is probably realistic. η_A tends to be higher for the internal reforming system because of the fewer auxiliaries and simplified controls. Unlike the previous case, η_T is theoretically limited by the requirement of thermal neutrality. Equation (6) shows how this is related to η_C , η_U , and η_E . Figure 5 shows this relationship graphically and indicates that adequate heat is available from the cell even at low heat exchange values. The apparent excess of heat, however, is balanced by losses from the cell which may impose a heat deficit. This is shown in Figure 6, which presents the components of heat balance around the internal reforming cell as a function of gross power output. The heat requirements for reforming are given for the theoretical limit of 100% conversion.

Allowing for heat input to the reformer plus losses to the cathode air streams and to the surroundings, a small heat deficit occurs. This can then be balanced by some form of heat exchange. Two possible schemes considered are: (a) inlet air to outlet air exchange to reduce air cooling; (b) outlet air to inlet methanol to reduce the vaporization load. Alternatively, if η_C is below 0.9, catalytic combustion of the residual fuel in the cell exhaust may be used, e.g., for fuel vaporization. This is the scheme employed in the present design study.

Table 2 shows values for component efficiencies equivalent to those presented in Table 1 for the external reforming system. Note that the heat exchange efficiency η_E is determined by assuming a recovery exchanger efficiency of 75% for the non-utilized cell heat losses. It can be seen that higher overall system efficiencies may be anticipated for the internal reforming system at all levels of development.

Table 2. Internal Reforming System - Component Efficiencies

	<u>Efficiencies</u>	<u>Theoretical Limit</u>	<u>Practical Limit</u>	<u>Present Design (State of the Art)</u>
Conversion	η_C	1.0	0.91	0.84
Cell	η_T	0.73	0.69	0.64
Auxiliaries	η_A	1.0	0.95	0.86
Heat Exchange	η_E	1.0	0.90	0.69
H ₂ Utilization	η_U	<u>1.0</u>	<u>0.97</u>	<u>0.95</u>
Net	η_N	0.83	0.66	0.50

6 KW DESIGN STUDIES

To permit a realistic comparison of the two approaches to be made, design studies of two complete 6kw systems have been made. The normal operating output of 6kw (net) was selected as being appropriate for probable initial commercial applications. The complete systems described have not yet been built, although extensive testing of the components and major sub-systems has been proceeding since 1962. As an example, Figure 7 shows a typical internal reforming bicell composed of two 5" x 5" anodes and a single porous nickel bicathode. Figure 8 shows an experimental 0.5 kw

multicell stack with associated instrumentation.

a. External Reforming: Figure 9 shows a simplified schematic of the external reforming system. Methanol/water is pumped to the reformer where it is first vaporized and then catalytically reformed. The reformer is operated at a temperature of 300°C, a pressure of 75 psig, and a space velocity of 1200 IHSV, † with heat supplied by catalytic oxidation of the extractor purge gases. Product gases, largely H₂ and CO₂ are purified in a palladium/silver diffuser containing 8 ft² of 1 mil foil and maintained at 300°C by the hot gases from the burner. The fuel cell employed operates at 75°C with circulated 5N KOH electrolyte. Both anode and cathode are lightweight "Teflon" †† TFE-fluorocarbon resin bonded electrodes operating at 1 psig differential pressure. In the present system, platinum activation is used but cheaper catalysts are under development. Figure 10 shows the current-voltage characteristic for the cell. Electrolyte-water concentration and temperature are controlled in separate subsystems through which the electrolyte is circulated. The cell module contains a total of 189 cells with a total electrode area of 64 ft² providing a gross power of 7 kw at normal operating load. The net thermal efficiency of the system at operating load is 40%. System specific weight and volume are 97 lbs/kw and 1.1 ft³/kw respectively.

Table 3 summarizes the weights and volumes of the major components.

Table 3. 6 kw External Reforming System - Component Parameters

<u>Component</u>	<u>Weight (lbs)</u>	<u>Volume (ft³)</u>
Fuel Cell	130	1.7
Reformer	61	0.77
Extractor	65	0.53
Battery	87	0.75
Miscellaneous Auxiliaries	<u>239</u>	<u>3.1</u>
Total System -----	582	6.85

b. Internal Reforming: Figure 11 shows a schematic of the internal reforming system. As discussed previously, thermal balance is achieved in the system by catalytic combustion of the cell exhaust gases to vaporize and superheat the methanol/water feed. The thermodynamic and kinetic factors involved in optimization of the cell operating temperature have already been mentioned. Other factors which must be considered are the requirements of heat transfer to the reaction zone and the need to minimize cell volume. As cell temperature is increased, the catalyst activity increases permitting a higher space velocity and thus a thinner catalyst bed for the same conversion level. This also results in increased heat transfer. Analysis of the present system indicated an optimum operating temperature of 225°C. Temperature control of the system is achieved by circulating oil through jackets around the cells. Water of reaction is removed from the cathodes via the excess air on a self-regulating basis. The air is scrubbed before entering the cells to prevent carbonate formation. Figure 12 shows the voltage-current characteristic for the cells. Operating point at rated load is 210 amps/ft² at 0.8 V. 121 cells

 † IHSV is the ideal hydrogen space velocity defined as the volume of hydrogen produced by stoichiometric conversion of the fuel supplied per hour divided by the reactor volume.

†† A DuPont registered trademark.

with a total area of 40 ft² provide a gross normal operating power of 7 kw. System net thermal efficiency at this operating point is 50%. Specific weight and volumes are 80 lbs/kw and 0.57 ft³/kw respectively. Weights and volumes of the major components are summarized in Table 4.

Table 4. 6 kw Internal Reforming System - Component Parameters

<u>Component</u>	<u>Weight (lbs)</u>	<u>Volume (ft³)</u>
Fuel Cell	284	1.5
Battery	87	0.75
Miscellaneous Auxiliaries	109	1.2
Total System ---	480	3.45

OVERLOAD AND CONTROL

The cell operating point is determined by the maximum overload required in a particular operation. In many applications, particularly electro-mechanical, the overload may be high but of relatively short duration. Under such conditions, an optimum for capital cost and size may be obtained by a hybrid combination of fuel cell and secondary battery. This battery supplies transient overloads and is automatically recharged by the fuel cell. The fuel cell itself may then be scaled to satisfy the integrated power requirement (i. e., total kwh/time) while operating at near peak power densities. This approach has been incorporated in both of the present system designs. It may be noted that a battery will in any case be required to provide the start-up power necessary for indirect systems. The battery capacity will be determined by either the overload requirements or the start-up demands. In the present design, lead acid batteries have been specified to provide 5:1 overload capability.

It is impossible in the present discussion to analyze the system controls in detail; however, some of the factors affecting response to varying loads should be mentioned. In a simple hydrogen/oxygen cell supplied from high pressure tanks, response is limited only by gas flow and regulator operation and is therefore quite rapid. With an indirect system, however, the change in load must be transmitted to each of the previous stages. Depending on the capacity and response of these stages, serious control lags may develop. To provide a smoother response, a small hydrogen surge tank has been incorporated in the external reforming design.

The control problem is minimized in the internal reforming system because of the closer integration of the reaction stages. In addition, the high hydrogen capacity of the palladium/silver membrane provides an effective surge capacity corresponding to approximately 6 coulombs/cm². This is roughly two orders of magnitude higher than for a platinum activated electrode.

CONCLUSIONS

An analysis of the various factors presented indicates that a selection between the external and internal reforming systems will depend largely on the requirements of the particular application. It has been shown that substantially higher system efficiencies are possible with internal reforming. This will be

obtained however at the expense of a higher capital cost resulting from the higher palladium content and more expensive materials of construction used in the system. Because of the fewer auxiliaries, the volume of the internal reforming system is substantially smaller, though system weights are similar. The superior response characteristics of this system may be important in variable load applications.

Considering future development, the efficiency of the external reforming system can be improved mainly by increasing cell operating voltages. On the other hand, to further improve the efficiency of the internal reforming system will require development of more active catalysts. This is particularly necessary if operation is to be extended to the use of hydrocarbon fuels. Capital cost reduction will require the use of thinner palladium membranes and higher operating cell current densities. Work along these lines is in progress.

REFERENCES

- (1) H. G. Oswin and S. M. Chodosh, "Fuel Cell Systems," Advances in Chemistry Series 47, p. 61 (1965).
- (2) A. J. Hartner and M. A. Vertes, London A. I. Ch. E. - I. Ch. E. Meeting, June 1965.
- (3) S. M. Chodosh and H. G. Oswin, Brussels Fuel Cell Symposium, June 1965.
- (4) M. A. Vertes and A. J. Hartner, Brussels Fuel Cell Symposium, June 1965.
- (5) D. P. Gregory, Present Symposium, ACS, September 1965.

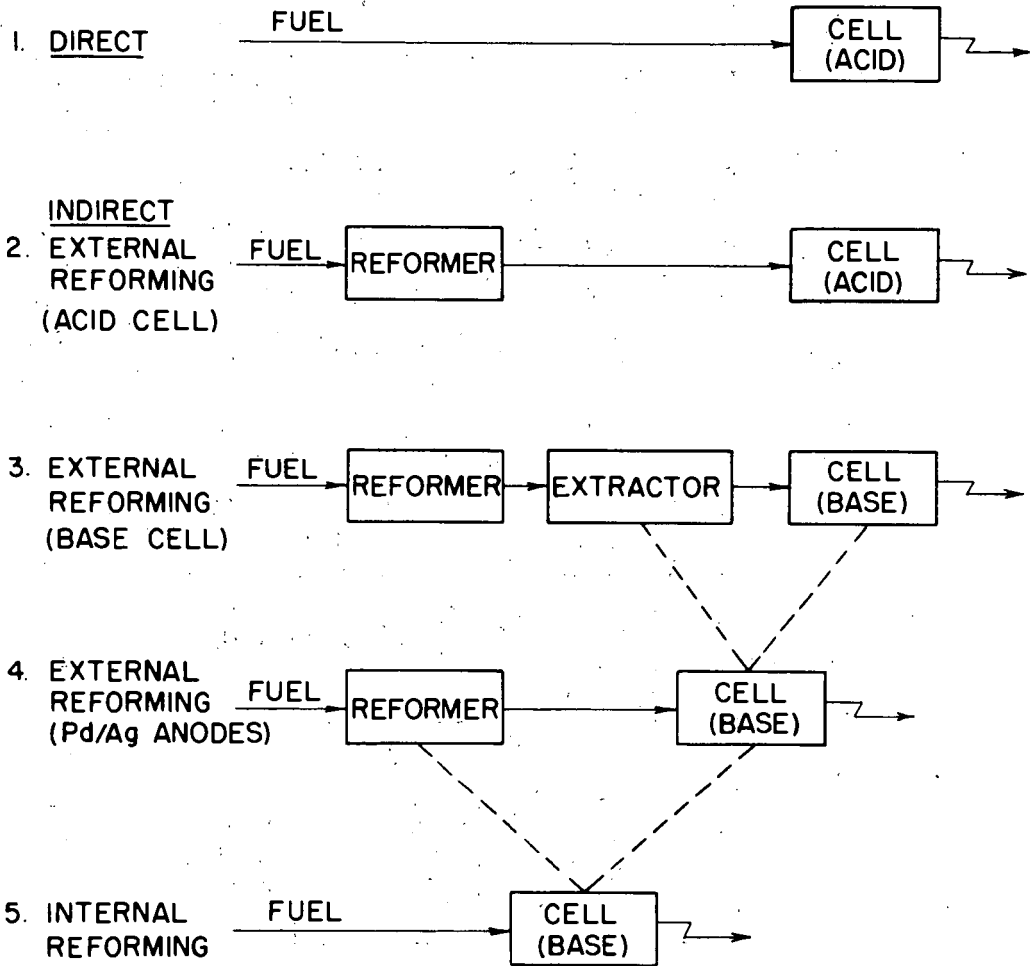


FIG. 1 CARBONACEOUS FUEL CELL SYSTEM OPTIONS

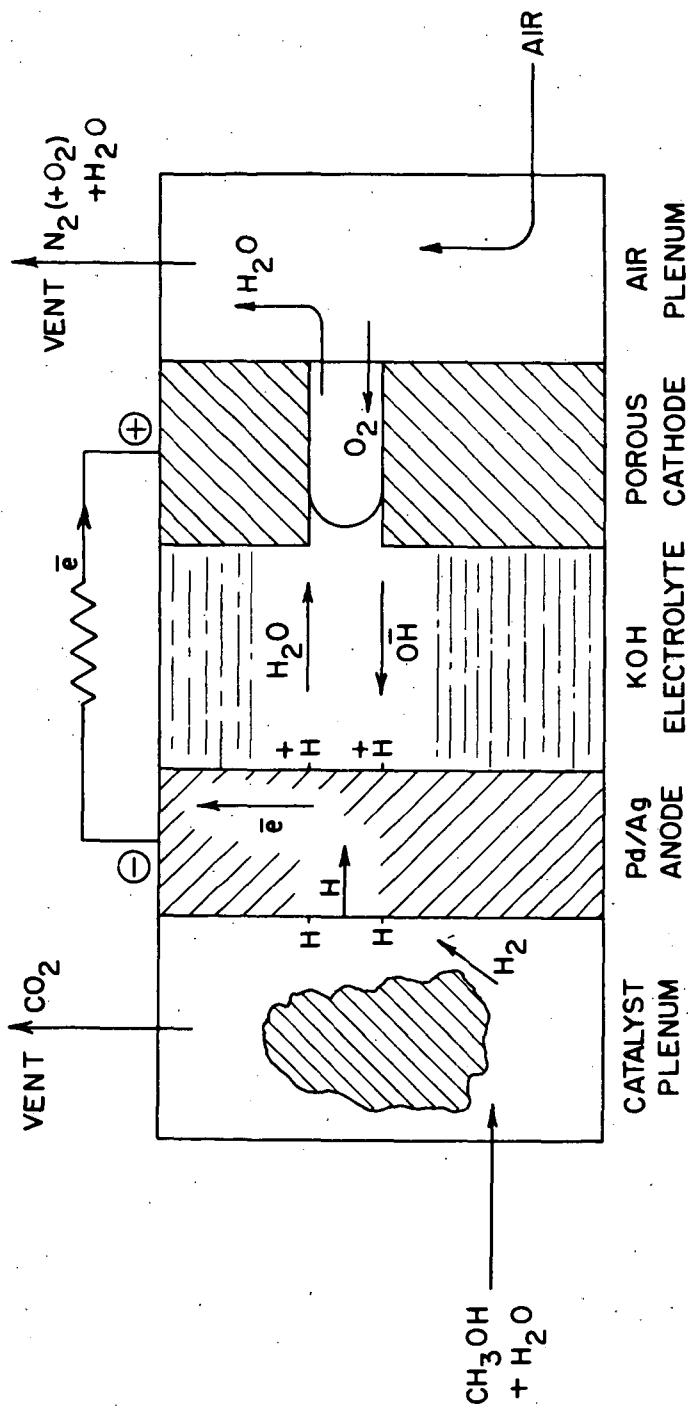
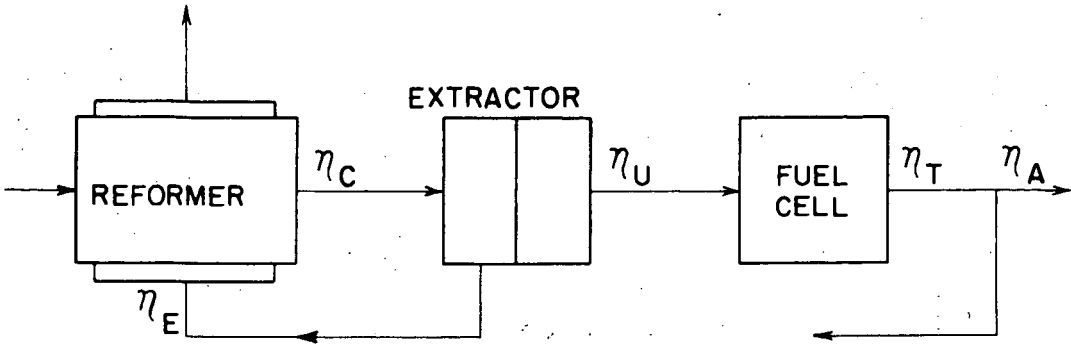
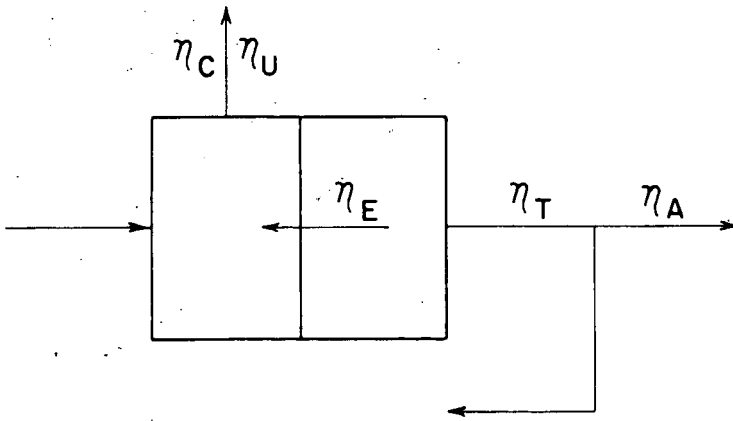


FIG. 2 OPERATING PRINCIPLE OF INTERNAL REFORMING CELL



(a) EXTERNAL REFORMING



(b) INTERNAL REFORMING

FIG. 3 ANALYSIS OF SYSTEM EFFICIENCIES

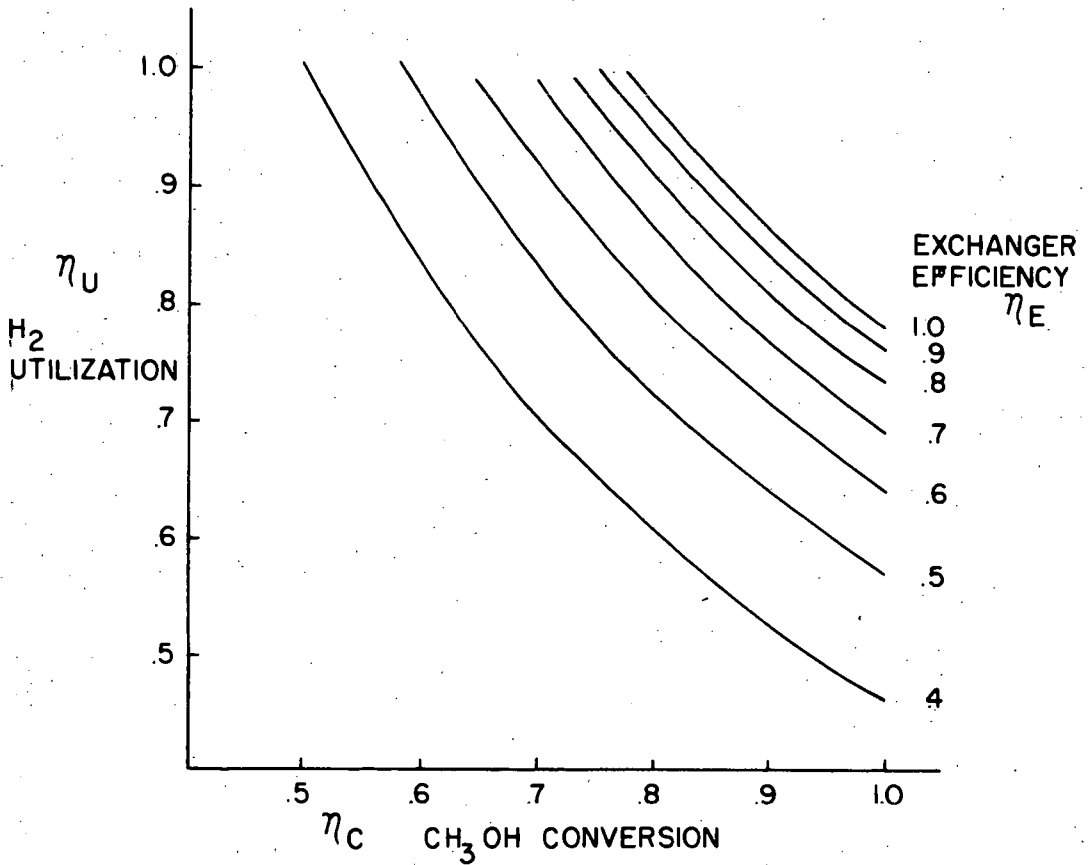


FIG. 4 CONDITIONS FOR THERMAL NEUTRALITY FOR EXTERNAL REFORMING SYSTEM

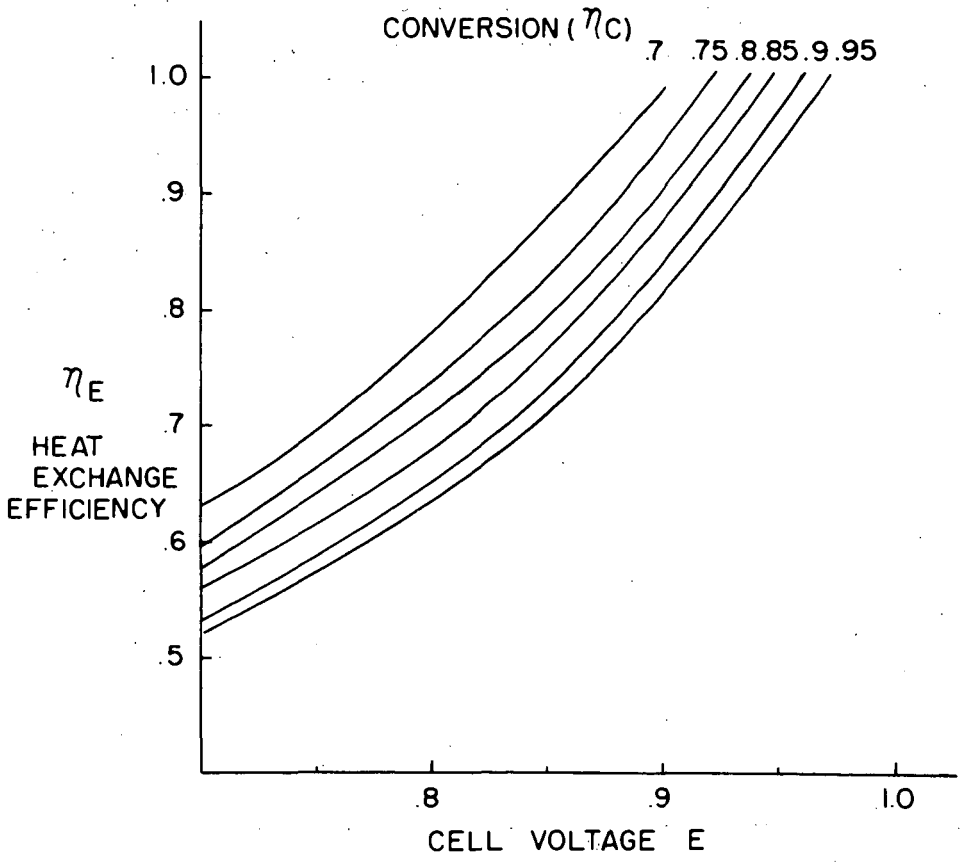


FIG. 5 CONDITIONS FOR THERMAL NEUTRALITY FOR INTERNAL REFORMING SYSTEM

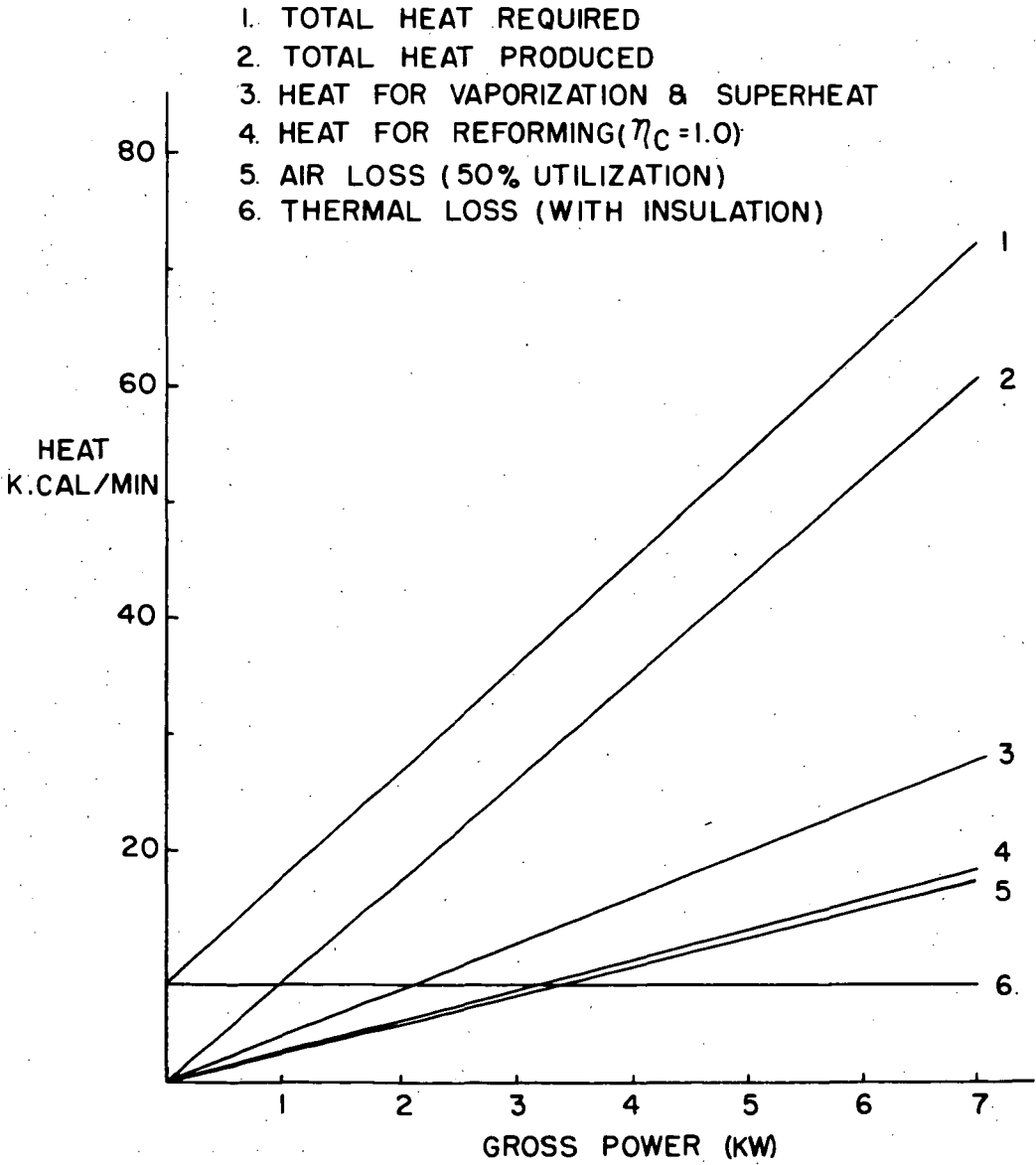


FIG. 6 HEAT BALANCE FOR INTERNAL REFORMING SYSTEM

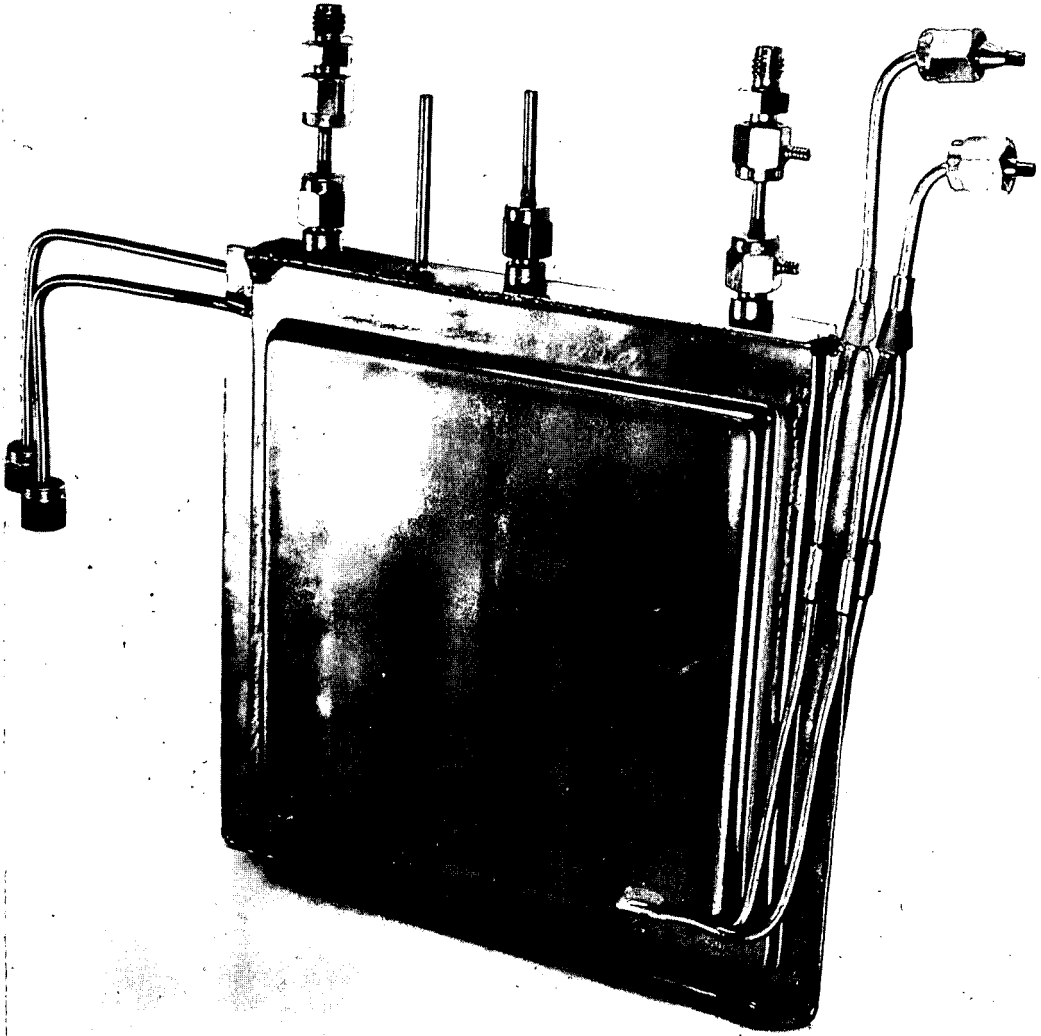


FIG. 7 METHANOL / AIR FUEL CELL

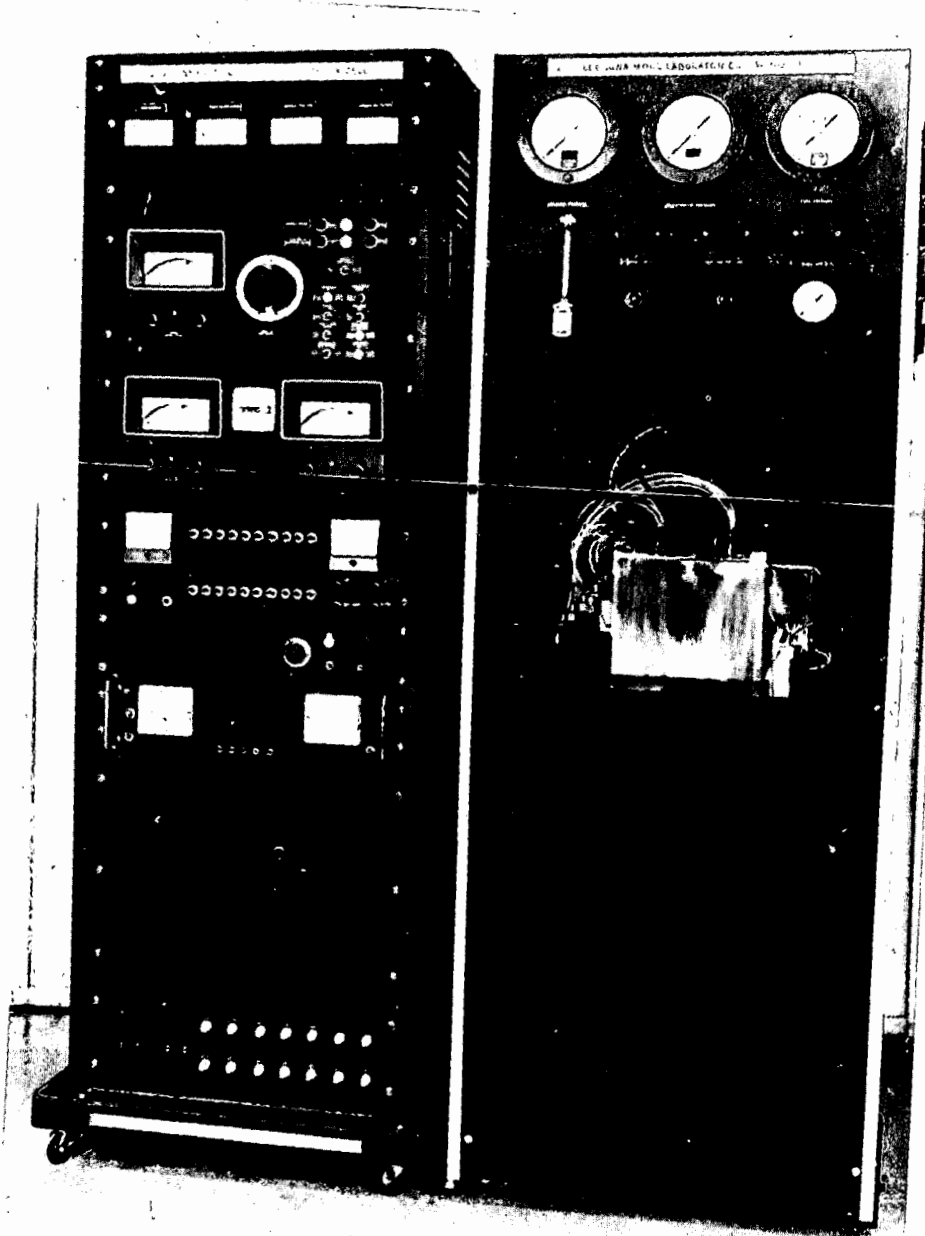


FIG. 8 EXPERIMENTAL 0.5KW INTERNAL REFORMING SYSTEM

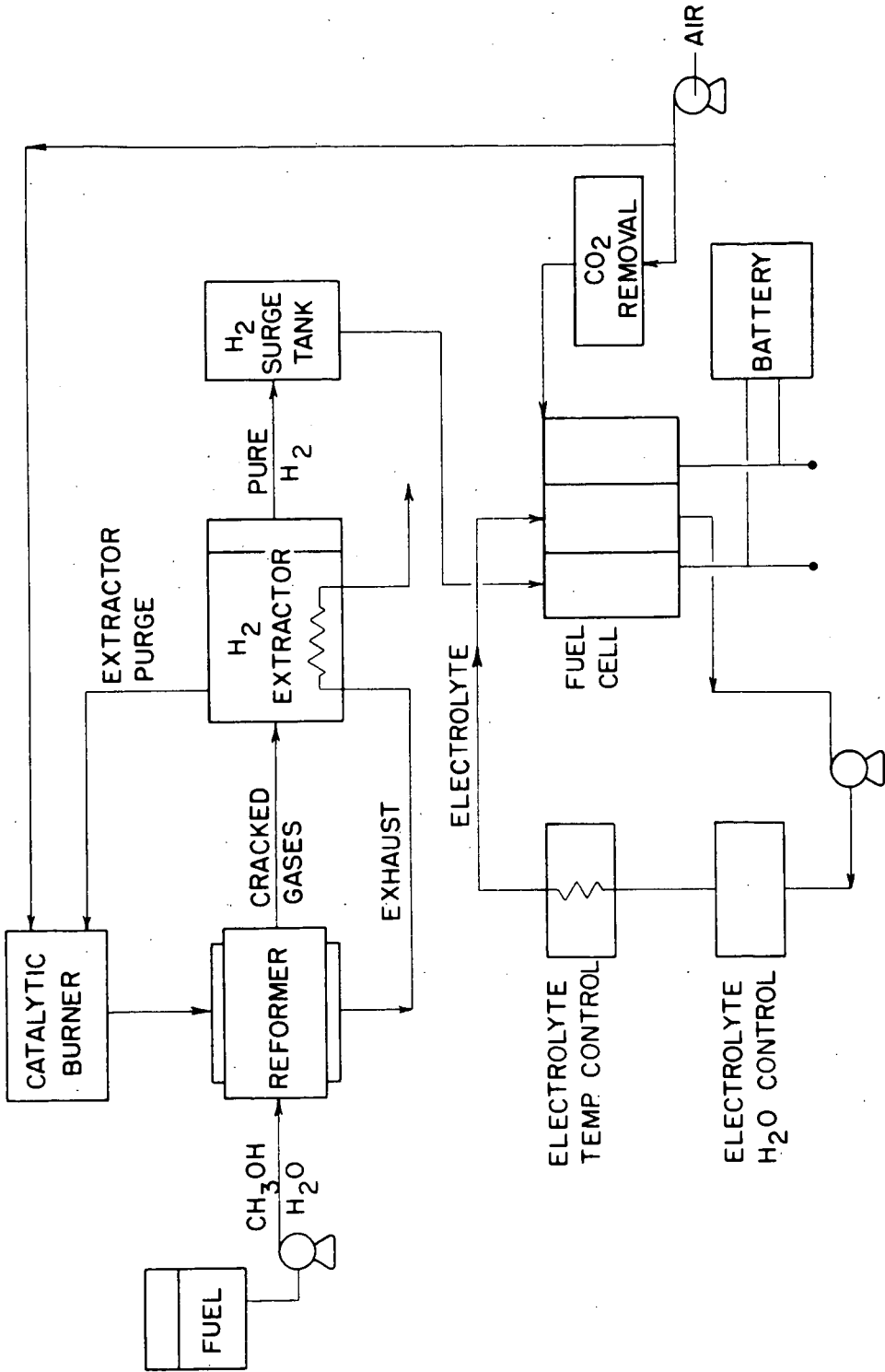


FIG. 9 SCHEMATIC OF EXTERNAL REFORMING METHANOL FUEL CELL

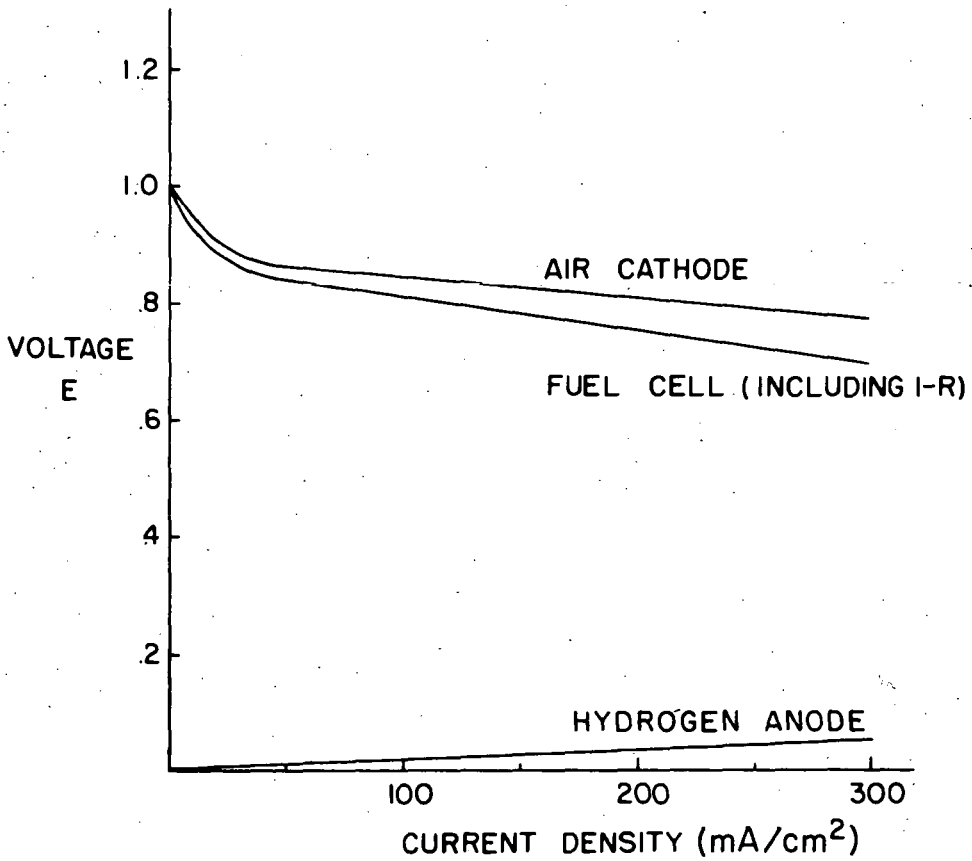


FIG. 10 E/I CHARACTERISTICS - HYDROGEN/AIR CELL

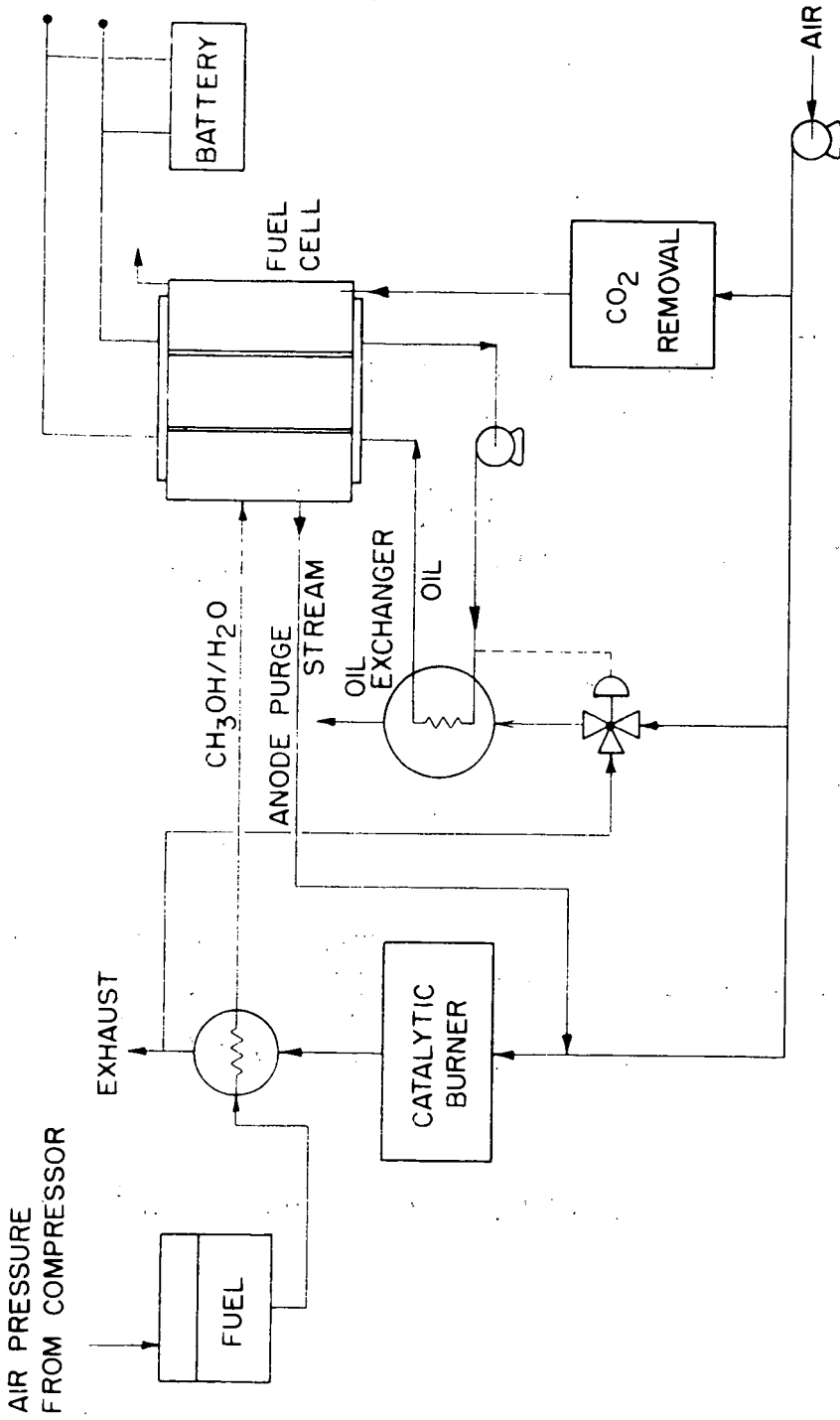


FIG. II SCHEMATIC OF INTERNAL REFORMING METHANOL FUEL CELL

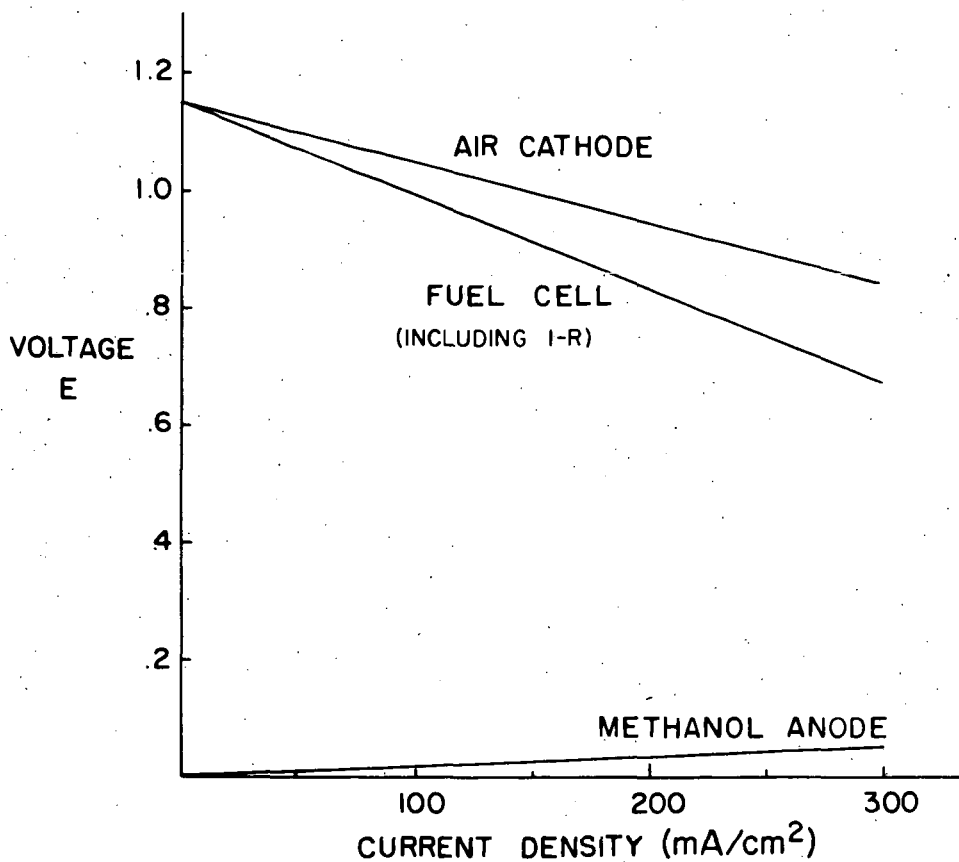


FIG. 12 E/I CHARACTERISTICS-METHANOL/AIR CELL

SOME ASPECTS OF MOLTEN CARBONATE FUEL CELLS

A.D.S. Tantram, A.C.C. Tseung and B. S. Harris

Energy Conversion Limited, Chertsey Road,
Sunbury-on-Thames, England

The ultimate aim of fuel cell development is a system of acceptable capital cost that can operate in an economic manner on low cost fuels. Although much effort has recently been put into investigating the alternative routes, the high temperature cell remains a favoured prospect.

Of the two main classes of high temperature cells (a) solid oxide electrolyte cells and (b) molten carbonate electrolyte cells, the latter has significant advantages in its lower temperature of operation and in the wider available choice of materials.

Work started at Soudes Place Research Institute and continued at Energy Conversion Limited, has investigated a wide range of different concepts of the molten carbonate cell. These may be broadly classified as follows:-

1. Free electrolyte cells.
2. Trapped electrolyte cells.
 - 2.1 Porous magnesia diaphragms.
 - 2.2 "Semi-solid" or "paste" electrolyte diaphragms.

Non-eutectic type.

Inert filler type.

Various combinations and compromises between these types are also possible.

In this paper we are concerned in particular with our experiences with cells based on the inert filler type of semi-solid electrolyte diaphragm.

Before discussing this work, it is worth summarising very briefly our main findings with the other types.

FREE ELECTROLYTE CELLS

The three-phase interface is established by the use of dual porosity electrodes run with a pressure differential. We had great difficulty in fabricating electrodes of sufficient strength at the operating temperature to withstand the necessary differential pressure. The factors contributing to this were:- the very high surface tension of the carbonate melt (see Table 1), the desirability of a small coarse pore size to obtain a high reaction area and, particularly with the cathode, limited choice of materials. From preliminary experiments with cell designs suitable for battery construction, it

was also clear that the problem of sealing the carbonate melt would be extremely severe.

Table 1. Surface Tension of Carbonate Melts, Dynes/cm.

°C	Li, Na, K 9, 6, 5 mol ratio	Li, Na 1 1
430	219.8	
480	217	
530	214	233
580	211	230.4
630	208.2	228

MAGNESIA DIAPHRAGM CELLS

In the absence of any commercial source, we developed our own porous magnesia diaphragms.

The main problem that we found with these cells was loss of electrolyte due to creep. It became clear that a much smaller pore size was desirable, coupled with very accurate control of the maximum pore size. This would prove very expensive in practice. An additional economic factor was the necessity for a machining operation on the sintered diaphragms. Sealing problems were also difficult.

SEMI-SOLID ELECTROLYTE. NON-EUTECTIC TYPE

This type¹ depends on choosing a carbonate composition that is well away from the eutectic, so that there is a range of temperature where the electrolyte body is semi-solid. An example is Li_2CO_3 78%, Na_2CO_3 12%, MgO 10%. The function of the small amount of magnesia in this context is to act as a nucleating agent to ensure the formation of small interlocking crystals when the electrolyte body solidifies after casting. The example given has a usable range from about 530°C (conductivity limit) to about 630°C (strength limit). It collapses under its own weight at 670°C and is completely molten at 690°C. Above this temperature, it can be cast into any desired shape and this facility is the main advantage of this type. We have successfully used this electrolyte in the form of discs, spun cast tubes and in a cell design involving the casting of the electrolyte around performed porous electrodes. The disadvantages are the narrow working temperature range and the fact that the solid:liquid ratio changes with temperature, making interface control difficult and uncertain.

SEMI-SOLID ELECTROLYTE. INERT FILLER TYPE

In the normal version an extremely intimate mixture of a carbonate eutectic and a substantial percentage of very finely divided inert filler (e.g. MgO) is densified to form an impervious electrolyte diaphragm.

General Properties

The physical properties are dependent, in particular, on the particle size of the inert filler and on the percentage used.

At the operating temperature, the carbonate component is molten and in this state the material is somewhat analogous to a clay-water system over a particular range of composition.

Under compression the material behaves in typical fashion, there being an initial elastic period (with some hysteresis) leading to a final yield point, which is quite high enough to make the material of practical use (e.g. >50 p.s.i. for 63% MgO). Compressive creep is extremely small, being undetectable in normal use. Figure 1 shows the integrity of a diaphragm after a 20-day cell test at 650°C, in which a sealing pressure of 10 p.s.i. was used.

Shear strength is, however, very low and shear stresses must be avoided in any cell or battery construction with this material.

Optimum composition is dependent in part on the filler particle size and represents a compromise between strength which increases with filler content and conductivity which decreases with filler content, e.g. for 50 w% MgO the diaphragm factor is 2.5 and for 63.5 w% MgO it is 4.0.

There are also rather less definable requirements associated with the setting-up of an optimum three-phase interface at the electrodes. Electrolyte retention is only a problem at the lower end of the range of usable filler content.

The forces holding these diaphragms together are almost entirely surface tension forces and depend upon there being, in practice, an extremely high meniscus length (molten carbonate - inert filler) at the surfaces of the diaphragm. This is demonstrated by the fact that a sample fully immersed in molten carbonate loses virtually all its compressive strength.

FABRICATION METHODS

Cold Pressing and Liquid Phase Sintering

It is not possible to produce high density diaphragms by this method, although rather better results are obtained if the sintering is carried out in vacuum. (See Figure 2).

Three steps normally take place in a liquid phase sintering. (a) Particle rearrangement under the influence of surface tension forces. (b) An increase in density by a solution and reprecipitation process. (c) Solid state sintering of the solid component. In the present case, we are liable to start with a continuous magnesia network which will resist (a). The solubility of magnesia in the molten carbonates is too low for (b) to appreciably occur and the temperature is too low for appreciable sintering of the magnesia (c). These factors explain why high density diaphragms cannot be made by cold pressing and liquid phase sintering.

Hot Pressing

(a) Above the carbonate melting point.

We have had little success with straight moulding of diaphragms by this method, due mainly to extrusion of the material between plunger and mould. Some experiments with injection moulding did, however, indicate that this would be feasible with high precision equipment.

(b) Below the carbonate melting point.

We find that just below the carbonate melting point the material exhibits a high degree of plastic flow and this method enables us to mould diaphragms to a high density without any of the problems of extrusion or sticking to the mould. The great advantage of this method is that it enables us to fabricate a wide variety of shapes to a finish as good as that of the moulding equipment. Figure 3 shows some electrolyte diaphragms made in this way. They are shown "as pressed," some of the graphite used as the mould release agent still being present. They are cavited to form the electrode gas space, baffled to give good gas distribution and have silver current collectors and connecting gaskets pressed on in the same operation. We have also found it possible to form gasporing in the same moulding operation. It is also possible to press on electrodes at the same time, thus giving a complete unit cell from one pressing operation. (Figure 4). We find, however, that the conditions normally used result in an excessive reduction in electrode porosity leading to poor performance. Subsequent attachment of the electrodes is therefore preferred.

Pretreatment of the material is important. The magnesia filler and the alkali metal carbonates are intimately mixed by ball milling and prefired at 700°C to 750°C. This prefiring treatment is to ensure intimate mixing, complete reaction of impurities and complete elimination of adsorbed water, (more about this later). It is important that the prefiring temperature be above the maximum ultimate cell operating temperature. This pretreatment is repeated at least once more. The material is then ground to below 20 mesh to provide the feed for the hot pressing operation. Alternatively, it may be further ground, cold pressed and sintered, to form a "biscuit" blank for the hot moulding operation.

The effects of some of the variables are shown in figure 2.

One of our standard compositions is 63.5% MgO, which was based on measuring the porosity of pure MgO hot pressed under the same conditions and computing the amount of molten carbonate necessary to just fill this porosity. We see that in practice (figure 2) much higher MgO contents can, in fact, be used due to the lubricating action of the carbonate component.

Our normal selected pressing conditions are 5 t.s.i. at 490°C when using binary eutectic (Na and Li carbonates) and at 385°C when using ternary eutectic (Na, Li, K carbonates).

Our density figures for the carbonate melts are:-(t in°C)

For Li, Na

1, 1 mol ratio, $2.030 - 4.30 \times 10^{-4}(t-500)$ g/cc

For Li, Na, K

9, 6, 5 mol ratio, $2.085 - 4.87 \times 10^{-4}(t-400)$ g/cc

Infiltration

An infiltration method has also been used successfully for the fabrication of electrolyte diaphragms. A cold pressed diaphragm of 100% magnesia will break up on infiltration, but the process may be successfully carried out if the starting material contains an appreciable percentage of the alkali metal carbonates. An example is as follows:-

A mixture of magnesia 63.5% with sodium-lithium carbonates pre-fired, ground and cold pressed at 10 t.s.i. This diaphragm is sintered at 600°C, cooled and placed on a prepressed disc of 100% sodium-lithium carbonate. The whole is then reheated to 600°C for half an hour. The additional carbonate infiltrates into the diaphragm as it melts. There is some danger that the infiltrating liquid will bypass some of the pores and leave these unfilled, but this can be overcome if the operation is carried out under reduced pressure, a carbon dioxide atmosphere being advisable. Excess electrolyte is ground off the diaphragm after cooling. The product contains 46 w% of the carbonate electrolyte, has a density of greater than 97% of the theoretical and the linear shrinkage is less than 0.5%.

Operating Experience

We will limit ourselves here to points that are specifically relevant to the use of semi-solid electrolyte. We have made and tested some 120 2-1/2" diameter cells (20 cm² active area) and about 60 of 4-1/2" diameter (80 cm² active area). We have also made some experimental stacks of 4-1/2" diameter, giving about 50 watts output. Figure 5 shows one of these stacks complete with heater and insulation.

A variety of electrode materials have been used, but a typical example would be -- for the anode, "B" nickel, granulated, presintered and graded to -100 + 120 mesh -- for the cathode, cosintered Ag/Cu₂O/ZnO (25/2.5/72.5% by wt.) and graded -100 + 120 mesh. In both cases these materials are made into a slurry with a silver suspension containing a temporary binder (giving 1% added silver) and applied to the faces of the electrolyte diaphragm in this form. The electrodes are then sintered in situ as the cell is brought up to operating temperature. Typical electrode thickness is 1 mm, porosity 50% on a 3 mm thick electrolyte diaphragm.

As the electrolyte component of the diaphragm melts, it expands to partially wet the electrode and a stable three-phase interface is set up. This process takes rather longer to equilibrate than one might imagine and is illustrated in figure 6, where the internal resistance of a new cell is followed over an initial temperature cycle of 2 hours duration. The extent and location of the three-phase interface will depend on the balance between the surface tension forces in diaphragm and electrodes. It will be affected in particular by the very fine microstructure in the electrode, for instance by the activation treatment mentioned later. These factors are difficult to control and this is one of the disadvantages of this type of cell construction.

Performance and Endurance

We must first of all distinguish between "unactivated" electrodes and those specially activated. The nickel anode may be activated in situ by a controlled partial oxidation, using a small percentage of oxygen in nitrogen such that about 5w% of the nickel is oxidised, followed by reduction with the fuel gas. The effect of such an activation is shown in figure 7.

An electrode activated in this fashion does, however, show a fall in activity with time and after about 60 hours the performance is the same as an unactivated electrode, which would remain unchanged over this period. We have experimented, with some success, with methods of stabilising this activation, but the long term results reported here refer to the lower level of performance. Figure 8 shows the performance obtained with an activated nickel electrode on pre-reacted methane-steam and on hydrogen. Figure 9 shows the effect of the fall in anode activity and the longer term performance deterioration discussed below.

Initial endurance tests with these cells showed that there was a progressive deterioration in performance occurring in the hundreds of hours region. The behaviour was not particularly reproducible and did not show any trend with temperature of operation or with current density and, in fact, similar results were obtained with cells left on open circuit for the bulk of the time. It was suspected that the fall-off was due to deterioration of the electrolyte diaphragms. Physical examination of the diaphragms after the tests, showed the presence of laminar faults. Examples of these are shown in figure 10. It should be noted that we have chosen particularly extreme examples to illustrate the phenomenon, the faults being usually considerably less marked. These faults result in (a) an increased internal resistance and (b) increasing inter-electrode leaks leading to falling performance. Using gas chromatographic techniques we were able to obtain a correlation between falling performance and increasing leaks. The procedure was as follows:-

With the cell on open circuit, hydrogen feed to the anode and air/carbon dioxide to the cathode, the nitrogen content of the anode effluent was analysed. This nitrogen could come by inter-electrode diffusion or by diffusion through a gasket leak from the external air. The cathode feed was then temporarily replaced by methane and the nitrogen estimation in the anode effluent was repeated. In this manner a semi-quantitative measure of both gasket and inter-electrode "leaks" could be obtained. The gasket leak did not normally alter with time and we were, in fact, able to eliminate this, by making the seal directly between the electrolyte diaphragm and the separator i.e. in effect by abolishing gaskets. Figure 11

shows an example of the correlation between falling performance and increasing inter-electrode leak.

Diaphragm deterioration was overcome by ensuring complete elimination of chemisorbed water from the material used for hot pressing. Any still present would be evolved during operation of the cell and initiate the lamination faults. These would tend to get worse with time, due probably to erosion effects arising from chemical combustion of the fuel and oxygen diffusing into the diaphragm. Water is very tenaciously held by magnesium oxide and much longer pre-firing times are necessary than might be thought. In addition, the pre-fired material will quite readily re-adsorb water and strict precautions have to be taken to ensure that this does not occur. Figure 12 illustrates the stable performance that can be obtained when strict attention has been paid to these factors. The increase in performance seen in the middle of this particular test was not explained. Finally figure 13 shows the absence of faults in an improved diaphragm after a cell test of 450 hours.

Conclusions

Practical cells, based on "semi-solid" electrolyte diaphragms, can be made with promising performance and endurance characteristics. Further improvements are desirable and there are indications that these can be achieved.

Careful battery design should be able to obviate the disadvantages of this type of cell and to exploit its advantages.

The hot pressing fabrication technique should be amenable to mass production methods, since the required conditions are not too far removed from existing plastic moulding practice. This could prove an important factor in achieving low capital cost.

THE ANODE MECHANISM

For the high temperature cell to fulfill its promise considerably higher power densities are required. To be able to take logical steps in this direction a better understanding of the electrode processes and their rate controlling steps is desirable. We are, therefore, taking a fresh look at this problem and the preliminary results are reported here. The anode process was chosen for the initial study, since in practical cells the greater part of the polarisation is normally at this electrode.

Experimental

The test cell used is shown schematically in figure 14. Also included, but not shown, were a reference electrode and a thermocouple pocket. Both the counter electrode and reference electrode were of platinum gauze partially immersed in the electrolyte and both were supplied independently with a 2.5:1 air - carbon dioxide mixture. The electrolyte was an equimolar mixture of sodium and lithium carbonates.

The positioning device enabled the electrolyte crucible to be raised or lowered thus, controlling the degree of electrode immersion. Starting with the electrolyte level below the bottom of the test electrode, the crucible is raised slowly until "first

touch" is registered by an electrical continuity test. The results quoted here are all with a further immersion of 0.1 inches. In addition to this there will be a meniscus about 0.25 inches high.

Initially both nickel and silver-palladium foils were chosen for examination, one point being that the large difference in possible hydrogen diffusion rates through the bulk metal could lead to instructive results. The foil electrodes were 0.005" thick and 1.15 cms wide. The silver-palladium used was the 23% silver alloy. The foils were used as received, with no pretreatment.

The anode compartment was swept with a large excess of hydrogen at 1 atm.

Results and discussion

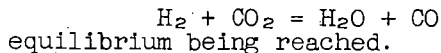
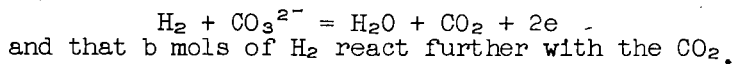
Figure 15 shows the corrosion curve for the silver-palladium obtained under "white spot" nitrogen, and indicates that only relatively low corrosion currents are possible in the potential range of interest.

Figure 16 compares the current voltage curves for hydrogen oxidation on nickel and silver-palladium at 550°C. The nickel curve was not very reproducible. The reproducibility of the silver-palladium curves is discussed later.

Figure 17 shows plots of E versus log i for hydrogen oxidation on silver-palladium at 550°C and 600°C respectively. It is seen that there is a very well defined linear portion extending over nearly two decades.

At this stage it was noticed that the relationship between E and i was very similar to that between E and x, where x describes the composition of a partially reacted fuel in the manner shown below.

Assume that we start with 1 mol of H₂ and that x mols react with CO₃²⁻,



For 1 atm total pressure, the partial pressures in the resulting mixture are therefore,

$$P_{H_2} = \frac{1 - (x + b)}{1 + x}, P_{H_2O} = \frac{x + b}{1 + x}, P_{CO_2} = \frac{x - b}{1 + x}, P_{CO} = \frac{b}{1 + x}$$

and we can write for the water gas equilibrium

$$\frac{(x + b) b}{[1 - (x + b)][x - b]} = K \dots \dots \dots (1)$$

At a given temperature this equation can be solved to obtain values of b to correspond with selected values of x. The corresponding partial pressures may then be derived and, from them, the corresponding values for E using the equation

$$E = \frac{RT}{4F} \log_e K_o P_{O_2}^* P_{CO_2}^* + \frac{RT}{2F} \log_e \frac{P_{H_2}}{P_{H_2O} P_{CO_2}} \dots\dots\dots(2)$$

$P_{O_2}^*$ and $P_{CO_2}^*$ refer to the partial pressures at the cathode. K_o is the equilibrium constant for $2H_2 + O_2 = 2H_2O$.

At a given temperature and for constant cathode conditions we can write

$$E = \text{Constant} + \frac{RT}{2F} \log_e \frac{[1 - (x + b)] (1 + x)}{(x + b)(x - b)} \dots\dots\dots(3)$$

It is found that the plot of E versus $\log_{10} x$ is linear over a wide range and it is the slope (S_x) of this plot that corresponded closely with the observed slopes (S_i) of the initial experimental E - $\log_{10} i$ plots at 550°C and 600°C. These figures are tabulated in table 2.

Table 2. Values of K, S_x , S_i , and α_x .

°C	K	S_x mV	S_i mV	α_x
550	0.219	197	197	0.414
600	0.295	226	233	0.383
650	0.385	246		0.372
700	0.49	262		0.368
887	1	336		0.343

α_x is the value derived from writing $S_x = \frac{2.3 RT}{2F\alpha_x}$

These considerations suggested the following picture. In the low current region (i.e. down to about 0.95v) the most important factor is the diffusion rate of reaction products away from the reaction site, on the immersed portion of the electrode, through the meniscus to the bulk gas. This rate should be proportional to the concentration difference and so the concentration of products at the reaction site has to build up appreciably before a reasonable diffusion rate is possible. This build up will affect the electrode potential in a similar manner to that defined by equation 3. As the current is further increased the rate of hydrogen diffusion to the reaction site would become the most important factor. Confirmatory evidence for this view is that silver-palladium, which has an additional route for hydrogen diffusion through the bulk metal, supports much higher currents than nickel.

A more precise statement of the hypothesis is as follows:-
At a given current the observed polarisation is due to the change in surface concentrations necessary to produce the diffusion rates of both reactants and products to meet the requirements of the processes occurring.

Making the following assumptions:-

The partial pressures of CO₂, H₂O and CO in the bulk gas (H₂ at 1 atm.) are all zero.

The surface concentrations at the reaction site can be described in terms of partial pressures, P_{H₂} etc., in atm.

The diffusion rates are directly proportional to the partial pressure differences.

Rate of discharge of CO₃²⁻ = i (CO₃²⁻ + H₂ = CO₂ + H₂O + 2e) fast.

Rate of formation of CO = y (H₂ + CO₂ = CO + H₂O) fast,

the rates being expressed in units of current, i.e. coulombs/sec. Then we can write,

Rate of H₂ in = i + y = k₁ (1 - P_{H₂}) hence P_{H₂} = $\frac{k_1 - (i + y)}{k_1}$

Rate of H₂O out = i + y = k₂ P_{H₂O} hence P_{H₂O} = $\frac{i + y}{k_2}$

Rate of CO₂ out = i - y = k₃ P_{CO₂} hence P_{CO₂} = $\frac{i - y}{k_3}$

Rate of CO out = y = k₄ P_{CO} hence P_{CO} = $\frac{y}{k_4}$

The k's involve the diffusion coefficient, Henry's law constant and the geometry of the diffusion path. The units will be coulombs. sec⁻¹ atm.⁻¹.

For the water gas equilibrium,

$$\frac{(i + y) y}{[k_1 - (i + y)][i - y]} = K. \quad \frac{k_2 \cdot k_4}{k_1 \cdot k_3} = K^1 \dots\dots (4)$$

For the cell e.m.f. at a given temperature

$$E = \text{Const} + \frac{RT}{2F} \log_e \frac{k_2 \cdot k_3}{k_1} + \frac{RT}{2F} \log_e \frac{k_1 - (i + y)}{(i + y)(i - y)} \dots\dots (5)$$

We cannot solve these equations without a knowledge of the k values, but a certain amount of information can be obtained using the analogy with the equations in x and b , (1) and (3), which can be solved. We find (a) that S_1 will be very little affected by the value of k_1 provided that k_1 is appreciably greater than $i + y$ i.e., provided we are not near the limiting current condition and (b) that S_1 will be appreciably affected by the value of K^1 . The extent of this variation can be seen by comparing the variation of α_x with K in table (2). To explain the experimental fit noted earlier, $\frac{k_2 k_4}{k_1 k_3}$ would have to be fairly close to 1.

Attempts to obtain confirmatory experimental results, however, met with some difficulty. In all cases a well defined linear range on the $E - \log i$ plot was found, the individual curves reproduced well with rising and falling current, and the values of S_1 in a given series increased with temperature. On the other hand the values for S_1 , obtained in different series, done for example on different days, showed a wide scatter. The following figures show the extremes recorded.

(a) At a given temperature (650°C)

Lowest $S_1 = 165$ mV , ($\alpha_1 = 0.555$)

Highest $S_1 = 530$ mV , ($\alpha_1 = 0.173$)

(b) At any temperature.

Lowest $S_1 = 147$ mV , ($\alpha_1 = 0.536$) at 520°C.

Highest $S_1 = 800$ mV , ($\alpha_1 = 0.121$) at 700°C.

At first sight it was difficult to explain these variations on the diffusion theory, since they implied a very wide variation in the value of $\frac{k_2 k_4}{k_1 k_3}$ and it was hard to see how this could occur.

$\frac{k_2 k_4}{k_1 k_3}$

It was, however, noticed that the value of S_1 was dependent on the history of the anode compartment conditions in the following manner. If the anode compartment had been left for a long period under pure hydrogen, low values for S_1 were obtained. If, however, it had been left under carbon dioxide before the tests with pure hydrogen, high values were obtained for S_1 . This observation suggested the following explanation. In the former case some decomposition of the carbonate electrolyte in the anode compartment will occur, leaving it CO_2 depleted and rich in M_2O . This will mean that there is a chemical sink available for the carbon dioxide, produced when taking a current, and would be expected to result in a very high value for k_3 (CO_2) as compared with diffusion through the liquid to the bulk gas. There would also be a tendency for $k_2(H_2O)$ to increase for the same reason, but since the equilibrium



is well over on the carbonate side we might expect the effect on k_2 to be considerably less marked. If this is true then we can see that the value of K^1 will be considerably reduced and this will result in an abnormally low value for S_1 . One can also postulate that when the anolyte has been under CO_2 , but starved of H_2O , similar considerations will dictate a low value for k_3 (CO_2) and a high value for k_2 (H_2O) due to the reverse of reaction (6) above. In this case therefore we would expect a high value for K^1 and hence S_1 . Confirmatory evidence is that, in the CO_2 deficient condition, unnaturally low open circuit voltages were observed on hydrogen. This is to be expected if the concentration of oxygen ions in the anolyte is increased⁽²⁾.

Finally the limiting current region was explored for various hydrogen-carbon dioxide mixtures on silver-palladium and the results are shown in figure 18. With pure hydrogen the limiting current region was very unstable.

Conclusions

It is possible to explain the experimental results in terms of a diffusion control mechanism, but further, more rigorously controlled experiments are necessary to obtain a valid quantitative correlation. We postulate that at a given current density the observed polarization is due to the change in surface concentrations necessary to produce the diffusion rates of both reactants and products to meet the requirements of the processes occurring. It follows that in the lower current density region the diffusion rates of the products are the dominant factors and that in the higher current density region the rate of hydrogen diffusion will become dominant. In the latter case the rate of diffusion of hydrogen through the bulk metal can be of great significance.

An essential part of the treatment is the assumption that the water gas shift occurs at the electrode surface and reaches equilibrium.

Any explanation in terms of activation control seems unlikely in view of the wide variation in α_1 that was found.

Partial decomposition of the anolyte could strongly influence the diffusion rates of CO_2 and H_2O .

The investigation will continue with studies on other metals and other fuels.

ACKNOWLEDGEMENTS

The authors wish to thank their colleagues, past and present, who have contributed to this work and the Board of Energy Conversion Limited for permission to publish.

REFERENCES

- (1) H. H. Chambers and A. D. S. Tantram, British Patent 806592.
- (2) J. Dubois and R. Buret, Bulletin de la Societe Chimique de France, 1963, p.2552.

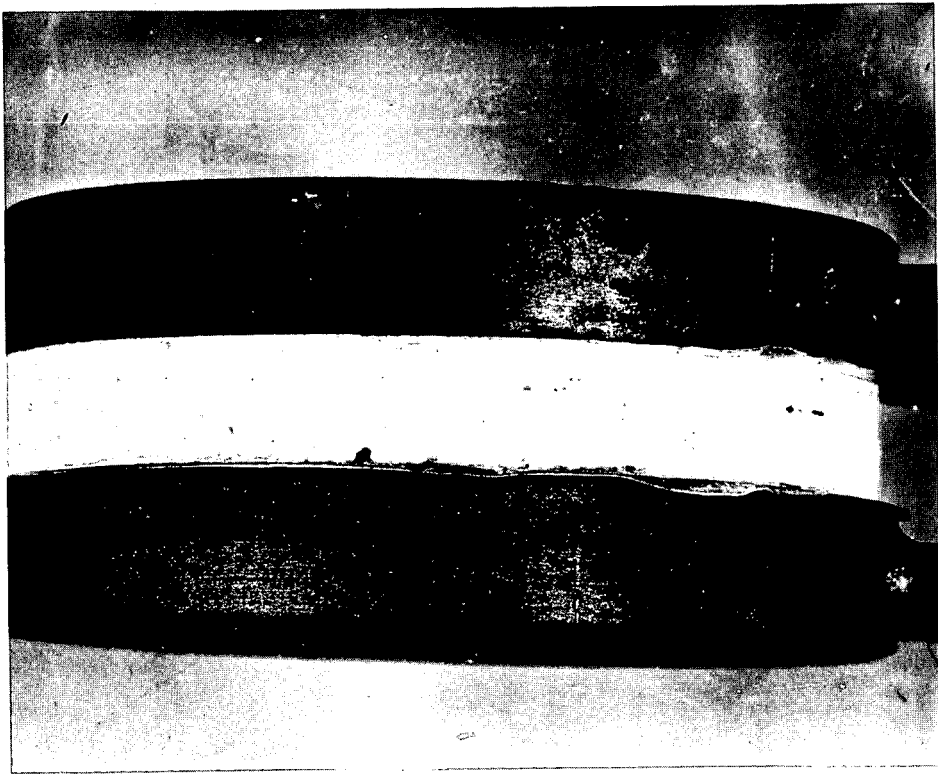


Fig. 1.-CELL AFTER 20 DAYS AT 650°C AND 10 PSI SEALING PRESSURE, SHOWING LACK OF DIAPHRAGM CREEP

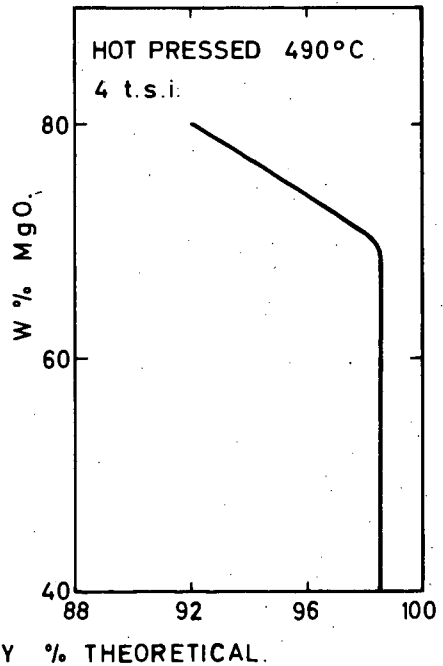
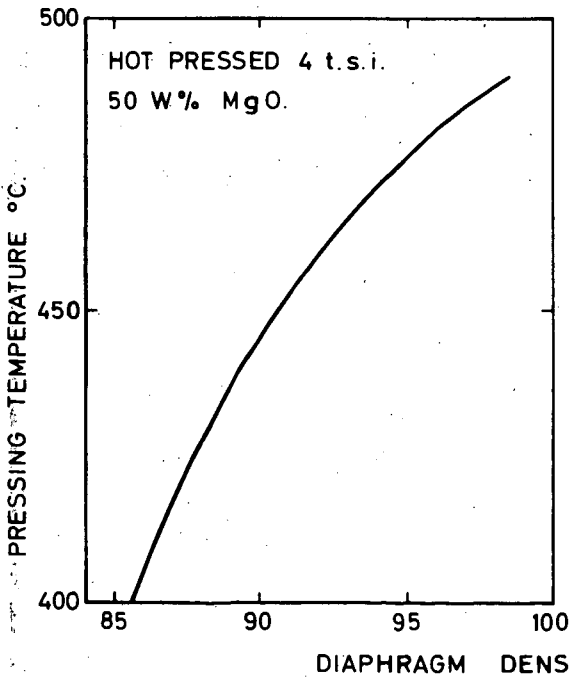
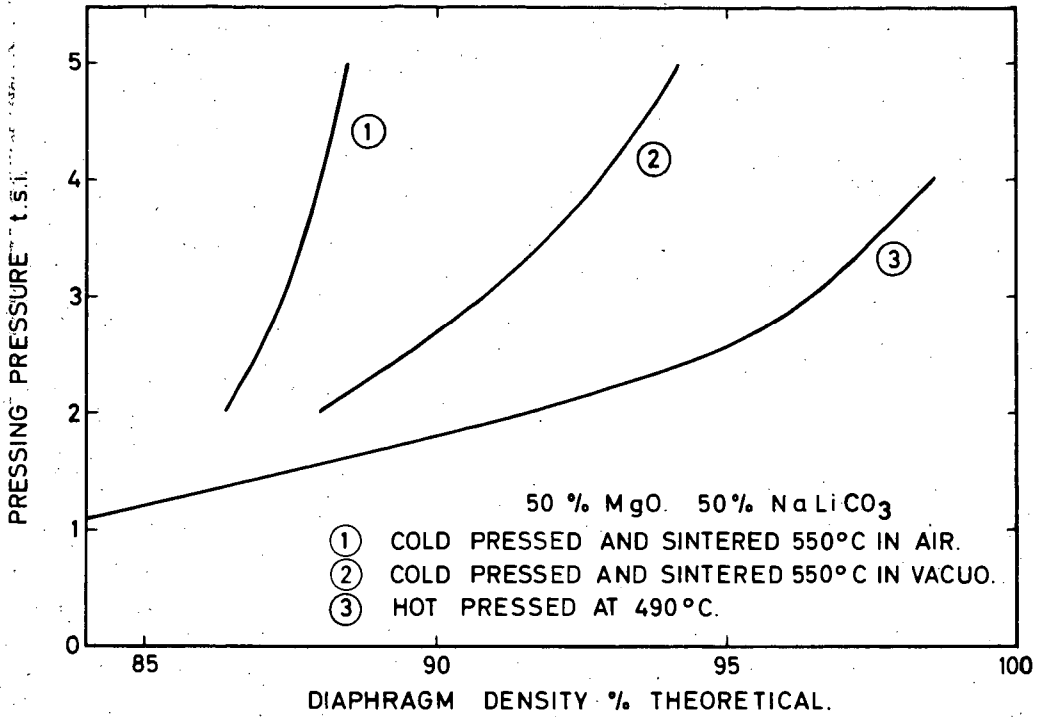


FIG. 2 THE EFFECT OF PRESSING CONDITIONS.

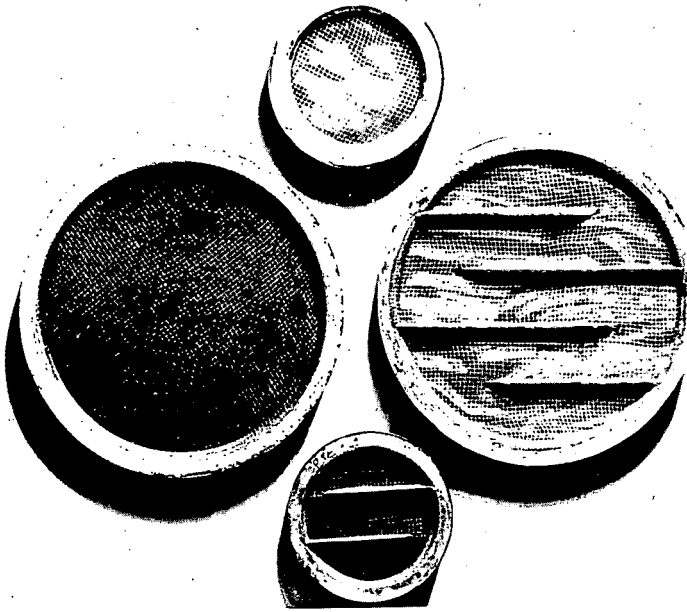


Fig. 3.-HOT-PRESSED ELECTROLYTE DIAPHRAGMS, 2.5" AND 4.6" IN DIAMETER



Fig. 4.-SECTION OF INTEGRAL CELL ELEMENT MADE BY SINGLE HOT-PROCESSING OPERATION

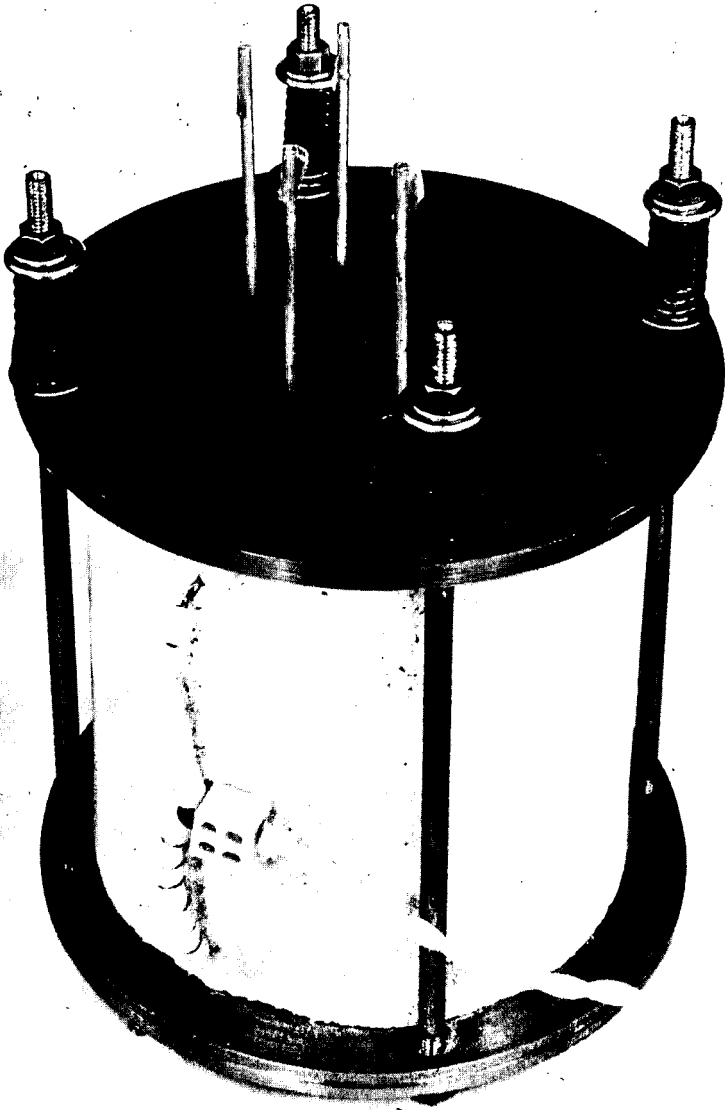


Fig. 5.- FIFTY-WATT BATTERY WITH HEATER AND INSULATION

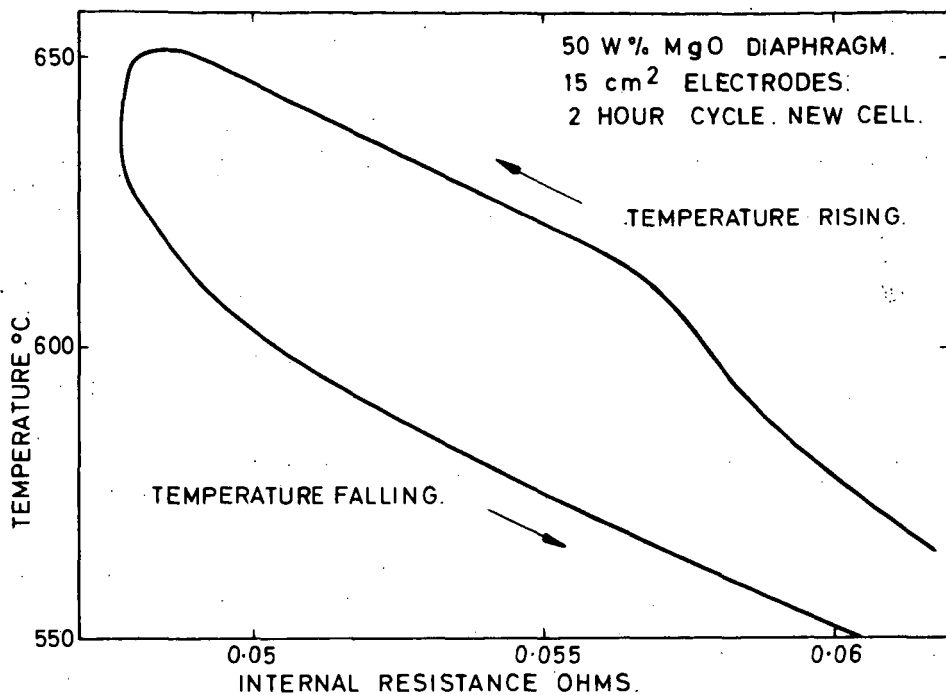


FIG. 6 ESTABLISHMENT OF 3 PHASE INTERFACE.

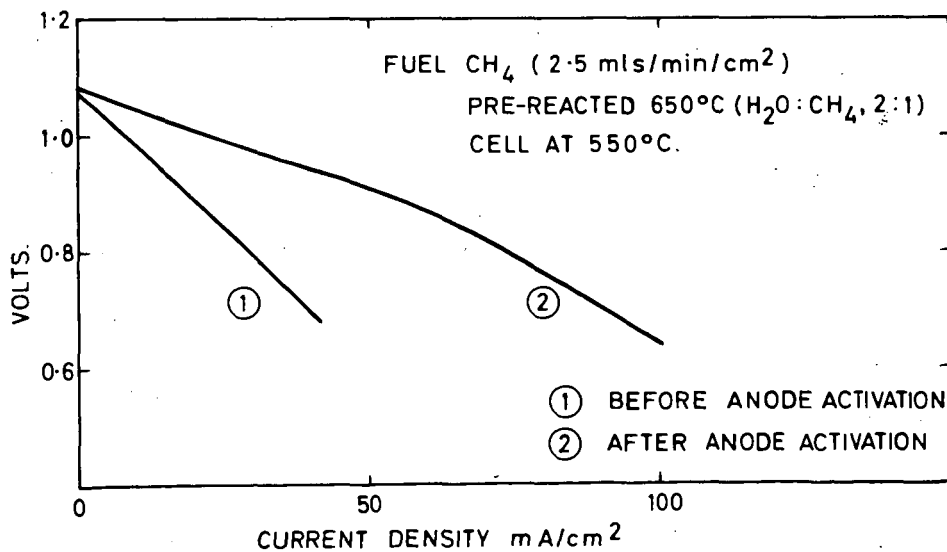


FIG. 7 EFFECT OF ANODE ACTIVATION.

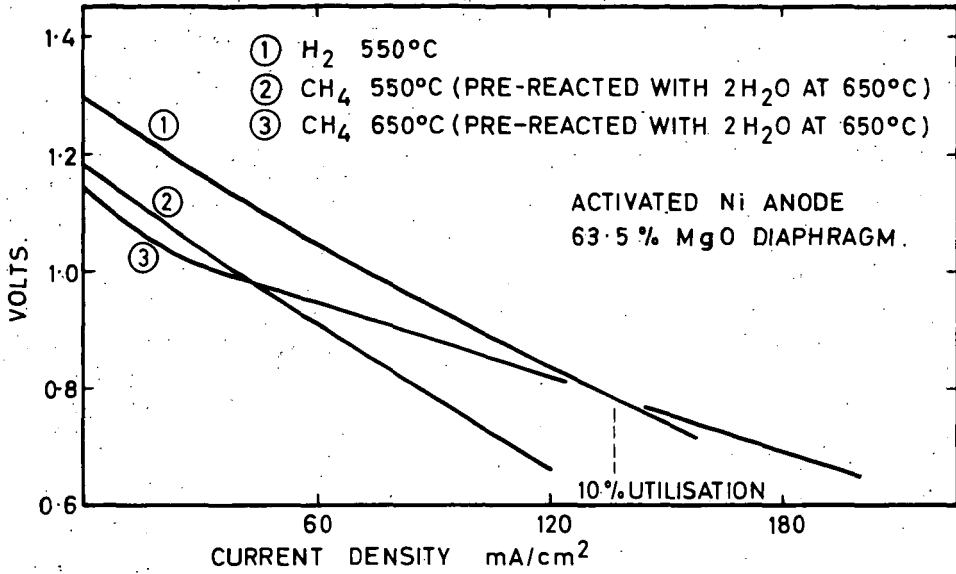


FIG. 8 INITIAL PERFORMANCE CELL H.P. 48.

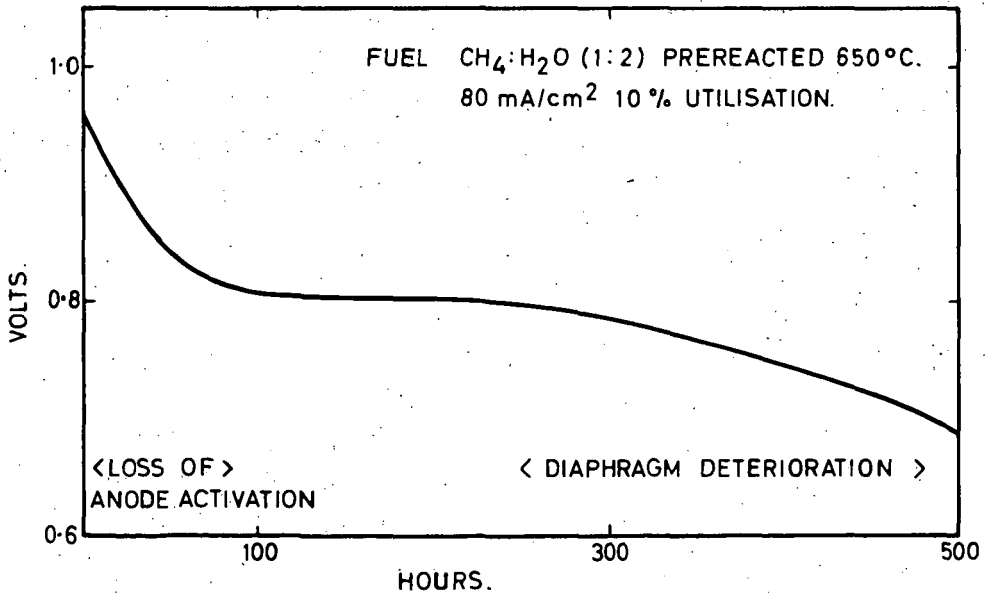


FIG. 9 ENDURANCE OF CELL H.P. 48 AT 650°C.

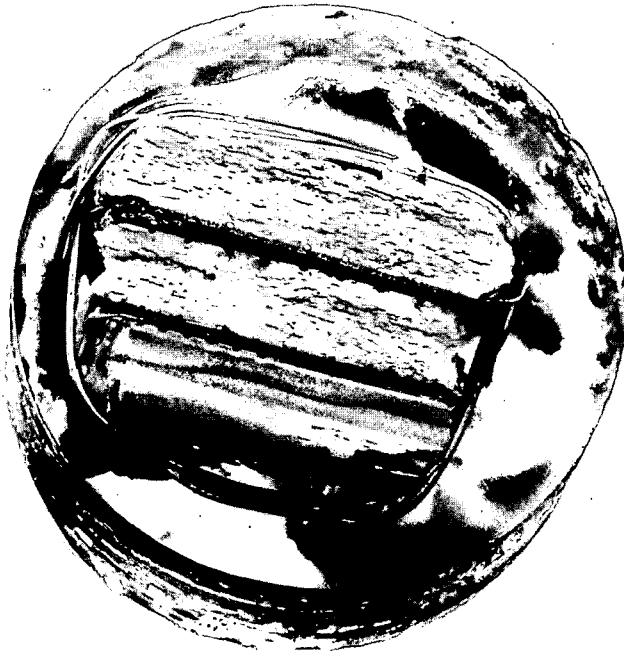


Fig. 10.-SECTIONS OF ELECTROLYTE DIAPHRAGMS AFTER 450 HOURS AT 600°C, SHOWING SEVERE LAMINAR FAULTS

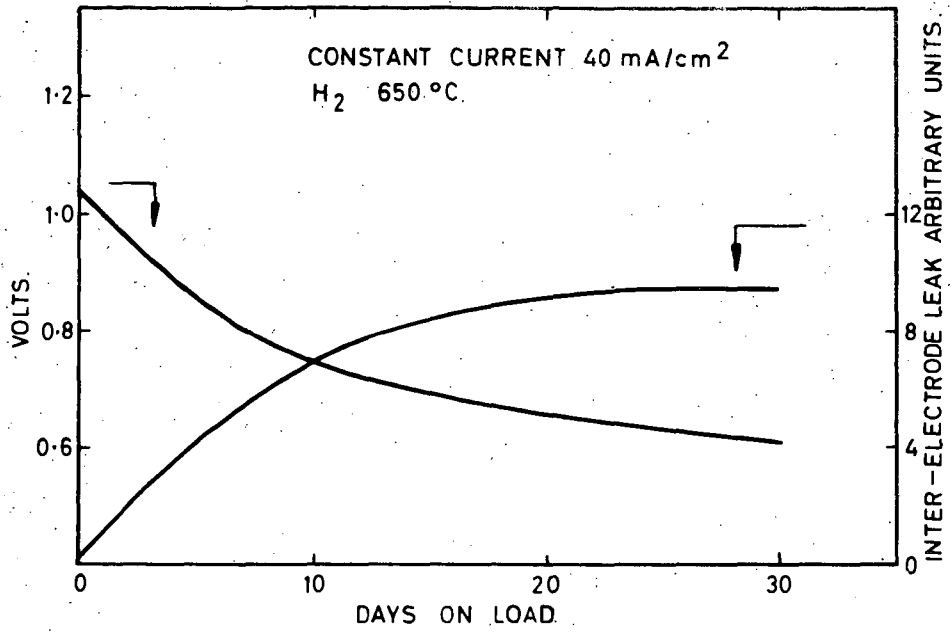


FIG. 11 DETERIORATING DIAPHRAGM. PERFORMANCE—LEAK.

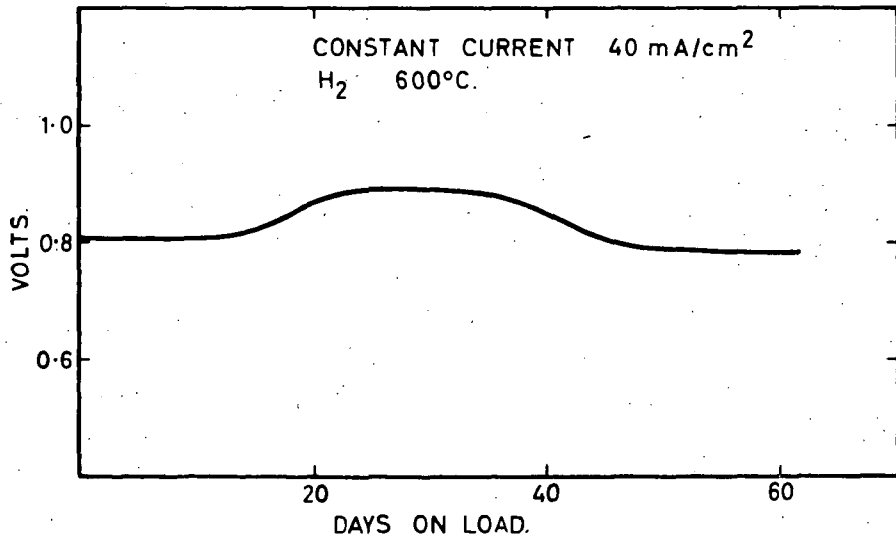


FIG. 12 IMPROVED DIAPHRAGM. ENDURANCE.

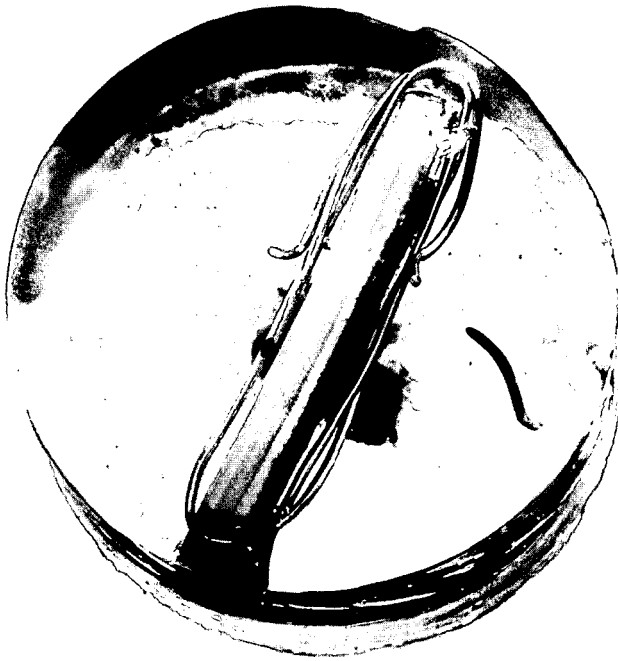


Fig. 13.-SECTION OF IMPROVED DIAPHRAGM AFTER
450 HOURS AT 600°C, SHOWING ABSENCE OF LAMINAR
FAULTS (see Fig. 10)

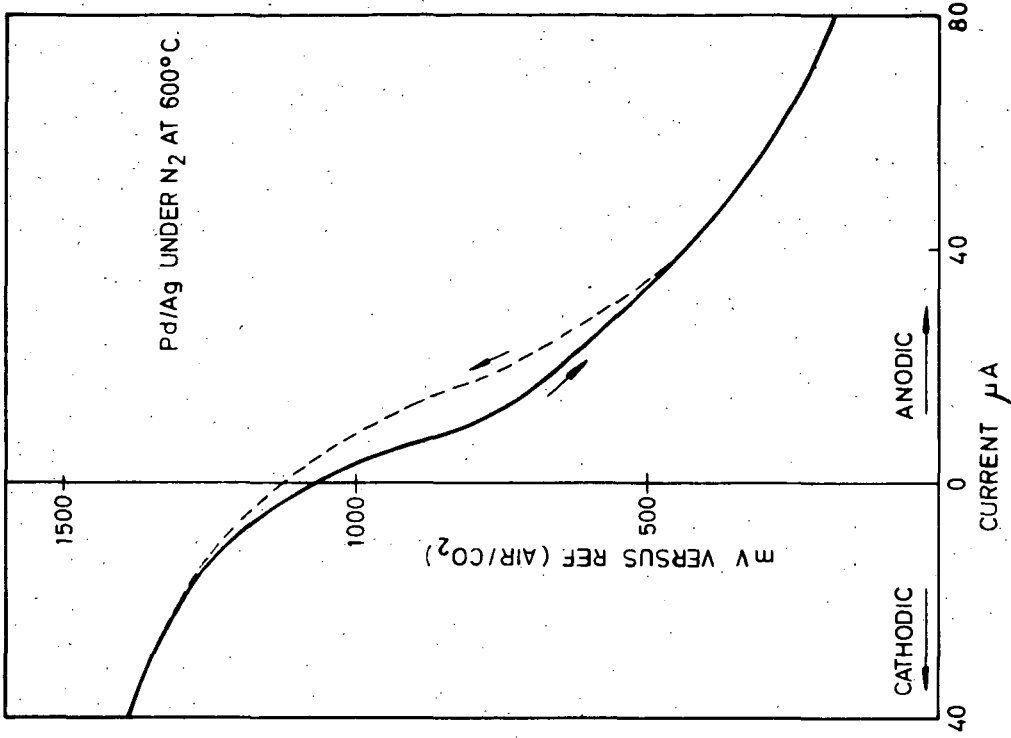


FIG. 15 CORROSION CURVE FOR Pd/Ag.

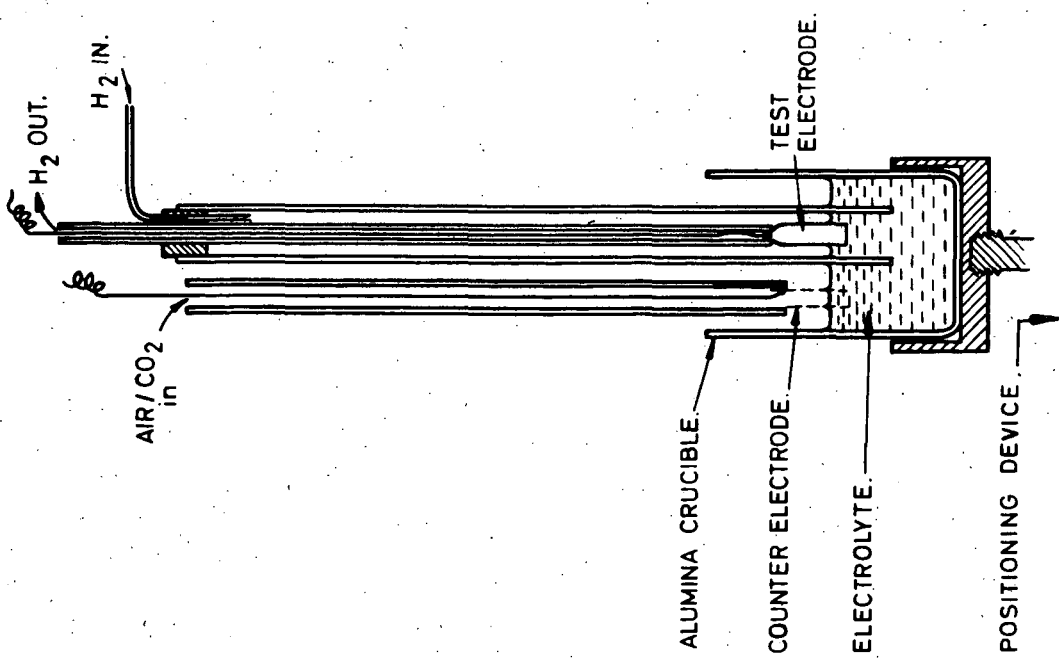


FIG. 14 SMOOTH ELECTRODE TEST CELL.

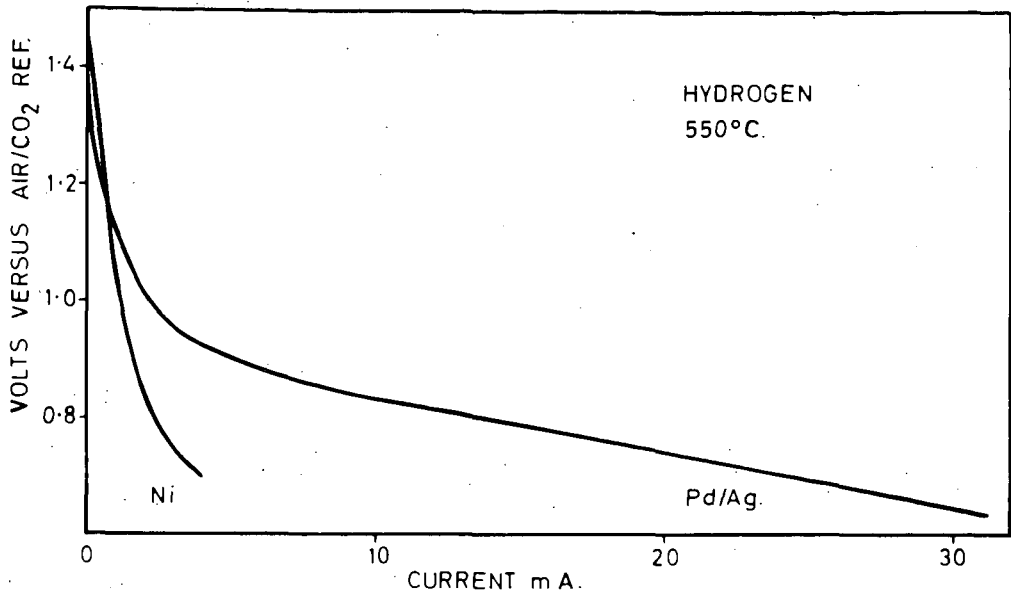


FIG.16 COMPARISON OF Ni AND Pd/Ag FOIL ANODES.

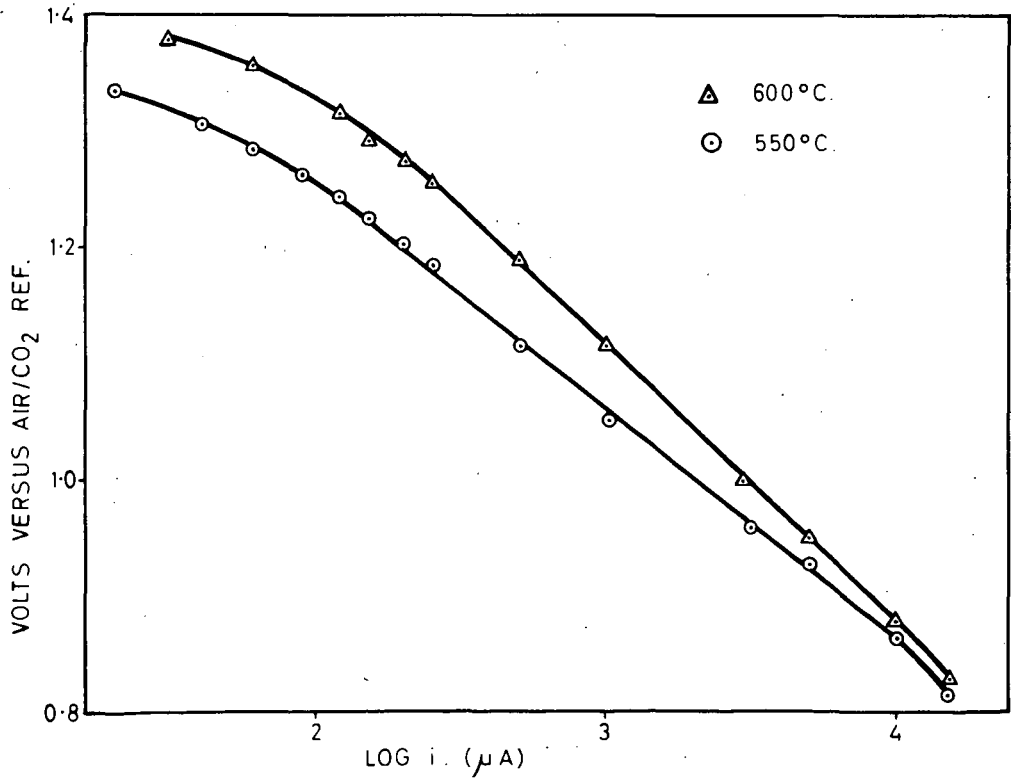


FIG.17 E-LOG i PLOTS. H₂ ON Pd/Ag.

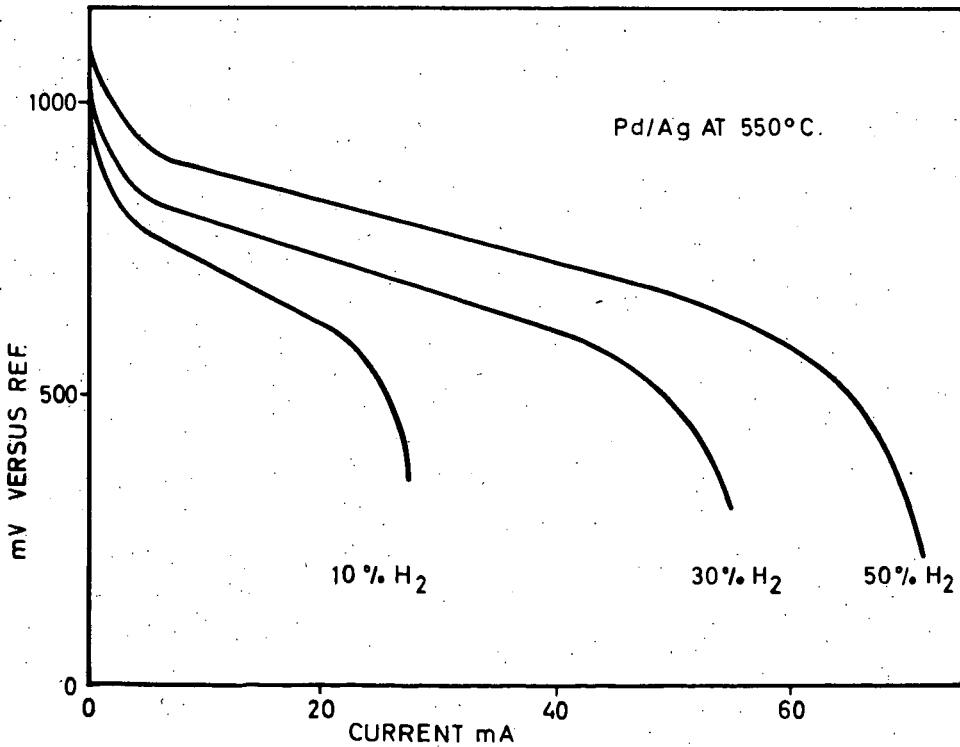
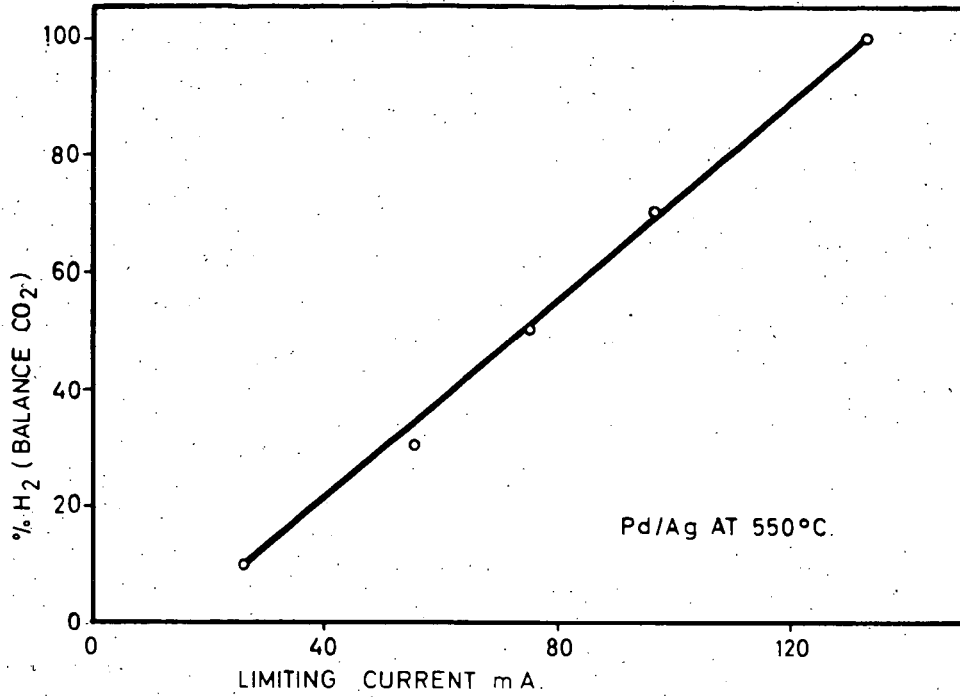


FIG. 18 LIMITING CURRENTS ON Pd/Ag.

THE DOUBLE-DUTY ANODE FOR
MOLTEN-CARBONATE FUEL CELLS

R. W. Hardy, W. E. Chase, and J. McCallum

Battelle Memorial Institute
Columbus, Ohio

INTRODUCTION

One of the principal objectives of research on molten-carbonate fuel cells¹⁻⁸ has been a battery which would operate on a carbonaceous fuel and air. Natural gas has been of special interest because of its low cost and wide availability.^{1,3,7,9} However, in the references cited it has been recognized that hydrocarbons do not supply much current when used directly in the fuel cell. There must be a preceding chemical step such as steam reforming or partial air oxidation to yield electrochemically active species, predominantly hydrogen and carbon monoxide. The requirements for effective steam reforming in a fuel cell were discussed in a previous paper,⁸ and the advantages of carrying out the steam reforming on the anode were described.

Three advantages are realized by steam reforming natural gas directly on the anode:

- (1) Good heat exchange between the exothermic electrochemical oxidation and the endothermic steam-reforming reaction.
- (2) Less steam required because product steam from electrochemical oxidation of hydrogen is available.
- (3) More extensive conversion of methane because products ($H_2 + CO$) are being consumed.

The possibility of realizing these advantages led to the first goal of electrochemical research. The goal was to obtain both reforming and electrochemical oxidation on the anode.

THE DOUBLE-DUTY-ANODE CONCEPT

The idea of carrying out steam reforming on the anode itself has been proposed by previous workers. Linden and Schultz suggest it in a patent,¹⁰ and Schultz et al.¹¹ describe results of some reforming experiments with methane-steam mixtures on nickel battery plaques. Sandler⁴ described results of experiments with mixtures of natural gas and steam reformed in a separate catalyst chamber in contact with the cell. Schultz's

data indicated that at 730 C, 15 mole percent hydrogen would be found in a mixture reformed on a nickel battery plaque, and 12 percent would be found when reforming on the electrode holder alone. The equilibrium composition is about 75 percent hydrogen. Thus, nickel battery plaques are not particularly effective. Sandler reported almost complete (i.e., equilibrium) conversion of methane to hydrogen on his unspecified catalyst at 580 C.

The performance of all-nickel porous bodies as steam reformers might be improved by forcing the steam-methane mixture through the pores of the coarse layer rather than simply passing the gas mixture along one face of the porous plaque and allowing the mixture to diffuse into the reaction zone. It was to obtain this "forced-by" operation that the double-duty anode shown in Figure 1 was designed. The term "forced-by" is used to distinguish this mode of fuel feed from other modes such as diffusion, "blow-through", and "dead-end".

The electrode is designed for use with a free electrolyte; therefore, it is a two-layer, double-porosity electrode. That is, there is a fine-pore layer which is flooded with electrolyte during operation, sealing one face of the coarse layer against gas leakage. By sintering the other face of the coarse layer to the electrode holder, a gas passage is formed so that fuel gas introduced at one edge of the electrode is forced through the coarse layer parallel to the electrolyte-gas interface and out the opposite edge. The use of forced flow requires that pressure drop be considered. For long flow paths, it would be impossible to maintain the meniscus in the fine layer near the exit edge without exceeding the bubble pressure near the inlet. A rule of thumb adopted for designing electrodes was that the pressure drop between the inlet and exit edges should not exceed 10 percent of the bubble pressure of the fine-pore layer.

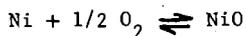
To meet the pressure drop requirements for large-area electrodes, a holder was designed which provided short flow paths without restricting the overall dimensions of the electrode. This design is shown in Figure 2. The fuel inlet and outlet channels are interlaced to force the methane-steam mixture through a section of the coarse layer.

OPERATIONAL LIMITS FOR DOUBLE-DUTY ANODE

Most fuel batteries to be economically successful must convert a large percentage of the fuel to electricity. This requires both extensive conversion of fuel to products and high electrochemical efficiency. While much emphasis has been placed on the latter condition (i.e., voltage efficiency), many investigators seems to have neglected, so far, the first requirement (i.e., extensive conversion). When the products of the electrochemical reaction are gases, not only does dilution of the fuel occur, but the products reduce the reversible potential as their concentration increases.

This was well emphasized by Broers and Ketelaar¹² and by Chambers and Tantram, who showed the effect of extent of conversion on the theoretical voltage of a cell.

Equilibrium gas compositions were calculated for each cell in a six-cell series-fed module (see Reference 8 for model). The calculated compositions for a 1:1 methane-steam mixture are given in Figure 3. It is apparent that most cells will be supplied with H₂ + CO if adequate reforming occurs. Double-duty anodes were operated on the composition corresponding to 70 percent electrochemical oxidation. This composition was designated "lean fuel gas". In the six-cell modules, the electrochemical consumption was projected as 84 percent; therefore, the last of the six cells must consume about half of the fuel value supplied to it. The goal established was 100 ma/sq cm at a potential more negative than -0.78 volt versus ORE* with 50 percent consumption of fuel. (The goal was also established on the basis of the design study.) This potential was chosen because nickel is thermodynamically stable to oxidation according to the reaction



at potentials more negative than -0.78 volt versus ORE when a_{NiO} = 1 (i.e., when the melt is saturated with NiO) and no other reactions occur.

The potentials calculated (assuming equilibrium) for the fuel mixture entering several cells are given in Table 1. Thus, the limitations imposed on the potential of the anode in the sixth cell by gas composition

TABLE 1. OPEN-CIRCUIT POTENTIAL OF FUEL GAS MIXTURES

Cell (of 6)	Open-Circuit Potential, at 1.4 Atm, vs ORE ^(a)
1 entering	-1.22
4 entering	-0.98
6 entering ("Lean Fuel Gas")	-0.91

(a) See footnote, page 5, for description of Oxygen Reference Electrode (ORE).

and by the nickel corrosion potential leave only 0.13 volt for polarization.

* Unpublished results. "ORE" is the Oxygen Reference Electrode, a reproducible, simple reference electrode for use in molten carbonates. It consists of a platinum wire spiral partially immersed in molten carbonate and bathed with a mixture of 70% CO₂ and 30% O₂. With proper construction and special attention to isolation of the electrolyte chamber from the bulk electrolyte, potentials are within 5 mv of the thermodynamically calculated values. It is reversible within the loading limits of a potentiometric recorder. In principle, this electrode is like those described by Stepanov and Trunov¹³ and by Janz and Saegusa.¹⁴

OPERATION OF THE DOUBLE-DUTY ANODE ON A
LEAN FUEL GAS MIXTURE

To establish that the proper flow pattern could be achieved, electrodes were operated on fuel mixtures containing hydrogen and carbon monoxide before using methane-steam mixtures. Experiments on stability of the forced-by mode were combined with experiments to determine the extent of the fuel utilization.

First experiments were performed with 2-sq-cm electrodes mounted in a holder of the type illustrated in Figure 4. The fuel gas was introduced at the arc-shaped recess on one side and was removed at the recess on the opposite side. Stability of the forced-by mode was established in several experiments where current densities up to 100 ma/sq cm were obtained at -0.78 volt versus ORE. Occasional flooding of the anode occurred when fuel pressure dropped accidentally or intentionally. Flooding was readily corrected by closing the exit line to force electrolyte out of the coarse-pore layer. No permanent loss of performance resulted from flooding. Thus, stable electrode operation is possible with the forced-by mode.

Most of the electrodes were operated for only a few hours at a given performance level to establish that the mode of operation was stable. Some failures occurred, resulting in loss of gas pressure. Failures were traceable to poor bonding of the electrode to the holder or of the coarse layer to the fine layer. But, satisfactory long-term performance was indicated by operating an anode for 11-1/2 days. Initially the electrode and associated tubing system showed little leakage, but at the end of 11-1/2 days the leakage of gas into the melt had become too great for further results to have practical significance. Performance remained the same throughout except during one purging required to remove a flooding condition. On lean fuel gas (18 percent H₂ + CO) the current density was 75 ma/sq cm at -0.80 volt versus ORE. Fifty to sixty percent of the fuel value was converted electrochemically throughout the 11-1/2-day operation. This established that good fuel utilization could be obtained along with adequate performance.

Cause of the gas leakage can be seen on the photograph in Figure 5. Two types of failure are apparent. The separation in the coarse layer seen in the section is responsible for the large bulge in the center. With active fuels which do not require steam reforming, separation has little effect on electrode performance. Separation is a mechanical problem and can be corrected by improved sintering technique and by the use of a mechanical support in the form of a honeycomb alumina separator between electrodes in a cell which reduces the unsupported span of the sintered structure.

Pockmarks and the small mounds of powder which appear predominantly at the edge of the electrode were the sites of gas leakage. The location of pits near the exit side and of powder deposits near the inlet side suggests that the gradient in reduction potential from inlet to outlet sides is the cause of this type of failure. A gradient in the reducing power of the gas phase will result in a similar gradient in the melt within the pores of the anode. In more oxidizing regions nickel dissolves; in more reducing regions it deposits. Small particles, released from the porous matrix at one point, are suspended in the melt and are incorporated in the surface where nickel ions deposit. Despite the potential seriousness of the loss of material, two measures can be proposed to reduce the transfer of nickel:

- (1) Provide more uniform gas distribution to minimize the reduction gradient across the anode.
- (2) Overlay the anode surface with a fine mesh screen to retain particles loosened by dissolution of nickel. Electroformed nickel screens of 1000 lines per inch are available and provide the equivalent of a specimen prepared by powder metallurgy with large particle-particle contact. Such screens have given satisfactory performance in short-time experiments where the screen was used as the fine-pore layer.

During the operation of this small (2-sq-cm) anode, a mass spectrometric analysis was made of a sample of exit gas. On a dry basis, 95 percent of the sample was carbon dioxide. The hydrogen-to-carbon monoxide ratio was 1 to 1.6, indicating that even without a special water-gas shift catalyst about one-third of the current was derived from carbon monoxide. This result means that it will not be necessary to convert all the methane to hydrogen, and the water-gas shift need not be complete.

A laboratory-model fuel cell having 18-sq-cm electrodes was used for several experiments with lean fuel gas. The anode holder of Figure 2 was used in the laboratory cell. Problems of sealing the cell against electrolyte loss were avoided by dipping both electrodes into a pot of molten carbonate. A reference electrode was included in the setup for recording single electrode potentials. The best performance obtained with one of these anodes on lean fuel gas was 25 ma/sq cm at -0.78 volt versus ORE for about two days. The performance of the 18-sq-cm electrode was somewhat low because of design and fabrication problems. Separation of the anode from the holder allowed fuel to bypass some sections of the electrode, resulting in a reduction of the effective area. Improvements in the design and fabrication are expected to bring the level of performance of the large anode up to that of the 2-sq-cm anode, or 100 ma/sq cm at -0.78 volt versus ORE.

STEAM REFORMING OF METHANE
ON ANODE STRUCTURES

After demonstrating that the double-duty anode would operate satisfactorily in the forced-by mode and that the lean fuel gas reaching the last of a series of six cells could sustain adequate current densities, the next step was use of a methane-steam mixture in the double-duty anode. A few experiments with nickel double-duty anodes revealed little activity for steam reforming, in general agreement with the work of Schultz et al.

A suitable steam-reforming catalyst was sought for incorporation into the nickel matrix. A survey of the literature revealed that a suitable supported catalyst should be nickel on periclase (natural magnesium oxide). Near-theoretical conversions of methane-steam mixtures to hydrogen and carbon monoxide were reported.¹⁵ Magnesium oxide is resistant to attack by molten alkali carbonates, as is nickel in the fuel atmosphere.

Several trial compositions lead to a suitable mixture of nickel and periclase powders which maintained structural integrity after pressing and sintering. The compact consisted of 15 weight percent periclase and 85 percent nickel. Both were in the form of 100-micron powders. After pressing and sintering under hydrogen, the compact was treated with nickel nitrate solution and dried on a hot plate. The nickel nitrate was decomposed and reduced simultaneously by heating in a hydrogen atmosphere to 760 C, slightly above the operating temperature of the cell.

Prior to making fuel electrodes, small-scale steam-reforming experiments were carried out with the catalyst-nickel powder mixture. The small-scale reformer consisted of a 1/8-inch Inconel pipe (0.269-inch ID) with brass tees silver soldered on each end. A 1/4-inch-OD Inconel tube with 200-mesh nickel screen over the end was inserted into the pipe. The pipe was oriented vertically in a 1-1/4-inch-diameter, 12-inch-long tube furnace, and 1.4-cm layer of unsintered nickel nitrate-treated mixture was packed onto the screen. The system was sealed well enough to keep the leak rate at only 1 ml of hydrogen in 13 minutes at 6 psig. The ends of the furnace were insulated, and heating tapes were used on the entrance line to keep the temperature above 100 C.

The usual test procedure was as follows: (1) purge this reactor with hydrogen, (2) heat to 760 C to decompose the nickel nitrate, (3) hold 1/2 to 1 hour at temperature to reduce the nickel oxide in the periclase, (4) adjust the temperature to the value shown in Table 2, and (5) purge from 4 to 6 hours with methane-steam mixture at the pressure shown before sampling the exit gas for analysis by mass spectrography.

The flow rate of the methane was adjusted to give a residence time of about 0.1 minute. A blank run was made with nickel powder in the reformer tube. Analytical results of these two experiments and the calculated equilibrium composition are given in Table 2.

TABLE 2. COMPOSITIONS OF MIXTURES RESULTING FROM
STEAM REFORMING OF METHANE

Condition	Pres- sure, psig	Tempera- ture, C	CH ₄	H ₂	CO	CO ₂	Percent- age Reaction (a)
Theoretical Equilibrium	5.9	727	7.8	69.2	20.8	2.2	74.6
Nickel Powder	5.5	732	97.5	0.3	0.8	0.3	1.1
Catalyst Mixture	5.6	727	9.4	68.8	17.9	3.9	70

(a) Calculated from:¹⁶

$$\% \text{ reaction} = \left[1 - \frac{\% \text{ CH}_4}{\% \text{ CH}_4 + \% \text{ CO} + \% \text{ CO}_2} \right] 100.$$

Percentage reaction, calculated by the equation of Arnold et al.,¹⁶ is a measure of methane reacted. The extent of the water-gas shift reaction cannot be measured by the equation. The results demonstrate the efficacy of the catalyst mixture for steam-reforming methane. A number of other experiments with differing amounts of catalyst and somewhat different temperatures and pressures also gave reaction percentages in the region of the theoretical values. These other experiments support the validity of the conclusion that the catalyst mixture is effective. The short residence time permits use of a 0.05 to 0.06-inch-thick coarse layer in an anode operating at 100 ma/sq cm. A small double-layer anode containing 15 weight percent catalyzed periclase in the coarse layer was also prepared. It was a structurally integral disc after pressing and sintering.

SUMMARY

Experiments have shown the feasibility of obtaining good steam-reforming activity from a supported nickel steam-reforming catalyst. It has also been demonstrated that such mixtures can be incorporated in a structurally integral two-layer electrode.

Anodes were designed for dual-purpose operation in a free-electrolyte molten-carbonate fuel cell. The ability of the anode structure to function properly with the forced-by fuel flow mode was demonstrated. Stable operation at 100 ma/sq cm at -0.80 volt versus ORE was obtained with a fuel mixture containing only 18 percent hydrogen and carbon monoxide. Such operation demonstrates that adequate performance can be obtained while electrochemically oxidizing 85 percent of the fuel value in a methane-steam mixture as required for the battery model discussed in an earlier paper. Further work is needed to establish long-time performance of the double-duty anode with methane-steam mixtures.

The authors wish to thank members of the Fuel Cell Research Group, who sponsored this work, for permission to publish.

REFERENCES

- (1) G.H.J. Broers, "High Temperature Galvanic Fuel Cells, Ph.D. Thesis from University of Amsterdam, 1958.
- (2) E. Gorin and H. L. Recht, Chem. Eng. Prog., 55, 51 (1959).
- (3) H. H. Chambers and A.D.S. Tantram, in "Fuel Cells" (G. J. Young, ed.), p. 94. Reinhold Publishing, New York, 1960.
- (4) Y. L. Sandler, J. Electrochem. Soc., 109, 1115 (1962).
- (5) I. Trachtenberg, J. Electrochem. Soc., 111, 110 (1964).
- (6) V. S. Daniel'bek, M. Z. Mints, V. V. Sysoyeva, and M. V. Tikhonova, in "Soviet Electrochemistry", Vol. 3, p. 173. Consultants Bureau, New York, 1961.
- (7) L. G. Marianowski, J. Meek, E. B. Schultz, Jr., and B. S. Baker, in "Proceedings of the 17th Annual Power Sources Conference" (PSC Publications Committee), p. 72. PSC Publications Committee, P.O. Box 891, Red Bank, New Jersey, 1963.
- (8) R. W. Hardy and J. McCallum, in "Fuel Cells" (prepared by Editors of Chemical Engineering Progress), p. 45. American Institute of Chemical Engineers, New York, 1963

- (9) G.H.J Broers, M. Schenke, and G. G. Piepers, Advanced Energy Conversion, 4, 131 (1964).
- (10) H. R. Linden and E. B. Schultz, Jr., U.S. Patent 3,146,131, August 25, 1964.
- (11) E. B. Schultz, Jr., K. S. Vorres, L. G. Marianowski, and H. R. Linden, in "Fuel Cells", Vol 2, (G.J. Young, ed.), p. 24. Reinhold Publishing, New York, 1963.
- (12) G.H.J. Broers and J.A.A. Ketelaar, in "Fuel Cells" (G. J. Young, ed.), p. 78. Reinhold Publishing, New York, 1960.
- (13) K. G. Stepanov and A. M. Trunov, Dokl. Akad. Nauk.SSSR, 142, 866 (1962).
- (14) G. J. Janz and F. Saegusa, "The Oxygen Electrode in Fused Electrolytes", Technical Report No. 13 (September, 1961), AD263952.
- (15) C. H. Riesz, H. A. Dirksen, and W. J. Pleticka, "Improvement of Nickel Cracking Catalysts", ICT Research Bulletin 20, Institute of Gas Technology, Chicago, 1952.
- (16) M. R. Arnold, K. Atwood, H. M. Baugh, and H. D. Smyser, Ind. Eng. Chem., 44, 999 (1952).

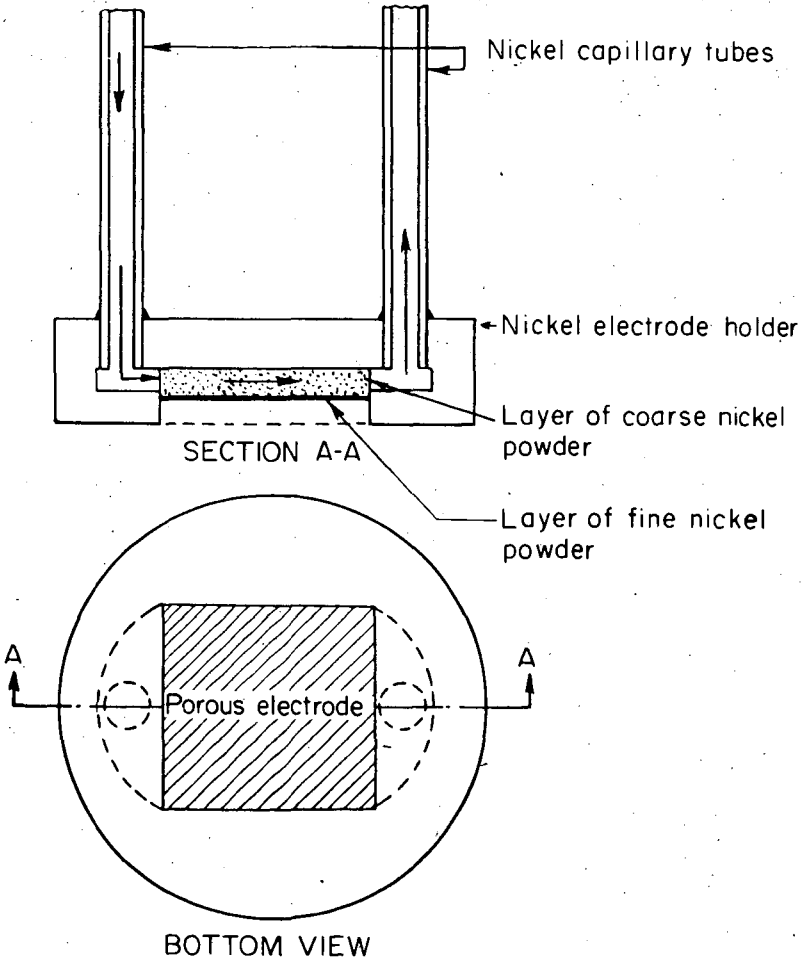
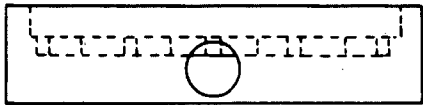
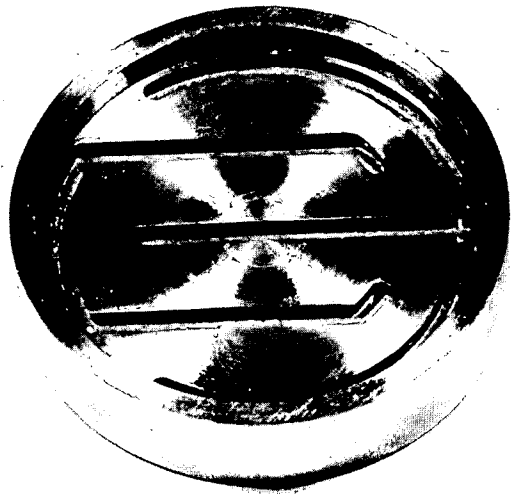
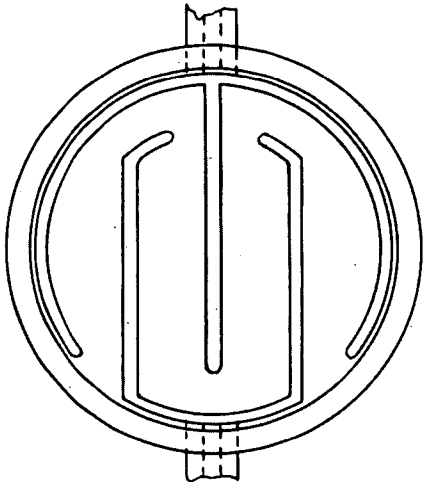


FIGURE 1. DOUBLE-DUTY ANODE DESIGN SHOWING FORCED-BY MODE.
(WHEN COARSE LAYER CONTAINS CATALYST THE ELECTRODE PERFORMS BOTH FUNCTIONS, STEAM REFORMING OF METHANE AND ANODIC OXIDATION OF FUEL.)



Anode Holder



FIGURE 2. HOLDER FOR LARGE DOUBLE-DUTY ANODES. ELECTRODE AREA 18 SQ CM.

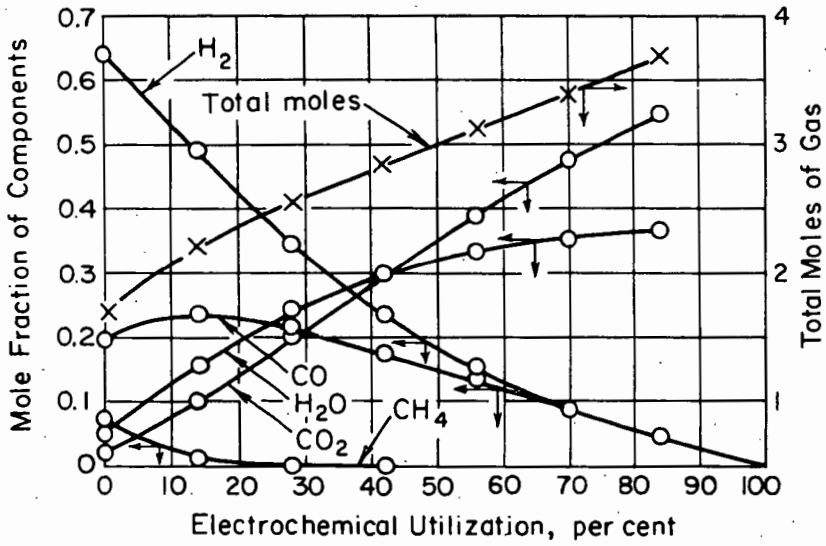


FIGURE 3. CALCULATED EQUILIBRIUM GAS COMPOSITION IN A FUEL BATTERY SUPPLIED WITH 1:1 METHANE:STEAM MIXTURE AT 1000 K AND 1.4 ATMOSPHERES.

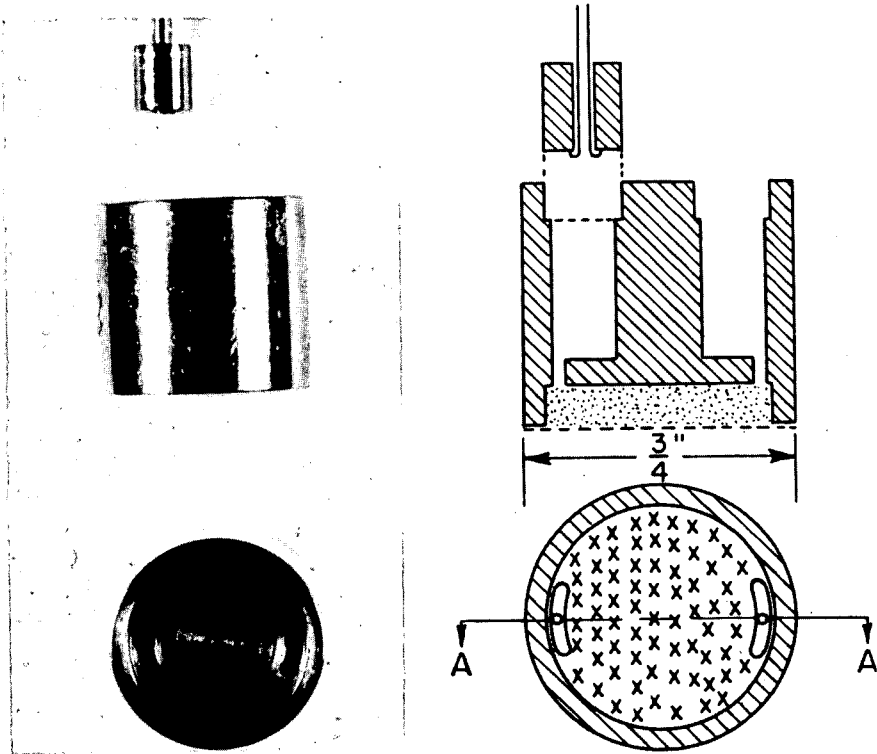


FIGURE 4. DETAILS OF 2-SQ-CM ANODES. ONE GAS INLET TUBE WITH FERRULE IS SHOWN.

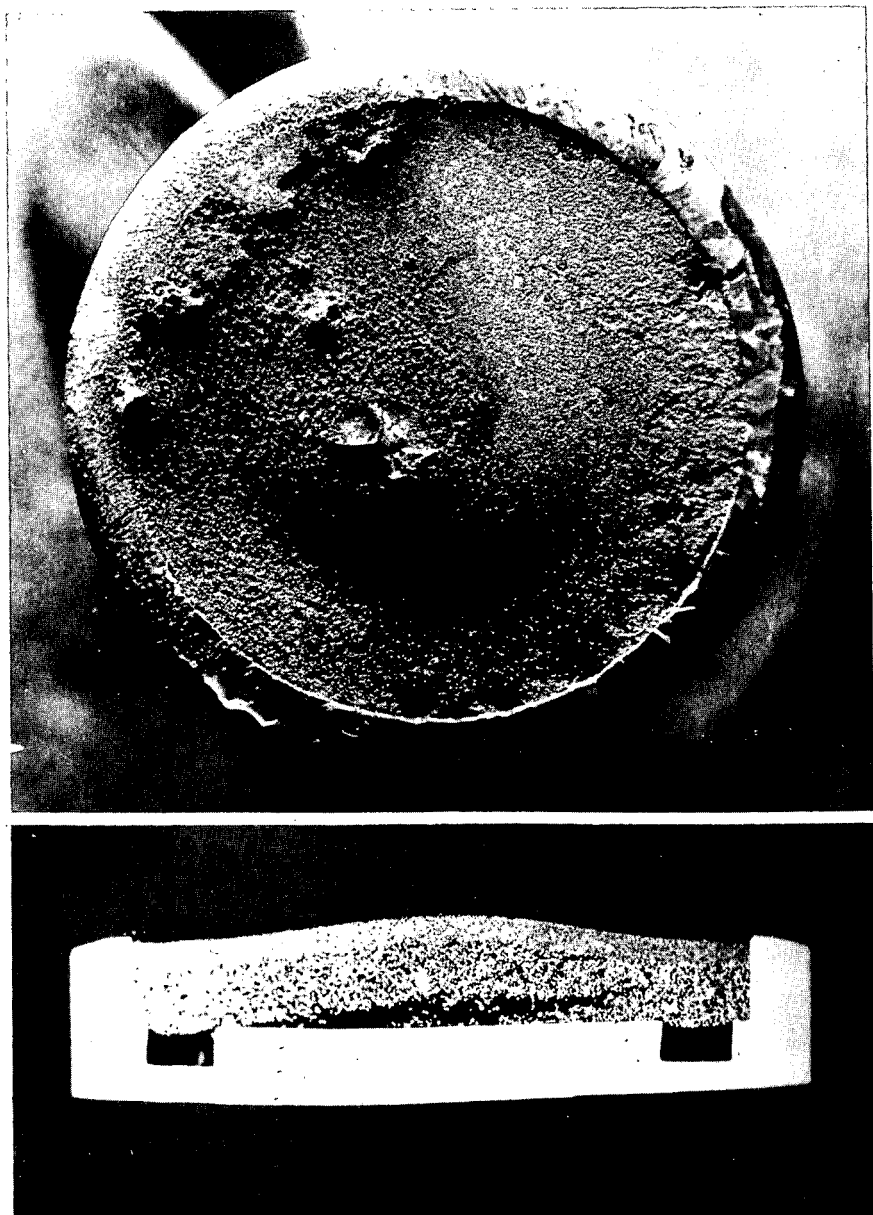


FIGURE 5. APPEARANCE OF A 2-SQ-CM ANODE AFTER 11-1/2 DAYS OF OPERATION ON LEAN FUEL GAS.

Long run experiments on high temperature
molten carbonate fuel cells

G.H.J. Broers and M. Schenke

Central Technical Institute T.N.O., The Hague, Netherlands *)

1. INTRODUCTION

Research on high temperature fuel cells of the molten carbonate electrolyte type, by the Dutch organisation T.N.O., was taken up in 1950. The development of this work has been described in a series of publications [1] - [6]. Comments on the work can also be found in [7] and [8].

A significant step towards the realisation of the strictly necessary gastightness was made by the application of the so-called paste electrolyte [4], [5]. It is obtained by blending an inert powdered solid such as MgO with a given amount of binary or ternary alkali carbonate mixture (Li_2CO_3 , Na_2CO_3 , K_2CO_3).

Above the eutectic melting point of the carbonates (500°C for Li-Na; 396°C for Li-Na-K) a stiff and dense paste can be obtained when the inert solid to carbonates weight ratio remains above a certain critical value. This value depends on the particle size (and shape) of the solid constituent and the composition of the carbonate mixture. As a rough-and-ready rule, a 50 solid/50 liquid weight ratio will yield a rather stiff paste when the particle size of the solid (MgO) is below 1 micron; but closer readjustments have to be made in accordance with the basic materials used. A too high liquid content will cause plastic flow, a too low one causes an unnecessarily high electrolyte resistance. Under optimal conditions, the specific resistance of a typical MgO/ternary carbonate paste is about two times as large as the corresponding pure liquid resistance (paste resistance $\sim 1.5 \Omega \text{ cm}$ at 700°C).

The experiments to be discussed here were all conducted on a laboratory scale. It was felt that technological development work was justified only if, in addition to leaktightness, the following demands could be satisfied:

- 1) a specific power output of at least 50 mW/cm^2 at 0.5 volt or better,
- 2) fuel and oxidant utilisation of at least 80%, at current densities of the order of 100 mA/cm^2 ,
- 3) a cell life of at least several months at the just mentioned power output, with the aim of reaching a life of the order of three years [6], [9] in future developments.

2. CELL CONSTRUCTION, ELECTRODES AND FUELS

For purposes of fundamental research, a high temperature cell should meet the following demands: 1. perfect gastightness; 2. absence of any parasitic current paths, such as caused by metallic gaskets in contact with the electrolyte; 3. reliable contacts between the electrodes and the electrolyte; 4. presence of a suitable reference electrode, connected to the system by some form of electrolytic bridge; 5. no galvanic contacts with the surrounding heating furnace; 6. appropriate means to know the degree of galvanic turnover, that is the ratio of the Faradaic current to the fuel and oxidant feed rate.

*) Correspondence on this subject to the laboratory address:
198, Hoogte Kadijk, Amsterdam-C, Netherlands.

2.1. Cells

The mentioned demands are satisfactorily met by the constructions shown in Fig. 1 and Fig. 2. In Fig. 1 the paste disc is pressed firmly against the inner wall of a high-purity Al_2O_3 tube at about 500°C . There is virtually no reaction between the alumina material and the carbonate melt when the former has been pretreated with a small quantity of molten carbonate for a few days. The working electrodes are pressed against the electrolyte by means of two additional Al_2O_3 tubes with a number of openings at the side of the electrodes, providing gas passages from inside to outside or conversely.

The pressing force on these tubes can be carefully controlled by means of springs with screw adjustments at their cold ends.

The reference electrode is a Pt or Au wire, dipping into a Al_2O_3 capillary filled with electrolyte paste. This "paste bridge" serves as a Haber-Luggin type connection to the disc surface. The phase boundary of the reference wire thereby is effectively screened from the electrolyte disc proper, and no ill-defined stray currents can pass through the reference wire, such as is most likely the case with so-called "idle electrodes". (The latter have their phase boundary situated direct in the current path between the working electrodes.) The reference is flushed with the same gas as the working electrode.

Two lead wires may be connected to each of the working electrodes, one serving as current lead and the other as potential lead. Resistance changes of each individual electrode can thus be measured too.

Fig. 2 depicts a simplified version of the cell of Fig. 1, being easier to assemble (as is evident from the figure). In this version, the reference electrode is a Pt wire wrapped around the outside of one of the gas sealing Al_2O_3 tubes. Use is made of the (in itself tedious) "creeping" effect of the carbonate melt along the wall of the tube. The "creeping film" stabilises within one or two days of cell operation (it comes to a stop at the colder parts of the tube) and forms a very effective electrolytic bridge between the wire and the ring-shaped periphery of the paste disc.

Whereas in Fig. 1 the reference potential is equal within ± 5 mV to the corresponding working electrode potential at open circuit, the reference potential in Fig. 2 depends on the gas atmosphere in the heating furnace. Addition of a small CO_2 flush to the air inside the furnace yields very stable potentials.

Great care must be taken to avoid direct contact between any hot parts of the cell and the (a.c. heated) furnace. The just mentioned "creeping" may otherwise lead to severe hum pick-up and electric leakage to either the a.c. mains or the ground.

2.2. Electrodes

The porous fuel electrodes discussed in this paper were all nickel specimens of various origin. Screens, sieve plates, sintered carbonyl nickel, nickel plates for secondary batteries and "fiber nickel" plates were used, as well as presintered nickel powder obtained by

* E.g. "Clevite" porous Ni; Clevite Corporation, Cleveland, Ohio, U.S.A.

** Huyck Corporation; Milford, Connecticut, U.S.A.

reduction of NiO with H₂. The commercially available types have no special advantages over Ni powder electrodes and are, at least at the present-day prices, by far too expensive to be used for anything else but research purposes.

The porous air electrodes were either of silver or copper oxide.

Silver electrodes were used in the form of wire screens and/or very thin layers of Ag powder (0.1 mm or less), adhered direct to the electrolyte surface.

The use of CuO as air electrode was reported by Justi and co-workers [7], [10], in connection with work on solid carbonate electrolyte fuel cells. In our case, commercially available CuO powder was mixed with some 10% of Cu powder. Small discs of about 1 mm thickness were pressed and subsequently sintered at 800°C in an air atmosphere. In the first few experiments, the discs were connected to all-copper current leads, in order to make sure that the electrochemical activity could be attributed solely to the CuO - Cu₂O system. In later tests, current leads of stainless steel or Pt wires were connected to the CuO material, thus avoiding gradual oxidation of the leads in long run experiments.

Whereas in low temperature cells the initially chosen porosity, pore size distribution and electro-catalytic activity of the electrodes is of crucial importance, a quite different situation exists in high temperature cells. Sintering effects, anodic dissolution and cathodic precipitation, and both surface- and bulk oxide formation under varying polarization strongly tend to alter the initial electrode structure. Figs. 3a and 3b show nickel anode specimens before and after use respectively. Initially, the commercially available material* had a porosity of 70% and a thickness of 1.0 mm. Fig. 3a is a microphoto of this material. Fig. 3b similarly shows the same material after 625 hours of continuous operation at 700°C and (nominally) 100 mA/cm², on an equilibrium mixture of H₂, CO, H₂O and CO₂. (iR-free polarization about +110 mV relative to open circuit.)

The thickness had shrunk to 0.6 mm (40% decrease) and a lateral shrinkage of about 15% was observed.

Evidently it is of no use to preselect electrode structures for high temperature cells on any basis different from long term operation experience. One might state that the high temperature cell tends to seek its own operating level, and not the one preferred by the investigator on the basis of initial electrode structures.

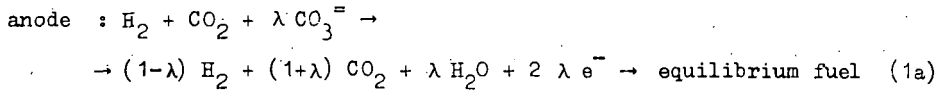
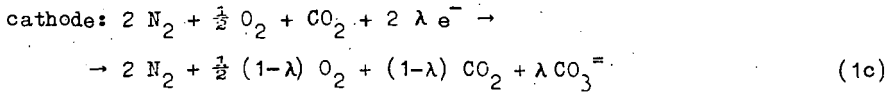
Also, conclusions about cell performances over periods of a few days have little meaning. Both overoptimistic and overpessimistic impressions may then result. An example of the latter will be shown in Sec. 3, Fig. 5.

2.3. Fuels

In most of the experiments a "standard fuel" of 1 mole of H₂ + 1 mole of CO₂ was used. The "standard oxidant" was 2.5 (vol.) air + 1 (vol.) CO₂. The feed rate was usually chosen in such a way that at 100 mA/cm², 10 per cent of the fuel and the oxidants were consumed. The cells were operated at atmospheric pressure.

*) Sintered nickel, type J.E.G.V.; Mond Nickel Company, London, England.

The overall cathodic and anodic reactions can be written as



λ is the conversion degree of the reactants; the composition of atmospheric air is taken for convenience as $2 N_2 + \frac{1}{2} O_2$.

Although the $1 H_2 + 1 CO_2$ fuel is not in thermodynamic equilibrium at the inlet of the cell, it turns out that at the Ni anode the equilibrium is indeed established. In the first place, the less convenient to handle fuel $1 CO + 1 H_2O$ yields the same open circuit potential as the former one. Secondly, this open circuit potential E is virtually equal to the value calculated on the basis of the equilibrium fuel composition and the Nernst law (decadic logarithm):

$$E \text{ (volts)} = E_o(H_2) + 0.992 \cdot 10^{-4} T \log \left[\frac{p_a(H_2) p_c^{\frac{1}{2}}(O_2) p_c(CO_2)}{p_a(H_2O) p_a(CO_2)} \right] \quad (2)$$

where p_a and p_c refer to anodic and cathodic partial pressures respectively.

For $\lambda = 0$ in eqs. (1c) and (1a), the calculated E values are 968 mV at $1000^\circ K$ and 980 mV at $700^\circ C$ [6]. The observed values at $700^\circ C$ are between 970 and 985 mV, apart from initial deviations due to "non-aged" Ni electrodes. It will be shown in Sec. 4 that the standard fuel can be considered as being oxidised already for 32% with regard to an "optimal fuel", just not depositing carbon at $1000^\circ K$.

In some of the experiments, $CH_4 + CO_2$ mixtures were used. Usually, equilibrium in that case is not established at the Ni electrodes, but insertion of a small amount of commercial Ni on MgO reform catalyst, in the anode space, is sufficient to yield equilibrium.

3. OPERATING CHARACTERISTICS AND POLARIZATION EFFECTS

The cells under discussion were all kept under a continuous current drain of 100 mA/cm^2 (whenever possible), unless current vs. voltage curves were measured. The latter measurements were carried out over time intervals of at least a full hour, so that a steady state was always achieved.

Individual electrode polarizations could be measured with the aid of the reference electrode, using a mercury-wetted relay for fast ($\approx 2 \text{ } \mu\text{sec}$) current interruption and a Tektronix type 535A oscilloscope to measure iR drops and potential/time transients. The method is essentially similar to the one described by Trachtenberg [11] and makes use of the "sweep delay" provision of the C.R.O. time base, to observe the magnitude of the iR break conveniently and quite sharply.

The principle of the measurement may be clear from Fig. 4a, where a typical course of the electrode potentials has been plotted on a linear time scale, for two different current densities before interruption.

Fig. 4b shows the corresponding cathodic and anodic transients plotted on a $t^{\frac{1}{2}}$ scale. The meaning of the partial linearity of these plots will be discussed hereafter.

Fig. 5 shows the steady state (iR free) potentials and the iR drop, as functions of the current density, of a cell at 740°C with a "fiber nickel" anode and a silver powder cathode. The x x points refer to the third day of operation. It is seen that the Ni anode potential positivates "dangerously" at about 80 mA/cm^2 , whereas the Ag cathode potential varies linearly with the current. Also, the open circuit voltage of the cell, 1035 mV , is too high, 960 mV being the true equilibrium value [6].

The open circle points, taken after 18 days of operation, reveal a rather striking improvement of the anode, now polarising linearly with the current up to 160 mA/cm^2 , where the polarization is $+105\text{ mV}^*$. The Ag cathode also shows some improvement, the polarization being -76 mV at 160 mA/cm^2 . The open circuit voltage now shows the proper value, 960 mV , indicating that the fuel gas attains true equilibrium at the "aged" electrode. The iR drop obviously has not changed during the operation period of 18 days.

The figure clearly shows the relative importance of electrode polarizations and iR drop; at 160 mA/cm^2 :

iR drop = 340 mV > anode polarization = 105 mV > cathode polarization = 76 mV .

Fig. 6a shows similar results for a cell with a CuO cathode on the 27th day of operation at 720°C . At 200 mA/cm^2 :

$iR = 325\text{ mV}$ > an.pol. = 102 mV > cath.pol. = 70 mV .

Both anodic and cathodic polarizations are linear with the current density.

Fig. 6b shows a number of terminal voltage vs. current density characteristics for the same cell, taken at different times and for different fuel feeds. The line 27 in Fig. 6b corresponds with Fig. 6a. Line 13, on $\text{CH}_4 + \text{CO}_2$, in the absence of a reform catalyst, reveals that in this case no equilibrium is established at the Ni electrode, otherwise a much higher open circuit potential would have been observed (about 1100 mV). Nevertheless, upon current drain a reasonable performance can be obtained. (Addition of a few tenths of a gram of reform catalyst in the anode space yields the calculated open circuit value and correspondingly improved results.)

The line 28, on pure hydrogen, was taken on the last day before deliberate termination of the test period, with the main purpose to test the leak-tightness. The very high open circuit potential (1470 mV) shows the absence of any significant leakage after 4 weeks of operation. Also the capability of the CuO cathode to deliver current densities of 250 mA/cm^2 at about 90 mV polarization (on air + CO_2) could be demonstrated by this test.

The use of thinner electrolyte discs (9 mm in the case of Fig. 5 and 6.5 mm at Fig. 6) yields improved performances. The results shown in Fig. 4a, for instance, were obtained with a paste disc of 5 mm thickness. The terminal voltage in this case is 695 mV at 129 mA/cm^2 and still 540 mV at 212 mA/cm^2 , with an iR drop of 282 mV in the latter case.

The given examples show that the purely resistive iR drop is always the predominant term in the total voltage drop of a current delivering cell. Nevertheless, the electrode polarization is by no means negligible, and therefore it is interesting to know whether it is mainly due to mass transport phenomena or to activation controlled processes (slow electron transfer, slow adsorption or desorption). A rather extensive study on this question has been

*) Polarization with respect to open circuit anode potential.

made by the present authors, but its details fall beyond the scope of this article and will be presented elsewhere [12].

Here it may be sufficient to note that d.c., a.c. and pulse methods, applied to both "flat" model electrodes (in the form of smooth wires or strips) and porous Ni and Ag electrodes, all point to mass transport controlled polarization (at least, above 600°C). Closer study reveals that the limiting factor is the presence of fluid electrolyte films on the surface of the electrodes, through which the reactant and product gases have to diffuse. At the Ni anode, the "off-diffusion" of the products CO₂ and/or H₂O through the film is rate determining, unless the H₂ partial pressure becomes very low (Sec. 4). At the Ag cathode the diffusion of either O₂ or CO₂ (depending on the relative partial pressures), is determining.

Evidence for the diffusion controlled character of the reactions at the porous electrodes is shown in Fig. 4b and Fig. 7. Though the porosity of the electrodes is ill defined, their properties may be approximated mathematically by the model of an "infinitely long" homogeneous transmission line [16].

Provided that the polarization tension at any spot on the phase boundary of the porous electrode is small enough as to yield an essentially linear relation between the instantaneous local tension and the corresponding current density, a mathematical analysis of the transmission line model yields the following results [12]:

- 1) Steady state. If the specific phase boundary resistance* of a planar electrode is R_b ($\Omega \text{ cm}^2$), the corresponding effective resistance R_p of a porous electrode is proportional to $\sqrt{\rho \delta R_b}$, where ρ is the specific resistance of the electrolyte film and δ its thickness.
- 2) Alternating current impedance. Similar to 1), if the phase boundary impedance of a planar electrode is $Z_b = A - jB$, where A is the real and B the imaginary component of Z_b and $j = \sqrt{-1}$, then the corresponding impedance Z_p of a porous electrode is proportional to $\sqrt{\rho \delta Z_b}$.
- 3) Galvanostatic transient response. It is well known that for a diffusion controlled process at a planar electrode, the overtension v , resulting from a short constant current pulse Δi , changes proportional to the square root of time:

$$v = \text{const. } \Delta i \sqrt{t}.$$

For the transmission line model of the porous electrode the corresponding relation can now be written as:

$$v = \text{constant } \Delta i \sqrt{\rho \delta t^{\frac{1}{2}}}$$

Now Fig. 4b depicts the course of anodic (porous Ni) and cathodic (porous Ag) polarization tensions after current interruption**, as functions of $t^{\frac{1}{2}}$. It is seen that the curves for both 129 mA/cm² (geometrical current density) and 212 mA/cm² show linear portions, as predicted by the latter formula. Moreover, the slopes of these linear portions are proportional with the current density, both for the anodic and cathodic curves. The anodic and

* The phase boundary resistance is defined as the ratio of polarization tension to current density. The concept is valid for small polarizations only ($\ll RT/F$).

** In order to observe the polarization change accurately, oscilloscopic traces were photographed over time intervals of 10^{-4} , 10^{-3} , 10^{-2} , 10^{-1} and 1 second.

cathodic slopes for the same current density, however, are different. It is seen that the anodic response is considerably more sluggish than the cathodic one.

The deviating initial part of the anodic curves (the first 5 milli-seconds) is probably due to the interference of double layer capacity effects.

Fig. 7 is a so-called Argand diagram of the impedance $Z_p = A_p - j B_p$ of a nickel brush electrode. In the diagram, the real part A of the observed electrode impedance has been plotted against the imaginary part B, for different a.c. frequencies between 10 c.p.s. and 50 kc.

For a purely diffusion controlled process at a planar electrode, the phase boundary impedance Z_b is the so-called Warburg impedance:

$Z_b = W_0 \omega^{-\frac{1}{2}} \exp - j \pi/4$; where W_0 is a constant, ω the angular a.c. frequency and $\pi/4 = 45^\circ$ the phase angle (arc tan B/A). According to 2), the corresponding impedance Z_p of the porous electrode should now be proportional to

$\sqrt{Z_b} = W_0 \omega^{-\frac{1}{4}} \exp - j \pi/8$. In the Argand diagram of the impedance vector end points, the latter expression is represented by a straight line with a slope $\pi/8 = 22\frac{1}{2}^\circ$, and $|Z_p| \omega^{\frac{1}{2}} = \text{constant}$. It is seen that the observed impedances satisfy these demands only approximately, with the greatest deviation at high frequencies. When, however, a correction is made for the influence of the double layer capacity (by standard vectorial subtraction methods) the cross-points are obtained, which satisfy the theoretical prediction very well. Similar results have been obtained for porous anodes with less ideal geometry than the brush form of the presented example.

The occurrence of the square root form $\sqrt{i\omega\delta}$ in the various expressions for the polarization implies that the measured polarization always includes a purely resistive contribution from the electrolyte film. Moreover, since the true phase boundary resistance R_b only appears as $\sqrt{R_b}$ in the expression for the steady state polarization of a porous electrode, the latter will be relatively insensitive to small variations of R_b , such as can be expected for slightly non-linear voltage-current relations. And finally, because RT/F at 1000°K has the large value of 87 mV, it is not very surprising after all that the observed steady state polarizations (Figs. 5 and 6) are essentially linear with the current density.

4. FUEL AND OXIDANT UTILISATION

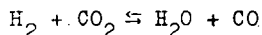
4.1. Oxidation of the fuel

In the experiments of Sec. 3, the fuel and oxidant utilisation was of the order of 10%, at about 100 mA/cm², relative to the feed. With regard to the fuel, the general course of its oxidation by CO_3^- ions can be visualised conveniently in the triangular C-H-O diagram of Fig. 8.

The "standard fuel" $1 \text{H}_2 + 1 \text{CO}_2$ is represented by P. Its oxidation (cf. reaction (1a), Sec. 2.3) proceeds along the straight line P - CO_3 , and would be completed at point P_e . Considering P as the initial fuel, its conversion degree λ at P is zero, and $\lambda = 1$ at P_e on the line $\text{H}_2\text{O} - \text{CO}_2$. The "optimal fuel", however, which can be oxidised along the same path, is represented by P_0 on the carbon deposition boundary (C.D.B.) curve [6], [13]. At 1000°K and 1 atm total pressure the composition of P_0 is 0.17 C + 0.63 H + 0.20 O. It is easy to show that, with respect to oxidation by CO_3^- ions, the standard fuel P is already oxidised for 32% when P_0 is taken as the initial fuel. If λ_0 represents the conversion degree of P_0 , then $\lambda_0 = 0.32 + 0.68 \lambda$ ($\lambda =$ conversion degree of P).

It is possible to calculate the theoretical (Nernst) EMF for any value of λ or λ_0 , by means of equation (2), Sec. 2.3 when the equilibrium compositions of the C-H-O gas phase on the line $P_0 - P_e$ are known. The author (Broers) has found a simple method [14] to calculate curves of constant CH_4 partial pressure (Fig. 8) and curves of constant EMF (Fig. 9) in the triangular diagram, so that the theoretical EMF values for different points on the line $P_0 - P_e$ can be read directly from it.

The CH_4 "isobars" of Fig. 8 show that at 1000°K , in the range of interest, $p(\text{CH}_4)$ is rather low, so that in good approximation only the equilibrium:



needs to be considered. This makes calculations of the equilibrium compositions along the path $P_0 - P_e$ fairly simple.

A still more convenient method involves the use of the diagram of Fig. 9. The curves in this figure permit a direct reading of the "excess EMF", ΔE (in millivolts), which has to be added to $E_0(\text{H}_2)$, cf. equation (2), to obtain the E value with regard to anodic gases. The cathodic contribution in (2) can of course be calculated straight forwardly.

The course of the theoretical EMF along the path $P - P_e$, i.e. $\lambda = 0$ to $\lambda = 1$, is shown in Fig. 11, upper curve. The cathodic partial pressures $p_c(\text{O}_2)$ and $p_c(\text{CO}_2)$ are kept constant (0.14 atm and 0.28 atm respectively), in agreement with the experimental set-up to be described.

Now the course of the practical cell terminal voltage as a function of λ was determined as follows. Suppose we have a battery of n cells, of equal surface area, connected in series. The fuel is passed through this battery in series flow. Then each cell converts a fraction $\Delta\lambda$ of the fuel, at equal current density. When the current is i , and the feed rate of the combustible part of the fuel mixture is equivalent to $n i$, $\Delta\lambda = 1/n$. The overall conversion degree at the entrance of cell k will be $\lambda = (k - 1)/n$, and at its exit $\lambda = k/n$. Thus, in principle the conversion would be complete at the exit of cell n . In practice this cannot be realised, since progressive fuel depletion and product accumulation tend to increase the (mass transfer controlled) polarization, so that in some given cell of the battery the actual current density becomes the limiting one.

Since no practical battery was available, relevant experiments were carried out with a single cell at 720°C , by means of a simulator technique represented in Fig. 10. When the standard fuel has been oxidised to a degree λ , reaction (1a), Sec. 2.3 has occurred.

In order to realise this reaction, the necessary amount of " CO_3^- ions" was supplied to the fuel in the form of gaseous O_2 and CO_2 (in the proper ratio), so that the latter gases reacted directly in the hot part of the anode tube with the incoming fuel, before reaching the electrode.

The supposed number of cells n was chosen as 10. At a cell current i the H_2 feed was evolved electrolytically at a current $10 i$, and the additional equal CO_2 feed (O_2 free) by accurate flow meter adjustment. O_2 simultaneously was evolved and supplied electrolytically at a current $10 \lambda i$, and mixed with an equivalent flow of $10 \lambda i \text{ CO}_2$ (the double amount of CO_2 against O_2 when expressed in moles/second). Thus the conversion

* Compare Fig. 2, $\text{O}_2 + \text{CO}_2$ entering through auxiliary inlet.

of the fuel could be adjusted quite accurately, by ammeter readings. The oxidant flow rate was held constant, at a large excess, in order to keep the cathode potential constant.

The results, at current densities of 62 mA/cm^2 and 125 mA/cm^2 are shown in Fig. 11. Since $\Delta\lambda = 0.1$ and e.g., at the entrance of cell no. 4, $\lambda = 0.3$, the voltage reading of cell 4 has been plotted at $\lambda = 0.35$. The actual voltages observed (full curves) have also been corrected for iR drop, yielding the dashed curves. It is seen that:

1. At 125 mA/cm^2 about 70% of the standard fuel (P in Fig. 8) can be utilised, or about 80% of the corresponding optimal fuel (P_0 in Fig. 8; λ_0 axis in Fig. 11). The partial pressure of the remaining fuel at $\lambda = 0.7$ is 0.11 atm.
2. At 62 mA/cm^2 , 90% of the standard fuel, or 93% of the optimal fuel can be utilised. The partial pressure of the remaining fuel at $\lambda = 0.9$ is 0.034 atm.
3. The difference between the theoretical E curve and the dashed curves, that is the polarization, appears to decrease with increasing fuel conversion, till close to the point where the current density becomes the limiting one.

This rather surprising phenomenon may be explained by the already known fact that not the fuel, but the products CO_2 and H_2O are rate controlling (Sec. 3), and that the overall rate of gas flow increases with increasing conversion (equation 1a). Probably the effect of the increasing CO_2 and H_2O partial pressures is counteracted so much by the increasing flow rate, that the overall effect is in favour of a polarization decrease. But finally the mass transport of the $\text{H}_2 + \text{CO}$ fuel, now at rather low partial pressure, takes over the role of the reaction products, and total depletion at the electrode surface starts very soon thereafter.

These observations clearly show that the attainable fuel utilisation is a pronounced function of the current density. In order to use the greatest possible fraction of the fuel feed, the current density in the "last cells" of the battery has to be decreased by increasing their surface area. Practically, this becomes a matter of optimising the increasing investment costs against the decreasing fuel costs. In this sense, the possibility of 90% fuel utilisation at (at least) about 60 mA/cm^2 seems a rather encouraging result.

4.2. Utilisation of O_2 and CO_2 **

The conversion at the cathode is given by equation (1c), Sec. 2.3.

The experimental measurement of the terminal voltage as a function of λ in an imaginary 10 cell series battery was carried out as follows:

1. Excess fuel (1 $\text{H}_2 + 1 \text{ CO}_2$) was used at the anode (about 10% conversion).
2. At cell current i , an electrolytically generated O_2 feed, $10(1-\lambda) i$, was led into the cathode space of the cell, together with:
3. A CO_2 feed (O_2 free) of $10(1-\lambda) i$, that is twice the O_2 flow rate in volume/sec.
4. A N_2 feed (O_2 free) held constant at 4 times the oxygen volume flow rate for $\lambda = 0$.

* Also to λ values not corresponding with integral cell numbers.

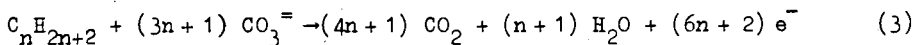
** The experiments described here and in Sec. 4.1 were carried out with one cell, with a Ag powder cathode and a "fiber nickel" anode. The measurements lasted 17 days in all.

The theoretical voltage as a function of λ was computed easily from the Nernst Law (equation (2), Sec. 2.3), using (1c) to calculate $p_c(O_2)$ and $p_c(CO_2)$. The results, at 720°C, are shown in Fig. 12, for current densities of 125 mA/cm² and 62 mA/cm². The dashed curves represent the iR free voltages. It is seen that:

1. At 125 mA/cm², about 85% of the "oxidant" $\frac{1}{2} O_2 + CO_2$ can be utilised. At this conversion, the remaining partial pressures are:
 $p(O_2) = 0.034$ atm; $p(CO_2) = 0.067$ atm.
2. Similarly at 62 mA/cm², about 95% utilisation is possible;
 $p(O_2) = 0.012$ atm; $p(CO_2) = 0.024$ atm.
3. By maintaining a slight excess of O_2 at 125 mA/cm², corresponding with $\lambda(O_2) = 0.80$, and studying the effect of $\lambda(CO_2) \geq 0.80$ solely, the dotted curve was found. Thus with regard to CO_2 conversion, about 90% can be utilised at 125 mA/cm².
4. Conversely, by keeping $\lambda(CO_2)$ at 0.80 and increasing $\lambda(O_2)$ beyond this value, about 93% O_2 utilisation could be reached. It seems therefore that in fact CO_2 is limiting when the stoichiometrical O_2/CO_2 ratio is used, but the match is rather close and may fall within the accuracy of the CO_2 flow meter calibration.
5. In contrast with Fig. 11, increasing conversion now brings about slightly increasing polarization, up till $\lambda \approx 0.75$. Since the overall flow rate in this cathodic case decreases with increasing λ , this is the result to be expected. Nevertheless, the polarization increase is enjoyably small.

From a purely theoretical standpoint, the maximum possible O_2 depletion from the air feed is not very important, though a great excess of air is definitely unwanted in connection with the heat balance of a battery system.

A quite different situation pertains to CO_2 depletion. Consider the (assumedly) complete combustion of a hydrocarbon C_nH_{2n+2} . The overall anode reaction is:



Now the oxidation products are to be recycled to the cathode, and mixed with air in such an amount that at least $(3n+1) CO_3^-$ can be formed and also utilised. Since $(4n+1) CO_2$ is available, its conversion degree should be at least:

$$\lambda(CO_2)_{cath.} \geq (3n+1)/(4n+1)$$

Thus the cathodic conversion degree of CO_2 should be better than 80% for methane fuel, and still better than 75% for higher hydrocarbons ($n \gg 1$). The experiments depicted in Fig. 12 show that conversion degrees of this magnitude can indeed be attained at current densities up to 125 mA/cm².

To the knowledge of the authors, experiments of the kind discussed here have not been reported earlier. Only Chambers and Tantram [15] reported data on H_2 conversion percentages, but did neither specify the current density nor the actual terminal voltages observed.

5. LONG RUN EXPERIMENTS AT CONSTANT CURRENT DENSITY (100 mA/cm^2)

In earlier work [5], [6], it was not possible to draw current densities of the order 100 mA/cm^2 for more than about 1 week. Improvement of the electrolyte paste properties eliminated the instability effects at current densities $> 25 \text{ mA/cm}^2$ virtually completely, so that a long run test at 100 mA/cm^2 could be carried out on a pair of small "twin cells" of 1 cm^2 surface area each.

Standard fuel and oxidant were used at 700°C , with 10% conversion relative to their feed rates. Both cells had "reinforced" Clevite porous nickel anodes (initially 70% porosity), which were used without any pretreatment. The cathodes were silver screens (0.5 mm wires with equally large spacings); cells constructed as shown in Fig. 1.

Fig. 13, upper section, shows the results over a 4600 hours period (after which the measurements were terminated deliberately), in terms of 1. terminal voltages, 2. iR free voltages, 3. open circuit voltages. The latter were observed only occasionally; see points indicated.

It is seen that:

1. The performances run rather similarly, the terminal voltages decreasing slowly from about 750 mV initially down to 470 mV at 4600 hours.
2. The iR free voltages become practically constant after $2-2\frac{1}{2}$ months, so that the electrode polarizations also become constant after that period. The cathodic polarizations (not shown separately from the anodic ones) stabilise to about 50 mV, the anodic ones to about 150 mV.
3. Initially there is an increase in polarization, which has to be ascribed to alterations of the porous Ni anodes. (Sintering effects, compare Figs. 3a-3b, Sec. 2.2). With respect to these alterations, "ageing" of the electrodes by a heat pretreatment at 800°C , in reducing atmosphere, is rather favourable.
4. The open circuit voltages (initially too high) attain the calculated value 980 mV within about 2 weeks, up till the end of the test. This indicates that the cells were still gastight after 6 months.

Analysis of the electrolyte pellets revealed that about 50 mole % of the initial carbonate content was lost after the 6 months period. In Fig. 13, lower section, the conductivity of cell 3 (cell 2 gives similar results) has been plotted as a function of the operating time. It is seen that, roughly speaking, the decrease of the conductivity is proportional with time, and that from 500 to 4500 hours a 50% decrease has occurred. This suggests that the only cause of the performance decrease, after the "stabilising period" of the anode, is due to slow vaporisation of the carbonate melt.

In principle, carbonate losses may occur by "creeping" as well as by vaporisation. In the conditions of the experiment, however, creeping of the Li-Na-K carbonate melt comes to a stop at the cold parts of the alumina tubes, within one or two days. Moreover, it is very unlikely that losses through creepage would alter the ratio of Li to Na to K.

The chemical analysis of the used electrolyte pellets, however, proved that the mentioned ratio had changed considerably. Initially the alkali atom fractions were : 0.37 Li, 0.39 Na, 0.24 K, whereas after 6 months they were : 0.47 Li, 0.36 Na, 0.17 K.

Thus the rate of K evaporation is the largest, that of Li the smallest one. Though the relative order of alkali carbonate stability is just the reverse with regard to CO_2 vapour pressure [1], it should be kept in mind that in the present experiments a relatively large CO_2 partial pressure was maintained all the time on both sides of the electrolyte pellet.

(A blank experiment with a liquid Li-Na-K carbonate mixture under CO_2 of 1 atm at 700°C , using a "cold finger" to condense the vapours, yielded qualitatively similar results. It took several weeks to collect a small quantity of condensed vapour.)

On the basis of the total amount of fuel and oxidant gases passed over the electrolyte pellets in the test period, it can be calculated that 1 mole of CO_3 was lost per (about) 10^5 moles of fuel, air and CO_2 . Thus the vaporisation rate is quite small.

This in turn would mean that a (more or less) continuous supply of fresh melt in very small quantities would result in a practically constant performance over a period of several times the one observed here, that is in the order of at least a few years.

In conclusion, it may be stated that with regard to power output, attainable gas utilisation and life of the essential cell components, the prospects of the high temperature fused carbonate cell are far more favourable than thought hitherto.

Only work on a larger scale can show whether the construction of batteries is technically, and if so, also economically feasible. The authors fully appreciate that this still a long way to go.

ACKNOWLEDGEMENT

The authors would like to thank their colleagues Messrs. G.G. Piepers, J. Marchés, C. van der Harst, N. van Bezooyen, B.W. Treijtel, C. van der Laan, H.J.J. van Ballegoy and H.E. Huynink for their aid in carrying out the experiments and their inventivity in solving many of the practical problems.

REFERENCES

- [1] G.H.J. Broers; "High temperature galvanic fuel cells"; thesis University of Amsterdam (1958).
- [2] G.H.J. Broers; Dechema Monographien Bd. 38, 277 (1960), Verlag Chemie G.m.b.H., Weinheim, W. Deutschland.
- [3] "Fuel Cells", Vol. 1, Chapt. 6. G.J. Young (Ed.), Reinhold, New York, (1960).
- [4] "Fuel Cells", Vol. 2, Chapt. 2. G.J. Young (Ed.), Reinhold, New York, (1963).
- [5] G.H.J. Broers; in "Fuel Cells, a C.E.P. Technical Manual", p. 90, Am. Inst. of Chem. Engineers, New York (1963).
- [6] G.H.J. Broers, M. Schenke and G.G. Piepers; J. Advanced Energy Conversion 4, 131 (1964).
- [7] E. Justi and A. Winsel; "Kalte Verbrennung - Fuel Cells", Chapt. 9.3. Steiner, Wiesbaden (1962).
- [8] "Fuel Cells"; W. Mitchell Jr. (Ed.); Chapt. 5 and Chapt. 9; Acad. Press. New York and London (1963).
- [9] R.W. Hardy and J. McCallum; in Reference [5], p. 45.
- [10] K. Bischof and E. Justi; Jahrb. Akad. Wiss. Lit. (Mainz), 250 (1955).
- [11] I. Trachtenberg; J. Electrochem. Soc. 111, 110 (1964).
- [12] G.H.J. Broers and M. Schenke; J. Advanced Energy Conversion; to be published.
- [13] E.J. Cairns, A.D. Tevebaugh and G.J. Holm; J. Electrochem. Soc. 110, 1025 (1963).
E.J. Cairns and A.D. Tevebaugh; J. of Chem. and Eng. Data 2, 453 (1964).
- [14] G.H.J. Broers and B.W. Treijtel; submitted to J. Advanced Energy Conversion.
- [15] H.H. Chambers and A.D.S. Tantram; in Reference [3], Chapt. 7, p. 105
- [16] R. de Levie, Thesis, University of Amsterdam (1963); Electrochim. Acta 8, 751 (1963).

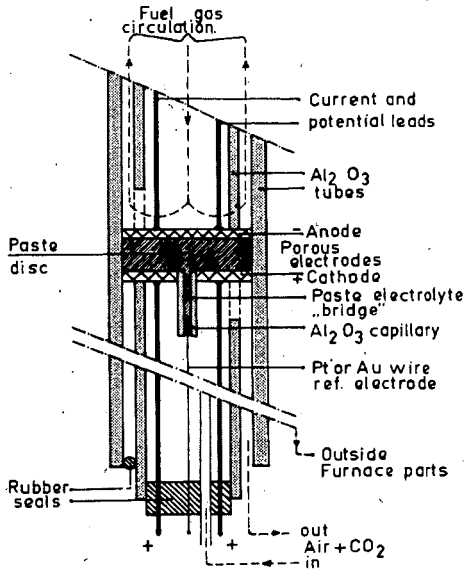


Fig.1 Disc cell with reference electrode for polarization and other fundamental studies.

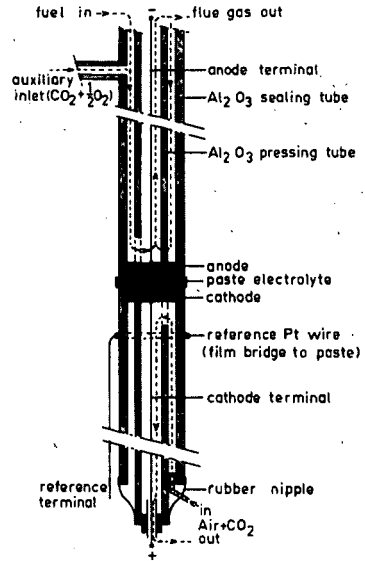


Fig.2 Simplified version of the cell cf. Fig.1.

Electrolytic bridge from reference wire to paste disc formed spontaneously by creeping of the molten salt.

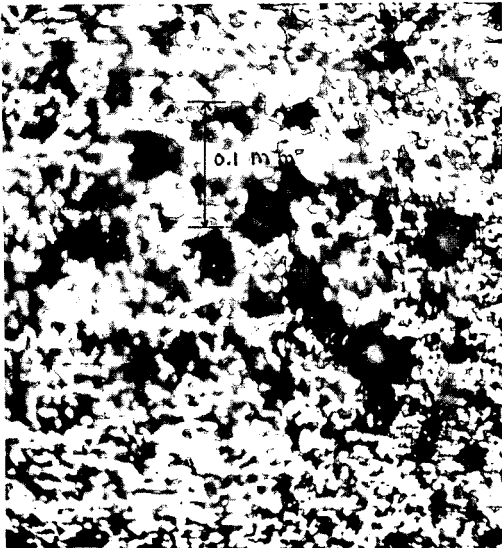


Fig.3a Porous Ni electrode (Mond Nickel Co.) before use. Magnification 125x, before final reproduction.

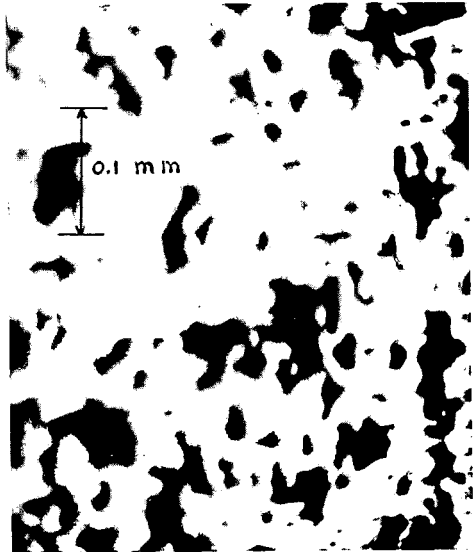


Fig.3b The same material after 625 hours of continuous anodic operation at 100 mA/cm², 700 °C.

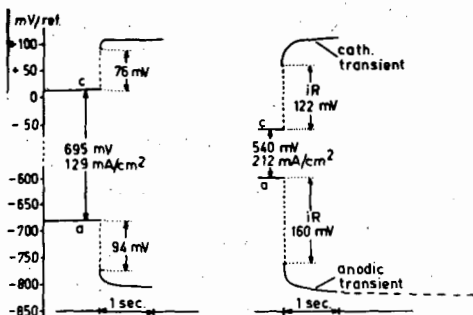


Fig. 4a.
Determination of iR drop and electrode polarization by means of fast current interruption ($< 2 \mu\text{sec}$).

Linear time scale.

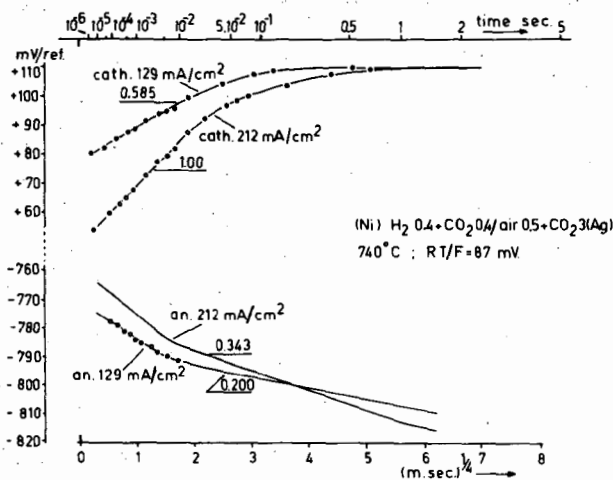


Fig. 4b.

Cathodic and anodic potential transients cf. Fig. 4a, but plotted on a $t^{1/2}$ time scale.

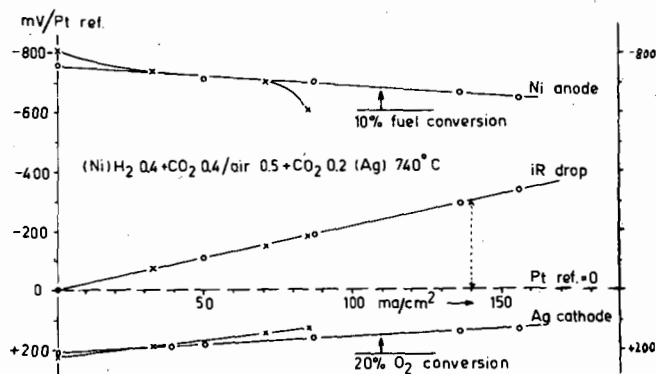


Fig. 5. Steady state (iR free) potentials and iR drop of a cell cf. Fig. 2, as functions of the current density. Cathode: Ag - powder, anode: "fiber nickel". x-x-x: 3rd day of operation; o-o-o-o: 18th day of operation.

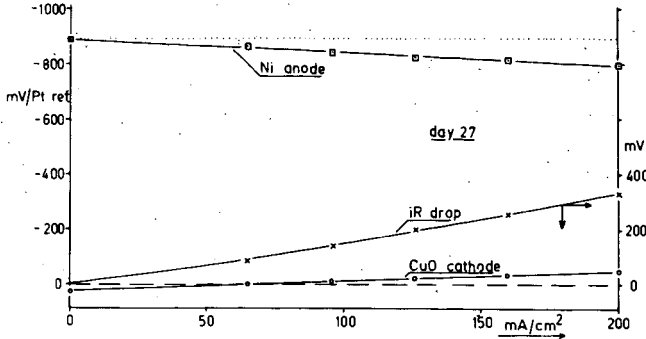


Fig. 6a. Steady state potentials and iR drop of a cell with CuO cathode and Ni anode, 27th day of operation.

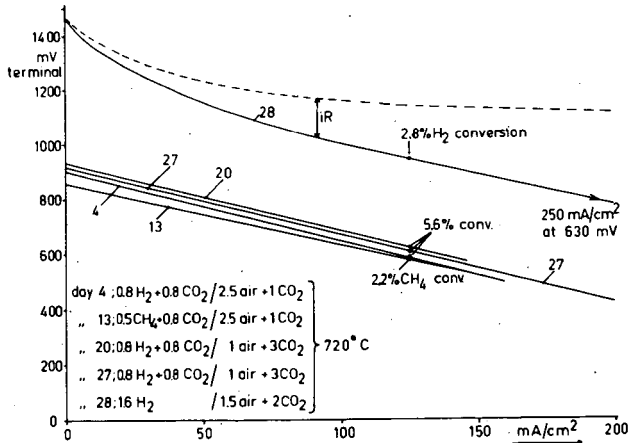


Fig. 6b. Terminal voltage vs. current density characteristics of the cell cf. Fig. 6a, over a 4 week period. No iR drop corrections, except upper curve (dashed).

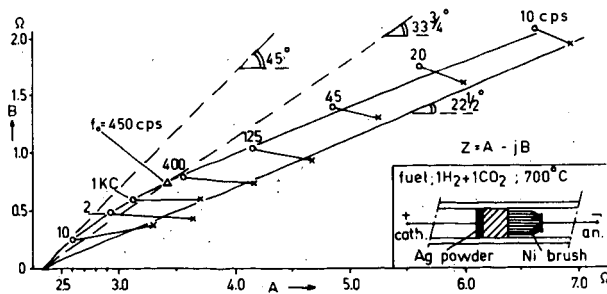


Fig. 7. A.C. impedance vector diagram (Argand diagram) of a nickel brush electrode, simulating an ideally homoporous system. o-o-o : points observed; x-x-x : impedances corrected for influence of double layer capacity. Drawn straight line : theoretical prediction for pure diffusion control; $22\frac{1}{2}^\circ$ slope, $|Z| \cdot f^{1/2} = \text{constant}$.

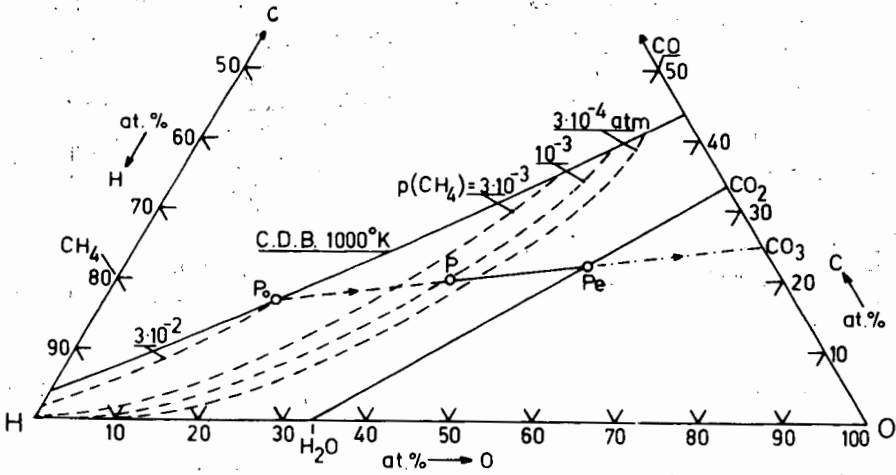


Fig. 8. C-H-O triangular diagram, representing at 1000°K and 1 atm : 1) Carbon deposition boundary (CDB) ; 2) Equilibrium partial pressure "isobars" of CH₄ (dashed); 3) Oxidation path PP_e of the standard fuel P, reacting with CO₃⁼ ions ; 4) Optimal fuel composition P₀ that may be oxidised along the same path. P corresponds with 32% oxidation of P₀ .

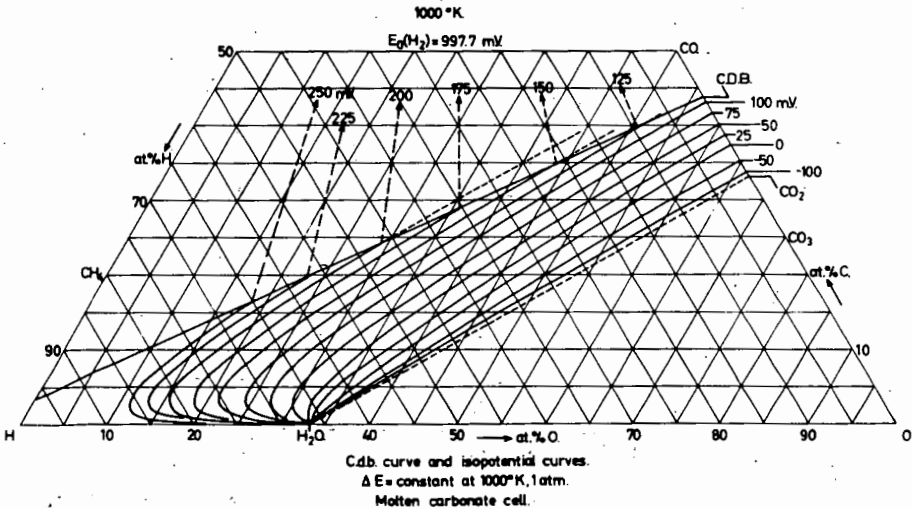


Fig. 9. C-H-O diagram with CDB and curves of constant EMF with regard to fuel composition, for molten carbonate cells at 1000°K, 1 atm. $E(\text{cell}) = E_0(\text{H}_2) + \Delta E(\text{anodic}) + \Delta E(\text{cath.})$; cf. Eq.(2). $\Delta E(\text{anodic})$ can be read directly from the diagram, in mV.

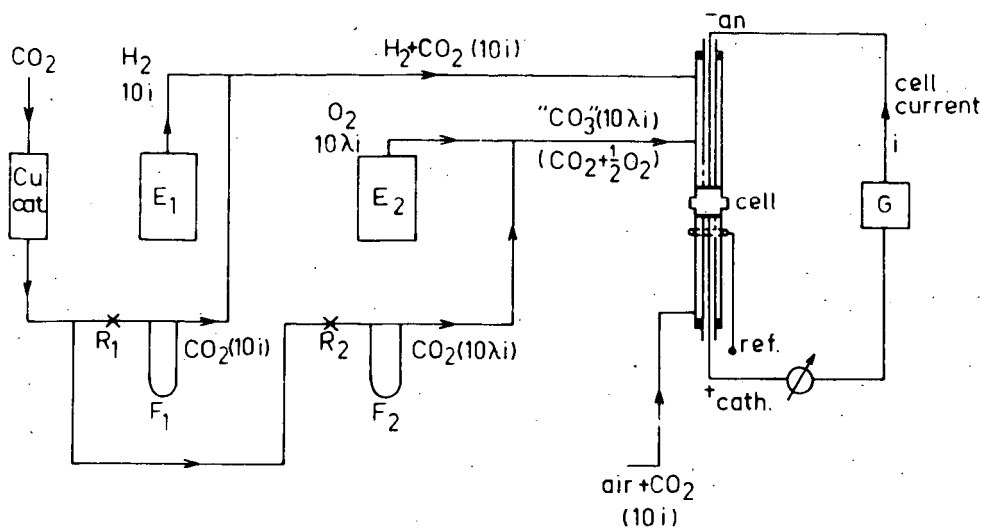


Fig.10. Determination of fuel utilization in an imaginary 10 cell series battery, by means of a single cell. E_1 : H_2 electrolyzer; E_2 : O_2 electrolyzer; F_1 and F_2 : CO_2 flowmeters with regulating valves R_1 and R_2 ; G : galvanostat. Cell cf. Fig.2.

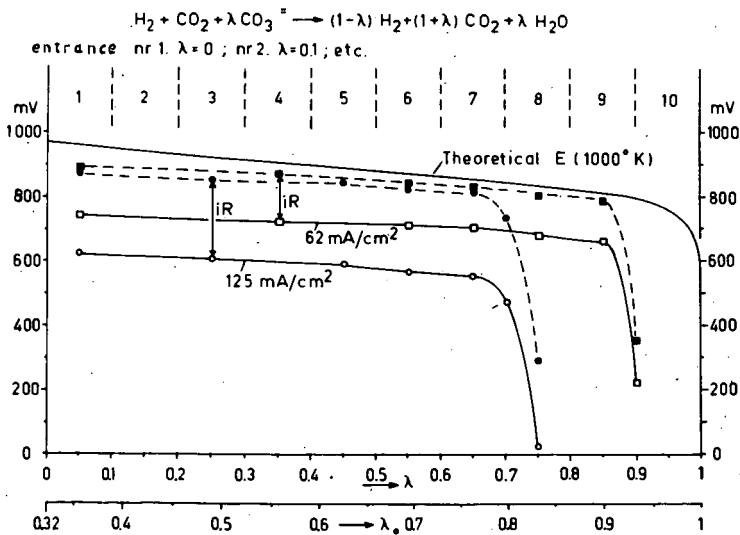


Fig.11. Results of fuel utilization experiments at 62 mA/cm^2 and 125 mA/cm^2 . λ is the conversion degree relative to point P in Fig.8, λ , similarly to point P, in Fig.8. Anode: "fiber nickel", cathode: Ag screen. $T=720^\circ\text{C}$. Theoretical E based upon equilibrium composition of the fuel mixture; derived from Fig.9 and Eqs.(1c) & (2).

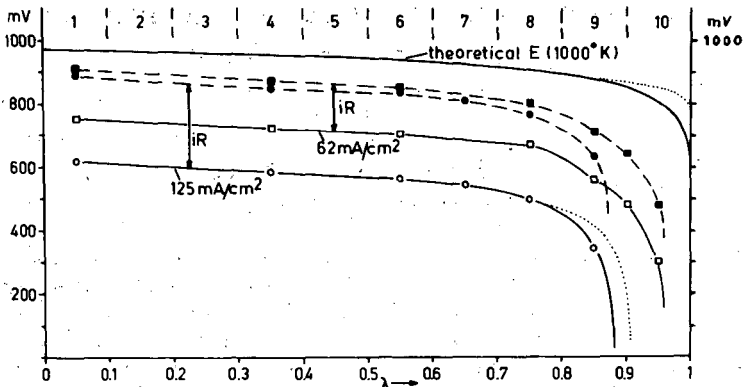
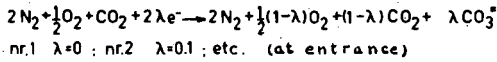


Fig.12.

Results of oxidant utilization experiments. Points indicated: equal conversion degrees of O_2 and CO_2 . Dot curve: $\lambda(O_2)$ held at 0.8, $\lambda(CO_2) \geq 0.8$. (Similarly for the theoretical E curve)

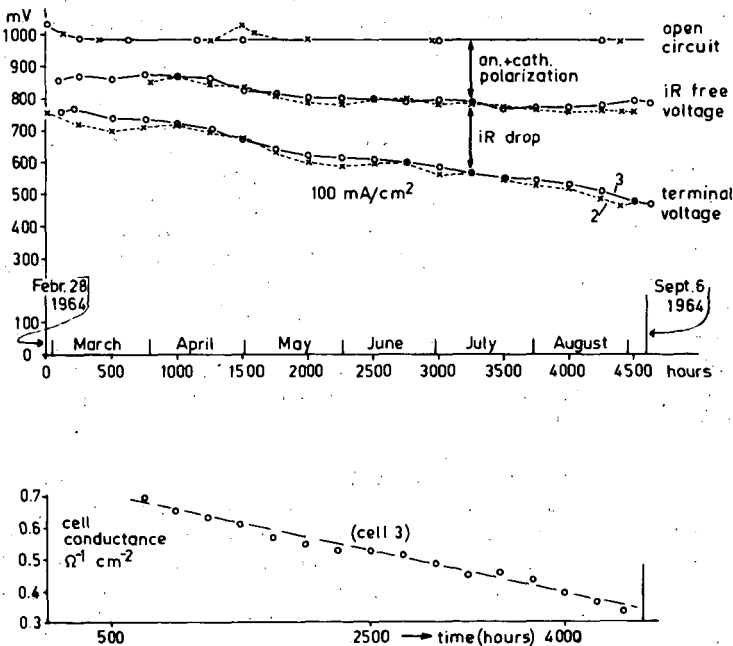


Fig.13.

Long run (6 months) output voltages of twin cells 2 (x-x-x) and 3 (o-o-o) at $700^\circ C$ and 100 mA/cm^2 continuously. Fuel: $1H_2 + 1CO_2$, 10% conversion; oxidant: $2.5 \text{ air} + 1CO_2$, 10% conversion. Anode: "Clevite nickel"; cathode: Ag screen. Lower section: decrease of cell conductance in the same period.

HYDROCARBON-AIR FUEL CELLS EMPLOYING SLURRIED MOLTEN CARBONATE ELECTROLYTES

Isaac Trachtenberg

Texas Instruments Incorporated, P. O. Box 5936
Dallas, Texas 75222

Fuel cells employing mixtures of molten alkali carbonates as the electrolyte have been described. These cells can be divided into three groups: those that employ a fixed ceramic matrix¹⁻³ impregnated with the electrolyte, a paste matrix⁴⁻⁶ consisting of a mixture of fine ceramic particles and the electrolyte that is preformed, and a free electrolyte^{7,8} with no matrix. In the first two groups, the ceramic-electrolyte body is the structural member and supports not only itself but also the electrodes. In the free electrolyte cells, the electrodes are the structural members and must to a great extent contain the very difficult to handle electrolyte. The slurried electrolyte cell described here takes advantage of the best of the cells mentioned above. There is no need for a pre-sintered or preformed ceramic-electrolyte body. The electrodes are the structural members. The ceramic particles serve as a separator and help contain the electrolyte. The electrolyte-ceramic slurry has no requirement for structural strength.

Cell Description

Figure 1 is a photograph of an actual test cell before operation. This unit consists of two cells connected electrically in parallel and is referred to as a 1 x 2 unit. The fuel gas supply flows between the two anodes. The unit is placed in a furnace chamber which contains the cathode gas supply. The cathodes are connected to the front plenum and the anodes to the rear plenum. The fuel gas plumbing is used for the current bus bar, and cell voltage is measured between the leads coming from the top of the front and rear plenums. A silver wire used as a third idling electrode is placed in the ceramic electrolyte reservoir cup. Each electrode is 1 in. x 4 in. Since there are two such electrodes in parallel, there is a total geometric electrode area of 8 sq. in., or 51.6 sq. cm, of each electrode (anode and cathode) in these units. Figure 1 shows only one of the two working cathodes.

A cutaway perspective of the unit is shown in Fig. 2. The primary anodes are not only connected together at the plenum but also have a corrugated nickel screen welded between them to yield a stronger structure, provide better distribution of the gases, and to serve as a secondary electrode. In the experiments described here magnesia particles are used to form the electrolyte slurry. When the unit is assembled, dry MgO of selected particle size (depending on the electrode structure) is placed between the working cathodes and anodes. A mixture of 50 mol % Li_2CO_3 and 50 mol % Na_2CO_3 is prepared, fused, broken into pieces about 2 to 10-mesh, and placed in the electrolyte reservoir cup. The entire assembly is placed in a furnace and raised to operating temperature. At about 500°C the electrolyte begins to melt and is drawn by capillary action up the MgO-filled alumina feed tubes and into the MgO particles between the working anodes and cathodes. Once the electrolyte has saturated the MgO, the additional electrolyte in the reservoir cup merely remains there until it is needed to replace any electrolyte which may evaporate from the slurry. This feature of the unit permits very easy and rapid addition of electrolyte to the unit when it is operated continuously for extended time intervals.

Experimental

The following discussion will pertain to the performance of several of the 1 x 2 units in which the structure of the electrodes was changed. In these experiments the gas supplies were held constant. The fuel gas supply was a simulated natural gas (CH₄) reformat consisting of approximately 80% wet H₂ and 20% CO₂. Previous experience with the simulated natural gas reformat has shown that this mixture is water-gas shifted in the steel plumbing to a nearly equilibrium (>90%) mixture of H₂, H₂O, CO₂, and CO at the operating temperature of the cell. The cathode gas supplied to the furnace chamber was 80% air and 20% CO₂.

The cells were under some load for more than 95% of the reported operating life. Operation of all the cells described was voluntarily terminated for postoperative examination while the cells were still performing at an acceptable level (>20 watts/ft²).

The data presented here were obtained from current-voltage (E-I) curves recorded daily except for some of the week ends. These traces were obtained from the working cathode versus the working anode and from the anode and cathode individually versus the third idling electrode. The latter curves were recorded to determine total polarization of the individual electrodes. Traces were obtained using either an EAI 1110 Variplotter or a Varian F80 X-Y recorder.

Current interruption studies similar to those previously reported^{1,3} for sintered matrix cells were performed. These studies continued to show that the total polarization is composed of two components, ohmic and concentration polarization. These interrupter studies also verified the 1000 cycle resistance measurements of the total internal cell resistance and determined the individual anode and cathode ohmic resistances.

Performance and polarization data as a function of operating time were presented to a 7040 computer to determine the best least mean square straight line, the standard error of the data points, and the standard error of the slope of the least means square line. The cell data treated in this manner include power density in watts/ft² at a fixed terminal voltage, open circuit voltage, total anode polarization, and total cathode polarization. Total anode and cathode polarization are defined as the difference between the potential versus the third idling electrode at open circuit voltage and that at the given current density. These data are discussed in detail in the following section.

Discussion of Results

Figure 3 shows two power versus hours of operation curves for 1 x 2 unit #47-47. This cell was operated at 600°C for 1100 hours before its operation was terminated voluntarily. It contains 120-mesh Ni screen primary and secondary anodes and silver-plated 120-mesh stainless steel cathodes. A secondary cathode of the same silver-plated material was also used on the cathode. (This secondary cathode can be seen on the cathodes in Fig. 10.) The MgO was sized so that it could be contained in the screens (>120-mesh). The data points shown were selected randomly and are representative of all of the points. The solid lines are the best least mean square line at the two cell terminal voltages of 0.5 and 0.7 volt respectively. The dashed line indicates the standard deviation of the points from the line. Although the line at 0.5 volt shows a slight increase in power and that at 0.7 volt exhibits a slight decrease in power as a function of hours of operation, neither observation is statistically significant. The errors in both slopes are greater than the slopes themselves (see Table I at the end of this section). Similar treatments of the open circuit voltage,

anode and cathode polarization at current densities up to 75 ma/cm^2 also exhibit no significant slopes.

From these data it is concluded that within the limits of reproducibility of cell performance from day to day there was essentially no change in performance for 1100 hours of operation.

Cell #47-53 was another 1 x 2 unit operated at 600°C . It contained primary anodes made by sintering presieved, highly active nickel particles onto 120-mesh nickel screen. No secondary electrodes were used in this unit. The cathode consisted of sintered presieved silver particles on 120-mesh silver-plated stainless steel screen. The MgO was sized to be contained by the electrodes. Figure 4 illustrates the power at 0.5 volt as a function of hours of operation. Cell operation was voluntarily terminated after 828 hours. Notice that the initial power density of 50 watts/ft^2 is about twice that of the preceding unit. Power density remained 42 to 48 watts/ft^2 for more than 400 hours of continuous operation. The decline in performance started just after 400 hours of operation and continued to about 500 hours, when it leveled out for the next 200 hours before resuming a slower rate of decline until operation was voluntarily terminated.

Figure 5 illustrates the effects on the open circuit voltage and the total polarization of both the anode and cathode at 75 ma/cm^2 . According to these data, the major cause of decline in power output of the cell was increased polarization of the cathode. There was essentially no change in the open circuit voltage during the entire operation. However, polarization on both electrodes did increase. Again notice that the cathode exhibits a distinct increase in polarization starting just after 400 hours and continuing to about 500 hours. The anode at the same time remained at worst unchanged, and at best it exhibited a slight decrease in polarization. However, the net result was a decrease in power output.

Postoperative examination of this cell showed that the sintered silver cathodes had undergone additional sintering sometime during their operating life with an accompanying decrease in surface area. The electrode appeared to be completely closed and the particles actually melted in spots. Little or no porosity remained. It is possible that a relay on the furnace temperature controller stuck, causing overheating so that the electrode continued to sinter. Some additional sintering was also observed on the nickel anodes, but these electrodes retained most of their original porosity.

Figure 6 illustrates the power at 0.5 volt versus-hours of operation for cell #47-140. This cell contained 120-mesh nickel screen primary anodes and 50-mesh nickel screen secondary anodes. The cathodes were silver-plated 120-mesh stainless steel screens. The plating was heavier than that used in cell #47-47.

From 100 to 500 hours of operation power output was at a level of 35 to 40 watts/ft^2 . Then it started to decline, reaching 22 watts/ft^2 at 1100 hours. The cell was terminated voluntarily after 1117 hours of operation.

The least mean square results are presented in Fig. 7 and Table I for open circuit voltage and polarization at 50 ma/cm^2 for both anode and cathode as a function of hours of operation. The order of contribution to the decline in power output of this unit are open circuit voltage, cathode polarization, anode polarization. Anode polarization, however, was higher from the start than is usually observed. This is attributed to the use of the 50-mesh nickel screen secondary electrode.

Examination of the electrodes after termination showed that the primary anode was flooded with electrolyte and had undergone appreciable oxidation. This oxidation is considered the cause for the decreased open circuit voltage, but is difficult to say which process occurred first. Previous experience with nickel anodes, however, has shown that nickel tends not to wet easily while nickel oxide does. The accompanying loss of active (for the fuel cell reaction) area may also account for the increase in anode polarization.

Several times during the operating life of this cell a small fire was observed on one of the cathodes. This fire was the result of fuel reaching the cathode. Although the fire did not cause the cell to fail, it did remove the silver plating in its vicinity. The redistribution of silver resulted in a loss of active cathode surface area, which could easily account for the increase in cathode polarization. Postoperative examination of these electrodes confirmed the silver redistribution. In many places the stainless steel screen was exposed to the electrolyte.

Silver migration on the electrodes and solubility in the electrolyte can be serious problems in any molten carbonate fuel cell. Migration can be retarded by preventing thermal and concentration gradients along the electrode. These gradients can be minimized by good heat management and gas distribution. The solubility aspects are a little more complicated. First, more silver must be present initially on the electrode than the amount required for good cathodes. Second, and more important, the solubility of silver can lead to dendrite formation, which can cause an electronic short and subsequent failure of the cell. In this respect the slurry-electrolyte system has an advantage over the other fixed matrix systems.^{3,4} Fixed matrix cells provide a mechanical support for the silver dendrites through the electrolyte. The slurry system provides little, if any, mechanical support for such dendrites; consequently, it has considerably less tendency to form shorts. Reliability testing of more than 200 cells containing slurried electrolyte revealed no failures because of any type of electronic shorting. This was not the case in previous experience with fixed matrix cells.

Cell #33-1 was very similar to #47-140, but both secondary and primary anodes were constructed of 120-mesh nickel screen. Figure 8 presents the power output at 0.5 volt and the anode and cathode polarization as a function of hours of operation. The open circuit voltage was constant during this period of operation. All data points for the power output are shown. The least mean square line exhibits an increase in power output with time; however, this slope is not significant (see Table I). The cell operated at an average power density of 36-37 watts/ft². It should be noted that both anode and cathode polarization decreased with time and that these slopes are significant (see Table I). However, when their variations are added to the other cell variables, no significant slope for power output is obtained.

At 582 hours of operation additional electrolyte was added to the reservoir cup. The power declined in 3 hours from 42.5 watts/ft² to 34.5 watts/ft². At 602 and 625 hours of operation it had declined further to 31.0 and 29.8 watts/ft². At the same time the polarization at 75 ma/cm² for the cathode started to decrease, while that of the anode increased. These observations may be explained on the basis that the additional electrolyte increased the wetting at both electrodes. In the case of the cathode the original wetting was less than optimum, while at the anode it was more than optimum.

This cell was allowed to operate for a total of 2000 hours before it was voluntarily terminated. Power output remained above 24 watts/ft² for the entire 2000 hours.

These data all point to the composition and structure of the cathode as the weakest point in the present cell structure and system. Current exploratory work is aimed at appreciably reducing or overcoming this limitation. Figure 9 represents a step toward increased power performance. At 0.60 volt this cell was producing 60 watts/ft². At maximum power its output approached 70 watts/ft². The total anode polarization was 110 millivolts at 100 amps/ft², while the cathode polarization was 260 millivolts at the same current density. Even in this cell the cathode presents the greater problem and the more promising area for future research.

Research on new electrodes is continuing. The slurry-electrolyte cell design and construction is relatively new, and at this writing the investigations are still on the lower portion of the learning curve. In little over eight months, progress has been made from a sustained steady performance of 15 to 20 watts/ft² to 35 to 40 watts/ft². It is difficult to project what the power output of similar cells will be in the future.

Multicell Unit

A view of a 3 x 2 unit is shown in Fig. 10. This unit consists of 6 cells. Essentially, it is three 1 x 2 units connected electrically in series. These units and some similar 2 x 2 units have been operated on a mixture of H₂, CO₂, and N₂ which simulates partial oxidation of JP-4.^{9,10} The CO₂ supply for the cathode is obtained by combusting the fuel gas effluent from the anodes in the furnace chamber. These units have had intermittent power output in the 40 to 60 watts/ft² range for short time intervals (6 to 24 hours), and 20 to 40 watts/ft² for hundreds of hours of operation. The cathodes employed in these units resemble those used in cell #47-47.

Figure 11 is a view of a 6 x 6 unit consisting of three parallel combinations of two 3 x 2 units in series.⁹ This unit contains one square foot each of anode and cathode. Power output has been as high as 33 watts at 3.0 volt and has remained between 25 and 30 watts for longer than 500 hours of operation.

Conclusion

Fuel cells employing a magnesia alkali carbonate slurry as the electrolyte have been successfully operated for extended time intervals. Continuous operation for more than 2000 hours has been achieved. Power output in small units operating on a simulated natural gas reformat fuel has been maintained at 35 to 40 watts/ft² for longer than 1000 hours. Multicell units have been operated on a simulated fuel representative of partial oxidation of JP-4 at nearly the same level.

New electrode compositions and structures in the initial research stage at this time are yielding power densities equivalent to 60 to 70 watts/ft².

There appears to be no fundamental reason why slurried molten carbonate fuel cell systems should not achieve significantly higher power densities and longer operating periods than those reported here.

Acknowledgements

The author acknowledges the work of J. K. Truitt and T. N. Hooper, who are responsible for the design concept of the slurried electrolyte cell system, the 3 x 2 and 6 x 6 units, and for permission to use photographs of these units. The author is also indebted to J. F. Haefling for assistance on the metallurgical portion and Roy Deviney who assisted in the experimental portion of this work.

References

1. Trachtenberg, I., J. Electrochem. Soc. 111, 110 (1964).
2. Truitt, J. K., Peattie, C. G. and Frysinger, G., "Proceedings of the 18th Annual Power Sources Conference," Power Sources Conference Publication Committee, 1964, p. 14.
3. Trachtenberg, I., in Advances in Chemistry Series #47, Fuel Cell Systems (American Chemical Society, Washington, D. C., 1965), p. 232.
4. Broers, G. H. J., Schenke, M. and Piepers, G. G., Advanced Energy Conversion 4, 131, 1964.
5. Baker, B. S., Marianowski, L. G., Meek, John and Linden, H. R. in Advances in Chemistry Series #47, Fuel Cell Systems (American Chemical Society, Washington, D. C., 1965), p. 247.
6. Broers, G. H. J. and Schenke, M., in Fuel Cells, Vol. 2, G. J. Young Ed. (Reinhold Publishing Corp., New York, 1963), p. 6.
7. Hart, A. B., and Powell, J. H., in "Batteries Research and Development in Non-Mechanical Power Sources," D. H. Collins, Ed. (The MacMillan Co., New York, 1963), p. 265.
8. Trachtenberg, I. and Haefling, J. F., unpublished results.
9. Truitt, J. K., Proceedings of the 19th Annual Power Sources Conference, 1965, in press.
10. Texas Instruments Incorporated, Final Technical Report for Contract No. DA-44-009-AMC-54(T). Prepared for U. S. Army Engineer Research and Development Laboratories, Fort Belvoir, Virginia, 12 March 1965.

TABLE I
Computer Results

Least Mean Square Fit of Data Presented in
Figures 3-8

Unit Number	Slope watts/ft ² /1000 hrs or volts/1000 hrs	Intercept watts/ft ² or volts	Std. Error of Slope watts/ft ² /1000 hrs or volts/1000 hrs	Std. Error of Observation watts/ft ² or volts
Dependent Variable*				
#47-47				
Power 0.7 v	-0.7	17.2	1.0	1.1
Power 0.5 v	1.5	25.8	1.5	1.7
#47-53				
Power 0.5v	-34.6	52	3.7	3.0
Open circuit voltage	-0.03	0.92	0.01	0.009
Anode-polarization 75 ma/cm ²	0.12	0.15	0.03	0.02
Cathode-polarization 75 ma/cm ²	0.22	0.05	0.09	0.07
#47-140				
Power 0.5v	-19.6	44	2.9	3.0
Open circuit voltage	-0.09	1.01	0.02	0.02
Anode-polarization 50 ma/cm ²	0.06	0.16	0.02	0.02
Cathode-polarization 50 ma/cm ²	0.07	0.13	0.01 ₅	0.01 ₅
#33-1				
Power 0.5v	1.0	36	3.1	4.8
Anode-polarization 75 ma/cm ²	-0.04	0.17	0.02	0.03
Cathode-polarization 75 ma/cm ²	-0.05	0.30	0.04	0.05

*Hours of operation is the independent variable.

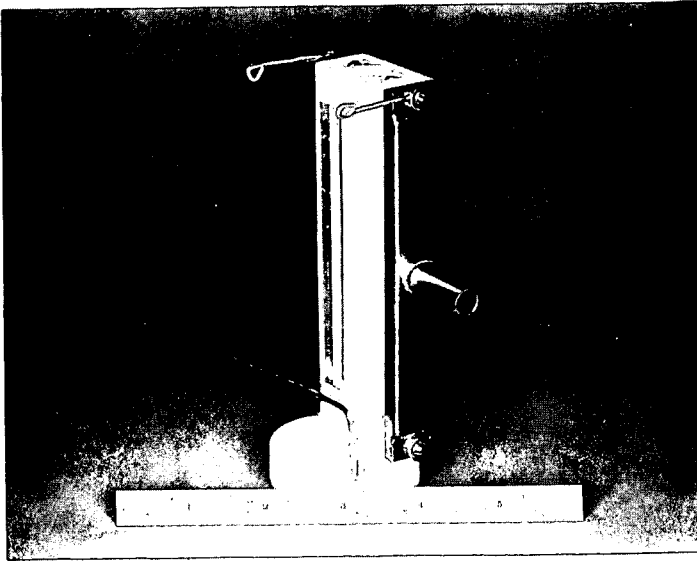


Fig. 1.-VIEW OF 1 x 2 UNIT SHOWING ONE WORKING CATHODE, THE IDLING ELECTRODE, AND THE ELECTROLYTE RESERVOIR.

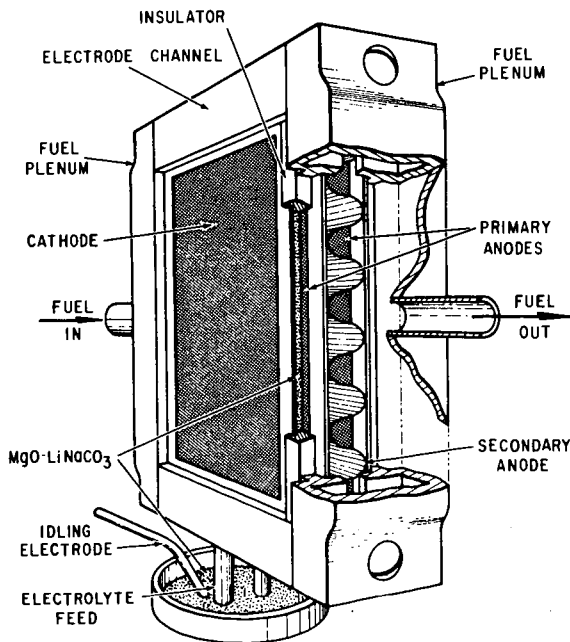


Fig. 2.-A CUT AWAY PERSPECTIVE OF A 1 x 2 UNIT.

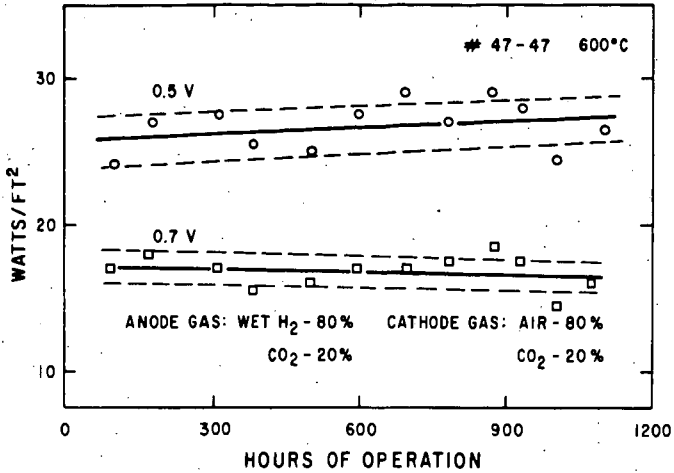


Fig. 3. -POWER OUTPUT AT CELL TERMINAL VOLTAGES (IR INCLUDED) OF 0.5 v. and 0.7 v. IS PLOTTED AS A FUNCTION OF HOURS OF OPERATION. SOLID LINES ARE THE BEST LEAST MEAN SQUARE FITS. DASHED LINES INDICATE THE STANDARD ERROR OF THE OBSERVATIONS FROM THE LINES.

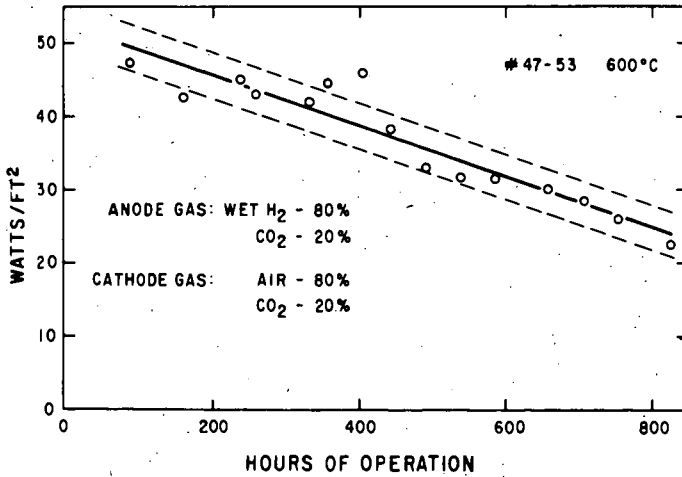


Fig. 4. -POWER OUTPUT AT A CELL TERMINAL VOLTAGE (IR INCLUDED) OF 0.5 v. IS PLOTTED AS A FUNCTION OF HOURS OF OPERATION. SOLID LINE IS THE BEST LEAST MEAN SQUARE FIT. DASHED LINES INDICATE THE STANDARD ERROR OF THE OBSERVATIONS FROM THE LINE.

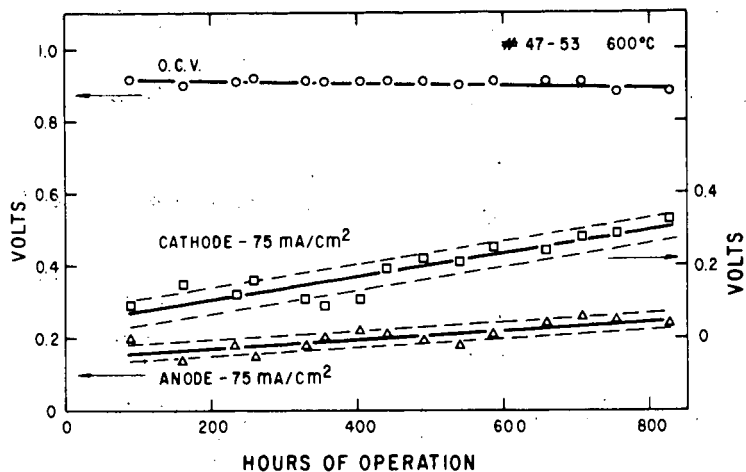


Fig. 5. -TOTAL CATHODE AND ANODE POLARIZATION INCLUDING IR AT 75 MA/CM² AND THE CELL OPEN CIRCUIT VOLTAGE ARE PLOTTED AS A FUNCTION OF HOURS OF OPERATION. SOLID LINES ARE THE BEST LEAST MEAN SQUARE FIT. DASHED LINES INDICATE THE STANDARD ERROR OF THE OBSERVATIONS FROM THE LINES.

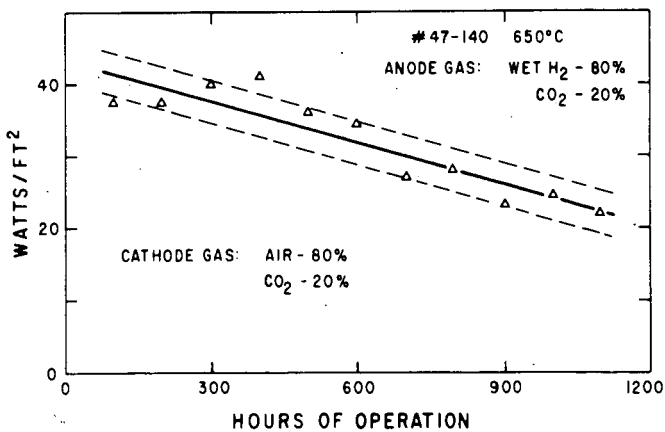


Fig. 5. -POWER OUTPUT AT A CELL TERMINAL VOLTAGE (IR INCLUDED) OF 0.5 v. IS PLOTTED AS A FUNCTION OF HOURS OF OPERATION. SOLID LINE IS THE BEST LEAST MEAN SQUARE FIT. DASHED LINES INDICATE THE STANDARD ERROR OF THE OBSERVATIONS FROM THE LINE.

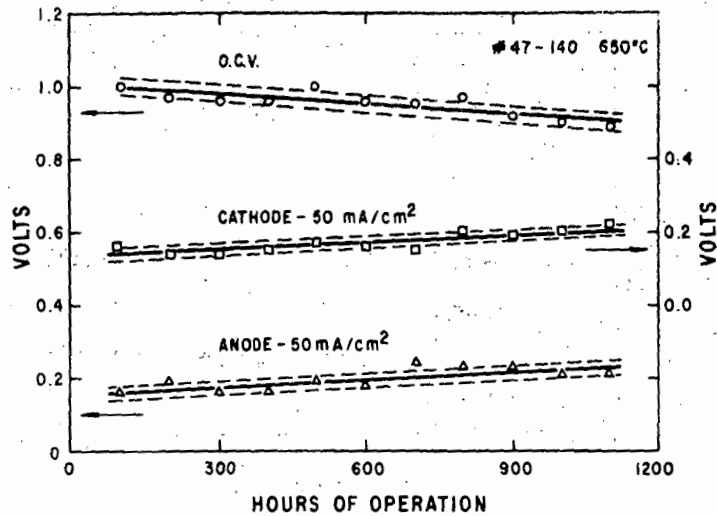


Fig. 7.-TOTAL CATHODE AND ANODE POLARIZATION INCLUDING IR AT 50 MA/CM² AND CELL OPEN CIRCUIT VOLTAGE ARE PLOTTED AS A FUNCTION OF HOURS OF OPERATION. SOLID LINES ARE THE BEST LEAST MEAN SQUARE FIT. DASHED LINES INDICATE THE STANDARD ERROR OF THE OBSERVATIONS FROM THE LINES.

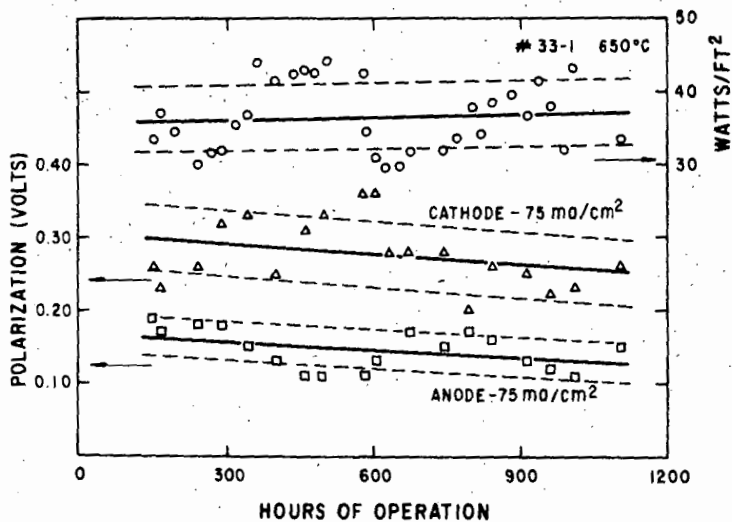


Fig. 8.-POWER OUTPUT AT A CELL TERMINAL VOLTAGE (IR INCLUDED) OF 0.5 v. AND TOTAL ANODE AND CATHODE POLARIZATION AT 75 MA/CM² ARE PLOTTED AS A FUNCTION OF HOURS OF OPERATION. SOLID LINES INDICATE THE STANDARD ERROR OF THE OBSERVATIONS FROM THE LINES.

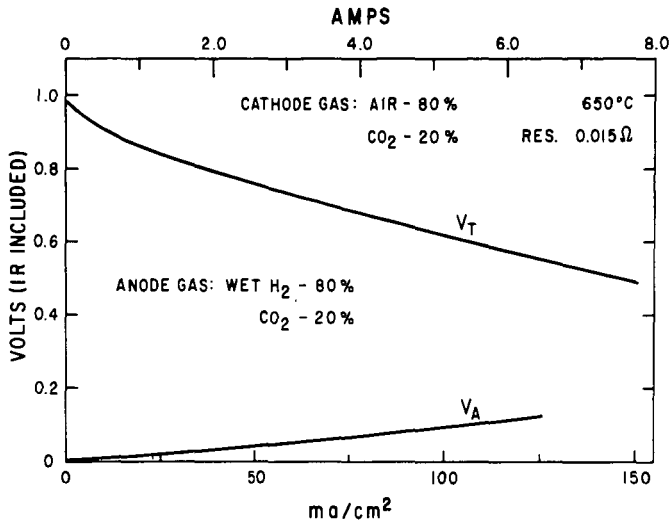


Fig. 9.- V_T IS THE CURRENT-VOLTAGE CURVE WITH IR INCLUDED. POWER OUTPUT IS 60 WATTS/FT² AT 0.6 v. CELL TERMINAL VOLTAGE. CURVE V_A INDICATES TOTAL ANODE POLARIZATION. AT 100 MA/CM² TOTAL ANODE POLARIZATION WITH IR IS 110 MILLIVOLTS.

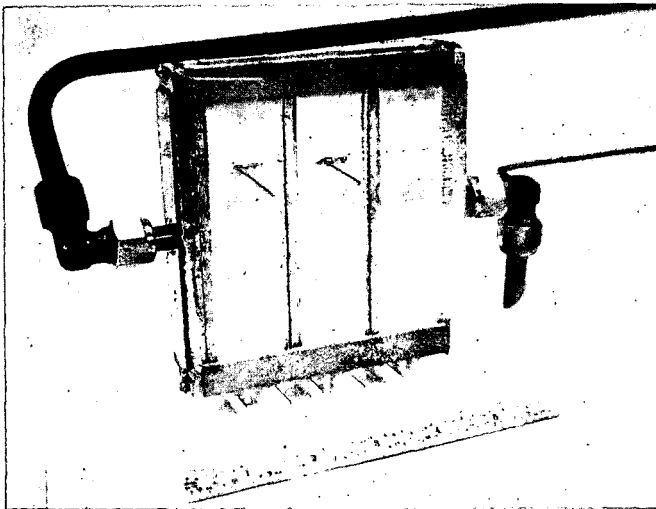


Fig. 10.-VIEW OF A 3 x 2 UNIT SHOWING HALF OF THE WORKING CATHODES.

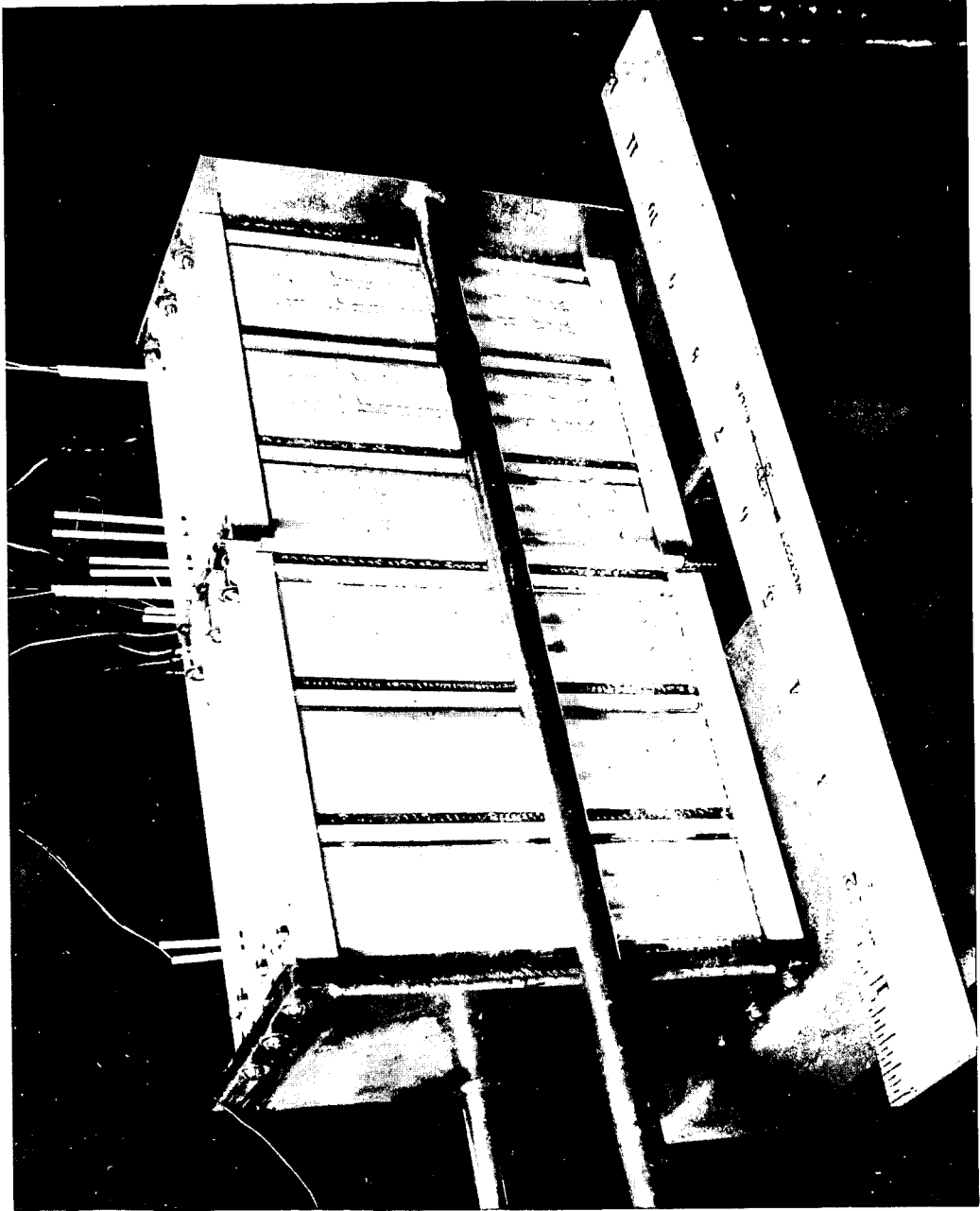


FIG. 11. -VIEW OF A 6 X 6 UNIT WITH THERMOCOUPLES ATTACHED TO SEVERAL OF THE WORKING ELECTRODES.

The Semi-Industrial Fuel Cell Element of the Gaz de France

A. Salvadori
Experimental and Research
Center No. 1 of the D.E.T.N. of
Gaz de France

INTRODUCTION

The studies undertaken by the laboratories of Gaz de France in the field of energy conversion have been carried out for almost four years in order to transform directly into electrical energy in a fuel cell the free energy of gases currently manufactured or distributed by this national service.

Massive quantities, relatively low prices and ease of transport of these raw materials encourage research towards perfecting industrial devices that would be simple, rugged, and inexpensive, but capable of yielding significant power. Relatively inert fuels are the usable gases: both natural gas either unreacted or catalytically steam reformed, and gas obtained by partial oxidation of gas and liquid hydrocarbons, nevertheless contain, although in small quantity, some impurities which seem to prohibit, to our knowledge, the use of sufficiently active, but sensitive catalysts which would allow functioning at moderate temperatures and in an aqueous environment. Under these conditions, it becomes necessary to counterbalance the catalytic effect by an increase in temperature and hence to operate in the presence of electrolytes made of molten salts. It seems better to make the best use of the notable advantages offered by the high temperatures providing the condition that the technological difficulties and the resulting corrosion problems can be solved.

The unavoidable heat release, provoked by any type of functioning cell, is all the more interesting to recover when the temperature of the system is high and when the dimensions of the battery are significant. The fuel cell then becomes a means of base production of electrical current which is located upstream in a complex. The other devices of this complex can use the thermal energy released by the cell.

1. PRINCIPLES OF OPERATION FOR AN INDUSTRIAL GENERATOR

Keeping these considerations in mind, the operating principle of an industrial generator can be defined in a general sense and thus serve as a constant objective towards which all investigations must be oriented.

The potential at the terminals of an elementary cell are low. For an installation to be of industrial interest it is necessary to group, in a unit well adapted to isothermal operation, the greatest possible number of elements. However, as these warm

each other, they must be spaced in the most judicious way so that the regulating fluid ensures as homogeneous a temperature as possible in all parts of the enclosure; for obvious reasons air used as an oxidant can be used for this role.

Two simple geometric forms may be considered a priori for the basic cells: the plane and the cylinder. We have deliberately set our choice on the latter for the following reasons: the thermal regulation of an assembly of bundles of the exchanger type is industrially well known; the practical construction of flat and thin electrodes of large area presents more difficulties than that of tubes; the high temperature construction in the shape of a filter press creates important sealing problems and prevents any possibility of replacing an element without a complete stop in the functioning of the battery; the phenomena of diffusion or creepage of the electrolyte at the joints or in any nonactive part of the cell may be easily eliminated in tubes by cooling of the involved extremity, at a temperature slightly below that of the melting point of the fused salts; the reacting gas supply is greatly simplified where all the cells have an electrode of the same sign in a unique enclosure containing the corresponding gas; the mechanical strength of a tube made by successive layers of the anode, of the electrolyte and of the cathode, is better than that of a plane surface made under identical conditions.

The construction of a cylindrical cell battery is advantageously made through a horizontal disposition of the elements inside a heated parallelepiped shaped container of which two opposite sides form supports and to which are fixed the ends of the cells bearing the different gas distribution systems and the current collectors. In order to determine orders of magnitude, the thickness of such an installation would be close to one meter, and its length and height would be a few meters. An unlimited number of cells may be used by placing them side by side separated by a passage large enough to conduct electric current of substantial size.

Figure 1 shows the sketch of an industrial unit which would function according to the above mentioned operating principles.

2. DESCRIPTION OF THE SINGLE CELL

The conception of an element must satisfy the technological constraints which have been enumerated and give an answer to the economic problems that the development of a new technology can create.

2.1 Choice of Materials

The materials with which the electrodes are made are generally expensive and rare, and it is necessary to use them in a small quantity and to build them by simple methods relying on industrial techniques that assure reproducible fabrication of several tens of thousand units. The three phase contact problem, gaseous (the reacting fluids), liquid (the electrolyte) and solid (the electrodes), has in the beginning of our work brought us to follow the method used very generally at the time, which consists of using porous metals and looking for their best operating conditions. Because, on the one hand, of the disadvantages that we have observed

in the utilization of a relatively thick layer, the accumulation in the pores either of products of combustion or nitrogen from the air, and on the other hand of the knowledge of the good diffusion at high temperature of gases through certain metals, we tried the use of these metals in thin compact sheets.

The diffusion of hydrogen through palladium and platinum is a phenomenon which has been known for a long time; further the systematic studies that we have made in this field have shown that the oxidant made of air to which carbon dioxide has been added passes sufficiently rapidly through thin silver sheets to give results at least as good as with the porous substances.

2.1₁ The Anode

In spite of above mentioned advantages, the utilization of palladium in a sheet cannot be considered for economical reasons, because it prohibits the use of any other fuel gas than hydrogen. For these reasons, the anode in our cells is always a graphite cylinder very lightly covered on the surface with palladium (close to 0.1 mg/cm^2).

Graphite has numerous advantages: good electronic conductance, very low expansion coefficient, relatively good mechanical strength and easy construction. Furthermore, in the reducing environment in which it is situated, it has never shown signs of deterioration.

2.1₂ The Cathode

Silver constitutes at the present state of our knowledge, the only metal usable as a cathode. But used as is and without preliminary precaution, in the presence of molten carbonates, it is subject to permanent corrosion. A systematic study has brought to light three principal aspects of the silver corrosion that can be summarized in the following manner; one of mechanical nature due to a degradation of the structure and which favors grain formation; another of a chemical nature which can be defined by a limited dissolution in the electrolyte; finally the third of an electrochemical nature making some silver precipitates appear in the electrolyte, which, because of convection currents and variable potential lines in the functioning cells, can settle at different points between the two electrodes.

However, our observations on the inhibiting role of combining with refractory oxides either in the electrolyte bath or in the cathode itself, have lead us to use a film of these oxides in order to materialize the idea of protecting the silver surface.

The film itself is made in a thin layer (0.1 mm) by flame spraying and offers all the qualities of a sheet.

2.1₃ The Electrolyte

Only electrolytes made of molten salts are usable. Among the different possible solutions, carbonates in a mixture judiciously chosen in relation to the temperature have been employed for CO_2 as one of the reaction products and its presence is favorable in particular to their thermal stability.

2.2 Employment of Materials

To satisfy the conditions preceedingly developed: compactness, facility of assembling, good mechanical resistance, small quantities of materials, easy industrial operation, we have studied in the most comprehensive way the best method of construction based on the following principles:

2.2₁ The Active Substance of the Cell (Fig. 2)

On the anode graphite finger palladium is deposited. A layer of refractory oxide, preferably of magnesia or stabilized alumina is deposited on the anode by flame spraying. This very thin layer, just thick enough to assure a good electric insulation contains the carbonates and thus serves as a support for the electrolyte. A silver-based thin film (0.1 to 0.2 mm) which constitutes the cathode is then deposited on the assembly. This metallic film is too thin to insure by itself a sufficient means for current removal and this is achieved by a silver wire fixed along the electrode which can be joined in a battery, to a central conductor.

2.2₂ The Top of the Cell (Figure 3)

The open extremity of the graphite finger is fixed in a brass piece which contains: an axial nozzle that penetrates to the bottom of the anode, its role is to feed fuel to the cell and to collect the anodic current; a radial nozzle through which the excess fuel that has not reacted carries away the products of the reaction water vapor and carbon dioxide.

This part of the cell, is connected to the wall of the exterior enclosure and is maintained at a lower temperature than that of the melting point of carbonates; they solidify and the creepage phenomena that would provoke their disappearance is prevented.

3. CONSTRUCTION OF A LABORATORY BATTERY USING SEMI-INDUSTRIAL ELEMENTS

The experimentation with single cells of various dimensions and method of construction proceeds in different directions with two goals; first to increase electrical performances, and second to prolong their life.

The present conception of the cells would allow a unit of dimensions which are already substantial and the battery that we have made could easily be built on a larger scale. But current densities of the order of 40 mA/cm² at 600 mV, and limited longevities, do not permit such an extrapolation.

However, the necessity to come out with a development of gas cells as quickly as possible has lead us to deal with problems created by the grouping of several elements. The latter are many and the following enumeration mentions only the principal ones:

1. Regulation of the unit temperature
2. Effective collection of the current

3. Evacuation and recuperation of the reaction products.
4. Controlled feeding of oxidant and fuel
5. Current Efficiency
6. Starting and stopping of the batteries
7. Analysis of results and evaluation of true efficiency

Accordingly the study and construction of a unit of large laboratory proportions already using some elements at the semi-industrial scale, has been undertaken in parallel with research on single cells.

3.1 Description of the Installation

3.1.1 Choice of the Number of Elements

In order to correspond to the hexagonal disposition generally adopted for the bundles of tubes, we have chosen 7 elements of which one is centrally located. It is necessary to place them in an oven that will insure their heating at the start and to compensate for heat losses while in operation.

3.1.2 The Oven (Figures 4 and 5)

It permits heating to 1000°C the volume containing the seven elements and can be placed under an oxidant pressure of a few tenths of a bar. It contains three superposed resistances, the wiring and regulation of which are independent, the lid of the oven is fixed and supports the tubular cells; the oven can be lowered to give access to the electrodes. The lower part can also be taken apart and easily repaired in the case of electrolyte leakage; it is provided, with devices that secure the positioning and support of the cathodes. This oven is also provided with auxiliaries that include:

1. An elevator assembly made of a platform capable of moving vertically which supports the oven.
2. A lifting crane for the block of cells.
3. The regulation of the independent electrical connections to the three heat zones.

3.1.3 Auxiliaries Insuring the Functioning of the Battery

First let us mention the inlet and outlet circuits of the reactants which present a certain complexity since they must insure constant flows, pressures and mixtures (case of the carbonated oxidant). Furthermore, the products of the reaction are collected and accounted for.

The problem resulting from the utilization of a current produced at several tens of amperes under some hundreds of millivolts has been solved through the use of a rotating device.

The oven is surrounded by a platform of dimensions large

enough to allow the technicians to work directly on the tops of the cells: all the controlling and measuring instruments are grouped at this level.

Figure 6 shows a general view of the system, it shows:

1. In the foreground the platform.
2. At the left, the oven.
3. At the right the instruments for measuring, controlling and fuel supply assembled on the same board.

3.1.4 Measuring Instruments

The gas reactants are supplied via classical laboratory flow meters, the water produced is retained by collectors followed by weighings: the carbon dioxide is sampled by a mass spectrometer (Fig. 7).

The overall electrical characteristics of the battery and those of each single cell are recorded continuously in order to obtain the most information from each experiment.

To account for results and to calculate the electrical and electrochemical performances of the installation, suitable meters are employed. Let us add that these measurements are completed by taking temperature at numerous points in the installation and inside each cell.

3.2 Experimental Results

The assembling of the complete installation has just been completed but its auxilliary apparatus for production of reformed gas that is intended for use with it, is not yet functioning. This installation has been in operation for too short a time to make it possible to publish definite results that ought to be further substantiated. As an example we shall give the results obtained during the first experiment with a set of 7 cells made under identical but not optimum industrial conditions.

3.2.1 Characteristics of a Single Cell

Total Length, mm	Diam., mm	Active Surface, cm ²	Weight, gm/cm ²			
			Cathode	Anode	Electrolyte	Refractory Oxide
800	18	220	0.130	graphite 0.55 palladium 0.002	0.048	0.170

3.2.2 Operating conditions

Oxidant air + CO₂ (30%); flow, 300 l/h under 150 m bars. The flow of air is relatively important due to the oversized dimensions of the oven. Fuel industrial hydrogen flow, 50 l/h under 130 m bars. In this experiment the hydrogen is not recycled after use. Temperature of operation: 600°C.

3.2_a Principal results obtained

This experiment was particularly aimed at determining the efficiency of series and parallel assemblies and in both cases the current potential curves shown on Figures 8 and 9.

The performances obtained with these cells made under poor conditions and for a relatively low test temperature are modest: 20A at 0.5v, which corresponds to a maximum power of 10w.

The duration of the experiment which was limited to approximately ten hours cannot be taken into consideration.

This experiment has shown, however, that the whole installation can satisfy all the technological objectives that we had defined. Furthermore, it will be possible to have twenty cells operate within the same dimensions and the same connections and the usable surface of each one of the cells may be further increased.

4. CONCLUSIONS

The conception of an elementary cell of semi-industrial dimensions which we have reached could, from the technological point of view, lead in the future, without major difficulty, to the construction of a pilot unit. Numerous problems for assembling and handling of materials were solved. They permit the construction of a battery which offers the possibility of studying the behavior of cells fabricated under various conditions, following operating methods apt to be used in industry.

Important progress has been made to considerably reduce the causes of corrosion (some silver cathodes preserved through combination with a coat of refractory oxide have shown no detectable sign of corrosion after operating for a few hundred hours). It is now necessary to ensure an industrial application that we consider, the construction of cells whose lifetime exceeds a year.

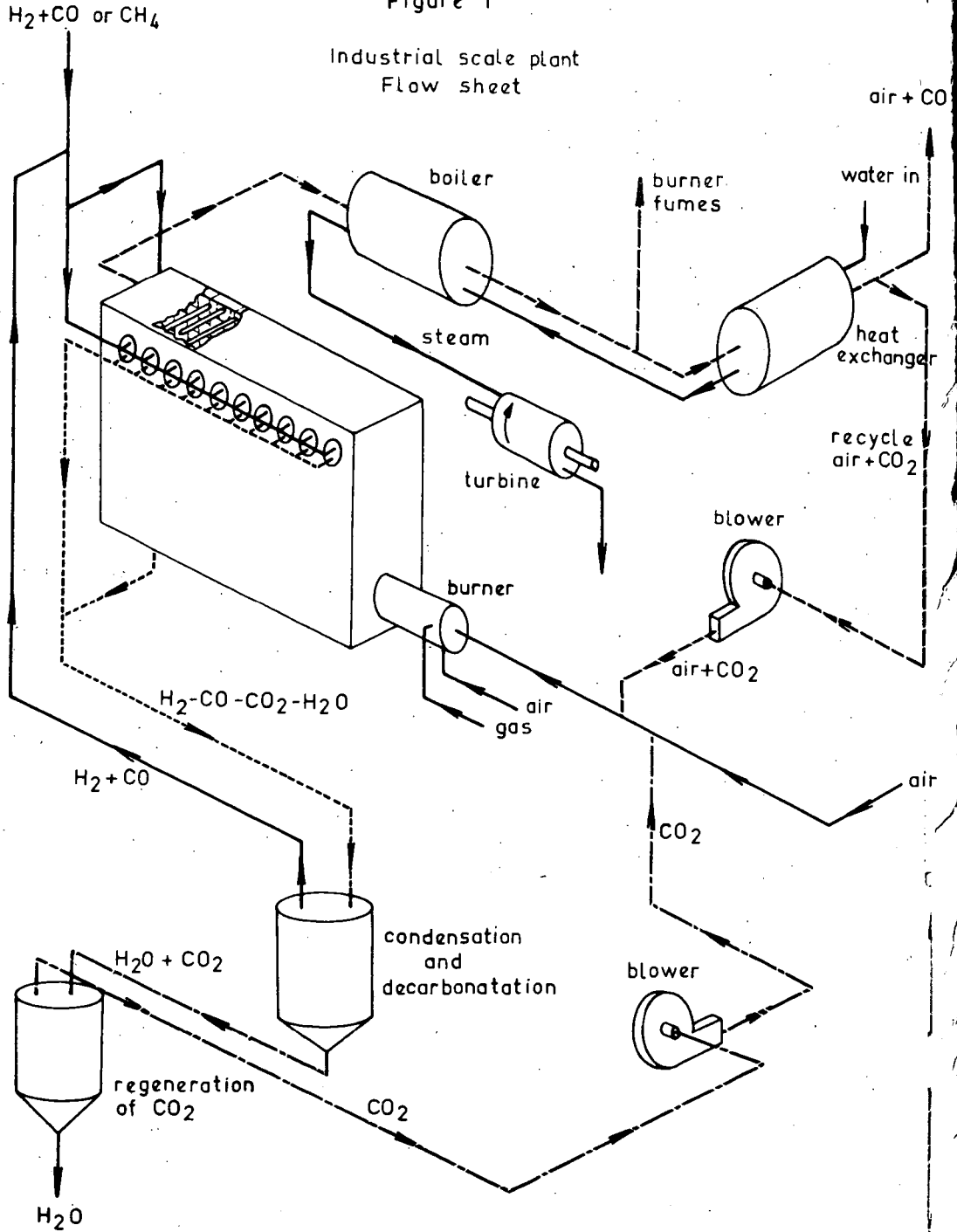
The current densities of some tens MA/cm² that we obtained from single cells are insufficient to make a powerful generator operate under advantageous conditions and compete with standard methods of power generation. We do not believe that this problem is impossible to solve in a reasonable period of time because it is difficult to imagine performance of high temperature cells being inferior to those of cold cells.

On the other hand the lifetime of gas cells which depends in particular, on many phenomena of corrosion, on the modification and the change with time of the properties of materials at various temperature, will require important efforts if the research is to be brought to the proper value.

For this purpose, Gaz de France is working in collaboration with specialized laboratories at universities or in industry and particularly with the Compagnie Generale d' Electricité. Gaz de France has obtained a research contract as a result of action of the committee for conversion of energy which is part of the General Delegation for Technical and Scientific Research.

Figure 1

Industrial scale plant
Flow sheet



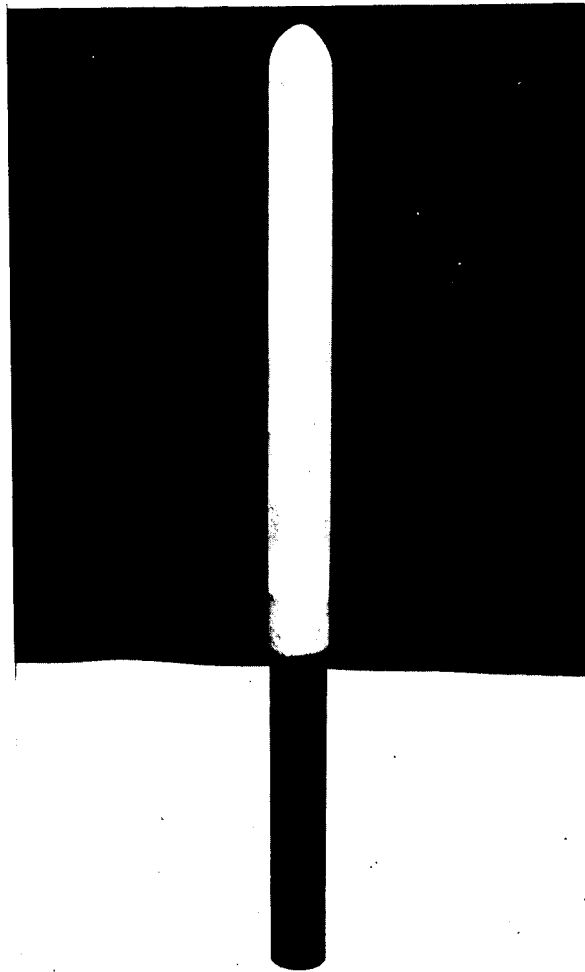


Figure 2: Main Section of a Single Cell

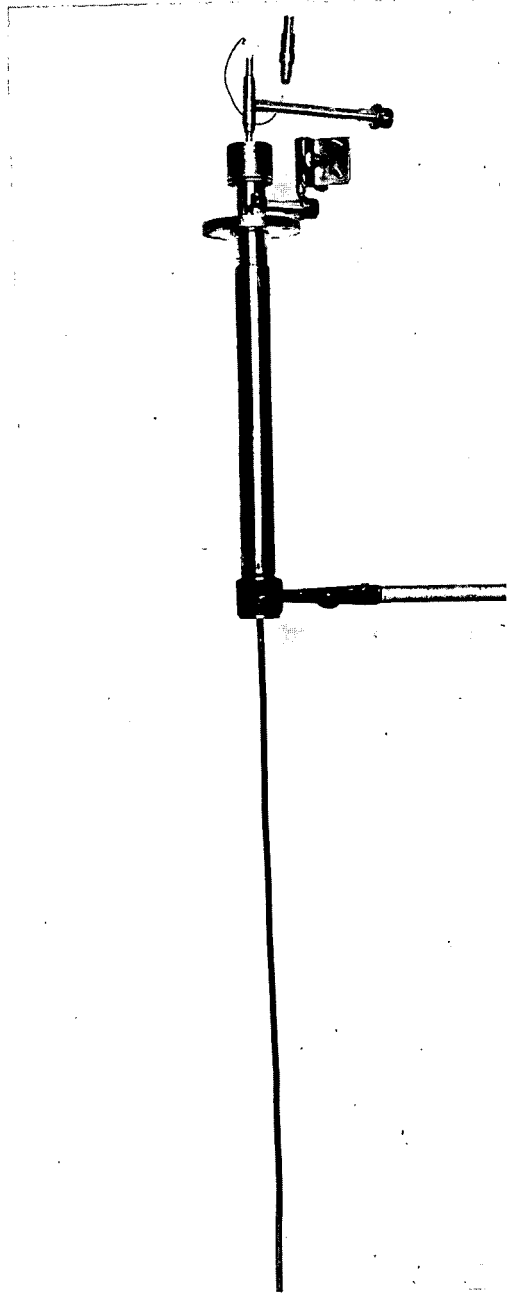


Figure 3: Top of a Single Cell

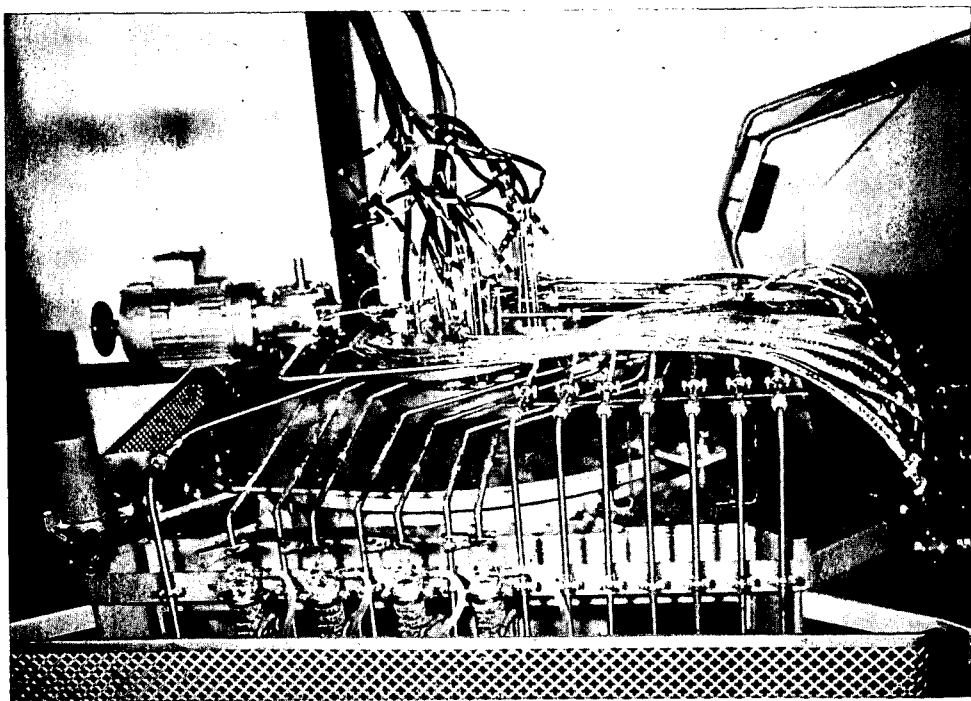


Figure 4: Seven-Element Battery, Top View

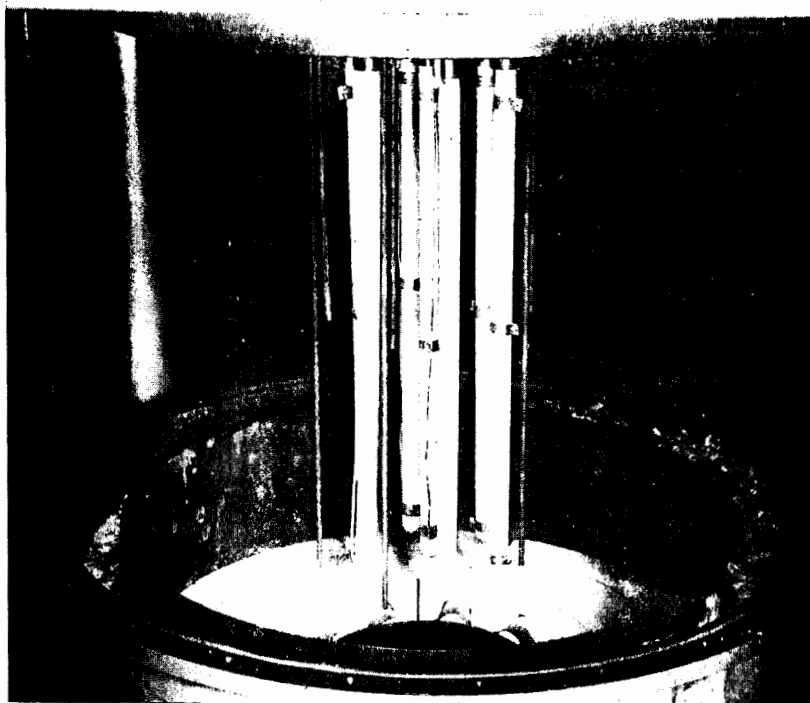


Figure 5: Seven-Element Battery, Bottom View

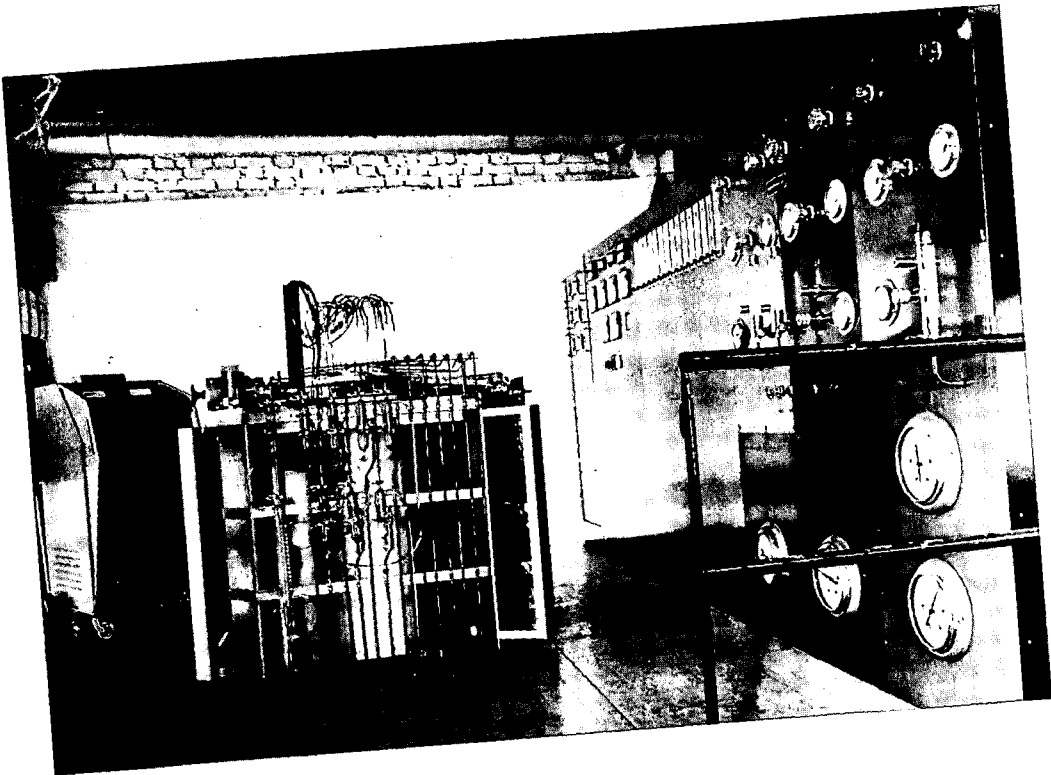


Figure 6: Total System

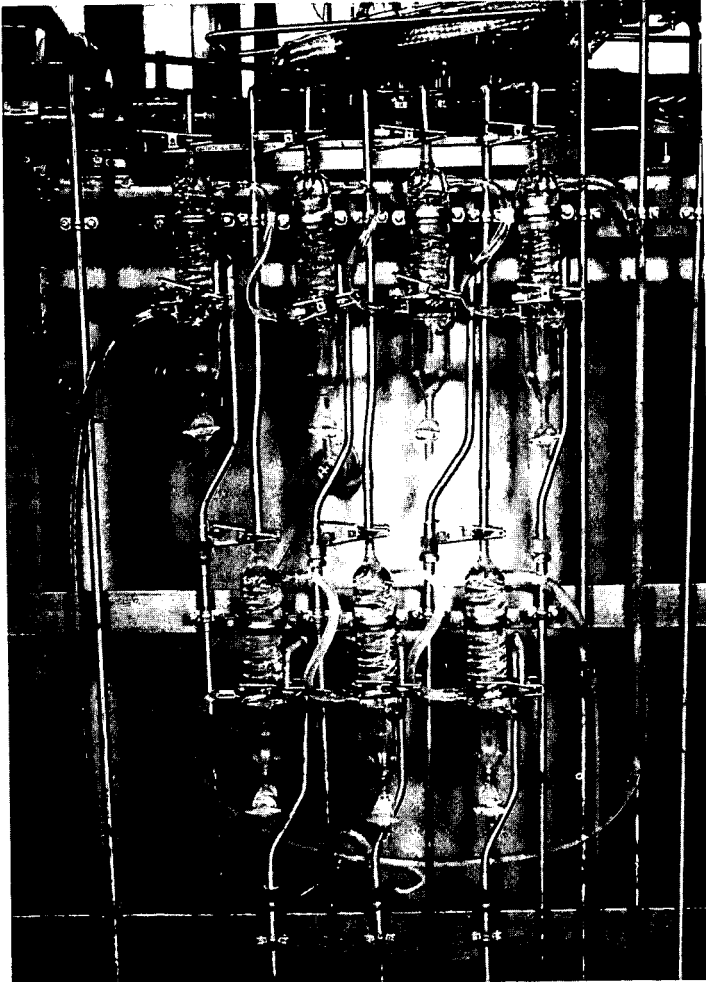
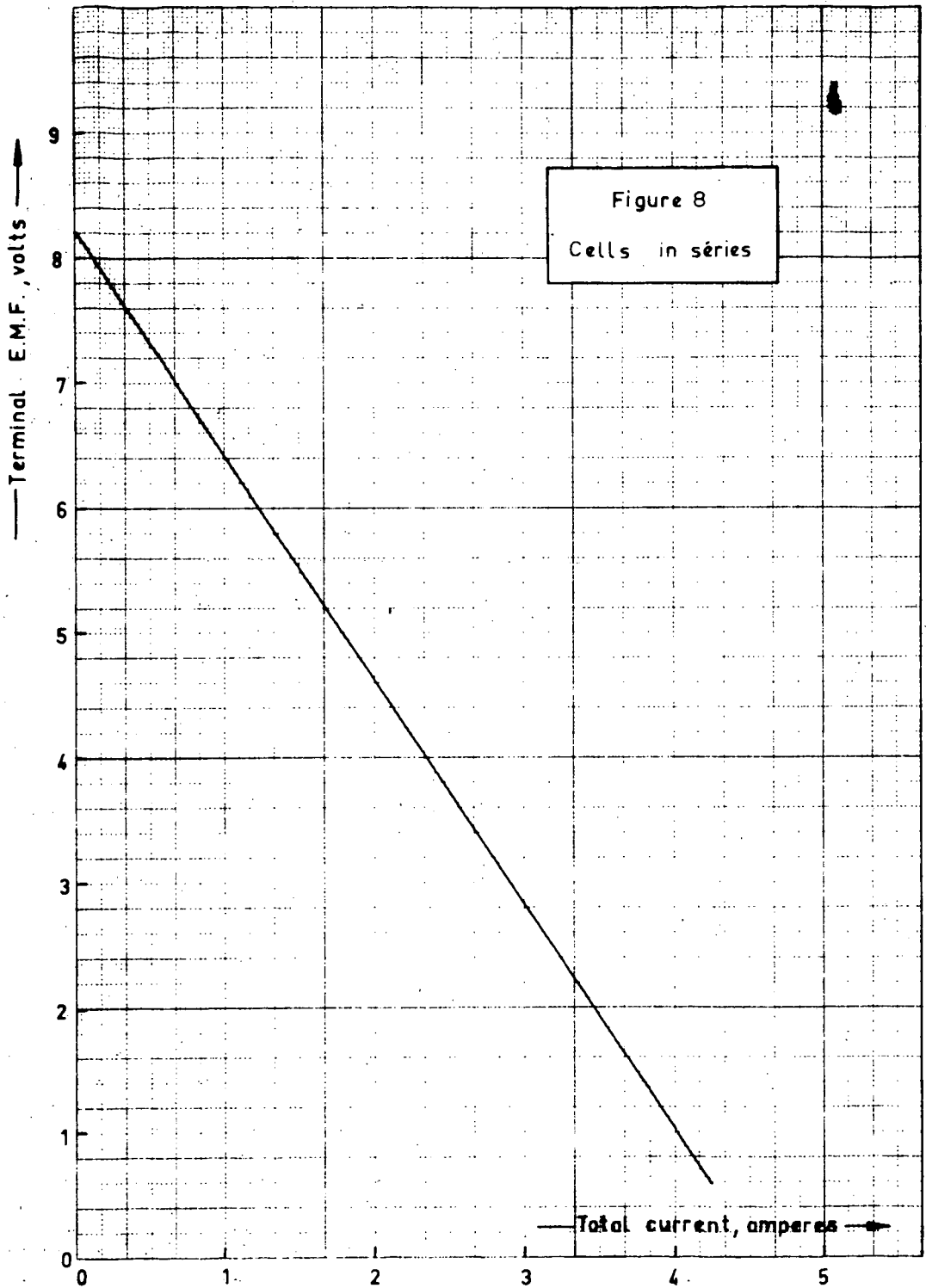
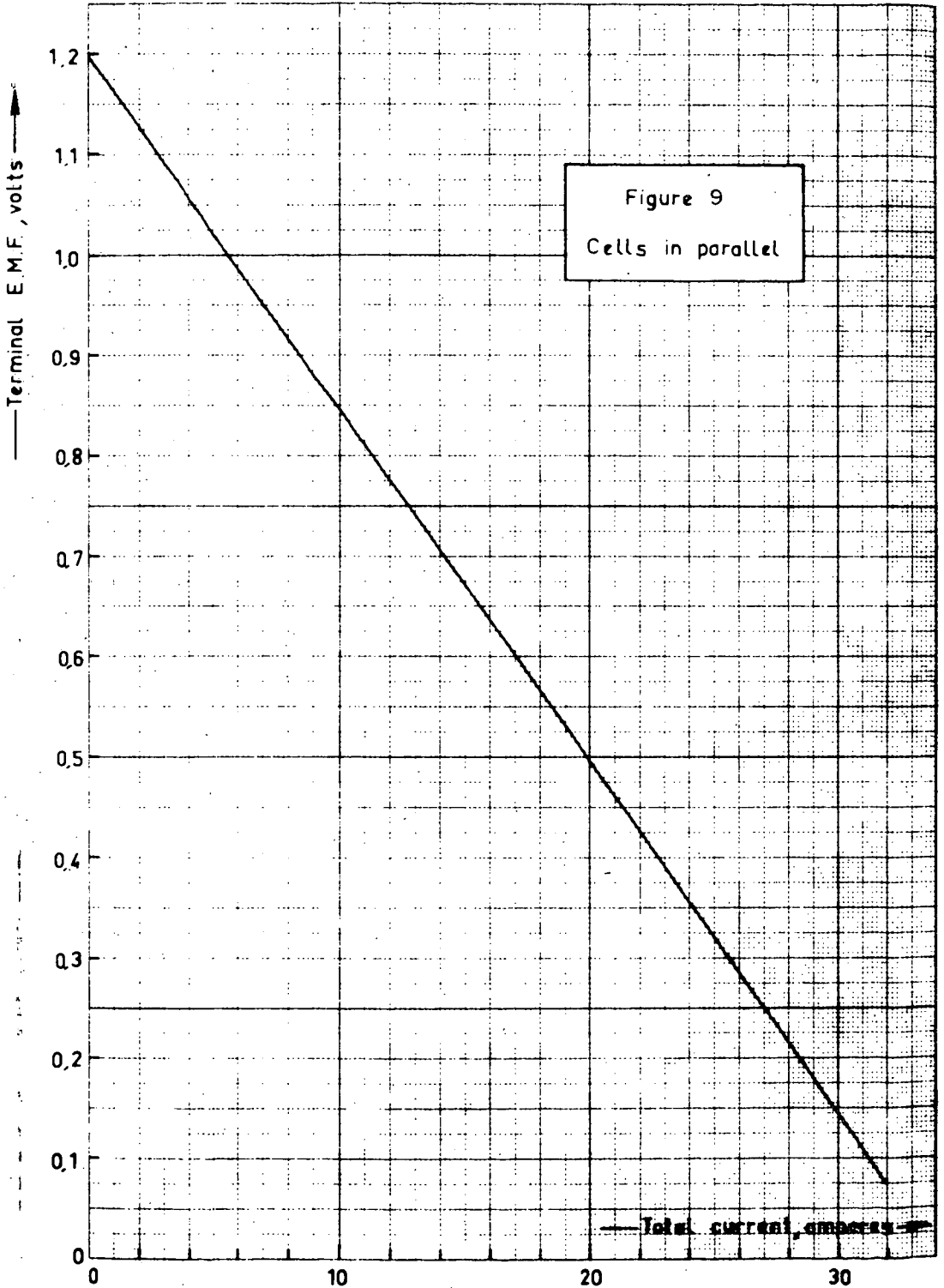


Figure 7: Recovery of the Reaction Products





ELECTRODE REACTIONS OF CO AND CO₂ IN MOLTEN CARBONATES

Alina Borucka

Cambridge University, Cambridge, England

ABSTRACT

Experiments have been made on the electrochemical reactions of CO/CO₂ gas mixtures at gold electrodes in molten ternary eutectic of lithium, sodium and potassium carbonates at temperatures up to 900°C. At zero applied current, the electrode potential depends on the partial pressures of CO and CO₂ according to the Nernst equation for the reaction: $\text{CO} + \text{CO}_3^{--2} = 2\text{CO}_2 + 2\text{e}^-$. Anodic current/potential relationships have been studied up to polarizations of 500 mV; similar measurements in the cathodic range have been made within the limits set by the Boudouard reaction.

MOLTEN CARBONATE FUEL CELL WITH WATER INJECTION

J. Millet

R. Buvet

Direction Des Etudes Et Recherches
De L'Electricite de France

17 Avenue de la Liberation
Clamart, Seine, France

1. INTRODUCTION

Since the end of the 19th century, using the chemical oxidation energy of fossil fuels has been considered in order to produce electrical energy directly from fuel cells.

The fact that a cell is more easily supplied with a gas especially a carbon containing gas has lead engineers to be interested for a long time in molten carbonates as an electrolyte. The first works of Ostwald (1) then those of Baur (2) and his co-workers were concerned with cells using gases which contain hydrogen and carbon monoxide.

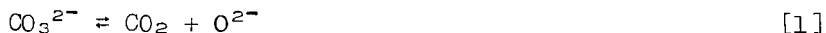
Davtyan (3) then Broers and Ketelaar (4) recommended a molten electrolyte fixed in a porous solid matrix. Gorin (5), Justi (6) and more recently many others such as Hart (7) and Salvadori (8) have also recommended the use of molten carbonates in fuel cells.

An important improvement has been brought forward these last few years, especially by Broers, in the performance of molten carbonate cells by adding carbon dioxide to oxygen feed.

2. USE OF AN ELECTROLYTE BUFFER

Several goals of our research group have been aimed at understanding the mechanism of exchange in the molten carbonates and the functioning of oxygen and hydrogen electrodes.

The carbonate solvent is entirely dissociated into the anion CO_3^{2-} and cations and the anion CO_3^{2-} is further dissociated according to the equilibrium:



The system $\text{CO}_3^{2-}/\text{CO}_2$ can thus be considered an acid-base system according to Lux (9) and Flood and Förland (10) with exchange of the O^{2-} ions.

To the equilibrium [1] there corresponds an equilibrium constant $K = \frac{C_{O^{2-}}}{P_{CO_2}}$ that Dubois (11) has found equal to 10^{-6} .

The solubility of CO_2 in carbonates has been measured

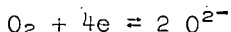
$$\frac{C_{O^{2-}}}{P_{CO_2}} = 10^{-4}$$

In these formulas the pressures are expressed in atmospheres and the concentrations of solutions in molarities.

A more recent work of Busson and Palons (12) on the potential at zero current of the oxygen electrode in the carbonates has made it possible to establish with precision the constant of equilibrium to be $K = 6$.

A solution of molten carbonates can be defined by the pO^{2-} , the negative logarithm of the concentration of ions O^{2-} .

The function of the oxygen electrode in the molten carbonates produces some O^{2-} ions.



In the vicinity of the oxygen electrode, the concentration of O^{2-} ions increases and this increase, inasmuch as it is not counter-balanced by diffusion, produces a polarization of the cell which can be called acidity polarization.

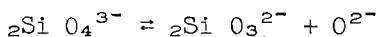
To bring CO_2 to the oxygen electrode, is to counter-balance the production of O^{2-} through the contribution of the acid part of the solvent, which as the effect of maintaining the pO^{2-} at a high value. This is a buffer effect. This effect may be visualized through Fig. 1. The diagram represents potentials of the oxygen and hydrogen electrodes as a function of pO_2 . The straight lines AC and BD are parallel and of slope $\frac{RT}{2F}$. The potential at zero current is the thermodynamic cell potential equal to AB and CD. If the hydrogen electrode operates at $pO^{2-} = 0$ and the oxygen electrode at $pO^{2-} = 6$, the potential of the cell is reduced to EB and the overpotential of acidity polarization is AE-A 600°. This overpotential is at the maximum of approximately $83 \text{ mV} \times 6 = 500 \text{ mV}$.

The pO^{2-} of the electrolyte of the cell can also vary at the fuel electrode through a contribution of CO_2 or of other products or where the pressure of CO_2 in the atmosphere rises above the electrolyte.

It is thus very important, in order to obtain a cell which operates in all circumstances, to maintain the pO^{2-} of the electrolyte constant on all parts of the cell.

Through association with the phenomena observed in aqueous solutions, we shall use weak acid systems relative to the solvent.

The orthosilicate metasilicate system fits very well:



The same applies to other salts exchanging the O^{2-} ion.

Our research has brought us to a much more simple and industrially profitable system. It is the water system.

3. WATER IN MOLTEN CARBONATES

Water has the properties of a weak acid in molten carbonates.

The properties of water may be summarized by the two equilibrium reactions:



The constants K_A and K_B are arranged to correspond respectively to these equilibria according to the relations:

$$\frac{P_{\text{CO}_2} \cdot C_{\text{OH}^-}^2}{P_{\text{H}_2\text{O}}} = K_A \quad [5]$$

$$\frac{P_{\text{H}_2\text{O}} \cdot C_{\text{O}^{2-}}}{C_{\text{OH}^-}^2} = K_B \quad [6]$$

These relations imply that the chemical potential of the solvent is constant, that is

$$C_{\text{OH}^-} \ll C_{\text{CO}_3^{2-}} \quad [7]$$

In an acid environment, the pressure of CO_2 determines the equilibrium potential, K being the equilibrium constant [1].

$$E = E_0 + \frac{RT}{4F} \log P_{\text{O}_2} + \frac{RT}{2F} \log P_{\text{CO}_2} + \frac{RT}{2F} \text{p}K \quad [8]$$

In the presence of a water system, the potential of the oxygen electrode is given by the relation:

$$E = E_0 + \frac{RT}{4F} \log P_{\text{O}_2} + \frac{RT}{2F} \log P_{\text{H}_2\text{O}} - \frac{RT}{F} \log C_{\text{OH}^-} + \frac{RT}{2F} \text{p}K_B \quad [9]$$

By varying the OH^- concentration and the partial pressures of water and oxygen in the atmosphere in equilibrium with the molten carbonates, we have shown that $p K_B$ is close to 5. We conclude that $p K_A = p K - p K_B = 1.5$ (by taking the reference states of gases at a pressure of one atmosphere).

There is a constant contribution of water vapor at the hydrogen electrode. On the oxygen electrode the contribution of water vapor has the effect of maintaining the basic electrolyte at a determined $p \text{O}^{2-}$ (below 6.2).

4. APPLICATION TO FUEL CELLS

The properties of a water system in carbonates have important consequences on the functioning of cells. They allow a reduction of the acidity polarization as does the carbon dioxide fed with oxygen. But as it was demonstrated by Hart (13), the use of carbon dioxide constitutes a heavy burden from an industrial point of view whereas the use of water would be much easier and cheaper.

In comparing the properties of similar elements of a cell fed on oxygen without any addition, with carbon dioxide and with water vapor, we were able to realize that the performances due to the addition of water are the best (Fig. 2).

The polarization is not only diminished by the contribution of water vapor (potential of zero current near 1 volt instead of 0.7 volt) but the current at the same cell potential is very superior to that obtained with the use of CO_2 . This phenomenon seems to be comparable with the increase of fluidness of molten carbonates in the presence of water.

Finally, the action of water as a weak acid allows the use of fuel gas containing carbon dioxide with an hydrogen electrode of porous material. Indeed, let us consider a cell functioning with a water pressure of 0.3 atm, in an hydroxyl ion environment.

Equation [5] gives 0.015 atm as a value of $p \text{CO}_2$ in equilibrium. Consequently, any fuel gas containing a weaker carbon dioxide partial pressure may be used without the risk of modifying the $p \text{O}^{2-}$ of the electrolyte.

5. MAKING OF PROTOTYPES

The preceding studies have first lead to tests on elements of cells of a few watts.

We are presently constructing several prototypes of a power close to 1 kw which vary in their geometric conception (vertical or horizontal electrodes) but have the same electrochemical conception.

The materials used are steel (25% Cr, 20% Ni) and dense alumina for the containers, thin sheets of palladium (50 microns) of an alloy of 24% silver-76% palladium for the fuel electrodes and silver and porous steel for the air electrodes. The electrolyte is a ternary eutectic of lithium, sodium and potassium carbonates functioning at 600°C. The fuel is a gas obtained through the reforming of natural gas and the oxidant air contains from 10 to 30% of water vapor.

The gases are fed at a pressure slightly higher than atmospheric.

Figures 3 and 4 are photographs of prototype elements with horizontal and vertical electrodes.

Naturally, these prototypes must be placed in an oven because their dimensions are too small to be autothermic.

The prototypes will give rise to a technico-economical study aimed at searching for the place of this system in the industrial production of electrical energy.

ACKNOWLEDGEMENT

The results which we presented are based on the work of a group of researchers which includes, besides the authors:

Mmes: Busson

Jacquin

Palons

Messrs: Barde

Dubois

Heuze

Legrauche

Bibliography

1. W. Ostwald
Z. Elektrochem. 1894 1 122
2. E. Baur
Z. Elektrochem. 1921, 27 194-199
3. O. K. Davtyan
Direct Conversion of Chemical Energy of Fuel into Electrical Energy, Moscow, 1947.
4. G. H. J. Broers, J. A. A. Ketelaar
(Young) Fuel Cells. Reinhold, New York 1960.
5. E. Gorin, H. L. Recht
Chem. Eng. Progress, 1959, 55 51-58
6. E. Justi, F. H. Spengler
U. S. Patent No. 2,830,109 1958.
7. A. B. Hart
Private communication. 1963.
8. A. Salvadori
Rev. Just. Franc. Petrole 1964, 19 144.
9. H. Lux
Z. Elektrochem. 1939 45 303.
10. H. Flood, T. Förland
Acta. Chem. Scand. 1947, 1 592-604, 79-798.
11. J. Dubois
Thesis, Paris 1964
12. R. Buvet, N. Busson, J. Millet, S. Palons
C.R. Sc. Acad in preparation
13. A. B. Hart, J. H. Powell, C. H. DeWhalley
Third Intern. Battery Symp. Bournemouth 1962.

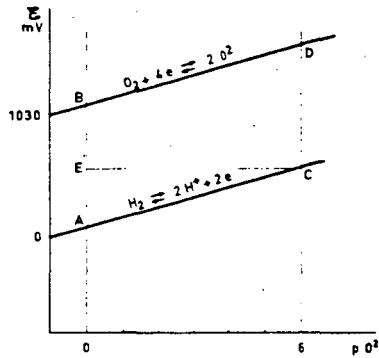


Fig.1 THERMODYNAMIC EQUILIBRIUM DIAGRAM IN MOLTEN CARBONATES

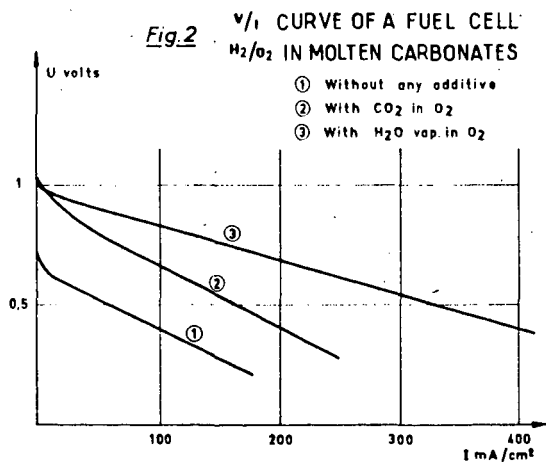


Fig.2 V/I CURVE OF A FUEL CELL H₂/O₂ IN MOLTEN CARBONATES



Fig. 3.-HORIZONTAL ELECTRODES PROTOTYPE

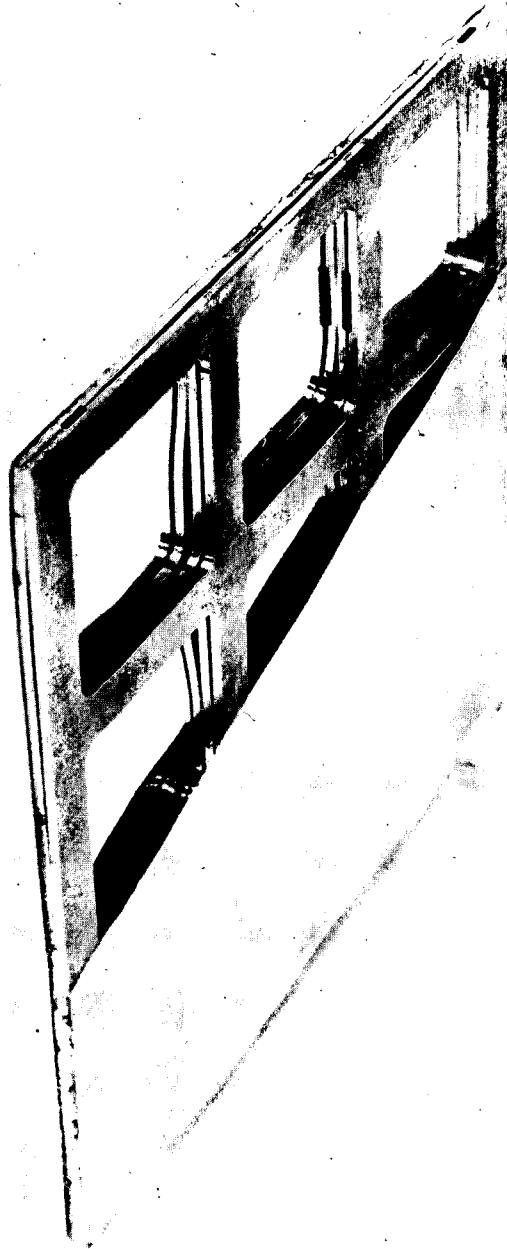


Fig. 4. -VERTICAL ELECTRODE PROTOTYPE

OPERATIONAL CHARACTERISTICS OF HIGH-TEMPERATURE
FUEL CELLS

B. S. Baker
L. G. Marianowski
J. Zimmer
G. Price

Institute of Gas Technology
Chicago, Illinois

INTRODUCTION

High temperature fuel cells have not received as much attention in the United States as their low temperature counterparts. As a result, from the viewpoint of a total system, the high temperature fuel cell is far less developed. The reason for this is simple. High temperature fuel cells are not as attractive for most military and space applications as low temperature fuel cells.

In Europe, especially in France, England, and Holland, a much larger portion of fuel cell development is directed toward commercial applications. The high temperature fuel cell is being more extensively investigated because it has a much more attractive economic potential. At the Institute of Gas Technology, interest in fuel cells is very definitely directed toward commercial goals. Emphasis on both high and low temperature fuel cell research is aimed at the development of inexpensive systems. This paper on the High-Temperature Molten Carbonate Fuel Cell reports on work which has been in progress at IGT since 1960. Details of much of this work already appear in the literature.¹⁻⁵

The principle advantages of the high temperature fuel cell are the elimination of expensive electrode catalysts from the system and the ability to operate with a variety of fuels and unpurified air.

However, raising the temperature to a typical figure of 900°F or above in a fuel cell which employs a water electrolyte would require a relatively high pressure system. This would be undesirable from both a technical as well as an economic viewpoint.

To avoid this difficulty, two solutions are possible. The electrolyte can be either 1) a salt that melts at a high temperature and which has a very low vapor pressure at this high temperature, or 2) an ion conducting solid used at still higher temperature (about 2000°F). Operating at this latter very high temperature requires the use of noble metals for stability rather than for catalytic purposes. This we want to avoid. For this reason, the fuel cell work at IGT is focused on the use of a molten salt electrolyte operating in the range of 900 to 1300°F.

The IGT molten carbonate fuel cell is patterned after the concept of Broers.⁶ In this system, a eutectic mixture of two or three alkali metal carbonates is mixed with an inert material such as a metal oxide. This forms a ceramic tile-like structure at room temperatures which becomes a non-Newtonian fluid or paste at the operating temperature.

In the IGT system, the paste electrolyte is held between a silver film cathode about 10 microns thick and a porous fiber nickel anode. The cathode is supported by a stainless steel grid. A complete fuel cell element of this type with an active area of one square foot is shown in Figure 1. These elements can be stacked in various ways to produce batteries of any voltage desired.

At the present time, the fuel for the IGT cell is reformed natural gas which is prepared by steam reforming in the presence of commercially available catalysts.

PERFORMANCE CHARACTERISTICS

Performance characteristics of high temperature molten carbonate fuel cells are usually inferior to those obtained in low temperature systems. Since the elevated temperature should improve reaction rate kinetics, an explanation for the poorer performance must be sought in terms of electrode properties and mass transfer processes. Low temperature fuel cell electrodes can be prepared with very high real to geometric surface areas. This may be achieved using high surface area carbons, nickels and precious metal blacks. In the high temperature cells, such active surfaces are unstable. They tend to sinter to form relatively low surface area electrodes.

A second factor affecting performance levels is the nature of the gas-liquid-solid interface at the electrode. In low temperature cells, it has been possible to achieve a relatively effective interface in terms of mass transfer properties, for example, a thin film of electrolyte on the bulk of the electrode, using either a double porosity electrode structure, waterproofing, ion exchange membranes, or matrices. In molten carbonate fuel cells, there has always been evidence of macroscopic flooding on electrodes which have been in operation for some time - e.g. over several hundred hours.

Broers⁷ and we at IGT⁸ have observed evidence for diffusion control in the liquid film for this type cell. Quantitative measurements in terms of film theory have not been possible because of lack of information on the solubility of hydrogen, oxygen, carbon monoxide, carbon dioxide, and water vapor in carbonate melts. Nevertheless, more effective use of electrode surface is clearly warranted.

To see if improved interfacial characteristics could be achieved, experiments at IGT have been conducted with a variety of matrix materials with different surface areas and particle sizes. The use of high surface area metal oxides has led to the development of cells which show no evidence of macroscopic flooding after prolonged operation. They have yielded performance characteristics of the type shown in Figure 2. Earlier performance levels are also shown in this Figure for comparison.

All tests at IGT are performed on hot pressed electrolyte discs. Those discs are prepared by pressing electrolyte powders at 8000 lbs/in² and 950°F. To prevent extrusion of the electrolyte between sections of the dies, aluminum discs are inserted in the pressing unit. The discs are designed to take advantage of the difference in coefficient of thermal expansion between the steel and aluminum to insure a seal tighter than that which could be achieved by mechanical tolerances alone. A thin palladium-silver foil is placed between the electrolyte powders and the aluminum to facilitate release of the electrolyte discs from the die assembly.

A series of experiments on different density fiber nickel electrodes shown in Figure 3, have yielded polarization characteristics shown in Figure 4. Higher density electrodes, such as 43 and 62 percent nickel, show a high level of polarization and the appearance of limiting currents. Electrodes having a density of 15, 20, and 33 percent yield equivalent performance within experimental error. These data were taken with cells having an electrode area of three square centimeters. Results have since been duplicated with cells having surface areas of 32 square centimeters. Cell lifetimes of 850 hours at the indicated performance level is the best achieved so far. These cells are still being tested. From these results, it appears that further optimization of electrolyte and electrodes may yield even better performance levels, placing a whole new perspective on the use of this type fuel cell system.

In the next sections the impact of these new polarization curves on heat transfer and overall system efficiency will be outlined.

HEAT TRANSFER

Considering the voltage characteristic shown in Figure 2, it is apparent that the maximum voltage-current performance is desired. The volume, weight, and cost of the fuel cell system is decreased. It is of interest, however, to examine the engineering implications especially as to how heat transfer is affected by the different voltage-current characteristics.

At IGT, we have considered the three dimensional heat transfer problem in a fuel cell battery.⁹ Figure 5, is a simplified diagram of the fuel cell. Heat transfer in such a cell depends mainly on such factors as battery dimensions, the voltage-current characteristic, the degree of fuel and air conversion, and the physical properties of the materials used to construct the cell. The complete problem is too broad to discuss here. However, in Figure 6 the temperature distribution within such a fuel cell is shown for the voltage-current characteristics of Figure 2. In all cases, the operating cell potential would be 800 millivolts.

It can be seen that the maximum temperature rise from the center of the battery to the assumed isothermal walls (in the case of the 1963 voltage-current characteristic) is only about 7°F. However, when the performance of the cell is improved (Best 1965), the maximum temperature rise increases to about 480°F. In practice, of course, the walls of the fuel cell would not be isothermal. Nevertheless, one can deduce from the experimental data that the low performance fuel cell would require the addition of heat to keep it at operating temperature. On the other hand, it would be necessary to remove heat from the system having the high performance characteristic.

This has been partly verified by constructing the 32-cell stack of elements shown in Figure 7. The performance of this battery was based on the 1963 characteristic. As expected, it was necessary to add heat to the system. The improved performance characteristics suggests another possibility. This is to incorporate reforming catalysts near the electrodes so that waste heat from the fuel cell can be used to sustain the endothermic reforming reaction. At the same time, this would provide a means for cooling the cell.

A further variation in cell performance is seen in Figure 8. Here the effect of conversion on temperature distribution is shown. In the direction of air flow (Z), it can be seen that as the conversion of oxygen is increased, two things happen. The first effect is a rise in the maximum temperature in the battery. This would be expected since less gas is available to remove heat. The second effect is somewhat less expected. The flow of gas through the cell causes a temperature distribution in the cell that is not symmetrical. Physically, this situation can be interpreted as follows: At a high rate of gas flow, heat is being removed from the section of the battery near the gas inlet and is being redistributed to the section near the outlet. In the case of a low rate of gas flow, complete symmetry in the Z direction can be expected.

The purpose of these heat transfer considerations was to determine some feeling for the size and shape of fuel cells which will be built at IGT within the next few years. More important, however, it permits assumptions on the nature of heat inputs in the system. It also establishes what the overall efficiency of such a system might be.

EFFICIENCY

In the high temperature molten carbonate fuel cell, a typical operating voltage that is compatible with the materials from which the cell is built is about 0.7 to 0.8 volts. From the previous discussion, we have seen that cells operating at this voltage level can be thermally self-sustaining. Thus, the overall efficiency of the system depends on the efficiencies of fuel and air conversion, and the reforming requirements. Air conversion is especially important in high temperature fuel cells where the heat content of the oxidant is substantial. In Figure 9, the overall efficiency of an external reformer-molten carbonate fuel cell is shown as a function of the efficiency of fuel and oxygen conversion. The oxidant is air.

For purposes of this example, it was assumed that 1) the external reformer was 60 percent efficient and 2) that no gas-to-gas heat exchange is possible but heat exchange from gas-to-boiling liquid is feasible. These assumptions are based on the need for unreasonably large gas-to-gas heat exchangers especially for low oxygen conversion. While such heat exchangers could be built, they would cost more than the fuel cell itself. However, from a practical viewpoint, steam generation is more feasible, and heat recovery for this purpose has been assumed.

It can be seen that at low oxygen conversion, the overall efficiency is not greatly affected by the efficiency of fuel conversion. It does become more important as the efficiency of the oxygen conversion improves. The reason for this is that when the fuel conversion is high, but the oxygen conversion is low, it is necessary to maintain a separate fuel supply to preheat the air. At low fuel conversion, the air can be preheated by burning spent fuel. The maximum efficiency for the external reforming system without gas-to-gas heat exchange will probably be between 35 and 39 percent.

In Figure 10, a similar analysis is made for an internal reforming system. In this case, the heat for the reformer is supplied by the polarization and entropic heats from the fuel cell. Again, the concept of gas-to-gas heat exchange for preheating feeds has been assumed to be impractical. The overall efficiency for this system is somewhat higher as might be expected. A figure of about 40-43 percent seems to be possible with present technology.

Finally, it should be noted that oxygen conversions higher than 60 percent may be possible in the future. In such a case, the efficiency of the overall system will be even higher. However, it is not likely to be greater than 50 percent unless low cost gas-to-gas heat exchangers can be developed.

ECONOMICS

The only real basis for economic evaluation of fuel cells at the present time is the cost of materials. Lack of knowledge and/or experience with manufacturing components and systems prohibits any more extensive analysis. To a certain extent, storage battery hardware can serve as a guide but this breaks down when confronted with a new component like the paste electrolyte in the high temperature fuel cell.

In an early publication³ we estimated the material costs of molten carbonate fuel cells and related these costs to the performance of IGT cells. Applying a similar method, we have once again presented our performance data in this fashion, (Fig. 11). Material costs are essentially the same as in the earlier publication. It can be readily seen that progress has been made which gives rise to considerable optimism for the economics of this type fuel cell. Typical performance characteristics indicate that material costs of about \$45 per kilowatt can be achieved and the best performance data reduces that figure to less than \$20 per kilowatt.

With respect to further improvement, we might look to using copper in place of silver at the cathode and to reducing the amount of stainless steel used for the current collector in the cell. Lifetime remains the big factor in the case of the molten carbonate fuel cell. Only more intensive experimental work can find a solution to this problem.

ACKNOWLEDGMENT

The high-temperature fuel cell research program at IGT is sponsored by the American Gas Association under its PAR (Promotion-Advertising-Research) Plan. The authors wish to thank the A.G.A. for allowing results of the program to be discussed in this paper.

REFERENCES CITED

1. Shultz, E. B., Jr., Vorres, K. S., Marianowski, L. G. and Linden, H. R., "High Temperature Methane Fuel Cell," in Young, G. J. Ed., "Fuel Cells," Vol. 2, 24-36. New York: Reinhold Publishing Corp., 1963.
2. Marianowski, L. G., Meek, J., Shultz, E. B., Jr. and Baker, B. S., "New Concepts in High Temperature Hydrocarbon Fuel Cells," Power Sources Conference 17, 72-75 (1963).
3. Baker, B. S., Marianowski, L. G., Meek, J. and Linden, H. R., "Further Developments in High Temperature Natural Gas Fuel Cells," Advances in Chemistry Series No. 47, 247-261. Washington, D. C.: American Chemical Society, 1965.
4. Baker, B. S., Marianowski, L. G. and Zimmer, J., "Design and Construction of a Molten Carbonate Fuel Cell Battery System," Paper presented at Delegation Generale a la Recherche Scientifique et Technique Symposium on Conversion des Energies, Paris, France, February 1965.
5. Baker, B. S., and Marianowski, L. G. "Operating Characteristics of an Economical High Temperature Fuel Cell" paper presented at the International Conference on Energetics, ASME meeting, Rochester, New York, Aug. 18-20, 1965.
6. Broers, G. H. J., "High Temperature Fuel Cells," Ph.D Dissertation, University of Amsterdam, The Netherlands, 1958.
7. Broers, G.H.J., and Schenke, M., "High Temperature Galvanic Fuel Cells," Final Report. File No. DA-91-591-EUC-1701.
8. Baker, B. S., IGT unpublished data.
9. Gidaspow, D. and Baker, B. S., "Heat Transfer in a Fuel Cell Battery," Paper presented at the Eighth National Heat Transfer Conference of the ASME and A.I.Ch.E., Los Angeles, Calif., August 8-11, 1965.

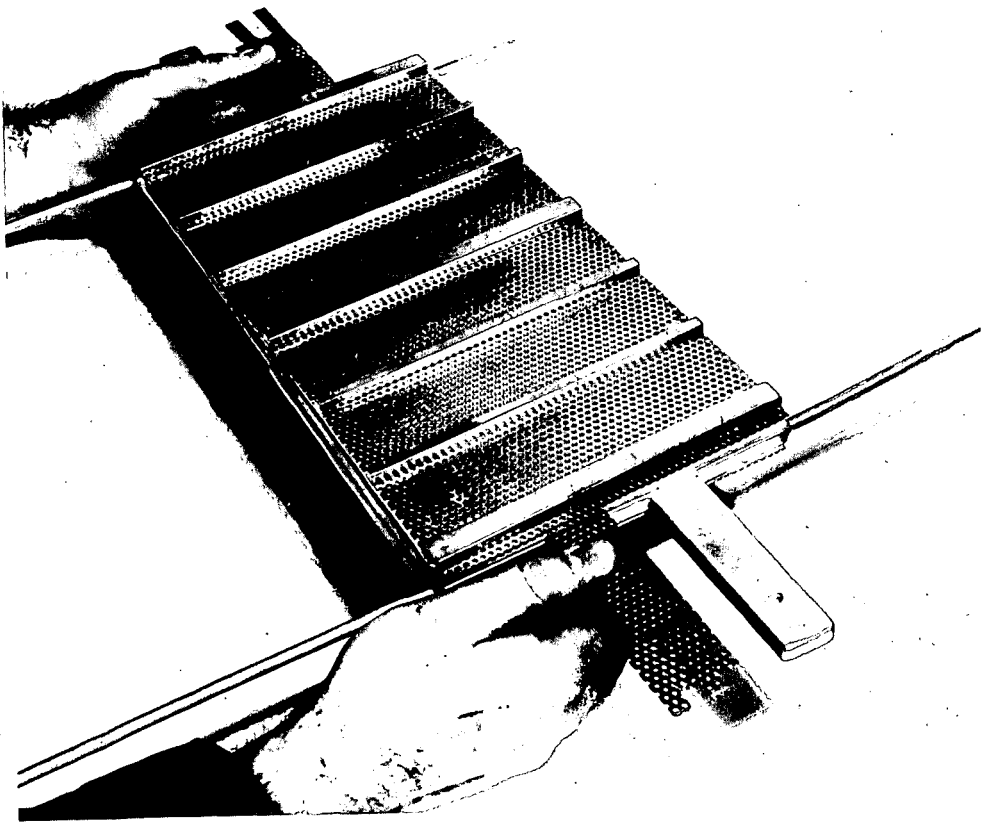


Fig. 1.-SINGLE ELEMENT OF IGT HIGH-TEMPERATURE FUEL CELL BATTERY

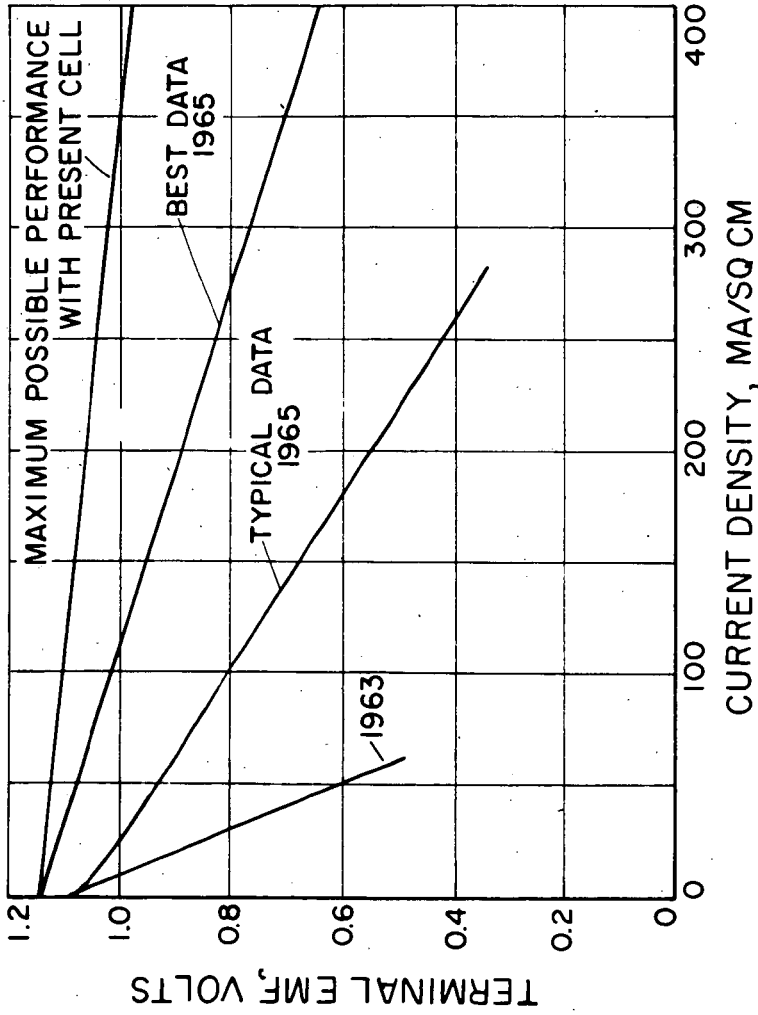


Fig. 2.-PERFORMANCE CHARACTERISTICS OF IGT MOLTEN CARBONATE FUEL CELL



15 %



20 %



33 %



43 %



62 %

Fig. 3. -DIFFERENT DENSITY FIBER NICKEL ELECTRODES USED IN IGT MOLTEN CARBONATE FUEL CELL (120X)

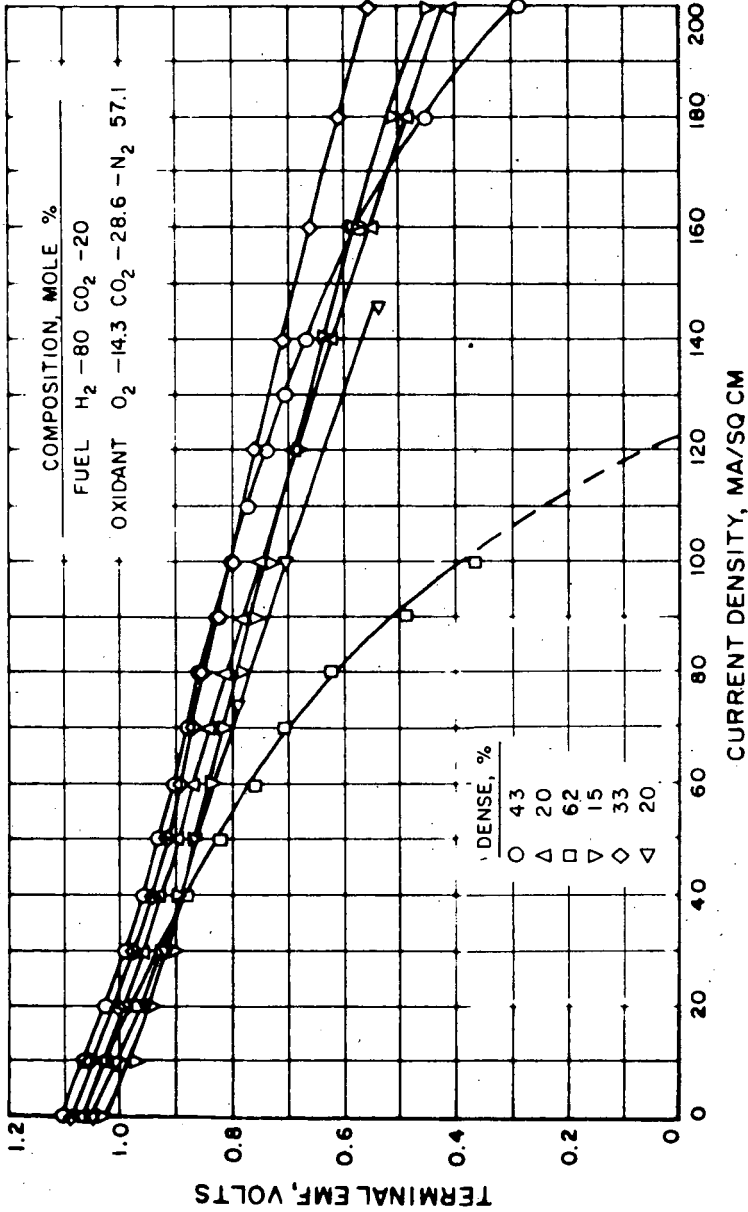


Fig. 4. -COMPARISON OF PERFORMANCE CHARACTERISTICS OF DIFFERENT DENSITY FIBER NICKEL ELECTRODES AFTER SEVERAL HUNDRED HOURS OPERATION

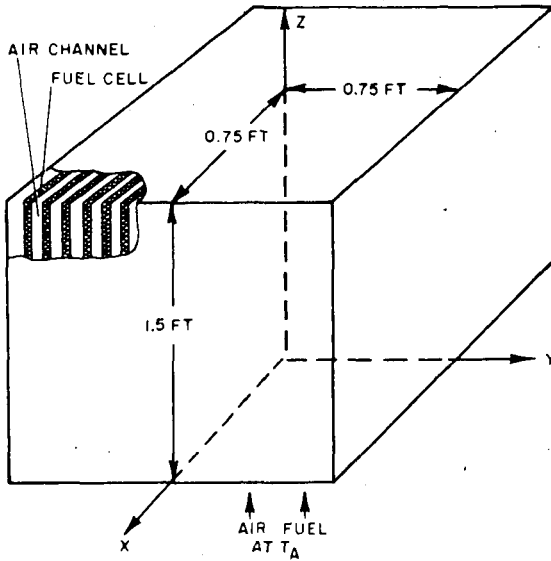


Fig. 5.-MODEL OF FUEL CELL BATTERY USED IN HEAT TRANSFER ANALYSIS

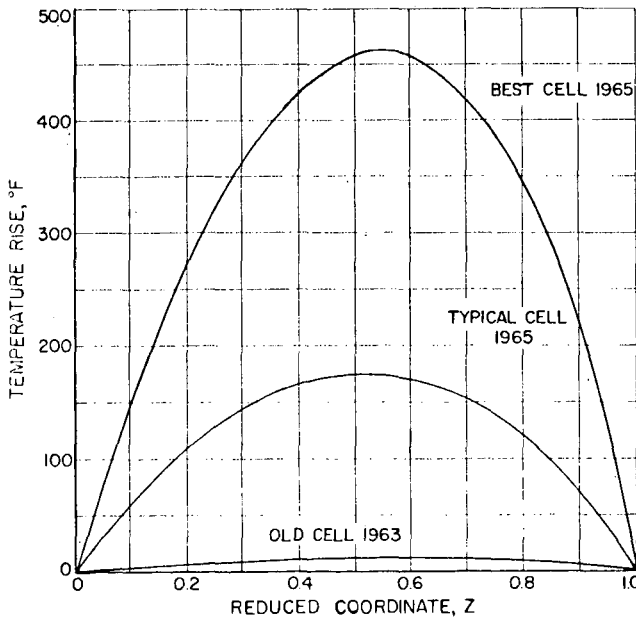


Fig. 6.-EFFECT OF POLARIZATION CHARACTERISTICS ON TEMPERATURE DISTRIBUTION. DIRECTION OF GAS FLOW.

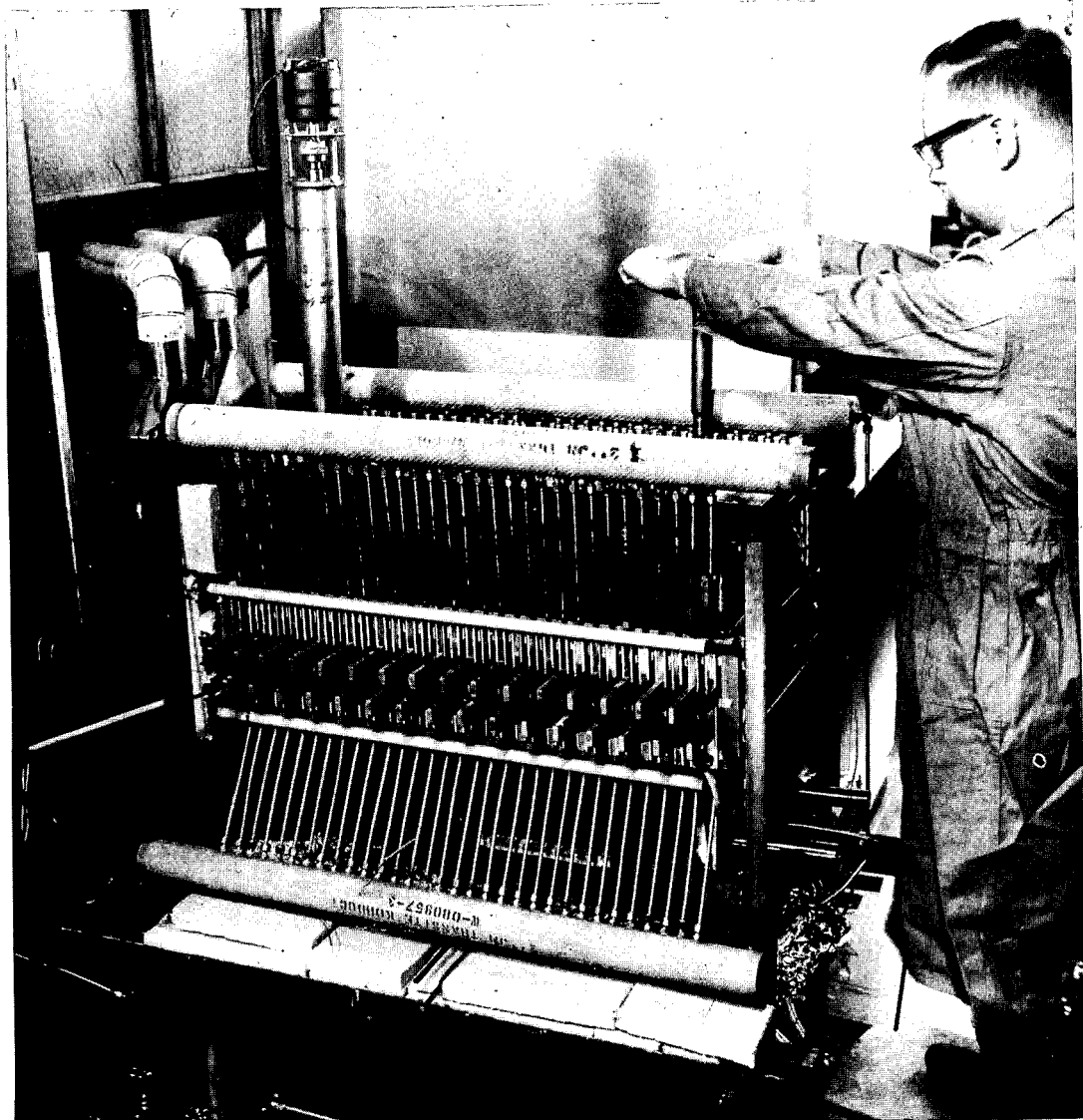


Fig. 7.-IGT 32-CELL HIGH-TEMPERATURE BATTERY

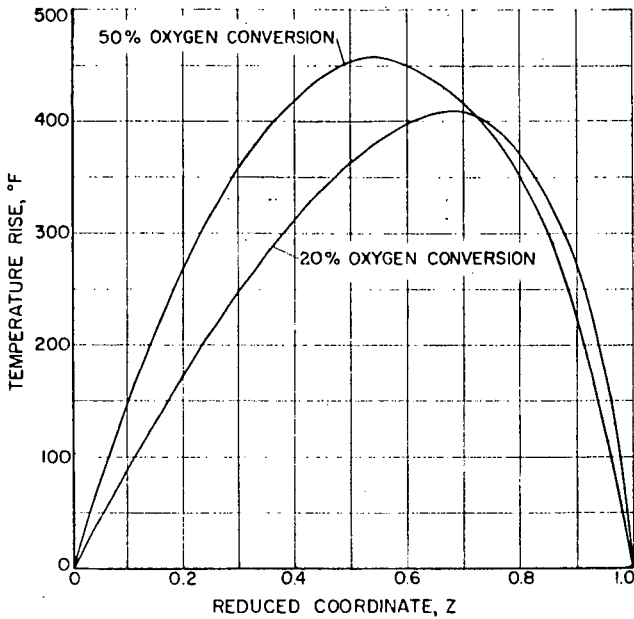


Fig. 8. -EFFECT OF AIR CONVERSION AT HIGH PERFORMANCE LEVELS ON TEMPERATURE DISTRIBUTION IN DIRECTION OF GAS FLOW

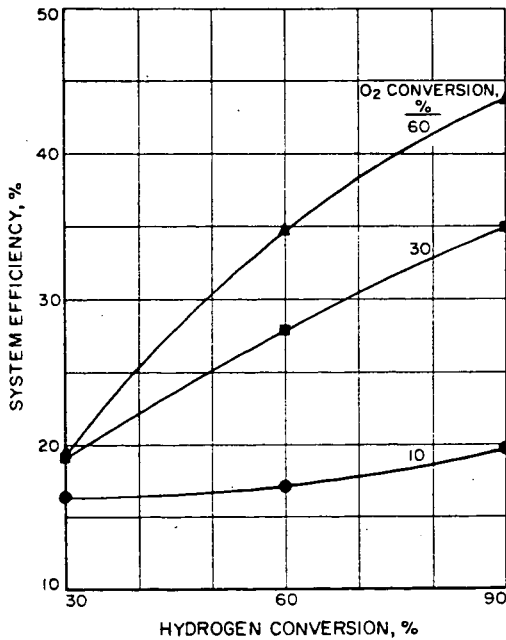


Fig. 9. -OVERALL SYSTEM EFFICIENCY AS A FUNCTION OF FUEL AND OXIDANT CONVERSION WITH AN EXTERNAL REFORMER

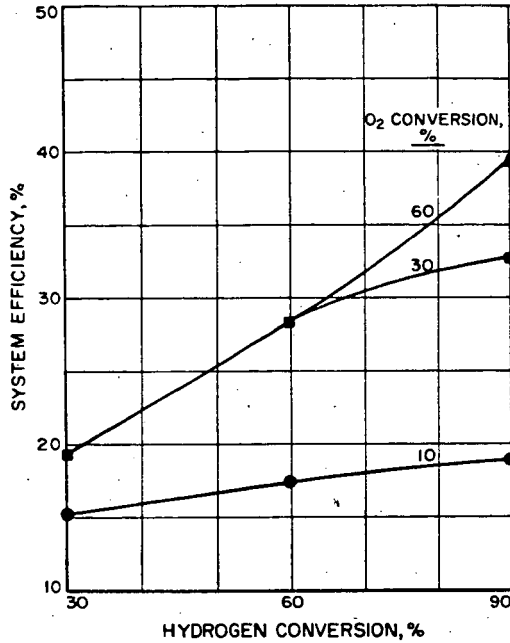


Fig. 10. -OVERALL SYSTEM EFFICIENCY AS A FUNCTION OF FUEL AND OXIDANT CONVERSION WITH AN INTERNAL REFORMER

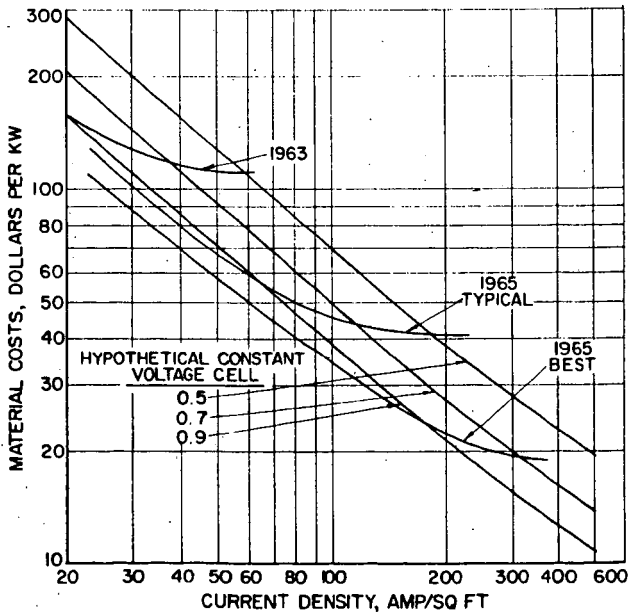


Fig. 11. -ECONOMICS OF MATERIALS USED IN HIGH TEMPERATURE MOLTEN CARBONATE FUEL CELLS

TESTING OF ELECTRODES FOR HIGH TEMPERATURE
SOLID ELECTROLYTE FUEL CELLS

E. F. Sverdrup, D. H. Archer, J. J. Alles, and A. D. Glasser

Westinghouse Research Laboratories
Beulah Road, Churchill Borough
Pittsburgh 35, Pennsylvania

INTRODUCTION

Fuel cell systems utilizing zirconium dioxide ceramic electrolytes are being developed both for electric power generation and for the electrolytic regeneration of oxygen from carbon dioxide-water vapor mixtures. Practical devices operate at temperatures in the vicinity of 1000°C in order to obtain high oxygen ion mobility in the electrolyte material. The measurement of the energy losses associated with electrode operation in air and fuel atmospheres under these high temperature conditions is the subject of this paper.

ELECTRODE PROCESSES IN THE SOLID ELECTROLYTE FUEL CELLS

A typical solid electrolyte fuel cell battery is shown in Fig. 1. It consists of a series of bell-and-spigot shaped cells which nest together to form a tube. A fuel stream is passed through the inside of the tube and air surrounds the outside. The steps involved in the reaction of the fuel and oxidant to produce reaction products and electric power can be visualized with the aid of Fig. 2. Oxygen molecules diffuse through the air to the air electrode surface where they dissociate and are adsorbed. Surface migration occurs over the electrode to sites at the electrode-electrolyte interfaces where, combining with two electrons from the electrodes, an oxygen atom becomes an O^- ion and enters an oxygen ion vacancy in the crystal lattice of the electrolyte. Oxygen ion transport through the electrolyte occurs. At the fuel electrode, oxygen ions leave the electrolyte give up electrons to the electrode and react with fuel species which have diffused to and been adsorbed on the fuel electrode surface. The products of the surface-reaction with the fuel are desorbed from the electrode and diffuse into the fuel reaction-product stream. The electrons that have been delivered to the fuel electrode pass through the conducting seal to the air electrode of the next cell where they again take part in the formation of oxygen ions. At the terminals of each cell a generated voltage appears (if the external electric circuit is open) which is given by:

$$E_g = \frac{RT}{4F} \ln \frac{P_{O_2H}}{P_{O_2L}}$$

E_g = open circuit voltage of the cell (volts)

R = gas constant, 8.134 (joules/°K-mole)

T = absolute temperature (°K)

F = Faraday number (96,500 coul/gm. equiv.)

P_{O_2H} = oxygen partial pressure at the air electrode of the cell

P_{O_2L} = oxygen partial pressure on the fuel electrode of the cell

This voltage reflects the reversible energy available from the isothermal expansion of an ideal gas between the two oxygen partial pressure levels. If the circuit is closed so that electric power is delivered to an external load, the voltage V_T appearing at the terminals of the cell is decreased by irreversible losses. If the battery operates at a load current I equal to the reaction of n_{O_2}

moles of O_2 per second ($I = 4F n_{O_2} \frac{\text{coulombs}}{\text{mole } O_2} \times \frac{\text{mole } O_2}{\text{sec}}$), then the

cell terminal voltage is decreased both by the ohmic resistance losses caused by the transport of electrons through the electrodes and $O^=$ ions through the electrolyte and by the irreversible losses associated with the transport of reactants and reaction products to and from the electrodes. Irreversible losses associated with the adsorption, desorption and surface reaction steps may also occur.

$$V_T = E_g - IR - V_p$$

V_T = terminal voltage of the cell (volts)

E_g = generated, open circuit, voltage of the cell (volts)

I = cell current (amperes)

R = total ohmic resistance between cell terminals, electrodes and electrolyte (ohms)

V_p = total voltage loss due to non-ohmic irreversible processes (volts)

The ohmic resistance loss "R" may be conveniently separated into components due to electron transport in the air electrode, the air electrode-to-electrolyte contact resistance, the ionic resistance of the electrolyte, the fuel electrode-to-electrolyte contact resistance, and the electronic resistance of the fuel electrode. Techniques have been developed for isolating and measuring these separately. The polarization voltage losses are not as easily separated but the overall potential loss associated with carrying out either the fuel or air electrode reaction can be measured as a function of the reaction rate (electrode current density) by measuring the non-ohmic potential drop between the appropriate electrode and the electrolyte.

AN APPARATUS FOR THE MEASUREMENT OF ELECTRODE LOSSES

Figure 3 is a schematic of an apparatus for measuring electrode losses. It consists of a furnace, a gas-tight system for reactant delivery and removal, and a number of spring-loaded probes

which bear on an electroded test sample. Each probe is a Pt-Pt 10% Rh thermocouple which can be used for sensing temperatures as well as potential. Fig. 4 is a photograph of the test cavity showing the probe arrangement. An electroded test wafer rests in the cavity and probes bear on both the upper and lower surfaces of the test specimen when the tester is assembled.

The probe arrangement shown in Fig. 4 and again in Fig. 5 allows a number of tests to be made. As can be seen from Fig. 5, the test sample is a wafer of the ceramic electrolyte with the electrode to be tested applied to one surface and a suitable counter electrode to the other surface. The electrode is applied as a band leaving a portion of the bare electrolyte surface exposed. Five probes bear on the electroded portion of each surface while the sixth probe rests on the electrolyte surface.

This choice of electrode and electrolyte probe locations allows the important electrode characteristics to be measured. The techniques involved are described in succeeding sections.

MEASUREMENT OF THE OHMIC LOSSES ASSOCIATED WITH ELECTRON TRANSPORT IN THE ELECTRODE

The losses which are associated with the transport of electrons along the electrode film to the sites where oxygen ions are formed depend on the electronic resistivity of the electrode material and on the geometry of the electrode. Expressions which take into account the non-uniform current density distribution in the electrode are easily derived but are less useful than the simplified approximation:

$$R_{\text{electrode}} = \frac{\rho_e}{\delta_e} \frac{\bar{l}_e}{\pi D}$$

where

ρ_e = electronic resistivity of the electrode material (ohm-cm)

\bar{l}_e = effective length of electron travel along electrode (cm)

δ_e = electrode thickness (cm)

πD = circumference of fuel cell (width of electrode) (cm)

As this expression shows, the parameter of interest to the fuel cell designer is the electrode resistivity divided by the electrode film thickness " ρ_e/δ_e ". This quantity is easily measured in the electrode tester by passing a current between two of the probes bearing on the electrode and measuring, potentiometrically, the potential drop across two other electrode potential probes. Solution of the two dimensional current flow problem for the geometry used allows the direct determination of ρ_e/δ_e from the measured ratio of voltage to current flow. Alternatively, the treatment of the potential problem by L. J. van der Pauw¹ allows ρ_e/δ_e to be calculated from measurements using four probes placed arbitrarily on the edges of an electrode film of arbitrary shape. The required measurements are indicated in Fig. 6. The two voltage-to-current ratios yield directly a value of the resistivity/thickness of the electrode film. In addition, the use of two differing current paths in the measurements allows major changes in the uniformity of the film during electrode operation to be easily detected. As an example of

these measurements, Fig. 7 compares the temperature dependence of a porous sintered platinum electrode and a fused platinum film electrode, as determined by the van der Pauw technique, with the calculated temperature variation of a sheet of bulk platinum having the same weight density. As would be expected from the character of the cross-sections of these films, shown in Fig. 8, the sintered electrode displays a ρ_e/δ_e about three times that of bulk platinum. The fused electrode film shows ρ_e/δ_e values about 1.5 times greater than bulk platinum. This increased effective resistivity gives some indication of the microporosity of the electrode film. Figure 7 also shows the irreversible increases in resistivity/thickness parameter displayed by both types of electrode when exposed to hydrogen-water atmospheres.

MEASUREMENT AND SEPARATION OF ELECTRODE TO ELECTROLYTE LOSSES

The voltage losses associated with the operation of an electrode are measured using the electrode tester by passing a current through the (electrode)-(electrolyte)-(counter-electrode) test wafer and measuring the voltage drop between two non-current carrying potential probes - one bearing on the test electrode and the other on the bare electrolyte. In practice current is introduced through the four probes located at the corners of the electrode and the potential is monitored between the center electrode probe and the electrolyte probe. The electrolyte probe, as shown in Fig. 5, is located as far as possible from the edge of the electrode. The direction of current flow determines the direction of oxygen ion transport and the reactions which take place at the test electrode. By appropriate choice of current direction and atmosphere either the air or the fuel electrode processes may be studied as illustrated in Fig. 9.

A Tektronix type 545 oscilloscope with a type D high gain differential input-d.c. amplifier is used to monitor the potential drop from the electrode to the electrolyte. The differential input rejects noise voltages common to both leads of the measuring circuit. The single trace mode of sweep operation is used and the gate output, a d.c. voltage of 30 volts which becomes available at the front panel of the scope when the sweep is initiated, is used in conjunction with a booster battery and a fast relay* to energize or de-energize the electrode current circuit. (Fig. 10) Oscilloscope traces such as are shown in Fig. 11 are obtained.

When the relay closes establishing current through the sample the electrode to electrolyte voltage rises to an intermediate value so rapidly that no trace can be detected on the oscillogram and then rises at a slower rate until the steady state potential drop corresponding to the given electrode current density is reached.

*C. P. Clare, Model HG 1202 - operating time 5 milliseconds with 52.5 volts step function voltage applied to the coil.

Similarly, when the relay opens, the potential decays almost immediately to an intermediate level and then more slowly to zero. The fast processes, which occur so rapidly that no trace is recorded on the oscillogram, are associated primarily with the resistive voltage drop occasioned by the passage of oxygen ions through the electrolyte. This can be seen by comparison of the magnitudes of the fast component of the potential drop with predictions of the electrolyte resistance based on the known resistivity of the electrolyte and the geometry of the sample. The strong temperature dependence of the electrolyte resistivity offers a convenient method of separating electrolyte resistance from other possible rapid polarization processes which would be expected to show a different temperature dependence.

An illustrative set of current interruption photographs taken on a fused-electrode test sample operating in oxygen at 900°C are shown in Fig. 12. The fast component of the total voltage drop across the specimen, V_{4-10} , can be scaled from the current interruption photographs and is 680 millivolts. Under the conditions of this test, a sample current of 1000 milliamps was being passed through the specimen. An overall "resistance" of 680 mv/1000 ma = 0.68 ohms is indicated. At 900°C the resistivity of $(ZrO_2)_{0.9}(Y_2O_3)_{0.1}$ electrolyte materials is 12 ohm-cm. The sample resistance calculated from geometry is then:

$$R_{4-10} = \frac{\rho_b \delta_b}{A} = \frac{12 (\Omega - \text{cm}) 0.09 (\text{cm})}{1.36 (\text{sq. cm})} = 0.80 \Omega \quad (1)$$

where ρ_b = electrolyte resistivity (ohm-cm)

δ_b = electrolyte thickness (cm)

A = electrode area (sq. cm)

The measured resistance is 85% of the resistance estimated from sample geometry. Measurements of total sample resistance were made at various temperatures between 800°C and 1000°C. The results are plotted in Fig. 13 and compared with calculated values based on sample geometry. As is evident from Fig. 13, the temperature dependence of the sample resistance is the same as that of the electrolyte, the total sample resistance remaining 85% of the calculated except at the lowest temperature - 800°C.

The accuracy with which electrode area can be measured is probably ±5% and the electrolyte resistance is known only to ±5%, so the agreement between the magnitude of the resistance characterizing the "fast process" polarization and the ohmic resistance of the electrolyte seems satisfactory.

MEASUREMENT OF THE ELECTRICAL POSITION OF THE ELECTROLYTE POTENTIAL PROBE

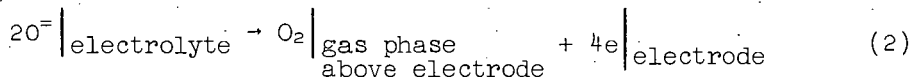
Figs. 12 and 13 illustrate the method used for establishing the electrical position of the electrolyte potential probe. If the electrolyte probe were positioned away from the edge of the electrode, at a distance which is large compared to the spacing between electrodes,

the ohmic resistance of the electrolyte included in measurement between electrode and probe would approach one half the total electrolyte resistance of the sample. In practice, it is difficult to achieve a separation between electrode and probe of more than twice the electrolyte thicknesses. It is also difficult to control the position of the probe with respect to the edge of the electrode. As a consequence, the electrical position of the probe does not usually fall in the center of the electrolyte. As Fig. 2 shows, in Test XXXII the probe was positioned electrically closer to the fused test electrode, the ratio of the resistance between this electrode and probe (R_{4-7}) and the total resistance (R_{4-10}) being $0.19/0.68 = 0.28$. Figure 12 demonstrates that this ratio remained constant, independent of test temperature and atmosphere.

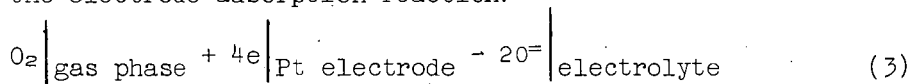
MEASUREMENT OF "SLOW" POLARIZATION PROCESSES

Figure 14 illustrates the usefulness of the current interruption technique in the investigation of electrode polarization. Here the polarization voltages of a particular electrode in oxygen and hydrogen-water atmosphere are compared. The electrode displays low polarization voltage losses when tested in oxygen atmospheres. In fuel atmospheres, large polarization losses, which decay on interruption of the current in times of the order 10 to 100 milliseconds, are typical. Volt-ampere characteristics of the electrode sample constructed from current interruption data taken in pure oxygen (Fig. 15) and in hydrogen (Fig. 16) are shown.

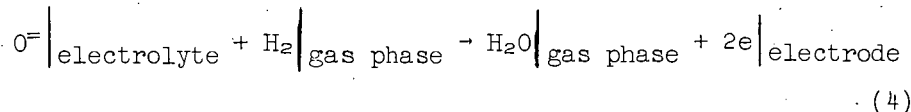
Evidently, the electrode desorption reaction:



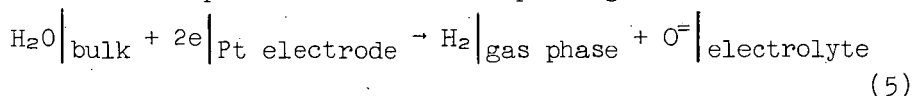
and the electrode adsorption reaction:



which take place in oxygen atmospheres are very nearly reversible even at current densities up to 750 ma/cm^2 . In fuel atmospheres the overall desorption reaction corresponding to reaction (2) is:



The overall adsorption reaction corresponding to reaction (3) is:



These reactions are not reversible at even moderate current densities. The degree of irreversibility corresponding to various current densities (i.e., reaction rates) has been measured over a range from zero to 750 ma/cm² and over the temperature range 1000°C to 750°C. The results of these tests are presented in Fig. 17.

Current interruption techniques have been used by others² to study the polarization behavior of molten carbonate cells at 600°C. Polarizations of 0.3 - 0.6 volt at current densities of 100 ma/cm² having decay times of over one second are observed at the hydrogen electrode. At the air electrode, polarizations of about 0.09 volts, with decay times between 10⁻² and 10⁻¹ seconds, are reported. These results may be compared with those presented in Figs. 14-17 which show hydrogen electrode polarizations of 0.05 volts with decay times of about 10⁻¹ seconds at 100 ma/cm². Air electrode polarizations are less than 10 mv and decay is less than 10⁻³ seconds.

ADDITIONAL CONSIDERATIONS IN THE INTERPRETATION OF ELECTRODE TESTER RESULTS HEATING EFFECTS ON THE SAMPLE CURRENT

Comparison of the current establishment and current interruption oscillograms of Fig. 11 shows that the current establishment oscillogram displays a resistive component of $\frac{500 \text{ mv}}{1450 \text{ ma}} = 0.34 \Omega$ while the current interruption photograph indicates a lowered resistive component of $\frac{400 \text{ mv}}{1450 \text{ ma}} = 0.28 \Omega$.

Measurements at other current levels indicate that the resistive voltage drop as measured from the current establishment photographs is directly proportional to current. Resistive drops measured from current interruption photographs depart from linearity at high electrode current densities. This difference may be attributed to heating of the sample by the passage of current. The strong temperature dependence of electrolyte resistivity causes appreciable changes in the sample resistance. Because polarization may also be strongly temperature dependent; this heating effect must be taken into account in obtaining polarization data such as is shown in Fig. 17. Since the sample is in thermal equilibrium with the tester furnace when current establishment oscillograms are taken, these oscillograms may be used to indicate the true resistance corresponding to the known sample temperatures. The major polarizations require times comparable to the thermal time constants of the system to reach equilibrium, hence their measurement from current-make oscillograms is not accurate. Current break oscillograms which yield the polarization corresponding to steady-state operation of the electrode at a given current density are more reliable. An estimate of the electrode operating temperature corresponding to a given current break oscillogram can be obtained by selecting the furnace temperature at which a current make oscillogram displays an equal resistive component.

ELECTRODE-TO-ELECTROLYTE CONTACT RESISTANCE

The existence of appreciable contact resistance between electrode and electrolyte due to the electrode contacting only a small fraction of the electrolyte surface can be detected using

current-make oscillograms and comparing the measured resistance with calculated values based on the sample geometry. The theoretical calculations of Eisenberg and Fick³ on the contact resistance of idealized contacts may be used to estimate the effective area of contact.

EFFECT OF HIGH ELECTRODE RESISTIVITY/THICKNESS PARAMETER

When the electrode resistivity/thickness parameter is less than one, the electrode surface can be considered an equipotential. A uniform current density in the electrolyte between the two electrode can be expected. If high resistance electrodes are tested, the assumption of uniform current density will not hold and care must be used in interpreting tester results. The electrode-to-electrolyte probe will then indicate the resistive and polarization drops associated with the reduced current density existing in the electrolyte near the electrode potential probe. A rough estimate of the actual current density at the probe may be obtained from the resistive component of the current interruption-oscillogram. A back-up current-distribution screen has been used in several experiments to make the electrode surface more nearly an equipotential and to obtain more reliable measurements of polarization.

CONCLUSIONS

An apparatus for the testing of electrode structures for high temperature, solid-electrolyte fuel cells has been described. Independent measurement of electrode resistivity/thickness and resistive and polarization voltage drops corresponding to electrode operation at various current densities (reaction rates), temperatures, and atmospheres have been carried out using current-interruption and current-establishment oscillograms. These techniques have proved useful and are being used in our efforts to develop low cost, long-life electrodes for solid-electrolyte fuel cells.

REFERENCES

1. L. J. van der Pauw, Philips Research Reports, 13, 1, 1958.
2. I. Trachtenberg, J. Electrochem. Soc., 3, 110, 1964.
3. M. Eisenberg and L. Fick, ACS Symposium on Recent Advances in Fuel Cells, 6, 46, 1961.

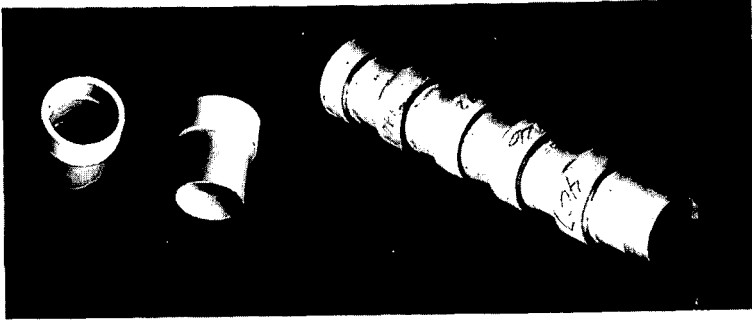


Fig. 1.-Bell-and-spigot fuel cells with five-cell battery assembly

1. Oxygen molecules diffuse through air to electrode surface
2. Adsorption and dissociation of O_2
3. Surface migration to reaction site
4. Oxygen combines with electrons from fuel side of previous cell forming O^{2-} ions
5. Ionic transport of O^{2-} through electrolyte
6. Deionization and surface reaction with fuel, delivery of electrons to the fuel electrode
7. Diffusion of fuel to fuel electrode surface
8. Adsorption of fuel on electrode, surface migration to reaction site.
9. Desorption of reaction product and diffusion into fuel stream

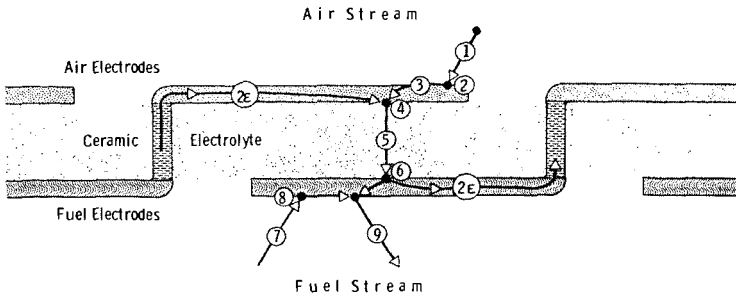
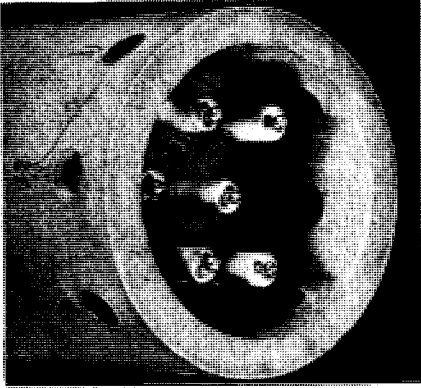
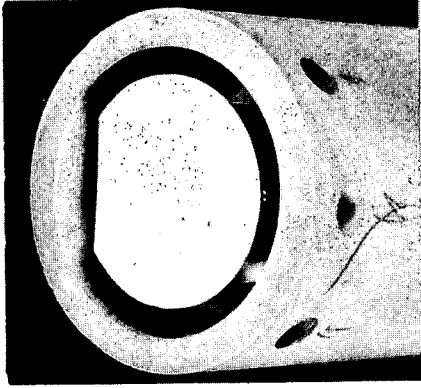


Fig. 2.-An electrode reaction process chain for solid electrolyte fuel cells



Water Cavity in Lava Tube, Showing Probes



Cavity with Electroded Water in Place

Fig. 4.-Internal views of electrode tester

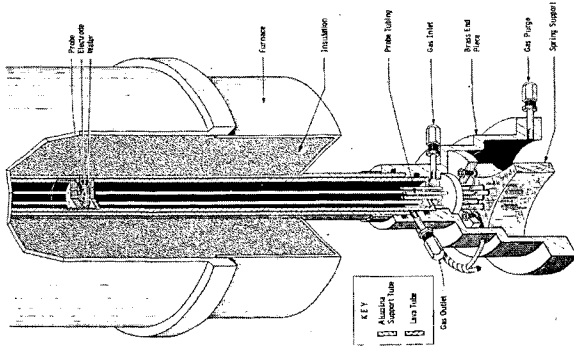


Fig. 3.-Cutaway drawing of electrode tester

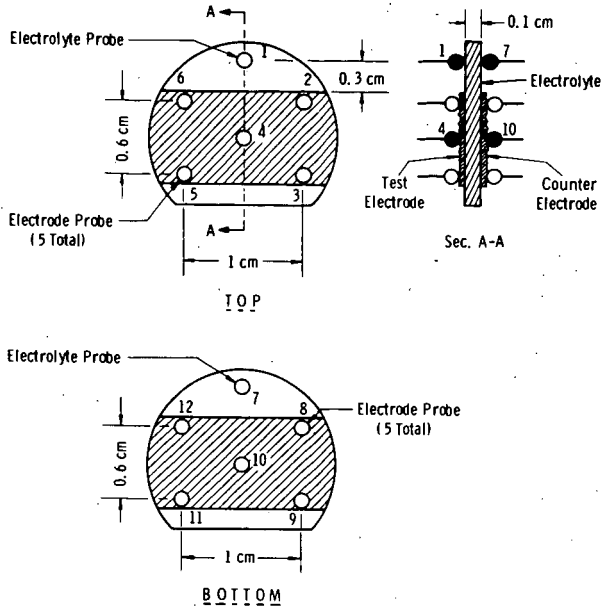


Fig. 5—Probe locations in the electrode tester

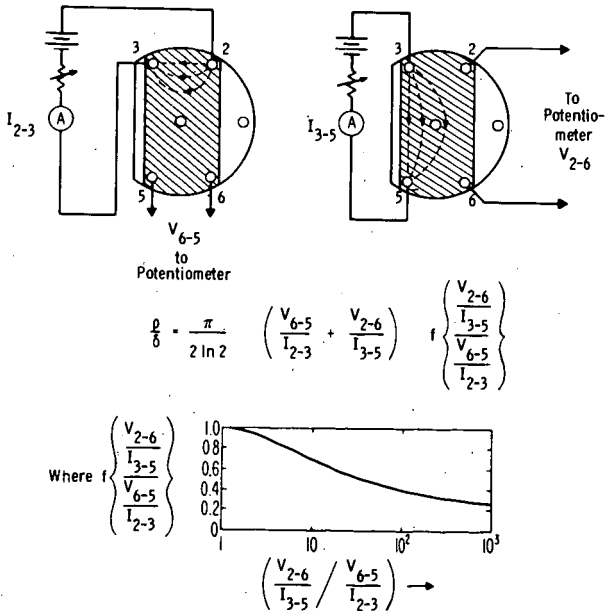


Fig. 6—Measurements to determine the electrode resistivity / thickness parameter using the van der Pauw technique

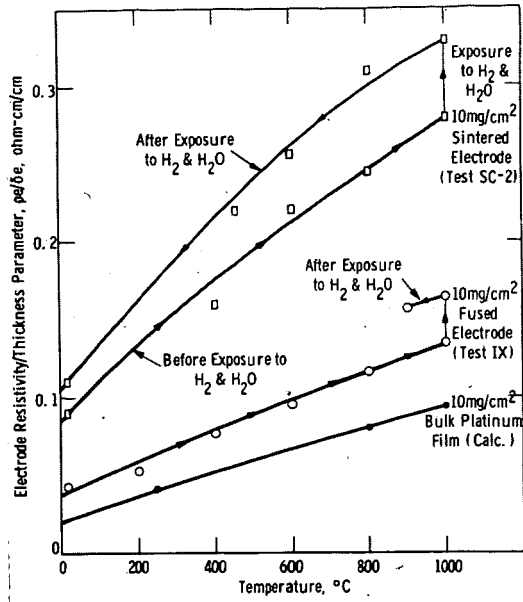
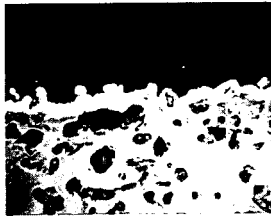
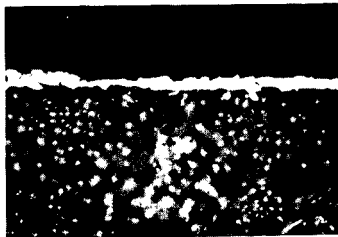


Fig. 7-A comparison of the temperature dependence of the resistivity/thickness parameter, (pe/be), for sintered and fused platinum electrodes



Sintered Platinum Electrode: 1000X



Fused Platinum Electrode: 1000X

Fig. 8.-Cross-section photomicrographs of platinum electrodes

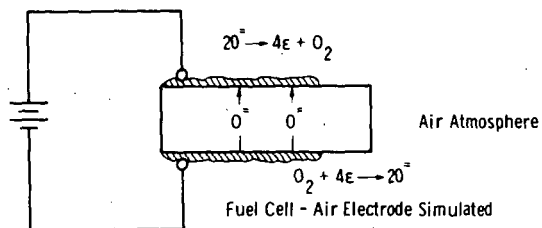
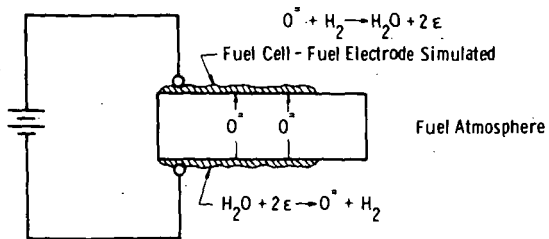


Fig. 9—Simulation of air electrode and fuel electrode operation by choice of current direction and surrounding atmosphere

Dwg. 746A197

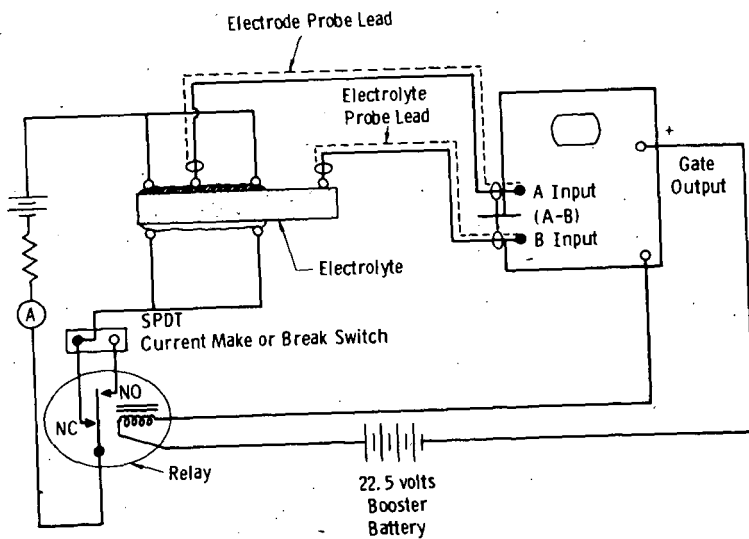
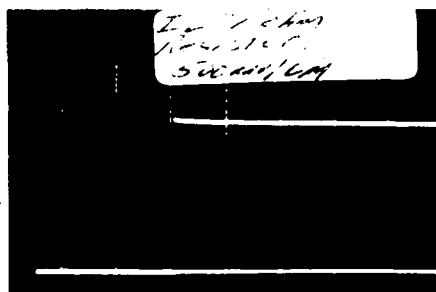
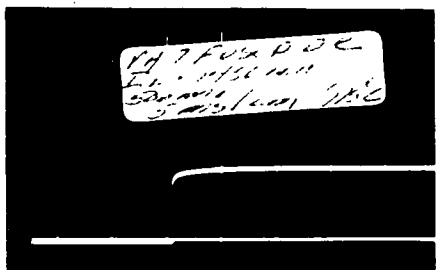


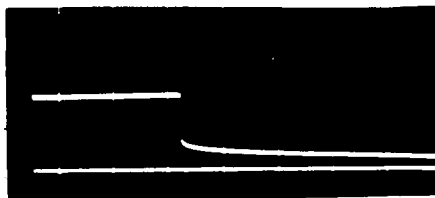
Fig. 10—Circuit used for electrode to electrolyte potential measurements



Sample Current
(Voltage Drop Across
a 1.00 ohm Resistor)



Current Establishment
Oscillogram



Current Break
Oscillogram

Vertical Scale: 500 mv/cm
Horizontal Scale: 5 msec/cm

Fig. 11—Current establishment and current interruption
oscillograms

Fused Platinum Electrode Test XXXIV
H₂ Saturated with H₂O at 26°C 975°C

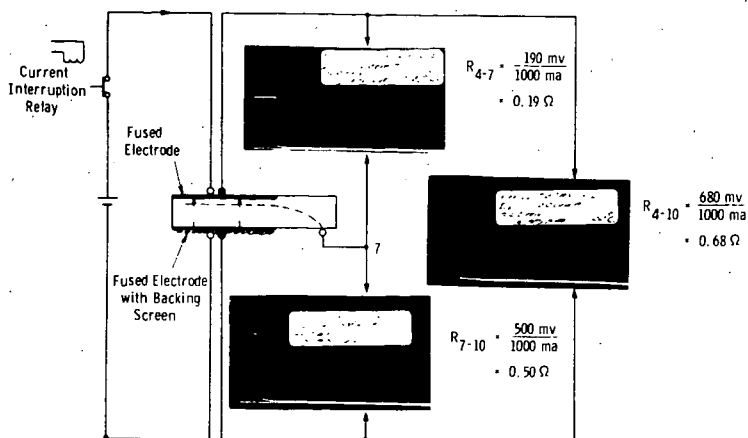


Fig.12—Illustrating method of measuring electrical position of electrolyte potential probe using resistive-component from current interruption tests

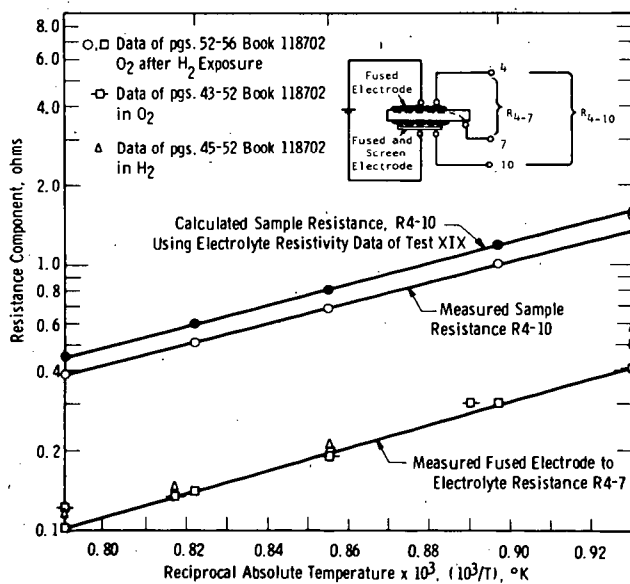
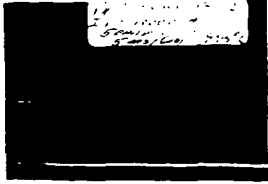
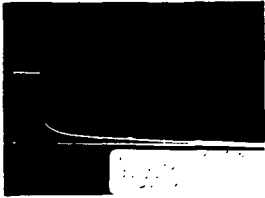


Fig.13—Measurements of the electrical position of the electrolyte potential probe



Fuel electrode performance in oxygen atmosphere
 Vertical scale: 100 mv/cm
 Horizontal Scale: 5 ms/cm
 Indicated R = 0.1 ohms
 Indicated polarization: 0 mv



Fuel electrode performance in hydrogen saturated with water at 70°C
 Vertical scale: 100 mv/cm
 Horizontal scale: 5 ms/cm
 Indicated R = 0.1 ohms
 Indicated polarization: 105 mv

Fig. 14—Electrical performance of fused electrode sample 517 desorbing in oxygen and hydrogen atmospheres
 Test XXXII Test Temp. 995°C
 Sample current 1.0 amperes
 Electrode current density 740 ma/cm²

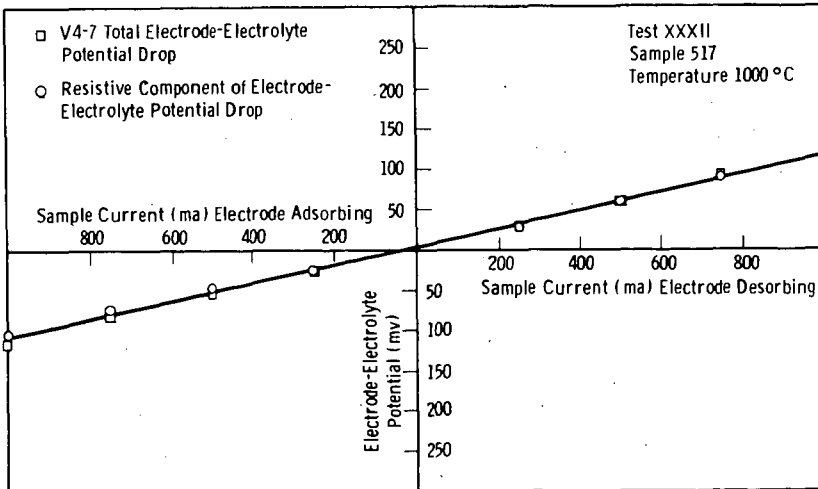


Fig. 15—Volt-ampere characteristic of fused electrode in an oxygen atmosphere

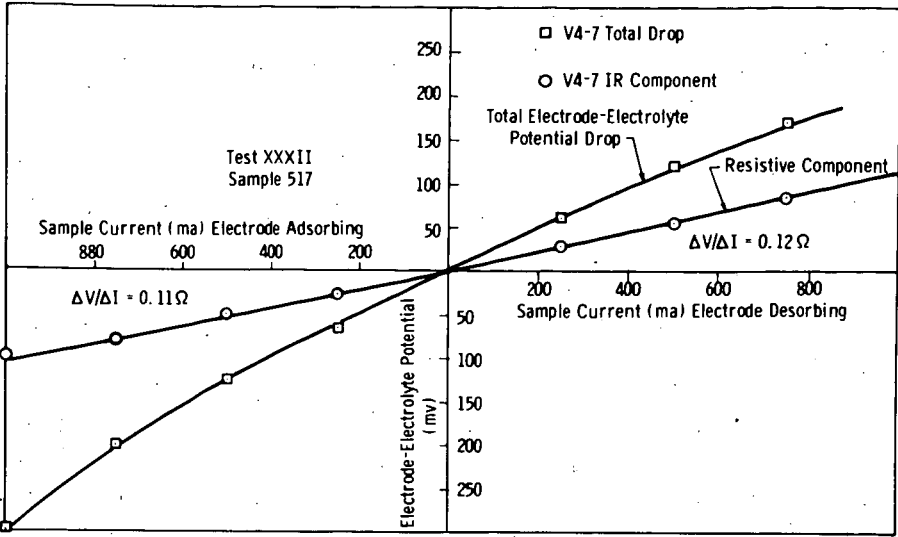


Fig. 16-Volt-ampere characteristic of fused electrode in H_2 and H_2O atmosphere at $1000^\circ C$

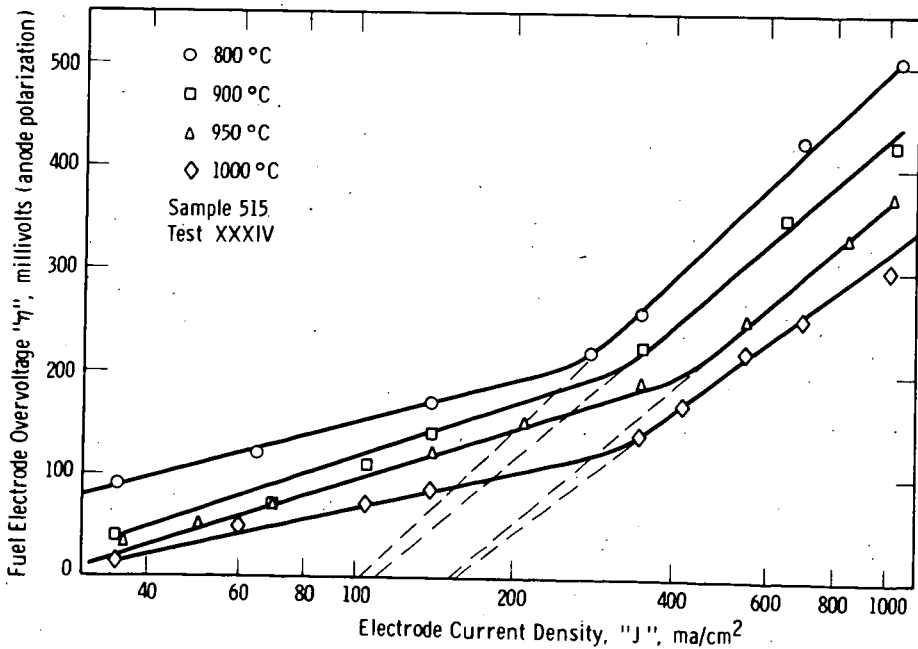


Fig. 17-Fuel electrode polarization as a function of electrolyte temperature

USING RADIOTRACERS TO STUDY HYDROCARBON ADSORPTION DIRECTLY AT ELECTRODES

R. J. Flannery and D. C. Walker

Research and Development Department, American Oil Company, Whiting, Indiana

INTRODUCTION

Recent research on low-temperature hydrocarbon fuel cells has revealed the importance of the role of adsorption in various electrode processes. Knowledge of the concentration and composition of adsorbed reactants, products, or intermediates on the electrodes and in the electrolyte is needed for a better understanding of such processes as electroreduction, electrooxidation, and formation of intermediates.

Programmed potential electrochemical techniques (1-3) have yielded some information about reactant adsorption by inference from oxidative stripping of the electrode, but no adequate techniques have been available to permit direct measurements while the cell is operating. However, the fact that radiolabeled organic molecules have been used successfully to detect adsorbed films on solid surfaces (4,5) has led to several studies of the use of radiotracer techniques for measuring electrode reactions. For example, workers at the University of Pennsylvania have used a thin, gold foil as an electrode and have counted activity through the foil (6), or have used a movable metal tape which is withdrawn from solution and counted (7,8). Such techniques have permitted studies of the adsorption behavior of some aromatics (9,10), olefins (11), and amines (6,7) on several metals. Nevertheless, the thickness of the metal foils limits the sensitivity of the former measurements, and the necessity of withdrawing the tapes prevents continuous samplings in the latter method.

To avoid these shortcomings, we have adapted a method that was developed by Cook (4) and later modified by Walker and Ries (5). In our adaptation, a metal film, deposited directly on a mica substrate, is made the electrode in a fuel cell, and the activity of a radiolabeled hydrocarbon is counted directly through the mica while the cell is operating. High sensitivity is possible because the metal film is only a few thousand angstrom units thick, and the very thin mica sheet absorbs little radiation compared with metals.

We have solved the major design problems associated with the technique. We have been able to produce stable, reusable, thin-film electrodes that are thin enough to allow high sensitivity in counting but thick enough to behave as equipotential electrodes. The cell is small enough to conserve the radiolabeled hydrocarbon, but is easy to fill and empty and is free of components that would adsorb fuel from the electrolyte. Air is excluded rigorously, and operation is confined to low temperatures to keep adsorption and oxidation rates low enough to be studied with 30-second counting periods.

This paper describes the design and operation of the cell and summarizes our studies of the adsorption and oxidation of various concentrations of radiolabeled n-butane at platinum electrodes in a sulfuric acid electrolyte at 25°C.

EQUIPMENT AND PROCEDURE

Apparatus

The adsorption cell and its associated electrodes are designed to minimize mixing of the anode and cathode products during electrolysis. As shown in Figure 1, the cell body is a shallow, 7-cc, glass cup, about 5 cm in diameter, to which two sidearms are attached. One sidearm is drawn to a fine tip within the cell (to serve as a Luggin capillary) and is equipped with a tapered joint to which an autogenous hydrogen reference electrode (12) is attached during electrolysis. The tapered joint is also used for attachment of a syringe by which the cell is filled or emptied. The other sidearm contains the platinum gauze electrode that serves as a cathode. The contents of the cell are magnetically stirred at 100 rpm.

The thin-film electrode, which serves as an anode, is mounted vertically to prevent accumulation of gas bubbles on its surface. It comprises a 2000-Å layer of platinum, bonded to a mica support by means of a 100- to 200-Å layer of tantalum on tantalum oxide. It is prepared as follows: A mounted piece of India Ruby Mica (Spruce Pine Co.), about 6 mils thick and 4.3 cm in diameter, is degreased in benzene, cleaned in chromate cleaning solution, mounted in a conventional sputtering apparatus (13), and evacuated overnight at 4×10^{-3} Torr. Then tantalum is reactively sputtered onto the mica in dry air at 0.05 Torr and 2200 volts at 10 ma for 7 minutes. The resultant layer is purged with oxygen-free argon, and the tantalum sputtering is continued in argon for 20 minutes. Finally, platinum is sputtered onto the tantalum in argon at 0.05 Torr and 1025 volts at 5 ma for 32 minutes.

Before the electrode is sputtered, the mica substrate is mounted between two metal rings, one of platinum and the other of Unalloy 50 (Fe-Ni), as shown in Figure 2. The rings are cemented to the mica with Pyrocera Number 95, vitrified at 450°C. After the sputtering, the finished electrode assembly is cemented to the cell with melted polyethylene. When the electrode is in position, the area of platinum exposed to the electrolyte is 15.94 cm², and the area of mica exposed to the counter is 11.33 cm². Measured from edge to center, the electrode has a resistance of about 1 ohm.

The counting equipment comprises a proportional counter (Model D-47, Nuclear Chicago Corp.) employing P-10 feed gas, and a transistorized scaler (Radiation Instrument Development Laboratories) with a print-out.

The potential of the thin-film electrode is controlled by a Brinkman Model 61-R fast-rise potentiostat in a conventional circuit. A galvanostat consisting of a helipot and a 90-volt battery is used for constant-current anodic or cathodic stripping. Potential during stripping is recorded on a 10-mv Brown recorder through a Keithly Model 610 electrometer.

Materials

The radiolabeled n-butane was obtained from the New England Nuclear Corporation. It had a C^{14} activity level of 1.9 millicuries per millimole and was used without further purification.

The sulfuric acid was J. T. Baker reagent grade.

Water for dilution was laboratory distilled water that had been redistilled twice from quartz into quartz receivers. It was deaerated by evacuation.

Stock solutions of butane were stored over mercury and transferred by displacement with mercury to prevent contact with air. All other reagents and solutions were deaerated before mixing, and transferred under purified argon.

The argon was purified by passage over copper turnings at 800°C.

Procedures

Preparation of Test Solution. Test solutions containing various concentrations of radiolabeled n-butane in 1N H_2SO_4 were prepared by diluting aliquots of the butane stock solution with oxygen-free electrolyte and oxygen-free, double-distilled water.

Counting Rate Calibration. Counting rates were calibrated against a standard source of known activity, and all data were corrected for attenuation of activity through the mounted thin-film electrode and for background and solution counts. Reported count rates represent true values at the electrode surface.

Determination of Electrode Area. To determine the actual surface area of the thin-film electrode, the surface was potentiostated at 1.2 volts in 1N H_2SO_4 for 3 minutes. Then the oxide was stripped galvanostatically at 2 ma ($125 \mu a/cm^2$). A sharp potential arrest was observed. The true area was calculated from the total number of coulombs required to strip the oxide. A factor of 0.3 millicoulombs/cm² derived from other work (14) was used.

Adsorption Measurements. In a typical adsorption run, the cell was filled with a blank 1N H₂SO₄ solution that contained no n-butane, and the thin-film electrode was pretreated (reduced) at 0.1 volt. Then the blank solution was replaced with the test solution, and the potential was controlled at one or more predetermined voltages while the adsorption at the thin-film electrode was measured in counts per minute per cm² of true electrode area. The reference electrode was operated at 5 ma/cm² in the same electrolyte (1N H₂SO₄).

RESULTS AND DISCUSSION

In the initial experiments, the adsorption of radion-n-butane in 1N H₂SO₄ at 25°C was studied as a function of time, electrode potential, and n-butane concentration. For a particular concentration of n-butane, electrolysis was started at 0.1 volt and adsorption was measured until an equilibrium value was reached. Then voltage was increased by 50 to 100 mv, and equilibrium adsorption was again noted. This procedure was repeated from 0.1 to 0.5 volt with 5×10^{-4} and 5×10^{-5} molal n-butane. For the latter solution, the voltage was then decreased in several increments.

As shown in Figure 3, equilibrium adsorption was negligible below 0.2 volt, showed a maximum at 0.3 volt, regardless of n-butane concentration, and again was negligible above 0.5 volt. However, when the voltage was decreased, less n-butane was re-adsorbed at 0.3 volt and more was retained at 0.1 volt.

Other workers (7,10) have found that the potential at which maximum adsorption of n-decyl amine and naphthalene occurs varies with concentration. They attribute this concentration dependence to variations in the electronic interactions of the pi electron system of the adsorbed molecules with the platinum. The fact that we observed no such concentration dependence may reflect a lack of electronic interaction between n-butane and the electrode.

Galvanostatic data show that at least part of the butane first adsorbed at 0.3 volt is displaced by hydrogen atoms adsorbed when the potential is switched to 0.1 volt. Anodic potential sweep data suggest that the butane adsorbed at 0.3 volt occupies sites normally involved in the second hydrogen wave (~0.35 volt) usually seen in potential sweep scans. The decrease in adsorption at higher voltages occurs because oxidation of n-butane begins to compete with adsorption above 0.3 volt. The subsequent change in the level of adsorption as the voltage was decreased indicates that an irreversible reaction occurs on the electrode above about 0.3 volt. For example, Figure 4 shows how the adsorption-time behavior of n-butane is affected by a change in potential. Here, equilibrium adsorption was established at 0.1 volt, and then the potential was increased 0.3 volt for several hours. When the potential was decreased to 0.1 volt, some of the n-butane was desorbed, but the equilibrium concentration retained on the electrode was much higher than the value measured initially at 0.1 volt.

Examination of the electrode as the potential was cycled repeatedly between 0.1 and 0.3 volt showed that such adsorption-desorption hysteresis is caused by the formation of a residue on the platinum. The residue forms slowly, will not hydrogenate off of the electrode at 0.1 volt, and will not wash off in blank electrolyte. However, it can be removed completely by oxidation at 1.2 volts.

In an effort to quantify the surface concentration of this residue, we first measured the maximum adsorption of n-butane as a function of concentration at 0.3 volt. Then we measured the amount of residue formed at each concentration as a result of repeated recycling between 0.1 and 0.3 volt. Based on the true surface area determined for the electrode, we were thus able to calculate the saturation adsorption of n-butane at 0.3 volt and relate it to the amount of surface covered by the residue. The concentration isotherms and the surface coverage data are shown in Figure 5 and Table I.

Results of the galvanostatic procedure used to measure the residues are illustrated in Figure 6. The residue-covered electrode was first potentiostated at 0.3 volt. The residue was then removed by oxidation at $63\mu\text{ a/cm}^2$, while the number of coulombs passed and the amount of C^{14} on the window were recorded simultaneously, starting at 0.3 volt and terminating at 1.2 volts. A blank galvanostatic curve in 1N H_2SO_4 was obtained to correct for coulombic contributions from double-layer charging and from oxidation of the platinum surface. Coulometric results were also normalized to the window area by using the ratio of window area (11.33 cm^2) to total area exposed to the electrolyte (15.94 cm^2). As the residue is oxidized, the C^{14} leaves the window presumably as C^{14}O_2 , and the count rate drops.

In Figure 6, count rate and total coulombs passed are plotted vs. potential. Oxidation of the residue begins above 0.65 volt as reflected in both curves. The initial negative values represent oxidation of hydrogen that was present on the electrode in the blank electrolyte at 0.3 volt but was not present on the residue-covered electrode. Some of the residue was much harder to oxidize and a little still remained at 1.2 volts in the scan. (The remainder can be oxidized if the potential is held constant for a time at 1.2 volts.)

As shown in Table I, if we assume that the n-butane molecules lie flat and occupy 29 \AA^2 , saturation is approached at a fractional coverage, θ , of 0.39. Whereas, if we take the value of $50\text{ \AA}^2/\text{molecule}$ commonly assumed in gas phase adsorption work where imperfect packing is concluded to occur, we find that θ is 0.98. In this work the actual area occupied by butane must be taken into account because the remaining free surface area is available to other solution species. Our data show that the amount of residue varies with the concentration and accounts for about 1/4 of the initial maximum amount of n-butane adsorbed at 0.3 volt. From the data for peak adsorption at 0.3 volt vs. concentration, an equilibrium constant calculated for the adsorption (7) gives $K_{\text{eq}} = 4.85 \times 10^{-4}$. The corresponding free energy of adsorption, ΔF_a , is 3 kcal/mole.

In our data for the oxidation of the residue, the count rate is directly related to the number of butane molecules originally adsorbed on the electrode. If these molecules were still intact they would yield 26 electrons each. The actual coulombic yields varied with the potential and reflected various states of oxidation of those portions of the residue removed with a given charge increment. In Figure 7, the number of millicoulombs measured is plotted against percent C^{14} removed. The curve appears to have four linear segments. On the basis of the count rate, the known specific activity, and 26 electrons per butane residue, 30 millicoulombs would be measured, and the average theoretical slope shown would be followed. The first two linear segments (45% C^{14} removal) have steeper slopes, reflecting partial oxidation of a substantial amount of the other 55% of butane-equivalent residue. The remaining 55% C^{14} is removed at a slope equivalent to one-half or less of the 26 electron slope, showing clearly the existence of an oxidized intermediate that is difficult to oxidize further. A total of 37 millicoulombs were passed in removing 80% of the residue.

CONCLUSION

The existence of the residue is interesting because previous (unpublished) work with various pulse techniques has shown that at higher temperatures there is a time-decay in oxidation rate which could result from decay of active sites, reduction of minor amounts of surface oxide (resulting from pretreatment techniques), or the formation of a residue which blocks catalyst sites. Our radiotracer data strongly support the latter. Additional experiments with stripping the residue have shown similar high initial and low final stripping rates. The partially oxidized material might be an unsaturated coke having a C/H ratio of about 1, perhaps similar to benzene. However, partially oxygenated species could also account for the observed state of oxidation. Assignment of an exact structure is not possible with the radiotracer method alone. Examination of residues from other fuel molecules, modification of the radiotracer technique to permit simultaneous C^{14} and H^3 measurement, or development of a spectroscopic method for examining the residue would be aids in that direction. Knowledge of the state of oxidation of the residue and its response to various treatments would be helpful for an understanding of the process of anodic oxidation of hydrocarbons at platinum. The radiotracer method can supplement conventional electrochemical measurements in that regard.

The radiotracer method should be used to study a number of problems in the fuel-cell area. Adsorption behavior should be studied for a variety of fuel types, such as alkanes, olefins, aromatics and naphthenes, and on other surfaces. Residues from oxidation of these fuel types and from reduction of radio-carbon dioxide should be examined in detail. Surface coverage and state of oxidation data for these reactants may reveal much about the structure and composition of surface species and their role in limiting the rate of the over-all process. Competitive adsorption in mixed liquid fuels should be explored, and the effect of poisons such as sulfur and arsenic on adsorption behavior should be assessed.

A general limitation exists with regard to the temperature range available for measurements. Adaptation of the cell and the counter

for use at higher temperatures is relatively easy to accomplish technically. But reaction rates for adsorption-desorption and oxidation increase with temperature. This eventually limits the method because feasible counting periods have a required minimum duration. For a given level of radio-activity, because of the irregular rate of decomposition of C^{14} , a minimum counting period is required to obtain small data scatter in repeated counts of the same source. For our work, 6 seconds produced some scatter. Appreciable increases in rates of sorption or oxidation processes would allow fewer samplings of count rate, eventually eliminating the possibility of simultaneous measurements.

In its present state of development, the method should accommodate acid and alkaline electrolytes and many non-aqueous electrolytes. A wide choice of electrode metals is possible. Mica is the preferred window material for hydrocarbons, but Mylar or Teflon may be useful with other reactants. Because the method has many potential applications, the cell structure should be chosen to suit the requirements of each system.

ACKNOWLEDGEMENTS

This work was financially supported by the Advanced Research Projects Agency of the Department of Defense as part of Project Lorraine under contracts DA-11-022-ORD-4023 and DA-49-186-AMC-167(X). Monitoring Agencies have been the U.S. Army Research Office (Durham), Harry Diamond Laboratories (U.S. Army Material Command) and the Marine Engineering Laboratories (U.S.N., Bureau of Ships). The assistance of B. Girman in preparation of samples is gratefully acknowledged.

LIST OF REFERENCES

1. S. Gilman, J. Phys. Chem., 67, 78 (1963).
2. S. B. Brummer and J. I. Ford, J. Phys. Chem., 69, 1355 (1965).
3. R. J. Flannery, G. Aronowitz, and D. C. Walker, Progress Report No. 1, Contract No. DA-49-186-AMC-167(X), (March, 1965).
4. H. D. Cook, Rev. Sci. Instr., 27, 1081 (1956).
5. D. C. Walker and H. E. Ries, Jr., ADVANCES IN CHEMISTRY, No. 43, American Chemical Society, 1964, pp. 295-301.
6. H. Wroblowa and M. Green, Electrochim. Acta, 8, 679 (1963).
7. J. O'M Brokris and D. A. J. Swinkels, J. Electrochem. Soc., 111, 736 (1964).
8. D. A. J. Swinkels, Ph.D. Dissertation, University of Pennsylvania, 1963.
9. M. Green and H. Dahms, J. Electrochem. Soc., 110, 466 (1963).
10. J. O'M Brokris, M. Green, and D. A. J. Swinkels, J. Electrochem. Soc., 111, 743 (1964).
11. E. Gileadi, private communication.
12. J. Giner, J. Electrochem. Soc., 111, 376 (1964).
13. L. Holland, "Vacuum Deposition of Thin Films," John Wiley & Sons, Inc., New York, 1958.
14. H. A. Laitinen and C. G. Enke, J. Electrochem. Soc., 107, 773 (1960); J. F. Connolly, private communication.

TABLE I
ADSORPTION AND AREA PER MOLECULE FOR VARIOUS CONCENTRATIONS OF n-BUTANE^a

n-Butane Concentration, Molal	Roughness Factor of Film-electrode ^b	Amount of Adsorption, C/M per cm ² true		Fractional Coverage, θ^e	
		Maximum ^c	Residue ^d	Maximum ^c	Residue ^d
7.1×10^{-6}	29.0	6	2	0.012	0.004
3.6×10^{-5}	26.3	58	14	0.12	0.028
7.1×10^{-5}	30.0	157	54	0.32	0.11
	30.9	153	50	0.32	0.10
2.1×10^{-4}	26.3	189	36	0.39	0.073
7.1×10^{-4}	29.0	189	27	0.39	0.054

- a. All measurements at 25°C in 1N H₂SO₄ at sputtered platinum electrodes.
- b. Determined by cathodic stripping of oxide.
- c. Initial adsorption at 0.3 volt vs. hydrogen, 11.3 cm² exposed electrode.
- d. Amount retained after repeated cycling at 0.1 and 0.3 volt, 11.33 cm² exposed electrode.
- e. Assuming molecules lie flat and occupy 29Å².

FIGURE 1
ADSORPTION CELL

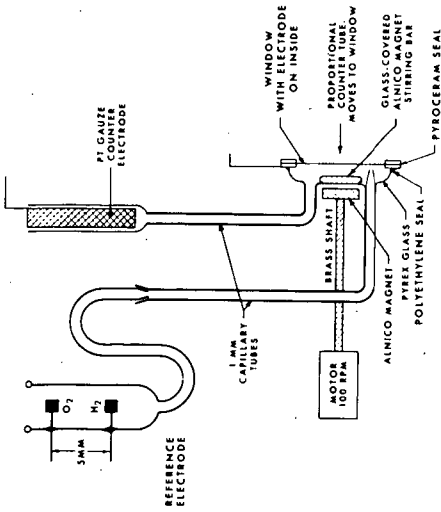


FIGURE 2
FILM-ELECTRODE MOUNTING

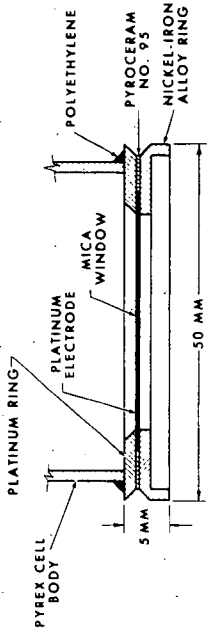


FIGURE 3
ADSORPTION OF RADIO n-BUTANE AS A FUNCTION OF POTENTIAL

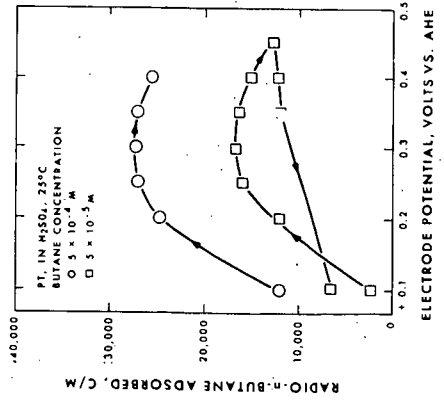
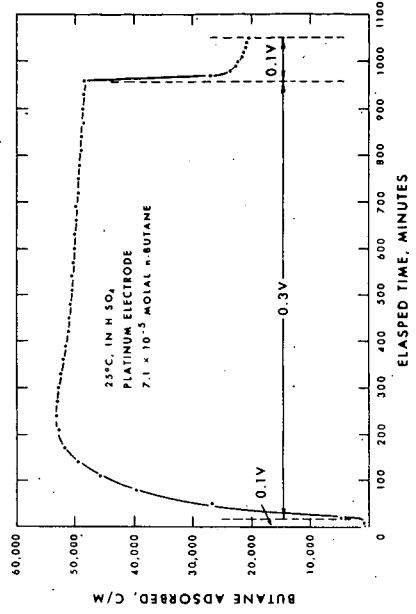


FIGURE 4
BUTANE ADSORBED VERSUS TIME AT CONTROLLED POTENTIAL



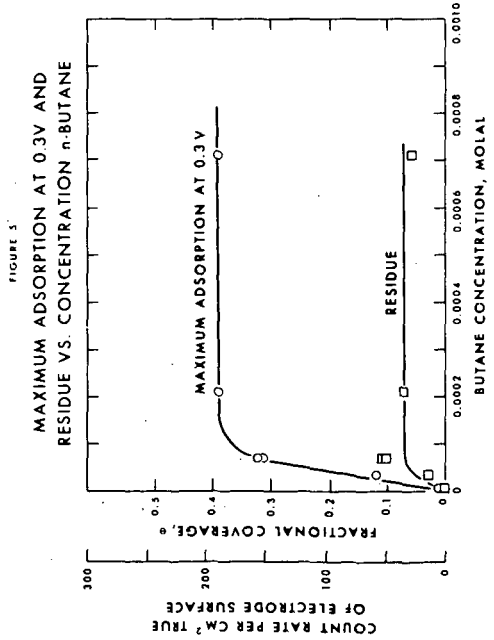
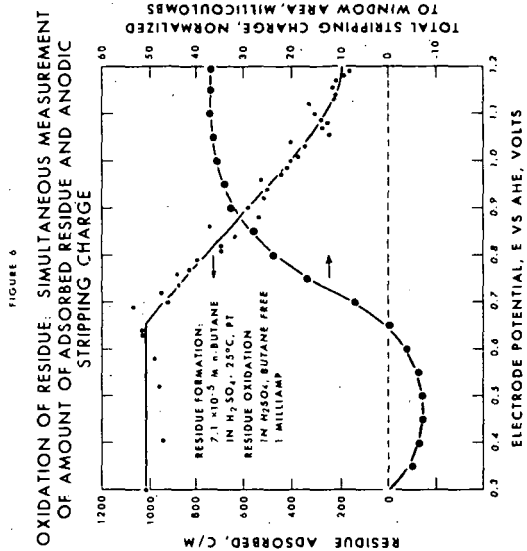


FIGURE 5
MAXIMUM ADSORPTION AT 0.3V AND RESIDUE VS. CONCENTRATION n-BUTANE

FIGURE 6
OXIDATION OF RESIDUE: SIMULTANEOUS MEASUREMENT OF AMOUNT OF ADSORBED RESIDUE AND ANODIC STRIPPING CHARGE

FIGURE 7
OXIDATION OF RESIDUE: ELECTRON YIELD AND POTENTIAL RANGE

THE STUDY OF HYDROCARBON SURFACE PROCESSES BY THE MULTIPULSE
POTENTIODYNAMIC (MPP) METHOD

S. Gilman

General Electric Research Laboratory
Schenectady, New York

INTRODUCTION

The ultimate goal of the hydrocarbon fuel anode researcher is to provide an intellectual basis for the enhancement of system reactivity. As a step toward that goal, we have undertaken the elucidation of the detailed mechanism of operation of a single well-defined system. The ethane-platinum system was chosen for its relative simplicity.

Other than mass transport, the significant reactions of ethane all occur on the platinum surface. Some of the reactions (such as electron transfer) will depend on the electric field strength and may be classed as electrochemical, others (e.g., possible cracking reactions) might be classed as surface-chemical, but in a general sense all are surface processes. It is immediately apparent therefore, that for mechanistic studies of organic electro-oxidation to have any basic significance, such studies must include characterization of the adsorption layer, preferably under anode operating conditions. Such studies come readily within the scope of electrochemical pulse techniques (1,2).

Since we are dealing with a complex adsorbate (ethane) and the platinum surface, we are actually dealing with not one, but a family of systems. Hence it is necessary to investigate a large number of C_1 and C_2 adsorbates (since these will yield pertinent surface species) as well as the adsorption of hydrogen, oxygen and anions. In this paper, we will stress the relationship of two sub-systems (ethylene and acetylene-platinum) to the ethane anode problem.

EXPERIMENTAL

Equipment and Chemicals

The electronic equipment, glass test vessel and electrodes have been described previously (3). The electrolytes used were 1 N perchloric acid and 85% phosphoric acid, each prepared from A.R. grade acid using triply-distilled water. The ethylene and acetylene used was Phillips Research Grade. Gas mixtures of ethylene or acetylene with argon were prepared from the Research Grade hydrocarbon, bottled and analyzed by the Matheson Co. The test electrode was a length of C.P. grade platinum wire sealed in a soft glass tube with 0.070 cm^2 of area exposed. The exposed end of the wire was sealed in a small bead of soft glass. The value of "saturation hydrogen coverage", S_{QH} , measured as previously (3) was $0.296 \text{ mcoul./cm}^2$, suggesting a "roughness factor" (R.F.) of 1.4 if 0.21 mcoul./cm^2 is taken to correspond to $R.F. = 1$. All measurements were made in a thermostatted air bath with control to $\pm 0.1^\circ\text{C}$.

Procedure

The potential functions employed are diagrammed in Fig. 1 (time axes not to scale). The procedure followed during each step of Fig. 1 is summarized in Table I along with the significance of the procedure. All potentials were measured against a reversible hydrogen electrode immersed in the adsorbate-free electrolyte.

RESULTS

I. Kinetics of Adsorption of Ethylene and Acetylene

Sequence I, Table I was employed in making these measurements. This sequence is similar to that previously used in the study of CO, (3) in that the passive "oxygen" film is used to hold off adsorption until reduced in step D. The duration of step B and the potential of step C have been decreased to avoid unnecessary exposure to oxidizing conditions (simply as a precaution) without any sacrifice of the surface reproducibility previously reported (3).

The charge corresponding to the oxidation of hydrocarbon adsorbed during step D may be measured by application of sweep E of sequence I, Table I. The traces of Fig. 2a and 2b were obtained at 30°C, using solutions of 1 N perchloric acid saturated with gas mixtures of 1.08% ethylene - 98.92% argon and 0.105% acetylene - 99.895% argon, respectively. The traces of Fig. 3 were obtained at 120°C using an 85% solution of phosphoric acid saturated with a gas mixture of 1.08% ethylene - 98.92% argon. For ethylene, trace 1 of Fig. 2a was obtained in the absence of ethylene, and serves as "solvent correction". The area included between trace 1 and any subsequent trace is a charge Q_{ENE}^* , which corresponds to the oxidation of the hydrocarbon adsorbed during step D of the sequence. For the sweep speed employed and for the concentration of hydrocarbon used, it may be calculated that the maximum amount of hydrocarbon which may arrive at the electrode (by linear diffusion) and be adsorbed and/or oxidized during step E, is small compared with that already adsorbed during step D. A similar charge, Q_A , may be defined for acetylene from Fig. 2b.

As for ethane (4) it has been found (5) that the charge defined by traces such as those of Fig. 3a and 3b decreases for sweep speeds over approximately 10 v./sec. This is due to retention of a portion of the ad-layer past the duration of the fast l.a.s. The smaller charge measured at higher sweep speeds may be "calibrated" however, so that higher concentrations of adsorbate may be investigated. We may write the expressions:

$$1) \quad Q_{ENE}^* = a Q_{ENE}$$

and

$$2) \quad Q_A^* = b Q_A$$

where Q_{ENE}^* and Q_A^* are the high-speed values of charge, and a and b are the proportionality constants relating these charges to the 10 v./sec. values. For example, for 1 N perchloric acid at 30°C, a and b were found to have the values 0.79 and 0.64, respectively for a sweep speed of 100 v./sec. (5). Plots of Q_{ENE} and Q_A vs $T_D^{1/2}$ obtained for the conditions of Fig. 2a and 2b appear in Fig. 4. The linear plots suggest diffusion-controlled adsorption. The relationship for semi-infinite linear diffusion is (3):

$$3) Q_{ENE} = 2n F C_{ENE} D_{ENE}^{1/2} \tau^{-1/2} \tau^{1/2}$$

where n = number of electrons to oxidize and desorb one molecule of adsorbed ethylene

D_{ENE} = diffusion coefficient of ethylene

C_{ENE} = bulk concentration of ethylene (mole/cm³)

and Q_{ENE} is expressed in coul./cm². A similar expression may be written for Q_A . For the ethylene data of Fig. 4, we choose

$C_{ENE} = 3.3 \times 10^{-8}$ mole/cm³ based on the solubility (3.04 x 10⁻⁶ mole/cm³, Ref. 6) at one atmosphere in 1 M sulfuric acid at 30°C and assuming applicability of Henry's Law

$D_{ENE} = 1.56 \times 10^{-5}$ cm²/sec. (the value for acetylene in water at 20°C, Ref. 7)

$n = 10$ electrons (assuming complete conversion of a surface C₂H₂ species to carbon dioxide and water)

From these values we obtain:

$$4) Q_{ENE} = 0.147 T_D^{1/2} \times 10^{-3} \text{ coul/cm}^2.$$

which exactly agrees with the experimental plot of Fig. 4. Considering the uncertainty in solubility and diffusion coefficient, the perfect agreement must be assumed to be fortuitous. The occurrence of reasonable agreement serves to establish that the adsorption is indeed diffusion controlled (under these conditions) and that the value of n chosen is probably correct to 20%. For the acetylene data of Fig. 5, we assume the same value of D and n as before. The concentration of acetylene is taken to be

$C = 3.68 \times 10^{-8}$ mole/cm³, based on the solubility in water at 30°C, Ref. 8) and assuming applicability of Henry's Law.

From these values, we obtain a theoretical value of:

$$5) Q_A = 0.164 T_D^{1/2} \times 10^{-3} \text{ coul./cm}^2$$

which is in excellent agreement with the slope of 0.160 of the plot of Fig. 4. Again, the perfection of agreement is probably fortuitous, but the general agreement supports the validity of the assumptions made.

One would not expect diffusion to a wire electrode to follow a linear diffusion law for more than a few seconds (9), which makes the linearity of the plots of Fig. 4 suspect. It is possible to check relationship (3) for values of T_D of less than one second, by using more concentrated solutions of the adsorbate and higher sweep speeds. Results (5) obtained in the fractional second range suggest diffusion-control up to approximately 80% of full coverage, followed by apparent activation control. This latter negative deviation oppose positive deviations from linear diffusion to keep the plots of Fig. 4 linear for large values of T_D .

II. Surface Coverage for Ethylene and Acetylene As A Function of Concentration and Potential.

Sequence II of Table II was employed for these measurements. Although the information required is the extent of adsorption during step E at potential U, steps D and F must be introduced to cope with the complication of surface "oxygen" and with irreversibility of adsorption, within regions of the potential range studied. The approach followed to obtain the data of Fig. 5 - 8, is as follows:

A. Maximum Adsorption at $0 < U \leq 0.6$ V.

1) Starting with Zero Surface Coverage -

T_D and T_F of sequence II, Table I were chosen as zero. The value of Q_{ENE} or Q_A was followed as a function of time at each concentration until a plateau value was reached. The adsorption time was then increased ten-fold to check on whether the maximum value had indeed been attained. An adsorption time somewhat larger than that required was then used to measure adsorption over the potential range. For 0.1% acetylene and 1% ethylene an adsorption time of 100 sec. was satisfactory. For 11% ethylene, 10 sec. suffices and for 0.01% ethylene 200 sec. with stirring suffices.

2) Starting with Full Surface Coverage -

At potentials other than approximately 0.2 - 0.4 v., there are processes of oxidation (high potentials) or hydrogenation-desorption (low potentials) competing with the adsorption process. Attainment of an equilibrium value is apparently very slow. It is possible that equilibrium surface coverage does not exist in the strict sense because of irreversibility in the adsorption, desorption and oxidation processes, further complicated by gradual changes in the structure of the ad-layer. Instead of awaiting apparent equilibrium, we may assume a "quasi-equilibrium" value to correspond to the average of the values achieved when the potential is applied alternatively, to the initially uncovered and fully-covered surface. The latter measurement is accomplished by choosing T_D at the value which results in full coverage for that concentration at 0.4 v. Potential U was applied for a similar length of time T_E , and the resulting decreased values of Q_{ENE} and Q_A were measured.

B. Maximum Adsorption at $U \geq 0.7$ v.

1) Starting with Low Surface Coverage -

At potentials above 0.7 v., the rate of reduction of the passive oxygen film introduced during step B is small (or zero), retarding adsorption. To compensate for this difficulty, T_D was chosen at 1 sec., during which time some (but not complete) adsorption of the hydrocarbon occurred. T_F was also set at 10 msec., to reduce surface "oxygen" deposited during step E, so that this would not interfere with subsequent determination of the surface coverage during the l.a.s.

2) Starting with Full Surface Coverage -

T_D was chosen at the value found to give full surface coverage at 0.4 v. This time also sufficed for complete reduction

of the oxygen film from step B. Step F was chosen at 10 msec. to prevent "oxygen" from interfering with the subsequent measurement of surface coverage.

III. Adsorption (l.a.s.) Traces for CO and Ethane.

Linear anodic sweep traces corresponding to CO surface coverage during adsorption and during oxidation of CO appear in Fig. 9a and 9b respectively. The characteristics of the electrodes used and the method of measurement were described previously (3,10). The sweep speed used was 360 v./sec. Fig. 9a corresponds to adsorption from 1 N perchloric acid saturated with a gas mixture of 1% CO - 99% argon. Fig. 9b corresponds to oxidation at 1.0 v. of a monolayer of CO adsorbed at 0.4 v. from the dilute CO solution. The temperature was 30°C in both cases.

Traces obtained during the adsorption of ethane from a 1 N perchloric acid solution saturated with pure ethane at 30°C, appear in Fig. 10. The conditions under which these traces were obtained were described previously (4).

The conditions under which the traces of Fig. 9 and 10 were measured are similar to those for ethylene and acetylene in that currents corresponding to organic oxidation, correspond only to material on the surface before application of the l.a.s.

DISCUSSION

I. Structure of Adsorbed Ethylene and Acetylene.

We will attempt to deduce certain aspects of the structure of the ad-layer on the basis of the results of measurement of the rate of adsorption, of the shape of the charge (surface coverage) potential plots and of the qualitative appearance of the adsorption (l.a.s.) traces.

A. Terminology Used In Describing the Adsorption Layer.

As there appears to be no generally accepted vocabulary for discussing the details of the ad-layer, the following terms and definitions have been adopted:

Stoichiometry of the ad-layer - The relative amounts of the various elements (carbon, hydrogen, oxygen, etc.) of the adsorbate present on the surface. This is not necessarily the same as the stoichiometry of any single surface species.

Stoichiometry of an ad-species - The relative amounts of the elements present in any particular ad-species. This does not reveal the actual number of atoms of each element in each species.

Composition of an ad-species - The number of atoms of each element present in the ad-species, other than those of the adsorbent. This may be represented as a chemical formula.

Structure of an ad-species - This includes its composition and the nature of the valences between each atom of the ad-species and the nature of each valence between the ad-species and the surface. The "gross" structure permits us to draw a qualitative

diagram showing the bond orientation of the atoms of the ad-species to each other and to the surface. For a heterogeneous surface, we must expect that for each "gross" structure, there will be a number (or perhaps a continuum) of "fine" structures. The fine structure includes information on bond length, bond strength, etc.

Structure of the ad-layer - This includes all information on the structure of the individual ad-species, and on the structure of the adsorbent surface.

As an example of the application of the above terminology, we may describe the structure of the CO ad-layer on Pt, suggested by Eischens and Plisken (11). The stoichiometry of the ad-layer, and the stoichiometry and composition of each ad-species corresponds to the formula CO. It has been suggested that the structure of one CO ad-species (linear) involves a bond from carbon to oxygen and a bond from carbon to one surface site. The structure for a second ad-species (bridged) involves a bond from carbon to oxygen and from carbon to two surface sites. This represents only gross structure since the variations in bond length and strength on various sites of the heterogeneous surface have not been taken into account. The gross structure of the ad-layer includes a certain proportion of the bridged and linear surface species.

B. Adsorption (l.a.s.) Traces for CO.

Results obtained for CO are helpful in demonstrating the effect of changing surface coverage on the characteristics of the adsorption trace of a relatively simple adsorbate. From Fig. 9a, we see that as the surface coverage (charge) with CO increases during adsorption, the shape of the trace changes and there is a marked shift of initial oxidation to the right on the potential axis. Such a shift could occur for a variety of reasons. For CO, it has been suggested that this is because the reaction mechanism involves surface sites not occupied with CO ("reactant-pair" mechanism, ref. 12). According to this explanation, the shift is not caused by a change in gross structure of the ad-species. The important point to be made here is that any attempt to identify an unknown surface species as CO on the basis of the adsorption trace, would be misleading unless comparison were made at (approximately) equal surface coverages. Since the adsorption trace is a highly complex representation of the electrochemical reactivity, it is important that all other conditions (sweep speed, temp., surface preparation) also be held constant. These principles will be used in attempting to arrive at the structure of the hydrocarbon surface species, below.

In the traces of Fig. 9b, the surface is initially covered with a monolayer of CO, and the coverage is progressively decreased by oxidation at 1.0 v. We see that the traces tend to shift back to the left on the potential axis, and when comparison is made at equal values of the surface-coverage, these traces are almost identical with the traces obtained during adsorption (Fig. 9a). Small variations may be due to corresponding variations in the fine structure of the ad-layer. This serves as fair evidence that the gross structure and in particular, the composition of the ad-species does not change at high potentials for this simple adsorbate.

C. Adsorption Traces at $0.2 \text{ v.} < U \leq 0.4 \text{ v.}$ for Ethylene and Acetylene in Perchloric Acid (30°C).

Fig. 2a presents l.a.s. traces ($v = 10 \text{ v./sec.}$) obtained during adsorption at $U = 0.4 \text{ v.}$, of ethylene from perchloric acid at 30°C . We see that a single broad wave was obtained, which shifts to the right on the potential axis with increasing surface coverage (charge). The shift is not as marked as for CO (see Fig. 9). Adsorption at the concentration of adsorbate used in Fig. 2a was complete within 25 sec. The trace for full coverage remained identical for up to 1000 sec., establishing constancy of the structure of the ad-layer over this period of time and at a potential of 0.4 v. Similar traces were obtained for this concentration at a sweep speed of $v = 100 \text{ v./sec.}$ These traces were then compared with those obtained using a ten-fold more concentrated solution for which full coverage is achieved within approximately 500 msec. The traces for identical surface coverage but different adsorption times could be exactly superimposed. On the basis of these experiments one may conclude that over the entire range of surface coverages the structure of the ad-layer remains constant from the fractional-second to the 1000 second range. Comparison of traces obtained at 10 v./sec. for $U = 0.2, 0.3$ and 0.4 v. reveal that the same statement may be made for each of these three potentials.

Traces for adsorbed acetylene appear in Fig. 2B. The dashed traces allow comparison of each trace with that of ethylene at a value of $Q_{\text{ENE}} = Q_{\text{A}}$ (to within 10%). We see that the comparable traces are almost identical. We tentatively conclude that the structure of the ad-species is the same for both adsorbates. The slight difference in the traces is ascribed to differences in fine structure of the ad-layer (perhaps a different distribution of species on the surface). Study of the traces reveals constant structure of the ad-layer over the same time and potential interval as for ethylene.

D. Adsorption Traces for Ethylene and Acetylene at $U \geq 0.5 \text{ v.}$ in Perchloric Acid (30°C).

Fig. 5a and 5b present l.a.s. traces for ethylene and acetylene respectively for values of U from 0.3 to 0.8 v. Traces 2 and 3 of each figure are included to emphasize that the adsorption of less material at 0.3 v. is reflected in a shift of the trace to the left on the potential axis. Traces 4 and 5 of each figure represent lower values of surface coverage (charge) than trace 3, but these traces lie to the right of trace 3. This shift to the right is clear indication that the structure of the ad-layer is different at the higher potentials. This change is first (barely) discernible at 0.5 v. One could argue that this represents only differences in the fine structure of the ad-layer. For example, the composition of the ad-layer might be the same as at lower potentials, but only sites involving relative inactivity (toward electrochemical oxidation) of the ad-layer might be covered. For CO, we have seen that there is no such marked change in reactivity of the ad-layer as we approach a given surface coverage alternatively from zero coverage at low potential, or from full coverage at high potential. By analogy, we conclude that the marked shifts in the traces of Fig. 3 correspond to gross changes in structure; namely, to changes in the composition of the ad-species. Hydrogen codeposition measurements support this view (5). One possibility is that de-hydrogenation of

the surface species leads to a stoichiometry approaching that of carbon. This choice is made tentatively, based on the observation that all oxygen-containing carbon compounds examined to date show higher reactivity than that suggested by traces 4 and 5 of Fig. 3.

E. Inferences from the Results of Measurement of Kinetics of Adsorption of Ethylene and Acetylene.

Thus far, the evidence suggests that identical ad-species are obtained upon adsorbing either ethylene or acetylene at potentials below 0.5 v. The simplest possibility for the stoichiometry of the ad-layer is therefore CH. Excellent agreement with diffusion theory was shown (in a previous section) if we assumed that 10 electrons are required for the oxidation-desorption of one mole of either adsorbate. This is precisely the electron requirement for conversion of the adsorbates to CO₂ and water through surface intermediates of CH stoichiometry. Since the solubility and diffusion coefficients could not be expected to be reliable to more than 20%, somewhat smaller ratios of hydrogen to carbon are also consistent with the kinetic observations. These observations fairly conclusively rule out the presence of any oxygen in the ad-species ($U < 0.5v.$), however, since this would drastically change the value of "n".

The composition of the ad-species obtained at low potential is suggested by results obtained by Niedrach (13). He found that hydrogenation-desorption of an adsorbed ethylene layer yielded predominately ethane, arguing for the conservation of the carbon-carbon bond. Hence at low potentials and temperatures we conclude that the ad-species have the composition C₂H₂. At higher potentials we tentatively conclude the formation of species of composition C₂H and C₂.

F. Structure of Ethylene Adsorbed at Temperatures Above 30°C.

The adsorption traces obtained at 60°C in perchloric acid were similar to those obtained at 30°C, with a slight shift of the traces to the left on the potential axis. As before, only one broad wave was apparent. Measurement of Q_{ENE} after an adsorption time of 8 sec. in a solution saturated with a gas mixture of 1.08% ethylene-98.92% argon, yielded a value 20% higher than the corresponding value at 30°C. This is a reasonable result if we assume diffusion-controlled adsorption (as at the lower temperature) and an increase in the diffusion coefficient of about 40%. Hence we conclude that the structure of the ad-species and the mechanism of adsorption is the same at 60° and 30° in perchloric acid.

For ethylene in phosphoric acid at 120°C, the adsorption traces (Fig. 4) are considerably different than in perchloric acid. Not only does oxidation of the ad-layer begin at lower potentials, but an inflection appears in each trace, suggesting two overlapping waves. This may be symptomatic of the formation of species containing a single carbon atom following rupture of the carbon-carbon bond. The values of Q_{ENE} obtained under these conditions do not have linear dependence on T^{1/2} and the adsorption is therefore relatively slow (compared with diffusion). Whereas the increased reactivity of the ad-layer is readily ascribed to the effect of increased temperature, the explanation for the slow kinetics of adsorption is not obvious. One possibility is that the surface species formed at this higher temperature tend to exert long-range ("poison") effects on the surface.

Another possibility is that adsorbed phosphate ions (14) influence the kinetics of adsorption.

G. Structure of Adsorbed Ethane.

Adsorption traces for ethane at 60°C in perchloric acid appear in Fig. 11. As previously (4) indicated, each trace consists of a peak lying at relatively low potentials and of a broad maximum which extends from about 0.8 v. to oxygen evolution potentials (at $v = 10$ v./sec.). The first peak is largely retained upon application of potentials approaching 0 v. Niedrach (15) has suggested that the first peak corresponds to C - 1 species. The broad maximum is removed by hydrogenation-desorption and it has already been suggested that this species has C_2H_2 composition on the basis of other evidence (4). This work tends to confirm that conclusion for potentials in the range 0.2 - 0.4 v. Since the evidence suggests that the C_2H_2 species convert (possibly further dehydrogenate) at higher potentials, this must also be true for the ethane system.

II. Dependence of Surface Coverage On Concentration, Potential and Temperature for Ethylene and Acetylene.

A. Significance of Q_{ENE} and Q_A .

In perchloric acid, in the potential range 0.2 to 0.4 v., the results suggest that the charges Q_{ENE} and Q_A correspond to the conversion of surface species of the composition C_2H_2 to CO_2 and H_2O . Hence we may write:

$$6) \quad Q_{ENE} = n \Gamma_{ENE} F = 10 \Gamma_{ENE} F$$

where Γ_{ENE} is the concentration of the ad-species in moles/cm², if Q_{ENE} is expressed in coul./cm² (of geometric area). Conversion to a "true area" basis may be made by dividing by the estimated surface R.F. of 1.4. A similar expression may be written for acetylene.

The fractional surface coverage with an adsorbate is commonly defined in terms of the experimental maximum value (although vacant sites may still exist). In terms of charge, we may write:

$$7) \quad \theta_{ENE} = Q_{ENE}/Q_{ENE(max.)}$$

where $Q_{ENE(max.)}$ is the largest plateau value observed on the charge-potential plots. A similar expression may be written for acetylene.

Since we suspect dehydrogenation of the ad-species at potentials above 0.4 v., the value of n of equation (6) may drop from 10 to a minimum of 8. This can introduce an error of no more than 20% in the estimation of either absolute or fractional surface coverage.

"Saturation" surface coverage (perchloric acid, 30°C) for ethylene and acetylene adsorbates corresponds to values of $Q_{ENE} = 0.64 \times 10^{-3}$ coul./cm² and $Q_A = 0.73 \times 10^{-3}$ coul./cm². These charges are equivalent to $\Gamma_{ENE} = 6.6 \times 10^{-10}$ mole/cm² (geometric area) or 4.7×10^{-10} mole/cm² (hydrogen or "true" area) and $\Gamma_A = 7.6 \times 10^{-10}$ mole/cm² (geometric area) or 5.4×10^{-10} mole/cm² ("true" area). From hydrogen codeposition experiments (5) only 75% of the hydrogen sites are obscured by C_2H_2 at full coverage using ethylene as adsorbate,

and 85% of the sites are obscured using acetylene as adsorbate.

B. Effect of Potential on the Surface Coverage for Ethylene and Acetylene.

From Fig. 7, we see that for both ethylene and acetylene, the surface coverage is constant over the potential range 0.2 to 0.4 v. For potentials below 0.2 v., the surface coverage drops off sharply. Burke et al. (16,17) have shown that the hydrogenation of ethylene and acetylene are diffusion controlled, and not quite diffusion controlled, respectively, at 0 v. It is the hydrogenation process, opposing the adsorption process, which causes the surface coverage to drop off at the low potentials. For both acetylene and ethylene, we note that different coverages are measured at a given potential, depending on whether the experiment is begun with zero ($T_p = 0$) or full surface ($T_p = 100$ sec.) coverage. The average value for each of the potentials probably approximates an equilibrium value.

The surface coverages obtained for ethylene and acetylene at potentials below 0.2 v. are noticeably different. This seems an anomaly if one accepts the conclusion that the composition of the ad-species is identical for both adsorbates. An explanation of this behavior is presented below.

Let us assume that adsorption must precede hydrogenation (in the limit, the surface coverage may be almost zero, however). For acetylene, the composition of the ad-species is the same as that of the adsorbate. At potentials below 0.2 v., there will be two competing reactions, i.e., the adsorption of C_2H_2 and the hydrogenation of surface C_2H_2 . Both rates may be expected to be a function of surface coverage and of potential. Starting with either the fully-covered, or uncovered surface, the system will attempt to reach equilibrium at a value of the surface coverage at which the two rates are equal. If the rates in question are complex functions of the surface coverage, and of the concentration of dissolved acetylene, equilibrium may be attained rather slowly, as seems to be the case.

For ethylene at potentials below 0.2 v., we might expect the operation of three kinetic processes, i.e., adsorption of ethylene to yield C_2H_2 surface species, hydrogenation of adsorbed C_2H_2 to yield ethane and (unlike the situation for acetylene adsorption), the hydrogenation of C_2H_4 (present at close to zero concentration on the surface) to yield ethane. Only the second process is held in common with the acetylene adsorbate system, hence one would expect to arrive at different equilibrium coverages for the two systems.

The lower values of surface coverage obtained (below 0.2 v.) for ethylene as compared with acetylene can be a consequence of a slower adsorption step, or of an appreciably larger rate for the reduction of the C_2H_4 species. Since the over-all rate of formation of ethane from ethylene is larger than for acetylene (14,15) the latter condition must be fulfilled. This is also an intuitive conclusion, if we accept the conclusion that the dehydrogenation of C_2H_4 to C_2H_2 on the surface is a spontaneous process throughout the potential range studied.

In the region of the flat plateau for ethylene and acetylene (Fig. 8) we see that the surface coverage for acetylene adsorbate exceeds that for the ethylene adsorbate by approximately 10%.

Hydrogen co-deposition experiments (5) reveal that only approximately 85% of the total (hydrogen) sites are covered even for the acetylene system. Since adsorption of ethylene requires a dehydrogenation on the surface (to C_2H_2) it seems reasonable to conclude that the surface might be sterically blocked at lower values of the surface coverage than for acetylene, for which system no surface dehydrogenation is necessary.

At potentials above 0.4 the surface coverage drops off with increasing potential for both acetylene and ethane. Both of these adsorbates undergo oxidation at these potentials. One might argue that full coverage should yet be attained unless the oxidation process were diffusion-controlled, because only then would it exceed the rate of adsorption. However, the rate of adsorption is only rapid at potentials within the range 0.2 - 0.4 v., where the ad-species are of constant composition. At potentials above 0.4, we have already seen evidence that the ad-species change composition. Results of measurement of rates of re-adsorption (5) suggest that as the potential increases, almost a combined monolayer of the hydrogen-poor species and surface oxygen results, with the latter contribution increasing with potential. The rate of adsorption from the point of incomplete coverage to full coverage is relatively slow. Since the rate of re-adsorption may be expected to depend also on the concentration of the adsorbate, we find the concentration-dependencies of Fig. 6.

C. Effect of Concentration of the Adsorbate On Surface Coverage.

For ethylene, the effect of concentration on Q_{ENE} (and hence on the surface coverage) is presented (perchloric acid at 30°C) in Fig. 6. In the (potential) region of maximum Q_{ENE} , we see that there is no methodical increase in surface coverage with concentration, of the type generally associated with the adsorption isotherms of systems exhibiting thermodynamically reversible adsorption. The maximum surface coverage is taken as essentially constant over the range of partial pressures covered. The average maximum value of Q_{ENE} is 0.62 mcoul./cm², with an average deviation of ± 0.02 mcoul/cm², or $\pm 3\%$ average deviation. The occurrence of full (effectively, since all adsorption sites are not necessarily covered) coverage at low partial pressures of adsorbate is not uncommon for systems which possess a high heat of adsorption.

In the potential range above 0.4 v., we see considerable effect of concentration on the surface coverage. The surface coverage at steady-state (assuming that such a state exists in practice for an ad-layer which may undergo continuous change in structure with time) would correspond to the value at which the rates of adsorption and of oxidation are in balance. Both of these rates may be complex functions of surface coverage, but the rate of adsorption must also be a function of concentration of dissolved adsorbate. Hence it is particularly the rate of adsorption which must decrease with decreasing concentration of adsorbate, and the surface coverage falls. It must be borne in mind, that in the range of potentials above 0.4 v., we are not dealing with diffusion-controlled rates of adsorption, as at lower potentials, since the structure of the ad-layer is more complex. It is probably the high rate of adsorption (relative to oxidation) that maintains a flat maximum over a wide range of potentials for the most concentrated adsorbate of Fig. 6, when the experiment is begun with full coverage. The slow approach toward equilibrium

is further argument against the shape of the surface coverage-potential plot's being determined by essentially electrostatic forces.

D. Effect of Temperature On Surface Coverage.

Fig. 8 reveals that at 60°, the maximum surface coverage achieved for ethylene is 5% higher than at 30°C. In either case, all adsorption sites are not fully occupied. One way in which the temperature may increase "full" coverage is to increase the mobility of the ad-layer, permitting closer packing of the ad-species.

It has already been noted that at 120°C and in phosphoric acid, the kinetics of adsorption and the composition of the ad-layer are complex. Values of Q_{ENE} up to 0.83 mcoul./cm² could be measured (adsorption for 100 sec.). If we assumed C₂H₂ composition of the ad-layer, this would be equivalent to 95% of full coverage (on basis of available hydrogen sites). It is not unlikely that the large value of charge actually corresponds to close packing of considerable C-1 species.

E. Comparison with the Results of Tracer Studies.

The adsorption of ethylene on platinized platinum (1 N sulfuric acid, 30 and 80°C) has been investigated by J.O'M. Bockris et al. (18), using tracer techniques. The results of this work disagree with those of our predecessors in several ways. An attempt to reconcile this disagreement appears below, on the basis that the only significant difference between the two systems is the surface roughness. Bockris (18) observes only a gradual increase of surface coverage with concentration from approximately 10⁻⁶ to 1.5 x 10⁻⁵ mole/l. bulk concentration of ethylene, with full coverage achieved at the higher concentration. In this work we attained full coverage at a concentration of 3 x 10⁻⁷ mole/l. (1.3 x 10⁻⁴ Atmos.). In our experiments, the adsorption was transport-controlled and required approximately 200 sec. for completion in a well-stirred solution (3 x 10⁻⁷ M./l.). By comparison, adsorption from a 10⁻⁶ M./l. solution would require 20 sec. for our system. For a platinized electrode with a R.F. of 100, as used by our predecessors, an equilibration time of 2000 sec., or approximately 30 minutes would be required. It is possible that such time durations were not allowed routinely. A second possibility is that the 100 fold greater rates of oxidation (on basis of geometric area) and hydrogenation-desorption encountered on the platinized electrode, tend to result in partial diffusion control for these reactions even at low potential, forcing the surface coverage down.

Bockris et al. (18), also found that maximum adsorption was attained only at higher potentials than in this work. The decrease in surface coverage encountered in this work, as the potential is lowered to less than 0.2 v., has been ascribed to the effect of the opposing rate of hydrogenation-desorption, which increases as the potential is lowered. For the platinized surface this rate would be increased 100-fold at comparable potentials. Such an enhanced rate might lead to sufficient depletion of the adsorbate to drive the surface coverage down at approximately 0.3 v., as found by Bockris.

III. Mechanism of the Electrochemical Oxidation of Hydrocarbons.

The studies of adsorption reported in this paper are a necessary preliminary to future detailed study of the mechanism and kinetics of the electrochemical oxidation of the hydrocarbons. It is possible at this time, however, to draw some qualitative conclusions on mechanism, based on the available information.

The rate of continuous oxidation of any complex molecule which yields a variety of surface intermediates, may be expressed in terms of the partial currents for each of "n" surface species:

$$8) \quad I_i = n_i F k_i f_i (\theta_1, \theta_2, \dots, \theta_n) g_i(U)$$

where n_i = number of electrons required to convert species "i" to the next identifiable surface species

k_i = appropriate rate constant

f_i = a function relating the current for species "i" to the surface coverage with the various species (assuming interaction)

g_i = a function relating the current to the applied potential for species "i"

Equation (8) also covers the situation for any reaction path requiring an adsorbed intermediate, even if the effective concentration of that species is vanishingly small. In addition there may be "m" reaction paths involving the initial reactant in the non-adsorbed state (Rideal-Eley as opposed to Langmuir-Hinshelwood mechanism, ref. 19):

$$9) \quad I_j = n_j F k_j h_j (\theta_1, \theta_2, \dots, \theta_m) j_j(U)$$

where the symbols have significances similar to those for equation (8). The total current may then be expressed as:

$$I = \sum_{i=1}^n I_i + \sum_{j=1}^m I_j$$

Since ethylene, acetylene and ethane all hold one group of surface species in common, we may discuss the qualitative dependence of the corresponding partial current on surface coverage, bearing in mind that this is a small part of a much larger problem area.

For the potential range 0.2 - 0.4 v. in perchloric acid, it appears that we have the common surface species C_2H_2 . The traces of Fig. 2 reveal that as the surface coverage with this species increases, the corresponding trace shifts to the right on the potential axis, or in other words, the initial oxidation becomes increasingly more hindered. One interpretation is that the electronic character of the surface changes with surface coverage. A more tangible possibility is that the transition state for oxidation of the surface species, involves surface sites not blocked by the hydrocarbon ("free" sites). The similar observation for CO (see Fig. 9) led to the suggestion of a "reactant pair" mechanism, involving adjacent sorbed CO and water molecules (3). For the complicated C_2H_2 structure there are several plausible explanations for similar dependence of oxidation rate upon free sites. These

include the requirement of extra sites for the rupture of carbon-carbon and carbon-hydrogen bonds. Additional information will be required before a conclusion may be reached in this area.

For the potential range above 0.4 v. (perchloric acid), the l.a.s. traces of Fig. 5 reveal that the ad-species formed at higher potentials undergo initial oxidation less readily than does the C_2H_2 surface species. On this basis it has already been suggested that the structure may be approaching C_2 stoichiometry at the high potentials. If this conclusion is correct, sequential dehydrogenation is one of the possible paths for the oxidation of all of the C - 2 hydrocarbons. It is apparently the path of smallest specific rate for ethane, for which a low potential wave appears in the l.a.s. trace (Fig. 10). For ethane, it has been suggested that an adsorbed ethyl radical is the common antecedent of both reaction paths (4). The more reactive path is believed to involve C - 1 species (15).

CONCLUSIONS

1. Under the conditions of our experiments, the adsorption of ethylene and acetylene from perchloric acid was diffusion-controlled. The early onset of diffusion control implies very rapid adsorption kinetics (equivalent to a first order electrochemical rate constant of greater than 0.1 cm/sec.) at low surface coverages.

2. The results of the adsorption measurements suggest that the composition of the ad-species for both ethylene and acetylene adsorbates is identical. In perchloric acid, at potentials of 0.4 v. or less, the ad-species has the composition C_2H_2 . At potentials above 0.4 v., the ad-layer becomes more refractory, possibly because of further de-hydrogenation of the acetylenic surface species. There is no evidence for conversion of the C_2H_2 species to more easily oxidized "oxygenated" species at moderate temperatures.

3. In phosphoric acid at 120°C, the kinetics of adsorption of ethylene follows a complex law. The structure of the ad-layer is also complex. It is possible that both temperature and specific anion effects play a significant role in the system.

4. The adsorption of ethane from perchloric acid is slow, and yields two categories of surface species represented as two "waves" on the linear anodic sweep traces. Wave I is not (significantly) desorbed at low potentials, and is comparatively electrochemically active (with respect to oxidation). Wave II is readily desorbed at low potentials and is identical with the acetylenic species obtained upon adsorbing ethylene or acetylene. At moderate temperatures, wave II does not convert to I at any appreciable rate and hence (in a sense) acts as an undesired residue as compared with wave I. The variation, with potential, of the composition of the ad-species represented by wave II is the same as that reported for ethylene or acetylene.

5. Full coverage of the surface is obtained (in perchloric acid) at partial pressures of ethylene as low as 10^{-4} atmospheres. The shape of the surface-coverage-potential plot for both ethylene and acetylene is consistent with a model such that the surface coverage is driven down at the low and high potential regions by rates of hydrogenation-desorption and of oxidation, which oppose

the rate of adsorption. In the high-potential region, the combined coverage of adsorption sites with multiply-bonded carbon species and with "oxygen" is high, even though the surface concentration of the organic species appears low on a Mole/cm² basis. The rate of adsorption of ethylene or acetylene on a surface partially covered with the high-potential carbon species is very slow compared with that on a surface partially covered with C₂H₂.

ACKNOWLEDGMENT

The author is pleased to acknowledge helpful discussions with L.W. Niedrach and D.W. McKee.

This work is a part of the program under contracts DA-44-009-AMC-479(T) and DA-44-009-ENG-4909, ARPA Order No. 247 with the U.S. Army Engineer Research & Development Laboratories, Ft. Belvoir, Virginia, to develop a technology which will facilitate the design and fabrication of practical military fuel cell power plants for operation on ambient air and hydrocarbon fuels.

REFERENCES

1. M.W. Breiter and S. Gilman, J. Electrochem. Soc., 109, 622 (1962).
2. S. Gilman and M.W. Breiter, J. Electrochem. Soc., 109, 1099 (1962).
3. S. Gilman, J. Phys. Chem., 67, 78 (1963).
4. S. Gilman, Fall 1964 Meeting of the Electrochemical Soc.; To be published.
5. S. Gilman, To be published.
6. Section on Hydrocarbon Solubilities in California Research Corp. Progress Report No. 10, Contract No. DA-49-186-ORD-929, April 1963.
7. "Chemical Engineers Handbook", ed. by J.H. Perry, McGraw-Hill Book Co., 1950.
8. H. Hiraoka, Rev. Phys. Chem. Japan, 24, 13 (1954).
9. "New Instrumental Methods in Electrochemistry", by P. Delahay, Interscience Pub., Inc., N.Y., 1954.
10. S. Gilman, J. Phys. Chem., 67, 1898 (1963).
11. R.D. Eishens and W. Pliskin, Advances in Catalysis, Vol. 10, Academic Press, Inc., N.Y. (1958), p.18.
12. S. Gilman, J. Phys. Chem., 68, 70 (1964).
13. L.W. Niedrach, J. Electrochem. Soc. 111, 1309 (1964).
14. S. Gilman, J. Phys. Chem., 68, 2098, 2112 (1964).
15. L.W. Niedrach, preprint of paper presented at this meeting.
16. L.D. Burke, C. Kemball and F.A. Lewis, Trans. of the Faraday Soc., 60, 913 (1964).
17. L.D. Burke, F.A. Lewis, and C. Kemball, Trans. Faraday Soc., 60, 919 (1964).
18. J. O'M. Bockris, B.T. Rubin and E. Gileadi, Fall, 1964 Meeting of the Electrochemical Soc.
19. "Catalysis by Metals" by G.C. Bond, Academic Press, N.Y. (1962).

Table 1.-PROCEDURES FOLLOWED DURING POTENTIAL SEQUENCES OF FIG. 1

Sequence	Fig.	Step (refers to Fig. 1)	Procedure	Purpose
I	1(a)	A	1. Potential normally held at 0.4 v. between experiments.	1. To minimize exposure of electrode and adsorbate to oxidizing or reducing conditions.
		B	2. Bubble gas* through solution with paddle-stirring for $T_B = 2$ seconds†.	2. To remove adsorbed materials from the surface, and to produce a passive film which blocks re-adsorption.
		C	3. Continue gas bubbling, and stirring for 1/2 minute. Stop bubbling and stirring and allow solution to become quiescent for 1 1/2 minutes. Total value of $T_C = 2$ min.	3. The passive film of step B is retained while desorbed materials and oxygen released during step B are swept into the bulk of the solution and diluted. The solution is allowed to become quiescent to restrict mass transport to ordinary diffusion in subsequent steps.
		D	4. The adsorption is allowed to proceed for T_D seconds.	4. The passive film is largely reduced during the first few milliseconds, allowing adsorption of the hydrocarbon from solution.
		E	5. Apply linear anodic sweep E of speed, v.	5. The amount of material adsorbed during time interval T_D may be determined from the l.a.s. trace.
II	1(b)	A - D	1 - 4. Same as for Sequence I.	1 - 4. Same as for Sequence I.
		E	5. The potential is raised (or lowered) to value U, for time T_E .	5. Further increase, or decrease occurs in the surface coverage acquired in step D.
		F	6. Apply l.a.s. F, of speed v.	6. The amount of material on the surface may be determined from the l.a.s. trace. This amount will be a function of T_D and T_E .

* The gas used was a designated mixture of argon and hydrocarbon.

† "T" with the appropriate subscript is the duration of any particular step.

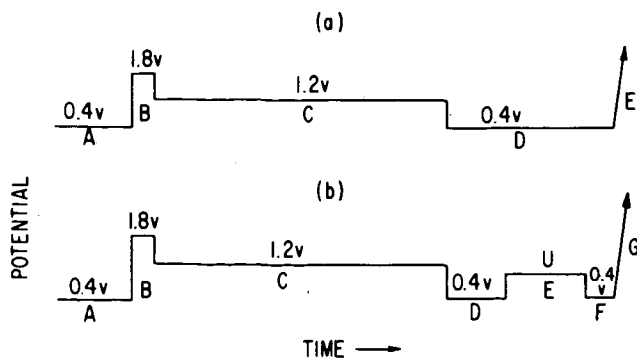


Fig. 1.-POTENTIAL SEQUENCES APPLIED TO THE TEST ELECTRODE (TIME AXES NOT TO SCALE).

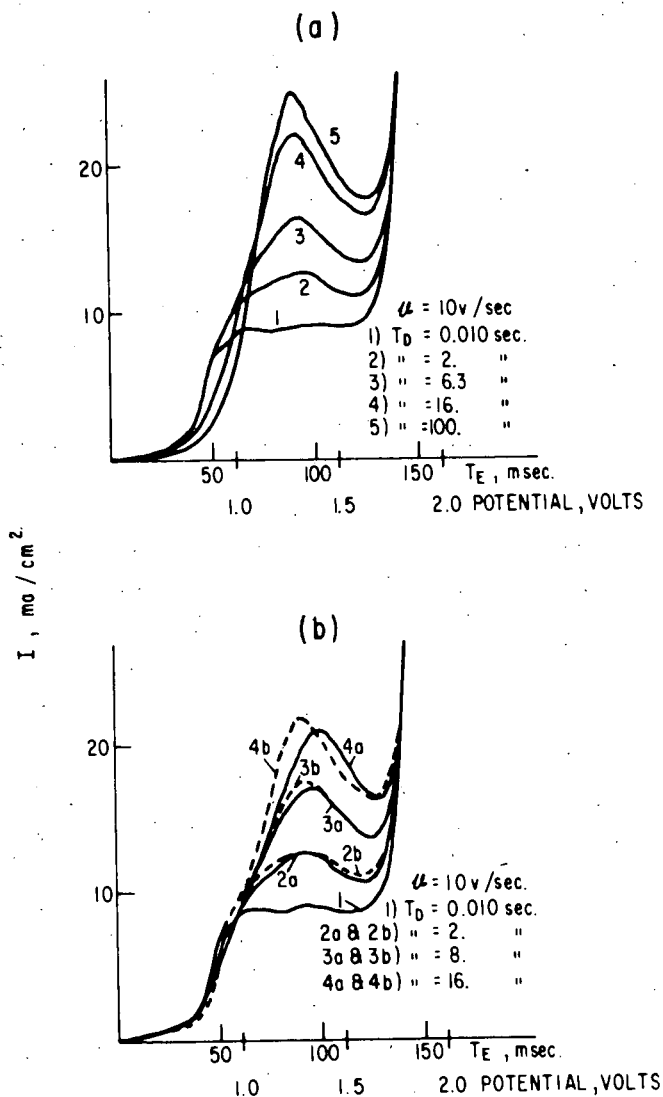


Figure 2. L.A.S. Traces Corresponding to the Adsorption at 0.4 v., of Ethylene and of Acetylene (1 N HClO₄, 30°C). Traces measured using Sequence I, Table I, with $v = 10 \text{ v./sec.}$ The traces of Fig. 2a and the dashed traces of Fig. 2b correspond to 10⁻² atmospheres of ethylene. The solid traces of Fig. 2b correspond to 10⁻³ atmos. of acetylene.

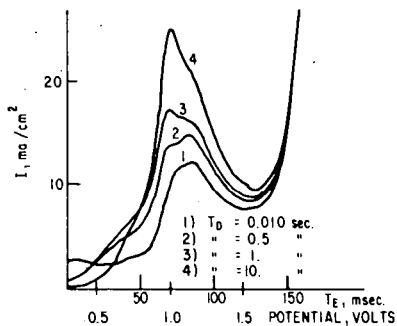


Fig. 3. -L.A.S. TRACES CORRESPOND TO THE ADSORPTION OF ETHYLENE FROM 85% PHOSPHORIC ACID AT 120°C (ETHYLENE p.p. = 10^{-2} ATMOSPHERES). TRACES MEASURED USING SEQUENCE I, TABLE I, WITH $v = 10$ v./sec.

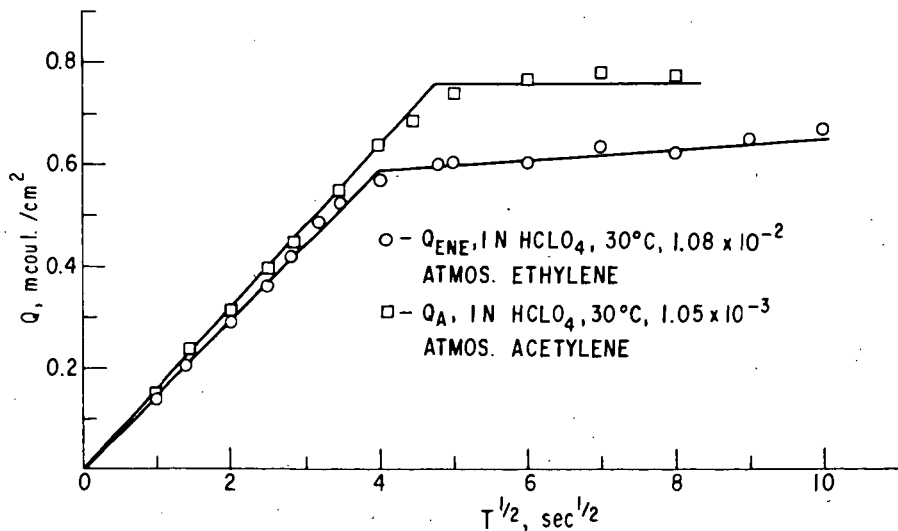


Fig. 4. -KINETICS OF ADSORPTION OF ETHYLENE AND OF ACETYLENE FROM 1 N HClO₄. THE ABSOLUTE SURFACE COVERAGE IS PROPORTIONAL TO THE CHARGE, Q (SEE TEXT).

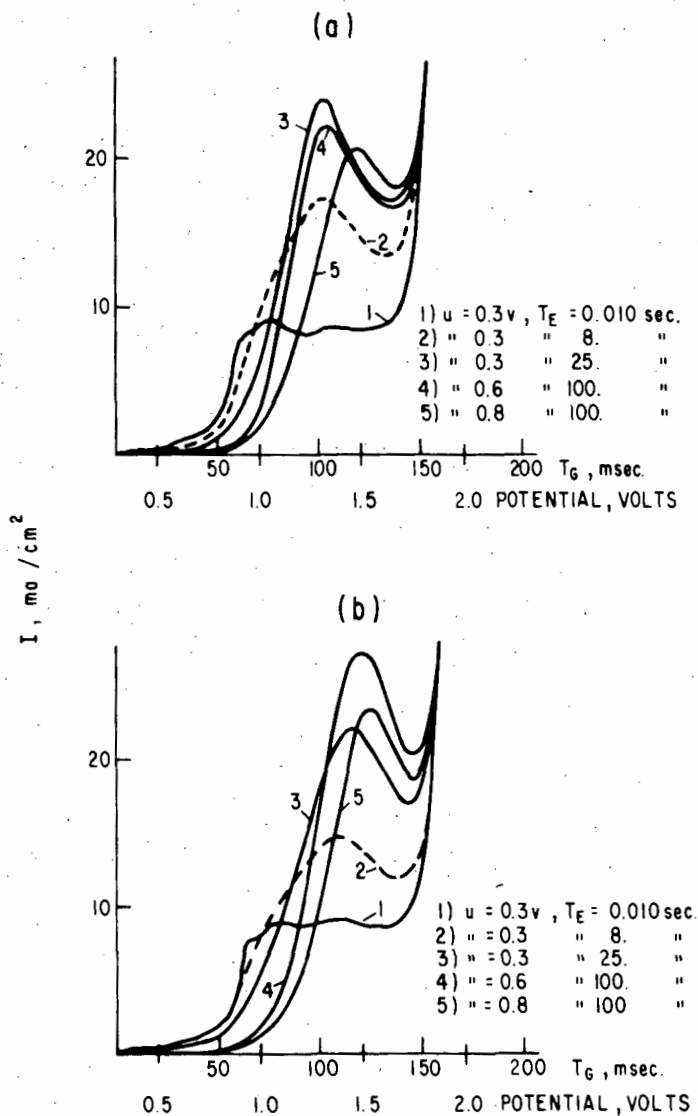


Figure 5. L.A.S. Traces Corresponding to the Adsorption of Ethylene and of Acetylene at Various Potentials (1 N HClO_4 , 30°C .). (a) p.p. of ethylene = 10^{-2} atmospheres, (b) p.p. of acetylene = 10^{-3} atmospheres. Traces measured using Sequence II, Table I, with $v = 10 \text{ v./sec.}$

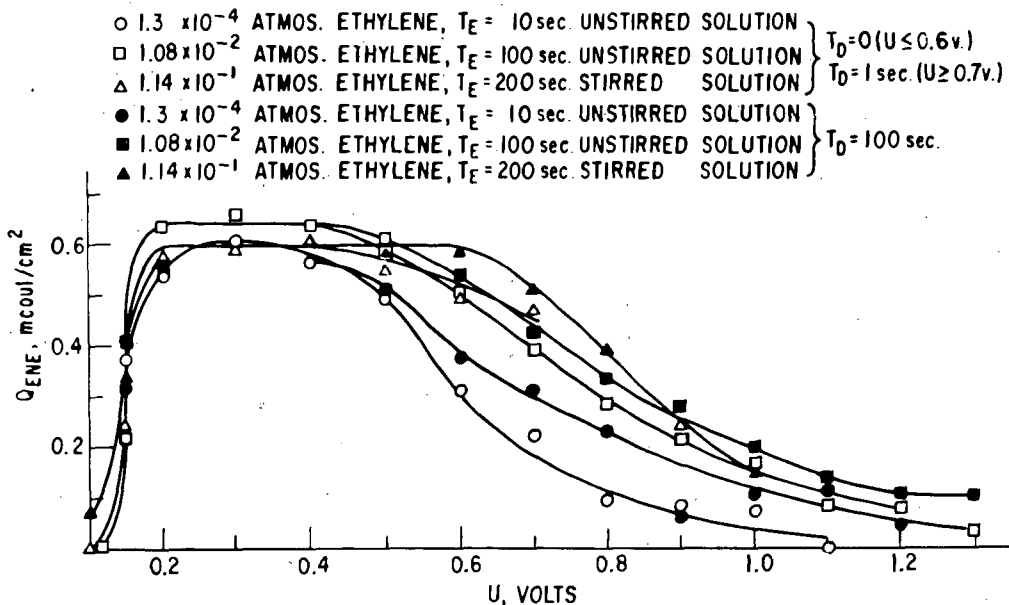


Fig. 6. -VARIATION OF SURFACE COVERAGE WITH ADSORBATE PARTIAL PRESSURE AND WITH POTENTIAL, FOR ETHYLENE (1 N HClO₄, 30°C). FRACTIONAL SURFACE COVERAGE MAY BE DERIVED BY NORMALIZING THE MAXIMUM CHARGE TO 1.

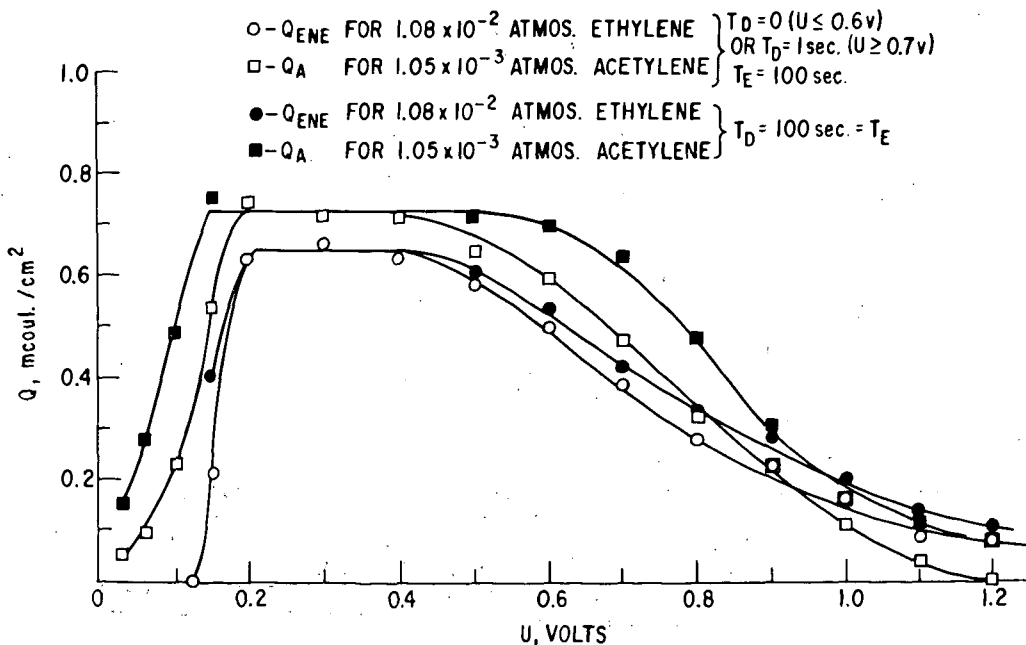


Fig. 7. -VARIATION OF SURFACE COVERAGE WITH POTENTIAL FOR ETHYLENE AND FOR ACETYLENE (1 N HClO₄, 30°C, ETHYLENE p. p. = 10^{-2} ATMOSPHERES, ACETYLENE p. p. = 10^{-3} ATMOSPHERES).

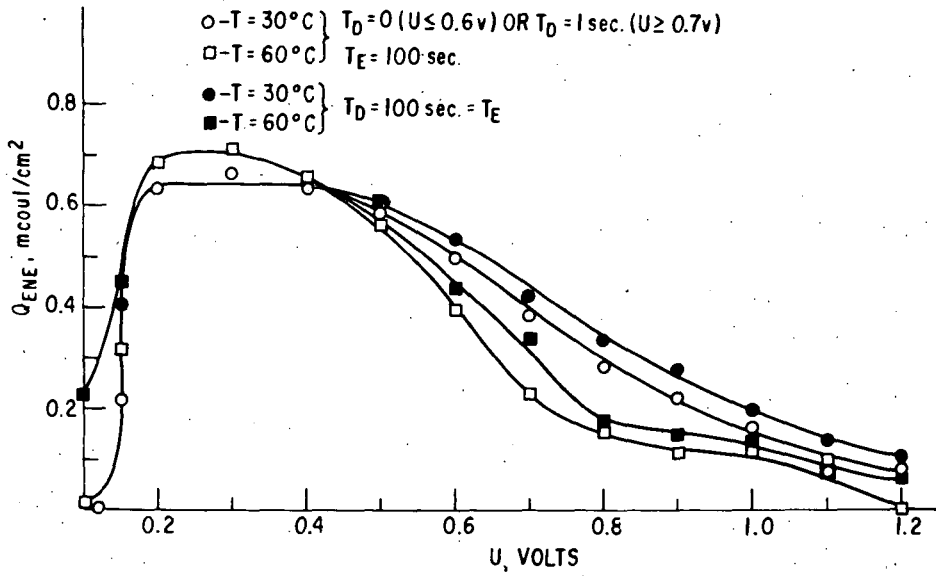


Fig. 8. -VARIATION OF SURFACE COVERAGE WITH POTENTIAL AND TEMPERATURE FOR ETHYLENE AND FOR ACETYLENE.

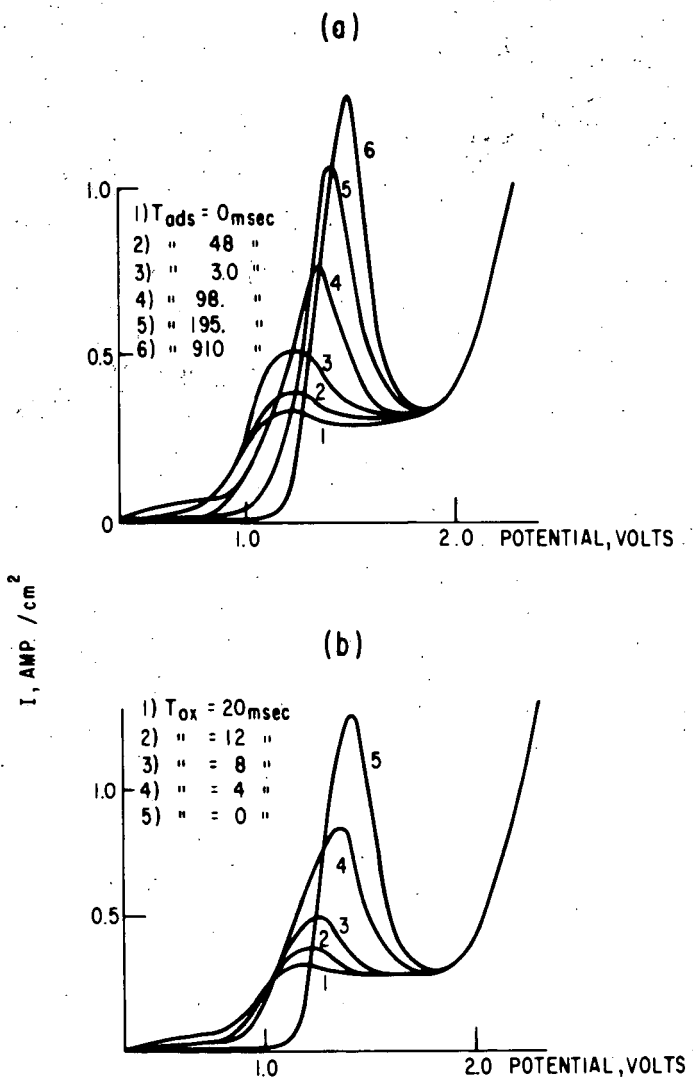


Figure 9. L.A.S. Traces for Adsorbed CO (1 N HClO₄, 30°C, CO p.p. = 10⁻² atmospheres, v = 360 v./sec.). (a) corresponds to the adsorption for time, T_{ads}; (b) corresponds to the oxidation for time T_{ox}, of a monolayer of CO.

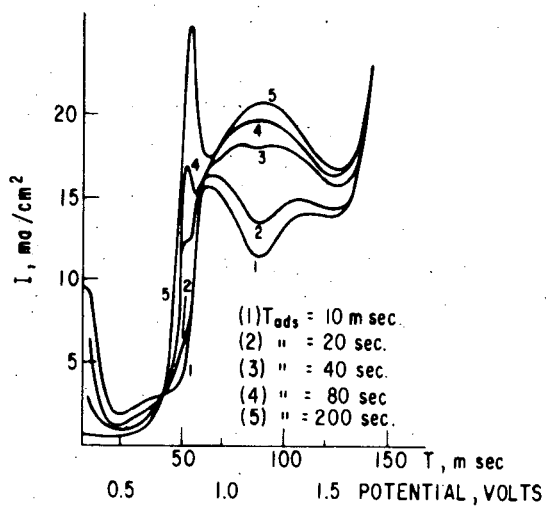


Figure 10. L.A.S. Traces Corresponding to the Adsorption of Ethane for Time, T_{ads} . (1 M $HClO_4$, $60^\circ C$, p.p. ethane = 1 atmosphere, $v = 10$ v./sec.).

MULTIPULSE POTENTIODYNAMIC STUDIES OF LOW MOLECULAR
WEIGHT HYDROCARBONS ON SEMIMICRO FUEL CELL ELECTRODES

L.W. Niedrach

General Electric Research Laboratory
Schenectady, New York

INTRODUCTION

Because of the limitations on the amount of information that can be obtained from polarization curves and material balances, it was felt desirable to study the behavior of hydrocarbon fuel cell anodes with multipulse potentiodynamic (MPP) techniques such as have been developed for microelectrodes(1,2). An additional purpose of the work was to compare observations upon fuel cell electrodes with similar observations with platinum wire microelectrodes. Such a comparison, which has been made in the case of ethane, has been described elsewhere(3).

In the course of fuel cell work it has been observed quite generally that the performances of all saturated hydrocarbons are similar although trends are evident as the molecular weight is changed. For this reason the three simplest hydrocarbons, methane, ethane, and propane, were used in this study as model compounds, and the more detailed work was confined to the first two fuels. A miniature version of a previously described(4) "conducting-porous-Teflon" fuel cell electrode (containing platinum black as the catalyst) was employed.

EXPERIMENTAL

A three-compartment, Teflon cell described elsewhere(3) was used in these experiments. The working electrode consisted of a 0.2 cm diameter Teflon-bonded, platinum black electrode(4). Both the hydrogen reference and the counter electrodes were platinized platinum flags. The former communicated with the working anode through a Luggin capillary. The cell was operated in an air thermostat, enabling control of temperature to within 0.1°C.

The 4.3 N perchloric acid electrolyte solution used for this work was prepared from reagent grade perchloric acid and quartz distilled water. Electrolytic grade hydrogen was used in the reference electrode chamber, and Phillips research grade hydrocarbons were used as the fuels. Tank argon, deoxygenated by passage over heated copper turnings, was used as the "fuel" for obtaining solvent blanks. Tank argon was also used for degassing the solution.

The electronic instrumentation and circuit have been described previously(1).

The potential-time sequence applied to the anode for adsorption studies at constant potential is shown in Fig. 1. The significance of the steps is covered below.

- A. Pretreatment step (15 sec) to remove oxidizable impurities and to produce a layer of "adsorbed oxygen" which serves to block fuel adsorption. The solution is vigorously stirred and purged with argon to remove molecular oxygen and oxidation products formed.

- B. Potential step, during which the oxygen layer formed in (A) is maintained, and the solution is purged for an additional 1 minute. The solution is then allowed to become quiescent for 1 minute.
- C. Reduction step (15 sec) during which the "adsorbed oxygen" layer is completely reduced within the allotted time. At this low potential (0.06 volt) the adsorption of the hydrocarbons is blocked. This step was included so that the reduction of the surface and the adsorption of the hydrocarbon would not occur simultaneously. However, omission of this step was found to have no detectable effect on the equilibrations, except for an initial current transient.
- D. Adsorption step, during which the hydrogen from (C) is rapidly oxidized, exposing a reproducibly clean surface for adsorption. The duration of this step is the adsorption time, T_D^* .
- E. Anodic sweep at 0.1 v/sec. The adsorbed fuel is oxidized and the surface covered with a layer of "adsorbed oxygen". Subtraction of the charge due to surface oxidation from the total charge yields the charge, Q_E , required to oxidize the surface species derived from the adsorbed fuel.
- E'. Alternative to (E), a cathodic sweep at 0.025 v/sec. which is used for determination of the "real" surface area of the electrode from the charge Q_{QH} corresponding to hydrogen deposition. In this case, argon is substituted for the hydrocarbon fuel.

When the sequence of Fig. 1 is terminated in Step (E') (linear cathodic sweep) a "hydrogen-deposition" trace may be obtained. From the charge, Q_{QH} , associated with this trace, the "real" area of the electrode may be derived(1). In the present work Q_{QH} was determined using a sweep rate of 0.025 v/sec. Over the useful range of $v = 0.01$ to 0.1 v./sec., Q_{QH} has been found reproducible to within 5% for this type of electrode(3). In calculating the "real" area of the electrode 0.21 mcoul/cm² was assumed to be the charge associated with one square centimeter(5).

For the determination of the charge, Q_E , associated with the oxidation of the adsorbed hydrocarbon species, the sequence of Fig. 1 terminating in step (E)(linear anodic sweep) was used. When argon is serving as the "fuel" the application of the pulse sequence to an electrode results in an "oxygen adsorption" trace. When a similar sequence is employed following an equilibration with a hydrocarbon fuel, a trace corresponding to oxidation of the fuel as well as the electrode surface is obtained. The closed area defined by the two traces may be used for the determination of Q_E (1). Actually the closed area corresponds to charge, $Q_{E'}$, which may include several terms:

$$Q_{E'} = Q_E + Q_{E''} + \Delta Q_{cap.} + \Delta Q_o \quad (1)$$

where Q_E = charge corresponding to oxidation of the hydrocarbon fuel adsorbed on the surface during step (D).

*The subscript here and for other time intervals refers to the step involved according to Fig. 1.

- $Q_{E''}$ = charge corresponding to fuel not adsorbed during step (D) but which oxidizes during step (E) with or without a preceding adsorption step.
- $\Delta Q_{cap.}$ = Difference in capacitive charges included under the "oxygen adsorption" and "fuel" traces due to differences in initial surface states.
- ΔQ_o = Difference in charges due to surface oxidation, included under "oxygen adsorption" and "fuel" traces.

It has previously been demonstrated, with ethane on smooth platinum, (2) that $Q_{E'} \approx Q_E$ if $v < 20$ v/sec. At higher values of v , $Q_{E'} < Q_E$, at least partially because some of the adsorbed fuel is retained on the surface during sweep (E). At the other end of the scale, it is important that the sweep speed not be so slow that appreciable re-adsorption of the fuel occur during step (E), and cause $Q_{E''} > 0$. For the present electrode the useful range of v was examined by adsorbing a fixed amount of ethane (corresponding to $\tau_D = 600$ sec) and measuring $Q_{E'}$ for a range of sweep speeds(3). The useful range was found to extend from approximately 0.1 to 0.4 v/sec., and in this range we assume $Q_E = Q_{E'}$. A sweep speed of $v = 0.1$ v/sec was used routinely in the present work.

Polarization curves were obtained in two ways. The first method involved application of Steps (A-D) of Fig. 1 before each measurement of current at a particular potential U . In the second method, steps (A-D) of Fig. 1 were applied only once, at the lowest values of U . The potential was then changed in increments and the current recorded for each potential after an apparent constant value was established. The two methods gave essentially identical results.

RESULTS

Traces obtained during linear anodic sweeps (l.a.s.) are shown in Fig. 2 for methane, ethane, and propane after equilibrations at 60°C at 0.3 and 0.4 volt. An argon blank is also included for comparison purposes. The ethane and propane show two types of oxidation waves. Wave 1 occurs at potentials below which (approx. 0.8 v) the electrode surface is itself oxidized. This first wave generally exhibits a well-defined peak. The second wave is more diffuse and extends all the way from approximately 0.8 volt to oxygen-evolution potentials. Methane differs markedly in that only wave 1 can be detected during oxidation of the ad-layer. Similar structures have been observed for the oxidation waves obtained for ethane adsorbed on platinum wire micro electrodes(2,6). These results imply a range of reactivities for a variety of ad-species on the electrode surface.

The adsorption of methane and ethane has been examined over a wider range of potentials than are shown in Fig. 2. In both cases a maximum value of Q_E occurs around 0.3 v. Below 0.1 volt, both adsorptions become negligible because of suppression by hydrogen on the surface. At potentials above 0.5 volt no ad-layer is observed for methane because of rapid oxidation following adsorption. Wave 1 for ethane becomes negligible at potentials above 0.6 volt and Wave 2 at potentials above 0.9 volt. The former wave, like that for methane, disappears because the ad-species associated with it are oxidized as rapidly as they appear on the surface. The latter wave disappears at the higher potentials because of rapid oxidation as well as

suppression of the adsorption rate.

Attempts to obtain similar data for ethylene with the Teflon-bonded electrodes have been unrewarding. Rates of adsorption are excessive for the low scan rates permissible with these electrodes, and re-adsorption prevents the accurate measurement of Q_E . With platinum wire microelectrodes, however, Gilman(6) has demonstrated that adsorbed ethylene and acetylene show only wave 2 at 60°C.

The effect of equilibration time on the l.a.s. traces for methane and ethane adsorbed at 0.3 volt is shown in Fig. 3. At 65°C, the single wave is evident for methane for equilibration times as long as one hour. In the case of ethane at 60°C, the ratio of the charges associated with wave 1 and wave 2 is not a sensitive function of the adsorption time. At 0.3 volt about 45% of the charge is associated with wave 1, and this value prevails up to a potential of 0.5 volt. At higher potentials the ratio declines rapidly.

At 0.3 volt, Q_E initially varies linearly with time but subsequently becomes linear with the logarithm of time for both methane and ethane. At 65°C the maximum (initial) adsorption rate for methane in terms of $\Delta Q_E/\Delta t$ is approximately 0.00015 mcoul/sec/cm² of "real" area. For ethane at 60°C, $\Delta Q_E/\Delta t$ is approximately 0.010 mcoul/sec/cm². At 25°C the rate for ethane is approximately one tenth that at 60°C. The rate for ethane at 25°C is too low for reliable measurement with the present system.

Because of the slow adsorption of methane, even at 65°C, an hour is required at 0.3 volt before "steady-state" coverage is approached. In the case of ethane, however, "steady-state" is essentially achieved within 10 minutes at 60°C. At higher potentials, e.g., 0.4 to 0.6 volt, methane also approaches steady-state within 10 minutes (but with lower surface coverages). At these potentials ethane reaches steady-state within a few minutes. More detailed treatment of the kinetics of these adsorptions are given elsewhere(3,7).

Figures 4 and 5 show the effect of temperature on the l.a.s. traces for methane and ethane. Because ten minute equilibrations were used in all cases, the traces do not all correspond to "steady-state" coverages, particularly at the lower temperatures. It is pertinent to note, however, that the wave for methane grows in very rapidly as the temperature is raised. Similarly, wave 1 for ethane becomes more pronounced at the higher temperatures - in this case at the expense of wave 2.

The nature of the species associated with l.a.s. waves 1 and 2 is of considerable interest. In view of past observations that the material associated with the first wave is resistant to removal by cathodic hydrogenation(6,8) and is probably partially oxygenated(8), several additional experiments were undertaken. To demonstrate that related, partially oxidized species do indeed oxidize further on the Teflon-bonded electrodes at 60°C over the same potential range as wave 1, the data in Fig. 6 were obtained. For this purpose, the electrode was equilibrated with CO (at 0.3 volt), CO₂ (at 0.06 and 0.2 volt) and argon saturated with formic acid vapor at 25°C (at 0.06 and 0.2 volt) prior to the l.a.s. It was further observed that the surface species from these equilibrations were not removed by cathodic hydrogenation.

To determine whether some of the species of wave 1 are removable by cathodic hydrogenation, and therefore probably unoxylated, additional cathodic hydrogenations were performed after equilibrations of the electrode with methane and ethane at several potentials. In these experiments sequence A-D of Fig. 1 was first followed. After adsorption for time, T_D , the potential was again stepped down to 0.06 volt for 2 to 5 minutes before application of the linear anodic sweep. The results of these experiments are summarized in Fig. 7 and Table I. It is clear that in each case a portion of the surface species was removed by this treatment. The amount removed decreased with increasing equilibration potential. In the case of the ethane all of wave 2 was removed by the hydrogenation treatment. The present results for ethane differ from those of Gilman(2) who performed similar hydrogenations with the wire micro-electrode after equilibrations at 0.4 volt. In that case no desorption of wave 1 species was observed after hydrogenation at 0.06 volt. The diffuse structure of the Teflon electrode as well as small differences in the catalytic behavior may account for the observed differences.

Table I

Effect of Cathodic Hydrogenation on Wave 1
($T_D = 5$ min; $T_{Hyd} = 5$ min)

	Methane 65°C		Ethane 60°C	
	0.3 volt	0.4 volt	0.3 volt	0.4 volt
Q_E^1 = initial; mcouls	4.0	2.8	10.1	8.0
Q_E^1 = after hydrogenation; mcouls	<u>2.5</u>	<u>2.3</u>	<u>3.8</u>	<u>5.5</u>
ΔQ_E^1 , mcouls	1.5	0.5	6.3	2.5
per cent removed	38	18	62	31

Another aspect of the problem that was given attention was the relationship between surface coverage and the polarization curves for methane and ethane. Such data for the two fuels, obtained at 65° and 60°C, respectively, are shown in Figs. 8 and 9. In these figures the abscissa is expressed in terms of the current density per cm² of "real" and "geometrical" area of the electrode. Therefore, the data may be related to the adsorption studies as well as performance curves for operating fuel cell devices.

The form of the polarization curves is typical of those for a variety of fuels when the data are obtained potentiostatically. Even hydrogen shows the minimum in the region from 0.9 to 1.4 volt on smooth platinum. Over the potential range from 0.3 to 0.45 volt, the curve for ethane has a linear Tafel region with a slope of 0.066 v/decade of current.

The surface coverages in these figures are expressed in terms of the charge per square centimeter of "real" area. The charge, Q_E^1 refers to that associated with wave 1, and in the case of ethane, Q_E refers to the total charge associated with the combined species of waves 1 and 2.

DISCUSSION

Among the present observations, those of most significance with regard to the performance of practical fuel cell anodes are the marked effects of temperature on the rates of adsorption and on the nature of the surface species as indicated by the l.a.s. traces. In the case of ethane, a ten-fold increase in the initial adsorption rate on a "clean" surface occurs in going from 25° to 60°C. A similar factor applies to the partially covered surface. The effect of temperature on the corresponding adsorption rate for methane appears to be even more pronounced although reliable data could not be obtained at 25°C. Such pronounced temperature coefficients for the adsorptions are reflected in the observed improvement in performance of hydrocarbon fuel cells with increasing temperature. In particular, they relate to the regions of "unstable" performance observed with saturated hydrocarbon fuel cells operating on resistive load.(9-11) Under these conditions, it will be recalled that at low current densities steady performance is obtained while at higher current densities the performance decays with time or, under certain conditions, oscillations set in(11,12). As a result of the increasing adsorption rates with increasing temperature, the region of instability occurs at continuously higher current densities as the operating temperature is increased.

When polarization curves are obtained potentiostatically, as in the present work, maximum currents are observed in place of the instability associated with resistive loads. It is of interest to compare the values of the maximum currents in Figs. 8 and 9 with those calculated from the observed adsorption rates on clean surfaces as measured at 0.3 volt.

In converting the adsorption rates to equivalent current densities, it must be recalled that the former are expressed in terms of the change in surface charge with time, $\Delta Q_E/\Delta t$. Allowance must therefore be made for any oxidation that occurred during the adsorption step itself; e.g., immediate oxidation of dissociated hydrogen. This may be done by multiplying $\Delta Q_E/\Delta t$ by the ratio of the charge associated with the hydrocarbon fuel molecule to that of the adsorbed species.

While the precise composition of the ad-layer has not been established for either methane or ethane, especially after short equilibrations, it is possible to calculate a range of limiting currents from the adsorption data at 0.3 volt. In the case of methane, depending upon whether the ad-layer is assumed to have an average composition approaching that of methyl radicals or that of a highly oxygenated species such as CO, the observed rate of adsorption would be equivalent to a steady state current density of from 0.15 to 0.6 microamps/cm² of "real" area. The observed value of 0.3 microamps/cm² is in good agreement in view of the evidence for a mixture of C₁ radicals and partially oxygenated species.

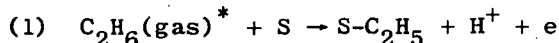
For ethane it is reasonable to bracket the composition of the ad-layer between one corresponding to C₂H₂ radicals and one corresponding to CO. This gives a range of current densities from 14 to 35 microamps/cm². In this case the observed maximum current of 2.5 microamps/cm² is much lower than the calculated value. This undoubtedly reflects the fact that at the potential of the maximum "steady-state" current some of the more refractory species are present on the surface and lower the adsorption rate relative to that on the "clean"

surface at 0.3 volt. The decline in the current density that occurs at higher potentials appears to reflect further reductions in adsorption rates as a result of such processes as "surface oxidation", anion adsorption, and stronger bonding of water to the surface. These processes would also contribute to the similar decline in methane performance at the higher potentials.

At low potentials, the effect of the adsorption rate on the polarization curve is minimal. Here it is clear that the overvoltage required for the further oxidation of surface intermediates to CO_2 is limiting. This is true, of course, under potentiostatic conditions as well as with the resistive loads of practical fuel cells.

With regard to specific mechanisms for the oxidation reactions, it would be premature to attempt to discuss them in any detail at this time. It is appropriate, however, to consider briefly some of the possible paths suggested by the available information. In particular, it is pertinent to speculate about the meaning of the two separate l.a.s. waves seen with ethane and propane, the single wave seen with methane, and the evidence for the partially oxidized surface species. In the discussion that follows, ethane will be used as the model with the expectation that higher molecular weight hydrocarbons will behave similarly. The behavior of methane, in turn will be somewhat simpler.

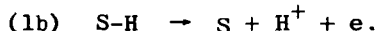
The initial step must certainly involve adsorption of the fuel on the electrode surface. On the basis of careful kinetic studies with ethane on wire microelectrodes, Gilman has concluded(6) that this primary adsorption step corresponds to the formation of an "ethyl radical" on the surface. This may be represented by



at potentials at which appreciable currents are drawn from the electrode. He points out that an equivalent route is given by

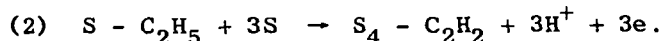


in which case the adsorbed hydrogen is rapidly consumed by the Volmer reaction:



At low potentials, of course, some of the hydrogen will remain adsorbed on the surface.

Gilman then reasons that the ethyl radical follows two paths. The first results in the formation of four surface bonds to the surface without rupture of the C-C linkage:

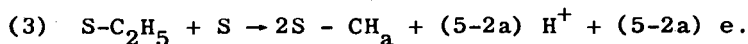


* More precisely, the gas will first dissolve in the electrolyte and be transported by diffusional processes to the electrode where it will adsorb from solution. While mass transport processes are not limiting in the work under discussion, it is obvious that they can become important under some conditions of operation. For practical fuel cell electrodes it is important that mass transport limitations be minimized.

This species is associated with wave 2 obtained with a l.a.s. and is identical with the single adsorbed species obtained when ethylene and acetylene are adsorbed(6). The present work is in accord with this interpretation, and cathodic hydrogenations of adsorbed ethane at 25°C have shown that the major material on the surface at that temperature corresponds to C₂ species, while those for propane correspond to C₃ species(8).

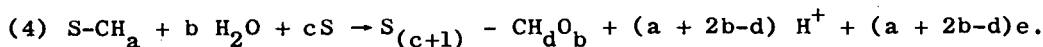
The second reaction path of the ethyl radical results in the formation of the material associated with wave 1, which Gilman also obtained for ethane on the platinum wire microelectrode. This wave he found, in contrast to wave 2, to be resistant to cathodic hydrogenation. He has also found that the species associated with wave 2 do not readily convert to those of wave 1.(6) In the absence of detailed kinetic data for the species associated with wave 1 Gilman did not speculate in detail on its identity.

The new data obtained with the Teflon-bonded electrodes are helpful in this area. The similarities between the single wave for methane and wave 1 for ethane strongly suggest that the second reaction path of the ethyl radical involves C-C bond fission as indicated in the following general equation:



This is in accord with the previous observation that C₁ species form during ethane (and propane) adsorption even at 25°C.(8) Grubb has also observed that on open circuit appreciable amounts of methane desorb from propane anodes in fuel cells operating at 65°C.(14) (The methylene radical with two carbon bonds to the surface may represent the principal species in parallel with the C₂H₂ of wave 2 which also has two surface bonds per carbon atom.)

The C₁ species in turn appear to react readily with water to form a partially oxygenated material which corresponds to the previously proposed "CO-like" species of Niedrach(8) and the "reduced CO₂" of Giner(15), and which Giner has also more recently found to be formed during the oxidation of hydrocarbons(16). The specific identity of the oxygenated species is as yet unknown and the reaction can therefore best be represented by:



That both the C₁ species and the partially oxygenated species are present on the surface and oxidize over the same potential range is indicated by the new hydrogenation experiments with methane and ethane. Since Eq. (3) represents a "cracking" reaction, and Eq. (4) a "re-forming" reaction, these observations suggest that it would be profitable to direct attention toward the study of the behavior of alternative catalysts in promoting such reactions.

With regard to the more refractory species of wave 2, which oxidize only at higher potentials, it is likely that an entirely different mechanism of oxidation prevails. This conclusion is based upon Gilman's observation that conversion to the species of wave 1 is slow(6). It is therefore likely that oxidative attack occurs before the C-C bonds are ruptured. This could result in the formation of alcohol-like species as intermediates. It should be emphasized, however, that such intermediates will undoubtedly be quite distinct from

those involved in the direct oxidation of alcohol-type fuels at moderate temperatures. The alcohol-like species derived from hydrocarbons would be strongly bound to the surface by multiple carbon-metal linkages, and hence complete oxidation to CO_2 would be assured. With alcohol fuels it is more likely that weaker bonds between the oxygen and the metal are involved. This is suggested by the incomplete oxidation to organic acids that is often observed with alcohols(17) at moderate temperatures. It is further supported by the behavior of alcohols towards deuterium exchange, where it is found that the hydroxylic hydrogen undergoes exchange most readily(18).

CONCLUSIONS

The behavior of saturated hydrocarbons on platinum catalyzed fuel cell anodes is strongly influenced by the rate of adsorption and the ability of the catalyst to promote "cracking" of C-C bonds as well as the reaction of C_1 radicals with water. Both the rate of adsorption and the catalytic activity of the platinum have pronounced positive temperature coefficients.

Species present on the electrode surface include C_1 radicals and partially oxygenated C_1 species in all cases. In the case of ethane and higher hydrocarbons multicarbon species are also present. These are strongly bound to the surface by multiple carbon-metal bonds and are relatively refractory.

After a primary adsorption step, at least two distinct reaction paths are followed by ethane and higher hydrocarbons. One path results in the formation of the relatively refractory species. The more desirable path results in "cracking" of the carbon chain to form the C_1 radicals and the partially oxygenated species.

Catalysts for hydrocarbon anodes should promote the cracking of higher molecular weight hydrocarbons to form C_1 radicals and also promote the reaction of these fragments with water.

In view of the many species present on the electrode surface and the changes in coverage and composition with temperature, potential, and time, much attention to analytic detail will be required before a definitive mechanism can be derived. All of these factors must be considered in valid interpretations of electrochemical performance data.

ACKNOWLEDGMENTS

The author is indebted to S. Gilman for many helpful discussions, and to I. Weinstock who provided some of the data.

This work is a part of the program under contracts DA-44-009-AMC-479(T) and DA-44-009-ENG-4909, ARPA Order No. 247 with the U.S. Army Engineer Research and Development Laboratories, Ft. Belvoir, Virginia, to develop a technology which will facilitate the design and fabrication of practical military fuel cell power plants for operation on ambient air and hydrocarbon fuels.

REFERENCES

1. S. Gilman, J. Phys. Chem., 67, 78 (1963).
2. S. Gilman, Electrochemical Society Washington Meeting, October 1964, Extended Abstracts of the Battery Division, p. 72;

Trans. Far. Soc., in press.

3. L.W. Niedrach, S. Gilman, and I. Weinstock, J. Electrochem. Soc., to be published.
4. L.W. Niedrach and H.R. Alford, J. Electrochem. Soc., 112, 117 (1965).
5. F.G. Will and C.A. Knorr, Z. Elektrochem., 64, 258 (1960).
6. S. Gilman, preprint, this meeting.
7. L.W. Niedrach, to be published.
8. L.W. Niedrach, J. Electrochem. Soc., 111, 1309 (1964).
9. W.T. Grubb, Proc. 16th Annual Power Sources Conference, Atlantic City, N.J., p.31 (1962).
10. L.W. Niedrach, J. Electrochem. Soc., 109, 1092 (1962).
11. M.J. Schlatter, in "Fuel Cell Systems" (R.F. Gould, ed.), p.292. Advances in Chemistry Series 47, American Chemical Soc., Washington, 1965.
12. H. Binder, et al., J. Electrochem. Soc., 112, 355 (1965).
13. S. Gilman, J. Phys. Chem., 67, 1898 (1963).
14. W.T. Grubb, J. Electrochem. Soc., 111, 1086 (1964).
15. J. Giner, Electrochimica Acta, 8, 857 (1963).
16. J. Giner, 15th Meeting CITCE, London and Cambridge, September 21-26, 1964, summaries of papers, p. xxix.
17. H. Binder, et al., in "Fuel Cell Systems" (R.F. Gould, ed.) p.283. Advances in Chemistry Series 47, American Chemical Soc., Washington, 1965.
18. G.C. Bond, 'Catalysis by Metals', Academic Press, New York, (1963) p.220.

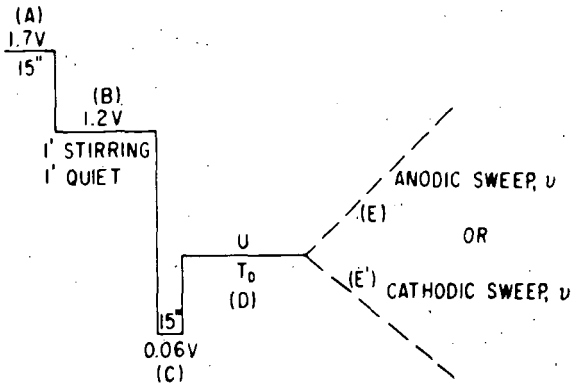


FIG. 1 POTENTIAL SEQUENCES APPLIED TO THE TEST ELECTRODE.

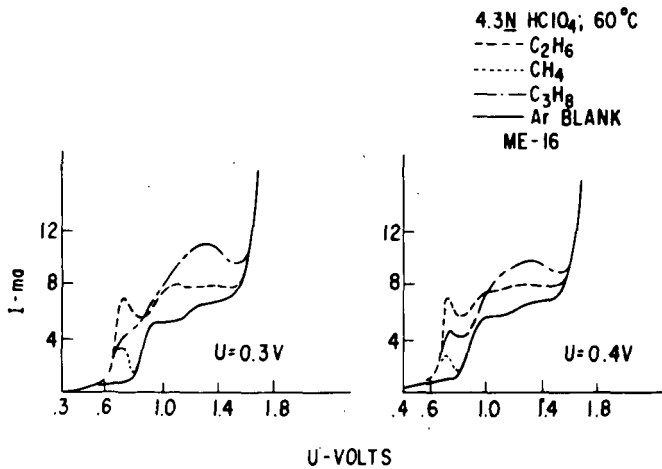


FIG. 2 CURRENT-POTENTIAL (TIME) TRACES FOR SEVERAL HYDROCARBON FUELS AFTER EQUILIBRATION AT DIFFERENT POTENTIALS.

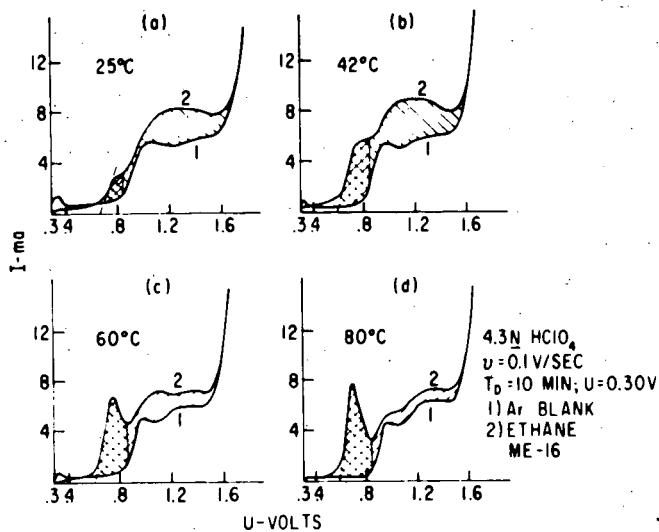


FIG. 5 CURRENT-POTENTIAL (TIME) TRACES FOR ETHANE ADSORBED AT SEVERAL TEMPERATURES.

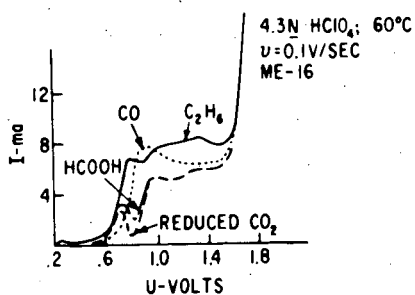


FIG. 6 CURRENT-POTENTIAL (TIME) TRACES FOR SEVERAL CARBONACEOUS MATERIALS ADSORBED ON PLATINUM.

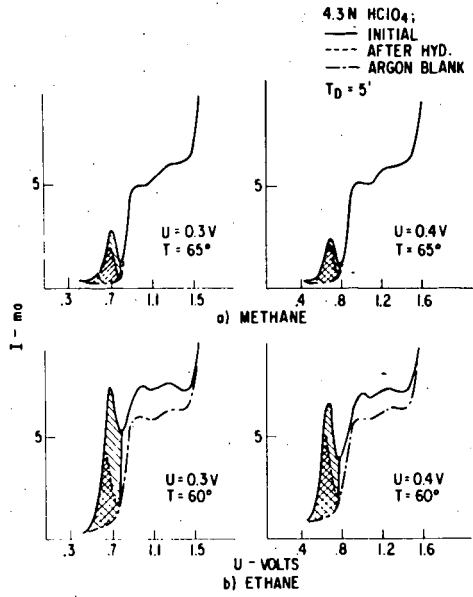


FIG. 7 EFFECT OF CATHODIC HYDROGENATION ON THE CURRENT-POTENTIAL (TIME) TRACES FOR ADSORBED METHANE AND ETHANE.

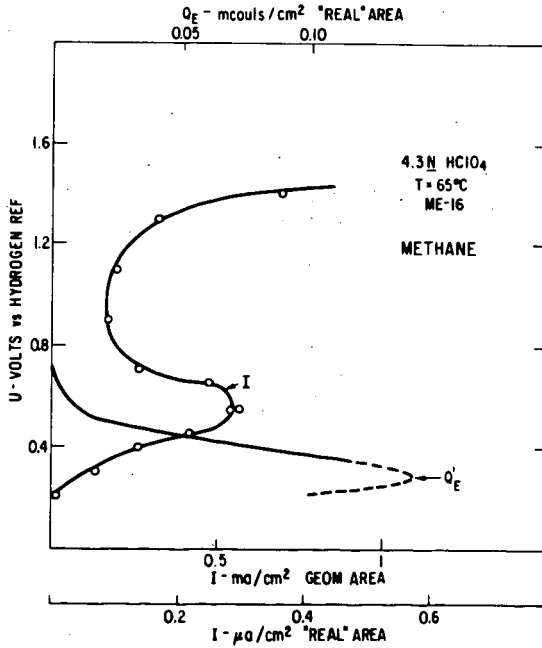


FIG. 8 POLARIZATION AND SURFACE COVERAGE CURVES FOR METHANE

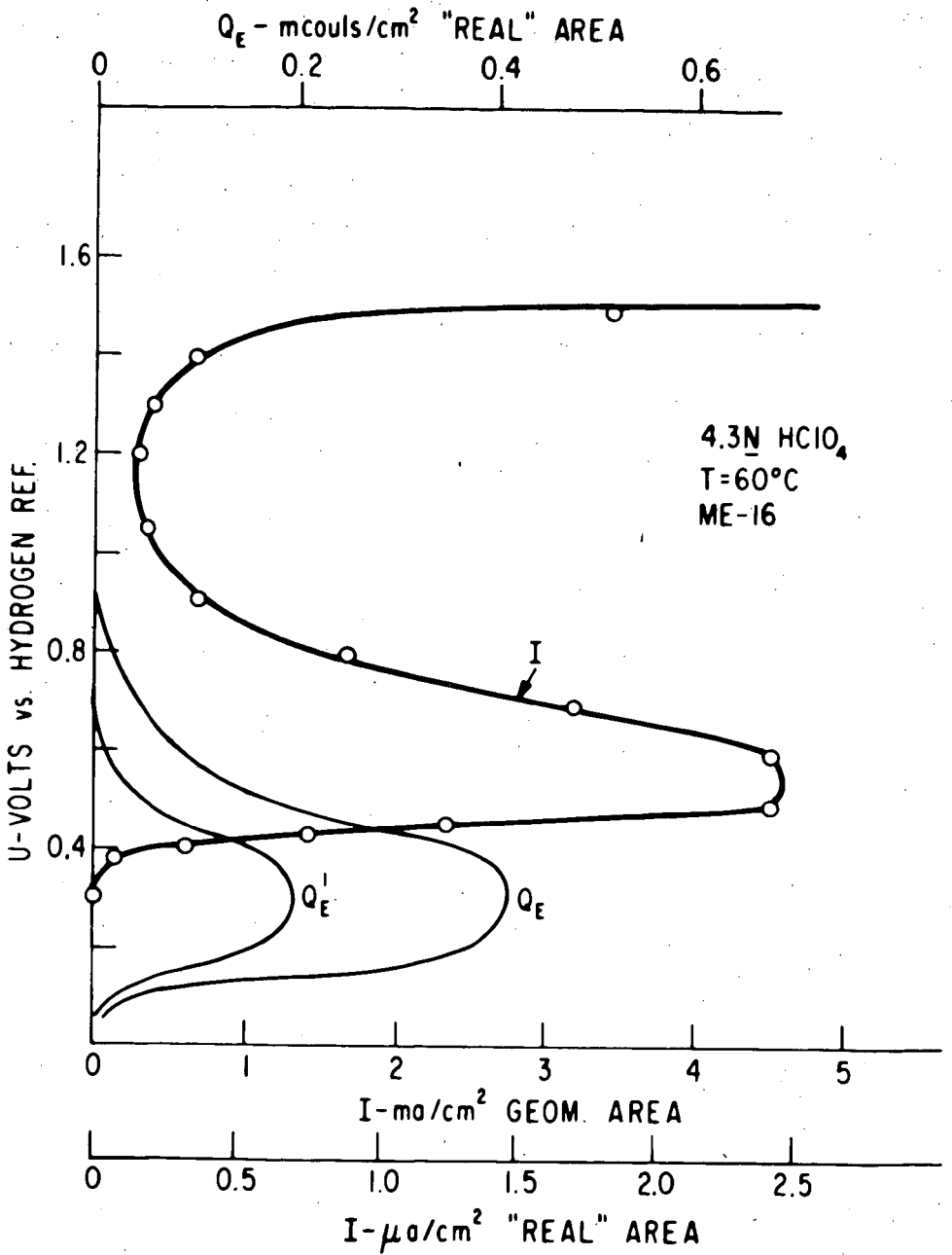


FIG. 9 POLARIZATION AND SURFACE COVERAGE CURVES FOR ETHANE.

STUDY OF HYDROCARBON OXIDATION BY EXPERIMENTAL
SEPARATION OF REACTION STEPS - 1. THEORETICAL
ANALYSIS AND ETHANE ADSORPTION ON PLATINUM.

M. BONNEMAY, G. BRONOEL, E. LEVART and A. A. PILLA - Laboratoire
d'Electrolyse, C.N.R.S., BELLEVUE - (S. & O.) -FRANCE.

INTRODUCTION

The study of electrochemical processes which involve two or more elementary reaction steps is at present of increased interest because of the development of fuel cells. The direct oxidation of hydrocarbons is a case in point since along with charge transfer, surface processes such as adsorption, desorption and possible conversion may take place. In addition to the above the effects of mass transfer may have to be taken into account. The analysis of such systems is difficult since most studies are undertaken with all of the processes occurring more or less simultaneously. Thus the surface reactions are all coupled with a diffusion step. Theoretical analysis is normally carried out under conditions either of semi-infinite linear diffusion or of known convection with all of the rate surface constants appearing as grouped constants in the resulting expressions. Separation of parameters is difficult and normally cannot be done without some degree of ambiguity. The work of Matsuda and Delahay¹ is an excellent example of the grouped parameter problem when relaxation techniques are employed. In addition the various mechanisms which have been proposed for the hydrogen evolution reaction and which all appear to provide at least partial explanations for this process are by now classic examples of parameter separation difficulties.

In order to study electrochemical reactions in which there is at least adsorption coupled with charge transfer such as the hydrogen evolution reaction, relaxation techniques have been extensively used. The main reason for their use is because they allow the quantity of hydrogen adsorbed at a given overvoltage to be evaluated. Charging curve²⁻¹², impedance measurements¹³⁻¹⁵ and the voltage sweep technique¹⁶⁻³⁰ have been employed. The determination of kinetic parameters using these methods is not, however, done without some degree of ambiguity, although the introduction of time as a variable normally renders the situation less complex since the number of simultaneous equations increases.

The fact, that the first step in the oxidation of gaseous reactants is normally one of adsorption allows the

possibility of separating this step from those succeeding it in time. This would allow independent analysis of the adsorption and possible conversion processes.

Such a technique necessarily involves time as a variable thus permitting a dynamic analysis of the reaction steps. It is thus a relaxation technique.

The direct electrochemical oxidation of hydrocarbons is receiving much attention at the present time³¹⁻⁴⁷. Probably the most important step in the oxidation and that most studied, is adsorption followed by possible conversion. Thus the aspect of catalysis in an electrochemical reaction is increasingly important. It is therefore of interest to be able to elucidate the process of adsorption so that the demand for new catalyst materials to be used in fuel cells may be, at least in part, met.

It is the purpose of this communication to describe a method whereby the reaction steps preceding charge transfer and desorption may be separated in time. A theoretical analysis of the method will be given and an example of its application will be made in a preliminary study of the adsorption of ethane and platinum.

THEORETICAL

In order to experimentally separate the reaction steps in the oxidation of a gaseous reactant it is necessary to allow the electrode to periodically be in the presence of gas then in the electrolyte. This may be carried out in the following way. The electrode under study is placed in a large circular insulated disc (making up only a small portion of this to avoid edge effects). The disc may then be rotated thus allowing the electrode to spend part of a rotation in the presence of the gaseous reactant and electrically insulated from the polarization circuit and the rest of the rotation immersed in the liquid where charge transfer and desorption may take place.

During the adsorption phase the electrode is covered with a thin film of liquid the thickness of which may be varied. There now exists a diffusion coupled adsorption process. Two methods by which this occurs may be envisaged. One is that in which the liquid film initially contains no gas so that this must first dissolve in the electrolyte then diffuse through the film with subsequent adsorption on the electrode surface. This case will be analyzed here. The second is to introduce on the electrode surface electrolyte previously saturated with the gas under study.

Adsorption then immediately starts with a diffusion layer gradually being created in the film. This case will be analyzed elsewhere.

The model used for the mathematical analysis given below is as follows. The film of electrolyte is of thickness δ such that finite linear diffusion is the sole mode of mass transfer. The dissolution of gas in the film occurs at $x = 0$ and is considered infinitely rapid, i.e. a concentration step function of time exists at the gas liquid interface.

The adsorption process occurs at $x = \delta$ following Langmuir kinetics which appears to hold for many adsorption processes in electrochemistry. The case in which Temkin kinetics prevail will be analyzed elsewhere. Thus the adsorption process is assumed to be given by:

$$\frac{d\Gamma(t)}{dt} = k_a (\Gamma_m - \Gamma(t)) C(\delta, t) - k_d \Gamma(t) \quad (1)$$

In order to take the diffusion process into account the Fick equation written for linear diffusion will be used.

$$\frac{\partial C(X, t)}{\partial t} = D \frac{\partial^2 C(X, t)}{\partial X^2} \quad (2)$$

This equation must be integrated using equation (1) from which the principal boundary conditions will be derived. The use of (1) as written prohibits the obtention of a closed form solution. This work is now in progress. Two cases which allow (1) to be simplified may be envisaged. If $\Gamma(t) \ll \Gamma_m$, then:

$$\frac{d\Gamma(t)}{dt} = k_a \Gamma_m C(\delta, t) - k_d \Gamma(t) \quad (3)$$

This simplification is probably fairly reasonable as far as hydrocarbons are concerned since their solubility in the aqueous solutions normally employed in fuel cells is small.

Further, the experimental technique, which is described in more detail below, allows measurements to be made at times sufficiently short so that this simplification may be fulfilled. If, in addition the adsorption process is sufficiently rapid, then:

$$k_a \Gamma_m C(\delta, t) = k_d \Gamma(t) \quad (4)$$

This, of course, is probably not true for hydrocarbon adsorption, but the case is of general interest and will be presented here.

a) Low coverage, rapid adsorption: The integration of (2) is carried out using the following initial and boundary conditions.

$$\begin{array}{ll} X = 0, t \geq 0 & C(0, t) = C_0 \\ X = \delta, t = 0 & C(\delta, t) = 0 \\ X = \delta, t > 0 & C(\delta, t) = \frac{D}{k} \Gamma(t) \end{array}$$

Since the surface concentration $\Gamma(t)$ is a function of the flux of the diffusing species at the electrode surface, then:

$$\Gamma(t) = D \int_0^t \frac{\partial C(\delta, t)}{\partial X} dt \quad (5)$$

The use of Laplace transformation leads to:

$$C(X, s) = \frac{C_0}{s} \left[\frac{\lambda \cosh \gamma(\delta - X) + \sinh \gamma(\delta - X)}{\lambda \cosh \gamma\delta + \sinh \gamma\delta} \right] \quad (6)$$

where $\gamma = s^{1/2}/D^{1/2}$ and $\lambda = D\gamma/Ks$.

This equation represents, in transformed state, the complete solution of equation (2) for these particular initial and boundary conditions. It can in principle be used in this form as was shown by Wynen^{4b} in a general study. Inverse transformation may be carried out by a method which has already been described elsewhere^{4a}. If, for a given film thickness observation is made at relatively short times, then:

$$\cosh \gamma(\delta - X) = \sinh \gamma(\delta - X) = 0.5 \exp \gamma(\delta - X) \quad (7)$$

and

$$\cosh \gamma\delta = \sinh \gamma\delta = 0.5 \exp \gamma\delta \quad (8)$$

Inverse transformation then gives:

$$C(X, t) = C_0 \operatorname{erfc} \left(\frac{X}{2D^{1/2}t^{1/2}} \right) \quad (9)$$

Equation (9) indicates that there is a certain time required before the adsorbant reaches the electrode surface since no adsorption parameter are present in the expression. The time constant for this process is approximately given by, $\tau = \delta^2/4D$. It is to be noted that this result is the same as would be obtained if the liquid film were of infinite thickness, thus attributing to the generality of the solution given by equation (6).

If for the same film thickness given above observation times are now longer, then, transforming (6) for $\Gamma(s)$:

$$\Gamma(s) = \frac{KC_0}{s} \left[\frac{\lambda}{\lambda \cosh \gamma\delta + \sinh \gamma\delta} \right] \quad (10)$$

and assuming that:

$$\sinh \gamma \delta = \gamma \delta + \frac{(\gamma \delta)^3}{6} \quad (11)$$

and

$$\cosh \gamma \delta = 1 + \frac{(\gamma \delta)^2}{2} \quad (12)$$

inverse transformation may be carried out giving:

$$\Gamma(t) = KC_0 \left[1 - \frac{6D}{\delta(6K+\delta)} \left(\frac{\delta^2 e^{-\frac{6Dt}{\delta^2}}}{6D} - \frac{\delta(3K+\delta) e^{-\frac{3Dt}{\delta(3K+\delta)}}}{6D} \right) \right] \quad (13)$$

Taking the first term of the series given in (11) and using (12) as is, one obtains:

$$\Gamma(t) = KC_0 \left(1 - \exp - \frac{2DT}{\delta^2 + 2K\delta} \right) \quad (14)$$

A still simpler expression may be obtained when the first term of both of the series given in (11) and (12) are used.

Thus:

$$\Gamma(t) = KC_0 \left(1 - \exp - \frac{DT}{K\delta} \right) \quad (15)$$

Equations (9) and (13) are the complete solutions for this particular diffusion adsorption process. They progressively characterize a pure diffusion then a diffusion - adsorption process. The transition between these two behaviors is particularly evident in equation (13) where it may be seen that the first exponential term contains only diffusion parameters, where as the second contains both diffusion and adsorption parameters. For relatively thinner and thinner films equation (6) is valid for only very short times, becoming effectively nonexistent for the thinnest films. Equation (13) may conveniently be replaced by (14) and then (15) for the thinner films indicating, as might be expected that the electrode surface becomes saturated with the adsorbing species more rapidly as the electrolyte film becomes smaller.

b) Low coverage, finite adsorption rate: This case is of greater interest here since it has been reported⁴⁷ that the rate of hydrocarbon adsorption is relatively slow. To integrate equation (2) the same initial and boundary conditions as those used previously will be assumed to be valid, except for the following:

$$X = \delta, t > 0 \quad C(\delta, t) = \frac{k_d}{K} \frac{d\Gamma(t)}{dt} + \frac{\Gamma(t)}{K}$$

In addition, equation (5) is also employed.

Laplace transformation results in an equation of the same form as that given in (6) where $\gamma = s^{1/2}/D^{1/2}$ and,

$$\lambda = \frac{(k_d + s)D\gamma}{k_d k_s}$$

Inverse transformation using the simplifications given in (7) and (8) results in equation (9), which is to be expected. Using the series expansions given in (11) and (12) the following equation results:

$$\Gamma(t) = KC_0 \left[1 - \frac{mn}{m-n} \left(\frac{e^{-mt}}{m} - \frac{e^{-nt}}{n} \right) \right] \quad (16)$$

where

$$m = \frac{6D^2 + 3D\delta^2 k_d + 6D\delta K k_d}{6D\delta^2 + K k_d \delta^3} - \frac{1}{2} \left[\left(\frac{6D^2 + 3D\delta^2 k_d + 6D\delta K k_d}{6D\delta^2 + K k_d \delta^3} \right)^2 - \frac{24D^2 k_d}{3D\delta^2 + K k_d \delta^3} \right]^{1/2}$$

Finally the series expansion used to obtain equation (15) gives:

$$\Gamma(t) = KC_0 \left[1 - \exp - \frac{Dk_d t}{D + k_d k \delta} \right] \quad (17)$$

It may be seen that essentially the same comments as those given earlier concerning the effect of the time of observation and the film thickness apply here. The main difference occurs of course in the time constant of the diffusion coupled adsorption process.

The analyses given above are of a very general nature and indicate that it may be possible to determine kinetic parameters specific to the adsorption process of any gaseous reactant. The experimental conditions may be chosen so that the simplest of the equations may be valid for most of the observation time, thus

facilitating the final calculations. In addition a theoretical study which will be presented elsewhere for the case in which the liquid film is initially saturated with gas shows that the equation valid for times during which equation (9) holds may be used in the calculation of $\Gamma(t)$ thus increasing the number of simultaneous equations.

EXPERIMENTAL TECHNIQUE

The exploitation of the equations given above necessitates an experimental determination of the amount of reactant adsorbed on the electrode after a given exposure time. This is most easily done by applying a potentiostatic pulse to the system once the electrode is immersed in the liquid. Integration of the resulting current-time curve allows $\Gamma(t)$ to be evaluated. Error due to double layer capacity current is greatly minimized because of the potentiostatic nature of the experiments.

The actual experimental cell will only briefly be described here. A detailed description will be given elsewhere. The electrode under study is placed in a non conducting disc, such as plexiglass or teflon, making up only a small portion of this so that the time between initial and complete immersion of the sample is negligible compared to the disc rotation speed. The level of the electrolyte in the cell may be varied so that many different exposure times may be obtained. Provision is made to vary the film thickness by means of a windshield wiper type arrangement. In addition it is possible to dry the electrode with a suitable hydrophilic material. A platinum counter electrode of large surface area is placed so that the working electrode is in a uniform potential field. Two auxiliary electrodes are placed in the cell such that any gas which enters the electrolyte is immediately oxidized, thus ensuring that the liquid film initially contains no gaseous reactant. A gold reference electrode found to be suitable for this work, is placed approximately 0.1 mm from the sample allowing potentiostatic conditions to be obtained rapidly. A saturated calomel electrode is also placed in the cell for standard comparison purposes.

The electronic circuit is shown in Fig. 1. The potentiostat P is a Tacussel PIT type having an amplifier rise time of about 30 nsec. In the work described below typical in circuit rise times are of the order of 700 nsec. The oscilloscope employed is a Tektronix type 555 having a dual beam and a dual time base. Plug in unit L is used to record the potential-time transient across the working electrode, W, and the reference electrode, S. Plug in unit D is used to record the current-time transient across resistance R. S₁ is a mechanical switch which operates as the electrode totally enters the solution. It serves to close the battery circuit which activates the mercury wetted Clare relay, S₂, thus allowing the pulse to be applied. It also triggers the oscilloscope slightly before the relay closes due to its approximately 2 m sec. reaction time. Proper synchronization of the two time bases allows pulses of the

type shown in Fig. 2 to be obtained. C is the counter electrode.

ETHANE ADSORPTION

To illustrate the method described above a preliminary study was made of the adsorption of ethane on a platinum electrode. Ethane was chosen since it is a relatively simple hydrocarbon and because it shows significant activity at low temperatures. In addition it has been studied by other workers³⁵⁻⁴⁷ thus allowing comparisons to be made.

The experiments were carried out using 5N phosphoric acid prepared from reagent grade acid and triply distilled water. The electrode was highly polished platinum of 0.5 cm² area. Ethane is obtained from "Société Air Liquide" and is of 99.99% purity. All measurements were made at 25^o ± 0.2^oC.

In order to ascertain that the quantity of current measured is actually that due to the adsorbed ethane pulses were applied to the system in an Argon atmosphere. The maximum pulse voltage always attained the same value as that employed for the ethane oxidation although the voltage difference was variable. This correction is rather important since there is a considerable amount of faradaic current even in the so-called double layer region indicating that the platinum electrode is certainly not inert. The difference between the current-time traces in argon and ethane may be seen in Fig. 3.

The (shaded area Fig. 3) charge, Q_E , corresponding to various ethane adsorption times is shown in Fig. 4. It may be seen that the adsorption times are relatively long, however, they follow to a good approximation an exponential curve. This would appear to indicate that the theory given above is obeyed. However, integration of equation (1) taking $C(\delta, t) = \text{const.}$ would also lead to exponential time behavior. In order to decide between pure adsorption control; or coupled diffusion-adsorption control experiments were carried out in which the film thickness was varied. In every case and even for the longest adsorption times Q_E depended upon the film thickness. It thus appears that the adsorption of ethane is partly diffusion controlled even when relatively thin films are present. It is to be noted that this does not indicate that there would be a limiting diffusion controlled current for all overpotentials in steady state fuel cell operation. It does, however, indicate that diffusion contributes to some extent to the total observed polarization and that higher hydrocarbon solubility would greatly increase performance.

It has been shown⁵⁰ that knowledge of the evolution of open circuit potential with adsorption time can provide information concerning adsorption especially if surface conversion exists. The experiments performed here give this data. Analysis of the potential-time curves for different exposure times indicates that the observed voltage difference is a direct measure of the equilibrium potential since the voltage base line varies with adsorption time and, because of the set up of the electric circuit, can only be due to different equilibrium potentials. A typical curve is shown in Fig. 5. It may be seen that there appears to be a slight arrest in the curve after approximately 10 min. exposure time. This function is a measure of

the extent of electrode surface coverage and indicates that there are probably two surface species one corresponding to low coverages and the other to high coverages. They are very probably related to the two peaks observed in the voltage sweep experiments used in similar studies and reported by Gilman⁴⁷.

In order to examine the behavior of these surface species and to obtain some indication of the processes which follow adsorption it is then necessary to examine the current-time curve obtained after application of the potential step function.

The first observation is that it appears fairly evident that the charge transfer and desorption processes take place much more rapidly than the adsorption and conversion processes. These latter then comprise the global rate limiting steps in the oxidation of ethane at these temperatures and indicate the importance of catalysis in this process.

Exploitation of the current-time curves may be carried out in the following way. If the current is due to the concentration of surface species then this should be an exponential function of time, thus:

$$i = A \exp - \beta t \quad (18)$$

where A contains electrochemical and proportionality constants and β represents the time constant for the charge transfer and desorption process. Semi logarithmic plots of the current time curves obtained in the presence of ethane show good linearity after the first 100 μ sec. No such linearity occurs for the curves obtained in an Argon atmosphere. These results indicate that diffusion control is nonexistent.

Examination of equation (18) shows that the intercept of the semi logarithmic plot should result in consistent values for the same surface species (taking into account surface concentration and overpotential).

Two sets of values were obtained corresponding to low and high coverages (See Fig. 5) indicating the presence of two surface species.

The study presented above is a preliminary one serving to give some indication of the potentialities of the method described in this work. It may be seen that a large variety of data may be obtained and that it is indeed possible to separate the two global processes occurring in the electrochemical oxidation of hydrocarbons. The results obtained are less ambiguous and it is hoped that future work will elucidate the phenomenon of catalysis in electrochemical processes.

ACKNOWLEDGEMENTS

The authors wish to thank O. Dupré La Tour for her verification of the algebra involved in this work. They also wish to thank E. Picq and G. Peslerbe for their considerable aid in the experimental work.

LIST OF SYMBOLS

- $\Gamma(t)$ = Surface concentration of adsorbing species at time t .
- Γ_m = Maximum surface concentration of adsorbing species.
- k_a = Adsorption rate constant.
- k_d = Desorption rate constant.
- $C(\delta, t)$ = Concentration of adsorbing species at electrolyte-solid interface.
- $C(X, t)$ = Concentration of adsorbing species at a point X within the liquid film.
- D = Diffusion coefficient of adsorbant.
- δ = Liquid film thickness and coordinate of electrolyte solid interface.
- X = Point within liquid film.
- K = $k_a \Gamma_m / k_d$.
- s = Laplace transform parameter.
- $C(X, s)$ = Concentration of adsorbing species after Laplace transformation at a point X within the liquid film.
- erfc = Error function.
- erfc = $1 - \text{erf}$.
- $\Gamma(s)$ = Surface concentration of adsorbant after Laplace transformation.
- C_0 = Initial gas concentration.
- Q_E = Charge corresponding to ethane surface concentration.

REFERENCES

1. Matsuda, H. and Delahay, P., Coll. Czechoslov. Chem. Commun. 25, 2977 (1960).
2. Slygin, A. and Frumkin, A., Acta Physicochim. URSS. 3, 791 (1935); 2, 819 (1936).
3. Ershler, B., Acta Physicochim. URSS. 7, 327 (1937).
4. Obrucheveva, O. and Burinsein, F., Doklady Akad. Nauk. SSSR. 63, 403 (1948).
5. Breiter, M., Knorr, C. A. and Völkl, W., Z. Elektrochem. 59, 681 (1955).
6. Giner, J., Z. Elektrochem. 63, 386 (1959).
7. Tyurin, Yu., Doklady Akad. Nauk. SSSR 126, 827 (1959).
8. Presbrey, C. H., Jr. and Schuldiner, S., J. Electrochem. Soc. 108, 985 (1961).
9. Bowden, F. P., Proc. Roy. Soc. 125A, 604 (1929).
10. Butler, J. A. V. and Armstrong, G., Ibid. 137A, 604 (1932).
11. Hickling, A., Trans. faraday. Soc. 41, 333 (1945).
12. Pearson, J. D. and Butler, J. A. V., Ibid. 34, 1163 (1938).
13. Eucken, A. and Weblus, B., Z. Elektrochem. 55, 114 (1957).
14. Breiter, M., Kammermaier, H. and Knorr, C. A., Z. Elektrochem. 60, 37 (1956); 60, 119 (1956).
15. Dolin, P. and Ershler, B., Acta Physicochem. URSS. 8, 747 (1940).
16. Will, F. and Knorr, C. A., Z. Elektrochem. 64, 258 (1960); 64, 270 (1960).
17. Franklin, T. C. and Cooke, S. L., Jr., J. Electrochem. Soc. 107, 556 (1960).
18. Kozawa, A., J. Electroanal. Chem. 8, 20 (1964).
19. Breiter, M., Electrochimica Acta. 5, 145 (1961).
20. Breiter, M., J. Electrochem. Soc. 109, 622 (1962).
21. Aston, J. G., J. Phys. Chem., 67, 2042 (1963).
22. Breiter, M., Electrochimica Acta, 8, 447 (1963).
23. Gilman, S., J. Electroanal. Chem. 7, 382 (1964).
24. Gilman, S., Nature, 203, 1130 (1964).

25. Breiter, M., *Electrochimica Acta*, 7, 25 (1962).
26. Magy, F., Horanyi, G. Y. and Vertes, G. Y., *Acta Chimica*. 34, 35 (1962).
27. Gilman, S., *J. Phys. Chem.* 67, 78 (1963).
28. Breiter, M., *Electrochem. Acta* 7, 601 (1962).
29. Breiter, M., *J. Phys. Chem.* 68, 2249 (1964).
30. Gilman, S., *J. Electroanal. Chem.* 7, 382 (1964).
31. Gilman, S., *J. Phys. Chem.* 67, 78 (1963).
32. Gilman, S. and Breiter, M. W., *J. Electrochem. Soc.* 109, 1099 (1962).
33. Grubb, W. T., *Nature* 198, 883 (1963).
34. Gilman, S., *J. Phys. Chem.* 68, 70 (1964).
35. Niedrach, L. W., *J. Electrochem. Soc.* 111, 1309 (1964).
36. Gilman, S., *J. Phys. Chem.* 67, 1898 (1963).
37. Murray, J. N. and Grimes, P. G., Private communication.
38. Jasinski, R., Huff, J., Tomter, S. and Swette, L., private communication.
39. Grubb, W. T. and Michalske, C. J., *Nature* 201, 287 (1964).
40. Grubb, W. T., *Ibid.* 201, 699 (1964).
41. Grubb, W. T. and Michalske, C. T., 18th Annual Proceeding Power Sources, Conference (1964).
42. Grubb, W. T., *J. Electrochem. Soc.* 111, 1086 (1964).
43. Wroblowa, H., Piersma, B. J. and Bockris, J. O'M., *J. Electroanal. Chem.* 6, 401 (1963).
44. Green, M., Weber, J. and Drazic, V., *J. Electrochem. Soc.* 111, 721 (1964).
45. Johnson, J. W., Wroblowa, H. and Bockris, J. O'M., *J. Electrochem. Soc.* 111, 863 (1964).
46. Giner, J., *Electrochimica Acta* 9, 63 (1964).
47. Gilman, S., G. E. Research Lab. rept. No. 65-RL-3870 C (1965).
48. Wijnen, M. D., *Rec. Trav. Chim.* 79, 1203 (1960).
49. Bonnemay, M., Bronoel, G., Levart, E., Pilla, A. A. and Poirier, E., *d'Ange d'Orsay, C. R. Acad. Sci. Fr.* 258, 4256 (1964).
50. Bonnemay, M. and Kagan, H. *Electrochimica Acta*. 9, 337 (1964).

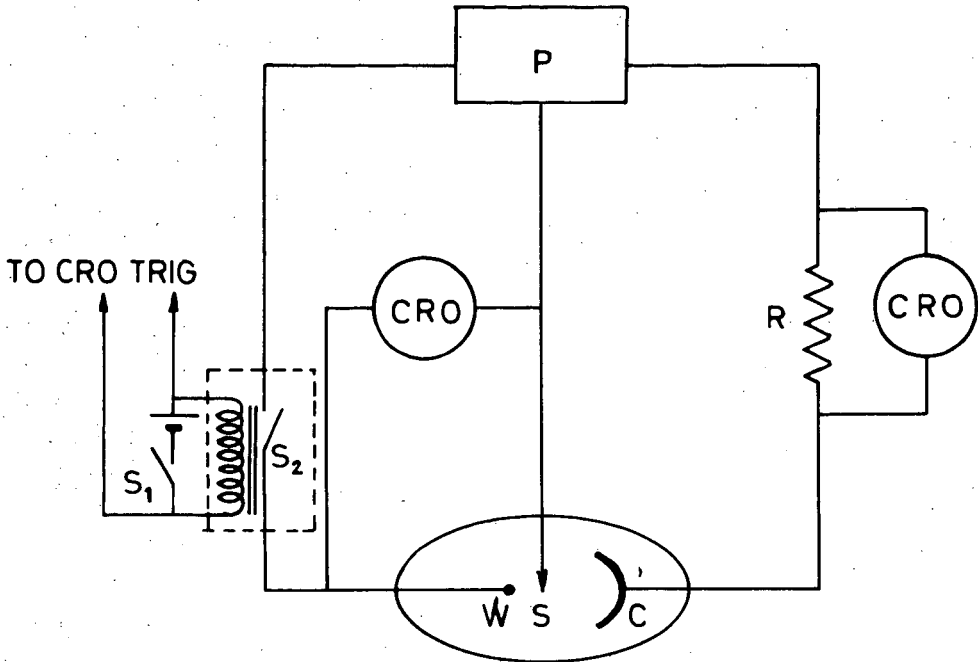


Fig. 1 - Electronic circuit for application of potential-time step functions.

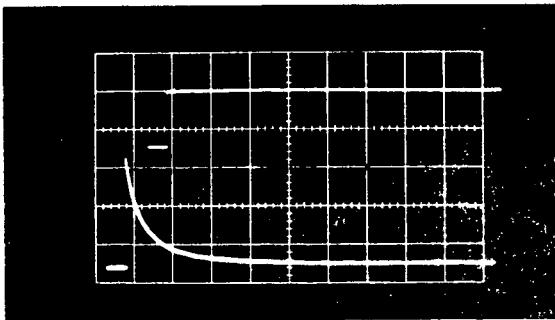


Fig. 2 - Upper curve : potential-time trace.
Lower curve : current time trace. Horizontal axis 1 m sec/cm, vertical axis 50 mV/cm.

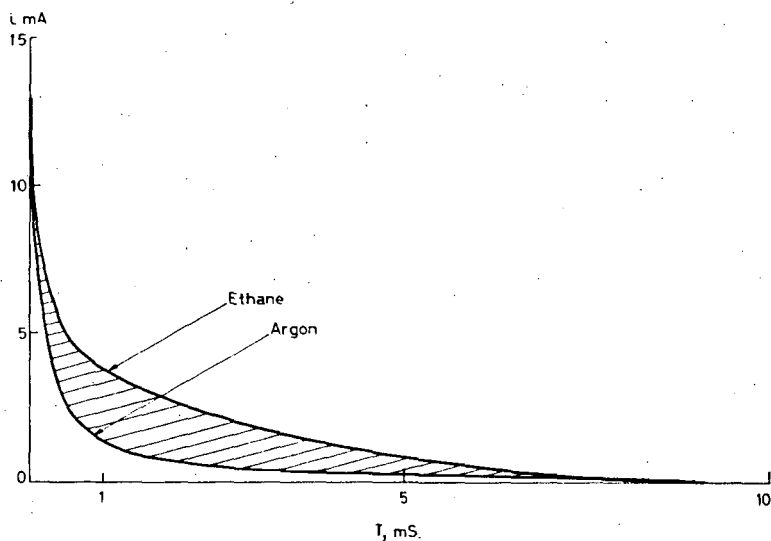


Fig. 3 - Current-time traces for Argon and ethane. Shaded area represents Q_E .

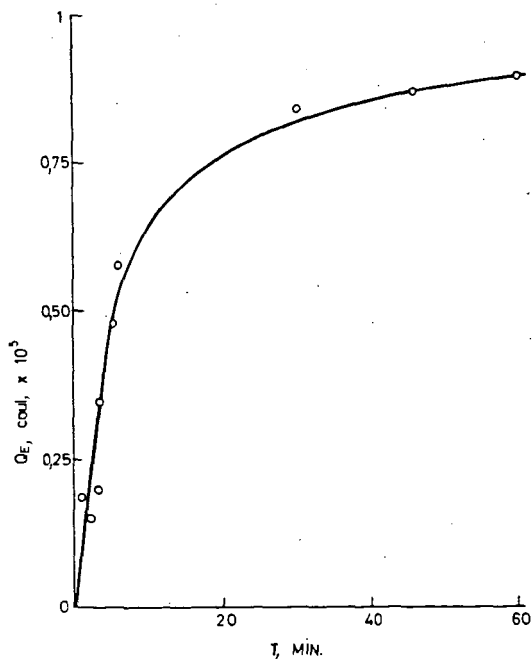


Fig. 4 - Variation of ethane surface coverage with time in adsorption phase.

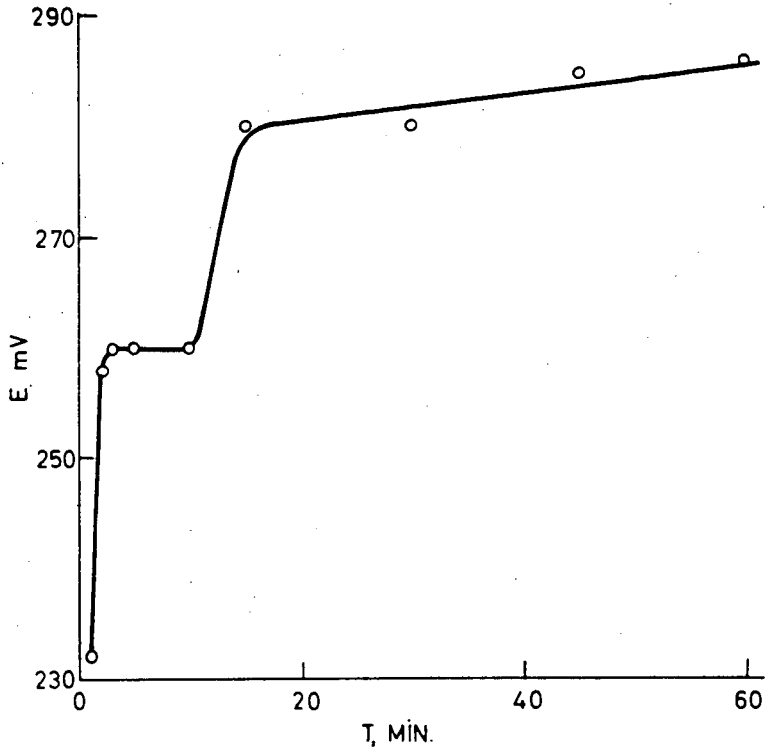


Fig. 5 - Variation of equilibrium potential with coverage.

ELECTROCATALYSIS AND HYDROCARBON OXIDATION

A. T. Kuhn, H. Wroblowa and J. O'M. Bockris

Electrochemistry Laboratory
University of Pennsylvania
Philadelphia, Pennsylvania 19104

EXTENDED ABSTRACT

An attempt is made to correlate the catalytic activities and physical properties of noble metal electrocatalysts, using ethylene oxidation at 80°C, in 1 N sulfuric acid as a test reaction. Relative catalytic activities are measured by a comparison of current values at an arbitrarily chosen potential.

A correlation was found between catalytic activity and both Latent Heat of Sublimation of the metal (L_s), which according to Pauling's formula reflects the adsorbate-adsorbent bond strength, and also the number of unpaired "d" electrons in the metal. Both of these parameters gave a "volcano" type relationship, when plotted against reaction rate.* (Figs. 1 and 2)

In both cases, Pt lay at the peak of the curve. Values of L_s for alloys were computed by assuming additivity of the L_s values of the components. Values of n_d , the number of unpaired "d" electrons, were obtained by using the values obtained for the first Period of Transition metals, and again assuming additivity in the case of the alloys.

In order to interpret the above relationships, the diagnostic criteria for mechanism determination were examined, and information on adsorption of ethylene was obtained elsewhere.¹ The results are shown in Table 1, A and B.

Oxygen coverage on the noble metals has been shown² to be proportional to the number of unpaired "d" electrons, and similar behaviour might be expected for ethylene. Thus on Gold, ethylene is known to be very slightly adsorbed¹, while on Platinum, the saturation coverage is that amount that might be predicted on the basis of 0.55 "d" electrons per Pt atom³. The apparent weak adsorption of ethylene on Rhodium, appears to result from competitive adsorption with oxygen, which is known to adsorb more strongly on this metal than on Pt⁴. The presence of less than 10% oxygen coverage is known to inhibit adsorption of organic species⁵.

* The almost identical behaviour of Au and Pd (see Table I A) suggest that under the conditions of the experiment, hydrogen or hydrogen containing species are absorbed in the Pd, thus filling the "d" band vacancies.

Table I A

Metal	Tafel Slope (mv)	i_{600}	$\frac{d \log i}{dP_{eth}}$	$\frac{d \log i}{dP_H}$	Reaction Products
Platinum	140	5×10^{-6}	-0.2	0	CO ₂
Palladium	190	2×10^{-7}	+0.5	0*	50% CO ₂ balance aldehydic
Rhodium	160	1×10^{-7}	+0.5	0	CO ₂
Iridium	160	3×10^{-7}	+0.5	0	CO ₂
Gold	200	2×10^{-7}	+0.5	0*	As Pd
Osmium	--	$< 1 \times 10^{-8}$	+ ?	--	--
Ruthenium	165	1×10^{-7}	+ ?	--	--
Silver	--	5×10^{-8}	+ ?	--	--
Mercury	--	$< 1 \times 10^{-8}$	+ ?	--	--

i_{600} denotes current at 0.6 volts vs R.H.E.

0* denotes that pH effect was zero in the range pH = 0 to 4.0. The reaction did not appear to proceed in alkaline solutions

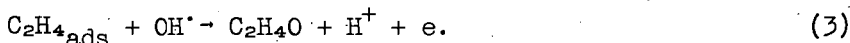
-- denotes parameter not measured due to experimental difficulties

+ ? denotes positive pressure effect of unknown magnitude

Table I B

Alloy	Tafel Slope	i_{600}	$d.i/d.P_{eth}$
Pd-Au 20-80 At% 46-54 At% 78-22 At%	2RT/F	6×10^{-7} 3×10^{-7} 4×10^{-7}	+ve \sqrt{p}
Rh-Pd 25-75 At% 50-50 At% 75-25 At%	2RT/F	7.0×10^{-7} 1.5×10^{-6} 3.0×10^{-6}	+ve
Cu-Rh 10-90 At%	2RT/F	4.0×10^{-6}	+ve \sqrt{p}
Cu-Au 25-75 At%	—	1×10^{-7}	—
Pt-Ru 80-20 At% 50-50 At%	2RT/F	8×10^{-7} 5×10^{-7}	+ve
Pt-Ni 85-15 At%	2RT/F	4.0×10^{-7}	—

In the case of Platinum, previously described by⁷, the following mechanism was suggested,



where step (2) was rate determining. This mechanism is obviously not applicable to other metals, where a positive fractional order of reaction with respect to ethylene indicates that an adsorbed organic species is involved in the rate determining step. In order to interpret the observed empirical rate equation:

$$i = k e^{\frac{FV}{RT}} p^{1/n} c_{\text{H}^+}^{-0.5} \quad (1)$$

Two mechanisms are proposed.

I. Radical Attack

In this mechanism, the sequence suggested above still applies, except that step (3) is now rate determining. Such a mechanism would give rise to an equation such as the above if coverage with OH[·] or O[·] were to change linearly with potential, as is often the case. The change of rate control from step (3) in the case of Au to step (2) for Pt and back to (3) for Rh, and the various factors controlling it, are considered in Table II.

TABLE II

Parametric Change	Forward Rate of (2)	Forward Rate of (3)
Increase in θ_{OH}	decreases	increases
Increase in θ_{eth}	decreases	increases
Metal-OH bond strength	increases	rises to max, then decreases.
Metal-ethylene bond strength	—	rises to max, then decreases.

Thus an optimum value exists, lying between the extremes of weak adsorption (not true chemisorption) and strong adsorption (immobile species, metal-adsorbate bond hard to break). The rate of step (3) will be highest on catalysts with high coverages of both adsorbed species, and intermediate values of bond strengths. It seems that Pt fulfills these conditions, having however a relatively slow rate for step (2) owing to the high coverage of ethylene.

This accounts for step (2) being rate determining. On gold, very low coverages and low bond strengths of adsorbed radicals result in step (3) proceeding slowly. The same is true on Rhodium, again because of very low ethylene coverage but also because of the much higher Metal-Oxygen bond strength. In both cases, step (3) becomes rate determining. The weakness of the Metal-Organic chemi-bond in the case of gold, is the probable reason for desorption of intermediates such as aldehydes, as opposed to the complete oxidation to CO₂ observed on other metals.

II. Electron Transfer from Organic Species

In this second possible mechanism, which has already been proposed for many oxygen containing organic species (6), the sequence is:



Such a mechanism is possible whenever zero or positive pressure effects with respect to concentration of organic species are observed.

An attempt to distinguish between mechanisms I and II is presently under way, involving H/D isotope effects.

References

1. B. Rubin, E. Gileadi and J. O'M. Bockris, To be Published.
2. M. L. Rao, A. Damjanovic and J. O'M. Bockris, J. Phys. Chem. 67, 2508 (1963).
3. E. Gileadi, B. Rubin and J. O'M. Bockris, J. Phys. Chem. In Press.
4. H. Dahms and J. O'M. Bockris, J. Electrochem. Soc. 111, 728 (1964).
5. M. Breiter and S. Gilman, J. Electrochem. Soc. 109, 1099 (1962).
6. V. S. Bagotskii and Yu. B. Vasilyev, Electrochimica Acta 9, 869 (1964).
7. H. Wroblowa, B. J. Piersma and J. O'M. Bockris, J. Electroanal. Chem. 6, 401 (1963).

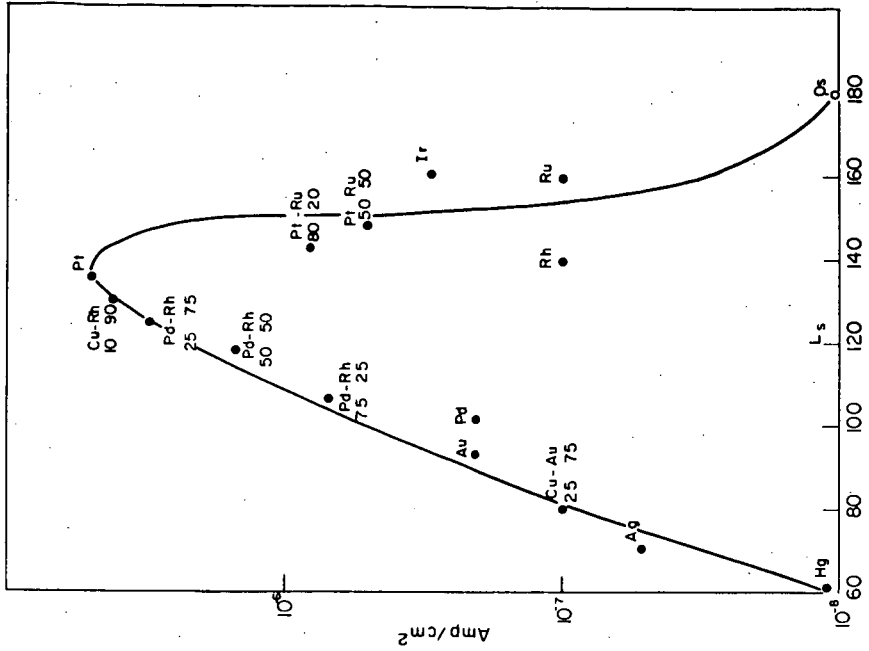


Fig. 2.-EFFECT OF LATENT HEAT OF SUBLIMATION ON CATALYTIC ACTIVITY

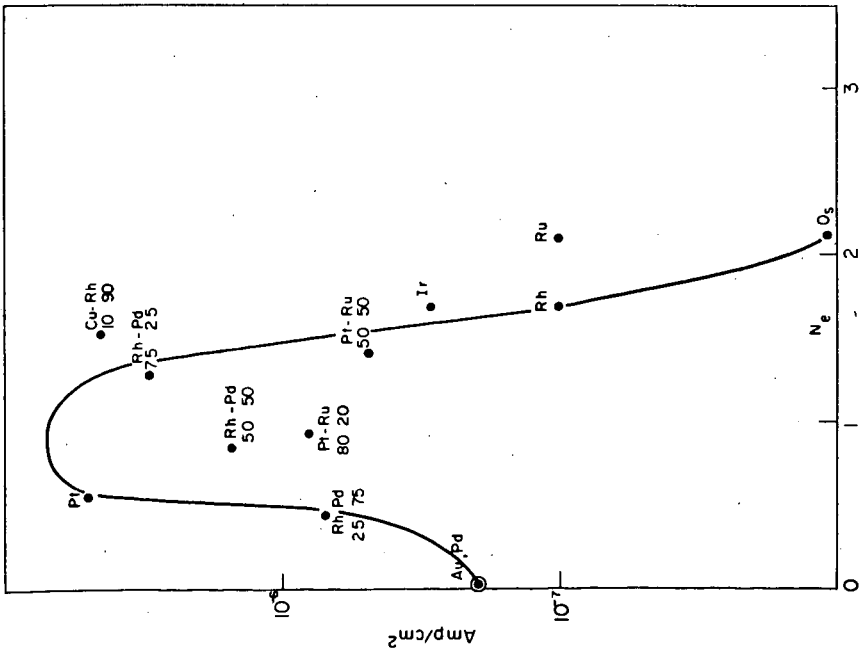


Fig. 1.-EFFECT OF UNPAIRED d ELECTRONS ON CATALYTIC ACTIVITY

Catalytic Electrodes for the Anodic Oxidation of Propane

J. D. Voorhies, J. S. Mayell and H. P. Landi

Central Research Division, American Cyanamid Company
Stamford, Connecticut

The complete electrochemical oxidation of simple hydrocarbons such as propane to CO_2 , protons and electrons can be accomplished in aqueous electrolytes with the proper combination of catalyst and temperature (1, 2). In fuel cell applications, an acidic electrolyte is usually required to reject the CO_2 produced at the anode, and a moderate temperature in the range of 100 to 200°C is necessary for an appreciable anode reaction rate. Under these conditions of temperature and acidity, anodic and chemical corrosion of electrocatalysts can be severe.

These adverse corrosion conditions limit the choice of electrocatalysts. In this investigation, some noble metals of Group VIII as pure metals, binary chemical codeposits and chemically reduced deposits on conductive substrates are considered. The object of this study was to evaluate the contribution of the chemical and physical properties of these electrocatalysts to their activity in the direct propane anode.

Two conditions of electrolyte and temperature were chosen, namely 85% H_2PO_4 at 140°C and 3N H_2SO_4 at 95°C . Under the first of these conditions, propane has shown a level of activity almost sufficient for practical fuel cells. The second set of conditions represents an objective in terms of reduction of general corrosion, better conductivity and possibly a superior oxygen electrode for combination with the hydrocarbon anode. Unfortunately, the temperature coefficient of the propane anode current going from 150 to 95°C is so large that the maximum anode power (milliwatts cm^{-2}) rapidly drops below a practical level. Anodic measurements in 3N H_2SO_4 have been useful, however, in evaluating electrocatalysts, principally because of a very characteristic limiting current density.

Experimental

All test electrodes consisted of a polytetrafluoroethylene (PTFE) bonded catalyst layer similar to those described previously (3, 4), a porous PTFE backing and a 45 mesh platinum collector screen. These three layers were compressed into a laminate as shown in Figure 1. Propane gas was fed through the electrolyte impermeable backing to the catalyst layer. The anode reaction occurs in this layer by virtue of intimate contact of reactant gas, liquid electrolyte and solid electrocatalyst. The collector screen serves to carry the current from the electrocatalyst to the external circuit.

The test cell was a spontaneous propane/oxygen cell operating under controlled resistive load. Anode potentials were measured with respect to a hydrogen reference electrode at room temperature using the same electrolyte as in the test cell. Connection to the test cell was made through a bridge and capillary system shown in Figure 2. Potential readings were obtained after three minutes at each resistive load setting. In the region of the limiting current observed in 3N H_2SO_4 at 95°C , these potential readings were unstable. Limiting currents measured by a potentiostatic technique using the Wenking 6LR potentiostat agreed well with those measured by the controlled resistive load technique.

A careful procedure for operation of these anodes was established in order to provide meaningful and reproducible values of anode potential and limiting current density. This involved reproducible preparation of the electrodes, pretreatment of the anodes consisting of high rate anodic oxidation of propane followed by open circuit equilibration with propane to an anode potential of about +0.1 volt versus the hydrogen electrode, adjustment of the propane flow rate and careful positioning of the potential measuring capillary at the center of and touching the collector screen. The cell contained a volume of electrolyte sufficient to provide water for the anode reaction and maintain a constant electrolyte composition. The reproducibility of anode potentials was about ± 10 mv and of the limiting current densities ± 1 mA cm⁻².

Catalyst Preparation

Borohydride reduction of the chloro complexes of the noble metals was frequently used to prepare catalysts. 5 to 10% aqueous solutions of NaBH₄ were added dropwise (3 to 6 ml/min) to solutions of the noble metals. In general, the reductions were carried out with the maximum possible dilution of the aqueous reaction mixtures and maximum rate of addition consistent with the size of the samples to be prepared. For deposition of platinum onto a conductive support, the support material was first suspended in water with stirring. Then a solution of chloroplatinic acid was added and allowed to contact the suspension for about 15 to 30 minutes prior to the initial borohydride addition. All finished catalysts were washed carefully to remove residual salts.

Anode Polarization at Platinum Black

Anodic potential versus current density plots which are representative of the behavior of platinum black/propane are shown in Figure 3. In 3N H₂SO₄ at 95°C, a well defined limiting current density of 28 mA cm⁻² (geometric current density) is observed for 20 mg cm⁻² of platinum black. However, the situation is not typical in that a rapid decrease in anode current is observed when the anode potential attains values above + 0.6 volt versus H.E. In this region platinum surface oxide formation may inhibit the propane anode process (5). The limiting currents cited herein refer to the point at which the anode potential changes by more than about 0.1 volt per 1 mA cm⁻² change in current density.

The source of the limiting current in 3N H₂SO₄ is believed to be some step in the electrode surface process rather than mass transport of propane to the surface. A diffusional limitation would be approximately described by a modification of the Nernst diffusion layer equation (6),

$$i_d = \frac{nFCD}{\delta}$$

where

i_d = diffusion limited current density (A cm⁻²)

D = diffusion coefficient of propane (cm² sec⁻¹)

δ = diffusion layer thickness (cm)

n = Faradays per mole = 20.

Since the real electrode area is about 4000 times the geometric area by an electrochemical measurement of surface area (7), and estimates of C and D are 2×10^{-7} moles/cc and 4×10^{-5} cm² sec⁻¹ respectively, the estimated diffusion layer thickness for $i_d = 28$ mA cm⁻² is 2 cm. This is obviously too thick by about two orders of magnitude. The conclusion is that the limiting current is not diffusion controlled in 3N H₂SO₄ at 95°C.

In 85% H_3PO_4 at 140°C, the anode polarization curve shows no limiting current in the region of spontaneous discharge of the propane/oxygen cell ($< 200 \text{ mA cm}^{-2}$). The anode potential at 20 mA cm^{-2} provides a meaningful figure of merit for an electrocatalyst and is used as such in Tables I and II. A polarization curve for the oxygen cathode in 85% H_3PO_4 at 140°C is also shown in Figure 3.

Unsupported Noble Metal Catalysts

Several platinum group noble metal catalysts as single metals or borohydride reduced binary codeposits were subjected to anode polarization tests. The results are shown in Table I. BET surface area measurements are included to show that the source of variations in performance is generally not the gross surface area of the catalyst. It may be argued that there are large differences in the real electroactive area for propane oxidation which account for the observed differences. This reasoning is difficult to refute without further studies, especially of propane adsorption.

In Table I, platinum is the most effective of the single noble metal catalysts while a codeposit of 75% platinum, 25% rhodium is apparently more active than either of the pure metals. However, borohydride reduction does not produce a black as active as those obtained from Engelhard. For this reason, the absolute activity of the best platinum-rhodium combination is less than that of the best platinum black.

Platinum Deposited on Carbides and Graphitic Carbons

The borohydride reduction of platinum onto the conductive substrates, graphite, titanium carbide and tungsten carbide produced catalysts with moderate activity for propane as shown in Table II. These supports were chosen for their electrical conductivity ($\sigma = 10^{-1}$ to 10^{-3} ohm cm when measured on compressed powders), corrosion stability and the possibility of cocatalysis.

The general effect of the conductive support is to improve the utilization of platinum at low loadings between 2.5 and 7.5 mg cm^{-2} of platinum. If there is a specific cocatalytic effect of the substrate, it is not large enough to be obvious from the data in Table II. A conductive support is necessary at low levels of platinum, as the utilization of unsupported platinum is already severely limited at 10 mg cm^{-2} .

The surface area and conductivity of the support are no doubt very critical, but commercially available carbides do not present a wide choice of these properties. Two sets of titanium and tungsten carbides were studied, I -325 mesh TiC and WC and II, 3-4 micron TiC and 1- 1.2 micron WC. The surface areas of these materials are somewhat anomalous in that the large particle size TiC (I) has a higher specific area than the smaller sized material indicating a difference in particle structure. Nevertheless, platinum catalysts prepared from all of these supports have similar activities with the WC supported material showing poor performance in hot phosphoric acid.

Graphitic carbons appear to be promising supports providing one can be found with sufficient stability to chemical and anodic corrosion. Stackpole 219XG has shown some corrosion stability (3). Cyanamid graphite has not been tested for this property. The relatively high surface area of the graphites allows a better distribution of metal catalyst than is available with the titanium and tungsten carbides.

Discussion

Owing to the corrosion limitations imposed on electrocatalysts for propene in hot acid electrolytes, the initial phase of this research effort has been directed toward metals of the platinum group. However, there are transition metals outside of the platinum group which have good corrosion stability, and there may be a number of binary or multicomponent alloys which have much better corrosion resistance than their pure metal constituents. Beyond chemical and anodic corrosion resistance, the problem is to find a catalytic source property or properties such as the proper 1) electronic configurations and energetics, 2) lattice spacings or 3) oxide coverage and structure. Unfortunately, the simultaneous combination of an effective catalytic source property with corrosion resistance is not easy.

The electrical conductivity of an electrocatalyst for a fuel cell electrode is a very critical problem. Fuel cell electrodes should be thin and are required to carry very high current densities. Under these conditions, it is necessary to have excellent electrical conductivity from a catalytic site to a collector point in the electrode structure. It is remotely possible that a non-conductive catalyst could be useful through catalysis of a purely chemical step in the electrode process, but this requires extremely efficient and rapid migration of intermediate species between conductive and non-conductive sites, a condition which is unlikely for complex hydrocarbon anode reactions. A possible exception is the case in which a non-conductive catalyst in the electrode promotes a low temperature water shift reaction of the hydrocarbon or one of the intermediates to produce hydrogen which would then serve as the active fuel.

The future of the direct hydrocarbon anode for fuel cells depends on significant improvement in one or more of the following areas:

- 1) better utilization of platinum or platinoid metals
- 2) new non-platinoid catalysts
- 3) new invariant electrolytes

Optimization of electrode and cell design is of great importance, but the catalyst and electrolyte problems remain the fundamental problems to be solved.

Acknowledgement

The authors are indebted to H. F. Eccleston for most of the electrochemical measurements and W. A. Barber and S. Arcano for preparation of catalysts.

References

1. W. T. Grubb and L. W. Niedrach, J. Electrochem. Soc. **110**, 1086 (1963).
2. C. W. Foust and W. J. Sweeney, in "Fuel Cells" (W. Mitchell, Jr., ed.) Chapter 9, Academic Press, New York, 1963.
3. R. G. Haldeman, et. al. in Advances in Chemistry Series, Number 47 "Fuel Cell Systems" pages 106-115, Copyright 1965 by the American Chemical Society.
4. L. W. Niedrach and H. R. Alford, J. Electrochem. Soc. **112**, 117 (1965).
5. L. W. Niedrach, J. Electrochem. Soc. **109**, 1092 (1962).
6. L. L. Bircumshaw and A. C. Riddiford, Quarterly Rev. **6**, 157 (1952).
7. J. S. Mayell and S. H. Langer J. Electrochem. Soc. **111**, 438 (1964).
8. General Electric Company, "Saturated Hydrocarbon Fuel Cell Program," Interim Report No. 1, Contract No. DA 44-009-AMC-479(T), pages 12, 26, April 1, 1964.

TABLE I
Unsupported Noble Metal Catalysts

<u>Electrode</u>	<u>Surface Area (BET)</u> <u>(m²/g)</u>	<u>3N H₂SO₄ @ 95°C</u> <u>Limiting Current Density</u> <u>(mA cm⁻²)</u>	<u>85% H₃PO₄ @ 140°C</u> <u>E₀ vs. H.E. @ 20 mA cm⁻²</u> <u>(mv)</u>
<u>Engelhard Blacks</u>			
Platinum (10) ¹	27	14	425
Platinum (20)	27	28	375
Ruthenium (20)	46	2	Current Limited
Rhodium (20)	4.3	1.5	Current Limited
Palladium (20)	28	ca. 1	-
<u>Borohydride Reduction</u>			
Platinum (10)	16	4	500
Platinum (20)	16	12	455
Pt (10) Rh (10)	29	4.5	-
Pt (15) Rh (5)	20	13	416
Rhodium (20)	26	2.5	-
Pt (9.5) Ir (0.5)	-	4	505

¹ - Values in parentheses are mg. of catalyst per cm² electrode area.

TABLE II

Platinum Deposited on Carbides and Graphites

Electrode ¹	Surface Area of Support (m ² /g)	3N H ₂ SO ₄ at 95°C Limiting Current Density (mA cm ⁻²)	85% H ₃ PO ₄ at 140°C E _a vs. H.E. at 20 mA cm ⁻² (mv)
Pt (2.5) ² TiC (7.5) I	4	-	715
Pt (5) Cyanamid Graphite (15)	11.4	7	481
Pt (5) Stackpole Graphite (15)	15	4	521
Pt (7.5) TiC (22.5) I	4	5	473
Pt (7.5) WC (22.5) I	0.11	4	Current Limited
Pt (7.5) Cyanamid Graphite (22.5)	11.4	9	445
Pt (7.5) TiC (22.5) II	0.43	5	Not Reproducible
Pt (7.5) WC (22.5) II	0.39	8	Current Limited
Pure TiC (10) I	4	-	ca. 700
Pt (10)	None	4	500

1 - The platinum was deposited by borohydride reduction in all cases.

2 - The values in parentheses represent the amount of material in the electrode in mg cm⁻².

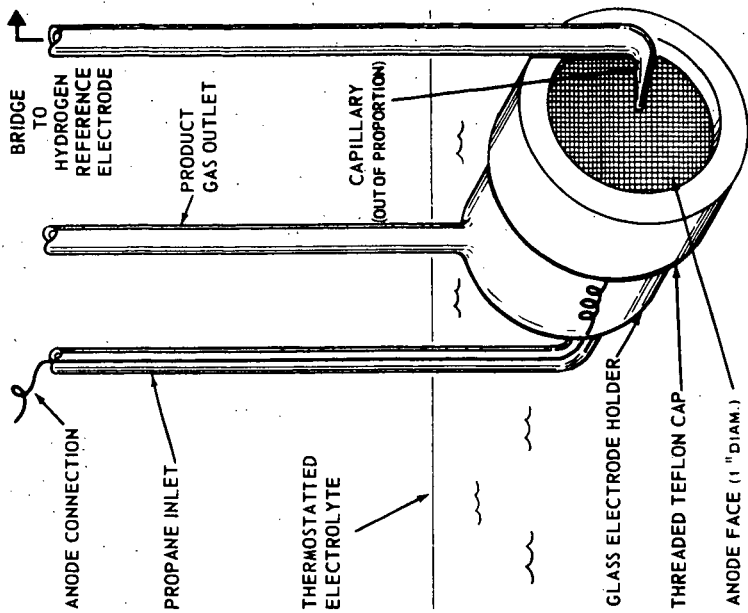


FIGURE 2 ANODE HALF CELL

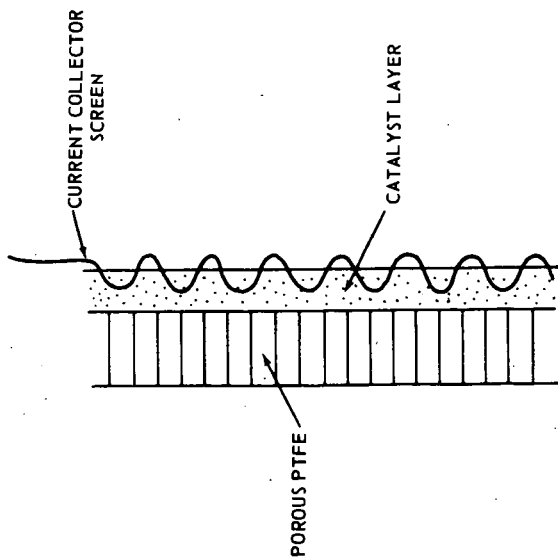


FIGURE 1 TEST ELECTRODE

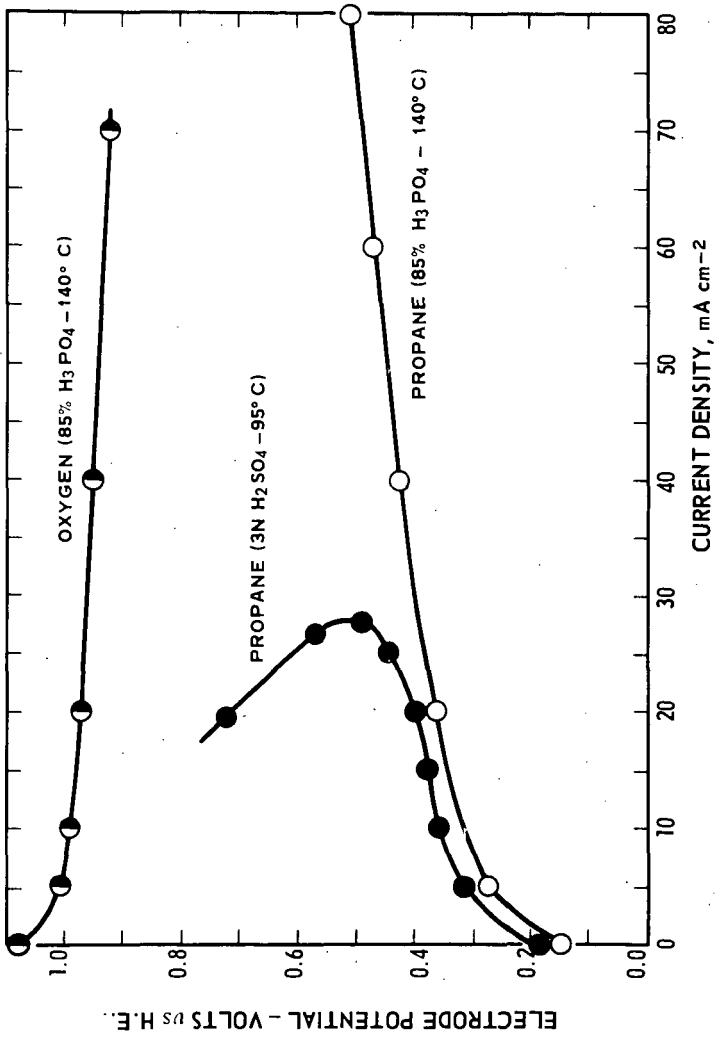


FIGURE 3 ELECTRODE POLARIZATION - CONTROLLED RESISTIVE LOAD

THE ADSORPTION AND OXIDATION OF HYDROCARBONS ON NOBLE METAL ELECTRODES
Part II.-PROPANE ADSORPTION ON SMOOTH Pt AT ELEVATED TEMPERATURES

by

S. B. Brummer and M. J. Turner

Tyco Laboratories, Inc.
Bear Hill
Waltham, Massachusetts

I. INTRODUCTION

The over-all aim of the present series of papers is to provide the basic scientific understanding of the functioning of a noble metal hydrocarbon anode. To this end, a study has been reported of the chemisorption of C_3H_8 from 13M H_3PO_4 solutions onto smooth Pt electrodes¹. In that work, measurements were reported for experiments made mainly at 80°C but some data were also taken at 110°C. In the present work, the previous experiments have been extended to 140°C, which is close to the region of effective operation of a hydrocarbon fuel cell². As will be seen, most of the conclusions of the previous work can be carried over to the higher temperature region although some modification of the views on the structure of the residues which are adsorbed is obtained from the experiments presented here.

II. EXPERIMENTAL

Most of the experimental procedures have been described previously^{1,3,4,5} and only the essential parts will be described here.

Experiments were carried out at 110°, 130°, and 140° ($\pm 0.5^\circ$) using electrolyte solutions of 13M H_3PO_4 purified with H_2O_2 ¹ saturated with N_2 or C_3H_8 , as required. The electrodes were Pt wires sealed in soft glass or, in experiments where very good approximation of semi-infinite linear diffusion was required, they were small flat flags. The electrodes were heated in an oxidizing gas flame, before use, to minimize surface roughening in the concentrated acid¹. Potentials were measured against the autogeneous H_2 reference electrode described by Giner⁶ and converted to the reversible hydrogen electrode in 13M H_3PO_4 at each temperature (R.H.E.).

Unless otherwise stated (cf. Glossary of Symbols), our results are expressed in terms of "real cm^2 ". A real cm^2 is defined in terms of the maximum cathodic galvanostatic charge for depositing H atoms on a clean electrode prior to H_2 evolution. It is assumed that this quantity, after correction for double layer effects, is 210 μ coulomb/ cm^2 (see reference (4) for a discussion of this point). This value of 210 μ coulomb/ cm^2 is taken as the reference value of Q_d^t at each temperature (cf. ref. (1)). A "clean electrode" is defined as one which has recently been anodized according to the procedure described below.

The basic experimental technique used in this study, as before¹, involves the rapid sequential manipulation of the electrode's potential so as to bring its surface, and the solution in its vicinity, into a reproducible and well-defined condition. This method has been used extensively by Gilman⁷ and the major departure from his procedure is the use of a galvanostatic pulse rather than a linear potential sweep to sample the surface. Prior to each measurement the electrode potential was raised to 1.35v. This allows the oxidation and desorption of adsorbed impurities and results in the formation of a passive oxide layer. During the first part of this treatment (1/2 min.), the solution in the vicinity of the electrode is vigorously gas-stirred to sweep away any desorbed impurities. Then the solution is allowed to become quiescent to establish the bulk concentration of C_3H_8 at the electrode (its reaction rate at 1.35v is very low). The oxide is reduced at 0.1v for 10 - 100 msec. and, since no C_3H_8 is adsorbed at 0.1v (see later), this brings the electrode into a clean and reproducible surface condition. The electrode is then brought to the potential of interest, E, for a time τ_E . Then an anodic or cathodic galvanostatic pulse is applied to sample the surface. This potential sequence is shown in Fig. 1.

To assist the presentation and discussion of the data, the symbols used in this paper are summarized in Table I.

III. RESULTS AND DISCUSSION

Anodic Charging Curves

In situ anodic stripping is one of the most direct and obvious methods of attempting to measure adsorption on a solid electrode and it has been used widely in the study of adsorption of organic substances on Pt (see, for example, references (3)-(5) and (7)-(12)). A considerable problem for smooth Pt electrodes is that at anodization rates which are fast enough to prevent significant re-adsorption during the pulse the oxidation of the adsorbate is usually pushed into the region of electrode oxidation. This complicates the interpretation of the charges obtained with anodic pulse methods. In addition to a charge, $Q_{\text{electrode}}$, due to oxidation of the electrode, some charge, Q_{dl} , also flows into the double layer. Charge may also be consumed in oxidizing material which diffuses up to the electrode during the pulse, $Q_{\text{diff}}^{\text{C}_3\text{H}_8}$. The total anodic charge under C_3H_8 in the potential region prior to O_2 -evolution

(cf. Fig. 2), $(Q_{\text{anodic}}^{\text{total}})^{\text{C}_3\text{H}_8}$, is then

$$(Q_{\text{anodic}}^{\text{total}})^{\text{C}_3\text{H}_8} = Q_{\text{ads}}^{\text{C}_3\text{H}_8} + Q_{\text{electrode}} + Q_{\text{diff}}^{\text{C}_3\text{H}_8} + Q_{\text{dl}} \quad (1)$$

The quantity of interest is the charge passed in oxidizing previously adsorbed C_3H_8 , $Q_{\text{ads}}^{\text{C}_3\text{H}_8}$, and it is clear that to determine it we must measure or eliminate the other quantities in equation (1).

$Q_{\text{diff}}^{\text{C}_3\text{H}_8}$ is small or negligible since we find that if τ_{ads} is short, viz. < 5 msec, so that an insignificant amount of C_3H_8 is adsorbed, $(Q_{\text{anodic}}^{\text{total}})^{\text{C}_3\text{H}_8}$ is the same as $(Q_{\text{anodic}}^{\text{total}})^{\text{N}_2}$. Evidently, even at elevated temperatures which are close to those obtained in a hydrocarbon fuel cell², C_3H_8 must be adsorbed before it can be oxidized and, as will be seen, there is no adsorption in the potential region of the anodic pulses (cf. Figs. 2 and 8).

Since Q_{dl} is likely to be relatively minor the major problem is the elimination of $Q_{\text{electrode}}$. In order to investigate a method of doing this, C_3H_8 was adsorbed for 10 sec. at 0.3 v at 130°C and $(Q_{\text{anodic}}^{\text{total}})^{\text{C}_3\text{H}_8}$ was measured as a function of the current density, i_a . This variation, is shown in Fig. 3 together with corresponding measurements made at 10 msec at 0.3 v under N_2 . It is seen that although both quantities depend strongly on i_a , their difference is independent of i_a over more than two orders of magnitude. The simplest way to account for this behavior is to assume that $Q_{\text{electrode}} + Q_{\text{dl}}$ are the same in N_2 and C_3H_8 . Then, as before (1),

$$(Q_{\text{anodic}}^{\text{total}})_{\text{C}_3\text{H}_8} - (Q_{\text{anodic}}^{\text{total}})_{\text{N}_2} = Q_{\text{ads}}^{\text{C}_3\text{H}_8} \quad (2)$$

The independence of the above difference on i_a could also be explained by assuming that $(Q_{\text{electrode}} + Q_{\text{dl}})$ varies with i_a but that previously adsorbed propane is desorbed during the measurement also as a function of i_a . These two effects would then have to be assumed to cancel when i_a is varied. This is most unlikely as the kinetics of these processes should vary rather differently with temperature and the non-dependence of $Q_{\text{ads}}^{\text{C}_3\text{H}_8}$ on i_a is known to occur at least from 80° to 130°. It seems clear then that the anodic charging method does give an accurate measure of the amount of oxidizable, adsorbed material. Subsequent measurements were made in the range of currents from 100-200 mA/cm² as was convenient.

Adsorption Kinetics at 130°C from Anodic Charging Curves

The variation of $Q_{\text{ads}}^{\text{C}_3\text{H}_8}$ with time of adsorption at various potentials is shown in Fig. 4. The data were obtained by extrapolating the $(Q_{\text{anodic}}^{\text{total}})_{\text{C}_3\text{H}_8}$ data to $\tau_{\text{ads}} = 0$ at each potential and subtracting the extrapolant from each of the values. This is more accurate than the above procedure of subtracting the 10 msec $Q_{\text{ads}}^{\text{C}_3\text{H}_8}$ values. We see that $Q_{\text{ads}}^{\text{C}_3\text{H}_8}$ increases with $\tau_{\text{ads}}^{1/2}$ independently of potential and, as at 80°C (1), this suggests that the initial adsorption onto a clean electrode is limited by diffusion in solution.

Assuming semi-infinite linear diffusion, with no retarding effect on the adsorption due to blockage by adsorbed material, the accumulation of material on the electrode is given by¹³

$$Q_{\text{ads}}^{\text{C}_3\text{H}_8} = 2n F \left[\frac{D_{\text{C}_3\text{H}_8}^{130^\circ}}{\pi} \right]^{1/2} C_{\text{C}_3\text{H}_8}^{130^\circ} \tau_{\text{ads}}^{1/2} \text{ coulomb/geom cm}^2. \quad (3)$$

The over-all reaction of C_3H_8 to CO_2 has been shown to be¹⁴



and n should therefore be 20. There is convincing evidence, both from earlier results¹ and from those given below, that n is 17 rather than 20. This assumes that the initially adsorbed material is propane which has lost about three H atoms upon adsorption and which is oxidized to CO_2 at high positive potentials. This argument also assumes that there is no turnover of adsorbed

molecules, i.e. no desorption. Then taking $C_{\text{C}_3\text{H}_8}^{130^\circ}$ as 6.8×10^{-8} moles/cm³¹⁵, and since the measured electrode roughness

was 2.0, we may use the initial slopes of Fig. 4 to calculate $D_{C_3H_8}^{130^\circ}$ as 5.0×10^{-6} cm²/sec. The value previously found at 80°C was 1.47×10^{-6} cm²/sec. Using Walden's rule, these predict 11.8×10^{-6} cm²/sec. and 9.3×10^{-6} cm²/sec for $D_{C_3H_8}^{25^\circ}$ in H₂O, respectively. These are reasonable values for $D_{C_3H_8}^{25^\circ}$ and in reasonable agreement with one another and they substantiate the conclusion that diffusion limits the initial adsorption on clean Pt.

As before, the rate of accumulation of adsorbed material on the electrode soon departs from diffusional limitation (Fig. 4). This occurs after about 6 sec, 2 sec and 0.4 sec at 0.22, 0.3 and 0.4 v respectively and takes place faster than at 80°C where the effect at corresponding potentials is significant after ~ 20-30 sec, ~ 10 sec and ~ 3 sec respectively.

As can be seen from Fig. 4, the concentration of oxidizable material becomes constant within 2 min. The values of $Q_{ads}^{C_3H_8}$ in Fig. 8 were thus taken after 2 min. of adsorption.

Adsorption Kinetics at 130° from Cathodic Charging

The purpose of cathodic charging curves is to examine the electrode surface for the presence of irreversibly adsorbed residues. Since most of the present studies of C₃H₈ adsorption were carried out at potentials in or close to the region of H-atom adsorption an additional potential step (1 - 10 msec at 0.5 v) was interpolated in the potential-time sequence just before measuring a charging curve. The purpose of this step was to displace any H-atoms, which might have been on the electrode at the lower potentials, prior to depositing H-atoms on the bare part of the electrode with the cathodic pulse. The duration of this step

was shown not to alter θ_H^t or $Q_{ads}^{C_3H_8}$. The variation of $\theta_H^{130^\circ}$ with time of adsorption and with potential is shown in Fig. 5.

At 130°C, and at 0.3 v and 0.4 v, θ_H^t decreases with $\tau_{ads}^{1/2}$ at essentially the same rate at each potential. This indicates, as did the anodic measurements, that adsorption is initially limited by diffusion in solution. Data at 0.2 v also follow a $\tau^{-1/2}$ relation but with a different slope. C₃H₈ is a sufficiently complex molecule that its mode of adsorption cannot be assigned a priori. Thus, each molecule of the adsorbed material could occupy one, two, three, or more Pt atoms on the surface. In order to discuss these possibilities, we calculate the diffusion-limited, adsorption rates for each mode of attachment.

The observed rate of accumulation of C_3H_8 is 1.42×10^{-4} coul/cm²/sec^{1/2}. If we take n as 17, this is equivalent to 5.2×10^{13} molecules/cm²/sec^{1/2}. Since 1 cm² is equivalent to 1.7×10^{15} atoms Pt, this corresponds

to $0.040 S \theta_H^{130^\circ} / \text{sec}^{1/2}$, where S is the number of Pt surface atoms occupied by each adsorbed C_3H_8 molecule. (Strictly, this should be $0.040 S \frac{17}{20-S}$ since n is a slight function of S , cf. equation (5).)

The data at 0.3v and 0.4v are well fitted by this equation for $S = 3$. At 0.2 v, the data follow the equation for 1 site adsorption. It seems then that the previous conclusions regarding the mode of adsorption as a function of potential are valid at 130°C. The

linearity of the $\theta_H^{130^\circ}$ vs. $\tau_{\text{ads}}^{1/2}$ plots over wide ranges of θ with no apparent effect from surface blocking, i.e. the absence of a $(1-\theta)$ term, is explained in terms of a long lived mobile adsorption-precursor state¹. The main adsorption process appears to be chemisorption but the precursor may involve a small quantity of physically adsorbed material.

Departure from linearity of the θ_H^t vs. $\tau_{\text{ads}}^{1/2}$ plots occurs after much longer times of adsorption than do the equivalent departures of the anodic charging data. Thus, at 0.4 v, 0.3 v, and 0.2 v, respectively, significant deviations occur at ~ 10 sec, ~ 30 sec, and (probably) 100 sec as against ~ 0.4 , 2, and 6 sec for the anodic data. As long as the adsorption follows the lines in Fig. 5, the rate of adsorption of C_3H_8 molecules is essentially equal to their rate of arrival at the surface, and the distribution of the adsorbed molecules is as described above. However, when deviations from the linearity of the cathodic data are found, the surface is becoming covered with the equilibrium, or at least steady state, concentration of C_3H_8 or related species at the particular potential of measurement. That this occurs later than the time required to reach saturation as judged by the $Q_{\text{ads}}^{C_3H_8}$ vs. $\tau_{\text{ads}}^{1/2}$ curves clearly indicates that the anodic and cathodic methods do not measure the same property of the adsorbate. This was noted previously and is also discussed below.

Experiments with Cl^- to Investigate Variation in Mode of Adsorption with Potential

As noted above, there is a dramatic change in the mode of attachment of C_3H_8 to a Pt electrode as the potential is raised from 0.2 v to 0.3 v. Thus, at all temperatures, each C_3H_8 molecule adsorbed at 0.2 v occupies one Pt surface atom and, at higher potentials, more than one. At 80°C and at 0.25 v, the adsorbate which is initially attached to one site per molecule, appears to change over to the 3-site species¹.

In order to account for the persistence of the singly-bonded species at 0.2 v, it is tempting to consider that the initial adsorption occurs via a primary carbon atom of the C_3H_8 since this would be relatively unlikely to yield a 3-site adsorbate. Similarly, the adsorption at 0.3 v and above might be assumed to occur via the secondary carbon atom. The variation of the mode of attachment of C_3H_8 with potential can then be seen as essentially the attempt by the electrode to act as an electrophilic substituent to the C_3H_8 . This explanation would gain in force if the potential of zero charge were in the vicinity of the changeover between the two kinds of adsorption.

An alternative explanation to account for the observations is to suggest that initial (1-site) chemisorption always occurs via the more reactive secondary carbon atom but that further (multi-site) adsorption requires the presence of high-energy adsorption sites on the Pt surface. At 0.2 v, most of these are still covered with H-atoms, at least initially. Thus, extensive 1-site adsorption occurs. Due to this 1-site adsorption, H-atoms would be displaced and, indeed, this is observed. However, by the time that this occurs there is so much C_3H_8 on the electrode that it is physically impossible for the singly-bound material to revert to the triply-bonded species. At 0.3 v, according to this explanation, almost all of the required deep energy wells are available and the progress from the 1-point attachment to the 3-point attachment can proceed.

In order to test these explanations, an experiment was devised in which Cl^- ion in solution was allowed to compete for the electrode with C_3H_8 . The specific adsorption of Cl^- on Pt is well known^{16,17} and this adsorption preferentially occupies the deep energy wells on the surface. Thus, the characteristic H-atom adsorption region is depressed to lower potentials¹⁸. On this rather oversimplified model one would expect that at, say 0.3 v, where the strongly adsorbed Cl^- successfully competes for the deep wells with the C_3H_8 , no deep wells will be available. If the second theory above is correct, this should lead to 1-site adsorption of C_3H_8 at all potentials. On the other hand the adsorption of Cl^- clearly moves the potential of zero charge to more negative potentials and even at 0.2 v the electrode will be anodic to the point of zero charge. Then on the basis of the first theory suggested above, the adsorption of C_3H_8 will occur on 3 sites even at 0.2 v.

The results of this experiment are shown in Fig. 6 for the adsorption of C_3H_8 at 0.3 v and 110°C. Evidently, the normal 3-site adsorption is progressively inhibited as more HCl is added to the H_3PO_4 . Also, the onset of chemisorption is considerably retarded and, as expected, the final adsorption of the C_3H_8 is less than usual. In addition, it was found that at 0.2 v in the presence of 0.17 mM HCl there was no change in the adsorption kinetics. The results thus indicate that the second theory above is closest to the explanation of the variation of the mode of adsorption with potential. However, the situation is somewhat more complex than is suggested by the above theories of the effect of Cl^- . Thus, assuming that all the added HCl is dissociated (which is hardly reasonable) and that, following

Gilman¹⁸, the rate of Cl^- adsorption is limited by solution diffusion and that each adsorbed Cl^- ion occupies 1 Pt surface site, we can calculate the times at which a monolayer of Cl^- should be present on the surface of the Pt. This is shown in Fig. 6 for $D_{\text{Cl}^-} = 2 D_{\text{C}_3\text{H}_8}$,

which is based on the ratio of the known value of D_{Cl^-} at 25°C in dilute solution¹⁹ and the value for $D_{\text{C}_3\text{H}_8}^{25^\circ}$ given previously. We see that particularly for the concentrated solutions of HCl the surface should be covered with Cl^- before almost any C_3H_8 has been adsorbed. Thus it is difficult to see why increasing the Cl^- concentration at this stage should make any difference. The answer probably lies in the fact that in the presence of C_3H_8 the Cl^- does not have the electrode all to itself and the C_3H_8 can effectively compete at least for some of the sites. It is apparent that when some Cl^- is adsorbed some C_3H_8 is adsorbed on 3-sites as before and some on fewer sites. Thus the slope of the $\theta_{\text{H}}^{1/2}$ vs. $\tau_{\text{ads}}^{1/2}$ line is decreased although the accumulation of C atoms on the surface is still governed by diffusion of C_3H_8 .

Despite these difficulties, it is quite clear that the model which is favored by the experiment is the one based on the active sites' occupancy with H atoms as a function of potential and, tentatively, we can conclude that adsorption involving 3-sites occurs with greater difficulty than the initial adsorption on 1-site. From the point of view of operating a fuel cell, it is not known which of the two species, 1-site or multi-site, is the more reactive but it is clear that we can modify the mode of attachment of the C_3H_8 by adding small quantities of appropriate anions to the electrolyte solution.

Extent of Adsorption as a Function of Temperature and Potential

In Fig. 7 we show the coverage of Pt with irreversibly adsorbed material in C_3H_8 -saturated solutions as a function of potential and temperature. (Data at 80° and 110° are from ref. (1).) The data at 0.25 v or greater refer to the steady state but at lower potentials the maximum adsorption has not been reached. This is because (cf. Fig. 5) the accumulation of C atoms is very slow (1-site) at low potentials. No attempt was made to obtain the limiting coverage at these potentials since it was thought that interference from adsorption of impurities would be considerable at the long times that would be involved. For this reason, the adsorption-potential curve has been represented by a dotted line in this potential region. It is evident that C_3H_8 adsorption occurs between 0.1 v and 0.7 v, with a maximum at about 0.3 v. The effect of temperature is small and within the experimental error.

The variation of the anodic charge with potential and temperature is shown in Fig. 8. The values were taken after 2 min of adsorption. Here, the data are in the steady state and it is evident that the adsorption increases rapidly from 0.1 to ~ 0.2 v and then slowly declines, becoming small or negligible at ~ 0.7 v. As before, the effect of temperature is small.

It will be seen in the next section that the correlation between the anodic and cathodic data is fairly good but we have not attempted to express the above adsorption data in the form of an isotherm related to $C_{C_3H_8}$ since it will be made clear that the material which is finally adsorbed on the electrode is not C_3H_8 as such.

Final Structure of "Adsorbed Propane"

It was seen earlier that the anodic and cathodic adsorbate vs. $\tau_{ads}^{1/2}$ curves deviate from linearity after different times of adsorption. In every case, at all temperatures and potentials, the anodic charge vs. $\tau_{ads}^{1/2}$ lines curve off first while the cathodic

curves indicate that in fact adsorption is continuing at the same rate. Previously¹ it was suggested that this results from the partial oxidation in the adsorbed state of the originally adsorbed material. Thus, less charge will be found in the ultimate oxidative measurement of the amount of adsorption with the anodic current pulse. This explanation fits all the observations which we presently have; for example, it accounts for the fact that the anodic charge tails off sooner at more anodic potentials and at higher temperatures. It also clearly demonstrates the dangers of attempting to characterize the adsorption in a complex system of this kind solely with anodic stripping.

If we take the limiting values of $Q_{ads}^{C_3H_8}$ and θ_H^t , at each potential, we can estimate the average oxidation state of the adsorbed material. The fraction of the H atom sites occupied by "adsorbed C_3H_8 " is then $(1 - \theta_H^t)$ and, when expressed in terms of the charge which would be involved in the oxidation of H atoms if they were on these $(1 - \theta_H^t)$ sites, this corresponds to $(1 - \theta_H^t) 210 \mu \text{ coul/cm}^2$. Since the oxidation of each H atom involves a single electron, the ratio of the limiting values of $Q_{ads}^{C_3H_8}$ and $(1 - \theta_H^t) 210$ yields the average number, $[e]$, of electrons involved in the ultimate, high-potential oxidation of the adsorbed material per Pt surface atom which it covers. This quantity is shown as a function of potential and temperature in Fig. 9 and we see that for $E \geq 0.3 \text{ v}$ $[e]$ is between 2 and 3 independent of temperature. The scatter is considerable as the limiting values of θ_H^t are difficult to estimate. Below 0.3 v, the adsorbed material is in a less oxidized condition. It may be recalled that the adsorption process is still continuing at these potentials so that the data shown in the figure will be somewhat higher than the values corresponding to the adsorbate at limitingly-long adsorption times. Consequently, the remaining discussion refers to data obtained at 0.3 v and above.

C_3H_8 dissociatively adsorbed on 3-sites per molecule and releasing $3H^+$ ions and 3 electrons (cf. equation (5)) should yield a material for which $[e]$ is 5.67. Therefore, the residue found cannot be C_3H_8 itself unless each adsorbed C atom is attached to about 2.8 Pt atoms (for $[e] = 2$). However, we can show that this is not likely for we observe in Fig. 5 that at these potentials the rate of accumulation of C atoms is just that given by the assumption that each C atom occupies 1 Pt surface atom (3-site adsorption). This process continues even when the adsorbate is being oxidized and unless it is assumed that the C atoms re-orient on the surface some time later, when both

θ_H^t and $Q_{ads}^{C_3H_8}$ have become constant, we may safely conclude that the adsorbed C atoms only occupy 1 Pt atom apiece. Then the observed final value of $[e]$ plus the observation that $[e]$ decreases during the process of adsorption suggest strongly that the adsorbate is gradually oxidized while it is on the electrode. The observation that $[e]$ is approximately constant over a range of potentials and temperatures suggests also that this residue is just a single species whose oxidation at higher potentials involves between 2 and 3 electrons per C atom. Such a hypothesis would agree with the results of Giner²⁰ and the value 2 for $[e]$ would recall suggestions that the final residue is something like CO (see ref. (21) for discussion of this suggestion for a similar system). However experiments we have carried out show that the composition of the adsorbate varies markedly with the potential of adsorption. This is totally unexpected from the data shown in Fig. 9.

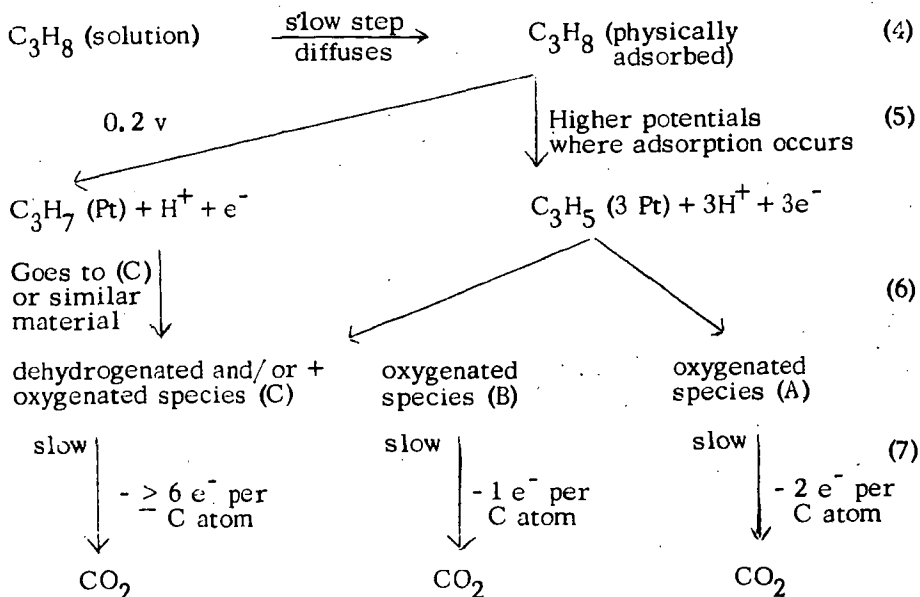
In order to trace the role played by the adsorbed intermediates in the over-all process an attempt was made to study their oxidation kinetics. The experiment consists of adsorbing material at a low potential and then displacing the potential so as to oxidize or displace the adsorbed material. A convenient potential for the latter purpose is 0.7 v, where there is insignificant oxide on the electrode to complicate the analysis. Both $Q_{ads}^{C_3H_8}$ and θ_H^t were followed as a function of time at 0.7 v and we find that the amount of adsorbate declines quite rapidly, becoming almost zero within 10 sec. The unexpected feature is the observation that $Q_{ads}^{C_3H_8}$ does not follow $(1-\theta_H^t)$ linearly with a slope corresponding to ~ 2 electrons per covered Pt atom. This is shown in Fig. 10 for adsorption at 130°C. Here, $\theta_{C_3H_8}$ is highest to the right of the figure and this corresponds to the condition of the adsorbate at 0.3 v. The removal of the adsorbed material is followed by tracing down the lines starting from the top right hand corner of Fig. 10. We see that most of the occupied Pt atoms are covered by a species for which $[e]$ is ~ 1 . However, the last part of the adsorbate to be removed, and hence the most difficult to oxidize, has a much higher value of $[e]$. The exact value of $[e]$ in this region cannot be estimated very accurately at this time and further experiments are in progress.

However, it is clear that a fraction of the C atoms (for 100 sec at 0.3 v, these cover ~ 5% of the total surface of the electrode) are in a considerably reduced state. Because of the high state of reduction of these species they contribute a large fraction of

$Q_{ads}^{C_3H_8}$. We cannot discriminate whether more than one such species is involved in this region, but it seems safe to hypothesize that we do not have alkyl radicals since these are presumably involved in the initial (rapid) adsorption and are then easily oxidized further. More likely, we have extensively dehydrogenated materials. For stabilization, these might involve attachment to more than 1 Pt site per C atom but this is not incompatible with the observations since only a small fraction of the C atoms would be involved.

Similar experiments on the adsorbate from 0.35 to 0.4 v (Fig. 10) show different effects. At 0.4 v, virtually all the adsorbed C atoms involve just about 2 electrons for their oxidation but at 0.35 v some of the C atoms are in a more reduced state. The increase in the amount of the more reduced (and yet harder-to-oxidize) residue with increasingly cathodic potential is expected.

These experiments demonstrate clearly the complexity of the species adsorbed on a Pt hydrocarbon anode and indicate that a careful and thoughtful approach must be used if we are to elucidate the path of the over-all reaction from C_3H_8 to CO_2 . Tentatively, we can suggest the following sequence for the adsorption-oxidation process:



At this time it appears from the number of electrons involved in reaction (7) that (A) may be a "CO-like" species, (B) a species similar to the formate radical and (C) is very likely a dehydrogenated species and may in fact arise from a small contribution, even at the higher potentials, from singly-bonded C atoms.

It is curious that the most highly oxidized residue (B) is found not at the highest potentials of adsorption but at an intermediate potential (0.3 v).

The distribution of these species on the electrode is demonstrably a function of potential and probably depends also on temperature and acid concentration. The description of the roles of these species in the over-all reaction is a first requirement in the understanding of the C_3H_8 oxidation mechanism and further studies on their oxidation kinetics will be reported subsequently.

IV. CONCLUSIONS

The results of the work reported here for C_3H_8 adsorption at 130 and 140°C largely confirm the previous results at 80 and 110°C¹ but some modification of the ideas presented earlier is required (see (5) below). The main conclusions are summarized below:

- (1) Anodic stripping yields a quantitative estimate of the amount of oxidizable material pre-adsorbed on the electrode.
- (2) The rate of adsorption is limited by diffusion in solution.
- (3) At 0.2 v, adsorption involves 1 surface site for each adsorbed molecule but at higher potentials 3 sites are used. Experiments with the addition of Cl^- indicate that this difference is related to the need for deep energy adsorption wells to convert (initial) 1-site adsorbate to 3-site attachment. It is suggested that these are covered with H atoms at 0.2 v and that this prevents significant 3-site adsorption.
- (4) The adsorbate is oxidized on the electrode and, thus, subsequent anodic stripping finds less material than expected. However, during this oxidation process, adsorption continues at the same rate and virtually none of the adsorbed and oxidizing C-atom centers is removed.

- (5) Because of this oxidation, residues whose final oxidation to CO_2 is slow accumulate on the electrode surface. The oxidation of these residues may be the rate limiting step in the conversion of C_3H_8 to CO_2 and, at potentials more anodic than 0.3 v, appears to involve about 2 electrons per covered Pt atom independently of potential and temperature. This suggests that the same species is involved under all conditions. Desorption experiments show clearly that this is not the case and that the composition of the residue depends on the potential of adsorption.

ACKNOWLEDGEMENTS

This work was supported by the U. S. Army Research and Development Laboratories, Fort Belvoir, Va., under Contract DA 44-009-AMC-410 (T).

REFERENCES

1. S. B. Brummer, J. I. Ford and M. J. Turner, in press.
2. W. T. Grubb and L. W. Niedrach, J. Electrochem. Soc., 110, 1086 (1963).
3. S. B. Brummer and A. C. Makrides, J. Phys. Chem., 68, 1448 (1964).
4. S. B. Brummer, J. Phys. Chem., 69, 562 (1965).
5. S. B. Brummer, and J. I. Ford, J. Phys. Chem., 69, 1355 (1965).
6. J. Giner, J. Electrochem. Soc., 111, 376 (1964).
7. S. Gilman, J. Phys. Chem., 66, 2657 (1962); 67, 78 (1963).
8. M. W. Breiter, Electrochimica Acta, 8, 447, 457 (1963).
9. T. Warner and S. Schuldiner, J. Electrochem. Soc., 111, 992 (1964).
10. D. R. Rhodes and E. F. Steigermann, J. Electrochem. Soc., 112, 16 (1965).
11. J. Giner, Electrochimica Acta, 8, 857 (1963); 9, 63 (1964).
12. M. W. Breiter and S. Gilman, J. Electrochem. Soc., 109, 622 (1961).
13. H. A. Laitinen and I. M. Kolthoff, J. Am. Chem. Soc., 61, 3344 (1939).

14. H. Binder, A. Kohling, H. Krupp, K. Richter and G. Sandstede, J. Electrochem. Soc., 112, 355 (1965).
15. Report by General Electric Co. on Contracts DA. 44.009-ENG-4409 and DA.44.009-AMC-479(T), dated Dec. 1964.
16. A. Slygin and A. Frumkin, Acta Physiochim., 3, 791 (1935).
17. A. Frumkin and A. Slygin, *ibid*, 5, 819 (1936).
18. S. Gilman, J. Phys. Chem., 68, 2098, 2112 (1964).
19. R. Parsons, "Handbook of Electrochemical Constants," published by Butterworth and Co., Ltd., London, England (1959).
20. J. Giner, Paper presented at C.I.T.C.E. meeting in London, England, September 1964.
21. S. B. Brummer, J. Phys. Chem., 69, 1363 (1965).

Table I. -GLOSSARY OF SYMBOLS

$C_{C_3H_8}^t$	Concentration of C_3H_8 at $t^\circ C$. (moles/cm ³).
cm ²	Unless otherwise stated, or in connection with $C_{C_3H_8}^t$ or $D_{C_3H_8}^t$, refers to real area which is defined as equivalent to 210 μ coulomb for Q_H^t .
$D_{C_3H_8}^t$	Diffusional coefficient of C_3H_8 at $t^\circ C$ (cm ² /sec).
E	Potential (v. vs. reversible H^+/H_2 (R.H.E.)).
[e]	The average number of electrons involved in the high potential oxidation of the adsorbate per Pt atom that it covers.
F	The Faraday.
geom cm ²	Geometric area of the electrode.
i_a	Anodic current density (amp/cm ²).
n	Number of electrons involved in oxidation of adsorbed species, see equation (3).

- Q Charge (μ coulomb/cm²).
- Q_{dl} Charge due to double layer charging during anodic galvanostatic transient.
- $Q_{electrode}$ Charge due to electrode oxidation during anodic galvanostatic transient.
- Q_H^t Maximum cathodic H atom charge on a clean electrode at $t^\circ\text{C}$.
- (Q_{anodic}^{total}) N_2 Charge passed during anodic galvanostatic transient in N_2 -saturated solution in potential region prior to O_2 -evolution ($\sim 0.8 - 1.8$ v depending on i_a).
- (Q_{anodic}^{total}) C_3H_8 Similar charge in C_3H_8 -saturated solution.
- $Q_{ads}^{\text{C}_3\text{H}_8}$ Charge to oxidize adsorbed C_3H_8 .
- $Q_{diff}^{\text{C}_3\text{H}_8}$ Charge due to oxidation of C_3H_8 diffusing up to electrode during anodic galvanostatic transient.
- S Number of surface sites occupied by each adsorbed C_3H_8 molecule
- t Temperature ($^\circ\text{C}$).
- θ_i Fraction of surface covered with species i .
- θ_H^t Ratio of the H atom charge under a given circumstance to the maximum value at the same temperature.
- τ Time (sec).
- τ_{ads} Time of adsorption.
- τ_E Time at potential E .
- τ_H Transition time during measurement of Q_H^t by galvanostatic pulse.

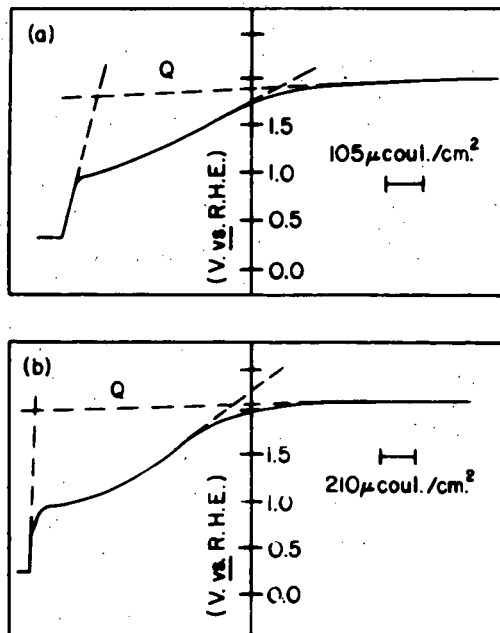
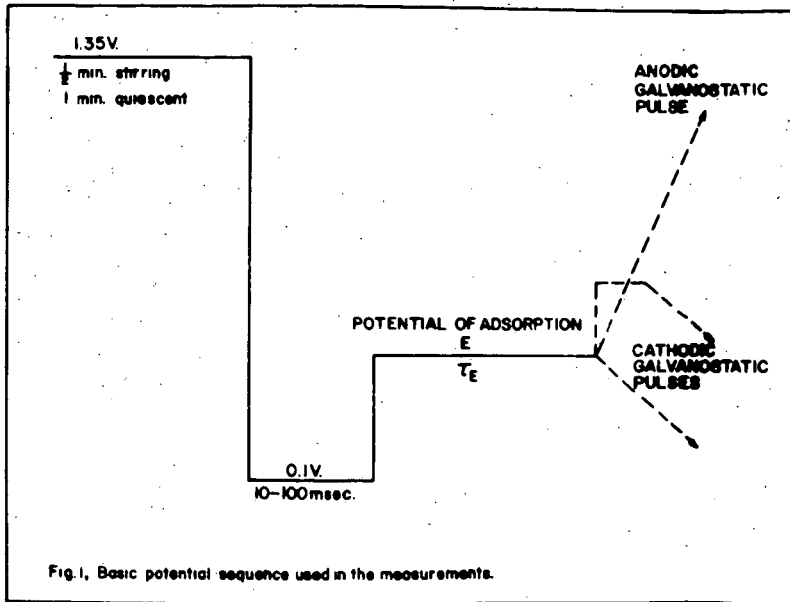


Fig. 2. Typical anodic charging curves at 130°C in presence of C_3H_8 . Curves were taken at 114mA./cm^2 (a) after 10 msec., (b) after 2 min. at 0.3V.

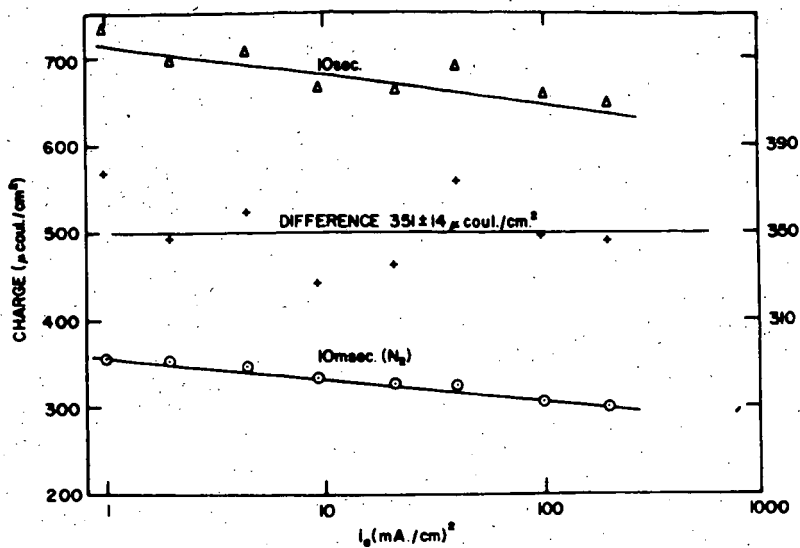


Fig. 3. Adsorption of C_3H_8 at 0.3V and 130°C. Δ , $(Q_{\text{ads.}}^{\text{total}})_{\text{C}_3\text{H}_8}$ after 10 sec.
 O, $(Q_{\text{ads.}}^{\text{total}})_{\text{N}_2}$ after 10 sec. +, DIFFERENCE = $Q_{\text{ads.}}^{\text{C}_3\text{H}_8} - Q_{\text{ads.}}^{\text{N}_2}$

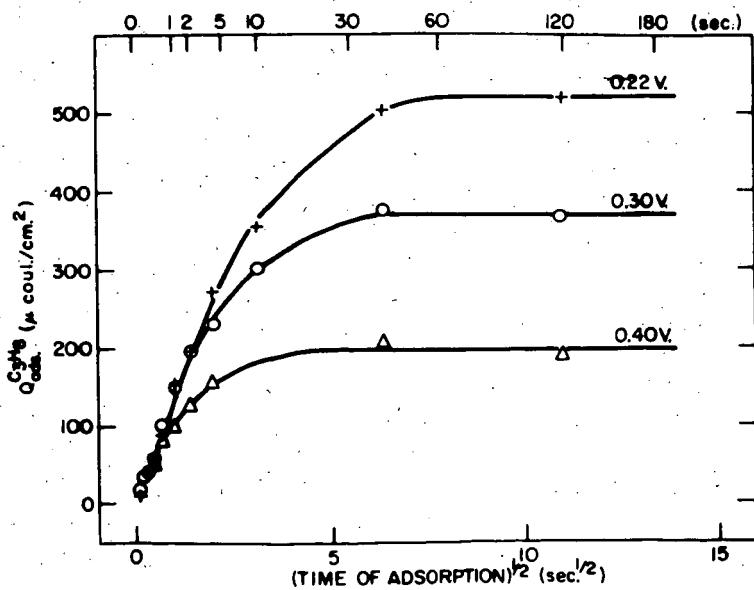
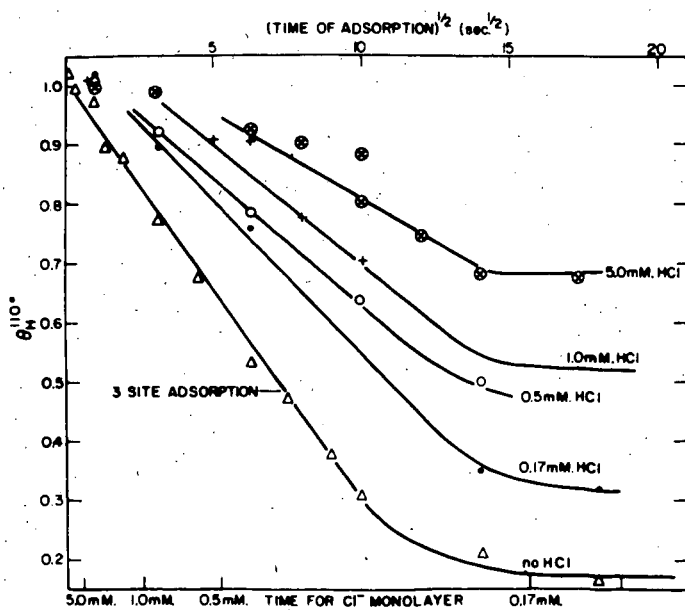
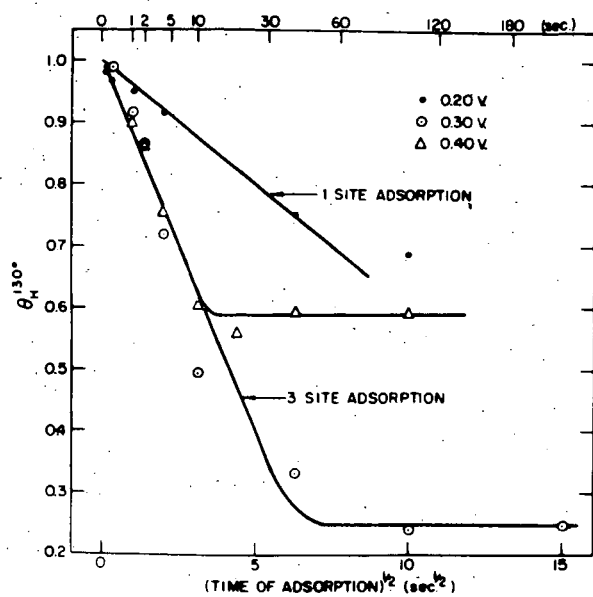


Fig. 4. Variation of $Q_{\text{ads.}}^{\text{C}_3\text{H}_8}$ with $T_{\text{ads.}}^{1/2}$ at 130°C.



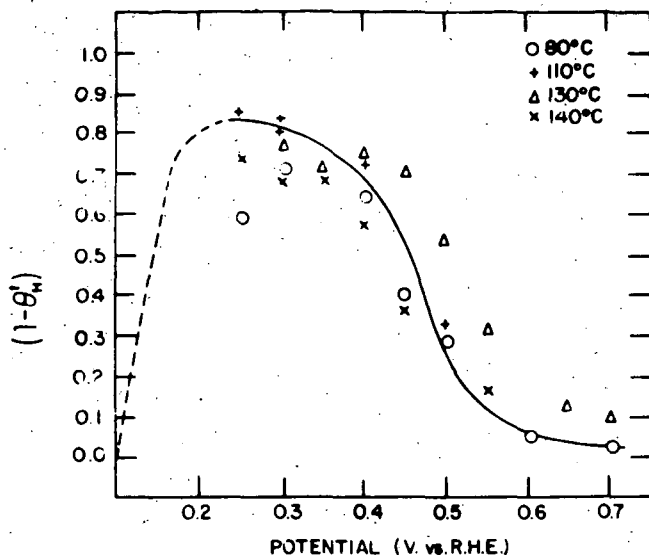


Fig. 7. Coverage of Pt with irreversibly adsorbed material as a function of potential and temperature.

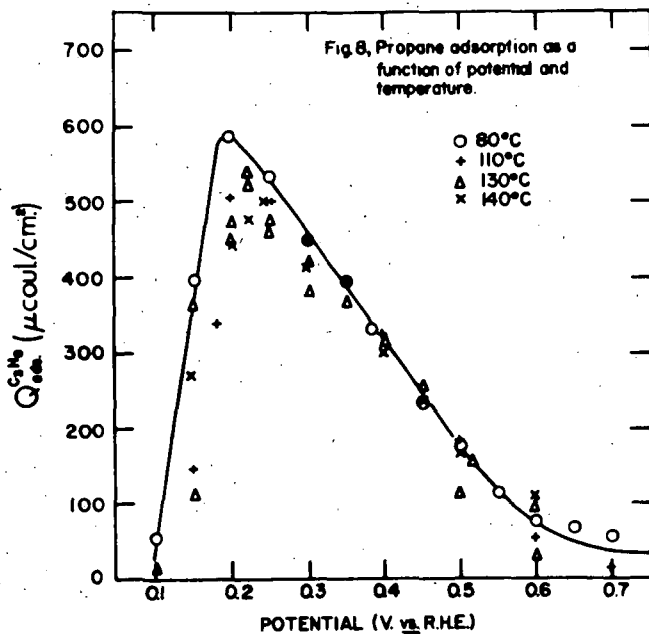


Fig. 8. Propane adsorption as a function of potential and temperature.

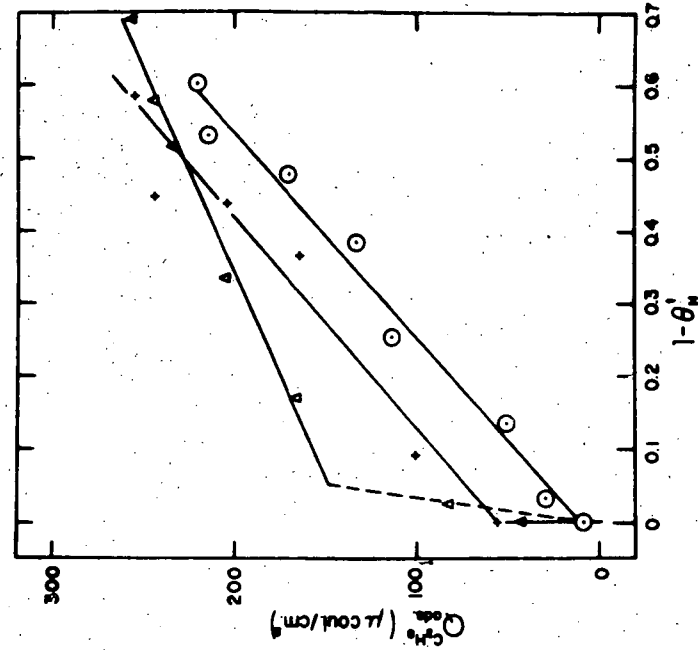


Fig. 10. Variation of the anodic charge with electrode coverage during desorption of 0.7V of material adsorbed at 130°C. Adsorption at 0.4V for 60sec. ○; 0.35V for 60sec. △; 0.3V for 100sec. ◇.

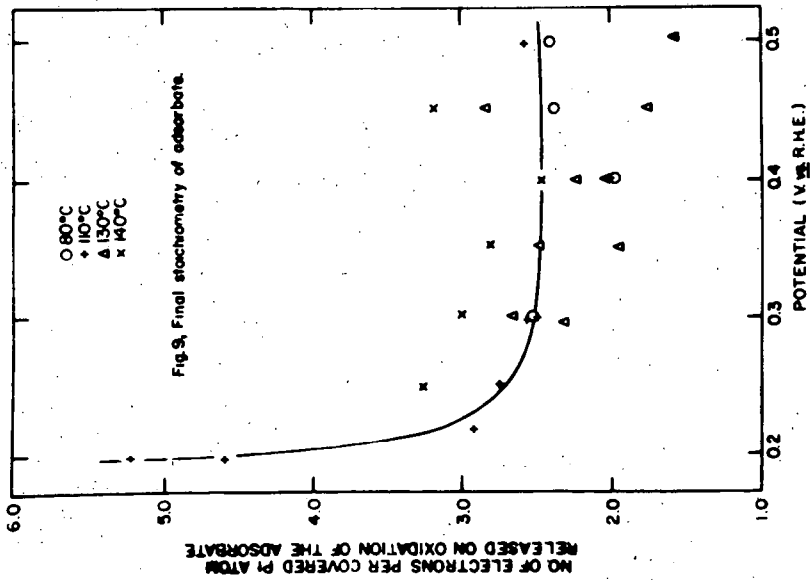


Fig. 9. Final stoichiometry of adsorbate.

RELATIVE REACTIVITIES IN THE DIRECT OXIDATION OF BINARY HYDROCARBON FUELS ON PRACTICAL ELECTRODES

H.J.R. Maget and P.J. Chludzinski

Direct Energy Conversion Operation, General Electric Co., Lynn, Mass.

INTRODUCTION

The direct oxidation of hydrocarbon fuels in presence of aqueous electrolytes and at temperatures less than 200°C has been extensively studied.¹ The interest of investigators has been mainly focused on pure paraffinic hydrocarbons. However, practical hydrocarbon fuels will probably be rather complex or at least consist of binary or ternary mixtures. If the reactivity of these fuels differs appreciably it can be expected that preferential anodic oxidation will correspond to the depletion of the more reactive species at the detriment of others. This, in turn, will result in an enrichment of the less reactive species. In addition, competitive adsorption and reactions are expected to take place on the electrode surface. These processes are not well known for complex mixtures. Relative reaction rates will also depend on anodic potentials, resulting in varying fuel reactivity, as the electrode surface potential varies with over-all currents.

The design of multi-cell stacks operating with fuel mixtures could be based on the least reactive species; gains in cell performance could be obtained if the behavior of various fuels could be understood.

It was decided to approach the problem by studying binary systems such as propane/octane, hexane/octane and heptane/octane. Individual constituents of these binary mixtures have been extensively investigated, and anode performance as a function of molecular chain length has shown that at 150°C in presence of phosphoric acid the fuel reactivity varies as: propane>hexane>heptane>octane.²

EXPERIMENTAL

The experimental work was conducted on porous platinum electrodes (geometric area: 50 cm²) prepared according to techniques described elsewhere.³ Phosphoric acid was used as the electrolyte at 150°C and concentrations ranging from 95-97 wt.%. High acid concentrations were chosen in order to operate the fuel at relatively low water vapor pressures, in equilibrium with the electrolyte. The electrolyte was pumped in the cell at flow rates sufficiently large to avoid thermal and concentration gradients. The counter-electrode operated on oxygen or air. Isothermal conditions were obtained by placing the complete cell in an oven, maintaining the cell temperature at 150 ± 2°C. Figure 1 represents

the single cell. Single electrode potentials (with and without ohmic contributions) were measured by means of a hydrogen reference electrode, located in the same environment (same temperature and electrolyte concentration).

The fuel (pure grade 99.9 mole %) was pre-mixed before entering the anode compartment. The fuel system, single-pass type, allowed the exit stream to enter a Perkin-Elmer 801 gas chromatograph, provided with a "hot" gas sampling valve and thermal conductivity cell. The chromatograph was calibrated with about 50 samples of chemical species and mixtures of species to determine separation time, peak heights, areas and the proper temperature of the column. The calibration was based on the area under the "peak" as described by a mechanical integrator on a Leeds-Northrup recorder.

Specific calibrations were conducted with known quantities of carbon monoxide, carbon dioxide, propane, hexane, octane, methane, air and mixtures of these constituents for a six foot, 1/8 inch O.D. column, packed with silica gel. Separation of air, carbon monoxide and methane could be accomplished at room temperature; carbon dioxide and propane at 150°C, and hexane and octane at 250°C. The carrier gas was helium, set at 30 cc/min. at 150°C, and although the chromatograph had flow compensators to keep carrier flow constant through the programmed temperature excursion the flow decreased somewhat at 250°C. Error was minimized by calibrating the chromatograph and running a fuel cell sample under the same conditions of temperature programming.

It was necessary to heat the sample valve, the sampling tube, and all fuel exhaust lines that were exposed to room ambient in order to prevent condensation of the higher boiling constituents. The lines were kept constant at about 150°C and monitored by thermocouples in various locations.

The anode exhaust was directed to a heated Teflon dehumidifier containing two chambers, one which trapped electrolyte leakage, and the other which contained phosphorous pentoxide to remove water vapor from the fuel exhaust before introduction to the silica gel column. The small fuel flows (approximately 0.02 cc/min.) were fed through a capillary tube flowmeter and the rates determined from pressure drops.

A schematic illustration of fuel feed and exhaust for the chromatograph system is shown in Figure 2. Helium was used to pressurize the fuel tank because its presence in the fuel would not be detected by the chromatograph. Pressure fluctuations due to the helium regulator were dampened by bleeding part of the helium to a water column. The bypass allowed the fuel feed line to the cell to be quickly filled prior to testing. The liquid fuel mixture was vaporized inside the oven in coaxial metal tubes, the inner tube supplying fuel to the hot outer tube, where it was "flash" vaporized. The system provided very satisfactory operation, with reproducible calibration and smooth, steady flow.

EXPERIMENTAL RESULTS AND DISCUSSION

1. Fuel and Oxidant Migration

Although fuel and oxidant solubilities are rather low at 150°C in concentrated phosphoric acid* (0.18 millimoles of propane/liter-atm., 0.34 millimoles of oxygen/liter-atm., approx. 0.03 millimoles of octane/liter-atm.), measurements were conducted to determine the rate of fuel loss and carbon dioxide evolution at the anode, due to chemical oxidation of the fuel. Results are reported in Table I.

Table I

Transport of Chemical Species Across the Electrolyte*

<u>Species at source electrode</u>	<u>Species at Counter-electrode</u>	<u>Transport Rate (moles/cm²-sec-atm) x 10¹⁰</u>
Octane	Helium	1
Octane	Oxygen	1
Carbon dioxide	Helium	4
Oxygen	Propane + Octane	52

*Electrode size: 50 cm². Electrolyte spacing: 3.2 mm. Phosphoric acid conc. 95-97 wt.% at 150°C. Species at source electrode at 1.0 atm.

In the case of oxygen transport measurements, the dissolved air in the fuel (about 0.2 mole %) was not a contributing factor to the oxygen content of the anode stream.

2. Electrochemical Oxidation of Pure Octane

Octane, at open circuit, showed a carbon dioxide content in the anode exhaust of 1%. If this is assumed to be chemical combustion from oxygen migrating from cathode to anode, it corresponds to a parasitic current density of 0.3 ma/cm². Pure octane, at 20 ma/cm² showed a fuel utilization and carbon dioxide production within 2% of the theoretical value. Corrected for chemical combustion, the agreement was within 1%.

3. Binary Fuel Mixtures

Attempts made to detect hydrogen, carbon monoxide or species other than the fuels fed into the anode chamber, were negative. Interfering peaks observed at low retention times, were identified as oxygen and/or nitrogen, due to oxidant migration from cathode to anode.

a. Propane/octane fuel mixtures.

The experimental results are reported in Figure 3

for the current contribution of propane as a function of log mean mole fraction of propane in the anode chamber. (Inlet concentrations are determined by flow rates, exit concentrations by gas chromatographic analysis. All data are corrected for the vapor pressure of water in equilibrium with the electrolyte.) The rate of propane oxidation is proportional to the mole fraction in the feed stream and also strongly dependent on the anodic potential, e.g. increasing the anodic potential induced a decrease in anodic propane current. This observation is in contradiction with the behavior of pure propane for increasing anodic potentials, at least up to potentials corresponding to oxygen deposition on the electrode surface. Linearity between propane current and gas phase composition is obtained up to average mole fractions of 0.3 to 0.4. At higher concentration, the electrode current is due entirely to the oxidation of propane. Similar observations can be made for octane, although the current due to octane oxidation increases with increasing anodic overvoltage, as expected. The behavior of this binary mixture is suggestive of species interaction and competition on the electrode surface.

Propane and octane currents can be represented by:

$$i_3/I = 740 e^{-11.6\eta_{x_3}} \quad 1.$$

and
$$i_8/I = 0.06 e^{6.0\eta_{x_8}} \quad 2.$$

where x_3 and x_8 represent the log mean mole fraction of propane and octane in the gas phase. At anodic over-potentials of 0.5 volts vs. H^+/H_2 , at which most of the experimental data was obtained, the currents can be expressed as:

$$i_3/I = 2.2 x_3 \quad 3.$$

and
$$i_8/I = 1.2 x_8 \quad 4.$$

b. Hexane/octane fuel mixtures.

All results reported in Figure 4 were obtained at anodic potentials near 0.5 volts vs. H^+/H_2 , necessary to achieve current densities up to 40 ma/cm^2 . Approximate linear relationships between current and gas phase

composition are obtained. The relative current contribution of octane is identical to that obtained for the binary propane-octane mixture. (i_8/I) is expressed by equation 4; for hexane:

$$i_6/I = 4.0 x_6 \quad 5.$$

c. Heptane/octane fuel mixtures.

The trends are similar to those obtained for the other binary mixtures (Figure 5). The current contribution of octane can be expressed by equation 4; for heptane:

$$i_7/I = 2.5 x_7 \quad 6.$$

4. General Relations

At high anodic overvoltage (0.5 volts vs. H^+/H_2) all current contributions can be represented by:

$$i_n/I = K x_n \quad 7.$$

where K represents a "fuel reactivity constant" representative of the molecular chain length of the paraffinic hydrocarbon.

Table II

Fuel Reactivity Constants for Various Fuels (at 0.5 volts vs H^+/H_2)

<u>Fuel</u>	<u>K-Value</u>
Propane	2.2
Hexane	4.0
Heptane	2.5
Octane	1.2

These results are presented in Figure 6. For hexane, heptane and octane the current contribution can be predicted from:

$$i_n/I = (13-1.5 n) x_n \quad 8.$$

where n represents the number of carbon atoms in the molecular chain. From pure fuel reactivity data reported by others², the expected reactivity constant for propane should be approximately $k_3 = 6.7$, whereas the measured value in the propane/octane mixture is only 2.2. This result may indicate competitive surface processes between hydrocarbon species of rather dissimilar chain lengths. C_1 and C_2 paraffinic hydrocarbons are expected to be less reactive than propane. C_9 and C_{10} n-paraffins are not expected to yield reactivity

constants appreciably different from n-octane.

The experimental results are presented in Figure 7 in terms of corrected current contributions, i.e. $i_p/13-1.5 n$ I vs. gas phase composition (using the experimental value of $K_3 = 2.2$ for propane). At present, the exact physical significance of the fuel reactivity coefficient is not clear.

CONCLUSION

The anodic electrochemical oxidation of binary fuel mixtures of hexane, heptane and octane can be predicted from the fuel gas phase composition and the relative reactivity of these fuels, which decreases with increasing chain length. The behavior of propane in propane/octane mixtures is unexpected, the propane reactivity decreasing with increasing anodic overvoltage.

ACKNOWLEDGMENT

This work is a part of the program under contract DA-44-009-AMC-479(T) with the U.S. Army Engineer Research & Development Laboratories, Fort Belvoir, Virginia, to develop a technology which will facilitate the design and fabrication of practical military fuel cell power plants for operation on ambient air and hydrocarbon fuels.

REFERENCES

1. Hydrocarbon-Air Fuel Cells, U.S. Army Engineer Research and Development Laboratories, Ft. Belvoir, Va., Contract No. DA-44-009-ENG-4909 and DA-44-009-AMC-479(T) - Reports 3 to 6.
2. Ibidem, Report No. 4
3. Niedrach, L.W. and H.R. Alford, Abstract No. 23, ECS Meeting, 1964, Washington, D.C.
4. Same reference as 1 - Report No. 6

PICTORIAL VIEW OF HYDROCARBON-AIR LIQUID ELECTROLYTE FUEL CELL TEST FIXTURE, SHOWING FLUID STREAMS

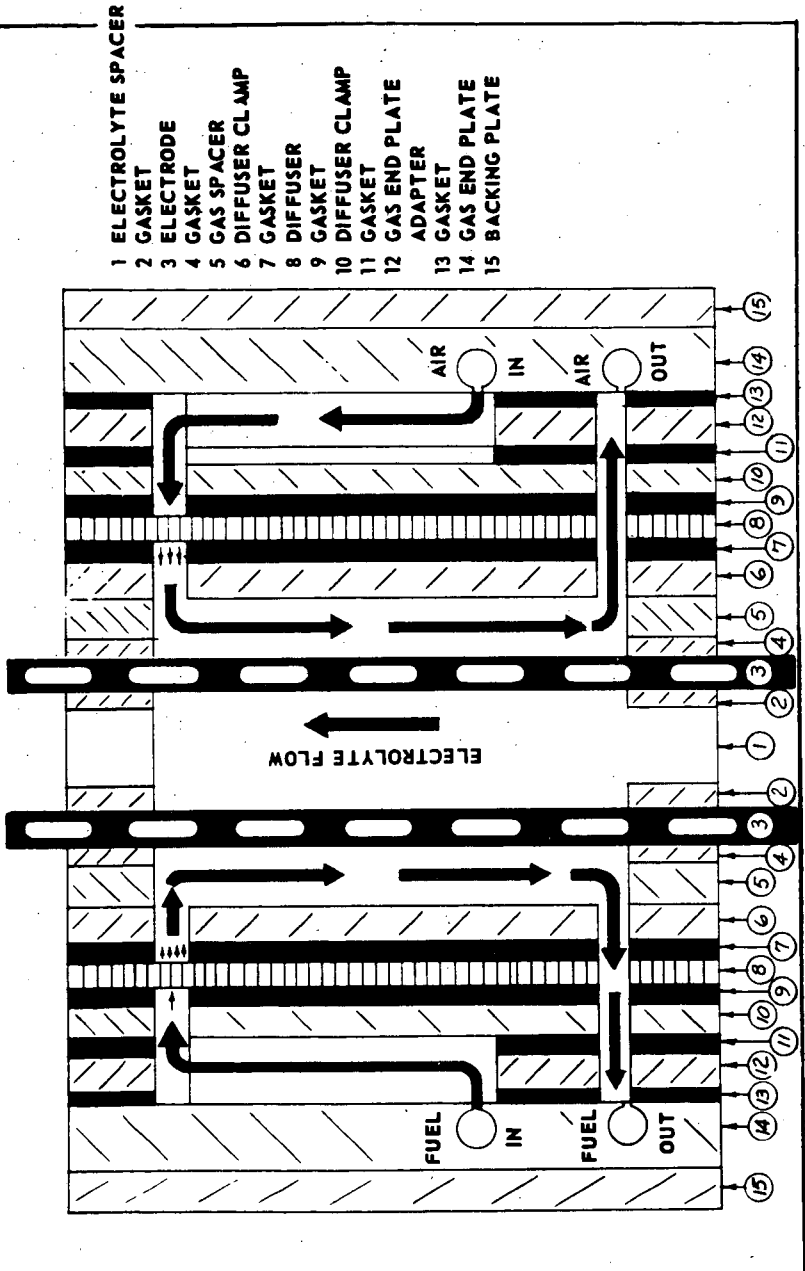


FIGURE 1

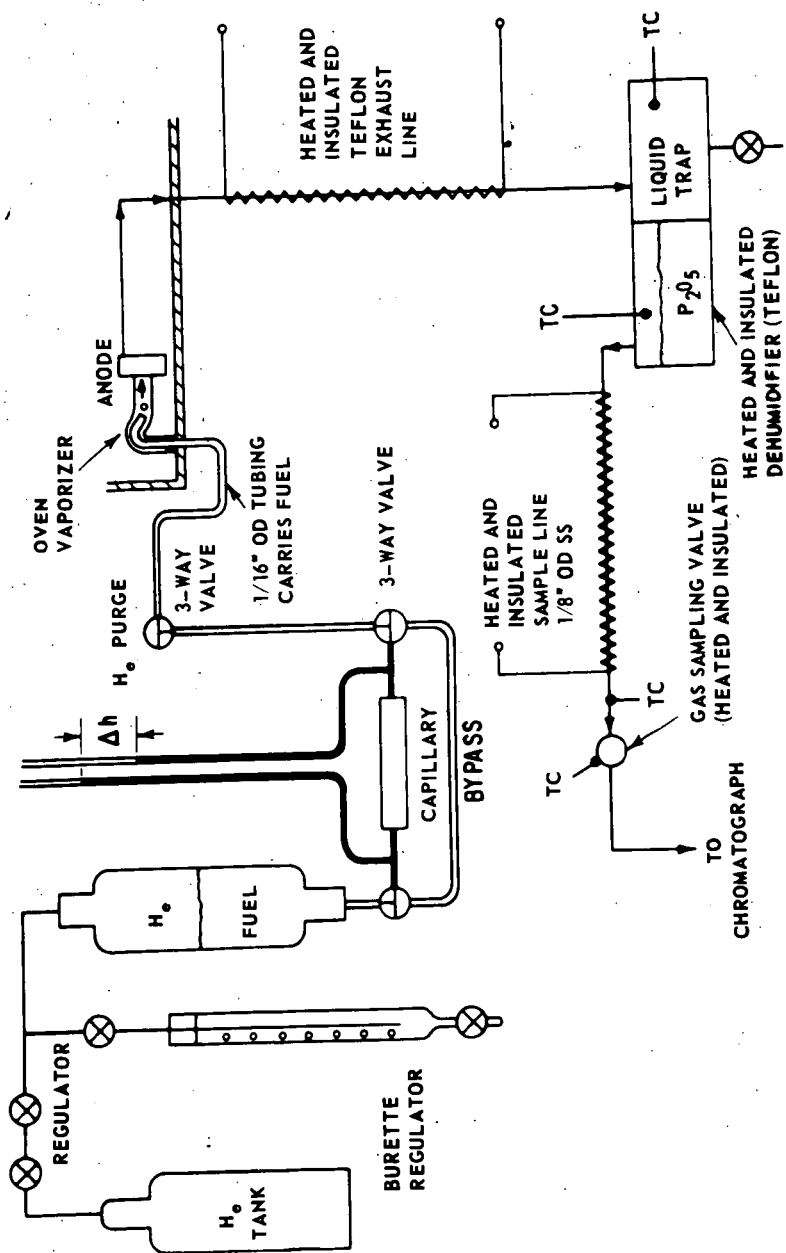


FIGURE 2 FUEL FEED AND EXHAUST FOR CHROMATOGRAPH SYSTEM FOR THE STUDY OF BINARY FUELS.

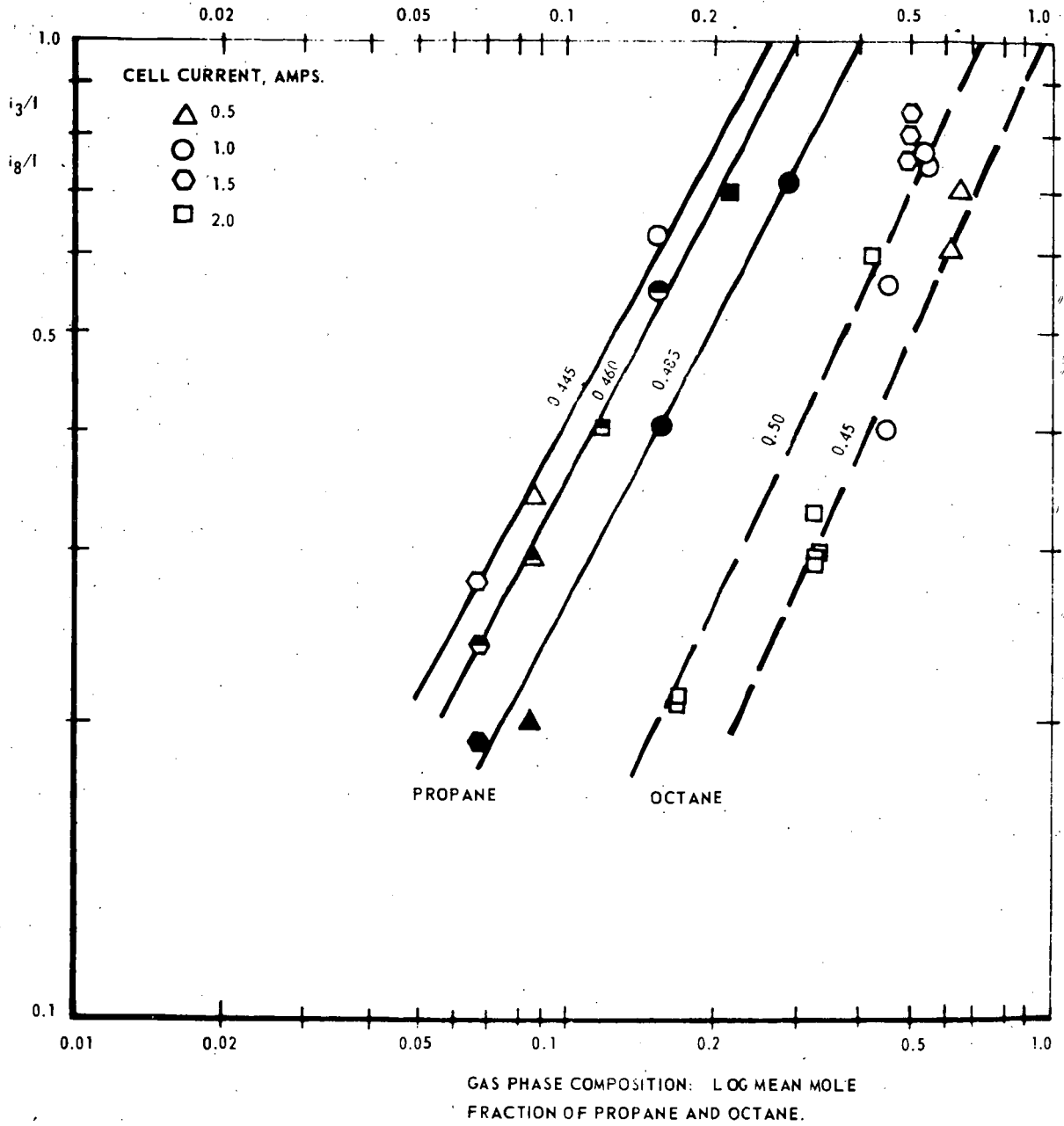


FIGURE 3: RELATIVE CURRENT CONTRIBUTION OF PROPANE AND OCTANE AS A FUNCTION OF ANODE POTENTIAL.

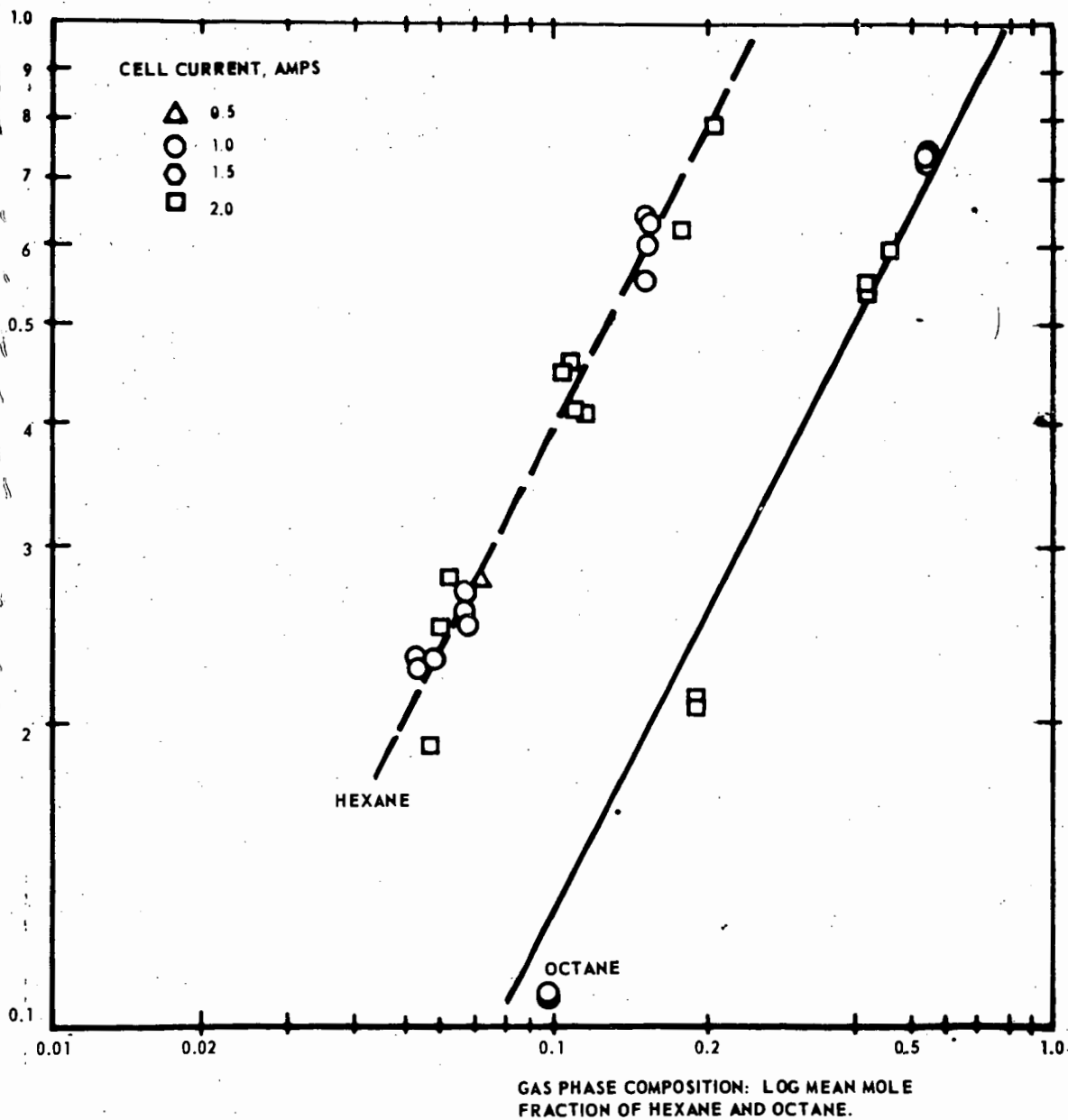


FIGURE 4: RELATIVE CURRENT CONTRIBUTION OF HEXANE AND OCTANE AT APPROX. 0.5 VOLTS ANODIC POTENTIAL.

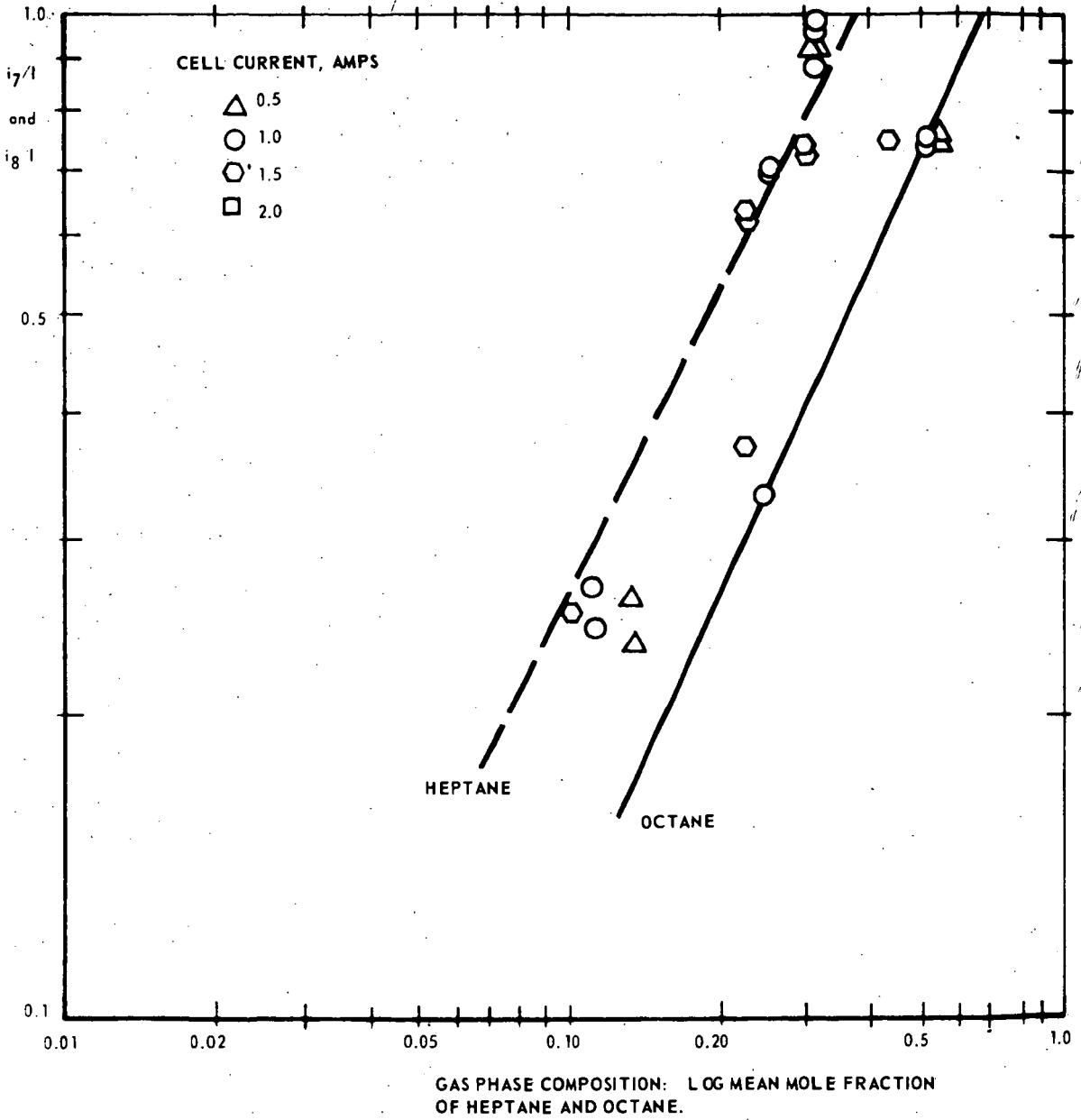


FIGURE 5: RELATIVE CURRENT CONTRIBUTION OF HEPTANE AND OCTANE AT APPROX. 0.5 VOLTS ANODIC POTENTIAL.

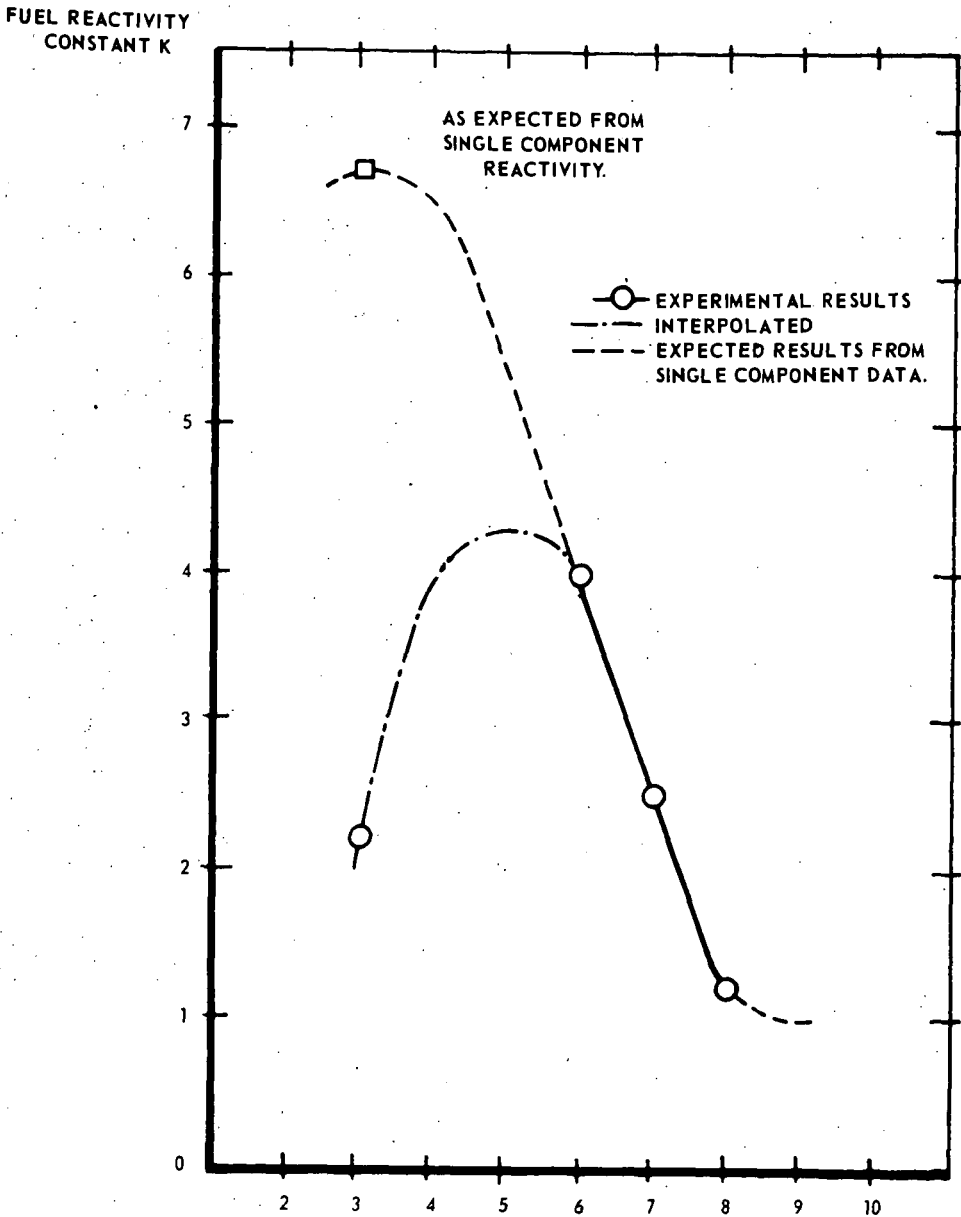


FIGURE 6: DEPENDENCE OF THE FUEL REACTIVITY CONSTANT K ON THE HYDROCARBON CHAIN LENGTH.

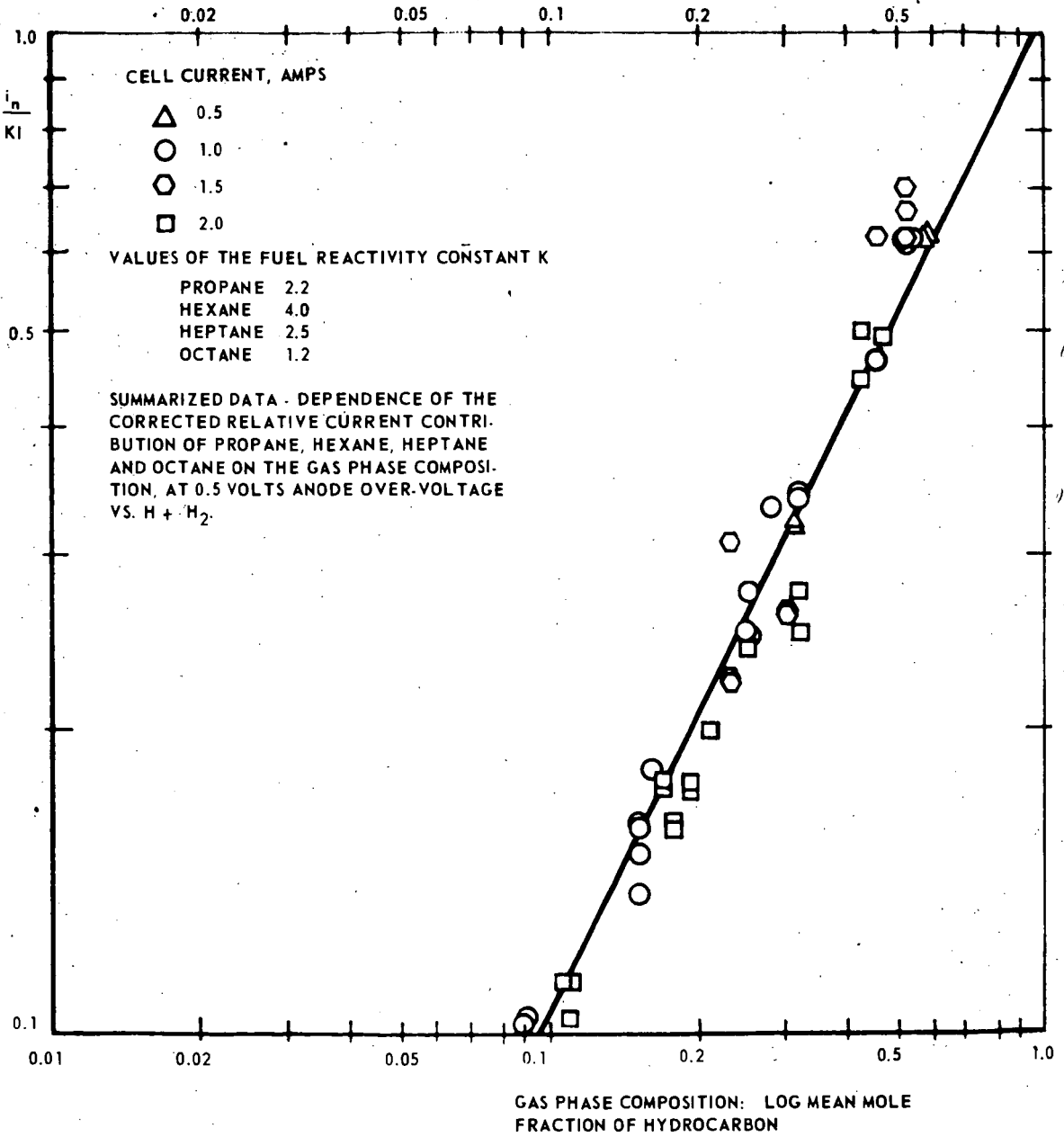


FIGURE 7

FLUORIDE ELECTROLYTES FOR SATURATED
HYDROCARBON FUEL CELLS

E. J. Cairns

General Electric Research Laboratory
Schenectady, New York

INTRODUCTION

The direct electrochemical oxidation of saturated hydrocarbons to carbon dioxide and water has been carried out at current densities in the vicinity of 100 ma/cm² only since 1963.¹⁻⁸ The most frequently investigated electrolyte in this connection has been phosphoric acid, primarily in the temperature range 150° to 200°C.¹⁻⁶ Although some success has been obtained with low molecular-weight hydrocarbons at about 100°C, this was at the expense of very high platinum loadings in the electrodes.^{7,8} It has been found recently that the system CsF-HF-H₂O provides electrolyte compositions with which current densities in excess of 200 ma/cm² can be obtained at 150°C, particularly with propane as the fuel.^{9,10} Further work with fluoride electrolytes disclosed that the HF-H₂O system showed good reactivity with saturated hydrocarbon fuels at temperatures in the range 80-110°C.¹⁰ All normal saturated hydrocarbons in the range C₁ to C₁₆ have shown reactivities within a factor of 20 to 50 of one another, both with the CsF-HF-H₂O and HF-H₂O electrolytes.¹⁰

Because of the strong effect of electrolyte composition on propane performance at 150°C,^{9,10} it was decided that a more thorough investigation of the effects of electrolyte composition and temperature on the kinetics of the anodic oxidation of propane was in order.

EXPERIMENTAL

In order to prevent any contamination of the electrolyte or electrodes, all portions of the apparatus which contacted the electrolyte were made of Teflon or platinum. The cell parts are shown in Figure 1. The end plates were Monel and did not contact the electrolyte. The gas compartments machined in the Teflon housing were 3 mm deep and of 11.38 cm² circular area. The electrodes used were Teflon-bonded platinum black supported by 45-mesh platinum screens, which also served as current collectors. The platinum black loading for the electrodes was usually 50 mg/cm², and the electrodes were prepared by procedures very similar to those in Reference 11. The center Teflon piece in Figure 1 served as the electrolyte compartment, and usually a piece having a 3 mm thickness was used. The cell parts were held together tightly by bolts; no gaskets were used since the Teflon parts formed a leak-tight seal to one another.

The electrolyte was prepared from Baker and Adamson reagent grade 48% hydrofluoric acid, having less than 20 ppm impurities; from cesium fluoride, synthesized with less than 100 ppm impurities by procedures already reported;^{12,13} and from quartz-redistilled water. To prepare electrolytes having fluoride concentrations higher than those accessible with the above reagents, pure, anhydrous HF was distilled from a tank of Matheson anhydrous HF, 99.9% min. purity. Electrolyte compositions were determined by acid-base titrations for HF, and by a gravimetric method for Cs as Cs₂SO₄; water was determined by difference.

The gases used were electrolytic grade oxygen, 99.6% minimum, and Matheson instrument grade propane, 99.5% minimum purity. For short experiments it was found that pre-saturation of the gases was not necessary in order to maintain the electrolyte composition constant. When necessary, presaturation could be accomplished by thermostatted water bubblers, in order to prevent possible deposition of carbon on the electrode surface.^{14,15}

Figure 2 shows a schematic diagram of the apparatus in which the cell was operated. The fuel feed rate was controlled via a needle valve and capillary-tube flowmeter in the case of gaseous fuels, and via a constant speed syringe drive in the case of liquid fuels. The fuel cell and identical reference cell were operated in a forced-convection air thermostat. The reference cell contained two high-area reversible hydrogen reference electrodes of Teflon-bonded platinum black. The exit gas streams from the cell passed through traps (to separate any liquid leaving the cell) and then to a gas chromatograph for analysis, as desired. The electrolyte was circulated slowly (about 2 to 3 cc/min) through the cells by gravity, and then returned to the reservoir by an all-Teflon pump. The electrolyte circulation system was kept closed to minimize evaporation.

The electrical characteristics of the anode, the cathode, and the cell as a whole were measured with the aid of a modified Kordes-Marko interrupter.^{16,17} The interrupter circuit yielded potential readings on a resistance-free basis, and all potentials of individual electrodes are so reported with respect to a reversible hydrogen reference electrode in the same electrolyte and at the same temperature. The current density-voltage data were taken at steady state (usually 2-5 minutes after a change in current) and in the order of increasing current density, starting at open circuit. Results for decreasing current densities were the same, except at current densities below about 2 ma/cm². Cell voltages, including resistive losses can be calculated from the reported IR-free values (E_{a-c}) using the expression

$$E = E_{a-c} - i\rho l \quad (1)$$

where i is the current density

ρ is the specific resistance of the electrolyte, 1-2 Ohm-cm

l is the inter-electrode distance, 0.3 cm.

Additional information concerning the experimental apparatus and techniques may be obtained from Reference 18.

The results reported below were gathered from a total of over 50 experiments using more than 20 cells, primarily with C₃H₈ as the fuel.

RESULTS AND DISCUSSION

CsF-HF-H₂O Electrolytes: There are two independent composition variables in the CsF-HF-H₂O system. The variables chosen to characterize the composition were the HF/(CsF + HF) molar ratio (or, alternatively, the F⁻/Cs⁺ equivalent ratio), and the mole percent H₂O. The effects of the two independent composition variables on the rate of anodic oxidation of propane were studied by preparing electrolytes of selected compositions and determining the current density-potential relationship for propane at various temperatures, most frequently at

150°C.

The propane performance at an electrolyte composition near the optimum for 150°C is shown in Figure 3. The maximum current density that could be supported under these conditions was 400 ma/cm², at an anode vs H₂ reference potential of 0.6 volt. For all the cells operated at 150°C, the best straight-line Tafel plots yielded an α_n value of 0.5 in the current density range of 40 to 250 ma/cm². In the current density range above 250 ma/cm², the anode performance could be improved by increasing the propane flow rate, up to a certain point, indicating a gas-phase mass transport limitation, rather than a kinetically limited current density.

The most striking relationship between electrolyte composition and propane performance at 150°C was found in a set of experiments which included electrolytes containing varying amounts of Cs₂CO₃ as an alternative to excess HF. The results are expressed in terms of the current density at an anode vs reference potential of 0.5 volt, as a function of the F⁻/Cs⁺ ratio, as shown in Figure 4. The water content was not the same for all of the experiments of Figure 4; the effect of this variable will be accounted for below. The data points in Figure 4 were obtained from several cells. Each datum point represents an average value for all cells operated at that particular F⁻/Cs⁺ ratio. Note that the break in the curve in Figure 4 is located at an F⁻/Cs⁺ ratio of about 1.2 rather than 1.0. At a F⁻/Cs⁺ ratio of 1.0, the pH is still greater than 7. The pH does not drop below 7 until the F⁻/Cs⁺ ratio exceeds about 1.2. The increase of performance with higher F⁻/Cs⁺ ratios is consistent with the idea that an acidic electrolyte is required for rapid oxidation of saturated hydrocarbons. The maximum rate of propane oxidation at E_{a-r} = 0.5 volt was 400 ma/cm², nearly 2 orders of magnitude greater than that observed for the alkaline system Cs₂CO₃-H₂O.¹⁹

It was found that the water content of the electrolyte also has an influence on the rate of propane oxidation, but its effect is much less than that of the HF/(CsF + HF) ratio. The separation of the effects of the two composition variables on cell performance was accomplished by an iterative data reduction procedure requiring a considerable number of data points. The value of HF/CsF = 2.0 was chosen for the point at which the effect of water content at 150°C would be determined, since this was in the vicinity of the best performance. The data in the range 1.8 < HF/CsF < 2.1 were normalized to HF/CsF = 2.0, and the effect of water content was established. The original data of Figure 4 were then normalized to an optimum water content of 12.5 mole percent and were replotted as shown by the solid line in Figure 5. The effect of water content at 150° is shown in Figure 6, for two values of the anode vs reference potential.

The results for other operating temperatures were reduced in a similar manner, using the iterative procedure. The final results for the effect of electrolyte composition on propane performance at several temperatures are shown in Figures 7 and 8. Some of the data used were not gathered at the temperature values selected for correlation. In these cases, the current densities were adjusted to correspond to the desired temperature, using the observed enthalpies of activation. These adjusted data points are indicated as extrapolated in Figures 7 and 8.

The results in Figures 7 and 8 show that for any temperature in

the range 90 to 150°C, the maximum propane performance can be obtained by using the highest HF/(CsF + HF) ratio possible, and a water content in the range 12-15 mole percent. In this way, current densities in excess of 400 ma/cm² at E_{a-r} = 0.5 volt and 150°C can be expected, in the absence of mass transport limitations.

It has been found that the HF/CsF ratio at any selected temperature has a maximum practical limit set by the boiling point of the electrolyte under the conditions of operation. For instance, a boiling point of 160°C was obtained for an electrolyte having 10 mole percent water and a value of 2.1 for the HF/CsF ratio. This limits the operating temperature at atmospheric pressure to about 150-155°C. At lower temperatures, higher HF/CsF ratios are possible. For example, values of 3.0 and higher may be obtained at 110°C.

The main virtue of the CsF is that of suppressing the vapor pressure of the HF by forming stable complexes such as CsF·HF, CsF·2HF, etc.,²⁰ raising the boiling point of the electrolyte. Therefore, higher operating temperatures can be used with a concomitant increase in current densities for the oxidation of saturated hydrocarbons. Alkali metal fluorides other than cesium fluoride or rubidium fluoride are not suitable substitutes because they are not soluble enough and do not reduce the HF vapor pressure sufficiently^{21,22} to allow significant performance improvements. Cesium fluoride was used in this work because of its greater abundance and therefore more favorable economics.

HF-H₂O Electrolytes: The rate of electrochemical oxidation of propane in the HF-H₂O system is affected by the composition of the electrolyte, and since there is only one composition variable, the optimum composition for a given temperature is easily established. The temperature range over which reasonable rates of oxidation were obtained was found to be from about 80°C to the boiling point. The HF-H₂O system forms a maximum boiling azeotrope at 37 mole percent HF, with a boiling point of 112°C,²³ thus setting the upper operating temperature at about 110°C.

The Tafel plots for a propane cell at 105°C, using a composition near that of the azeotrope, are shown in Figure 9. The performance at 105°C is not as high as the best obtained at 150°C (see Figure 3), but only a moderate performance premium was paid for a 45°C decrease in operating temperature. The maximum current density observed (130 ma/cm²) was set by the gas-phase diffusional resistance of the Teflon film on the anode, as shown by the fact that higher maximum current densities were observed when thinner Teflon films were used. The effects of both temperature and HF-H₂O electrolyte composition on cell performance are summarized in Figure 10. The dotted portions of the curves indicate those compositions which have a boiling point below the indicated temperature and hence are only accessible at pressures above atmospheric. Since the optimum composition (25-30 mole percent HF) is not far from that of the azeotrope, it has been found convenient to use the azeotrope for routine fuel cell operation.

Enthalpies of Activation and Tafel Slopes: The enthalpy of activation for the overall anode reaction was obtained from a plot of the logarithm of the current density at a fixed anode overvoltage versus the reciprocal of the absolute temperature. The enthalpy of activation was determined over the temperature range 80 to 170°C and over the composition range from no added HF to pure HF. The results

are shown in Figure 11. It was found that the temperature range had no effect on the enthalpy of activation, but that there was a sharp transition from a value of 3.7 kcal per mole to 18 kcal per mole at a $\text{HF}/(\text{CsF}+\text{HF})$ ratio of about 0.66, which corresponds to $\text{CsF}\cdot 2\text{HF}$. The higher enthalpy of activation indicates that the highest operating temperature possible should be used, but only up to the point of being able to maintain a $\text{HF}/(\text{CsF}+\text{HF})$ ratio above 0.66.

The values of αn obtained from the Tafel plots over the temperature range 80° to 170°C are summarized in Figure 12. The closed points indicate those data which were normalized with respect to electrolyte composition effects. At low temperatures (below 130°C), the Tafel plots usually showed two straight-line regions, a low slope (high αn) at low current densities ($<10 \text{ ma}/\text{cm}^2$) and a high slope (low αn) at high current densities ($>20 \text{ ma}/\text{cm}^2$). For temperatures above 140°C , only one Tafel slope was observed, with a value of αn near 0.5.

The composition effect on Tafel slopes is shown for various temperatures in Figure 13. At 150°C , for electrolytes of low HF content, the Tafel curve shows two slopes, which eventually yield to a single slope of $\alpha n \approx 0.5$ at high HF contents. For the higher $\text{HF}/(\text{CsF}+\text{HF})$ ratios at lower temperatures, however, the two-sloped Tafel curve persists. Only slight changes of Tafel slope with water content have been observed. In general, the best propane performance is associated with compositions which show a high enthalpy of activation and αn values of 0.5 and higher. By suitably adjusting electrolyte compositions and temperatures, the optimum performances shown in Figure 14 were obtained. The 150°C curve was obtained using an electrolyte of the composition shown in Figure 3.

CONCLUSIONS

The relationships between the rate of the electrochemical oxidation of propane on platinum black and electrolyte composition for the systems $\text{CsF}-\text{HF}-\text{H}_2\text{O}$ and $\text{HF}-\text{H}_2\text{O}$ have been established. Maximum propane fuel cell performance at a given temperature in the range $90 - 150^\circ\text{C}$ is obtained with the maximum $\text{HF}/(\text{CsF}+\text{HF})$ ratio, at an optimum water content of 12 to 15 mole percent, for the range $\text{HF}/\text{CsF} = 2.0$ to 3.0 . Operating temperatures down to 80°C are feasible for the $\text{HF}-\text{H}_2\text{O}$ system, while retaining good propane performance. Power densities (on an IR-free basis) of $80 \text{ milliwatts}/\text{cm}^2$ at 150°C and $30 \text{ milliwatts}/\text{cm}^2$ at 105°C are possible in optimum composition fluoride electrolytes.

ACKNOWLEDGMENTS

It is a pleasure to thank E.J. McInerney, A.M. Breitenstein, and L.D. Sangermano for their contributions to this work. Helpful discussions were provided by W.T. Grubb and E.L. Simons.

This work is a part of the program under contracts DA-44-009-AMC-479(T) and DA-44-009-ENG-4909, ARPA Order No. 247 with the U.S. Army Engineer Research & Development Laboratories, Ft. Belvoir, Virginia, to develop a technology which will facilitate the design and fabrication of practical military fuel cell power plants for operation on ambient air and hydrocarbon fuels.

REFERENCES

1. General Electric Company, Press Release (April 23, 1963).
2. W.T. Grubb and L.W. Niedrach, J. Electrochem. Soc., 110, 1086 (1963).
3. H.G. Oswin, A.J. Hartner and F. Malsapina, Nature, 200, 256 (1963).
4. W.T. Grubb and C.J. Michalske, Nature, 201, 287 (1963).
5. R. Jasinski, J. Huff, S. Tomter and L. Swette, Ber. der Bunsengesellschaft, 68, 400 (1964).
6. W.T. Grubb and C.J. Michalske, J. Electrochem. Soc., 111, 1015 (1964).
7. H. Binder, A. Kohling and G. Sandstede, paper presented at Washington, D.C. meeting of the Electrochem. Soc., Abstract No. 11 (Oct. 1964).
8. H. Binder, A. Kohling, H. Krupp, K. Richter and G. Sandstede, J. Electrochem. Soc., 112, 355 (1965).
9. E.J. Cairns and G.J. Holm, paper presented at the Washington, D.C. meeting of the Electrochem. Soc., Abstract No. 30, (Oct. 1964); see also extended Abstracts of the Battery Division.
10. E.J. Cairns, paper presented at the San Francisco meeting of the Electrochem. Soc., Abstract No. 140, (May 1965); see also extended Abstracts of the Electro-Organic Division.
11. L.W. Niedrach and H.R. Alford, J. Electrochem. Soc., 112, 117 (1965).
12. E.L. Simons, E.J. Cairns and L.D. Sangermano, Gen. Elec. Research Laboratory Report No. 64-RL-3689C (June 1964).
13. E.L. Simons, E.J. Cairns and L.D. Sangermano, Electrochem. Tech., 2, 355 (1964).
14. E.J. Cairns, A.D. Tevebaugh, and G.J. Holm, J. Electrochem. Soc., 110, 1025 (1963).
15. E.J. Cairns and A.D. Tevebaugh, J. Chem. Eng. Data, 9, 453 (1964).
16. K. Kordesch and A. Marko, J. Electrochem. Soc., 107, 480 (1960).
17. E.J. Cairns and A.D. Tevebaugh, Saturated Hydrocarbon Fuel Cell Program, Technical Summary Report No. 3, Part I - Task IV, Jan. 1 - June 30, 1963, Contract No. DA-44-009-ENG-4909, ARPA Order No. 247, Project No. 8A72-13-001-506, USAERDL.
18. E.J. Cairns and D.C. Bartosik, J. Electrochem. Soc., 111, 1205 (1964).
19. E.J. Cairns and D.I. Macdonald, Electrochem. Tech., 2, 65 (1964).

20. R.V. Windsor and G.H. Cady, J.A.C.S., 70, 1500 (1948).
21. G.H. Cady, J.A.C.S., 56, 1431 (1934).
22. E.B.R. Prideaux and K.R. Webb, J. Chem. Soc., 1937, 2.
23. R. Vieweg, Chem. Techn. 15, 734 (1963).

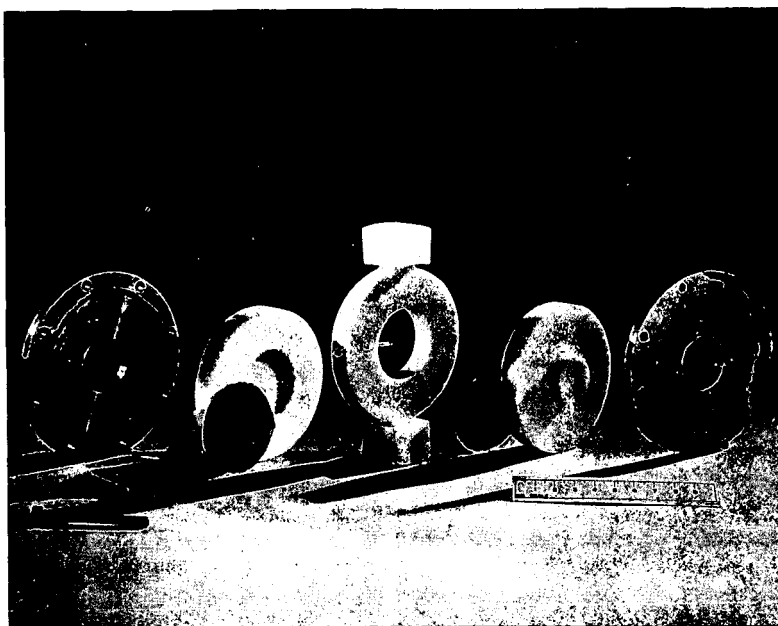


Figure 1. Photograph of cell parts.

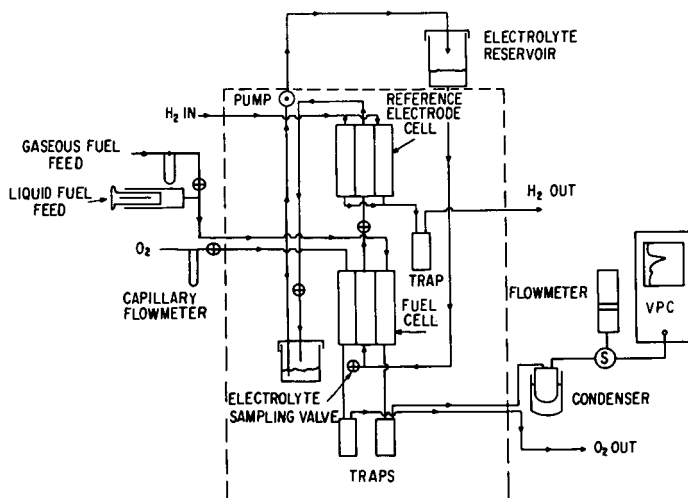


Figure 2. Schematic diagram of fuel cell apparatus.

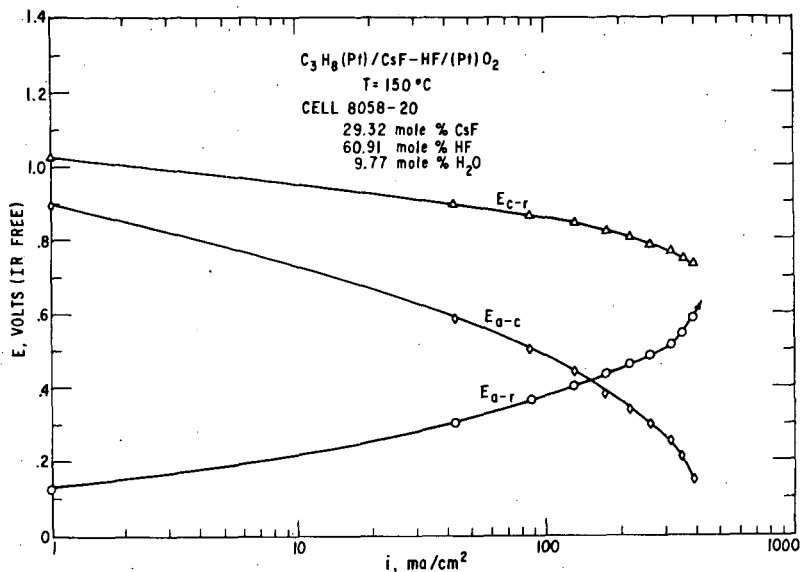


Figure 3. Propane performance at 150°C using CsF·2.1 HF + 15 mole percent water as electrolyte.

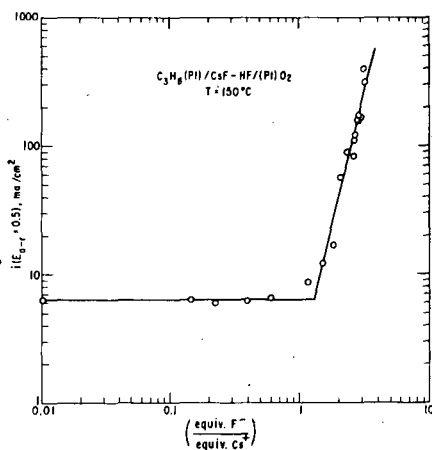


Figure 4. Effect of F^-/Cs^+ ratio on propane current density at $E_{a-r} = 0.5$ V; 150°C.

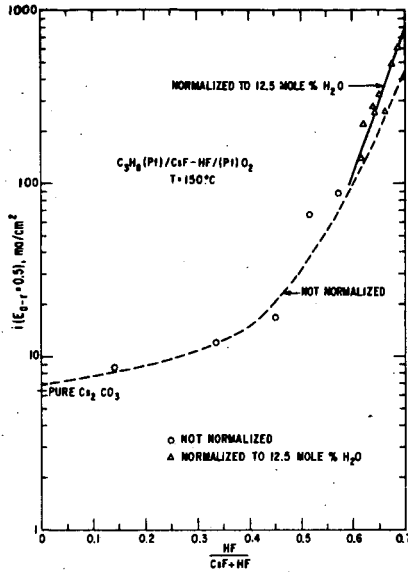


Figure 5. Effect of electrolyte HF content on propane performance for: Δ 12.5 mole % H_2O ; \circ variable water content; $150^\circ C$.

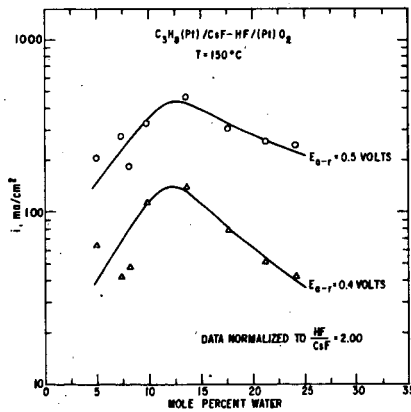


Figure 6. Effect of electrolyte water content on propane performance for: \circ $E_{a-r} = 0.5$ V; Δ $E_{a-r} = 0.4$ V; at $150^\circ C$ and $HF/CsF = 2.00$.

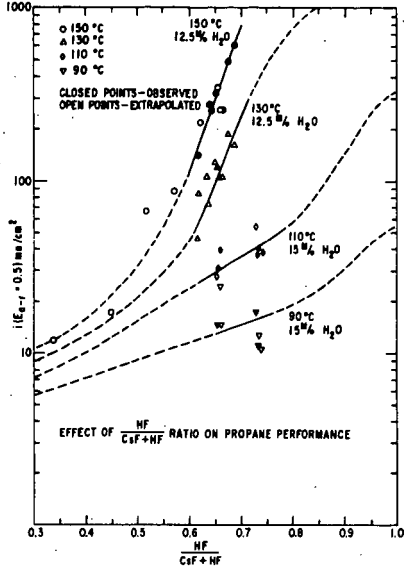


Figure 7. Effect of electrolyte HF content on propane performance for various temperatures and water contents.

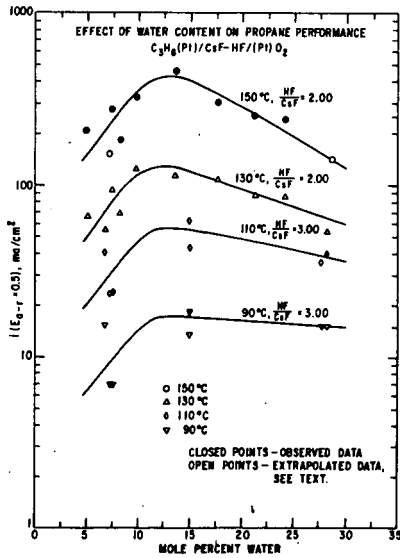


Figure 8. Effect of electrolyte water content on propane performance for various temperatures and HF contents.

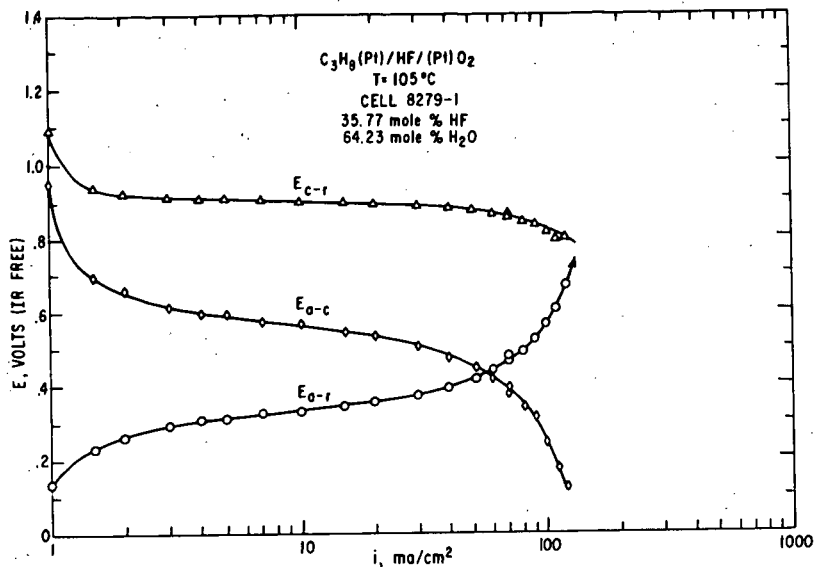


Figure 9. Propane performance at 105°C with 37 mole % HF electrolyte.

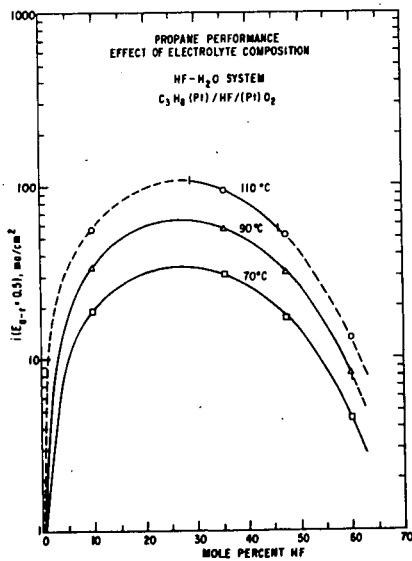


Figure 10. Effect of $HF-H_2O$ electrolyte composition on propane performance at various temperatures.

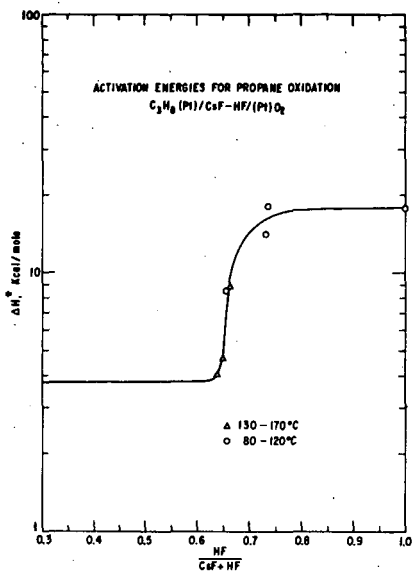


Figure 11. Effect of electrolyte composition on enthalpy of activation for propane oxidation.

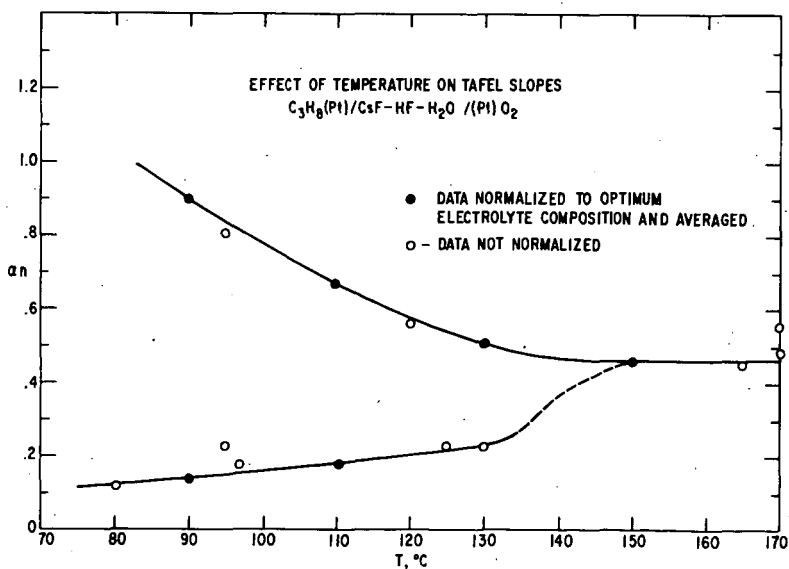


Figure 12. Effect of temperature on values of αn obtained from Tafel plots of propane performance.

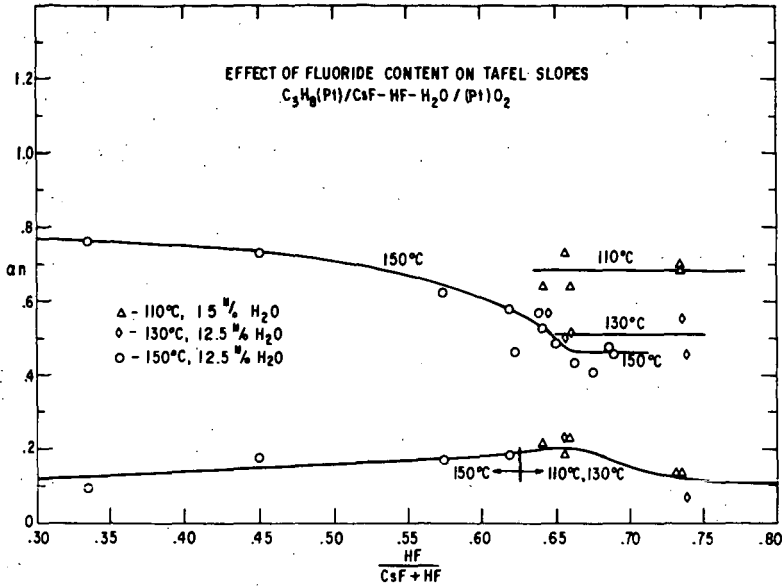


Figure 13. Effect of electrolyte composition on value of αn for various temperatures.

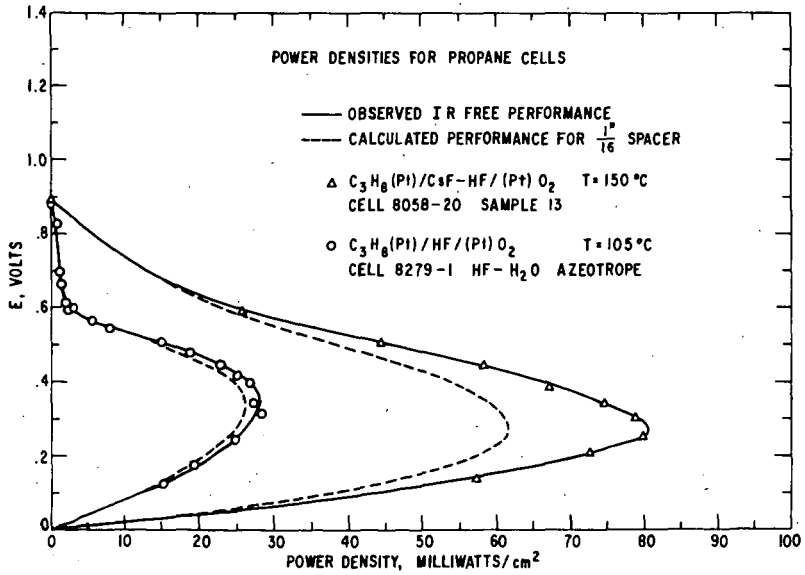


Figure 14. Propane performance at optimum electrolyte compositions for 150° and 105°C.

THE APPLICATION OF INORGANIC MEMBRANES IN HYDROCARBON FUEL CELLS

C. Berger, Ph. D.
M. P. Strier, Ph. D.

Astropower Laboratory
Missile and Space Systems Division
Douglas Aircraft Company, Inc.

1.0 INTRODUCTION

The expansion of laboratory efforts in fuel cells in the last several years has been noted for its urgency and aggressiveness. Three broad categories of fuel cell systems have evolved - the ion membrane, the liquid electrolyte (including electrolytes absorbed in asbestos) and high temperature electrolytes including fused salt matrices and ceramic bodies.

In this paper we shall concentrate on the activities of our laboratories in the area of inorganic ion exchange membranes. For those readers desiring to establish a background in the various organic membrane fuel cell types suitable references are available (1, 2, 3, 4, 5).

It is interesting to note that the first synthetic ion exchangers were also inorganic, i. e., the synthetic zeolites or Permutits⁽⁶⁾. The subsequent development of the organic exchanger resins, with emphasis on practical applications, completely dominated the field of ion exchange chemistry, and it was not until recently that, for the reasons mentioned below, there has been a resurgence of interest in inorganic exchangers and membranes.

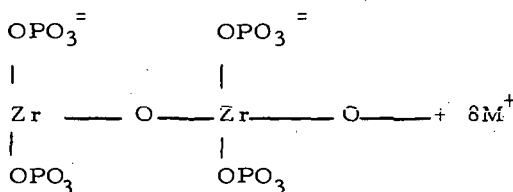
During recent years there has been considerable research on inorganic cation exchangers. The heteropolyacid salts, such as ammonium phosphomolybdate, and the acid salts of hydrous oxides, such as zirconium phosphate have proven to be particularly interesting and their investigation by numerous researchers has been well documented in a monograph by Amphlett⁽⁶⁾. Much less attention has been given to inorganic anion exchangers. Kraus, et al,⁽⁷⁾ as well as Amphlett, ⁽⁸⁾ have investigated the anion exchange properties of various hydrous oxides, particularly the quadrivalent metal oxides, such as ZrO_2 , SnO_2 , ThO_2 , and TiO_2 . Duwell and Shepard⁽⁹⁾ have prepared mixed hydrous oxides anion exchangers in which a second cation of higher valence than the parent cation is introduced into the structure, the resulting net positive charge being balanced by the presence of exchangeable anions. Schoenfeld⁽¹⁰⁾ has done similar research on mixed oxide anion exchangers and has studied the relation between capacity and drying temperature of the precipitated gel.

Preliminary efforts in developing and characterizing inorganic membranes were made by Dravnieks et al⁽¹¹⁾, and Hamlen⁽¹²⁾. Membranes produced during these investigations were essentially non adherent compacts or membranes produced by using teflon as a sintering adhesive. These experimental materials were suitable for obtaining some analytical values but lacked the strength to serve as practical fuel cell membranes. Moreover, they possessed no capability for extended operation at higher temperatures such as $90^\circ - 150^\circ C$. The latter capability is particularly of interest since the temperature range mentioned apparently is at least a minimal practical requirement for hydrocarbon utilization in phosphate based fuel cells⁽¹³⁾. Another implied requirement and one that indeed is most important is the

ability to retain water in the membrane so that efficient electrolyte conductance can be established. It is toward these ends and the attainment of high strength, and high electrolytic conductance and good water retention that the Astropower Laboratories has striven^(14, 15). A good measure of success has been achieved and the results are reported below.

The principal membrane activity has been focused on the inorganic polymer, $ZrPO_4$. Essentially, the reason for our interest in this polymer is that a good deal of laboratory information exists relative to this material and considerable success has been achieved in these laboratories in developing strong conductive zirconium phosphate. The phosphate group as noted above appears to have interesting properties in hydrocarbon oxidation⁽¹³⁾.

Tests of the cation exchange capacity of zirconium phosphate in these laboratories have duplicated results of other investigators^(7, 8). The structure of zirconium phosphate as an inorganic polymer with exchangeable H^+ ions attached to fixed ionic groups has been proposed by other investigators as⁽¹⁶⁾,



where the M^+ are hydrogen ions or exchangeable cations attracted to the negatively charged phosphate groups. It seems reasonable to assume that there are two exchange sites per phosphate group, corresponding to the two dissociable hydrogens, and this assumption was the basis for calculating the theoretical cation exchange capacity of 13.3 meq/g. Table I indicates the theoretical and actual capacities of three cation exchangers⁽¹⁷⁾. The observed capacity of 3.2 meq/g at pH 6, however, would seem to indicate that only one hydrogen per phosphate group is replaceable, and hence the maximum attainable capacity may be 6.65 meq/g. Kraus⁽⁷⁾ has made similar observations concerning the number of replaceable hydrogens.

Clearly a number of acid salts may have utility as hydrogen-oxygen fuel cells as well as having applications in hydrocarbon fuel cells. The investigation of such salts has been performed in these laboratories⁽¹⁵⁾ and by European investigators⁽¹⁸⁾. The latter made successful fuel cell membranes from tin and titanium phosphates by joining the particulate phosphates with organic binders such as carboxymethyl cellulose. The membranes gave satisfactory results at 25°C but do not appear satisfactory for applications at elevated temperatures.

The use of solid acid phosphate membranes has advantages over liquid phosphoric acid as an electrolyte medium for hydrocarbon oxidation. Principally, these are compactness, position insensitivity, and, in particular, lack of corrosive attack. In the investigation of these membranes several technical factors have combined to furnish us with a good solid electrolyte for hydrocarbon utilization and testing. These are:

1. Special techniques for forming strong cohesive membranes⁽¹⁵⁾.
2. The attainment of high conductivities⁽¹⁴⁾.

3. The ability, if required to implant catalyst materials directly in the membrane^(14, 15).
4. The incorporation of water balancing agents, which enable the fuel cell electrolyte to operate as high as 150°C⁽¹⁵⁾.
5. Hydrolysis tests indicating the inherent stability of the inorganic phosphate membrane⁽¹⁴⁾.

2.0 EXPERIMENTAL

2.1 Membrane Preparation - Non-Sandwich Type

A 1:1 - mixture ratio of ZrO_2 and H_3PO_4 was prepared and sintered at a temperature of 500°C. The sintered materials were crushed and ground to minus 80 mesh and mixed with equal parts of H_3PO_4 and "Zeolon H" a Norton Company sieve material. The "Zeolon H" is one of a group of water balancing agents developed and used at Astropower Laboratory in these experiments⁽¹⁵⁾. These mixtures were dried for 16 hours at 130°C and then granulated to minus 32 plus 80 mesh. Next, they were pressed at 15-ton load into 2-in. diameter membranes having the thickness of the order of 0.7 mm. Finally they were sintered at temperatures of 500°C for two hours. The transverse break strengths of these resulting membranes were determined and were about 5000 psi \pm 100. The resistivities of the membrane was about 4 ohm-cm at 110°C and 100% R. H.

2.2 Membrane Preparation - Sandwich Type

Basically, this technique involves the formation of a fuel cell membrane catalyst composite consisting of three layers of material which are pressed and sintered together. The center layer is comprised of membrane material similar to the mix described in 2.1, and the two outer layers which are bonded to the center layer are mixtures of the same membrane material and platinum black. The composite three-sectional membrane was formed in the following manner:

A weighed amount of the platinum-bearing material is placed in the pressing die, followed by a layer of the membrane material and a second layer of the catalyst-bearing material. The top punch is then inserted and the assembly (two-inch diameter) is pressed at 15 tons total load. After pressing the composites are placed on flat, smooth refractory plates and sintered in air for two hours at 500°C. After cooling to room temperature, the composite membrane-catalyst wafer was impregnated with 85% phosphoric acid, oven-dried at 120°C and sintered at 500°C for two hours. This impregnation procedure was repeated two more times.

2.3 Fuel Cell Assembly and Operation

A design of a typical fuel cell unit is shown in Figure 1. Assembly of the fuel cell is performed by placing either type of membrane in the recessed metal casing which has been treated with a film of silicone resin. Platinum or palladium powder is sprinkled on both surfaces of the membrane and screen electrodes pressed up against the catalyst on either side. When sandwich membranes are used, additional catalyst is not required. The catalyst loading is a total of .025 g. cm^{-2} . The O-rings are put in place and the assembly bolted together. The flow rate of the hydrocarbon is 2 cm^3 min^{-1} and for oxygen 4 cm^3 min^{-1} . The entire configuration is operated in an oven in the temperature range 50° - 150°C.

3.0 RESULTS

The performance of the fuel cell configuration when fueled with hydrogen and oxygen were encouraging in proving the capability for operation of the "water" balanced zirconium phosphate in the temperature range extending from about 50°C to 150°C. Some of the results obtained for the hydrogen-oxygen system are shown in Figure 2. The duration of the fuel cell performance depicted graphically range from 300 - 1000 hours⁽¹⁴⁾. The stable performance of the system over the 50°C - 150°C led us to believe that it was suitable for preliminary tests as a hydrocarbon fuel cell.⁽¹⁵⁾

Efforts were then initiated with hydrocarbon fuels and oxygen. These were ethane, propane, butane and propylene. Pertinent data is shown in Figure 3 for propylene, Figure 4 for ethane, Figure 5 for propane and Figure 6 for butane. Polarization points were recorded after five minutes of stabilized performance.

4.0 DISCUSSION

Figure 2 is illustrative of the fact that the membrane system employed is functional over the range 50° - 150°C. Attempts to move to higher temperatures have led to deterioration of fuel cell performance. This can be attributed to the lack of effectiveness of the "water balancing" agent contained in the membrane. A secondary effect, perhaps, is that the partial pressure of water in the vicinity of the electrode-catalyst may thereby become considerably higher, making access of the hydrocarbon and oxygen to the reaction interface more difficult.

Figure 3 for propylene indicates that performance of the hydrocarbon fuel cell appears to improve with elevated temperature, (as would be anticipated) until the vicinity of 150°C is attained. This does not preclude improved performance (with temperature) but indicates that a satisfactory electrolytic conductive mechanism could not be maintained at 150°C due to "water balancing" agent deficiency. Tests in these laboratories⁽¹⁵⁾ have indicated that other "water balancing" materials may be more effective.

5.0 CONCLUSIONS

1. The essential element in the maintenance of an electrolytic conductance in a fuel cell membrane at elevated temperatures is the presence of a water balancing agent. An exception may be that the membrane itself may have this property.
2. Phosphate based inorganic membranes serve as a suitable electrolytic environment for hydrocarbon oxidation in fuel cells between 100 - 150°C.

6.0 ACKNOWLEDGMENTS

We wish to express our appreciation for the laboratory efforts contributed by A. Rosa and G. Belfort in the various aspects of our hydrogen-oxygen fuel cell work and our hydrocarbon fuel cell endeavors. We also wish to express our appreciation for the support of the Astropower Laboratory, Missile and Space Systems Division, Douglas Aircraft Company, for their support of our effort in hydrocarbon fuel cells and the National Aeronautics Space Administration, Lewis Research Center, Cleveland, Ohio, for their support of our hydrogen-oxygen fuel cell efforts under Contract NAS 7-6000 (1962 -).

TABLE I
THEORETICAL AND OBSERVED CAPACITIES
FOR INORGANIC CATION EXCHANGERS

<u>Gel</u>	<u>Assumed Mathematical Ratios for Calculating Theoret. Capacity</u>	<u>Molecular Weight</u>	<u>Theoret. Capacity</u>	<u>Observed Capacity (meq/g)</u>
Zirconium phosphate	$\begin{array}{c} \text{H}^+ \\ \text{H}^+ \text{OPO}_3^- \\ \\ \text{-Zr-O-} \\ \\ \text{H}^+ \text{OPO}_3^- \\ \\ \text{H}^+ \end{array} \quad n$	301n	13.3 (6.65)*	3.2
Zirconium tungstate	$\begin{array}{c} \text{H}^+ \\ \text{H}^+ \text{OWO}_3^- \\ \\ \text{-Zr-O-} \\ \\ \text{H}^+ \text{OWO}_3^- \end{array} \quad n$	605n	3.3	2.1
Thorium phosphate	$\begin{array}{c} \text{H}^+ \\ \text{H}^+ \text{OPO}_3^- \\ \\ \text{-Th-O-} \\ \\ \text{H}^+ \text{OPO}_3^- \\ \\ \text{H}^+ \end{array} \quad n$	442n	9.05 (4.52)*	2.0

*Value in parentheses represents theoretical capacity if only one hydrogen ion per phosphate group is exchangeable.

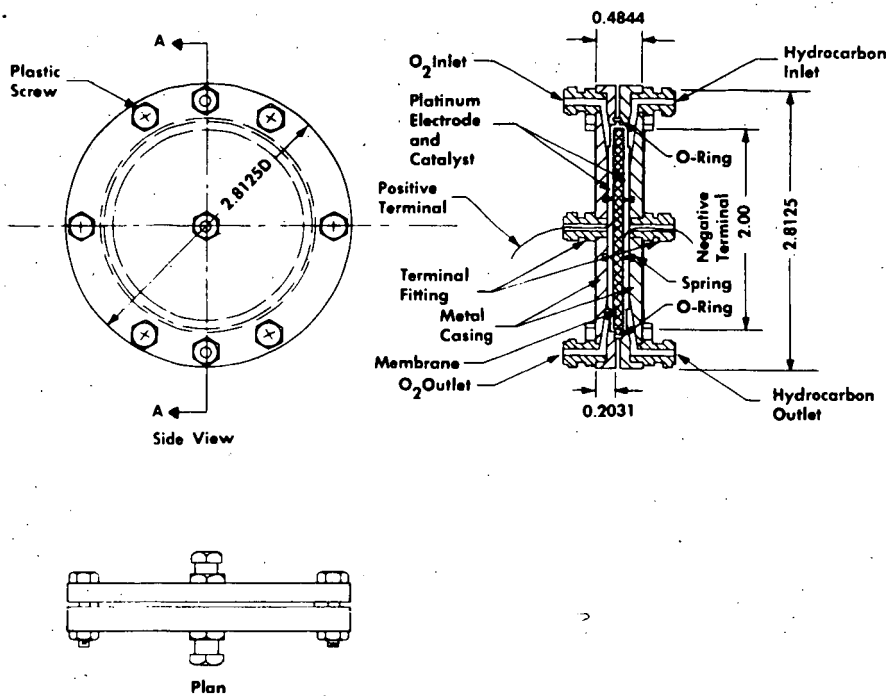


Figure 1. Hydrocarbon Test Fuel Cell

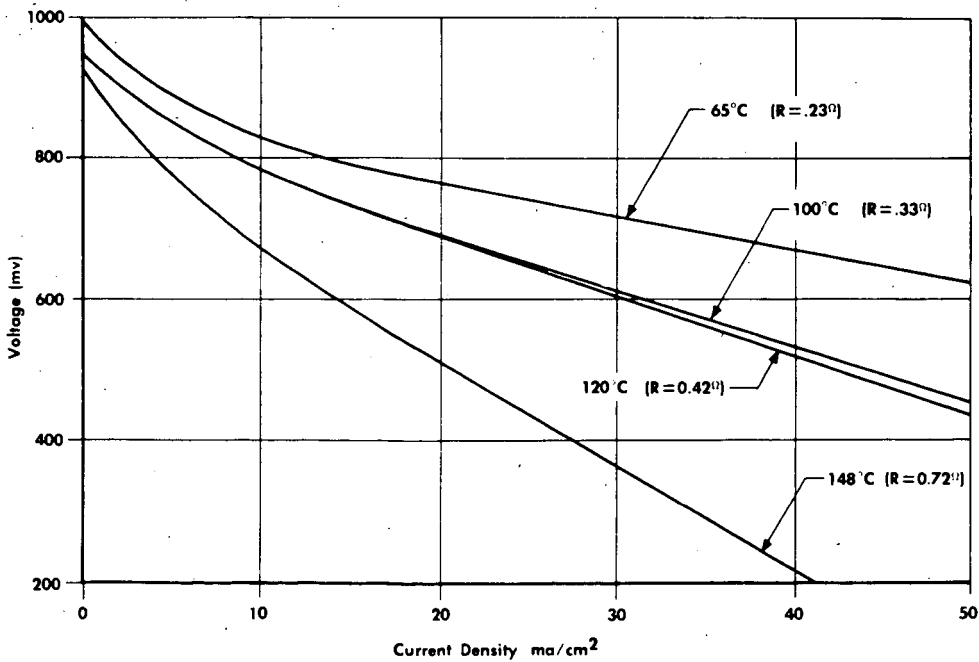


Figure 2. Polarization Curves for Hydrogen-Oxygen Inorganic Membrane Fuel Cell

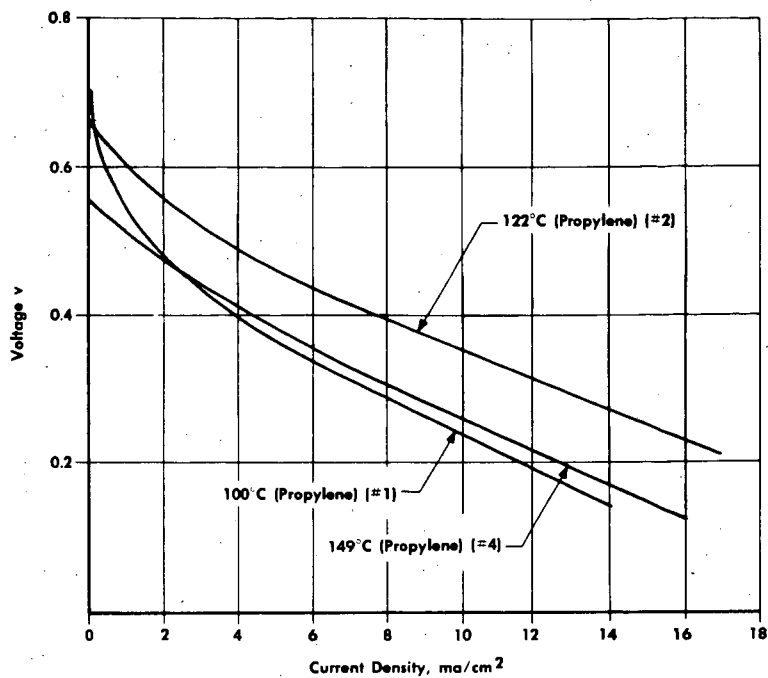


Figure 3. Polarization Curves for Propylene-Oxygen Inorganic Membrane Fuel Cell

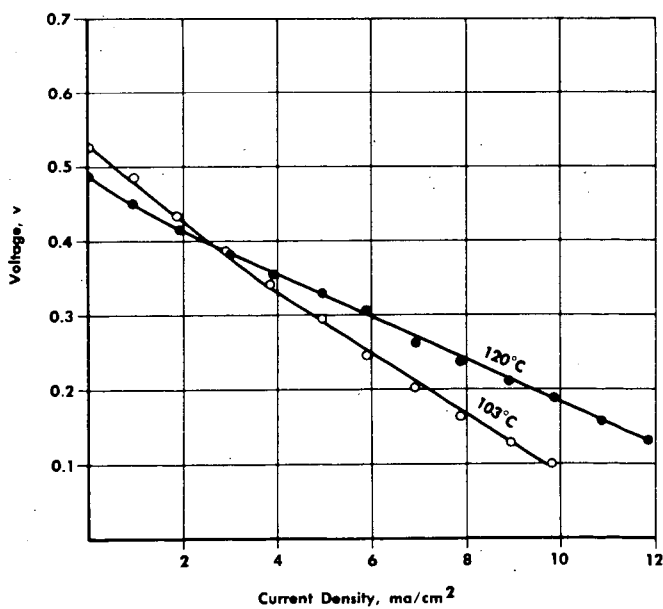


Figure 4. Polarization Curve for Ethane-Oxygen Inorganic Membrane Fuel Cell

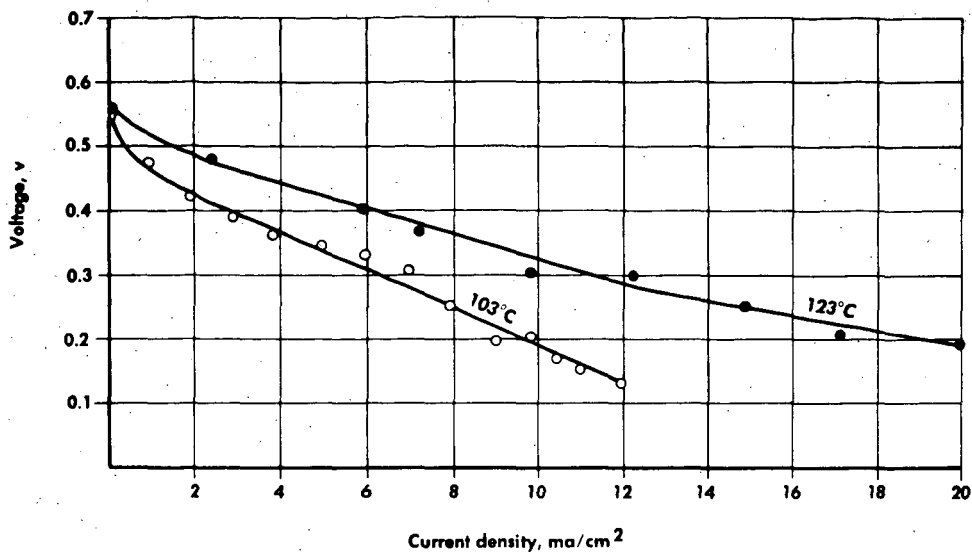


Figure 5. Polarization Curves for Propane-Oxygen Inorganic Membrane Fuel Cell

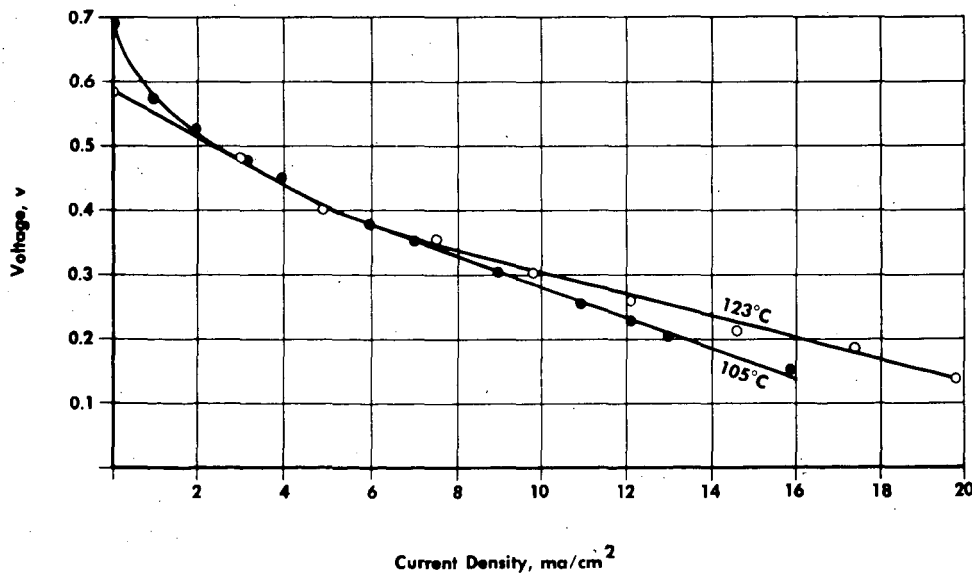


Figure 6. Polarization Curves for Inorganic Membrane Butane-Oxygen Fuel Cell

OPERATING CHARACTERISTICS OF PALLADIUM-SILVER ANODE ON IMPURE HYDROGEN STREAMS

S.M. Chodosh, N.I. Palmer, H.G. Oswin

Leesona Moos Laboratories
Division of Leesona Corporation
Great Neck, New York

INTRODUCTION

The practicality of using non-porous hydrogen diffusion anodes in fuel cells has been described by Oswin and Chodosh⁽¹⁾, Elmore and Tanner⁽²⁾. The advantages in manufacture and operation of these electrodes are considerable and have stimulated work on these palladium membrane electrodes to lower electrode costs and permit their use with cheaper fuels than pure H₂. Modifications of the electrode surfaces have been developed to extend anode performance and permit wider application of the non-porous anode.^(3, 4, 5,)

Most of the work has been related to the palladium-silver alloys which appear to be remarkably suited for fuel cell applications. A unique property of the alloys is their selective permeability to hydrogen, and some of the metallurgical factors involved have been discussed by Makrides⁽⁶⁾. Recently von Sturm and Kohlmüller⁽⁷⁾ using palladium membranes have derived a relationship between concentration polarization (with respect to H atoms), the membrane thickness, current density and partial pressure of hydrogen in the gas phase. In this work, however, the membrane surfaces were activated by an undisclosed technique, and the effects of the surface activation are not apparent.

Although originally conceived⁽⁸⁾ for use with relatively pure H₂ streams, the greatest potential application of palladium-silver anodes is with carbonaceous fuels. To obtain efficient anode performance with carbonaceous streams, there are two prime requirements:

1. The electrode must exhibit high limiting currents with low partial pressures of hydrogen, and
2. The electrode must be stable in the presence of materials other than hydrogen. Specifically, the limiting currents (H₂ flux) at low p_{H₂} values must not be lowered significantly by gases and substances present or formed in the fuel streams.

The palladium-silver anode can be used in a fuel stream in at least two ways. The fuel can be externally reformed, to provide a gas rich in free hydrogen which is then circulated behind the Pd-Ag electrode and the hydrogen extracted electrochemically. In this case the external reformer is operated at a higher temperature than the fuel cell. The fuel cell with palladium-silver anode can then be operated at any convenient temperature.

The second method of operation which has been developed recently^(9, 10) consists of reforming the fuel stream to hydrogen in the anode chamber behind the palladium alloy membrane. This "internal reforming" process requires operating the fuel

cell at a temperature high enough to reform the fuel rapidly: the endothermicity of this process is satisfied by the polarization losses in the fuel cell itself. Continuous extraction of H_2 down to lower than equilibrium values of p_{H_2} permits very efficient utilization of the fuel.

Before either of these types of fuel cell could be developed; however, it was necessary to provide a highly efficient H_2 -extracting anode⁽¹⁾ with low sensitivity to contaminant gases.

The work presented here describes progress with this type of anode and some of the preliminary studies carried out with various types of H_2 -containing streams.

EXPERIMENTAL PROCEDURES

The experiments were performed at 200°C in 75% potassium hydroxide. Potential measurements were made versus a reversible 75 Pd/25 Ag/hydrogen reference electrode in the same electrolyte, and all values reported are on the E_h scale. A Luggin capillary was employed at the surface of the membrane to measure anode potential. Studies for the most part were conducted on one inch diameter, 1.5 mil and 5 mil thick 75% palladium - 25% silver membranes operating against a Pt mesh counter electrode. The experimental apparatus is presented in Figure 1. All anodes studied were activated as described in the following section.

ELECTRODE PREPARATION

Many activation procedures have been investigated at Leeson⁽⁵⁾ in an attempt to improve operating parameters such as limiting current density, polarization, and stability. The activation procedure used in this work was satisfactory and entirely reproducible.

75 Pd/25 Ag membranes were first abraded with 50 micron aluminum powder. The membranes were then cathodized in 5% KOH solution using two Pt mesh counter electrodes to maintain proper geometry: this cathodization resulted in the saturation of the membrane structure with hydrogen. The structures were then immersed in a 2% palladium chloride solution (2-molar HCl) for approximately 4 minutes. The hydrogen previously introduced into the lattice chemically reduces the palladium ions from the plating solution to form a palladium black on both of the membrane surfaces; the quantity of black deposited was a function of plating time and anode thickness. This procedure resulted in an adherent, active palladium black; most structures studied had activations of approximately 4 to 5 milligrams per square centimeter. Although the amount of Pd activation is not a critical factor over the range $\sim 1-15 \text{ mg/cm}^2$ ⁽⁵⁾ the 5 milligram level of activation was arbitrarily selected for experimental convenience.

THE EFFECT OF HYDROGEN PARTIAL PRESSURE

The driving force for the diffusion of hydrogen through the metal lattice is the differential activity of hydrogen, and it was important at the beginning of this study to determine the relation between hydrogen partial pressure, limiting current density and polarization. This was desirable since in later studies it permitted separation of the relative effects of partial pressure and impurities. This data was obtained using streams containing predetermined mixtures of hydrogen and nitrogen. A low

utilization was used to simulate a constant partial pressure of hydrogen across the membrane. Using structures of 15, 10, 5, 3 and 1.5 mils in thickness and partial pressures of .025, .125, 0.25 and 2.5 psia hydrogen, the relationship shown in Figure 2 was obtained. Figure 2 indicates that down to 2.5 psia the process is bulk controlled over the range of thicknesses studied. At lower pressures, a degree of surface control is evident. Corresponding polarization data is shown in Figure 3. The variation of OCV with H_2 partial pressure follows the Nernst relationship within experimental limits.

As with any electrode operating on an impure reactant, the concentration of reactive species in the stream (in this case hydrogen) will decrease during passage over the electrode. The concentration of hydrogen in the exit purge stream should ideally approach zero, and the extent of approach will be determined by the ability of the electrode to operate at a low effluent concentration of hydrogen. The actual partial pressure of H_2 (over a given range) behind the electrode will be determined by the extent of back-mixing within the anode gas chamber. This will be a function of the geometry of the chamber, the gas flow-rates and the electrode current density. The mixing profile was not determined in these preliminary studies.

Hydrogen utilization studies were conducted employing a stream of 70% hydrogen and 30% nitrogen. The relationship between utilization and I_{lim} was determined experimentally by fixing the current density and reducing the flow to the newer stable value. An overall hydrogen mass balance was established by analyzing the composition of the effluent gas. This analysis was performed continuously by a thermal conductivity cell.

Measurements were taken at current densities of 139, 179 and 487 mA/cm² with an inlet hydrogen partial pressure of 25 psia. At the lower current densities hydrogen utilizations of 90% were observed. This value fell to 80% when the current density was increased to 487 mA/cm². Since this is below the limiting current range at moderate H_2 partial pressures, polarization was virtually unchanged over the range of utilizations studied. These results established that low polarization and high hydrogen utilization could be obtained simultaneously when operating on impure hydrogen streams.

It was next necessary to determine the extent to which this result is dependent on the identity of the particular impurities. The following sections present the data related to the ammonia-, methanol-, and hydrocarbon-derived streams.

AMMONIA-CONTAINING STREAMS

Simulated "cracked" NH_3 streams containing 2 to 5% NH_3 , and a balance of hydrogen and nitrogen in a ratio of 3 H_2 :1 N_2 were used. The fuel was prepared by introducing NH_3 into a 75% H_2 , 25% N_2 stream; the concentration of ammonia in the effluent was determined by adsorption in 0.856 N H_2SO_4 and titration with 0.01 N NaOH.

The effect of 3 H_2 :1 N_2 streams containing 4.3% and 2.2% NH_3 on anode polarization and limiting current density is shown in Figure 4, and it is apparent that:

1. At similar limiting current densities (350 mA/cm²), a hydrogen utilization of 75% is obtained with the ammonia-free stream compared to a hydrogen utilization of 54.7% for the 4.3% NH_3 feed.

2. Reducing the ammonia concentration to 2.2%, it is possible to increase the hydrogen utilization to 74.4% with only a slight reduction in limiting current (325 mA/cm²). Operation at these conditions for a period of 9 hours produced no change in I_{lim} or polarization.
3. A return to operation with pure hydrogen/nitrogen mixtures after exposure to ammonia resulted in a fairly rapid (but not instantaneous) return to the original performance level, indicating the reversibility of the ammonia effect.

From these results, it is evident that ammonia exerts a more profound influence on hydrogen anode performance than does nitrogen in similar concentrations. The ammonia clearly influences not merely the hydrogen partial pressure but also the adsorption kinetics on the palladium surface. This would be expected in view of the known adsorption of ammonia on transition metals. On the other hand, its demonstrated reversibility indicates that ammonia cannot be regarded as a strong poison. For good H₂ utilization at high current densities, the temperature and space velocity in the ammonia cracker must be optimized to maintain the NH₃ concentration below 2%.

SIMULATED METHANOL REFORMER STREAM

The cracking of methanol to yield CO + H₂ followed by the shift reaction with water to yield CO₂ + H₂ provides a gas of the approximate composition 70% H₂, 23% CO₂, 1 - 2% CO + unreacted methanol and water. The effects of these various compounds on anode behavior is discussed below:

1. Effect of CO₂

Streams of 75% H₂, 25% CO₂ have been studied. CO₂ behaves as a totally inert diluent, and limiting current density is a function only of the reduction in hydrogen partial pressure. No poisoning effects with CO₂ have been observed on structures operated for periods of hundreds of hours.

2. Effect of CO

The initial exploratory studies employed a stream of 75% H₂, 20% CO₂, and 5% CO. This amount of CO is substantially greater than that normally expected from methanol reformed at 250°C.

The experimental procedure employed was as follows: (1) an anode was operated in pure H₂ measuring polarization and limiting current density; (2) at 150 mA/cm² using the H₂, CO₂, CO stream and a given vent rate (hydrogen utilization) the polarization was observed over a half-hour period with the following results:

<u>% Hydrogen Utilization</u>	<u>Increased Polarization After 1/2 Hour Under Load</u>
8.33	no change
20	no change
33	no change
38.1	7 mV
57.1	23 mV

It is apparent that CO has an increasingly deleterious effect on anode polarization as the utilization is increased. This is also demonstrated by its effect on limiting current densities as seen in Figure 5. Increasing the utilization at 150 mA/cm² from 8.33% to 38.1% halved the limiting current density; this is greater than can be expected from the presence of an inert diluent, demonstrated in the previous H₂/N₂ utilization studies.

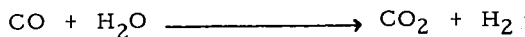
It was also observed when changing from a CO-containing stream to pure H₂ that recovery of the initial limiting current could be obtained, but only after extensive purging with pure H₂. This indicates that the CO is strongly, but not irreversibly adsorbed onto the gas side surface.

Further studies were then conducted on streams containing 0.01, 0.1 and 1% CO in the presence of H₂O and CO₂. Water was included since it was expected to be present normally in the low temperature shift effluent. Each experiment was conducted for the period of time it took to either double the initial polarization at 150 mA/cm², or 50 hours, whichever came first. H₂ utilization was maintained at 50%.

The results of these experiments are summarized in Table 1 below:

Gas (°C)	Composition(%)				The Effect of CO on Anode Polarization		Electrode Diameter(in.)
	CO	CO ₂	H ₂ O	H ₂	Poisoning Under Load (Hours Required To Double Polar.)	Recovery (Hrs. of H ₂ Purge Needed)	
200	0.01	0	0	Bal.	slow (~20)	slow (~10)	1 & 5
	0.1	0	0	Bal.	rapid (< 1)	slow (~10)	1 & 5
	0.1	0	2	Bal.	none (> 50)		1
	1	0	2	Bal.	none (> 50)		1
	0	26	0	Bal.	none (> 50)		1
	0.1	25	0	Bal.	rapid (10 - 20)	slow (~10)	1
	1	25	0	Bal.	rapid (< 10)	slow (~10)	1

The data shows clearly that CO (either alone or in the presence of CO₂) poisons the gas side reaction, but that in the presence of water (~2%), no deterioration in anode polarization is observed. This is explained by the shift reaction occurring on the gas side of the palladium black activated membrane:



The effect of this process can be measured by the observation that as little as .01% CO is deleterious when present in the dry form, whereas 1% CO can be safely tolerated in the presence of water.

EFFECT OF METHANOL AND H₂O

The effect of the expected concentration of unreacted methanol (1 - 2%) and H₂O (1 - 2%) in the reformer stream was evaluated. The desired hydrogen stream was synthesized by passing hydrogen through a glass absorption column containing the proper H₂O/methanol composition. The stream composition was analyzed by

gas liquid chromatography. Using streams containing the desired impurity content, an anode was kept under a load of 150 mA/cm^2 for 25 hours with a vent rate equivalent to 50% H_2 utilization. Potential under load was steady for the period studied, and polarization curves indicated no change in limiting current density after this exposure to the impure stream. The utilization was increased to 80% at the same load with no change in stability. Subsequent runs using actual (internally) reformed methanol showed no poisoning of the anode over periods exceeding 200 hours. These experiments were carried out at $200 - 250^\circ\text{C}$ with hydrogen utilization of 80 - 90% and current densities of 150 mA/cm^2 .

EFFECT OF CH_4

Dependent on the efficiency of reforming, substantial concentrations of saturated hydrocarbons may be encountered when operating on fuels such as kerosene, gasoline, etc. Methane in particular will be present, even with methanol feed, due to the methanation of carbon monoxide. Tests with CH_4 showed it to be an inert diluent.

UNSATURATED HYDROCARBONS

Unsaturated hydrocarbons may be present in significant quantities either as impurities in the feed, or as a result of partial dehydrogenation during the reforming process. It was considered possible that because of their tendency to chemisorb on transition metals, some poisoning of the H_2 diffusion process might be observed. Tests, however, failed to confirm this, and stable operation for the periods specified was observed with ethylene. However, a reduction in the limiting current was noted which corresponded almost exactly to the loss of hydrogen required for hydrogenation of the unsaturated species. The original polarization and limiting current conditions were observed immediately on restoring the hydrogen partial pressure.

OTHER SPECIES - ACTUAL REFORMER STREAMS

Additional qualitative experiments have indicated that severe and irreversible poisoning can occur in the presence of significant quantities of acetylene or of sulfur. The exact limits of tolerance for these species have not been established, but operation with actual reformed streams from both methanol and hydrocarbon fuels in internal-reforming cells has shown no gas-side deterioration over operating periods of 500 hours. From this it can be concluded that any species generated during reforming but not explicitly considered in these studies must be present in low concentrations which do not noticeably affect the diffusion process.

DISCUSSION

The data presented clearly show that a suitably prepared palladium-silver anode can be used efficiently to extract hydrogen from impure streams within certain limits.

The limits of operation are set by the temperature (fixed in these studies at 200°C), the required H_2 utilization, i.e., exit p_{H_2} , and the reversibility of the chemisorption of various impurity species.

H_2 utilization at fixed current density is a function of p_{H_2} , flow rate and the extent of impurity adsorption. The data obtained with H_2/N_2 mixtures show that below $p_{\text{H}_2} = 2.5 \text{ psia}$, gas-phase adsorption is limiting. When poisons which can be strongly

adsorbed are present in the hydrogen, a significant fraction of the surface is covered by the poisoning species even when $p_{H_2} = 2.5$ psia. Under these conditions, the surface (hydrogen - adsorption) process is rate-limiting at higher partial pressures of hydrogen. Only when p_{H_2} is high enough so that H_2 competes successfully for surface sites with the poisoning species and causes an increase in Θ_H is there any reduction in the extent of limitation by the surface step.

N_2 , CO_2 , H_2O , CH_4 and CH_3OH do not appear to affect the p_{H_2} - limiting current relationship and all of these species act as inert diluents: they are likewise known not to chemisorb strongly on metals such as palladium.

Ethylene appears to be an intermediate case. The evidence (rapid desorption) is that it does not chemisorb strongly under these conditions and hydrogenates very rapidly to ethane which by inference must be completely inert. By contrast, acetylene is an irreversible poison; this is explainable by its tendency to form strongly-bonded, surface species on most Group 8 metals. Neither acetylene nor ethylene have been observed in steam-reformed effluents and are not considered to be likely poisons.

Ammonia, known to chemisorb extensively, but reversibly on Pt and Pd, is tolerable up to the level of 2% of the stream content.

The case of carbon monoxide is very important from a practical point of view since the most efficient shift catalysts in use today cannot reduce CO below 0.1% level at useful space velocities. In the absence of water it is demonstrated that CO chemisorbs strongly and extensively on the palladium surface, significantly lowering Θ_H and limiting currents. In the presence of water vapor, however, this is not the case, and the palladium acts as a remarkably good shift catalyst, so that limiting currents are unaffected. Thus, by inference, Θ_H must be higher and Θ_{CO} smaller than when water is absent. In turn, this would imply that the rate of the shift reaction is far greater than the rate of adsorption of CO.

In recent practice^(9, 10) it has been demonstrated that the anodes can be operated efficiently for long periods on reformed streams of methanol/water and hydrocarbon/water. Under these conditions⁽⁹⁾, the membrane surface is exposed to mixtures of CO, CO_2 , H_2 , H_2O and fuel: the composition of this gas at any point on the surface being determined by temperature, space-velocity, pressure and the extent of back-mixing. The least favorable case (for H_2 adsorption on the membrane surface) exists at the exit point where the values of p_{CO} , p_{CO_2} will be highest and p_{H_2} lowest. Operating at conditions where 85% of the methanol has been decomposed and 90% of the resulting hydrogen 'extracted' by the anode, the anode has operated without increased polarization at exit values of $p_{CO} > 1\%$. This seemingly high level of p_{CO} can be tolerated since it is unstable with regard to the shift equilibrium:



Thus, when the CO is adsorbed on the palladium surface, it is unstable, and rapidly converts to CO_2 and H_2 since the palladium is an efficient shift-promoting catalyst under these conditions.

Sulfur, especially in the form of H_2S , is of course one of the most strongly adsorbed poisons on metal surfaces. Experience has shown, however, that all reforming catalysts are sensitive to sulfur poisoning, and fuel streams must be pre-treated to

remove sulfur in order to obtain good reformer-catalyst lifetimes. In this respect, the pre-treatment of fuel and the removal of sulfur traces by the reformer catalyst significantly reduce the chance of sulfur-poisoning of the palladium membrane by the H₂ stream, and the quantitative tolerance of the membrane surface to sulfur is therefore of academic interest at this point.

It is apparent that from a practical point of view, the non-porous diffusion anodes when operated under correct conditions can provide very efficient fuel utilization at high current densities, and that they are operable in the presence of a wide variety of impurities and by-products of fuel-reforming.

REFERENCES

- (1) H.G. Oswin and S. M. Chodosh "Non-Porous Hydrogen Depolarized Anodes for Fuel Cells," Fuel Cell Systems, R. Gould, editor, Advances in Chemistry Series, No. 47, ACS Applied Publications, (1965).
- (2) G.V. Elmore and H.A. Tanner, J. Electrochem. Soc. 108 : 669 (1961)
- (3) S.M. Chodosh and H.G. Oswin "The Activation of Non-Porous H₂/Pd-Ag Fuel Cell Anodes," "Journées Internationale D'Etude Des Piles a Combustible," Brussels, June 1965. French Patent #1,354,685.
- (4) A. Kussner and E. Wicke, Z. Physik. Chem. 24 : 152 (1960).
- (5) L. Lederer and N.D. Green, Electrochim Acta 8 : 883 (1963).
- (6) A.C. Makrides, Quarterly Progress Reports 1 through 5, Contract DA-49-186-ORD-982 (1962 - 1964).
- (7) F. von Sturm and H. Kohlmüller, Naturwiss. 52 : 31 (1965).
- (8) U.S. P. 3,092,517.
- (9) A.J. Hartner and M.A. Vertes "Methanol In-Situ Reforming Fuel Cells," A.L. Ch. E. - L.Ch. E. Meeting, London, June 1965.
- (10) M.A. Vertes and A.J. Hartner "Internal Reforming Fuel Cells," "Journées Internationale D'Etude Des Piles a Combustible," Brussels June 1965.

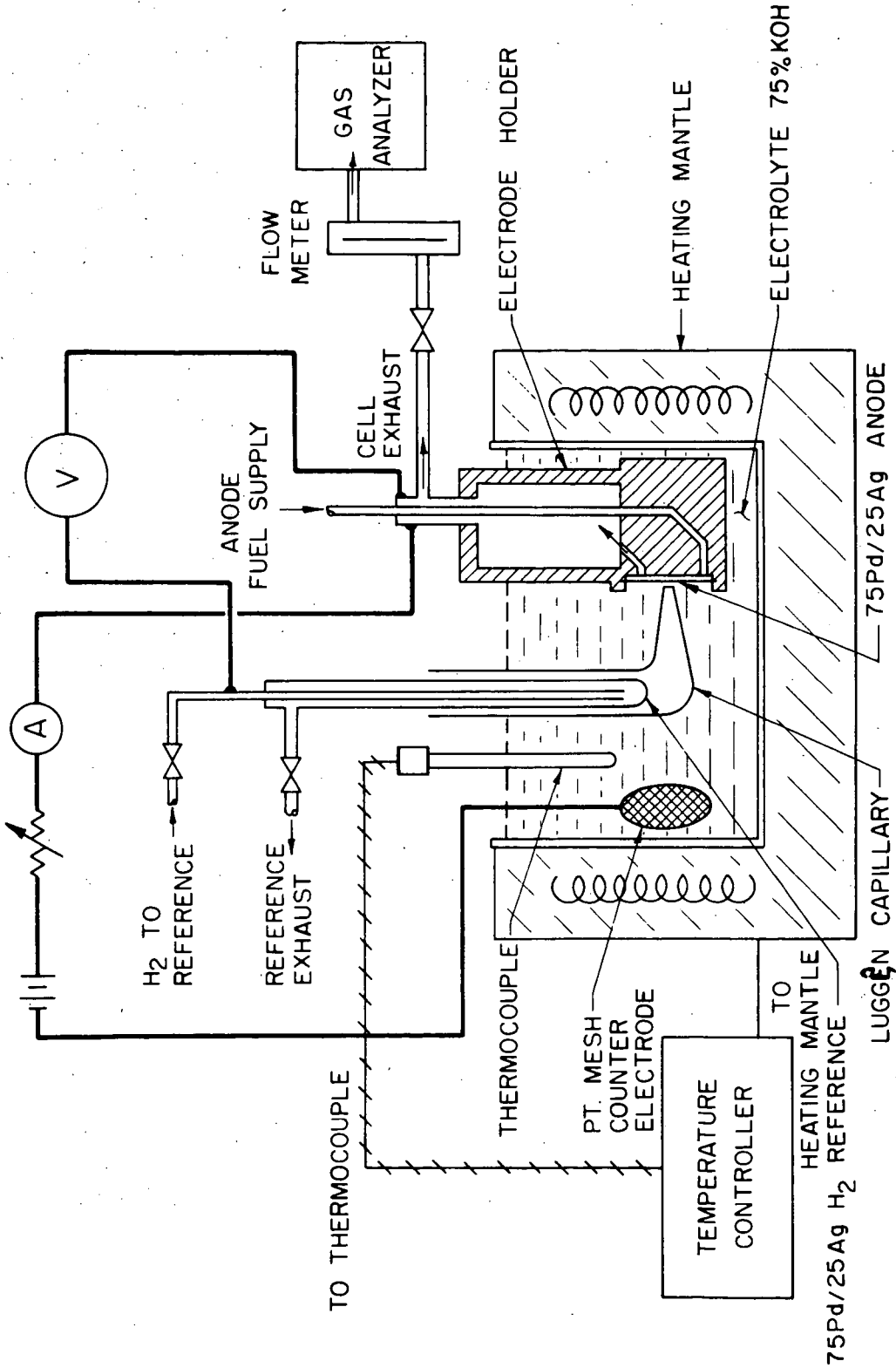


FIG. 1 EXPERIMENTAL APPARATUS

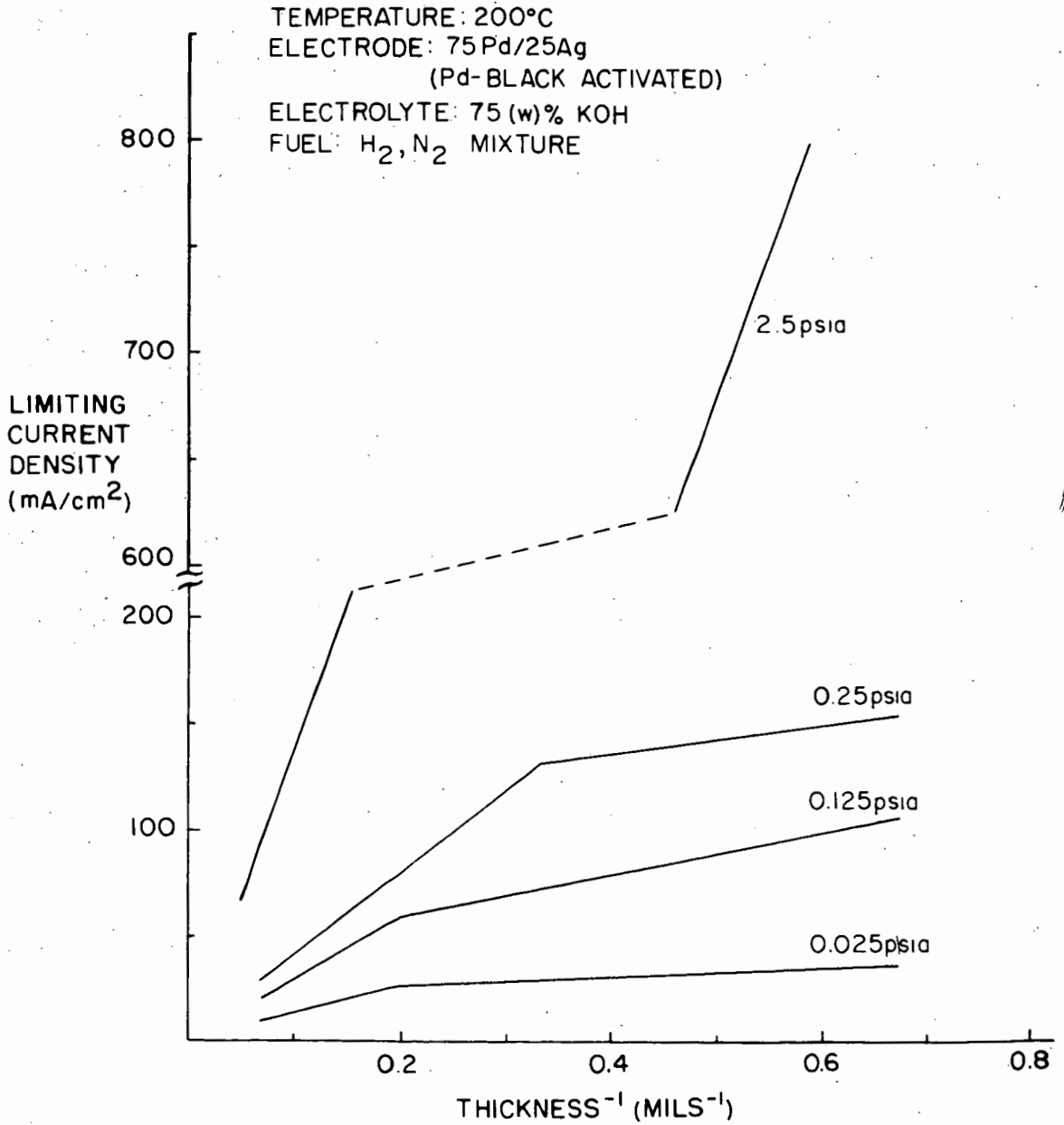


FIG.2 EFFECT OF PH₂ AND ELECTRODE THICKNESS ON LIMITING CURRENTS OF Pd/Ag ANODE

TEMPERATURE: 200°C
ELECTRODE: .0015", 75Pd/25Ag
(Pd-BLACK ACTIVATED)
ELECTROLYTE: 75 (w)% KOH
FUEL PRESSURE: 10 psig
FUEL: H₂, N₂ MIXTURE
FLOW RATE OF FUEL: 1025 cc/min/cm²

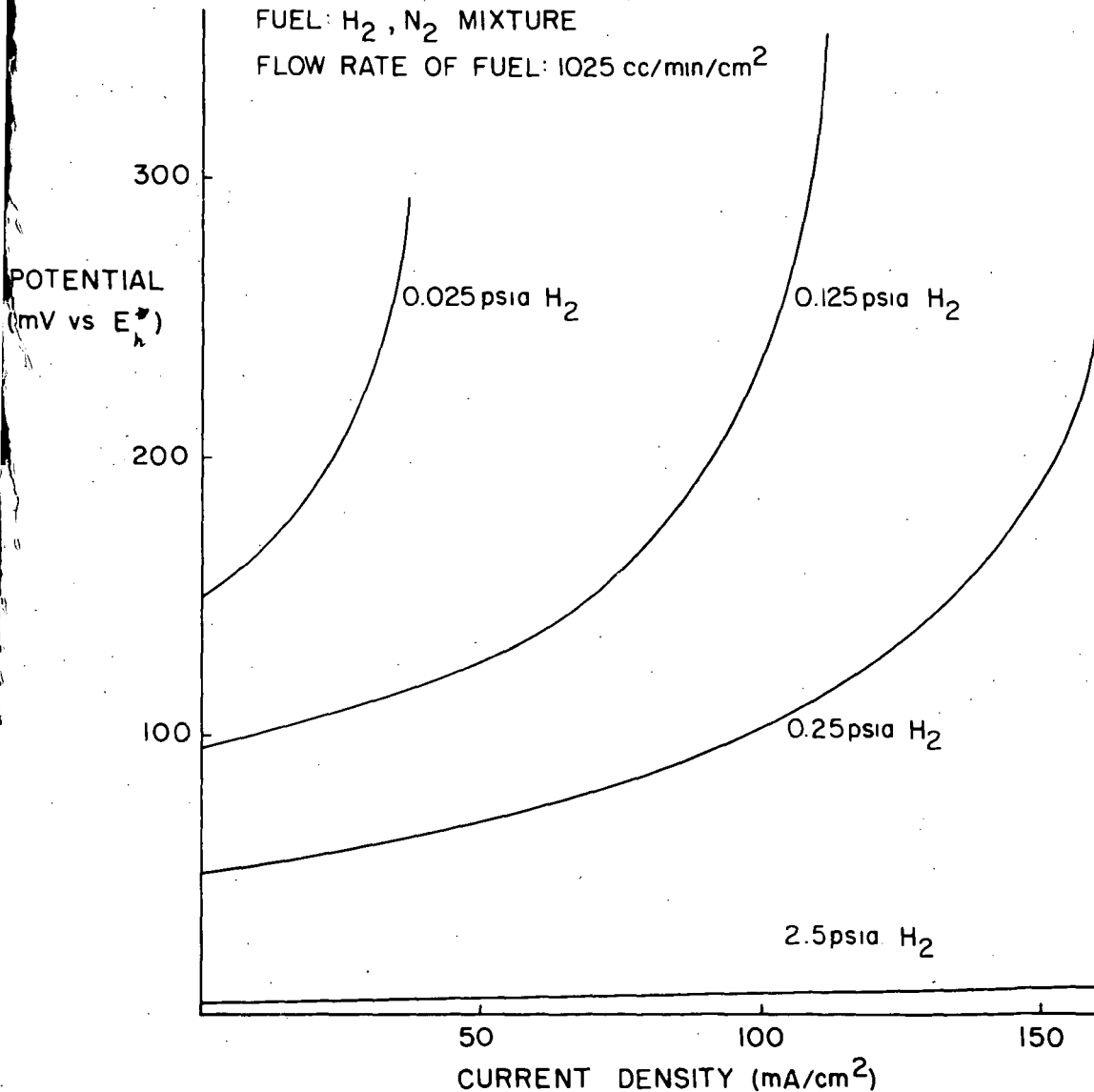


FIG. 3 POLARIZATION OF ANODES OPERATING AT LOW PARTIAL PRESSURES OF HYDROGEN

TEMPERATURE: 200°C

ANODE: .0015", 75 Pd/25 Ag

(Pd-BLACK ACTIVATED)

ELECTROLYTE: 75 (w) % KOH

FUEL PRESSURE: 25 psig

CURVE FUEL MIXTURE

VENT RATE (cc/min)

CURVE	FUEL MIXTURE	VENT RATE (cc/min)
1	100% H ₂	3
2	75% H ₂ , 25% N ₂	54
3	75% H ₂ , 25% N ₂	10
4	71.1% H ₂ , 23.7% N ₂ , 4.3% NH ₃	11
5	73.3% H ₂ , 24.4% N ₂ , 2.2% NH ₃	5

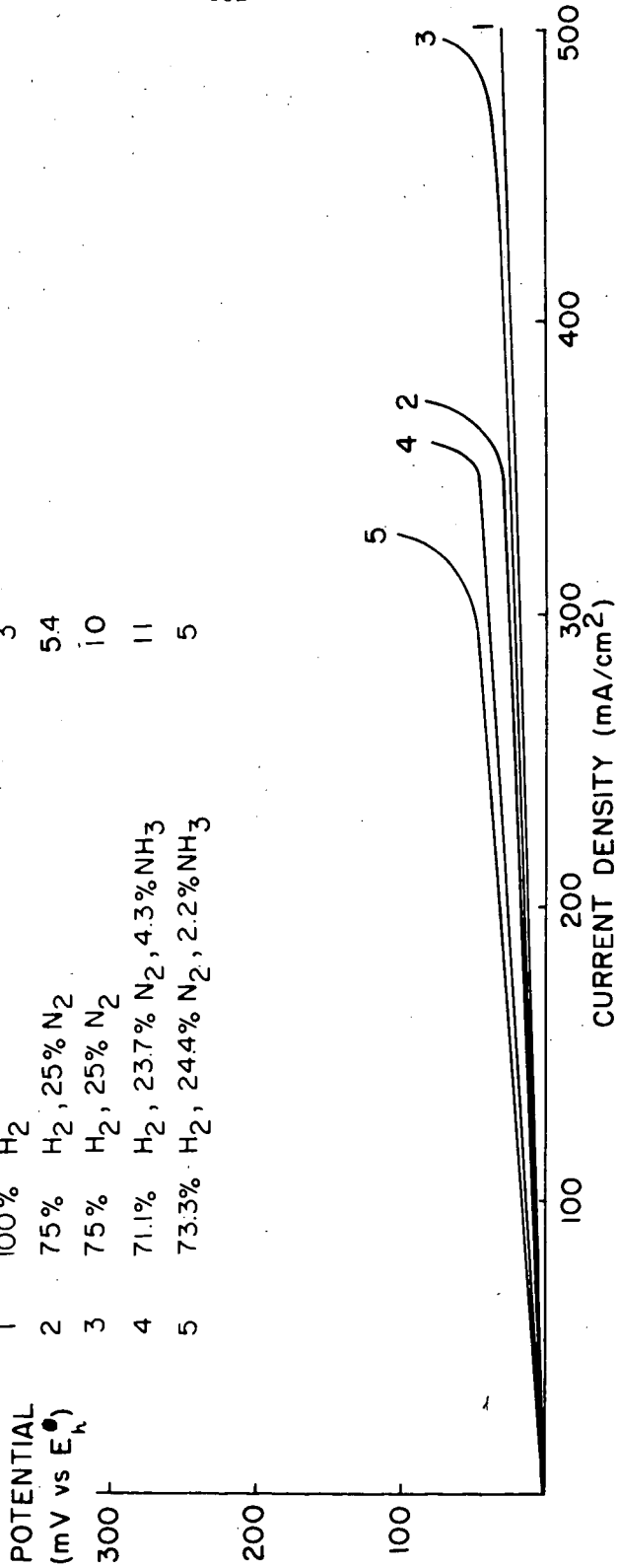


FIG. 4 ANODE POLARIZATION WITH NH₃/H₂ STREAMS

TEMPERATURE: 200°C
 ANODE: .0015", 75 Pd/25Ag
 (Pd-BLACK ACTIVATED)
 ELECTROLYTE: 75(w)% KOH
 FUEL PRESSURE: 25 psig
 FUEL MIXTURE: 75% H₂
 20% CO₂
 5% CO

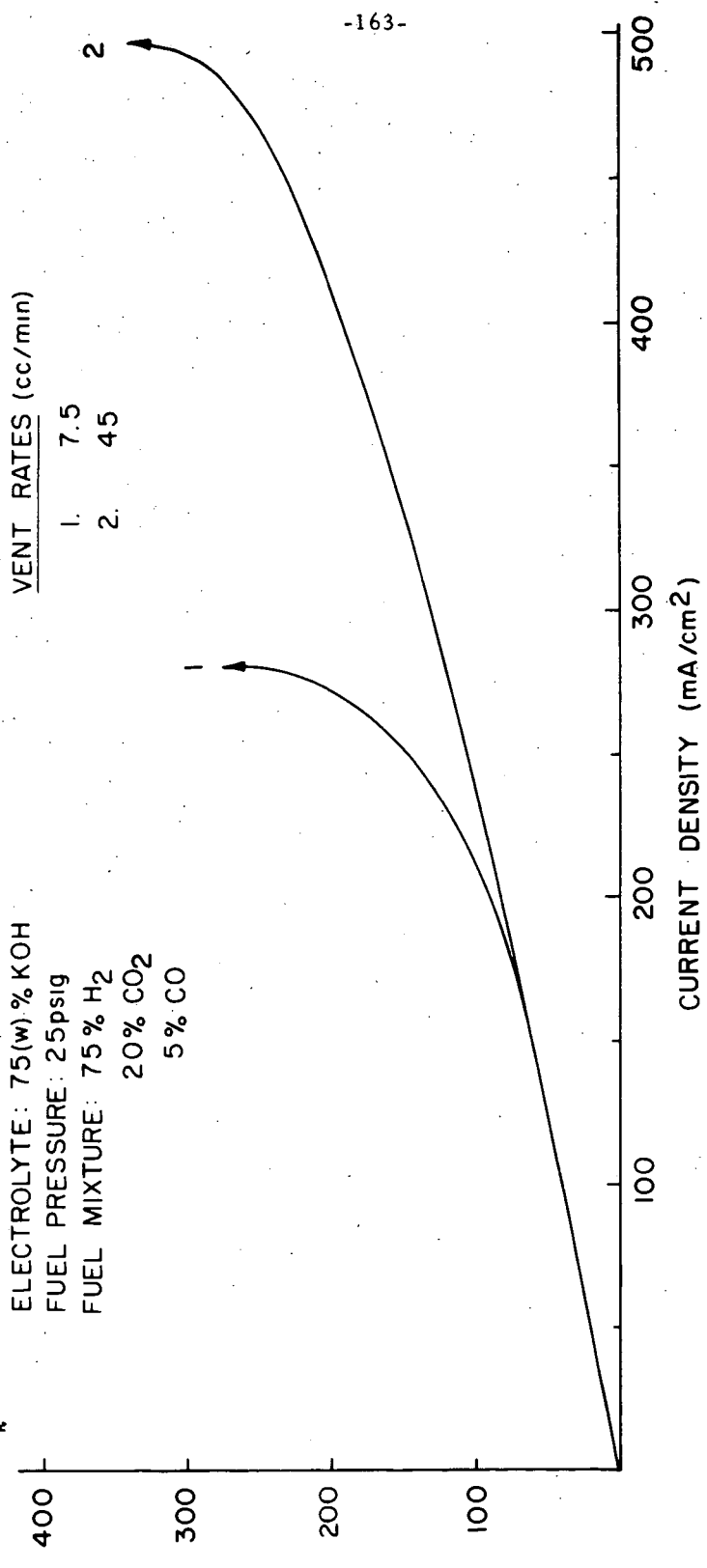


FIG. 5 ANODE POLARIZATION WITH CO/CO₂/H₂ STREAMS

FEASIBILITY STUDIES ON A HYDROCARBON FUEL CELL

D. P. Gregory and H. Heilbronner

Pratt & Whitney Aircraft
Division of United Aircraft Corporation
East Hartford, Connecticut

INTRODUCTION

Work has been reported on several different types of hydrocarbon fuel cells, including those operating with molten carbonate electrolytes, and those with aqueous acid electrolytes at lower temperatures. Both of these cells suffer from serious corrosion problems, and also indicate that their operating efficiency may remain low because of (a) heat losses from the carbonate cell, and (b) high polarization of the anode in the acid cell.

Since one of the major claims of the fuel cell is its high efficiency, it is well to examine carefully the overall efficiency of any hydrocarbon fuel cell, considering both the operating cell voltage and the utilization efficiency of the fuel.

One of the most efficient fuel cells is the modified "Bacon" cell, a H_2/O_2 cell operating with nickel electrodes at 4-500°F in concentrated alkaline electrolyte. This cell has exhibited current densities of over 300 asf at 1.0 volt at which voltage most other cells are barely producing any current at all. However, the alkaline electrolyte precludes the direct use of a carbon-containing fuel.

Previous work has been reported (1) on the use of palladium membrane anodes in 400°F KOH-electrolyte fuel cells. Such an anode, permeable to hydrogen only, permits the use of impure hydrogen, containing CO_2 and CO , and high currents and efficiencies have been demonstrated. More recently (2) a cell has been described in which methanol and steam are reacted on a catalyst in contact with a palladium membrane anode. At 400°F, this reaction proceeds rapidly, almost to completion.

One can also consider the use of a hydrocarbon in a cell of similar configuration (3). Hydrocarbon-steam reactions take place on cheap nickel catalysts, and the use of thin palladium-silver alloy film anodes, paired with a nickel cathode, presents the concept of a relatively cheap and highly efficient hydrocarbon fuel cell, in which the reforming catalyst does not have to be compatible with the electrolyte.

The Internal Reforming Anode Concept

Figure 1 represents a schematic of the "internal reforming anode cell."

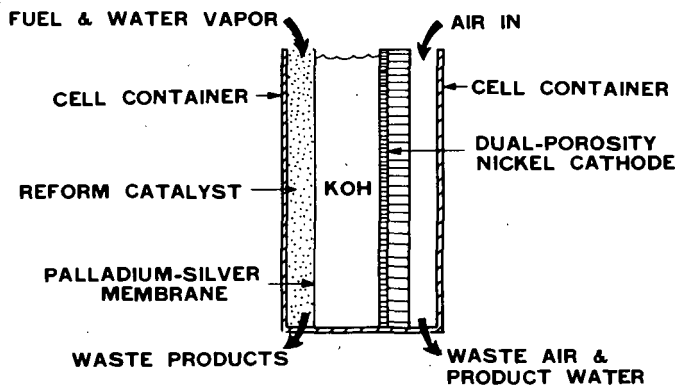


Figure 1. Schematic Diagram of Hydrocarbon-Air Fuel Cell

Hydrocarbon/steam mixture is fed into the gas-space of the cell which is packed with catalyst. Hydrogen, CO and CO₂ are produced. The hydrogen permeates through the palladium anode and enters into a conventional fuel cell reaction. The other electrode is a biporous oxidized nickel structure fed with CO₂-free air.

Hydrocarbon-steam reforming reactions are normally carried out at temperatures around 1500°F. The Bacon fuel cell, however, is limited to a maximum temperature of about 500°F, by the maximum service temperature of the Teflon insulating gaskets, and by the onset of unacceptable corrosion rates at the cathode. At 500°F the equilibrium hydrogen production from a hydrocarbon will be very low, and one might predict very poor fuel utilization. As current is drawn from the cell, however, hydrogen is extracted from the equilibrium mixture, forcing the reaction to proceed. In this way, it is theoretically possible to obtain 100% conversion of the fuel, even at 500°F. The rate of the reaction, however, at such a low temperature is completely unknown, and can only be found by experiment.

Experiments were set up, therefore, to test the feasibility of this cell concept, operating on a number of different hydrocarbon fuels. Primarily, it was required to know if the hydrogen production reaction could proceed fast enough at these temperatures to sustain useful currents, and if hydrogen could be extracted through the palladium anode at a high enough rate to obtain high fuel utilization.

Apparatus

A rectangular anode holder was constructed as shown in Figure 2.

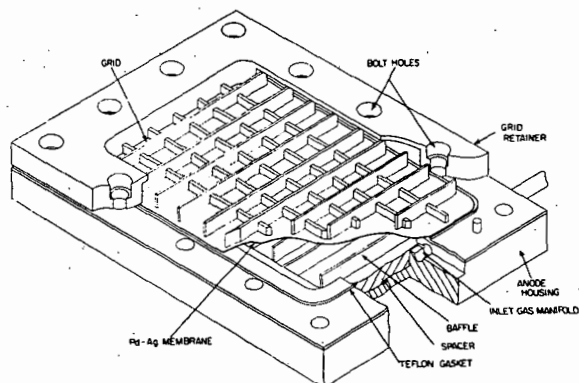


Figure 2. Cutaway of Anode Assembly

The palladium-silver alloy foil was clamped across the face of a shallow recessed plate, to form a closed cavity. This cavity was packed with a commercial supported-nickel reforming catalyst. Gas was fed in and taken out by two galleries along opposite edges of the cavity. The palladium foil was prevented from bowing inwards by the catalyst and outwards by a nickel criss-cross grid.

This anode holder was immersed in a tank of 85% KOH maintained at 500°F, and a dual-porosity nickel cathode welded into a dished plate to form a gas cavity, was suspended close to the anode from a lid which sealed the KOH from the air. Figures 3 and 4 show this arrangement clearly. A 1/8" diameter palladium-silver tube, fed with hydrogen, was suspended from the lid to serve as a reference electrode.

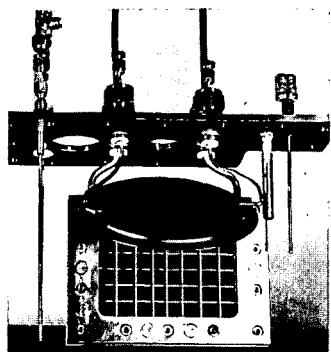


Figure 3. Hydrocarbon Fuel Cell Assembly with Cathode Bent Back

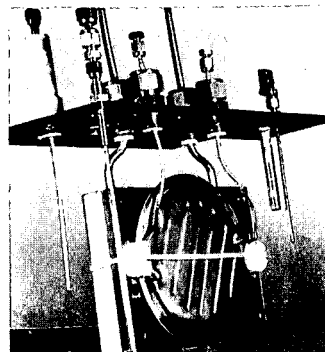


Figure 4. Hydrocarbon Fuel Cell Assembly

The anode was supplied with an accurately metered mixture of hydrocarbon and steam, preheated to 500°F. The exit gas was cooled, passed through a palladium-tube hydrogen detector, and analyzed by means of a chromatograph. Flow rates were recorded by a bubble meter at the exit, and the system pressure was controlled by a manostat in the vent line. A schematic of the system is shown in Figure 5.

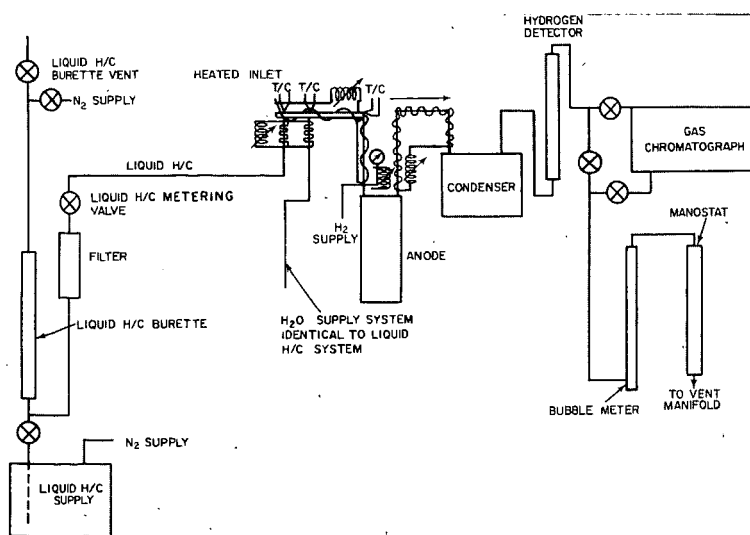


Figure 5. Schematic of Hydrocarbon Anode System

RESULTS

The cell was operated on n-octane, methane and a commercial kerosene fuel, JP-150, with very encouraging results. Figure 6 shows half-cell and full-cell polarization curves for octane-air. The electrode spacing was 0.59 inch. It will be seen that 80 amps/ft² was obtained at a cell terminal voltage of 0.75V, with a fuel flow corresponding to a utilization of 45%.

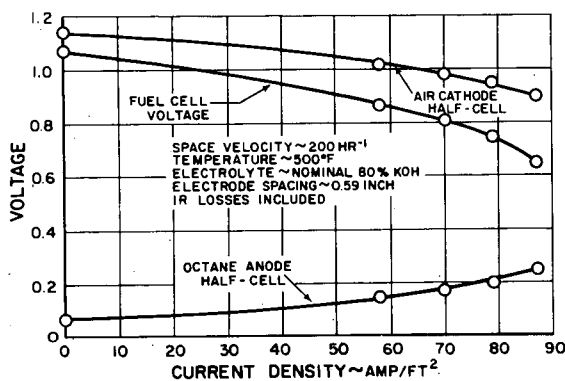


Figure 6. Experimental Performance of Air-Octane Fuel Cell

Under similar conditions, methane also gave 80 amps/ft² at 0.75 V and 45% fuel utilization, and JP-150 gave 68 amps/ft² at 0.75 V at 35% utilization (Figure 7).

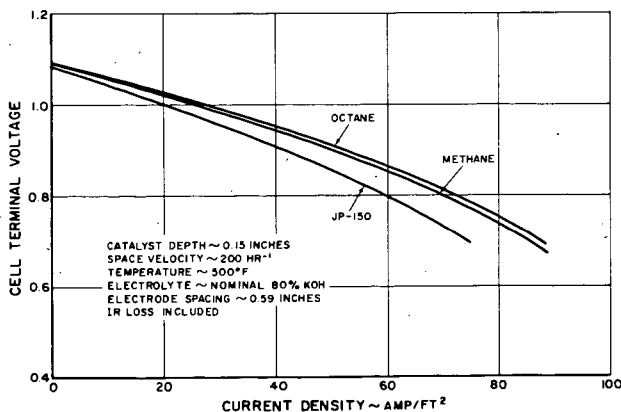


Figure 7. Comparison of Various Fuels in the Internal Reforming Cell

In order to increase the fuel utilization, it is necessary to reduce the fuel flow rate. To study the effect of fuel flow rate on current density, the anode was maintained at a constant polarization, (0.15 V from an unpolarized hydrogen electrode). There is a direct relationship between the fuel flow rate, current density, and fuel utilization. As fuel flow is increased, unless a higher current flows, the utilization simply falls off. Figure 8 shows fuel flow (ideal hydrogen space velocity) plotted against current density. The sloping lines are lines of constant utilization.

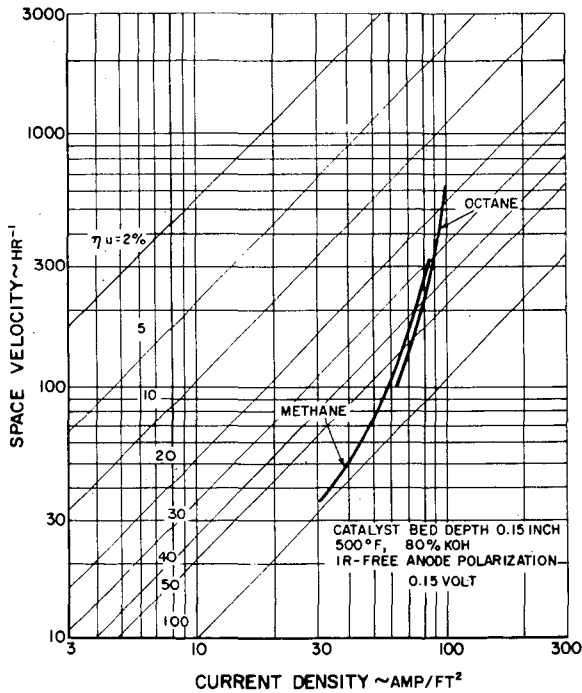


Figure 8. Relationship Between Fuel Flow Rate, Current and Fuel Utilization for Constant Anode Polarization of 0.15 Volts

The curves on Figure 8 indicate the variation of current with varying fuel flow at a fixed polarization for octane and methane. The curves would be displaced slightly to the left for lower polarizations and vice-versa. It was possible to run the cell on methane with a 70% fuel utilization; but in order to achieve the highest utilizations, the penalty in current density became severe. In other words, the current is limited by the fuel supply when higher utilizations are attempted. This suggests that the catalytic production of hydrogen is too slow to sustain high currents and utilizations.

If the rate of the catalytic reforming reaction is limiting, an improvement in performance might be expected by using a thicker catalyst bed. Figure 8 was obtained with a catalyst bed thickness of 0.15 inches. The anode was made in such a way that bed thicknesses of 0.30" and 0.60" could be obtained. Increasing the bed thickness to 0.60" did indeed give higher current densities, up to 175 amps/ft², at the same space velocity and polarization. However, in order to obtain the same space velocity with a larger bed volume, higher actual fuel flow rates were required, and this had the effect of reducing the fuel utilization to about 30%.

It became clear at this point that considerable optimization of anode design would have to be done in order to trade-off between the currents, cell volumes and efficiencies associated with varying the catalyst bed thickness.

Since the effect of the quantity of the catalyst is so marked, a study was made of the reforming reaction itself, in order to see how its kinetics were affected by the extraction of hydrogen. This study was carried out by analysis of the exit gases vented from the anode.

Using n-octane as fuel, we consider the following possible reactions:

1. Fuel conversion to CO and H₂.
2. Shift of CO to CO₂ (assumed complete at this temperature).

3. Conversion of CO and H₂ to form methane.
4. Extraction of hydrogen by the anode process. (Figure 9)

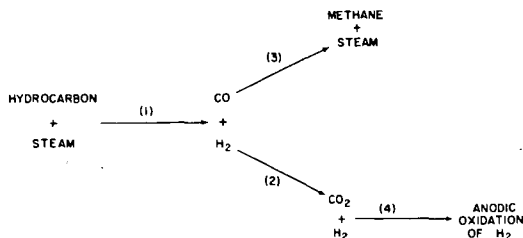


Figure 9. Schematic of Reaction Paths

The third reaction is an undesirable one, since it removes hydrogen from the equilibrium mixture. It is catalyzed by the same catalysts that promote the desirable reaction (1).

First, we studied the amount of unconverted fuel appearing in the exhaust. This gives a measure of the rate of reaction 1. We were surprised to find that although no unreacted fuel is found at first, it begins to show up after about 5 hours, progressively increasing, indicating that the catalyst decays quite rapidly. Figure 10 shows the decrease of the fuel conversion with time. Notice that the decay is not so apparent when the cell is on load - when the fuel utilization of the cell reaches 50%, a much higher proportion of the fuel fed in is converted. This would be expected since the effect of extraction of hydrogen is to increase the rate of the hydrogen-forming reaction.

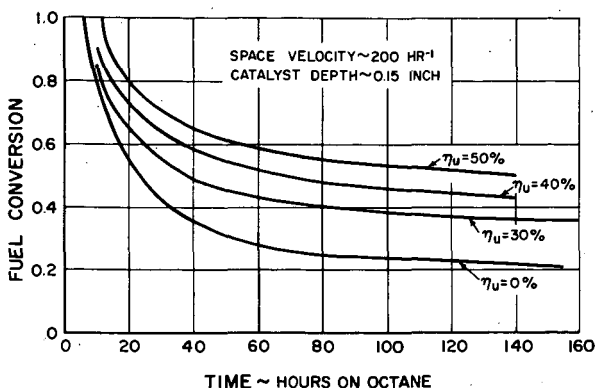


Figure 10. Comparison of Catalyst Aging Effect on Octane Fuel Conversion at Utilization Efficiencies of 0, 30, 40 and 50 Percent

Secondly, we observed the amount of methane appearing in the cell exhaust. This gives an indication of the rate of reaction 3. Figure 11 shows the "Reform Conversion" as it changes with time. The "Reform Conversion" is the proportion of the converted fuel which produces hydrogen, rather than methane. In the ideal case it is 1.0. It will be seen that at no-load conditions, the reform conversion remains low, indicating most of the fuel is being converted to methane.

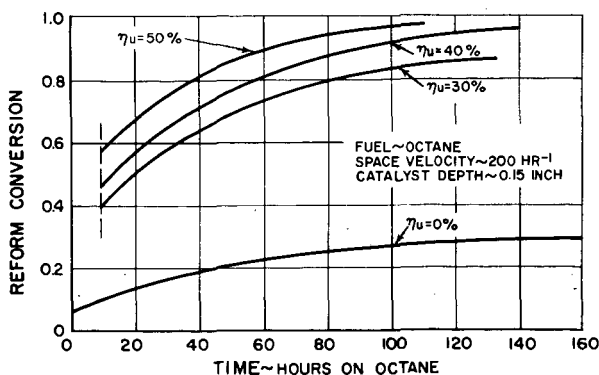


Figure 11. Comparison of Catalyst Aging Effect on Reform Conversion at Utilization Efficiencies of 0, 30, 40 and 50 Percent

When hydrogen is extracted from the equilibrium, all processes producing hydrogen tend to be favored. This includes the reverse of the methane-producing side reaction, so methane formation is suppressed. This is shown on Figure 11, where the initial "Reform Conversion" is as high as 0.55 when the fuel utilization is 50%. The Reform Conversion increases with time as the catalyst decays. Since less hydrogen is produced, so a higher proportion of it gets extracted by the anode, and the tendency for methane formation becomes less.

The most important conclusion here is that the catalytic reaction changes radically with hydrogen extraction, so that little useful information will be learned from studying the reaction in a conventional reactor.

Thirdly, attention was paid to the hydrogen content of the exhaust stream. This gives an indication of the rate of reaction 4. Figure 12 shows that over 90% of the hydrogen produced in the catalyst bed is extracted as "current" through the anode, and the amount increases slightly with time.

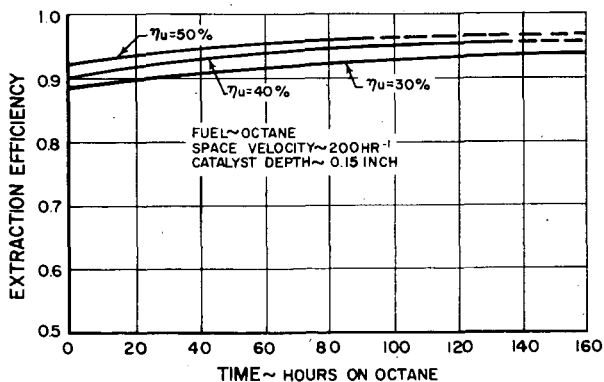


Figure 12. Comparison of Catalyst Aging Effect on Extraction Efficiency at Utilization Efficiencies of 30, 40 and 50 Percent

The sum total of these time effects on the performance of the cell is not very marked. As the catalyst decays, more unreacted fuel is vented. Of the hydrogen formed, less is reconverted to methane, and the total hydrogen production remains almost constant. The net result of this is that the cell performance, as measured by current density at a given polarization, only falls slowly for 50 hours or so, then begins to decrease as the catalyst decay becomes really severe. This is illustrated in Figure 13. This accounts for the fact that the cell appears to be stable for short term operation, though examination of the vent gases would show a dramatic change during the first 24 hours of operation.

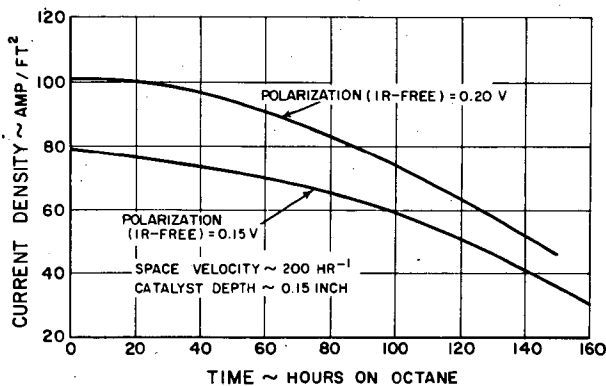


Figure 13. Comparison of Catalyst Aging Effect on Current Density with Octane Fuel at APV = 0.20

In the case of methane fuel, a much reduced decay rate was observed. A cell was run for a total of 730 hours at a constant anode potential of .015V. The current density changed only from 65 amps/ft² to 50 amps/ft² and the fuel utilization from 80% to 60%. The methane system exhibits another clear difference over liquid hydrocarbons: There is no complication of the methane-producing side reaction, and the equilibrium partial pressure of hydrogen for any degree of extraction may be calculated thermodynamically. By comparing the performance of an internal reforming anode with that

of a palladium anode fed with hydrogen at the calculated equilibrium partial pressure, it should be possible to examine the rates of the reform reaction and the extraction process separately. This work is at present in progress.

CONCLUSION

This work has shown that the demonstrated performance of the internal reforming hydrocarbon cell, in terms of current-voltage curves and utilization efficiency, is superior to that of other direct hydrocarbon systems.

However, a closer look at the system indicates that one can easily be misled by a single consideration of current-voltage curves for hydrocarbon fuel cells. Consideration of the fuel utilization efficiency requirement dictates that the higher current densities demonstrated may be unfeasible from an efficiency standpoint. There will be a difficult optimization process between cell volumes, catalyst bed thickness, maximum current density and cell efficiency. This optimization will vary for different catalysts, operating temperature and cell design, so cannot be attempted at this stage.

With present technology the current density obtainable at overall cell efficiencies of greater than 60% are still below 100 a/ft^2 and have to be increased before a commercially attractive cell can be built. Present indications are that the catalytic reforming of the fuel at 500°F is limiting the reaction, so that improved catalysts will be needed. The catalyst used in this work not only had too low an activity at 500°F, but also decayed rapidly with time at this temperature. Up to now there has never been an incentive to develop catalysts for this reaction for a thermodynamically unfavorable temperature region.

All of the work reported here was done with 1.5 mil thick foil anodes. A reduction of thickness by a factor of 3 to 5 may be needed to obtain economic feasibility. Such a reduction in thickness will also bring about higher current densities due to higher

hydrogen transport, so another optimization of material cost, power density and technical fabrication will be required.

During the operation of the internal reforming cell, we have learned that time-decay effects can be far from obvious, and only a careful monitoring of all the separate processes going on in a complex system can show whether a decay effect is occurring. Otherwise a decay may be compensated by another variable for long periods of time, only to appear as a performance loss at a later point.

In conclusion, the authors would like to thank Messrs. T.G. Schiller, W. Levins, G. Smarz, J. Allison and others who have contributed to the work described in this paper. We would also like to acknowledge the U.S. Army Engineer Research and Development Laboratory, under whose contract DA-44-009-AMC-756(T), part of this work was carried out, and thank the management of Pratt & Whitney Aircraft for their permission to publish the results.

REFERENCES

1. Oswin, H.G. and Chodosh, S.M., "Non Porous Hydrogen Depolarized Anodes for Fuel Cells," in Fuel Cell Systems. R. Gould, Editor. Advances in Chemistry Series, No. 47, ACS Applied Publications, 1965.
2. Palmer, N.I., Vertes, M.A. and Liebermann, B. - to be published at the 1965 Fuel Cell Symposium of the A.C.S.
3. Vertes, M.A. and Hartner, A.J., "Internal Reforming Fuel Cells" - presented at the S.E.R.A.I. conference on fuel cells, Brussels, June 1965.

Studies on the Fuel Electrodes of Liquid Fuel Cells

Masaru Yamano and Hironosuke Ikeda

Sanyo Electric Co., Ltd. Research and Development Center, Osaka, Japan

(1) Introduction

Various activation catalyst metals have been used as the electrodes of alkaline liquid fuel cell (1), (2), (3). However, some ambiguity exists as to what the properties of such activation catalyst metals are and in what state and to what liquid fuels these electrodes are actually suited.

The present authors have used typical alkali-resistant metals, i.e. Au, Ag, Pt, Pd, Ni and Cu as catalyst metals, and formaldehyde (4), hydrazine (5), (6) and methanol, which are conventional and typical fuels as liquid fuels in consideration of reaction velocities (7). They have examined various combinations of these liquid fuels with the above-mentioned catalyst metals and studied the resulting polarization characteristics.

In the experiment performed, the electrodes prepared by forming various catalyst metal powders under the pressure of 2 tons/cm² were immersed in a mixture of each of the fuels tested and an alkaline electrolyte, and the resulting polarization characteristics were measured.

The results have shown that Pt, Pd and Au powders which have high oxygen over-potentials and low hydrogen potentials are preferred. Then, the authors have prepared such powders having different surface areas, and studied the resulting polarization characteristics.

Lastly, with the electrodes prepared by forming the activation catalyst powders of Pt and Pd having the surface areas of 32.9 m²/gr. and 31.8 m²/gr., respectively, polarization characteristics were measured in mixtures of the alkaline electrolyte and various mono, di, tri and polyhydric saturated alcohols having different numbers of carbon atoms to find the manner in which the activation catalysts would act upon the different fuel alcohols.

(2) Experiment

(2.1) Preparation of Metal Powders

The following metal powders were used:

- a) Copper Powder; purity 99.97%, electrolysis.
- b) Iron Powder; purity 99.992%, carbonyl iron powder (Mond Chemical).
- c) Nickel Powder; purity 99.998%, carbonyl nickel powder (Mond Chemical B type).
- d) Silver Powder; purity 99.97%, by dissolving 10 gr. AgNO₃ in 10 cc. pure water, adding 50 cc. HCHO and 85 cc. 50% KOH while cooling, allowing to stand for 2 hours, washing and drying.

- e) Palladium Black; purity 99.98%, by dissolving 10 gr. PdCl_2 in 20 cc. 5% HCl, adding 50 cc. 30% HCHO and 87 cc. 50% KOH while cooling, allowing to stand for 2 hours, washing and drying.
- f) Gold Black; purity 99.96%, by dissolving 10 gr. HAuCl_4 in 200 cc. pure water, adding 55 cc. 33% HCHO and 92 cc. 50% KOH while cooling, allowing to stand for 2 hours, washing and drying.
- g) Platinum Black; purity 99.975%, by dissolving 10 gr. H_2PtCl_6 in 200 cc. pure water, adding 60 cc. 33% HCHO and 98 cc. 50% KOH, allowing to stand for 2 hours, washing and drying.
- h) Heat-treated Powders; each of the above blacks was heat-treated in nitrogen gas at 200° , 400° and 600°C . for 20 minutes.
- i) Thermodecomposed Powders; purity Pd 99.98%, Pt 99.995%, Au 99.96%, heating H_2PtCl_6 , PdCl_2 , and HAuCl_4 , respectively, at 500°C . in an electric furnace, followed by thermodecomposition in nitrogen gas for 20 minutes.

2.2) Preparation of Activation Catalyst Metal Electrodes

Each of the test electrodes was prepared by weighing 300 mg. of metal powder and forming it under the pressure of 2 tons/cm² into a disc, about 15 mm. in diameter and about 0.5 mm in thickness.

2.3) Method of Measurement

a) Measurement of Surface Areas

In order to ascertain the relationship between the surface areas and electrode characteristics of the various metal powders prepared in (2.1) (i.e. the black, the heat-treated and the thermodecomposed samples), the surface area of each test electrode was measured by B.E.T. method.

b) Measurement of Polarization Characteristics with Various Fuel Electrodes.

Each of the test electrodes prepared as per (2.2) was immersed in a mixed solution containing 10 parts of 25% aqueous solution of KOH and 2 parts of each fuel and the polarization characteristics on anodic oxidation were measured with an opposite electrode of Ni plate. With a reference electrode of Hg/HgO 1N-KOH, polarization characteristics at various current densities were measured at 20°C . Fig. 1 shows the experimental arrangement used.

(3) Results of Measurements

(3.1) Measurement of the Surface Areas of Various Metal Powders

The results are given in Table 1.

Organically reduced powders are generally known as metallic blacks and have comparatively large surface areas. Reductions in surface area due to heat-treatment are linearly distributed. The samples prepared by thermodecomposition of metallic salts show

smaller surface areas at the same temperature of heat treatment.

(3.2) Polarization Characteristics with Various Activation Catalyst Metals

For the purpose of ascertaining the properties of various activation catalyst powders, i.e. Pt, Pd, Au, Ag, Ni and Cu, the powder surface area of 0.18 to 0.75m²/gr. was selected so that the influences due to variety in surface area might be minimal.

a) Formaldehyde

With various electrodes prepared as per (2.2), polarization characteristics were measured in a mixture of 10 parts 25% KOH and 2 parts formaldehyde at current densities of 0-100 ma/cm². The results are shown in Fig. 2. The order of increasing polarization is Au, Pt, Pd, Ag, Ni and Cu.

b) Hydrazine

Polarization characteristics were measured in the same manner as above by immersing each metal powder electrode in a mixture of 10 parts 25% KOH and 2 parts hydrazine. The results have shown that Ni, Pt and Pd powders exhibits superior characteristics. (See Fig. 3).

c) Methanol

In a mixture of 10 parts 25% KOH and 2 parts methanol, polarization characteristics were measured in the same manner as above. It will be apparent from Fig. 4 that Pt, Pd and Au are superior in that order. The other metals showed quite unsatisfactory results.

(3.3) Polarization Characteristics by Surface Area with Pt, Pd and Au Electrodes

a) Formaldehyde

The Pt, Pd and Au blacks prepared as per (2.1), each having a various surface area, were used as electrodes and polarization characteristics were measured with respect to formaldehyde. Fig. 5 shows the relationship between the polarization potentials of the Pt, Pd and Au electrodes on anodic oxidation at the current density of 500 ma/cm² and the surface areas of those activation catalyst metal powders.

For all of Pt, Pd and Au, the difference in surface area of the electrode does not exert any great influence. If the electrode is made of a powder which surface area is about 1.0 m²/gr., there will be a relatively low degree of polarization on anodic oxidation even at 500 ma/cm² and invariably satisfactory results are obtained with any of the above-mentioned catalyst metals.

b) Hydrazine

The Pt, Pd and Au blacks prepared as per (2.1), each having a various surface area, were used as electrodes and polarization characteristics were measured with respect to hydrazine in the same manner as (2.2). Fig. 6 shows the relationship between the polarization potential of the electrodes on anodic oxidation at 200 ma/cm² in hydrazine and the surface areas of the electrode metals. In the case of Pt, there was no significant difference in characteristics due to changes in surface area, just as it was the case with formaldehyde. However, with the Pd electrodes, there was found a slightly significant influence, for the electrode potential was altered more appreciably within the range of 8.54 m²/gr. - 1.67 m²/gr. than within the range of more than 8.54 m²/gr. Moreover, with respect to Au, the influence of smaller surface areas was conspicuous and when it was less than 1.0 m²/gr., the degree of polarization was inordinately high.

c) Methanol

The Pt, Pd and Au blacks prepared as per (2.1), each having a various surface area, were used as electrodes and polarization characteristics were measured with respect to methanol in the same manner as (2.2). Fig. 7 shows the relationship between the electrode potential in methanol on anodic oxidation at the current density of 100 ma/cm² and surface areas of those catalyst metal powders.

Compared with formaldehyde and hydrazine, the influences of differences in surface area were conspicuous for all the Pt, Pd and Au electrodes. Among them, the influences were relatively minor in the case of Pt, while a slightly higher degree of polarization was observed in the case of Pd. With respect to the Au electrodes, which generally have smaller surface areas, considerably high degrees of polarization were observed on anodic oxidation at 100 ma/cm². Within the range of surface areas which could be measured, there was a greater influence of changes in surface area of Au powders than in the case of Pt and Pd.

(3.4) Polarization Characteristics with Various Electrodes in Saturated Alcohols

Polarization characteristics were measured with Pt and Pd black electrodes in various saturated alcohols and their isomers.

a) Pt Electrode Characteristics by the C-number of Mono, Di and Tri, and their isomers.

- (i) With the Pt black electrodes prepared as per (2.1) and (2.2), polarization characteristics on anodic oxidation were measured to ascertain the influences of the C-numbers of mono, di and trihydric alcohols and the isomers of monohydric alcohol. Fig. 8 shows the characteristics obtained with monohydric alcohols having different C-numbers and their isomers. In Fig. 9 are shown the polarization characteristics with dihydric alcohols having different C-numbers. Fig. 10 shows the influences of trihydric alcohols

As regards monohydric alcohols, the C-number range surveyed was from C_1 to C_{10} ; dihydric alcohols from C_2 to C_{10} ; trihydric alcohols from C_3 to C_5 . According to Fig. 8, it is found that the greater the C-number is, the higher the degree of polarization is. As regards their isomers, the degree of polarization increases in the order of iso, sec and tert, and extremely high degrees of polarization are obtained with propyl and higher alcohols. With regard to di and trihydric alcohols (See Fig. 9 and 10.), the degree of polarization increases in C-numbers as it is the case with monohydric alcohols. In the case of dihydric alcohols, high degrees of polarization are obtained with C_5 and up. In regard to trihydric alcohols, the degree of polarization is relatively low up to C_5 .

(ii) Pt Electrode Characteristics with Various Saturated Alcohols, Each Containing the Same Number of C and OH.

With the same Pt black electrode as (a-i), polarization characteristics were measured for mono to hexahydric alcohols, each containing the same number of C and OH. It will be apparent from Fig. 11 that the degree of polarization increases in the order of mono, di and trihydric alcohols, but that in the case of polyhydric alcohols, even hexahydric alcohols shows a relatively low degree of polarization.

b) Pd Electrode Characteristics by the C-number of Mono, Di Tri and Polyhydric Alcohols and their Isomers.

1) With the Pd black electrodes prepared as per (2.1) and (2.2), polarization characteristics on anodic oxidation were measured to ascertain the influences of the numbers of C atoms contained in mono, di and trihydric alcohols. Fig. 12 shows the influences of the C-numbers of monohydric alcohols and their isomers. Similar influences for dihydric alcohols are illustrated in Fig. 13 and Fig. 14 relates to trihydric alcohols. It will be apparent from Fig. 12, 13 and 14 that just as with the Pt black electrode mentioned-above, the greater the C-number is, the higher the degree of polarization is, and that as regards the various isomers, the degree of polarization is higher in the order of iso, sec and tert.

The degree of polarization is pronounced with propyl and higher alcohols. In the case of dihydric alcohols, the degree of polarization is conspicuously high for C_5 and up, while trihydric alcohols show relatively low degrees of polarization up to C_5 , just as it is the case with the Pt black electrode.

ii) Pd Electrode Characteristics for Various Alcohols, Each Containing the Same Number of C and OH.

With the same Pd black electrodes as (b-i), polarization characteristics were measured for mono to hexahydric alcohols, each having the same number of C and OH. (See Fig. 15) The degree of

polarization is higher in the order of CH_3OH , $\text{C}_2\text{H}_4(\text{OH})_2$, $\text{C}_3\text{H}_5(\text{OH})_3$ and so on, although it is still relatively low even in the case of hexite.

(4) Discussion

In order to ascertain the characteristics of various activation catalyst metals as electrodes, we have selected certain metals on the basis of their chemical reactivities in mixtures of an alkaline solution and various liquid fuels, and studied the polarization characteristics of the above activation catalysts for different fuels. The fuels used are those which are readily miscible with electrolyte KOH. Thus, we have used formaldehyde which is capable of undergoing Cannizzaro's reaction, hydrazine which is partially decomposed in the presence of catalysts, and methanol which is only sparingly decomposed in the presence of the catalysts. Considering the characteristics of various electrode metals with respect to formaldehyde, as will be apparent from Fig. 2, any of the metals tested is useful. However, the order of preference is Au, Pt, Pd, Ag, Ni and Cu, and it is found that even if a metal having somewhat high hydrogen over-potential, e.g. Ag, is employed a satisfactory result may still be obtained so long as it also has a sufficiently high oxygen over-potential. In other words, a high oxygen over-potential is a primary requirement.

It will be seen from Fig. 5 that since only minor differences in characteristics are attributable to differences in surface area of catalyst metal, the only requirement for the electrode is that it should be an effective current collector. From the polarization characteristics for hydrazine, it is found that whereas only unsatisfactory results are obtained with Ag which exhibits relatively good characteristics with formaldehyde (Fig. 3), considerably better results are obtained with Ni. It is presumed, therefore, that in addition to a high oxygen over-potential, a low hydrogen over-potential is essential. Furthermore, in view of the catalytic decomposition of hydrazine, it is thought that sufficiently satisfactory polarization characteristics are obtained when the surface area of the catalyst metal powder is larger than $1.0 \text{ m}^2/\text{gr}$. (See Fig. 6)

With regard to methanol, it will be apparent from Fig. 4 that better results are obtained in the order of Pt, Pd and Au, while the other metals are quite unsatisfactory in respect of polarization characteristics. Thus, in addition to the above-mentioned requirement of high oxygen over-potential and low hydrogen over-potential, it is found that, as will be seen from Fig. 7, the greater the surface area of the activation catalyst metal is, whether it is Pt or Pd, the more satisfactory the polarization characteristics are. At least, within the range of measurement described above, a logarithmically linear relation holds between polarization potential and the surface area of the activation catalyst metal. It will also be seen that to activate methanol, a surface area of more than about $20 \text{ m}^2/\text{gr}$. is required. Thus, by selecting a large surface area, the catalytic oxidation may be accelerated.

Then, with the so-called metal black electrodes of Pt and Pd powders having maximal surface areas, we have studied the influences

on polarization characteristics of the number of C atoms in various mono, di, tri and polyhydric alcohols. Pt and Pd exhibit the same tendency, and the degree of polarization increases in higher alcohols of each group. As regards their isomers, the degree of polarization is higher in the order of n, iso (8), sec and tert. On the other hand, even when the C-number is large, polyhydric alcohols, which contain many OH groups, shows only low degrees of polarization and therefore, can serve as effective fuels. Especially satisfactory results are obtained when given alcohol contains the same number of C atoms and OH groups, e.g. in the case of methanol, ethylene glycol, glycerin, erythrite, adonite and mannite. (See Fig. 11 and 15.) It is presumed, therefore, that when the activation catalysts of Pt and Pd are used as electrodes, the OH groups have an important role on the anodic oxidation of alcohols, improving their polarization characteristics. With respect to hydrocarbons, it is presumably difficult to be activated even if the surface area of Pt or Pd is made extremely large. Thus, it is preferable to employ alcohols whose numbers of C atoms and OH groups are the same or not substantially different. If Pt and Pd black electrodes are used as activation catalysts, polyhydric alcohols having substantially the same number of C atoms and OH groups will prove to be effective fuels for a liquid fuel cell.

(5) Acknowledgement

The authors wish to thank Mr. Kenichi Toyota and other associates of Sanyo Electric Co., Ltd. - Research and Development Center for their assistances in the experimental work. Thanks are also due to Miss Reiko Kihara for her assistance in manuscripts.

(6) References

- (1) J. E. Wynn, Proc. 14th Power Sources Conference (1960).
- (2) U. S. Pat. 2925454.
- (3) P. G. Grimes et al, Proc. 15th Power Sources Conference (1961).
- (4) H. Ikeda, 5th Symposium by the Chem. Soc. of Japan (1964).
- (5) H. Hunger, Proc. 13th Power Sources Conference (1959).
- (6) B. Baker and E. Eisenberg, Extended Abstracts of Electrochem. Soc. 113 (1962).
- (7) T. Hayashi, 4th Battery Symposium by the Chem. Soc. of Japan (1963).
- (8) Y. Miyake et al, 31st Meeting by the Electrochem. Soc. of Japan (1964).

Table 1.-SURFACE AREA OF VARIOUS METAL POWDERS

condition kinds of metal	Powder reduced by formaldehyde (m ² /g)	Powder by heat treating metal black			direct thermo decomposition of metallic salts(m ² /g)
		200°C 20 ^{min} (m ² /g)	400°C 20 ^{min} (m ² /g)	600°C 20 ^{min} (m ² /g)	
Pt	32.9	15.54	8.18	2.74	0.18
Pd	31.8	20.7	8.54	1.67	0.20
Au	3.55	2.56	1.345	0.735	0.02
Ag	0.19				

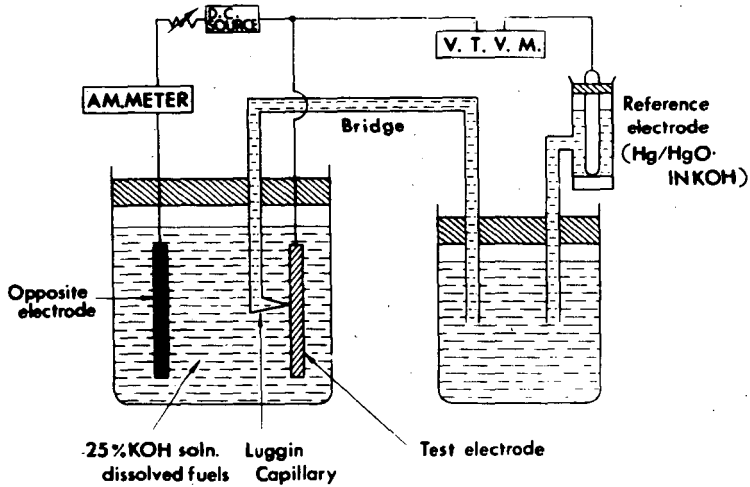


Fig. 1.-EXPERIMENTAL ARRANGEMENT FOR MEASUREMENT OF ANODIC POTENTIALS

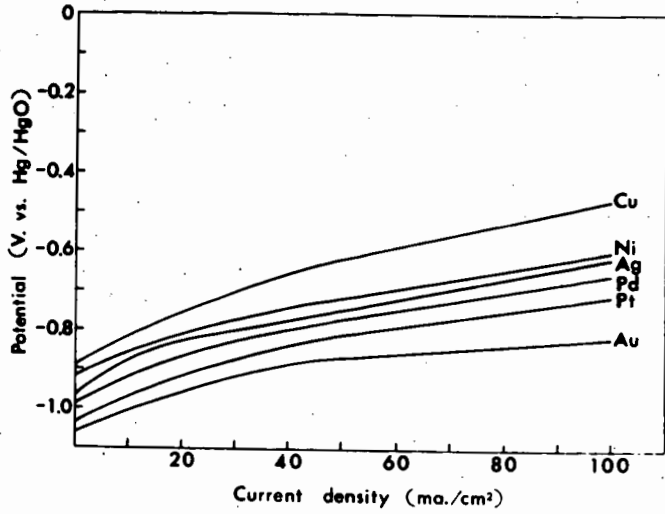


Fig. 2.-ANODIC OXIDATION POTENTIALS OF VARIOUS ACTIVATION CATALYST METALS IN FORMALDEHYDE

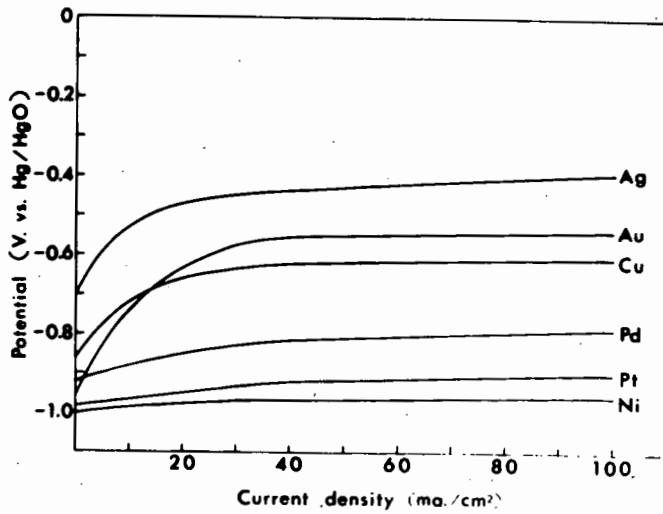


Fig. 3.-ANODIC OXIDATION POTENTIALS OF VARIOUS ACTIVATION CATALYST METALS IN HYDRAZINE

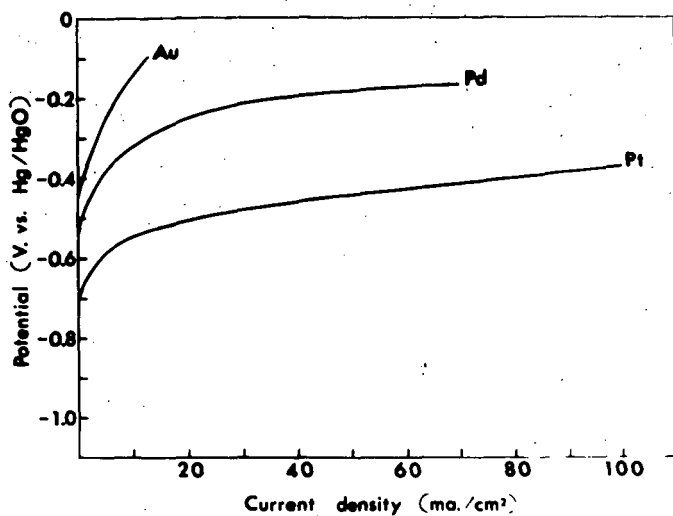


Fig. 4.-ANODIC OXIDATION POTENTIALS OF VARIOUS ACTIVATION CATALYST METALS IN METHANOL

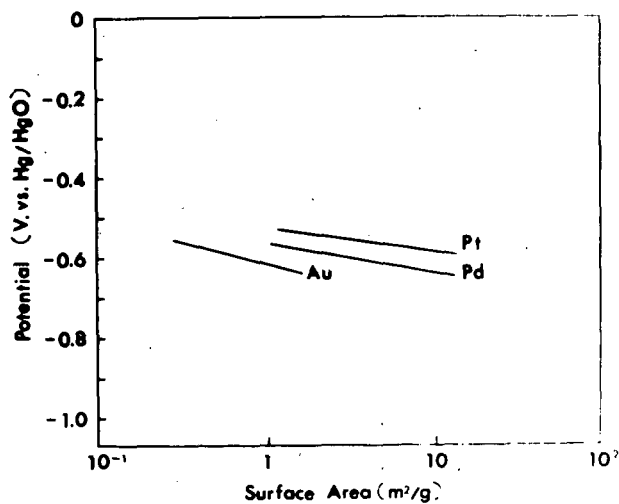


Fig. 5.-ANODIC OXIDATION POTENTIALS vs SURFACE AREA OF Pt, Pd, AND Au IN FORMALDEHYDE AT CURRENT DENSITY OF 500 MA/CM²

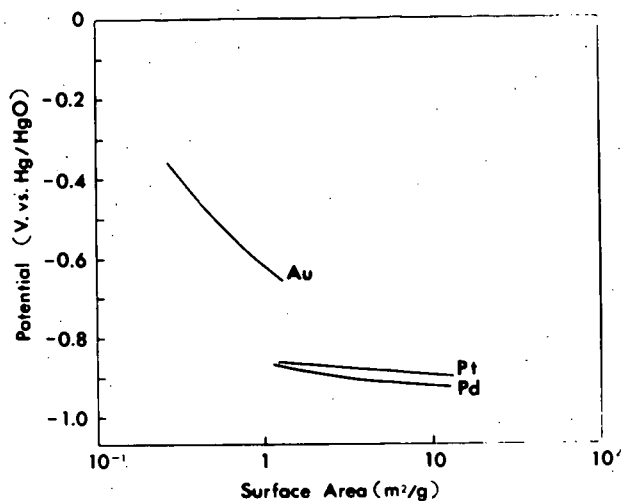


Fig. 6. -ANODIC OXIDATION POTENTIALS vs SURFACE AREA OF Pt, Pd, AND Au IN HYDRAZINE AT CURRENT DENSITY OF 200 MA/CM²

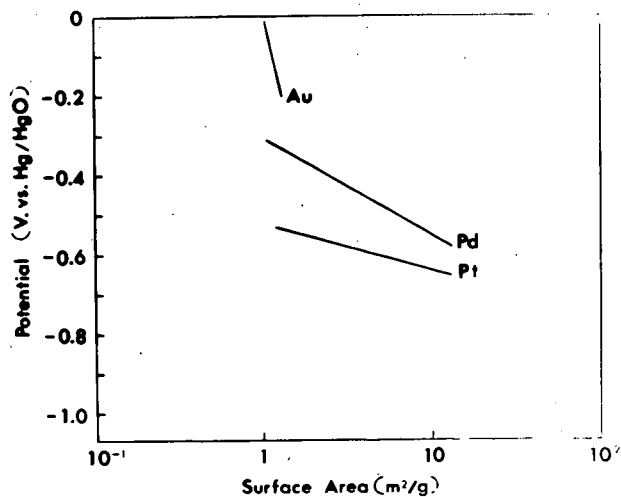


Fig. 7. -ANODIC OXIDATION POTENTIALS vs SURFACE AREA OF Pt, Pd, AND Au IN METHANOL AT CURRENT DENSITY OF 100 MA/CM²

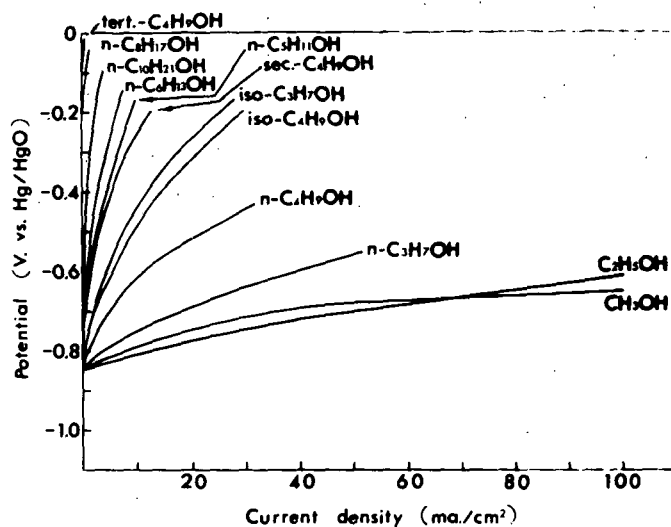


Fig. 8. -Pt ANODIC POTENTIALS WITH THE C-NUMBER AND THEIR ISOMERS OF MONOHYDRIC ALCOHOLS

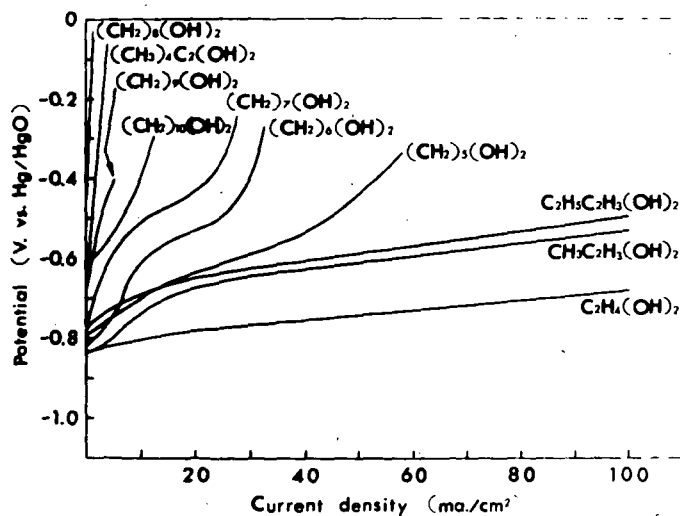


Fig. 9. -Pt ANODIC POTENTIALS WITH THE C-NUMBER OF DIHYDRIC ALCOHOLS

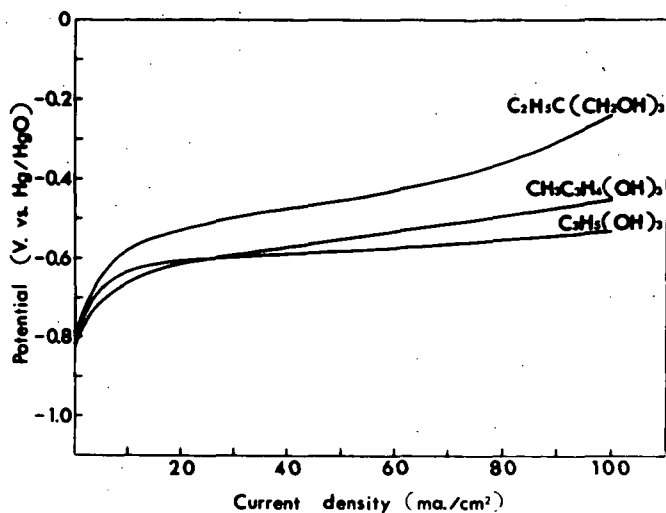


Fig. 10.-Pt ANODIC POTENTIALS WITH THE C-NUMBER OF TRIHYDRIC ALCOHOLS

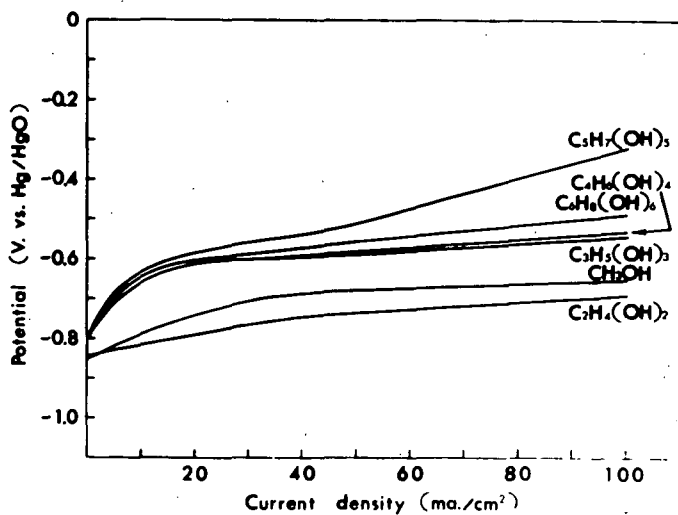


Fig. 11.-Pt ANODIC POTENTIALS WITH VARIOUS ALCOHOLS EACH CONTAINING THE SAME NUMBER OF C AND OH

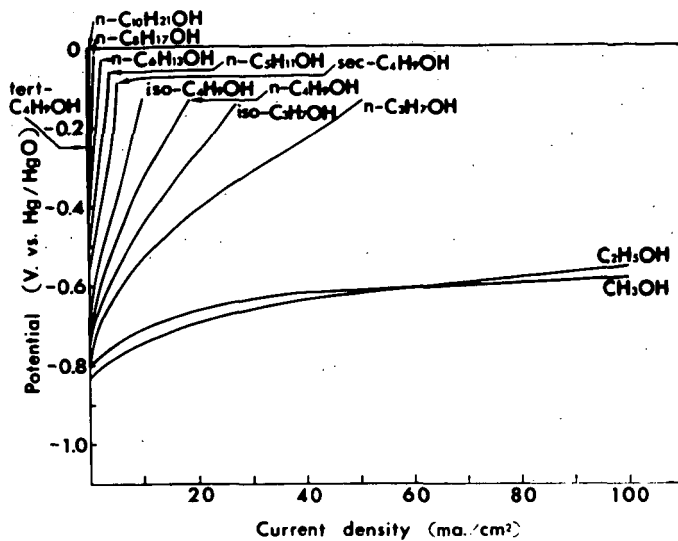


Fig. 12.-Pd ANODIC POTENTIALS WITH THE C-NUMBER AND THEIR ISOMERS OF MONOHYDRIC ALCOHOLS

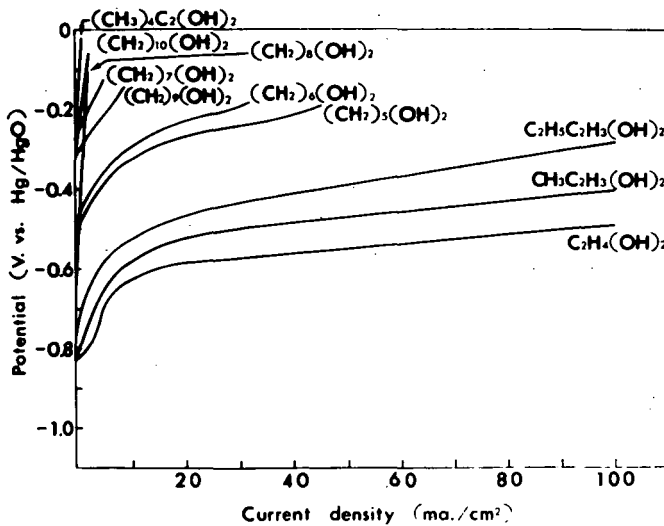


Fig. 13.-Pd ANODIC POTENTIALS WITH THE C-NUMBER OF DIHYDRIC ALCOHOLS

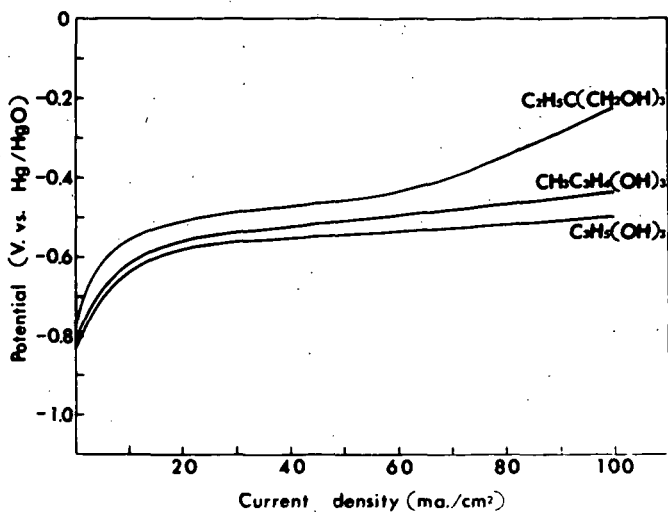


Fig. 14.-Pd ANODIC POTENTIALS WITH THE C-NUMBER OF TRIHYDRIC ALCOHOLS

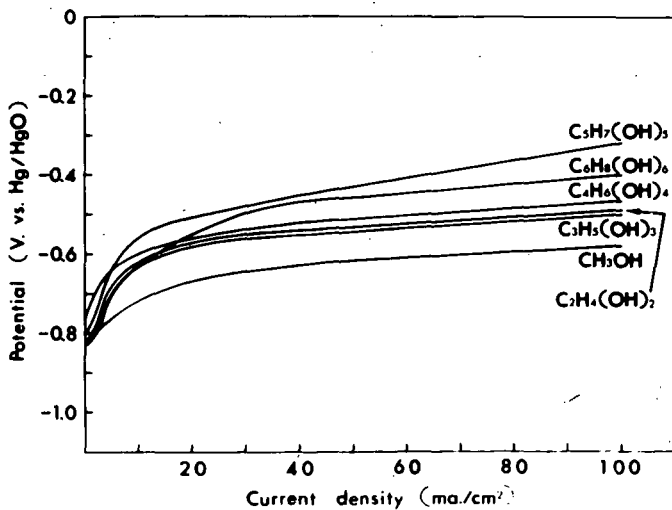


Fig. 15.-Pd ANODIC POTENTIALS WITH VARIOUS ALCOHOLS EACH CONTAINING THE SAME NUMBER OF C AND OH

THE ELECTROCHEMICAL OXIDATION OF HYDROCARBONS;
NATURE AND ACTIVITY OF ELECTRODEPOSITED
PLATINUM BLACKS CONTAINING VARYING AMOUNTS OF LEAD

Raymond Thacker

Research Laboratories, General Motors Corporation, Warren, Michigan

INTRODUCTION

The electrochemical oxidation of hydrocarbons, such as propane, at relatively high rates necessitates the use of a finely divided platinum catalyst.¹⁻⁵ Other materials that have been tried, namely, palladium,⁶⁻⁹ nickel,⁶ silver,⁹ cobalt molybdate,¹⁰ and nickel boride,¹¹ although showing some activity, are not as satisfactory. In a recent paper¹² it was indicated that high rates of oxidation can be sustained only if large amounts of platinum (>35 mg./cm.²) are used. Smaller amounts (9 mg./cm.²) do not perform quite as well. A question that immediately arises is whether surface area is the sole criterion for electrochemical activity. From the experimental fact that electrodes containing the same amount of platinum have a variable activity, it might be suggested that there is some other important physical property playing a significant role.

At this time, only a few attempts have been made to investigate the role of the catalyst in organic electro-oxidation.^{13, 14} Dahms and Bockris¹⁴ made a comparative study of the anodic oxidation of ethylene on bright metal electrodes made of Au, Ir, Pd, Pt, and Rh in M sulfuric acid at 80° C. No attempt appears to have been made to determine the reasons for the catalytic activity of the finely divided metals, particularly of platinum. Joncich and Hackerman¹⁵ have studied the relationship between the surface area of electrodeposited platinum black and concentration of chloroplatinic acid plating solution, current density, time, and geometry of the electrode system. Among other things, they showed that for a particular solution and system there is an optimum current density which gives the maximum surface area. In an earlier paper, Bianchi¹⁶ showed that the character of electrodeposited platinum black can be profoundly altered by the inclusion of heavy metal ions in the plating solution. Pb, Hg, Cd, and Tl inclusions in the deposit led to an increase in the lattice parameter, whereas Cr, Mn, Fe, Co, Ni, Cu, Zn, and Pd led to a decrease. Sb, Bi, Sn, As, and Au, although altering the appearance of the deposit, had no effect on the lattice parameter.

Since a hydrocarbon electrode reaction involves an initial adsorption step, it would appear that the lattice spacing of the catalyst is important. By using electrodeposited platinum black containing various inclusions, it is possible that some indication of the effect of lattice spacing in electro-organic reactions might be obtained.

The work reported here consists of an investigation of the effect of lead content on the nature of electrodeposited platinum, and the activity of these deposits toward the electrochemical oxidation of ethane, ethylene, propane, propylene, and n-butane in 5M H₃PO₄ at 80° C.

EXPERIMENTAL

The cell used in this work is shown in Fig. 1 (a). It consisted of a Pyrex glass tube, 12 cm. long and 3.5 cm. in diameter, with a coarse glass frit, H, sealed into it, 2 cm. from the bottom. Two glass tubes, A and B, 8 mm. outside diameter, each having a 7/25 socket sealed to the ends, were connected to the cell, one below the frit and the other 2 cm. from the top. These tubes were used for admitting and venting gases, as indicated in the figure. The cell top contained four 7/25 sockets

which supported three working electrodes, F, and a reference electrode, C. The working electrodes consisted of a platinum wire, 1 cm. long and 0.5 mm. in diameter, sealed through a 7-cm. long tube, which was connected to a 7/25 through-cone. The reference electrode, a Beckman saturated calomel electrode with a fiber junction, was connected to the cell through a salt bridge containing the same electrolyte. The salt bridge was comprised of a 7/25 through-cone and a closed, electrolyte-lubricated stopcock, D. The tip of the bridge tube was drawn down and then bent up to prevent gas bubbles from getting into it. The counterelectrode, G, consisted of a close fitting, 2-cm. long platinum gauze (50 mesh) cylinder. A platinum lead connected to this electrode was sealed through a small side tube at the upper end of the cell. About 40 cc. of electrolyte was used in the cell, and this occupied a little over half the volume above the frit. The gases before admission to the cell were passed through a similar vessel containing the same electrolyte, in order to saturate them with water vapor. Both the cell and the water vapor gas saturator were maintained at $80^{\circ} \pm 1^{\circ}$ C. in a water bath controlled by an Electromax temperature controller. The water level in the bath was maintained by a simple float valve.

Before a run, the cell and saturator were cleaned by soaking in concentrated nitric acid for about 2 hr. They were then thoroughly washed with copious amounts of distilled water. To remove the acid from the frits, large amounts of distilled water were drawn through them with a water pump. Finally, after soaking in distilled water for some time, they were washed with triply distilled water. During the washing of the cell and the saturator, the working electrodes were prepared, and the electrolyte was purified by pre-electrolysis.

The working electrodes were cleaned by heating to a white heat followed by immersion in concentrated nitric acid. After repeating this operation several times, the electrodes were washed in triply distilled water. They were then coated with platinum black by electrodeposition using a small cell, shown in Fig. 1 (b). The working electrode, F, was mounted vertically inside the center of the small glass thimble containing 2.5% chloroplatinic acid and a small concentration of lead acetate. A small, 1-cm. long platinum gauze (50 mesh) cylinder, G, which fitted closely inside the thimble was used as a counterelectrode. The platinum wire lead of the counterelectrode was sealed through the bottom of the thimble. The working electrode was platinized at a current density of 10 ma./cm.² for 1 hr. During this interval it was alternately anodized and cathodized for periods of 1.5 min. by using a timer and reversal switch. The plating solution was discarded after the preparation of each electrode and was replaced by unused stock solution.

The electrolyte was pre-electrolyzed in a single compartment cell which was provided with gas inlet and outlet tubes. It held 65 cc. of electrolyte. The cell top was a 24/40 through-cone, which had two 6-mm. outside diameter tubes connected to the lower side. Platinum wire leads were sealed through these tubes. One was spot-welded to a 5-cm. long platinum gauze (50 mesh) cylinder from which a section had been removed, and the other wire was placed vertically inside the cylinder. Before use the pre-electrolysis cell and electrodes were cleaned as described above. The 5M H₃PO₄ used here was pre-electrolyzed for 60 to 100 hr. at a total current of 40 ma. using the platinum wire as the anode. The anodic current density was 62.5 ma./cm.². The electrolyte was stirred with nitrogen during the pre-electrolysis. With this arrangement, it was considered that oxidizable material would be removed at the anode, but would not be converted to the reduced state at the cathode because of the larger area and hence lower current density.

The gases were supplied to the cells through polyethylene tubes, and ground glass joint connectors were used throughout. Glass tubing was sealed to the polyethylene tubing with molten polyethylene.

The sources and grades of the materials were: hydrocarbons - Matheson, C.P. grade; nitrogen - Matheson, pre-purified grade; and phosphoric acid - Baker, analytical reagent grade.

RESULTS AND DISCUSSION

The electrodeposited platinum blacks were characterized by measurements of the lead content, crystal structure, and surface area. For the first two, the deposits were prepared on two platinum foils, 1 cm.² in area, which were mounted 1 cm. apart in a cell similar to that shown in Fig. 1 (b) except that it did not contain a cylindrical platinum gauze counterelectrode. The current density (10 ma./cm.²); time of plating (1 hr., during which time the electrodes were alternately anodized and cathodized as described above), temperature (25° C.), and concentration of chloroplatinic acid solution (2.5%) were identical with the conditions used in preparing electrodeposited platinum blacks on platinum wires (geometric area of 0.16 cm.²) for the electrochemical measurements. The only difference between the several deposits was the amount of lead acetate contained in the chloroplatinic acid solutions. This was varied between 0 and 0.2%.

In the first two columns of Table I are shown the lead acetate concentrations and the appearances of the deposits, respectively. It will be seen that lead acetate concentrations between 0.003 and 0.05% gave black, powdery deposits, the degree of subdivision diminishing with increasing concentration, whereas lead acetate concentrations between 0.075 and 0.2% gave grey, compact deposits. The deposit prepared in the absence of lead acetate was grey and compact and was similar in appearance to those obtained with the higher lead acetate concentrations. The coulombic efficiencies, as shown in the third column of Table I, were close to 40% for all of the deposits.

The deposits prepared by Bianchi¹⁶ using the same lead acetate concentrations were different from those described here in that they were black and very powdery, the degree of subdivision increasing with concentration. Two reasons can be presented for the differences, namely, that Bianchi used a lower concentration of chloroplatinic acid solution (1%) and a much higher current density (625 ma./cm.²). A lower coulombic efficiency (≈3%) was reported. In the present work, it was shown that current densities greater than 10 ma./cm.² gave rise to much gassing and a finer black deposit which tended to appear in the electrolyte as a colloidal solution. Hackerman¹⁵ has also shown that variations in the nature of electrodeposited platinum black can result from changes in concentration and current density.

The lead content of the deposits was determined by a nondestructive X-ray fluorescence method using a standard thin film flat specimen technique.¹⁸ A calibrated set of standards for this method was obtained by atomic absorption analysis of chemically stripped deposits. The Pb/Pt atomic ratios were calculated from the analytical data and are shown in the fourth column in Table I. In Fig. 2 is shown the plot of Pb/Pt atomic ratio vs. lead acetate concentration. It will be seen that this ratio increases almost linearly up to a lead acetate concentration of 0.08%, whereafter it tends to a constant value at higher concentrations. The deposits prepared from solutions containing 0.075, 0.1, 0.15, and 0.2% lead acetate have similar Pb/Pt atomic ratios and, as might be expected, have a similar appearance.

All the deposits gave Debye Scherrer diffraction patterns, indicating that they were crystalline. In contrast, Bianchi¹⁶ found that the powdery deposits obtained with lead acetate concentrations from 0.08 to 0.15% gave no lines which he concluded was a result of the deposits being in a state of colloidal dispersion. An appreciable line broadening, which tends to increase with lead content, is evident in the present results, suggesting that the crystallite sizes are smaller in the higher lead containing deposits. A line shift was also observed in going from the deposit containing no lead to the one having a Pb/Pt ratio of 0.0021 and remained

constant with further increases in this ratio, in contrast to the gradual increase observed by Bianchi.¹⁶ It would appear that the lattice constant of the lead containing deposits is greater than that of pure platinum, but it does not increase with increasing Pb/Pt atomic ratio. The diffraction patterns contained several unidentified lines which could very well be explained by a solid solution of lead in platinum, in agreement with data reported in the literature.¹⁶

Two methods were used to determine the areas of the platinum black electrode deposits supported on platinum wires (geometric area = 0.16 cm.²). The electrodes used for this purpose were those used later in an investigation of the electro-oxidation of hydrocarbons. In the first method, the area of the deposits was determined from the charge required to form a monolayer of oxygen atoms in a triangular sweep measurement.¹⁹ In general, the electrodes were cleaned by soaking in concentrated nitric acid for 15 min., followed by washing with copious amounts of distilled water and finally with triply distilled water. They were then immersed in nitrogen stirred 5M H₃PO₄ at 80° C. contained in the cell and were held for 1 min. at 1.4v vs. NHE (Normal Hydrogen Electrode)* and then for 1 min. at 0v using an electronic potentiostat.²⁰ A triangular voltage sweep was then applied potentiostatically to the electrode at a sweep rate of 20 mv./sec. Typical curves, dashed and dotted lines, shown in Fig. 3, were obtained for deposits having Pb/Pt atomic ratios of 0.0021 and 0.0256, respectively. The oxidation peaks at 1.08v are the result of the formation of a monolayer of oxygen atoms on the electrode surface,²¹ and the reduction peaks at 0.76v are the result of the removal of this monolayer. The area under the peaks was measured by tracing them from the photographs of the oscilloscope traces onto vellum having a uniform weight, and then weighing the appropriate cuttings. The areas under the oxidation and reduction peaks were almost identical, as would be expected. In calculating the areas of the electrodes, it was assumed that there is one oxygen atom per surface platinum atom and that there are 1.6×10^{15} sites per square centimeter.²² The areas of the electrodes (apparent area = 0.16 cm.²) are shown in the fifth column of Table I.

The second method, attempted to determine the areas of the electrodes, consisted of the measurement of double layer capacities using a single pulse technique.²³ The differential capacity was calculated from the relationship $C = i/\frac{dv}{dt}$, where i is the apparent current density and $\frac{dv}{dt}$ is the slope of the photographed trace on the oscilloscope screen. A similar procedure to that described above was used to prepare the electrodes before application of a constant current pulse. The electrode potential after the pretreatment was about 680 mv. In order to check the method and to obtain a standard of comparison, measurements were made on a bright platinum wire (geometric area = 0.16 cm.²). The average of several determinations was 36 $\mu\text{f}/\text{cm}^2$, and if a roughness factor of two is assumed, then the value of 18 $\mu\text{f}/\text{cm}^2$ obtained is in excellent agreement with those quoted in the literature.^{23, 24} Although the method worked very well with the bright metal, it was less successful when applied to the finely divided metal. For one thing, because of the larger areas, and therefore larger double layer capacitances, the slopes of the potential-time traces, even for large current densities (375 ma./cm.²) were very small and could not be measured very accurately. Furthermore, the traces showed a continuous curvature even after short intervals ($\approx 10 \mu\text{sec.}$) from the start of the pulse, thus making it extremely difficult to determine the relevant slope. However, a procedure was developed which was used for all of the deposits. With it the deposit having a Pb/Pt atomic ratio of 0.0021 was found to have a double layer capacitance of 854 $\mu\text{f}/\text{cm}^2$, which is in good agreement with the value reported by Tarmy et al.²⁵ at the same potential. This agreement, however, may be entirely fortuitous, as the electrodeposited platinum black used by Tarmy, who did not give any details, may have been different from the one used here. Generally the areas calculated from the double layer capacities were of the same order of magnitude as those determined by the triangular sweep method, but the values were slightly lower.

*All subsequent potentials are vs. NHE unless the contrary is stated.

The lack of agreement between the two methods might be due to the difficulties encountered in applying the double layer capacity method.

In Fig. 4 is shown the plot of real area, as determined by the triangular sweep method, vs. Pb/Pt atomic ratio. It will be seen that the electrode having a Pb/Pt ratio of 0.0021 had the largest area. As the atomic ratio increases the area decreases, reaching a minimum at an atomic ratio of 0.021. The area increased slightly at higher values of the atomic ratio. The electrode containing no lead had an area between those having atomic ratios of 0.0021 and 0.021.

The activity of the several deposits toward the electro-oxidation of the hydrocarbon gases was determined using the triangular sweep method.¹⁹ A sweep rate of 20 mv./sec. was used. The same set of electrodes was used for all of the five gases--ethane, ethylene, propane, propylene, and n-butane. However, the following procedure was used in switching from one gas to another in order to remove adsorbed species on the electrodes from the previous gas. The electrodes were held at 1.4v for 1 min. and then at 0v for 1 min. using a potentiostat before applying the triangular voltage sweep. Typical curves for propylene, full line, and dash-dot-dashed line for electrodeposits having Pb/Pt atomic ratios of 0.0021 and 0.0256, respectively, are shown in Fig. 3. The oxidation peaks at 0.75v are the result of the electro-oxidation of propylene, and the areas under these peaks in millicoulombs are used here as a measure of the electrode activity. These areas were measured by the method described previously. The areas under the oxidation and reduction peaks at 1.08 and 0.76v, respectively, were also measured.

In Fig. 5 is shown a plot of hydrocarbon oxidation (area under the oxidation peaks) vs. the Pb/Pt atomic ratio. The first thing that is evident is that ethylene and propylene are electrochemically oxidized more extensively than ethane, propane, and n-butane for all values of the atomic ratio. The curves for ethane, propane, and n-butane are identical, whereas those for ethylene and propylene differ slightly. All the gases show a maximum at an atomic ratio of 0.0021, the values for propylene and ethylene being more than four times that for the saturated hydrocarbons. At higher atomic ratios the degree of oxidation diminishes, the decline being greater for ethylene and propylene. The electrodeposit containing no lead was almost as active as that having an atomic ratio of 0.0256 in the oxidation of ethylene, ethane, propane, and n-butane. Propylene was exceptional in that the electrodeposit having an atomic ratio of 0 was almost as active as the one having a ratio of 0.0021.

Comparing Fig. 4 and 5, it is seen that the variation in degree of hydrocarbon oxidation with Pb/Pt atomic ratio closely parallels the variation of real area with this ratio. In Fig. 6 the degree of hydrocarbon oxidation vs. real area is shown. It will be seen that the degree of oxidation of the unsaturated hydrocarbons increases proportionately with real area, but that of the saturated hydrocarbons does not. In the latter case, it appears that there is some other factor limiting the oxidation as the area is increased. The data presented illustrate that area is important in the electro-oxidation of hydrocarbons and that it tends to mask any other important factors such as the effect of lattice parameter.

An important consideration in organic electro-oxidation reactions is the role of chemisorbed oxygen. On platinum, oxygen chemisorption begins at a potential of 800 mv.,^{26, 27} as shown by the dashed and dotted lines in Fig. 3. The oxidation peaks of ethane, propane, and n-butane, which occur at 0.56, 0.59, and 0.56v, respectively, do not overlap the peak for "O" formation at 1.08v, but the peaks for ethylene and propylene, which occur at 0.71 and 0.77v, respectively, do. It is seen in Fig. 3 that the oxidation peak at 1.08v and the reduction peak at 0.76v in the propylene curves are, respectively, greater and smaller than the corresponding peaks in the nitrogen curves. The effect becomes smaller with increasing Pb/Pt atomic ratio. It appears that propylene is oxidized in the potential region where "O" chemisorption takes place and the latter is inhibited, since a smaller oxygen

reduction peak is observed. Ethylene behaves similarly to propylene, except that the effect described is more pronounced. Propane and n-butane are similar in that the peaks at 1.08 and 0.76v are identical with the corresponding peaks in the nitrogen curves, suggesting that oxidation of the hydrocarbons does not take place in the oxygen chemisorption region. In fact, the hydrocarbon reactions appear to be inhibited by surface oxygen.¹² Ethane behaves differently from the other four hydrocarbons in that the peaks at 1.08 and 0.76v are both greater by the same amount than the corresponding peaks observed with nitrogen. It is suggested that this is due to the reversible formation of an oxidation product of ethane in the oxygen chemisorption region.

CONCLUSIONS

1. The lead content of electrodeposited platinum black, prepared from 2.5% chloroplatinic acid at a current density of 10 ma./cm.² for 1 hr. increases with lead acetate concentration. The Pb/Pt atomic ratio increases almost linearly up to a lead acetate concentration of 0.08%, whereafter it tends to a constant value with further increases of concentration.

2. The real area of the platinum black electrodeposits is a maximum at an atomic ratio of 0.0021.

3. The degree of hydrocarbon oxidation varies with Pb/Pt atomic ratio as does the real area, and the effect is much greater for ethylene and propylene than for ethane, propane, and n-butane. The electrodeposits having a Pb/Pt atomic ratio of 0.0021 have the greatest activity.

4. Other factors, such as lattice parameter, that might be important in the electro-oxidation of the hydrocarbon gases are masked completely by the area effect.

5. Ethylene and propylene continue to be oxidized in the potential region where oxygen is chemisorbed on platinum. In the process oxygen chemisorption is inhibited. The electro-oxidation of propane and n-butane is inhibited by surface oxygen.

ACKNOWLEDGMENT

The author is grateful to the following people of the General Motors Research Laboratories: Dr. J. P. Hoare, for many helpful comments; Mr. A. C. Ottolini, Mr. H. A. Jones, and Dr. J. L. Johnson, for doing the analytical work; and Miss F. A. Forster, for making the X-ray measurements.

REFERENCES

1. W. T. Grubb and L. W. Niedrach, *J. Electrochem. Soc.*, 110, 1086 (1963).
2. W. T. Grubb and C. J. Michalske, *Nature*, 201, 287 (1963); *J. Electrochem. Soc.*, 111, 1015 (1964).
3. W. T. Grubb, *Nature*, 201, 699 (1964).
4. H. G. Oswin, A. J. Hartner, and F. Malaspina, *Nature*, 200, 256 (1963).
5. H. Binder, A. Köhling, H. Krupp, K. Richter, and G. Sandstede, Paper presented at Electrochemical Society Meeting, Toronto, 1964, Abs. No. 11.
6. V. R. José and V. D. Long, *J. Appl. Chem.*, 64 (1964).
7. L. W. Niedrach, *J. Electrochem. Soc.*, 109, 1092 (1962).
8. M. J. Schlatter, "Fuel Cells," Vol. 2, Ed. G. J. Young, Reinhold Publishing Corp., (1963), p. 190.

9. R. Thacker and D. D. Bump, *Electrochem. Technol.*, 3, 9 (1965).
10. C. E. Thompson, United States Patent 3,116,169, Dec. 31, 1963.
11. R. Thacker, *Nature*, In press.
12. R. Thacker, Paper presented at Electrochemical Society Meeting, Washington, D. C., 1964, Abst. No. 9.
13. E. Müller, *Z. Elektrochem.*, 29, 264 (1923); *ibid.*, 33, 561 (1927).
14. H. Dahms and J. O'M. Bockris, *J. Electrochem. Soc.*, 111, 728 (1964).
15. M. J. Joncich and N. Hackerman, *J. Electrochem. Soc.*, 111, 1286 (1964).
16. G. Bianchi, *Annali Di Chimica*, 40, 222 (1950).
17. R. Thacker, *J. Chem. Ed.*, In press.
18. T. P. Schreiber, A. C. Ottolini, and J. L. Johnson, *Appl. Spectros.*, 17, 17 (1963).
19. F. G. Will and C. A. Knorr, *Zeit. für Elektrochemie*, 64, 258 (1960).
20. J. L. Griffin, J. P. Hoare, and R. Thacker, To be published.
21. W. Nestorova and A. Frumkin, *Zhur. Fiz. Kim.*, 26, 1178 (1952).
22. A. Hickling, *Trans. Far. Soc.*, 41, 333 (1945).
23. J. P. Hoare, *Electrochim. Acta*, 9, 599 (1964).
24. M. C. Banta and N. Hackerman, *J. Electrochem. Soc.*, 111, 114 (1964).
25. B. L. Tarmy *et al.*, ASTIA Report No. AD 432865, Dec. (1963).
26. K. J. Vetter and D. Berndt, *Z. Elektrochem.*, 62, 378 (1958).
27. W. Böld and M. Breiter, *Electrochim. Acta*, 5, 145 (1961).

TABLE I

PROPERTIES OF PLATINUM BLACK ELECTRODEPOSITS

<u>Lead Acetate Concentration in Plating Solution (%)</u>	<u>Appearance of Deposits</u>	<u>Coulombic Efficiency (%)</u>	<u>Atomic Ratio (Pb/Pt)</u>	<u>Real Area Per Geometric Area of 0.16 Cm.² (cm.²)</u>
0	Grey, compact		0	57.3
0.003	Black, very powdery	40.6	0.0021	85.4
0.01	Black, very powdery	35.9	0.0041	81.4
0.05	Black, powdery	37.2	0.0143	41.7
0.075	Grey, compact	41.6	0.0208	36.7
0.1	Grey, compact	41.6	0.0230	47.4
0.15	Grey, compact	39.8	0.0247	
0.2	Grey, compact	38.4	0.0256	47.4

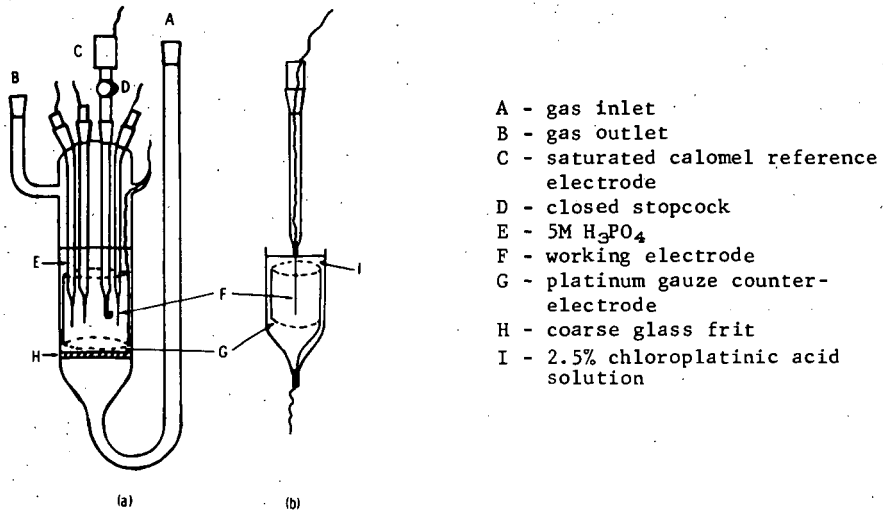


Fig. 1. (a) Electrochemical cell. (b) Working electrode preparation cell.

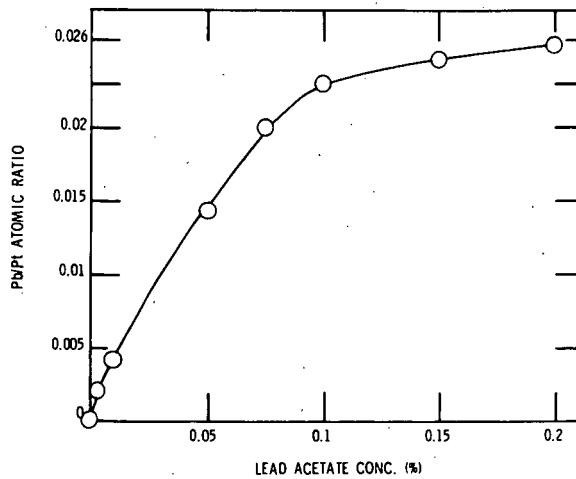


Fig. 2. Pb/Pt atomic ratio of electrodeposited platinum black prepared from 2.5% chloroplatinic acid solutions containing different lead acetate concentrations.

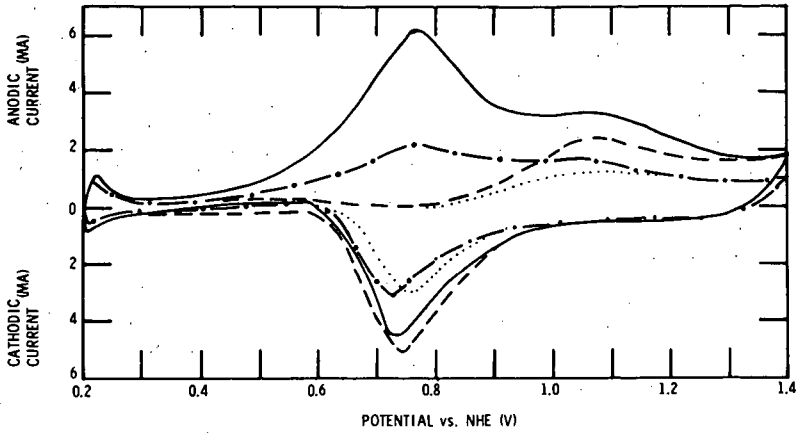


Fig. 3. Potential sweep curves on electrodeposited platinum black, in 5M H_3PO_4 , at 80° C. Full line - propylene, dashed line - nitrogen, Pb/Pt = 0.0021; dash-dot-dashed line - propylene, dotted line - nitrogen, Pb/Pt = 0.0256.

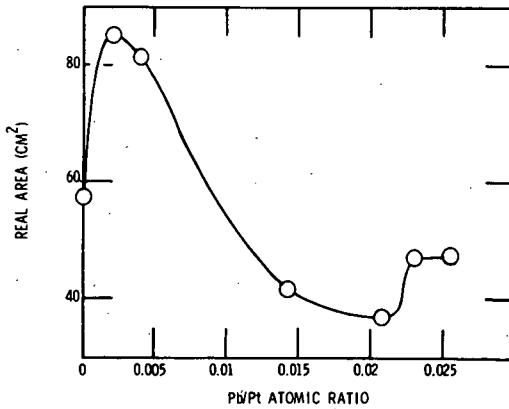


Fig. 4. Real area of electrodeposited platinum black prepared from 2.5% chloroplatinic acid solutions containing different lead acetate concentrations. Variation with Pb/Pt atomic ratio.

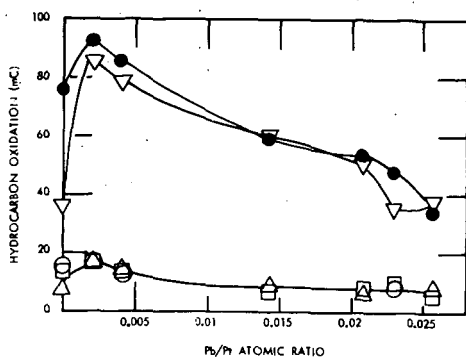


Fig. 5. Hydrocarbon oxidation ($5\text{M H}_3\text{PO}_4$, 80°C .) on electro-deposited platinum black prepared from 2.5% chloroplatinic acid solutions containing different lead acetate concentrations. Variation with Pb/Pt atomic ratio. \square , ethane; \circ , propane; \triangle , n-butane; ∇ , ethylene; \bullet , propylene.

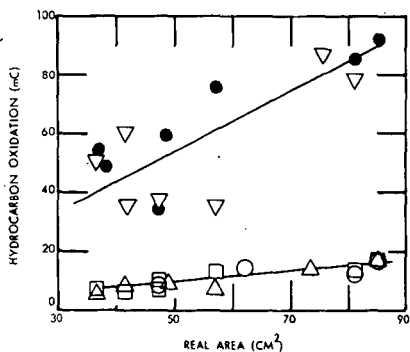


Fig. 6. Hydrocarbon oxidation ($5\text{M H}_3\text{PO}_4$, 80°C .) on electro-deposited platinum black prepared from 2.5% chloroplatinic acid solutions containing different lead acetate concentrations. Variation with real area. \square , ethane; \circ , propane; \triangle , n-butane; ∇ , ethylene; \bullet , propylene.

ANODIC OXIDATION OF HYDROCARBONS

M. L. Savitz, R. L. Januszkeski
G. R. Frysinger

U. S. Army Engineer Research and Development Laboratories
Fort Belvoir, Virginia 22060

The anodic oxidation of hydrocarbons is of particular interest for direct generation of electrical power from a liquid fuel in a fuel cell. The U. S. Army Engineer Research and Development Laboratories (USAERDL) are engaged in a program in combination with industrial and university workers to better understand the mechanism by which hydrocarbons react at fuel cell electrodes. Grubb (1) has examined the oxidation of hydrocarbons from methane to hexadecane as a function of chain length, structure, and unsaturation in Neidrach-Alfred electrodes (2) in phosphoric acid electrolyte at 150°C. Saturated hydrocarbons were most active with unsaturated, branched and cyclic compounds less active.

The ultimate potential of fuel cell power supplies is related to the performance which can be achieved at an electrode surface. Reaction paths and the rate limiting steps must be understood for aliphatics, olefins, aromatics, and oxygenated compounds if versatile electrode structures are to be devised. Currently, several investigations are being performed to determine the mechanism of anodic oxidation of hydrocarbons in acid solution - some of the results to be reported in other papers at this symposium.

Investigations of the mechanism of anodic oxidation of octane in concentrated H_3PO_4 at 130 and 150°C have been initiated in our laboratory and preliminary results are presented.

Experimental

A standard three compartment electrochemical cell (3) was used for oxidation and adsorption studies. The working electrode was either a platinized-platinum electrode or bright platinum electrode of thermocouple grade platinum. Both electrodes had geometric area of 0.5 cm². The bright electrode was flame-treated before each experiment to minimize change of electrode area in concentrated H_3PO_4 at high temperatures (4). The reference electrode consisted of a platinized platinum electrode which was cathodically polarized with help of another platinized platinum electrode in the same compartment as described by Giner (5). The counter electrode was of platinized platinum maintained in an argon atmosphere. To remove

impurities from the H_3PO_4 it was necessary to reflux it with 30% H_2O_2 solution for 24 hours and distill off water until the desired acid concentration was obtained. Chromatographic grade octane (99+ mole %) was injected into the working compartment with a syringe, and constant composition was maintained by bubbling argon through a presaturator containing octane at a temperature slightly lower than its boiling point.

In order to obtain a reproducible surface for adsorption studies, the electrode was pretreated with a series of potential steps and then maintained at a fixed potential for varying times before examining the surface state of the electrode with an anodic or cathodic pulse. Essentially the electrode was held at 1.35 V for 1 minute - the last 30 seconds without stirring, at 0.1 V for 30 msec. and then at a fixed potential for from 10 msec to 10 minutes before applying the transient pulse (4). Figure 1 indicates the circuit for the programmed electrode pretreatment. First the 1.35 V (V_1) is applied to the cell by adding onto the internal pre-set potentiostatic voltage (V_3). Trigger Circuit Number 1, manually operated, then activates a ramp generator; the Hg-wetted relay number 1 opens switch 1A and closes 1B and obtains 0.1 V (V_2). After 30 msec, SCR circuit number 1 is activated, opening relay switch 2A and closing 2B, returning the cell to V_3 for from 10 msec to 10 sec before SCR circuit number 2 fires, activating Hg-wetted relay 3, closing switch 3 and firing the constant current. Manual operation of the galvanostatic relay was employed where times at V_3 exceeded 10 seconds. Figure 2 shows the position of the programmed circuit in relation to the potentiostatic input.

Results and Discussion

The adsorption of octane has been studied at 130°C in 85% H_3PO_4 with anodic and cathodic galvanostatic charging curves. Brummer has found that anodic charging gives a reliable estimate of the amount of oxidizable material adsorbed on the electrode for propane in H_3PO_4 from 80-130°C (4). In order to know about the amount of species irreversibly adsorbed on the electrode, cathodic charging curves are also needed.

In the octane studies at 130°C on bright platinum the measurement of the difference between Q_{ads}^{octane} and Q_{ads}^{argon} with anodic charging curves and Q_H from cathodic charging curves with and without octane was found to be relatively independent of current density from 540 microamp/cm² to 150 ma/cm². A current density of 45 ma/cm² was chosen

for the measurements. A plot of the charge Q_{ads}^{octane} from anodic charging at 130° on bright Pt in 85% H_3PO_4 with the time of adsorption at various potentials is shown in Figure 3. The charge occurring from oxidation of the electrode in H_3PO_4 under argon has been subtracted from the charge obtained with octane. Initially Q_{ads}^{octane} increases linearly with square root of time independent of potential from 0.1 to 0.5 V. This indicates that adsorption is initially limited by diffusion of the reactant in solution. The adsorption appears diffusion controlled for about 3 sec at 0.2 V, 2 sec at 0.3 V, 1 sec at 0.1 and 0.4 V, and 500 msec at 0.5 V. The rate then decreases and the concentration of adsorbed species reaches a constant maximum value in about 30 seconds. The value is maintained for at least 10 minutes except at 0.1 V where the charge begins to decrease after 2 minutes. The maximum amount of adsorption appears at 0.2 and 0.3 V. There is much less adsorption at 0.6 V, and at 0.7 V the adsorption with octane is only negligibly different from that under argon. From Figure 3 the initial slope of the Q_{ads}^{octane} vs $t_{ads}^{1/2}$ is 2.88×10^{-4} coul/cm²/sec^{1/2}. Since the electrode had a roughness factor of 1.24, the initial slope is 3.58×10^{-4} coul/geom cm²/sec^{1/2}. The diffusion constant D octane can be calculated from the equation (6):

$$Q_{ads}^{octane} = 2nF D^{1/2} \pi^{-1/2} C t^{1/2}$$

where n is the number of electrons released in the oxidation of adsorbed species which for the complete oxidation of octane to CO_2 would be 50, F is Faraday number, C is the concentration of octane in mole/cm³. Using 6.72×10^{-9} moles/cm³ for the concentration of octane at $130^\circ C$ (7), the diffusion constant for octane is found to be 9.6×10^{-5} cm²/sec. This value appears high in that the diffusion coefficient found for diffusion in a liquid is usually from 0.5 to 4×10^{-5} cm²/sec (8). Brummer (4) reports $D_{propane}^{130}$ of 5×10^{-6} cm²/sec. Octane would be expected to have a lower value thus a slower rate of diffusion rather than faster. An increase in carbon chain length normally causes a decrease in diffusion constant e.g. ethanol, 1.28×10^{-5} cm²/sec, n-propanol 1.1×10^{-5} cm²/sec, n-butanol $.96 \times 10^{-5}$ cm²/sec, (9).

One possible explanation for this would be that very little octane is being oxidized or is being only partially oxidized at $130^\circ C$ and n is less than 50. Current-potential studies of the oxidation of octane at constant potential on a bright Pt electrode at $130^\circ C$ yielded only a few microamp/cm² of current. With a platinized platinum electrode, with a roughness factor of 500, only 60 microamp/geom. cm² of current were obtained. Other studies have shown the oxidation of octane at $150^\circ C$ in Teflon bonded cells to be only 1/5 that of propane (1). Since octane with 8 carbon atoms is a hydrocarbon even more complex than propane the formation of any intermediate might cause decomposition of octane into smaller saturated, unsaturated, or cyclic compounds and/or oxygenated species. Since octane at $130^\circ C$ is only $4^\circ C$ above its boiling point, the assumed concentration value used in the diffusion calculation might not be accurate for the length of the experiment. However, as long as an octane presaturator was used during a run, the data recorded at the beginning was reproducible over the elapsed time span of an experiment. The results were

reproducible in three different experiments within 10%.

The above points are being investigated further at 130°C and experiments are being extended to 150°C where a greater extent of octane oxidation is expected.

Figure 4 gives the variation of anodic charge of octane with time of adsorption for platinized-platinum under conditions similar to those of bright platinum. A straight line is obtained but the rate of diffusion appears more potential dependent and its rate controlling for a longer period of time. At 0.2 and 0.3 V adsorption appears diffusion controlled for 60 sec, at 0.4 for 80 sec and at 0.5 V 120 sec. In the case of the bright platinum, the rate deviated from diffusion earlier at more anodic potentials (0.5 and 0.4) whereas here the lower potentials deviate earlier. Maximum adsorption, however, is still obtained at 0.2 and 0.3 V.

Cathodic charging curves were obtained to give an indication of the amount of irreversibly adsorbed material on the electrode. The electrode was pretreated as for the anodic charging curves and again held at a fixed potential for from 10 msec to 10 minutes. For potentials below 0.4 V, a potential step at 0.5 V was substituted for 0.1 V (V_2) and was applied for 10 msec after the fixed potential (V_3) instead of before as V_2 was. This step removed any H atoms which might have accumulated on the electrode surface (4).

From the cathodic pulse the degree of coverage Θ_H equal to the ratio of the H atom charge Q_H^{octane} to maximum value Q_H^{argon} at the same temperature can be obtained. A measure of the fraction of surface covered by adsorbed hydrocarbon is obtained from $1 - \Theta_H^{\text{octane}}$ (10). The variation of Θ_H^{octane} on bright platinum in 85% H_3PO_4 at 130°C with time of adsorption is shown in Figure 5. Θ_H^{octane} decreases linearly with $t^{1/2}$ indicating that adsorption is initially limited by diffusion in the solution. The rate appears more potential dependent than that from anodic charging curves and linearity persists for longer times than in the cathodic charging - 7 seconds at 0.2 V and 0.4 V, 11 seconds at 0.3 V and 0.5 V. The maximum degree of coverage ($1 - \Theta_H^{\text{octane}}$) from cathodic curves, taken after 2 minutes, at which point Q_H is constant, occurs at 0.2 V which corresponds to the anodic charging curve results. Using the results obtained with anodic charging the number of Pt sites occupied by adsorbed organic can be determined.

The observed rate of accumulation of adsorbed organic species from Figure 3 was 2.88×10^{-4} coul/cm²/sec^{1/2}. This would be equivalent to 3.58×10^{13} molecules/cm²/sec^{1/2} if n is 50. Since 1.3×10^{15} atoms/cm² of Pt or 2.10×10^{-4} coul/cm² corresponds to a monolayer of H (10), this corresponds to about $0.03 \Theta_H^{130}$ /sec^{1/2} if the adsorption of a octane molecule involves only 1 Pt atom for adsorption and would be $0.24 \Theta_H^{130}$ /sec^{1/2} for 8 sites. From Figure 5, it appears that 8 site adsorption is occurring at 0.2 V, 6 site at 0.3 and 0.4 V, and 3 site at 0.5 V. These results differ from propane where 1 site adsorption has been found to occur at 0.2 V and 3 site adsorption at potentials greater than 0.3 V (4). The octane results are tentative and the additional information mentioned earlier which will be obtained may clarify some of the differences.

References:

1. W. T. Grubb, Hydrocarbon Phosphoric Acid Fuel Cells, 18th Annual Power Sources Conferences, Atlantic City, May 1964.
2. L. W. Neidrach and H. R. Alfred, Jr. J. Electrochem. Soc. 112, 117 (1965).
3. S. B. Brummer and A. C. Makrides, J. Phys. Chem. 68, 1448 (1964).
4. S. B. Brummer, J. I. Ford, M. J. Turner, in press.
5. J. Giner, J. Electrochem. Soc. 111, 376 (1964).
6. H. A. Laitenen and I. M. Kolhoff, J. Am. Chem. Soc. 61, 3344 (1939).
7. J. Paynter and D. MacDonald, unpublished results.
8. P. A. Johnson and A. L. Babb, Chem. Rev. 56, 387 (1956).
9. Chemical Engineers Handbook, McGraw-Hill, New York, New York (1963) 14-25.
10. S. Brummer, J. Phys. Chem. 69, 562 (1965).

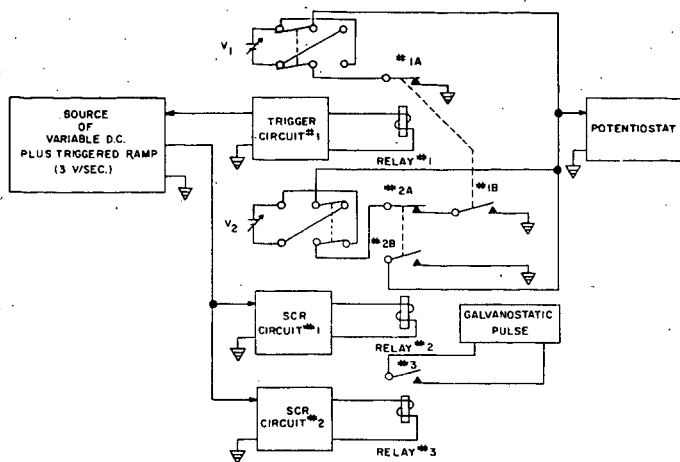


Figure 1 CIRCUIT FOR POTENTIAL STEP PRETREATMENT OF THE ELECTRODE

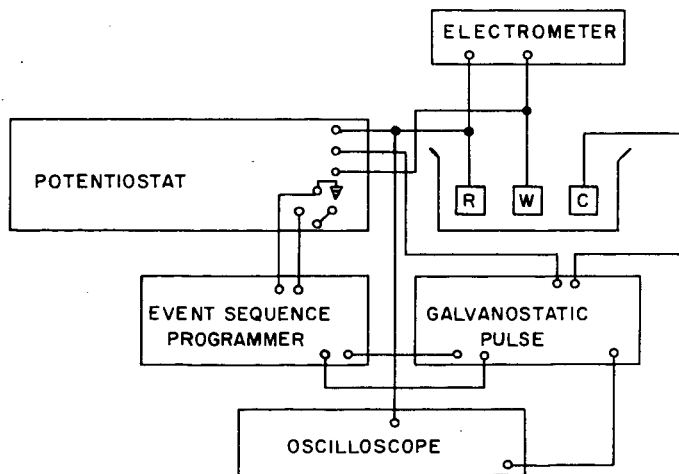


Figure 2 BLOCK DIAGRAM FOR ADSORPTION STUDIES

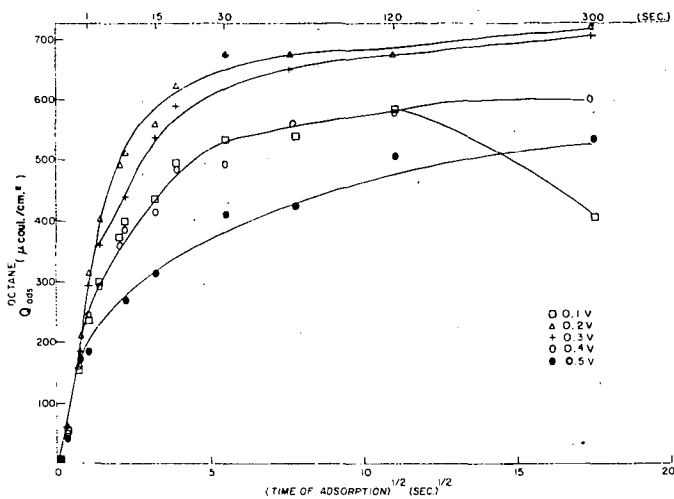


Figure 3 VARIATION OF Q_{ads}^{octane} WITH $t_{ads}^{1/2}$ AT 130° C WITH BRIGHT Pt ELECTRODE

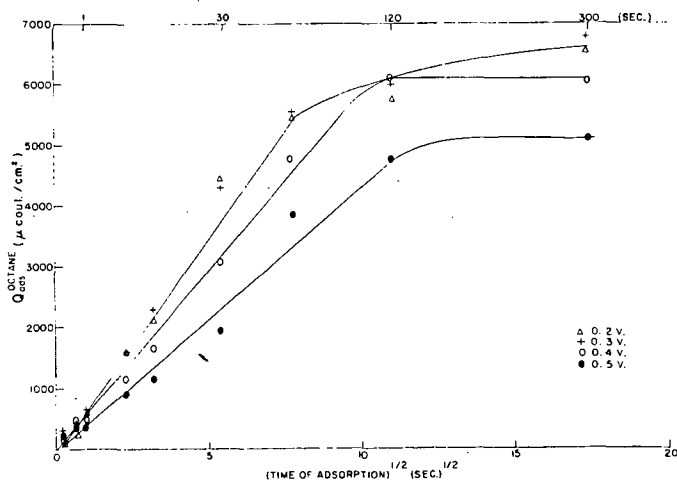


Figure 4 VARIATION OF Q_{ads}^{octane} WITH $t_{ads}^{1/2}$ AT 130°C WITH PLATINIZED-PLATINUM ELECTRODE

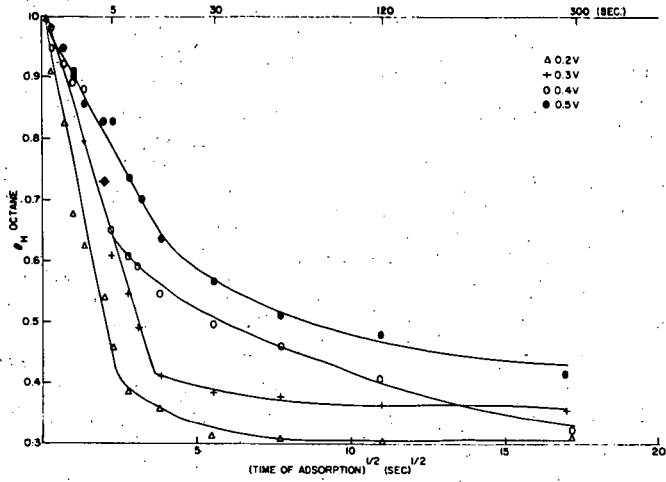


Figure 5 VARIATION OF θ_H WITH $\tau_{ads}^{1/2}$ AT 130°C WITH
BRIGHT Pt ELECTRODE

Limiting Processes at Hydrocarbon Electrodes

J. A. Shropshire, E. H. Okrent, H. H. Horowitz
Esso Research and Engineering Company

The development of an efficient low temperature, aqueous, hydrocarbon-air fuel cell has been the subject of intensive investigation in recent years. Saturated hydrocarbons would be well suited to commercial fuel cells because of their low cost and high availability. Liquid hydrocarbons are especially preferable because they are easily handled, easily separated from the products of combustion, carbon dioxide and water, and because of their low solubility in the electrolyte, not likely to be oxidized at the cathode.

While the earliest demonstration of the electrochemical activity of a saturated hydrocarbon was made with a non-noble catalyst(1), commercially promising current densities were not observed until electrodes with heavy platinum loadings, thirty and more milligrams per cm^2 --were used (2,3). However, hydrocarbon fuel cells will require a reduction in catalyst cost of at least two orders of magnitude before they are commercially practical. One way to achieve this cost reduction is to find an active non-noble catalyst. Efforts along these lines are in progress in several laboratories. A second approach is to improve the utilization of the present catalyst, thereby reducing its requirement per kilowatt of power. To accomplish this end it is necessary to know what processes are limiting the performance of the present hydrocarbon electrodes. In line with this objective, the aim of the present study was to determine whether the steady state performance of operating anodes is limited by the intrinsic electrochemical activity of the catalyst or whether physical factors exert important effects.

This problem is complicated by the fact that the optimum electrodes are complex porous structures consisting of hydrophobic and hydrophilic materials exposed to both fuel and electrolyte. Their activity may be limited by loss of useful electrode area through a failure to be wet by electrolyte, or through total flooding by electrolyte leading to lengthy fuel diffusion pathways. In addition, temperature gradients and the evolution of reaction products may give rise to continuous changes in the location of the fuel-electrolyte interface, which may further complicate the picture(4). These effects are superimposed on the chemical and electrochemical processes occurring on the electrode surface, such as the chemisorption of the fuel and the charge transfer processes associated with its oxidation.

Because of the many possible limiting processes caused by the superposition of physical and chemical variables, relatively little mechanism work has been done on porous diffusion electrodes operating with immiscible fuels. Typical chemical studies have been done on bulk metals (5) or electrodeposited blacks (6). Studies of physical variables have involved model studies of menisci (7) or studies with soluble fuels dissolved in electrolyte which is flowed through the porous electrode (8). The present study attempts to determine which of the many possible physical and chemical processes limits the activity of porous wetproofed electrodes operating on hydrocarbon fuels, and describes some new physical aspects of their operation.

Approach

A number of platinum black catalysts were prepared using different chemical reducing agents. These were formed into porous, wetproofed, interface-maintaining electrodes and tested for steady state performance on butane gas. The activity varied widely, even when corrected for variations in surface area. Next the intrinsic electrocatalytic activities of the catalysts were compared by measuring their ability to oxidize preadsorbed butane. This was done using a voltage-scanning technique under conditions where physical factors limiting the access of fuel to the surface could have no effect. At the same time various physical properties of the catalysts were measured to determine whether these would correlate with the steady state performance. Finally, additional observations of surface effects were made which led to the recognition of a new phenomenon which may be very important in the operation of hydrocarbon electrodes.

Experimental

Preparation and Evaluation of Platinum Catalysts

Five platinum blacks were prepared using various chemical reducing reagents. In addition, a sample of commercial platinum black was included in the study. Each of these was formed into an electrode simply by mixing with Teflon emulsion and hot pressing into a 50 mesh tantalum screen. This type of electrode was chosen because of its ease of preparation and good reproducibility. Optimum electrode formulations perform better than any reported here, giving 100 ma/cm² at 0.18 volts polarization and 300 to 400 ma/cm² limiting current on butane at 150°C. However, preparation variables must be much more closely controlled with these electrodes to achieve reproducible results.

The electrodes were tested for activity using butane fuel and 14.7 molar phosphoric acid electrolyte at 150°C. A driven "half cell" was used in which the electrode was mounted in a glass flange with 5.7 cm² exposed to electrolyte on one side and gaseous fuel on the other. The electrode polarization was measured by means of a calomel-Luggin capillary reference system which was precalibrated against a reversible hydrogen electrode in the same system. Experimental points were run galvanostatically until the polarization reached a constant value. Runs lasted from one to five days.

The activity of the catalysts varied by a factor of fifty, whereas the surface areas, measured electrochemically, varied by only a factor of three, as shown in Table 1. The logarithmic standard deviation of the current densities, measured in a related study, corresponded to $\pm 1.6\%$. Thus, the desired wide range of activity was achieved. The next question to be answered was whether the fiftyfold activity variation could be ascribed to differences in the intrinsic chemical reactivity of the catalysts.

Table 1

Activity of Platinum Blacks

<u>No.</u>	<u>Reducing Agent</u>	<u>Current Density at 0.4 volts Polarization (ma/cm²)</u>	<u>Electrochemical Surface Area meters²/gm*</u>
1	Formaldehyde	2.5	8.9
2	Hydrogen	6	22.5
3	Potassium Borohydride	15	13.4
4	Lithium	19	26.9
5	Commercial (Engelhard) Platinum (Repeat Runs)	92, 90	23.7
6	Formaldehyde + Protective Colloid	130	21.8

* Obtained from voltage scan measurements (see below) assuming theoretical monolayer is 239 m²/gm, based on 100, 110, and 111 planes weighted according to their X-ray peak intensities.

Evaluation of Intrinsic Electrochemical Activity

A. Indications of Electrochemical Rate Limitations

Before examining the adsorption-oxidation results it should be pointed out that the steady state performance curves gave definite indications of chemical and electrochemical rate limitations. Typical performance curves at both 100° and 150°C showed a Tafel-like region, of slope approximating 0.13 volts per decade, followed by a limiting current region (Figure 1). The energy of activation in the Tafel region was about 18 kcal/mole while that in the limiting region was 10 to 12 kcal/mole (Table 2).

Table 2

Summary of Butane Reaction Parameters

<u>Parameter</u>	<u>Tafel Region</u>	<u>Limiting Region</u>
Tafel Slope (volts/decade)	0.12-0.14	(∞)
Activation Energy (kcal/mole)	17-19	10-12

The slope of $2 RT/F$ is consistent with the proposals that the oxidation of the platinum surface (9) or the rate of water discharge (5) is limiting in the Tafel region. In the limiting current region an activated step occurring before the electrochemical steps, not involving electron transfer, is indicated to be rate limiting. This could well be the chemisorption of the fuel. True diffusion limited rates, encountered in the adsorptions to be described below, had a very low activation energy.

Assignment of chemical rate limitations to the steady state curves does not preclude the coexistence of physical limitations in the different catalysts. These could shift the curves without changing their shape by making more or less surface area available for reaction. Nevertheless, evidence of the existence of electrochemical rate limitations in the low polarization regions justifies the use of the adsorption-oxidation technique described below.

B. Adsorption-Oxidation Studies

A measure of the intrinsic electrochemical activity of the catalysts was obtained by forming them into totally flooded electrodes and measuring the rate at which they oxidized preadsorbed butane, per unit surface area. The total amount of butane adsorbed at saturation coverage could also be used as a measure of one of the catalytic parameters affecting steady state activity. In this way catalyst structure problems, which limit the accessibility of the fuel or the electrolyte to the surface of the catalyst, were avoided.

Fifty milligrams of the catalyst to be tested were mixed with 5 mg of emulsified Teflon and pressed at 200 psi into a fifty mesh platinum screen attached to the face of a 2 cm^2 platinum foil. This amount of Teflon was sufficient to bind the catalyst to the "flag" electrode, but since it was not sintered or subjected to high pressures it did not wetproof the electrode. The flag, mounted on the end of a long platinum wire, was suspended in 3.7 molar sulfuric acid held at 80°C . Reference and counter electrodes were also mounted in the cell. The potential between the reference and working electrodes was controlled by means of a Duffers Model 600 potentiostat and driven in triangular voltage sweeps by a Servomex Low Frequency Wave Form Generator. Current-voltage diagrams were recorded on a Moseley Model 135 x-y Plotter. The sweep range was from 0.15 to 1.45 volts versus reversible hydrogen in the same electrolyte. Typical scans with and without adsorbed butane are shown in Figure 2. Integration of the area under the oxide reduction peak on the cathodic sweep gave a measure of the platinum surface area. Butane peaks were obtained after exposing the wetted electrode to gaseous butane in the space above the electrolyte. When butane was passed over the surface of the electrolyte with the flag totally immersed, no appreciable butane peaks could be obtained within exposure times of one hour, due to its low solubility.

This fact made possible a very convenient adsorption-oxidation procedure: The flag electrode was pulled out of the electrolyte until only the lower edge of the platinum foil, an area without catalyst, was immersed in electrolyte. The potential of the electrode could thus be fixed during the adsorption period by the potentiostat. Since only very small currents passed through the wetted layer it is felt that the potential was in relatively good control during the adsorption period. The potential during the adsorption was set at 0.0 volts versus calomel or 0.15 volts versus reversible hydrogen under these conditions. At the end of the adsorption period the electrode was totally immersed in the electrolyte and within one minute thereafter was subjected to anodic and cathodic scans, with the assurance that no significant amount of butane could be adsorbed during the scan period. The number of coulombs in the butane peak was obtained by integration, taking the butane-free base curve into account. Using this technique, fairly rapid adsorption rates could be obtained. These rates were about an order of magnitude less than those obtainable in wetproofed porous electrodes and were clearly diffusion limited, showing a 0-2 kcal activation energy and an approximately linear proportionality of coulombs versus square root of time. These rates were therefore not used in the analysis. Only the total number of coulombs and the shape of the oxidation curve were used as criteria of catalytic activity.

The electrochemical surface areas of the catalysts, as determined from the number of coulombs in the oxide reduction peak, varied by a factor of three as shown in Table 1. However, the ratio of the butane peak at saturation to the oxide reduction peak was virtually constant for all the catalysts at 1.58 with a standard deviation of 0.13. Assuming 26 electrons involved in butane oxidation and 2 in oxide reduction this result indicates 8 platinum sites per butane molecule or one carbon atom per 2 platinum atoms in the surface, independent of the platinum reduction technique.

An index of the rate of the electrochemical oxidation was obtained for all of the catalysts by comparing the observed current at 0.45 volts polarization from butane theory at fixed initial fractional coverage. However, minor variations in the shapes of the curves made this measurement somewhat irreproducible. Therefore, the butane oxidation peak was integrated to 0.45 volts polarization and the catalytic activity expressed in terms of the fraction of the initial adsorbed butane burnt off to 0.45 volts polarization as a function of the initial butane coverage. This method was shown to be able to detect differences in activity: Varying the temperature from 60 to 150°C (using phosphoric acid in the latter case) produced large variations in this ratio. Nevertheless all of the catalysts tested here showed essentially the same relation between fraction reacted at 0.45 volts and initial fractional coverage, indicating all had roughly the same intrinsic electrochemical activity per unit surface area (Figure 3).

From Figure 3 it is also noted that the fraction reacted at 0.45 volts polarized declined severely with increasing butane coverage. This lends credence to the hypothesis that a reaction such as oxidation of, or water discharge on, the uncovered platinum sites is rate determining.

Regardless of the mechanism, however, it is concluded that electrochemically, all of these high surface area catalysts are essentially identical.

Physical Examination of the Catalysts

Following the finding that the intrinsic electrochemical activity of the catalysts could not account for the variation of their steady state performances, they were next examined for variations in their physical properties. The properties measured were: crystallite size by X-ray line broadening; bulk density after the settling of aqueous suspensions; B.E.T. nitrogen surface area; the pore volume by nitrogen capillary condensation; and the appearance of the agglomerates under the electron microscope (Table 3).

Table 3

Catalyst Characterization

Sample No. (1)	Bulk Density ⁽²⁾ (gm/cm ³)	Crystallite Size ⁽³⁾ (Å)	B.E.T. Surface Area (m ² /gm)	Pore Volume ⁽⁴⁾ (cm ³ /gm)	Current Density at 0.4 volts Polarization(ma/cm ²)
1	0.27	62	8	0.03	2.5
2	0.65	35	10	0.05	6
3	0.99	82	7	0.13	15
4	0.65	50	26	0.19	19
5	0.46	77	28	0.39	92, 90
6	0.55	45	30	0.40	130

(1) As given in Table 1.

(2) After 24 hours settling of an aqueous suspension.

(3) By X-ray line broadening.

(4) By equilibration with liquid nitrogen in a liquid nitrogen bath.

The physical properties in general varied by a greater factor than the intrinsic electrochemical activities. In particular the pore volume could be correlated with the steady state activity, the more open structures giving the higher activities (Figure 4).

Electron microscope examination of the catalysts provided further evidence of their structural variation. While quantitative comparisons were not possible there appeared to be definite differences in appearance between the low activity, low pore volume catalysts and the high activity, high pore volume materials. The latter were characterized by a lacy agglomerate structure with the individual crystallites forming a network of low coordination number. The poorer catalysts had much less lacy material, large dense areas and some indications of well formed edges of relatively large crystals. The best and the worst catalysts are compared in Figures 5 and 6.

It, thus, appears that the fiftyfold variation in steady state catalytic activity was due not to changes in chemical reactivity of the catalyst surfaces, but to changes in the physical nature of the catalysts, having to do with the openness of the structure and the ease of diffusion within it.

Operation of Porous, Hydrophobic Electrodes

The finding that physical parameters governed the operation of hydrocarbon electrodes led naturally to a consideration of their physical mode of operation, and to what may be an important new phenomenon. There have been two general approaches to the understanding of the operation of porous diffusion electrodes. One involves diffusion of the dissolved fuel into the porous structure flooded with electrolyte (8). The other considers pores containing meniscuses such as are illustrated by the model experiments of Will (7). Diffusion alone, without flow, cannot account for the activities observed. A simple calculation shows that the butane can penetrate only about 5 microns into the structure by diffusion alone from the surface, since its solubility is so low, relative to the reactivities shown in Figure 1. The importance of internal meniscus formation is cast in doubt by the facts that liquid and gaseous decane give about equal performance (Figure 7), whereas the electrolyte meniscus is inverted in going from gaseous to liquid hydrocarbon fuels. Whereas for gases the electrolyte meniscus is concave upwards, for liquid hydrocarbons it is concave downward. That is, the platinum is preferentially wetted by the hydrocarbon. (See Appendix I and Figure 8 for details).

The phenomenon of gasification, or boiling, within the pores of a wetted hydrophobic matrix, at temperatures far below the normal boiling point, may help explain how fuel penetrates into the depths of porous electrodes, and why gases and liquids perform equally well. It has been observed that certain Teflon-wetproofed electrodes mounted in their normal operating configuration, begin to spontaneously emit a stream of bubbles on the electrolyte side, when the temperature is raised to within 30° of the normal electrolyte boiling point. This phenomenon will occur in the absence of any pressure excess on the fuel side, and will even overcome a considerable electrolyte head. It is observed even with liquid decane in the fuel chamber. It can be shown thermodynamically that the boiling point of a liquid in a porous hydrophobic matrix can be lowered by 30° and more, due to the preferential wetting of the surface by gas rather than liquid. (See Appendix II for derivation and example illustrating the effect.) However, the thermodynamics do not explain the continuous bubble release observed in certain electrodes. This may be due to temperature and pressure gradients, turbulence and pore junctions within the electrode.

In any case, a picture of hydrocarbon electrode operation is proposed in which localized electrolyte boiling within the small hydrophobic pores provides a stream of vapor which carries the gaseous or vaporized fuel into the depths of the catalyst bed. Thus, the contact area magnification necessary to provide adequate diffusion into a relatively thick electrode is obtained. Menisci exist transiently along the stream of bubbles, continually being renewed by their passage. In a sense, the "dynamic interface" referred to as necessary for the operation of electrodes for immiscible fuels is thus set up. This phenomenon may explain why electrode activity has been observed to rise to a maximum about 8° below the boiling point of the electrolyte (2).

Summary and Conclusions

A series of platinum blacks prepared with different reducing agents showed a fiftyfold variation in steady anodic activity with butane at 150°C. The intrinsic electrochemical activity of the catalysts as measured by their ability to oxidize preadsorbed butane, however, was shown to be essentially equal. The observed activity was shown to be a function of the physical structure of the catalyst as determined by internal pore volume measurements and electron microscopy. It appears then that the different reducing agents either did not affect the growth and morphology of the platinum crystallites or that these factors have little effect on chemical reactivity. The reducing conditions did have marked effects on the way the crystallites agglomerated, however. Pore volumes varying from 60 to 900% of the solids volume were achieved. This in turn had a marked effect on performance, the finer more open structures giving the best performance.

The results indicate that with unsupported platinum catalysts physical variables affect performance more than chemical. Further understanding of the physical operation of porous electrode is therefore desirable. One or two aspects of this problem have been treated here. The meniscus shape within the pores is probably not critical since a liquid hydrocarbon fuel, with an inverted meniscus, gave activities essentially identical to the same fuel in the gas state. The solubility and diffusion mode of fuel transport from the surface of the catalyst bed is inadequate by itself to account for the observed activities. The phenomenon of internal gasification caused by a lowering of the boiling point of the electrolyte due to its being present in a high surface area, hydrophobic bed helps account for the activity. It can provide a large area increase by exposing the deep innards of the catalyst bed to gaseous fuel.

There are important implications of this work in the development of new electrode catalysts: It is clear that steady state performance testing will not necessarily detect catalysts of intrinsically greater chemical reactivity. As a corollary, catalysts with superior intrinsic activities will not necessarily operate best in finished electrodes. Probably the physical structure of new catalysts will have to be optimized individually to secure optimum performance.

Acknowledgment

The work reported in this paper was made possible by the support of the Advanced Research Projects Agency under Order No. 247 through the U.S. Army Electronics Laboratories (Contract No. DA 36-039 AMC-03743(E)). Permission to publish is gratefully acknowledged.

References

1. C. E. Heath and C. H. Worsham in "Fuel Cells", Vol. 2, (G. J. Young, Ed.) p. 182, Reinhold (1963).
2. W. T. Grubb and C. J. Michalske, J. Electrochem. Soc., 111 447 (1964); Ibid., 1015 (1964).
3. H. Binder, A. Köhling, H. Krupp, K. Richter, and C. Sandstede, J. Electrochem. Soc., 112 355 (1965).
4. H. A. Liebhafsky, E. J. Cairns, W. T. Grubb, and L. W. Niedrach in "Fuel Cell Systems", (R. F. Gould, Ed.), p. 116, Advances in Chemistry, No. 47, A.C.S. (1965).
5. H. Wroblowa, B. J. Piersma and J. O'M. Bockris, J. Electroanal. Chem., 6, 401 (1963).
6. J. A. Shropshire, J. Electrochem. Soc., 112 465 (1965).
7. F. G. Will, J. Electrochem. Soc., 110 145 (1963).
8. L. C. Austin, P. Palasi and R. R. Klimpel, in "Fuel Cell Systems", (R. F. Gould, Ed.); p. 35, Advances in Chemistry, No. 47, A.C.S. (1965).
9. T. C. Franklin and C. Liang, Report No. 2, Air Force Contract A-F. 19 (604)-8414, August (1962).

Appendix I

Evidence for Inverted Meniscus with Liquid Hydrocarbons

As was demonstrated by F. Will with hydrogen,⁽⁷⁾ an area of increasing current output is obtained as a potentiostatted plate or wire electrode is withdrawn from submersion in an electrolyte up through the fuel-electrolyte interface. This is because the meniscus is concave upwards and forms along the partially protruding surface. With liquid hydrocarbons, however, an area of increasing current density was observed as the bottom of an electrode was lowered from total submersion in the fuel through the electrolyte interface. This phenomenon was more easily observed in the presence of a surfactant where the active area extended as much as one cm. below the nominal interface. Figure 8 illustrates the data with liquid heptene-2 at 80°C. The film of heptene was observable under the electrolyte by means of the phenomenon of total reflectance at an angle of 70 to 80° from the normal.

Thus, there is no doubt that the liquid hydrocarbon-electrolyte meniscus is concave downwards into the electrolyte, along the electrode face. Consideration of the wetting properties of platinum makes this result seem reasonable. Sulfuric acid or phosphoric acid wets clean platinum foil. However, liquid hydrocarbons displace the electrolyte. A platinum foil immersed in decane was not wet by a droplet of 3.7 M sulfuric acid. Instead of spreading it remained on the surface as a globule with a very high contact angle. On the other hand, a droplet of decane placed on the under surface of a platinum foil immersed in electrolyte spread on it immediately, displacing the electrolyte from the surface. This phenomenon has not been studied as a function of potential but it is known that platinum is more hydrophobic at reducing potentials than at oxidizing.

Appendix II

Thermodynamics of Boiling Point
Lowering in a Hydrophobic Matrix

A porous hydrophobic body is considered to be totally immersed in a vessel of electrolyte, which has filled all the pores. Within the porous body the liquid is in equilibrium with a bubble of its own vapor. The vapor is not at the external pressure, however. A difference in pressure between the external and vapor pressures is necessary to maintain the liquid within the hydrophobic matrix.

$$P_v = P_o + (\gamma_{gs} - \gamma_{ls}) \sigma \quad (1)$$

where P_v = pressure of vapor within matrix

P_o = external pressure (1 atm)

γ_{gs} = gas solid interfacial tension

γ_{ls} = gas liquid interfacial tension

σ = surface to volume ratio of matrix

Equation (1) will be recognized as that used in porosimetry, where ΔY , which is negative in this case, is written as $\gamma_{gl} \cos \theta$ (θ is the contact angle), and σ for pores of radius r equals $2/r$. Establishment of equilibrium within the porous body requires that the temperature be lowered until the vapor pressure of the liquid equals that given by equation (1). The exact thermodynamic treatment is quite complex, but an approximate idea of the size of the effect can be obtained from the Clausius-Clapeyron equation in the form:

$$\frac{dP}{dT} = \frac{\Delta H}{TV_v} \quad (2)$$

where T is the equilibrium temperature (boiling point)
 ΔH is the heat of vaporization of the liquid
 V_v is the molar volume of the vapor

Combining [2] with the differential of [1], using the gas law for V_v , and integrating, one finds that:

$$\frac{1}{T_B} - \frac{1}{T} = \frac{R}{\Delta H} \ln \left(\frac{P_o + \sigma \gamma_{gl} \cos \theta}{P_o} \right) \quad (3)$$

where T_B is the boiling point when σ is zero. Since $\cos \theta$ is negative for hydrophobic matrices $T < T_B$. In heavily loaded platinum black electrodes, for example, σ can be $10^6 \text{ cm}^2/\text{cm}^3$. To obtain a 20°C lowering of the boiling point in this case, a weighted average value of θ of only 90.4° is required. Excessive wetproofing in a region of the electrode can give values of $\sigma \gamma_{gl} \cos \theta$ greater than one atmosphere. The pores in this region will remain free of liquid at all temperatures. Apparently the proper wetproofing is achieved by correct blending and sintering of the platinum and Teflon.

Figure 1

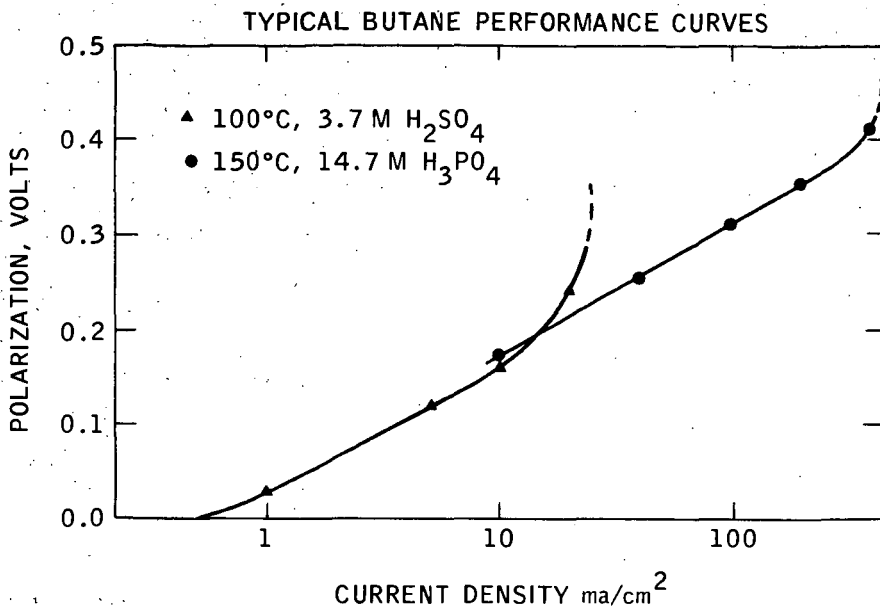


Figure 2

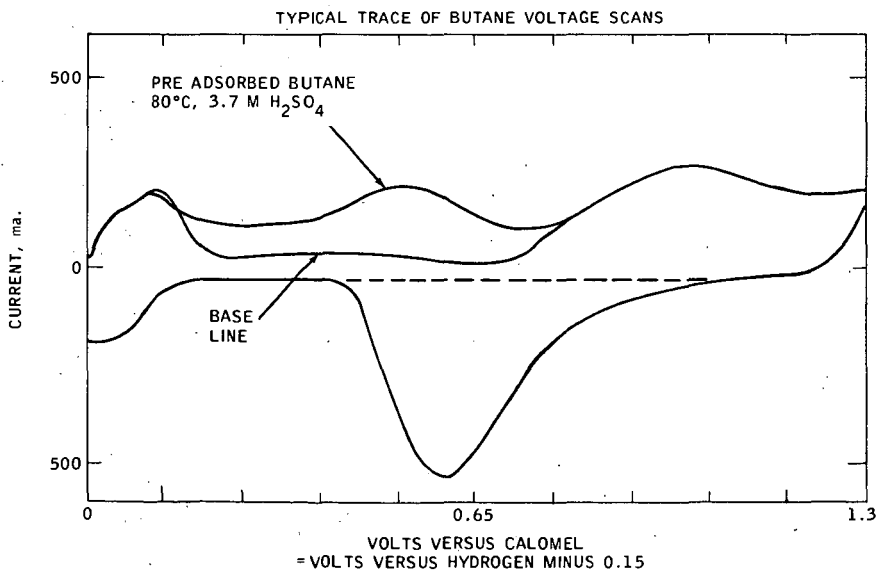


Figure 3
FRACTION BUTANE REACTED VERSUS INITIAL COVERAGE

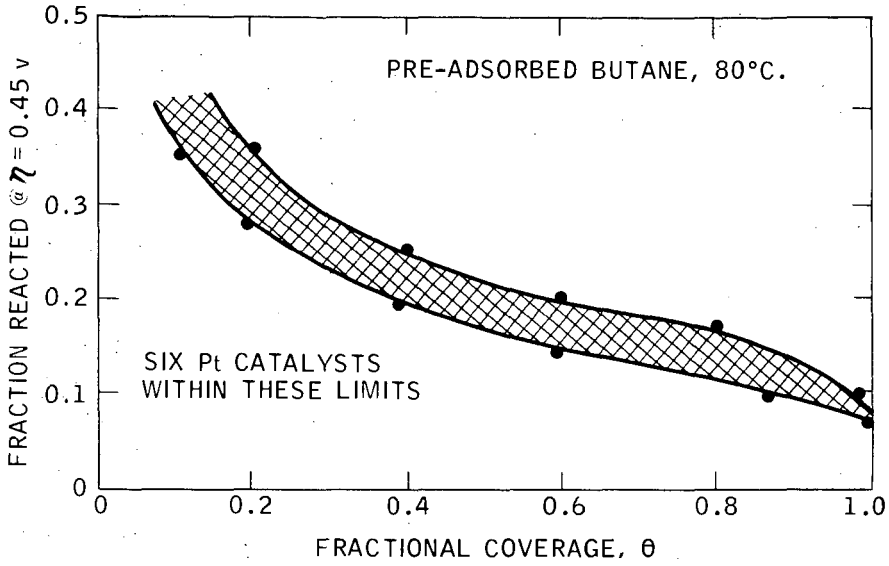


Figure 4
BUTANE PERFORMANCE CORRELATES WITH PORE VOLUME

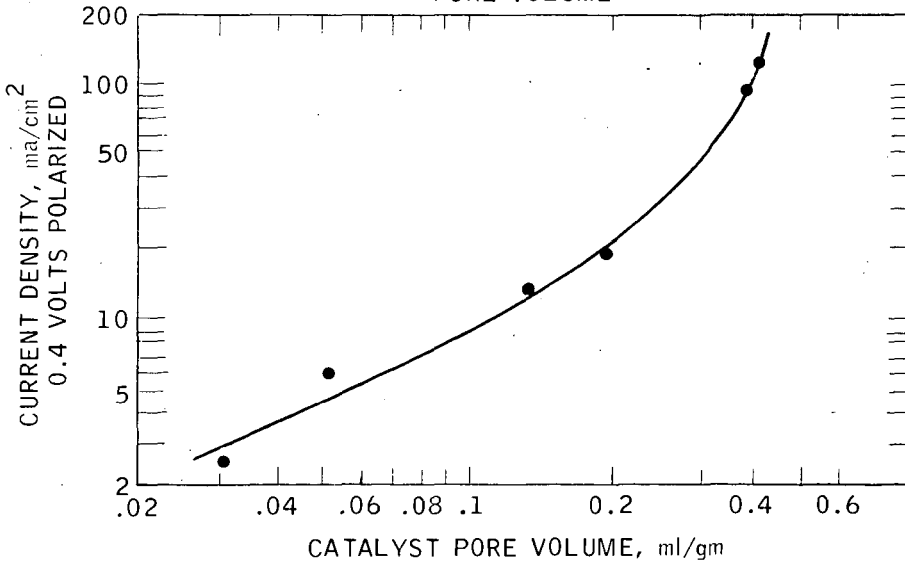


Figure 5
ELECTRON MICROGRAPH OF
HIGH PERFORMANCE CATALYST
PORE VOLUME = $0.4 \text{ cm}^3/\text{gm}$



Figure 6
ELECTRON MICROGRAPH OF
POOR CATALYST
PORE VOLUME = $0.03 \text{ cm}^2/\text{gm}$



1 MM = 300\AA

Figure 7

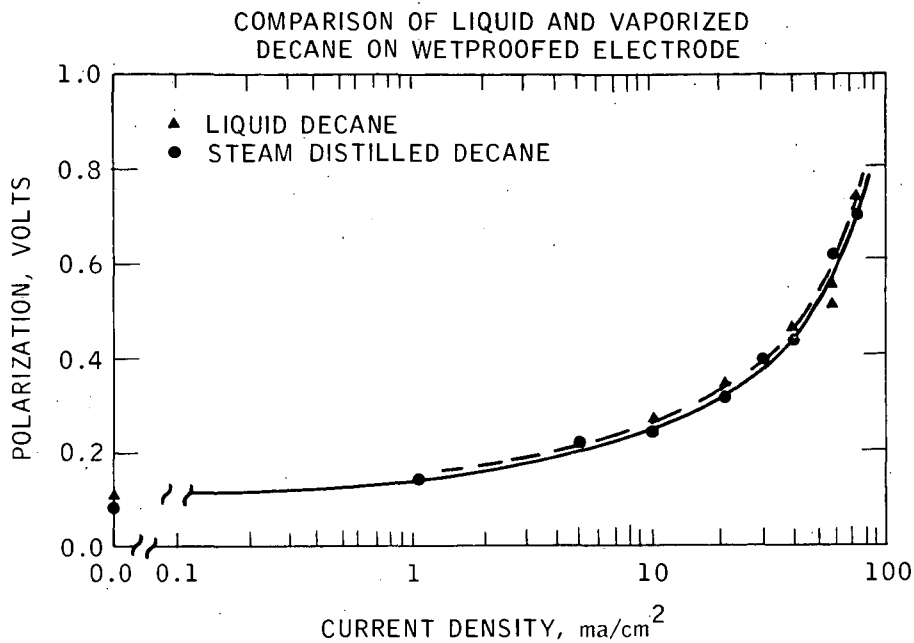


Figure 8

